

See discussions, stats, and author profiles for this publication at: <https://www.researchgate.net/publication/261758280>

# Nondestructive evaluation and health monitoring of highway bridges

Thesis · December 2000

---

CITATIONS

10

---

READS

21

1 author:



[Victor J. Hunt](#)

University of Cincinnati

69 PUBLICATIONS 565 CITATIONS

SEE PROFILE

# UNIVERSITY OF CINCINNATI

November 13 \_\_\_\_\_, 2000

I, Victor J. Hunt,  
**hereby submit this as part of the requirements for the  
degree of:**

Doctorate of Philosophy (Ph.D.)

**in:**

Electrical and Computer Engineering and Computer Science

**It is entitled:**

Nondestructive Evaluation and Health Monitoring

of Highway Bridges

**Approved by:**

Arthur Helmicki

Patrick Garrett

Marios Polycarpou

David Brown

Bruce Walker

Michael Lenett

**Nondestructive Evaluation and Health Monitoring of Highway Bridges**

A dissertation submitted to the

Division of Research and Advanced Studies  
of the University of Cincinnati

in partial fulfillment of the  
requirements for the degree of

DOCTORATE OF PHILOSOPHY (Ph.D.)

in the Department of Electrical and Computer Engineering and Computer Science  
of the College of Engineering

2000

by

Victor J. Hunt

B.S.E.E., University of Cincinnati, 1988

M.S., University of Cincinnati, 1991

Committee Chair: Arthur J. Helmicki, Ph.D.

# Nondestructive Evaluation and Health Monitoring of Highway Bridges

## Abstract

This research seeks the rational organization and integration of nondestructive evaluation (NDE) technologies, the methods of structural identification, and concepts of reliability and fault detection, each according to its merits, within a system devoted to monitoring the state-of-health of an instrumented structure. A global NDE methodology has been developed based upon the structural identification concept, employing *truckload testing, modal testing, and instrumented monitoring* as its principal experimental tools. The test results are transformed to both strain influence lines and modal flexibility, which have been demonstrated to be a conceptual, quantitative, comprehensive, and damage-sensitive signature. These parameters also provide an accurate condition index, since it may be used to conveniently obtain the stress profiles and deflected shapes of a bridge under any loading pattern. The capacity rating for the instrumented section and/or an estimation of the remaining fatigue life for the instrumented member/connection based upon the relevant AASHTO codes can be obtained immediately following the controlled truckload testing of the bridge.

This methodology has provided several unique deliverables to the aforementioned field of expertise:

1. The application, verification, and assessment of truckload testing, modal impact testing, and long-term monitoring procedures, as well as their necessary sensor types and positioning, for several highway bridges.

2. A reduced set of quantitative models for the estimation and identification of single and multiple span beam response to truckload and impact in both the time and frequency domains.
3. The quantitative evaluation of the most promising damage indices for the detection of induced damage-types on a decommissioned specimen.
4. The quantitative identification of AASHTO condition indices and their requisite assumptions from the acquired field data.

The most important contribution of this research is an objective technique for the accurate field identification of bridge parameters (specifically, strain influence lines and modal flexibility) which not only provide for the timely assessment of structural condition but are also sensitive to typical damage scenarios. These results are achieved without a finite element model, but can also serve to calibrate such a model for greater spatial precision and the investigation of other possible damage scenarios, repair/retrofit schemes, and other structural considerations.



## **PREFACE - NATIONAL SIGNIFICANCE AND RESEARCH SCOPE**

The National Science Foundation (NSF) and the Federal Highway Administration (FHWA) have advocated the concept of an intelligent infrastructure for some time with many initiatives. The Civil Infrastructure Systems (CIS) Task Group was established in January, 1992, to represent a broadbased, multi-disciplinary approach towards a solution for the nation's deteriorating and inadequate infrastructure. Due to prohibitive maintenance costs, the task group stressed the need for intelligent renewal which uses limited resources in a cost-effective manner. This necessarily requires a concurrent research initiative to adapt and focus existing knowledge on the monitoring and evaluation of existing structures for their maintained longevity. A grant announcement (NSF 92-56) called for the systems analysis and innovative design of an intelligent structure which would:

- Integrate sensor innovations, microelectronic systems, and diagnostic signature analysis
- Provide accurate evaluation of condition, residual strength, and remaining life
- Explore the application of new materials, such as fiberglass composites

The University of Cincinnati Infrastructure Institute (UCII) has over ten years of experience in the research of assessment technologies for structures, including:

- Loads and natural hazards (service, fatigue, strength, and extreme-event limit states)
- Nondestructive evaluation via controlled truckload and modal testing
- Long-term monitoring and on-line prediction of needed maintenance
- Advanced on-site instrumentation systems and smart materials

- Destructive testing, damage process mechanisms and evaluation of remaining service life
- Characterization of performance under extreme events and acceptable risk
- Interdependence and collocation of infrastructure systems
- Geographical information systems
- Social and economic effects

Three instrumented, steel-stringer bridges in Cincinnati have served as an on-going testbed for UCII research since 1995. Each has been fitted with a custom on-site monitoring system in order to record the effects of the environment, traffic, and our annual regimen of bridge tests. Moreover, one has been subjected to controlled damage and will permit evaluation of different hypotheses on damage detection. Together, they represent the birth, life, and demise of a typical steel-stringer bridge in Ohio.

Steel-stringer bridges, the most common bridge in Ohio, have and will continue to be an important bridge type for UCII. We have examined the before, during, and after effects of the largest truckload in Ohio history (352 ton) as it crossed three critical steel-stringer bridges in Toledo. Several of these bridges were tested and/or monitored during the recent construction of Fort Washington Way along the riverfront in downtown Cincinnati. Six specimens of a thirty bridge project have been truckload and modal impact tested for the beginnings of a statistical database for these bridge types in order to facilitate their general rating, overload routing, maintenance planning, and inventory management by the Ohio Department of Transportation (ODOT).

Other bridge types have also come under our investigation in recent years. A fiber-reinforced polymer (FRP) composite bridge in Dayton is currently being evaluated for its long-term and reliable application for the infrastructure. A cantilever truss bridge in Ironton, built in 1922 over the Ohio River, is presently under our “microscope” due to concerns regarding its present load and fatigue capacity.

Given the synergy of the on-going research and test specimens, the expressed objective for UCII research is the systematic and integrated development of an optimal field testing regimen and a long-term on-site health monitor for highway bridges with a major emphasis on steel-stringer bridges. While the concept of an intelligent structure is not new, many of the issues that need to be resolved are not all recognized. Further, real-life implementation of well-researched concepts is still a major challenge.

The basic issues that are obstructing this research goal include:

- Limitations in sensor and data-acquisition technologies
- Limitations in state-of-the-art field experimentation
- Optimal integration of human and machine intelligence, specifically:
  - Accumulated heuristic know-how and experience on bridge engineering
  - Structural testing results and on-line instrumented monitoring data

The final product is envisioned as an on-site continuous health monitor which:

- Acquires sensor data at variable sampling speeds,
- Communicates with peripheral devices such as a video camera or traffic scale,
- Provides a graphical interface via Internet and phone line with a remote engineer,
- Performs simple range and other checks for sensor faults,
- Identifies parameters for a simple beam or grid model of the bridge,
- Detects any structural degradation or damage via thresholds,
- Has an open architecture for future expansion or connection.

This research is meant to complement and extend the work currently funded by the Ohio Department of Transportation, the Federal Highway Administration, the National Science Foundation and other agencies. The UCII researchers have developed a rational, global condition assessment technique that addresses the conceptualization and measurement of several unknowns for bridges, which include:

- A lack of quantitative knowledge on the as-built state parameters (e.g., initial stresses, strains and displacements, local and global stiffness) and their variation over time;
- A lack of clear and quantitative definitions for the performance parameters (e.g., reliability, functionality, serviceability, safety, lifecycle cost, etc.) and relationships between the state and performance parameters;
- A lack of a clear and complete understanding of the phenomena which influence the state-of-force in a bridge; which lead to changes in state parameters; and/or which lead to a decrease in performance.

This research has and will be conducted collaboratively by a multi-disciplinary team of electrical, mechanical, and civil engineers bringing together knowledge and experience from the areas of space system health monitoring, mechanical modal testing and control, and bridge structural behavior and performance.

# **Nondestructive Evaluation and Health Monitoring of Highway Bridges**

## **Acknowledgements**

I would like to express my deepest gratitude and respect for my friend and advisor, Dr. Arthur Helmicki, for his unending support and guidance through some very tough times in my personal, professional, and academic matters over the past years. For this research, he particularly helped talk through and promote several of the signal processing and systems integration concepts that are now presented in this dissertation. I wholeheartedly acknowledge the very important contributions of my friend and colleague, Dr. Michael Lenett, who was always ready to help with the many theoretical and practical matters that developed every day in the laboratory or in the field. His experience and sound judgement were critical in the evaluation and implementation of the structural engineering concepts and indices explored in this research. I must thank my fellow student and dreamer, Dr. Ahmet Turer, for his unending imagination and contributions to the research. Constantly driven by creative yet boundless ideas, he was a powerful motivator to think big and reach even farther. His early work on the identification of the influence line and the assessment of partial composite action are clearly reflected in my applications here.

Of course, there are no words that can do justice to the encouragement and support of my dear family. When the days seemed long and uncertain, my mother spoke of small measured steps and my father had such faith in my future that all seemed possible. My brother and sister continue to lead by example and the wisdom and humor of my grandparents were like music to the soul. My son, Tyler, has brought unbelievable love and joy into my life; any troubles slip away with him by my side. My tight network of friends, also known as the “uncles”, have been a

constant reprieve from the weekly grind. This past year, I have been blessed with an angel and her wonderful daughter to make each day special and to dream again of tomorrow. All in all, life is good.

Here, I pay tribute to my past colleagues and students who have worked on the many research projects at the University of Cincinnati Infrastructure Institute. I recall the great fun and experience that I gained when working with Dr. Alper Levi, Mr. Kirk Grimmelman, Mr. Ray Barrish, and Mr. Mike Shell during the construction of HAM-126-0881. The damage assessment project for HAM-561-0683 would not have been possible without the efforts of Mrs. Ann Griessmann, Dr. Necati Catbas, and our unique panel of experts. There were significant contributions to our very first instrumented monitor of HAM-42-0992 by Mr. Yong Gao, Mr. Er Zhong, Mr. Srinivas Iyer, Dr. Daniel Farhey, Mr. David Corni, and Mr. Bob Fitzpatrick. The original investigator for these projects was Dr. A. Emin Aktan; I thank him for the opportunity to begin my research in this field and for his confidence in my abilities to simultaneously manage all of these projects and more during his tenure at the University of Cincinnati. Also, he fostered a new appreciation in me for the art, science, and architecture of highway bridges.

This research was supported by the Ohio Department of Transportation (ODOT) and the Federal Highway Administration (FHWA). Mr. Dalal, Fagrell, Moore, Waheed, and Welker of ODOT Bridge Bureau; Mr. Campbell, Eltzroth, and Spinosa of ODOT District 8; and Mr. Rodriguez and Shamis of Ohio FHWA have extended their confidence in this endeavor and for that I am very grateful. I would especially like to thank Mr. Vikram Dalal for his continuous support through many contracted projects with the University. I also acknowledge the valuable input provided by

Dr. Chase of FHWA Headquarters and the Office of Research at Washington, D.C., and Drs. Chong and Liu of the National Science Foundation.

Lastly, I would like to thank the committee members for this research. Each of you has provided me with your valuable time, experienced advice, and thoughtful regard in this and other matters over the past years and for that I am indebted to you.

# Nondestructive Evaluation and Health Monitoring of Highway Bridges

## Table of Contents

<b>LIST OF TABLES</b>	<b>vi</b>
<b>LIST OF FIGURES</b>	<b>viii</b>
<b>1. INTRODUCTION</b>	<b>1-1</b>
1.1. FIELD OF EXPERTISE	1-1
1.2. BACKGROUND	1-3
1.2.1. <i>The Crumbling Infrastructure</i>	1-3
1.2.2. <i>Diagnostic Load Testing</i>	1-8
1.2.3. <i>Modal Impact Testing</i>	1-11
1.2.4. <i>Finite Element Modeling</i>	1-13
1.2.5. <i>Systems Identification Approach</i>	1-16
1.2.6. <i>Consensus Terminology for Structural Systems</i>	1-20
1.3. OBJECTIVE AND EXPECTED SIGNIFICANCE OF THE RESEARCH	1-23
1.3.1. <i>Instrumented Monitoring of a Bridge in Service</i>	1-26
1.3.2. <i>Lifetime Monitor of a Constructed Bridge</i>	1-29
1.3.3. <i>Validation of Tools Via Damage Simulation Project</i>	1-39
1.4. PROBLEM STATEMENT AND RESEARCH DELIVERABLES	1-41
<b>2. ANALYSIS AND IDENTIFICATION OF A HIGHWAY BRIDGE UNDER TRUCKLOAD</b>	<b>2-1</b>
2.1. ELASTIC DEFORMATION OF A BEAM WITH A SINGLE SPAN UNDER QUASI-STATIC EQUILIBRIUM	2-2
2.1.1. <i>Ideal Beam Response to a Slowly Moving Point or Axle Load</i>	2-8
2.1.2. <i>Ideal Beam Response to a Slowly Moving Truckload</i>	2-18

2.2.	ELASTIC DEFORMATION OF A BEAM WITH MULTIPLE SPANS UNDER QUASI-STATIC EQUILIBRIUM	2-22
2.2.1.	<i>Ideal Multi-Span Beam Response to a Slowly Moving Point or Axle Load</i>	2-23
2.2.2.	<i>Ideal Multi-Span Beam Response to a Slowly Moving Truckload</i>	2-32
2.3.	ELASTIC DEFORMATION OF A BEAM WITH A SINGLE SPAN UNDER DYNAMIC CONDITIONS	2-37
2.3.1.	<i>The Conventional MKC Lumped Mechanical Model - Temporal and Frequency Domains</i>	2-37
2.3.2.	<i>The Generalized MKC Distributed Model – Spatial, Temporal and Frequency Domains</i>	2-41
2.4.	ELASTIC DEFORMATION OF A SINGLE SPAN UNDER DYNAMIC CONDITIONS	2-49
2.5.	THE COUPLED DYNAMIC INTERACTION OF BEAM AND LOAD	2-51
2.6.	FIELD IDENTIFICATION OF BRIDGE INFLUENCE LINES	2-53
<b>3.</b>	<b>CONDITION ASSESSMENT OF A HIGHWAY BRIDGE UNDER TRUCKLOAD</b>	<b>3-1</b>
3.1.	SECTIONAL INDICES FOR CONDITION ASSESSMENT UNDER TRUCK AND LANE LOAD	3-7
3.1.1.	<i>Maximum Stress in the Outer Fiber (i.e., Bottom Flange)</i>	3-7
3.1.2.	<i>Modal Frequencies, Shapes, and Weighting</i>	3-10
3.1.3.	<i>Curvature</i>	3-11
3.1.4.	<i>Neutral Axis Location</i>	3-13
3.1.5.	<i>Truckload Moment</i>	3-15
	Method 1: Fully Composite with Nonzero Axial Force	3-17
	Method 2: Fully Composite with No Axial Force	3-18
	Method 3: Partially Composite with No Axial Force	3-21
	Method 4: Noncomposite with Axial Force	3-23
	Example Estimation of Moments for Truckload Test of HAM-126-0881	3-24
	Comparison of Analysis Methods by Simulating Stages of Composite Action	3-29
3.1.6.	<i>Distribution Factor</i>	3-30
3.1.7.	<i>Impact Factor</i>	3-33
3.1.8.	<i>Capacity Load Rating</i>	3-36
	Working or Allowable Stress Method	3-36
	Limit States or Load Factor Method	3-37

Inventory and Operating Load Ratings	3-38
Ultimate Moment by the Four Analysis Methods	3-40
Deadload Moment by the Four Analysis Methods	3-42
Truck Liveload Moment and Rating by the Four Analysis Methods	3-43
Example Truck Liveload Moment and Rating for HAM-126-0881	3-45
Lane Liveload Moment and Rating by the Four Analysis Methods	3-56
Example Lane Liveload Moment and Rating for HAM-126-0881	3-58
Event (e.g., construction) Moment and Rating by the Four Analysis Methods	3-64
Environmental (e.g., thermal) Moment and Rating by the Four Analysis Methods	3-65
3.1.9. <i>Remaining Fatigue Life</i>	3-69
<b>4. DAMAGE ASSESSMENT OF A HIGHWAY BRIDGE UNDER TRUCKLOAD</b>	<b>4-1</b>
4.1. LOCAL NONDESTRUCTIVE DIAGNOSTIC TECHNIQUES (NDT) FOR HIGHWAY BRIDGES	4-4
4.1.1. <i>Ultrasonic Evaluation</i>	4-5
4.1.2. <i>Half-Cell Potential</i>	4-5
4.1.3. <i>Acoustic Emission</i>	4-6
4.1.4. <i>Radiographic Testing</i>	4-6
4.1.5. <i>Impact-Echo Techniques</i>	4-6
4.1.6. <i>Infrared Thermography</i>	4-7
4.1.7. <i>Ground Penetrating Radar</i>	4-7
4.1.8. <i>Surveying</i>	4-8
4.2. GLOBAL NONDESTRUCTIVE DIAGNOSTIC TECHNIQUES (NDT) FOR HIGHWAY BRIDGES	4-8
4.2.1. <i>Modal Analysis</i>	4-8
4.2.2. <i>Diagnostic Load Testing &amp; Instrumented Health Monitoring</i>	4-10
4.3. INDUCED DAMAGE EXPERIMENTS FOR CLOSED BRIDGE SPECIMEN	4-12
4.3.1. <i>Sectional Indices for Damage Assessment under Instrumented Monitoring</i>	4-17
4.3.2. <i>Sectional Indices for Damage Assessment under Static Truckload</i>	4-20
4.3.3. <i>Sectional Indices for Damage Assessment under Modal Impact</i>	4-23

4.3.4.	<i>Sectional Indices for Damage Assessment under Crawl-Speed Truckload</i>	4-25
	Maximum Stress for Bottom Flange Sensors	4-26
	Capacity Load Rating for Instrumented Sections	4-29
4.3.5.	<i>Sectional Indices for Damage Assessment by Finite Element Model</i>	4-33
4.3.6.	<i>Sectional Indices for Damage Assessment by Visual Inspection</i>	4-37
<b>5.</b>	<b>HEALTH MONITORING/MANAGEMENT SYSTEM FOR HIGHWAY BRIDGES</b>	<b>5-1</b>
5.1.	EXISTING SYSTEM FOR THE HEALTH MONITORING OF A STEEL-STRINGER BRIDGE	5-5
5.1.1.	<i>Local Data Acquisition</i>	5-7
5.1.2.	<i>Coordinated Platform</i>	5-10
5.1.3.	<i>Qualitative Decisions</i>	5-18
5.2.	FUTURE IMPROVEMENTS TO THE BRIDGE HEALTH MONITORING SYSTEM	5-19
5.2.1.	<i>Autonomous Operation</i>	5-21
5.2.2.	<i>Parameter Processing, Display, and Archival</i>	5-23
5.2.3.	<i>Relevant Health Decision Algorithms</i>	5-26
5.3.	BRIDGE MANAGEMENT SYSTEM	5-31
5.3.1.	<i>Qualitative or Heuristic Knowledge Base</i>	5-32
5.3.2.	<i>Adaptive or Neural Algorithms for Learning</i>	5-34
5.3.3.	<i>Statistical Knowledge Base of Common Bridge Types</i>	5-36
<b>6.</b>	<b>CONCLUSIONS</b>	<b>6-1</b>
6.1.	GENERAL OVERVIEW OF THE RESEARCH	6-1
6.2.	SPECIFIC REVIEW OF THE DISSERTATION	6-5
<b>7.</b>	<b>REFERENCES</b>	<b>7-1</b>

<b>A1.</b>	<b>APPENDIX: Elastic Deformation at the Middle of a Single Span Beam Under Crawl Truckload</b>	<b>A1-1</b>
<b>A2.</b>	<b>APPENDIX: Elastic Deformation at the Quadrant of a Single Span Beam Under Crawl Truckload</b>	<b>A2-1</b>
<b>A3.</b>	<b>APPENDIX: Elastic Deformation of the End Span of a Three Span Beam Under Static Equilibrium</b>	<b>A3-1</b>
<b>A4.</b>	<b>APPENDIX: Elastic Deformation of the Middle Span of a Three Span Beam Under Static Equilibrium</b>	<b>A4-1</b>
<b>A5.</b>	<b>APPENDIX: Elastic Deformation of the End Span of a Three Span Beam Under Crawl Truckload</b>	<b>A5-1</b>
<b>A6.</b>	<b>APPENDIX: Elastic Deformation of a Single Span Beam Under Dynamic Truckload</b>	<b>A6-1</b>
<b>B1.</b>	<b>APPENDIX: Design Calculations For Constructed Bridge, HAM-126-0881</b>	<b>B1-1</b>
<b>C1.</b>	<b>APPENDIX: Optimization of the Data Acquisition System, Optim Electronics MEGADAC</b>	<b>C1-1</b>

# Nondestructive Evaluation and Health Monitoring of Highway Bridges

## List of Tables

TABLE 1-1A: PERCENTAGE OF DEFICIENT BRIDGES	1-4
TABLE 1-1B: BUDGET FOR DEFICIENT BRIDGES	1-4
TABLE 3-1: SOME COMMON LINEARIZED CONDITION INDICES FOR CONSTRUCTED FACILITIES	3-2
TABLE 3-2: THEORETICAL AND IDENTIFIED PARAMETERS FOR TEST TRUCK ON BRIDGE, HAM-126-0881	3-28
TABLE 3-3: THEORETICAL AND IDENTIFIED PARAMETERS FOR HS20 TRUCK ON BRIDGE, HAM-126-0881, UNINTENDED COMPOSITE ACTION IS ALLOWED FOR IDENTIFIED PARAMETERS AT LIMIT STATES	3-54
TABLE 3-4: THEORETICAL AND IDENTIFIED PARAMETERS FOR HS20 TRUCK ON BRIDGE, HAM-126-0881, COMPOSITE ACTION AS DESIGNED IS ENFORCED FOR IDENTIFIED PARAMETERS AT LIMIT STATES, ULTIMATE CAPACITY IS LIMITED AS PER NONCOMPACT BUT COMPOSITE SECTION	3-55
TABLE 3-5: THEORETICAL AND IDENTIFIED PARAMETERS FOR HS20 TRUCK ON BRIDGE, HAM-126-0881, COMPOSITE ACTION AS DESIGNED IS ENFORCED FOR IDENTIFIED PARAMETERS AT LIMIT STATES, ULTIMATE CAPACITY IS LIMITED AS PER NONCOMPACT BUT COMPOSITE SECTION, MEASURED DEADLOAD AND OTHER CONSTRUCTION STRESSES ARE USED	3-66
TABLE 3-6: THEORETICAL AND IDENTIFIED PARAMETERS FOR HS20 TRUCK ON BRIDGE, HAM-126-0881, COMPOSITE ACTION AS DESIGNED IS ENFORCED FOR IDENTIFIED PARAMETERS AT LIMIT STATES, ULTIMATE CAPACITY IS LIMITED AS PER NONCOMPACT BUT COMPOSITE SECTION, MEASURED CONSTRUCTION AND ENVIRONMENTAL STRESSES ARE USED	3-67
TABLE 3-7: LIMIT TEST OF STRESS RANGE FOR INFINITE FATIGUE LIFE OF DETAIL CATEGORY	3-72
TABLE 3-8: DEADLOAD TEST OF TENSILE STRESS FOR INFINITE FATIGUE LIFE OF DETAIL CATEGORY	3-72
TABLE 3-9: REMAINING FATIGUE LIFE FOR CRITICAL SECTIONS OF HAM-126-0881	3-73

TABLE 4-1:	COMPARISON OF ANALYTICAL SECTION PROPERTIES AND STRAINS	4-19
TABLE 4-2:	CONDITION SUMMARY OF POSITIVE MOMENT REGIONS BEFORE FLANGE CUT, HAM-561-0683	4-31
TABLE 4-3:	CONDITION SUMMARY OF POSITIVE MOMENT REGIONS AFTER FLANGE CUT, HAM-561-0683	4-31
TABLE 4-4:	CONDITION SUMMARY OF CRITICAL REGIONS BEFORE FLANGE CUT, HAM-561-0683	4-31
TABLE 4-5:	CONDITION SUMMARY OF CRITICAL REGIONS AFTER FLANGE CUT, HAM-561-0683	4-31
TABLE 4-6:	DESIGN VALUES OF CRITICAL REGIONS, HAM-561-0683	4-31
TABLE 4-7:	CONDITION SUMMARY OF FE MODEL BEFORE FLANGE CUT, HAM-561-0683	4-35
TABLE 4-8:	CONDITION SUMMARY OF FE MODEL AFTER FLANGE CUT, HAM-561-0683	4-35
TABLE 4-9:	MODIFIED SUMMARY OF CRITICAL REGIONS BEFORE FLANGE CUT, HAM-561-0683	4-36
TABLE 4-10:	MODIFIED SUMMARY OF CRITICAL REGIONS AFTER FLANGE CUT, HAM-561-0683	4-37
TABLE 5-1:	REQUIRED BANDWIDTH FOR BRIDGE HEALTH MONITORING SYSTEM	5-14

# **Nondestructive Evaluation and Health Monitoring of Highway Bridges**

## **List of Figures**

FIGURE 1-1: TOOLBOX OF NDE METHODS AND TECHNOLOGIES	1-2
FIGURE 1-2: BRIDGE CONSTRUCTION TIMELINE	1-4
FIGURE 1-3: BRIDGE INSPECTION REPORT	1-5
FIGURE 1-4: SILVER BRIDGE COLLAPSE IN 1967	1-8
FIGURE 1-5: AASHTO TRUCK AND LANE LOAD RATINGS FROM INFLUENCE LINE	1-10
FIGURE 1-6: MOBILE LABORATORY FOR MODAL IMPACT TESTING OF HIGHWAY BRIDGES	1-12
FIGURE 1-7: CALIBRATION OF FINITE ELEMENT MODEL WITH BRIDGE TEST RESULTS	1-15
FIGURE 1-8: MULTI-SYSTEM CONCEPTUALIZATION OF INTELLIGENT INFRASTRUCTURE	1-17
FIGURE 1-9: NDT REGIMEN OF STRUCTURAL EVALUATION	1-18
FIGURE 1-10: LIFETIME ASSESSMENT OF STEEL-STRINGER BRIDGES	1-18
FIGURE 1-11: HIERARCHICAL MONITOR SYSTEM FOR HIGHWAY BRIDGES	1-20
FIGURE 1-12: SYSTEM AND STRATEGY FOR INSTRUMENTED HEALTH MONITORING	1-23
FIGURE 1-13: NATIONAL TEST SITES IN CINCINNATI, OHIO	1-26
FIGURE 1-14: IMPLEMENTED BRIDGE HEALTH MONITOR, HAM-42-0992	1-28
FIGURE 1-15: TYPICAL RESPONSES TO TRAFFIC AND LONG-TERM ENVIRONMENTAL INPUTS	1-28
FIGURE 1-16: INSTRUMENTATION, TESTING, AND MONITORING OF THE CONSTRUCTION AND SERVICE OF A STEEL- STRINGER BRIDGE	1-30
FIGURE 1-17: INSTRUMENTED MONITORING OF DEADLOAD STRESSES	1-32
FIGURE 1-18: INSTRUMENTED MONITORING OF CROSSFRAME WELD STRESSES	1-33
FIGURE 1-19: INSTRUMENTED MONITORING OF BEARING WELD STRESSES	1-34
FIGURE 1-20: COMPARISON OF AASHTO DESIGN MODEL AND ACTUAL FIELD EXPERIMENT	1-35
FIGURE 1-21: DYNAMIC RESPONSE OF BRIDGE, HAM-126-0881	1-36
FIGURE 1-22: DYNAMIC RESPONSE OF BRIDGE, HAM-42-0992	1-36
FIGURE 1-23: SUMMARY OF LIFETIME STEEL STRESSES FOR BRIDGE, HAM-126-0881	1-37
FIGURE 1-24: MODAL IMPACT TEST SYSTEM FOR DETECTION OF INDUCED DAMAGE	1-40

FIGURE 1-25: BRIDGE GIRDER CONDITION INDICATOR AND TRUCKLOAD VERIFICATION	1-41
FIGURE 1-26: INSTRUMENTED HEALTH MONITOR FOR BRIDGE, HAM-126-0881	1-45
FIGURE 2-1: SIMPLY SUPPORTED BEAM	2-2
FIGURE 2-2: BENDING THEORY FOR A SIMPLY SUPPORTED BEAM	2-3
FIGURE 2-3: EQUILIBRIUM OF FORCES FOR A UNIT CROSS SECTION OF BEAM	2-7
FIGURE 2-4: TRUCKLOAD RESPONSE DETERMINED FROM INFLUENCE LINES	2-10
FIGURE 2-5: MOMENT AND DEFLECTION FOR A POINT LOAD AND THE UIL AT MIDSPAN OF AN IDEAL BEAM	2-11
FIGURE 2-6: MOMENT AND DEFLECTION FOR A SIMULATED TRUCKLOAD AT MIDSPAN OF AN IDEAL BEAM	2-11
FIGURE 2-7: DEFLECTION MAGNITUDE AND PHASE FOR POINT LOAD OF SIMPLE BEAM AT 10MPH	2-13
FIGURE 2-8: MOMENT MAGNITUDE AND PHASE FOR POINT LOAD OF SIMPLE BEAM AT 10MPH	2-13
FIGURE 2-9: DEFLECTION MAGNITUDE AND PHASE FOR POINT LOAD OF SIMPLE BEAM AT 50MPH	2-14
FIGURE 2-10: MOMENT MAGNITUDE AND PHASE FOR POINT LOAD OF SIMPLE BEAM AT 50MPH	2-14
FIGURE 2-11: MOMENT MAGNITUDE AND PHASE FOR POINT LOAD OF QUARTER SPAN AT 50MPH	2-15
FIGURE 2-12: DEFLECTION MAGNITUDE AND PHASE COMPARISON OF FT AND FFT FOR POINT LOAD AT 50MPH	2-17
FIGURE 2-13: MOMENT MAGNITUDE AND PHASE COMPARISON OF FT AND FFT FOR POINT LOAD AT 50MPH	2-17
FIGURE 2-14: DEFLECTION MAGNITUDE AND PHASE FOR TRUCKLOAD OF SIMPLE BEAM AT 10MPH	2-18
FIGURE 2-15: MOMENT MAGNITUDE AND PHASE FOR TRUCKLOAD OF SIMPLE BEAM AT 10MPH	2-18
FIGURE 2-16: DEFLECTION MAGNITUDE AND PHASE FOR TRUCKLOAD OF SIMPLE BEAM AT 50MPH	2-19
FIGURE 2-17: MOMENT MAGNITUDE AND PHASE FOR TRUCKLOAD OF SIMPLE BEAM AT 50MPH	2-19
FIGURE 2-18: DEFLECTION MAGNITUDE AND PHASE COMPARISON OF FT AND FFT FOR TRUCKLOAD AT 50MPH	2-22
FIGURE 2-19: MOMENT MAGNITUDE AND PHASE COMPARISON OF FT AND FFT FOR TRUCKLOAD AT 50MPH	2-22
FIGURE 2-20: SIMPLY SUPPORTED BEAM WITH THREE SPANS	2-23
FIGURE 2-21: MOMENT AND DEFLECTION FOR A STATIONARY POINT LOAD AT 1 <sup>ST</sup> MIDSPAN OF A 3-SPAN BEAM	2-25
FIGURE 2-22: MOMENT AND DEFLECTION FOR A MOVING POINT LOAD AT 1 <sup>ST</sup> MIDSPAN OF A 3-SPAN BEAM	2-25
FIGURE 2-23: MOMENT AND DEFLECTION FOR A SIMULATED TRUCKLOAD AT 1 <sup>ST</sup> MIDSPAN OF A 3-SPAN BEAM	2-25
FIGURE 2-24: DEFLECTION MAGNITUDE & PHASE FOR POINT LOAD OF 1 <sup>ST</sup> MIDSPAN OF 3-SPAN BEAM, 10MPH	2-26

FIGURE 2-25: MOMENT MAGNITUDE & PHASE FOR POINT LOAD OF 1 <sup>ST</sup> MIDSPAN OF 3-SPAN BEAM, 10MPH	2-26
FIGURE 2-26: DEFLECTION MAGNITUDE & PHASE FOR POINT LOAD OF 1 <sup>ST</sup> MIDSPAN OF 3-SPAN BEAM, 50MPH	2-27
FIGURE 2-27: MOMENT MAGNITUDE & PHASE FOR POINT LOAD OF 1 <sup>ST</sup> MIDSPAN OF 3-SPAN BEAM, 50MPH	2-27
FIGURE 2-28: DEFLECTION MAGNITUDE AND PHASE COMPARISON OF FT AND FFT FOR POINT LOAD AT 50MPH	2-31
FIGURE 2-29: MOMENT MAGNITUDE AND PHASE COMPARISON OF FT AND FFT FOR POINT LOAD AT 50MPH	2-31
FIGURE 2-30: DEFLECTION MAGNITUDE & PHASE FOR TRUCKLOAD OF 1 <sup>ST</sup> MIDSPAN OF 3-SPAN BEAM, 10MPH	2-32
FIGURE 2-31: MOMENT MAGNITUDE & PHASE FOR TRUCKLOAD OF 1 <sup>ST</sup> MIDSPAN OF 3-SPAN BEAM, 10MPH	2-32
FIGURE 2-32: DEFLECTION MAGNITUDE & PHASE FOR TRUCKLOAD OF 1 <sup>ST</sup> MIDSPAN OF 3-SPAN BEAM, 50MPH	2-33
FIGURE 2-33: MOMENT MAGNITUDE & PHASE FOR TRUCKLOAD OF 1 <sup>ST</sup> MIDSPAN OF 3-SPAN BEAM, 50MPH	2-33
FIGURE 2-34: DEFLECTION MAGNITUDE AND PHASE COMPARISON OF FT AND FFT FOR TRUCKLOAD AT 50MPH	2-36
FIGURE 2-35: MOMENT MAGNITUDE AND PHASE COMPARISON OF FT AND FFT FOR TRUCKLOAD AT 50MPH	2-36
FIGURE 2-36: MKC PARAMETER ESTIMATION FROM TIME OR FREQUENCY DOMAINS	2-38
FIGURE 2-37: MAGNITUDE AND PHASE OF DYNAMIC EXCITATION OF IDEAL BEAM FROM POINT LOAD, 50MPH	2-45
FIGURE 2-38: MAGNITUDE AND PHASE OF FREE DECAY OF IDEAL BEAM AFTER POINT LOAD, 50MPH	2-46
FIGURE 2-39: MAGNITUDE AND PHASE OF FULL DYNAMIC RESPONSE OF IDEAL BEAM TO POINT LOAD, 50MPH	2-46
FIGURE 2-40: DYNAMIC DEFLECTION OF IDEAL BEAM TO POINT LOAD, 50MPH	2-47
FIGURE 2-41: DYNAMIC MOMENT OF IDEAL BEAM TO POINT LOAD, 50MPH	2-48
FIGURE 2-42: DEFLECTION MAGNITUDE AND PHASE COMPARISON OF FT AND FFT FOR POINT LOAD, 50 MPH	2-49
FIGURE 2-43: TIME RESPONSES AND UIL FOR CRAWL TRUCKLOAD TEST OF BRIDGE, HAM-42-0992	2-54
FIGURE 2-44: FREQUENCY RESPONSES AND UIL FOR CRAWL TRUCKLOAD TEST OF BRIDGE, HAM-42-0992	2-54
FIGURE 2-45: COMPARISON OF STATIC, CRAWL-SPEED, AND SIMULATED TRUCK RESPONSES	2-56
FIGURE 2-46: COMPARISON OF MEASURED VS. SIMULATED RESPONSE OF DUMP TRUCK AT 40 MPH	2-58
FIGURE 2-47: COMPARISON OF MEASURED VS. SIMULATED RESPONSE OF TANDEM TRUCK AT 40 MPH	2-59
FIGURE 2-48: TIME RESPONSES AND UIL FOR CRAWL TRUCKLOAD TEST OF BRIDGE, HAM-126-0881	2-61
FIGURE 2-49: FREQUENCY RESPONSES AND UIL FOR CRAWL TRUCKLOAD TEST OF BRIDGE, HAM-126-0881	2-61
FIGURE 2-50: INFLUENCE LINES FOR ALL TRAFFIC SENSORS OF BRIDGE MONITORING SYSTEM, HAM-126-0881	2-62
FIGURE 2-51: SIMULATION OF INFLUENCE LINE USING SCALED MOMENT EQUATIONS FOR IDEAL BEAM	2-63
FIGURE 2-52: COMPARISON OF MEASURED VS. SIMULATED RESPONSE OF DUMP TRUCK AT 50 MPH	2-65

FIGURE 2-53: COMPARISON OF MEASURED VS. SIMULATED RESPONSE OF TANDEM TRUCK AT 50 MPH	2-66
FIGURE 2-54: COMPARISON OF MEASURED VS. SIMULATED RESPONSE OF SEMI TRUCK AT 50 MPH	2-67
FIGURE 3-1: FILTERED TRUCKLOAD RESPONSES FOR CRITICAL CROSS-SECTIONS OF HAM-126-0881	3-8
FIGURE 3-2: INFLUENCE LINES FOR CRITICAL CROSS-SECTIONS OF HAM-126-0881	3-9
FIGURE 3-3: NEUTRAL AXIS LOCATION DURING TRUCKLOAD OF HAM-126-0881	3-14
FIGURE 3-4: IDEAL BEHAVIOR FOR A FULLY COMPOSITE AND NONCOMPOSITE SECTION OF EAST SPAN	3-15
FIGURE 3-5: FIRST METHOD OF ESTIMATING THE SECTION MOMENT FOR EAST SPAN	3-17
FIGURE 3-6: MEASURED STRAIN PROFILE FOR FULLY COMPOSITE SECTION OF HAM-126-0881	3-18
FIGURE 3-7: SECOND METHOD OF ESTIMATING THE SECTION MOMENT FOR EAST SPAN	3-19
FIGURE 3-8: MEASURED STRAIN PROFILE FOR PARTIALLY COMPOSITE SECTION OF HAM-126-0881	3-20
FIGURE 3-9: THIRD METHOD OF ESTIMATING THE SECTION MOMENT FOR EAST SPAN	3-22
FIGURE 3-10: FOURTH METHOD OF ESTIMATING THE SECTION MOMENT FOR EAST SPAN	3-24
FIGURE 3-11: EFFECTIVE DECK WIDTH AND RCA FOR TRUCKLOAD TEST OF HAM-126-0881	3-26
FIGURE 3-12: ESTIMATED MOMENT OF MIDDLE SPAN FOR TRUCKLOAD TEST OF HAM-126-0881	3-26
FIGURE 3-13: ESTIMATED MOMENT OF EAST SPAN FOR TRUCKLOAD TEST OF HAM-126-0881	3-27
FIGURE 3-14: ESTIMATED MOMENT OF EAST PIER FOR TRUCKLOAD TEST OF HAM-126-0881	3-27
FIGURE 3-15: COMPARISON OF ANALYSIS METHODS FOR VARIOUS STAGES OF COMPOSITE ACTION	3-30
FIGURE 3-16: IMPACT FACTOR FOR VARIOUS TRUCKLOAD TESTS OF HAM-126-0881	3-35
FIGURE 3-17: AASHTO TRUCK AND LANE LOAD SPECIFICATIONS	3-44
FIGURE 3-18: LIVELOAD STRESS AND MOMENT OF SIMULATED HS20 TRUCKLOAD FOR THE MIDDLE SPAN	3-46
FIGURE 3-19: RATING FACTORS OF SIMULATED HS20 TRUCKLOAD FOR MIDDLE SPAN	3-47
FIGURE 3-20: SUMMARY OF CONDITION ASSESSMENT RESULTS FOR MIDDLE SPAN	3-47
FIGURE 3-21: LIVELOAD STRESS AND MOMENT OF SIMULATED HS20 TRUCKLOAD FOR THE EAST SPAN	3-48
FIGURE 3-22: RATING FACTORS OF SIMULATED HS20 TRUCKLOAD FOR THE EAST SPAN	3-49
FIGURE 3-23: SUMMARY OF CONDITION ASSESSMENT RESULTS FOR EAST SPAN	3-49
FIGURE 3-24: REDUCED RATING FACTORS FOR UNINTENDED COMPOSITE ACTION IN EAST SPAN	3-51

FIGURE 3-25: LIVELOAD STRESS AND MOMENT OF SIMULATED HS20 TRUCKLOAD FOR THE EAST PIER	3-52
FIGURE 3-26: RATING FACTORS OF SIMULATED HS20 TRUCKLOAD FOR THE EAST PIER	3-53
FIGURE 3-27: SUMMARY OF CONDITION ASSESSMENT RESULTS FOR EAST PIER	3-53
FIGURE 3-28: LIVELOAD STRESS AND MOMENT OF SIMULATED HS20 LANELOAD FOR THE MIDDLE SPAN	3-59
FIGURE 3-29: RATING FACTORS OF SIMULATED HS20 LANELOAD FOR THE MIDDLE SPAN	3-59
FIGURE 3-30: LIVELOAD STRESS AND MOMENT OF SIMULATED HS20 LANELOAD FOR THE EAST SPAN	3-60
FIGURE 3-31: RATING FACTORS OF SIMULATED HS20 LANELOAD FOR THE EAST SPAN	3-61
FIGURE 3-32: LIVELOAD STRESS AND MOMENT OF SIMULATED HS20 LANELOAD FOR THE EAST PIER	3-62
FIGURE 3-33: RATING FACTORS OF SIMULATED HS20 LANELOAD AND FIRST POINT LOAD FOR THE EAST PIER	3-63
FIGURE 3-34: RATING FACTORS OF SIMULATED HS20 LANELOAD AND BOTH POINT LOADS FOR THE EAST PIER	3-63
FIGURE 3-35: SUMMARY OF CONDITION ASSESSMENT FOR CRITICAL SECTION OF HAM-126-0881	3-68
FIGURE 3-36: SUMMARY OF INSTRUMENTED MONITORING FOR CRITICAL SECTION OF HAM-126-0881	3-69
FIGURE 3-37: EXAMPLE CALCULATION OF REMAINING FATIGUE LIFE FOR MIDDLE SPAN	3-72
FIGURE 4-1: GENERAL PLANS FOR HAM-561-0683	4-13
FIGURE 4-2: LOCATION AND TYPES OF DETERIORATION FOR HAM-561-0683	4-14
FIGURE 4-3: INSTRUMENTATION PLAN FOR HAM-561-0683	4-15
FIGURE 4-4: CALENDAR, TYPES, AND LOCATION OF INDUCED DAMAGES FOR HAM-561-0683	4-16
FIGURE 4-5: INSTRUMENTED MONITORING OF FLANGE CUT FOR HAM-561-0683	4-18
FIGURE 4-6: ESTIMATED SECTIONAL PROPERTIES DUE TO INDUCED DAMAGES	4-19
FIGURE 4-7: DEFLECTION PROFILE FOR FLANGE, WEB, AND CROSSFRAME CUTS OF HAM-561-0683	4-21
FIGURE 4-8: STRAIN PROFILES FOR FLANGE, WEB, AND CROSSFRAME CUTS OF HAM-561-0683	4-22
FIGURE 4-9: CORRELATION OF DEFLECTION PROFILES FOR TRUCKLOAD AND MODAL TESTS	4-23
FIGURE 4-10: BRIDGE GIRDER CONDITION INDICATOR OF DAMAGE SCENARIOS FOR HAM-561-0683	4-25
FIGURE 4-11: INFLUENCE LINE BEFORE AND AFTER FLANGE CUT FOR BOTTOM FLANGE OF SOUTH SPAN	4-27
FIGURE 4-12: INFLUENCE LINES BEFORE AND AFTER FLANGE CUT FOR BOTTOM FLANGE OF OTHER SPANS	4-27
FIGURE 4-13: INFLUENCE LINES BEFORE AND AFTER FLANGE CUT FOR BOTTOM FLANGE OF PIERS	4-28

FIGURE 4-14: CALIBRATION OF THE FINITE ELEMENT MODEL FOR HAM-561-0683	4-34
FIGURE 4-15: SUMMARY ASSESSMENT FOR INDUCED DAMAGE PROJECT, HAM-561-0683	4-40
FIGURE 5-1: HEALTH MONITORING SYSTEM FOR BRIDGE, HAM-126-0881	5-3
FIGURE 5-2: HEALTH DECISION STRATEGY FOR BRIDGE, HAM-42-0992	5-4
FIGURE 5-3: SYSTEM HIERARCHY FOR A BRIDGE, HAM-126-0881	5-5
FIGURE 5-4: PARAMETER ACCURACY FOR WEIGH-IN-MOTION SCALES	5-10
FIGURE 5-5: SYSTEM DIAGRAM FOR INTERNET COMMUNICATION	5-13
FIGURE 5-6: REMOTE INTERNET DISPLAY OF BRIDGE CONDITION, HAM-126-0881	5-15
FIGURE 5-7: INFORMATION SOURCES AND REQUIRED STORAGE CAPACITY	5-16
FIGURE 5-8: EXAMPLE DISPLAYS OF MAXIMUM STRESS FOR TRAFFIC AND ENVIRONMENTAL MONITORING	5-24
FIGURE 5-9: EXAMPLE DISPLAY FOR MAXIMUM SHIFT IN NEUTRAL AXIS	5-24
FIGURE 5-10: EXAMPLE DISPLAY FOR UNIT INFLUENCE LINE	5-25
FIGURE 5-11: EXAMPLE DISPLAY FOR MODAL PARAMETERS	5-25
FIGURE 5-12: THRESHOLDING FOR DAMAGE DETECTION	5-29
FIGURE 5-13: HIERARCHY OF DAMAGE INDICATOR THRESHOLDS	5-29
FIGURE 5-14: EXAMPLE DISPLAY OF SENSOR CONDITION STATUS	5-30
FIGURE 5-15: MANAGEMENT DECISION TREE FOR IDENTIFIED STRUCTURAL CONDITION STATES	5-33
FIGURE 5-16: STATISTICS FOR STEEL-STRINGER BRIDGES IN OHIO	5-37
FIGURE 5-17: STATISTICAL CONFIDENCE FOR SAMPLE SIZE	5-39

# **Nondestructive Evaluation and Health Monitoring of Highway Bridges**

A Dissertation by

Victor J. Hunt

## 1. Introduction

### 1.1. Field of Expertise

This interdisciplinary research draws heavily from several engineering sciences: structural identification, reliability or risk evaluation, nondestructive testing, and health monitoring. Structural identification has been defined as: “the development of an analytical conceptualization of a structure, or region thereof (including supports and continuity), and quantifying, testing, improving, and validating the resulting analytical model by correlating response simulated by the model with those of the measured structure [Ibanez, 1972].” Reliability evaluation involves the prediction of an adverse event or trend (e.g. structural collapse, member deterioration) and the probable timing, magnitude, and effect this event or trend will have on the structural capacity, local member stiffness, and other parameters of interest [Yao, 1985 and 1996]. Nondestructive testing (NDT) is the accurate measurement of the state parameters of an existing structure, accounting for design details, deterioration, damage, repair, environmental and operational conditions [NSF, 1992 and 1993]. This testing can yield better results with a controlled experiment, but oftentimes this is not possible with a large structure due to the necessity of its continued operational use.

In this context, health monitoring is the rational organization of the above technologies, methods, and concepts each according to its merits within a system devoted to monitoring the state-of-health of a structure. This monitoring system may sit resident and on-line at the site of a structure in order to provide continuous assessment of its performance; or, the monitoring system may represent the remote bureau of responsible engineers and inspectors which is the typical practice of the present day. In either case, this system takes a hybrid approach for structural monitoring where emphasis is placed upon the optimum interconnection and interaction of several NDE methods and technologies of merit for the given structure (see Figure 1-1).

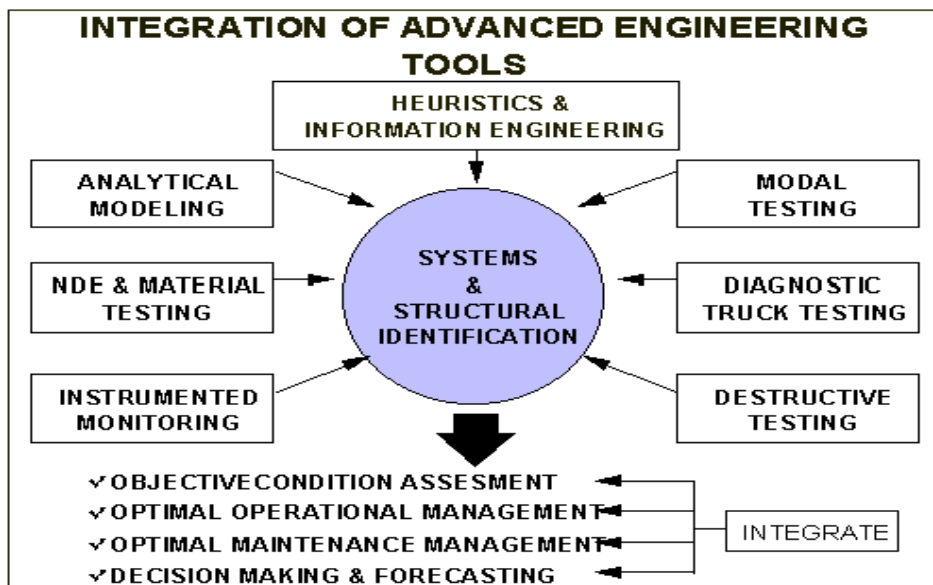


**Figure 1-1: Toolbox of NDE Methods and Technologies**

While these concepts have been known for many decades, the experimental and analytical tools for a meaningful and practical application to civil structures such as bridges or buildings has only recently emerged. Increased computational capability in desktop and site computing hardware has resulted in significant progress in algorithm development and testing [Ghanem, 1995,

Shinozuka, 1995, and Aktan, 1998b]. Instrumentation and data-acquisition hardware which has been custom-designed for the operating range of civil structures and which can withstand the environmental rigors of the infrastructure has become commercially available [Massicotte, 1994, Alamapalli, 1994, Hunt, 1994, Levi, 1996, Aktan, 1998a, Lenett, 2000a]. Truck and other load testing has been refined to a quick and efficient method of identifying structural condition and capacity rating of highway bridges [Lichtenstein, 1998, Schulz, 1995, Levi, 1997, Turer, 1999, Lenett, 1999d and 2000b]. An established art-science in the mechanical and aerospace fields of engineering, modal testing and vibrational analysis has become an invaluable tool for the damage detection, capacity rating, and seismic vulnerability estimation of civil structures [Lenett, 1997, Aktan, 1997b, Natke, 1988, and Doebling, 1996]. With the above methods and technologies, this research is dedicated to a solution for the nation's crumbling infrastructure.

## 1.2. Background

### 1.2.1. The Crumbling Infrastructure

Following World War II, the United States rapidly developed and industrialized the current infrastructure system for transportation, power, and communication (see Figure 1-2). This system has served as a common network for American civilization (e.g. commerce, defense, government, entertainment, media, etc.), joining homes and cities with the fabric of modern technology. The infrastructure is now decaying because of age, deterioration, misuse, lack of repair, accidental damage, and improper design for current demand. Through deregulation,

several utilities such as the phone and power companies have successfully maintained and even improved their facilities. However, the nation’s highways and other public structures remain under governmental control and are funded through taxes. The Federal Highway Administration (FHWA) estimates that 35% of the bridge inventory is currently deficient due to either structural or traffic inadequacy and that this has led to a seventy-eight billion dollar backlog of needed maintenance (see Table 1-1) [FHWA, 1993].

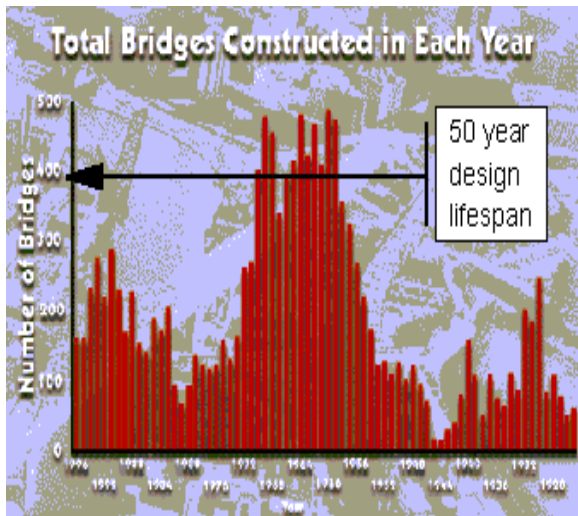


**Figure 1-2: Bridge Construction Timeline**

Federal Highway System	Amount	Total%
Bridge Inventory	575,583	100
Deficient Bridges	199,277	35
• Structural Deficient	118,563	21
• Functionally Obsolete	80,714	14

**Table 1-1a: Percentage of Deficient Bridges**

Federal Highway System	Amount
Repair All Deficiencies	\$78B
• Average Annual Cost	8.2B
Current Annual Spending	5.0B

**Table 1-1b: Budget for Deficient Bridges**

One common issue in civil infrastructure systems is the need to monitor, assess, and diagnose structural integrity of the global structure and in its various local components. To avoid hazardous collapse and/or disruption of the service, officials must evaluate the expected useful life of the structure and plan repair or renewal accordingly. Subjective or inaccurate condition assessment has been identified as the most critical technical barrier to effective infrastructure management [Clinton, 1993]. For example, since 1971, conditions of highway bridges are typically expressed in terms of subjective indices which are based on visual inspections alone

[AASHTO, 1983 and 1989, see Figure 1-3]. The difficulties of visually inspecting and evaluating an aging constructed facility accurately and completely, even when this may be conducted by experienced engineers, are well-known [FHWA, 1993]. NDE technologies of a rigorous and objective nature are sought to quantitatively identify and evaluate the condition or health of highway structures.

BRIDGE INSPECTION REPORT

BR-85 REV. 02-95

BRIDGE NUMBER HAM 00561 0693 CINCINNATI YEAR BUILT     

ROUTE      UNIT     

DOT 08 BRIDGE TYPE STEEL/BEAM/CONT TYPE SERVICE 2 51 LONGVIEW STAT HOSPITAL DR

DECK	Some Material Spalls with Exp. Rebar, cracks	3	Major Abut Cracking; Core Holes;	41	3
1. FLOOR SURFACING	Cracking & some 1-COMC	8	2. WEARING SURFACE	Water Spalls-ASPHA	41
3. CRACKS - DIAGONAL	Core Holes	2	4. MEDIAN		47
3. CURBS, SIDEWALKS & WALKWAYS	1-COMC/1-COMC	9	6. DRAINAGE	Water stands on deck & leaks through	45
5. RAILING	Has 7' fencing attached	10	8. SUMMARY		44
7. EXPANSION JOINTS	Closed both Exps 2-STL SLOG	11	10. BEAMS/GIRDERS/SLABS	OR FULL-IEP AT Abut 1-STL	45
9. ALIGNMENT	MAX. SPAN=90	12	11. DIMENSIONS	or CROSSFRAMES TOT. LGTH=133	13
11. DIMENSIONS		13	13. FLOOR BEAMS		14
13. FLOOR BEAMS		14	14. FLOOR BEAM CONNECTIONS		47
15. TRAFFIC	ALL TRAFFIC FOR Experimental	15	16. DIAGONALS		48
17. END POSTS	U.C. Piers, Victor Hunt	16	18. TOP CHORD		49
19. LOWER CHORD		17	20. LOWER LATERAL BRACING		50
21. TOP LATERAL BRACING		18	22. SWAY BRACING		51
23. PORTALS		19	24. BEARING DEVICES	FRACK - Rust at Abut 2-SLOG	52
25. ARCH		20	26. ARCH COLUMNS or HANGERS		53
27. SPANREL WALLS		21	28. PAINT	TYPE: U YEAR=87	54
29. PINS/HANGERS/HINGES		22	30. FATIGUE PRONE CONNECTIONS		55
31. LIVE LOAD RESPONSE	Closed to All Traffic (?)	23	32. SUMMARY		56
33. ABUTMENTS	Abut Cracking with Unsound	24	34. ABUTMENT SEATS	CRACKS - Spalls	57
35. PIERS	2-COMC	25	36. PIER SEATS		58
37. BACKWALLS	Unsound beneath	26	38. WINGWALLS		59
39. FENDERS and DOLPHINS	SPANS=3	27	40. SCOUR		60
41. SLOPE PROTECTION	PIERS=2	28	42. SUMMARY		62
43. CULVERTS	1-COMC	29	44. ALIGNMENT		63
45. GENERAL		29	46. SEAMS		64
47. HEADWALLS or ENDWALLS		31	48. SCOUR		65
49. GENERAL		32	50. SUMMARY		66
51. CHANNEL		33	52. PROTECTION	X	67
53. WATERWAY ADEQUACY		34	54. SUMMARY		68
55. APPROACHES	Major Cracking - Settlement	35	56. APPROACH SLABS	Cracking & Settlement	69
57. GUARDRAIL	Post Rotten & Missing G.R. on Ground	36	58. RELIEF JOINTS		70
59. EMBANKMENT	BRDG. WIDTH=26	37	60. SUMMARY PCT. LEGAL	ISD?	71
61. NAVIGATION LIGHTS	MVC ON=9999 UND=1408	38	62. WARNING SIGNS	"STOP" - BRIDGE CLOSED	72
63. SIGN SUPPORTS		39	64. UTILITIES		73
65. VERTICAL CLEARANCE		40	66. GENERAL APPRAISAL & OPERATIONAL STATUS		74
67. INSPECTED BY	R. Hoefler	76	68. REVIEWED BY		78
70. DATE	05/14/96	86	72. SURVEY		92

DOT 2852 Photos Taken

USE REVERSE SIDE FOR ADDITIONAL DETAILS

Figure 1-3: Bridge Inspection Report

Current health evaluation and damage detection methods are either visual or localized experimental technologies such as local instrumentation, acoustic, ultrasonics, impact-echo, radar, x-ray, infrared, magnetic or thermal fields, eddy-current, etc. However, a clear distinction between global and local state properties does not always exist. For example, flexibility or stiffness may be expressed in terms of a large number of reference/discrete systems for the same structure. Mode shapes may be of displacement or strain, and frequencies and mode shapes may correspond to global, mixed or local modes. In general, the responses and coordinates which may be considered global depend on the constructed facility. If the critical deterioration mechanisms or the critical regions and responses have not yet been established, local scans and measurements can not feasibly and effectively address the problem of global condition and damage assessment. Even if it was possible to conduct a complete local scan in spite of the large numbers and sizes of typical constructed facilities, for effective management we would also need to understand how local damage affects the complete system performance.

Controlled structural testing, measurement and performance evaluation are well established and have been the cornerstone of the civil engineering profession for centuries [Aktan, Bahkt, Bertero, Cantieni, DeWolf, Fisher, Lichtenstein, Moses, Newmark, Nowak, etc.]. Recent efforts in the literature have been directed towards characterization of the observed ambient and/or service response of the structure (i.e. its healthy condition) and identifying the effect of specific damage events or deterioration mechanisms upon this characterization. Here, the term “characterization” is broadly used to encompass the efforts of mechanical, geometrical, qualitative, fuzzy, neural or any other form of response model for the structure. These characterizations are quite varied as a complete understanding of structural response is not

possible due to its highly complex behavior and the lack of sufficient computing power, including the following concerns: nonlinearity, coupled or composite assembly of elements and members, time variance, statistical nonstationarity, incomplete observability of both input and output sets, lack of mechanical reciprocity, six degrees of displacement and rotational freedom, multi-dimensional state space behavior, etc.

Much of the knowledge regarding the evaluation of structural behavior remains uncaptured in the form of “know-how” or “rules-of-thumb.” The federal government mandated biannual inspection of all highway bridges after the collapse of the Silver Point Bridge over the Ohio River in 1967 (see Figure 1-4). Inspectors are trained to grade each bridge and its major structural components on a scale of 0-9 according to their arms-length appearance [AASHTO, 1983]. This inspection is still quite subjective and will vary with the extent of the inspector’s experience and affiliation [Lenett, 1999d]. It is more desirable to couple this visual inspection with a more detailed investigation of the soil-foundation-structure system, material sampling and testing, properly designed sensitivity analyses, and, if warranted, load and/or vibrational modal testing, by an experienced structural engineer. However, such inspections are more expensive and the numbers and sizes of commonly recurring types of infrastructure components do not permit most inspections to be carried out by experienced engineers.



**Figure 1-4: Silver Bridge Collapse in 1967**

### 1.2.2. Diagnostic Load Testing

Truck, proof, or other load testing of highway bridges has usually been reserved as an area of academic research due to the complexities, cost, and disturbance to service of such a field experiment. However, when a structure's computed capacity is less than the desired level of performance, it is usually beneficial to the owner to objectively identify the actual structural response to controlled loading experiments. The constructed bridge will have many inherent mechanisms to resist the applied load and which are generally not considered in the analysis of its capacity. These identified mechanisms include the actual load distribution, impact factor,

unintended composite action, participation of superimposed deadload, material properties, unintended continuity, participation of secondary members, effects of skew, effects of deterioration and damage, unintended bearing restraint, and environmental effects such as thermal stresses [Lichtenstein, 1998]. The AASHTO *Manual* envisions the future use of diagnostic tests under truckloads for load rating [AASHTO, 1994].

Fatigue evaluation of highway bridges is also of great concern to the bridge engineer, particularly with older monumental structures that have undergone several episodes of rehabilitation or with suspect connections which were designed before the recent investigation of such phenomena [Fisher, 1984]. Many loading repetitions are required at suspect members, welds, or connections in order to produce a fatigue failure at some time in the future. Generally, all truck loading stresses, whether above or below the allowable range, cause fatigue damage that could result in a fatigue failure. In contrast with the design rating which defines the largest allowable load corresponding to permanent structural damage, the effects of fatigue loading can best be defined in terms of the total life of the bridge for the given spectrum of service stresses that it experiences each day. To study the fatigue susceptibility of a bridge, the engineer must have the most realistic and precise information to make an accurate assessment, particularly when the live load stresses are used in the cubic equations of the AASHTO code. It would be extremely time-consuming and nearly impossible to attempt to account for all variables in a conventional computer analysis. The only way to obtain precise service information is through continuous field monitoring of the local stress field upon and adjacent to the suspect members, connections, or welds.

One conceptual signature that represents bridge condition and can be determined from a truckload test is the fundamental structural parameter of the unit influence line, the characteristic response at any instrumented bridge node due to the position of a unit load. Here, the unit load is defined to be a truck axle of one kip total weight and the loading path is considered to be that of a typical tandem or semi truck driven in the marked lane(s). It has been demonstrated that the strain (or stress) influence line is a damage sensitive index by conducting truckload tests on decommissioned concrete and steel highway bridges which were loaded to various damage states [Levi, 1997, and Turer, 1997]. Turer (1999) showed that the decomposed unit influence line and its utility to estimate the future effects of proof or “superloads” can provide an accurate and conceptual health index for a structure. This research will demonstrate how the influence line can be reliably identified from controlled or service loadings and then used to immediately provide a capacity rating for the instrumented section and/or an estimation of the remaining fatigue life for the instrumented member/connection based upon the relevant AASHTO codes (see Figure 1-5).

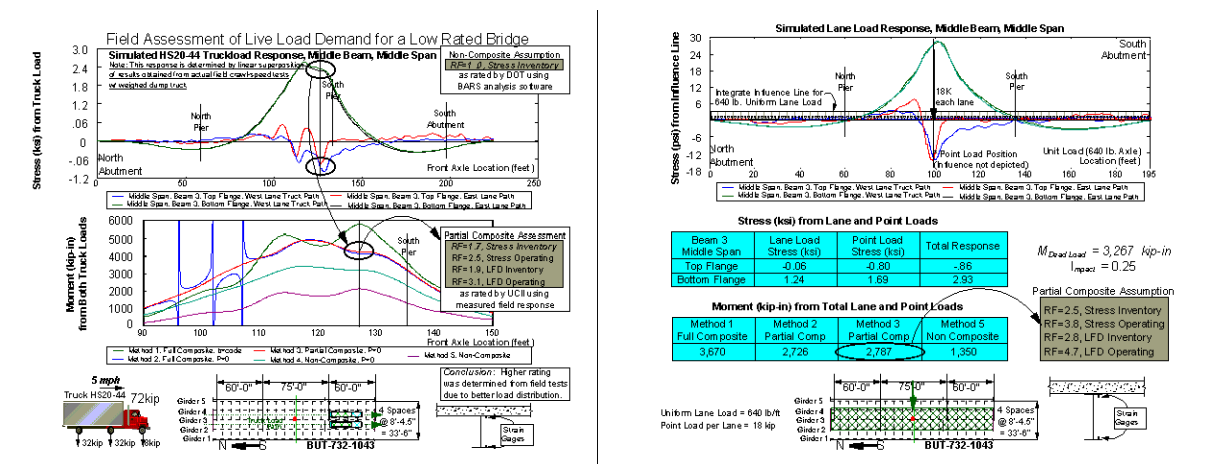
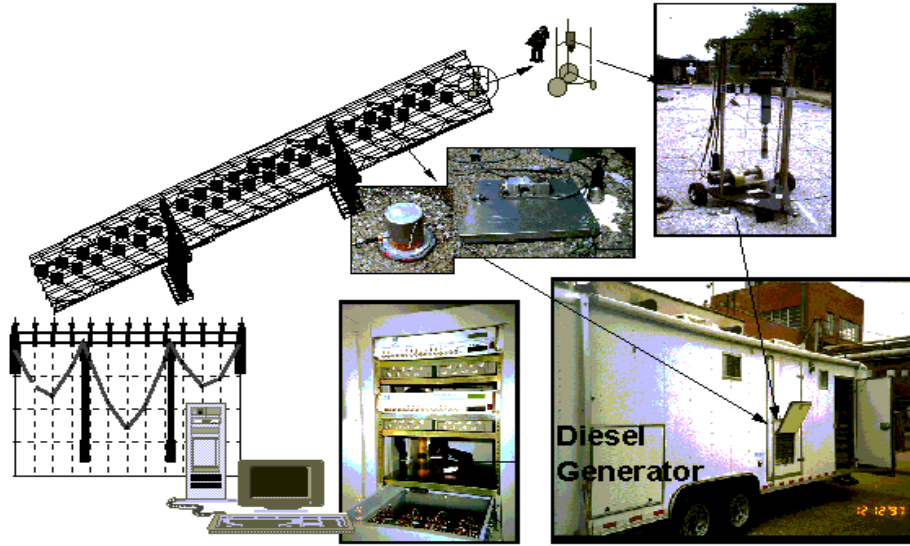


Figure 1-5: AASHTO Truck and Lane Load Ratings from Influence Line

### 1.2.3. Modal Impact Testing

The work towards modal characterization or identification has been largely the result of knowledge transferred from other industries. For example, modal testing and instrumented monitoring have been used extensively for the structural identification and health monitoring of automobiles [Allemang and Brown, 1982], offshore oil platforms [Vandiver, 1975 and 1977], and the NASA space shuttle [Helmicki, 1991, 1993, and 1994]. The conventional mechanical model of modal or vibrational testing consists of a second-order, linear dynamical state space governed by the  $n$ -dimensional matrices of mass  $M$ , stiffness  $K$ , and damping  $C$  [Allemang, 1994]. The order,  $n$ , of these matrices will depend upon the spatial distribution of the coordinates at which we desire to express the structures displacements and the overall size of the structure. Accelerometers are positioned at the coordinates to measure the structure's vibrational response to an applied impact from a custom hammer instrumented with a load cell (see Figure 1-6). Generally, no access below the bridge is required and the bridge may be impact tested in parts so that one or more lanes may remain open to traffic. Frequency domain representation of the measured signals allows immediate derivation of bridge flexibility at the instrumented coordinates by employing a modal parameter estimation algorithm in the spatial domain, known as the Complex Mode Indicator Function (CMIF) [Catbas, 1997].



**Figure 1-6: Mobile Laboratory for Modal Impact Testing of Highway Bridges**

Many global condition indices may be conveniently measured or extracted by conducting a modal test. The basic concept is that modal parameters, such as frequencies and mode shapes, are a function of the physical properties of the structure and their dynamical interrelation. Any changes in the measured modal parameters is, therefore, due to some change in the structural properties and is considered as damage. For example, relative frequency changes between different modes have been used in crack detection [Adams, 1978; Cawley, 1979; Ju, 1986 and 1993; Meneghetti, 1993]. DeWolf, however, reported good correlation and a linear relationship between ambient temperature and the fundamental frequency of a bridge. Shifts in the higher-frequency bending modes obtained via local instrumentation, such as strain gages, have been proposed to be more sensitive to the onset of member cracking [Begg, 1976]. Stubbs compares the distribution of flexural strain energy, as related to the measured member curvature, of a mode shape along a beam-element before and after damage. Sanayei suggested that the stiffness coefficients and other parameters established for the elements could serve as condition indices.

It has been demonstrated that modal flexibility is a damage sensitive index by conducting modal tests on decommissioned concrete and steel highway bridges which were loaded to various damage states [Toksoy, 1993 and 1994; Aktan, 1994a and 1996c, Lenett, 1997]. Zhang (1993) showed that the uniform load surface and its curvature can provide an accurate and conceptual health index for a structure. A derived flexibility matrix with the appropriate spatial resolution can be used to virtually simulate the deflection basin and influence lines for any span and under any loading pattern upon the bridge. It is possible to check this for spatial anomalies for directly assessing condition even without a prior experiment. Spatial comparison-checks include: the flexibility of support conditions, the flexibility of symmetric points, the flexibility of similar bridges which are known to be healthy, or the flexibility of a rational analytical characterization. However, the more definitive use of flexibility is that it serves as a baseline for future reference. Any changes in the local flexibility of redundant structures serve as sensitive and reliable indices for damage.

#### 1.2.4. Finite Element Modeling

A common shortcoming in civil engineering education, research and practice has been a lack of emphasizing the differences between modeling an actual constructed facility for condition assessment as opposed to modeling a non-existing facility for design. Condition assessment of an existing constructed facility is best served by discrete, geometric models taking advantage of any heuristic knowledge-base and, ideally, experimental data from field tests of the structure. Turer has developed a user-friendly software package to automate the development of finite element (FE) models given user input of key bridge parameters [Turer, 1997]. The prototype Windows-

based software will permit an engineer to interactively generate a customized grid or the full finite element model for a given steel-stringer bridge by describing the geometry, dimensions, member, sub-structure and support properties, as prompted by the software. All available information (e.g., the original design, fabrication/shop drawings, construction, inspection, rating and maintenance records, existing conditions as documented by arms-length-inspection, etc.) can be utilized in the construction of a preliminary model without idealizing geometric attributes. General information about the bridge (such as age, climate, traffic load, etc.) should also be documented, so as to build a knowledge base for future bridge management systems. Bound-sensitivity analyses of the most consequential parameters (or parameter groups) allow greater understanding of measured phenomena and also permit the use of the FE model for designing controlled experiments such as truck-load or modal testing. The FE model serves to establish the frequency band of interest, frequency resolution, truck-load positions or modal impact grid, and the reference locations and orientation.

Advanced measurement technologies are then critical for accurate geometric modeling as even an experienced inspector may not fully conceptualize complex geometric details or be able to differentiate between cosmetic versus structurally critical details. In order to perform FE model calibration, certain structural and material properties within the model, such as moments of inertia and concrete modulus of elasticity, etc. will be selected as variables. The idealized internal continuity and external boundary conditions are replaced by appropriate translational and rotational springs to better simulate the local kinematics which have critical impact on the global responses. As field data becomes available, the preliminary FE model of a tested bridge is

calibrated to conform to the experimentally determined dynamic characteristics, flexibility, peak strains, deflections, influence lines, etc. (see Figure 1-7).

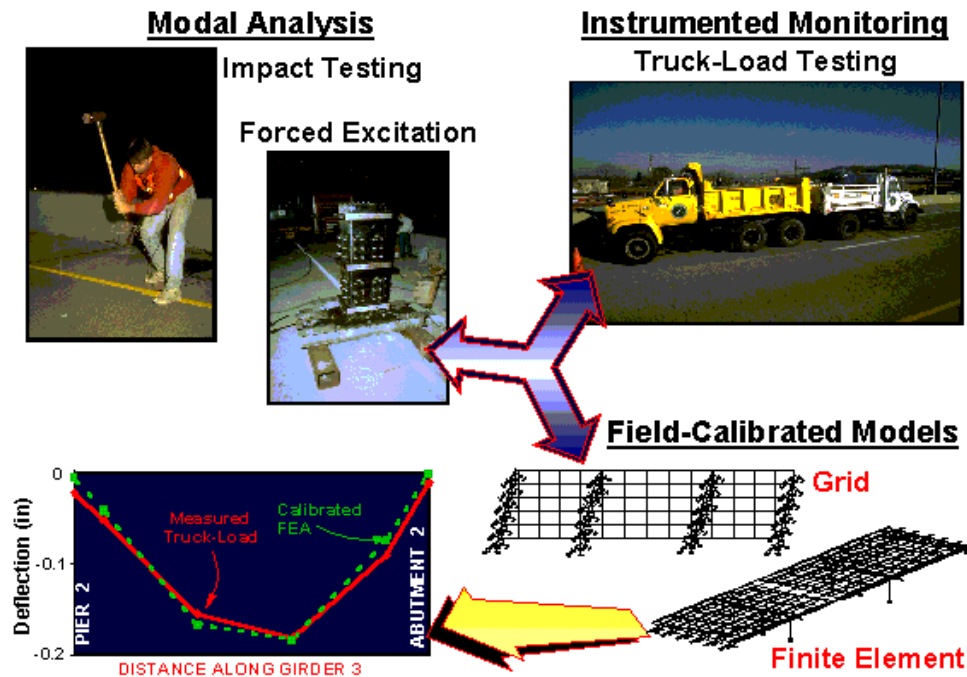


**Figure 1-7: Calibration of Finite Element Model with Bridge Test Results**

In addition, modeling assumptions such as linearity, elasticity, reciprocity, stationarity, and others are verified by the field tests. The field-calibrated FE model now accurately simulates the element stiffnesses and local kinematics at the exterior and interior supports as well as connections. If damage has been diagnosed, this step permits localizing it. In this manner, the actual state and all the critical behavior mechanisms are captured and simulated accurately for the entire structure. Load ratings for a test bridge are then computed from the calibrated FE model. If future bridge conditions such as sudden damage, advanced deterioration, or planned rehabilitation are to be considered, then the FE model provides the ideal tool to approximate and assess such events.

### 1.2.5. Systems Identification Approach

The millions of miles of bridges, combined with the need to respond swiftly to accidental damage, has also lead several federal institutions to pursue the instrumented monitoring of highway roads and bridges. It is envisioned that the intelligent infrastructure of the future (Figure 1-8) will include a sensor system (System #7) which will monitor structural condition (System #5), and alert officials (System #3) in case it is decided (System #9) that the reliability of the structure (System #6) is reduced to an unacceptable level. At a minimum, it has been established that an instrumented bridge health monitoring system will be comprised of a collection of sensors and data-acquisition hardware which will act to collect, archive, and possibly telemeter various bridge measurements such as strains, deflections, accelerations, temperature, rotation, and others. These measurements will, in turn, be used by bridge engineers to complement the subjective visual inspections and must be sufficient to characterize the structure's response (System #8) to its ambient loading environment (System #4) in order to assess structural integrity. In addition, a dedicated monitor would facilitate an on-going regimen of objective NDE tests (System #2) such as truckload and modal impact experiments with minimal interruption to its service (see Figure 1-9). Detected anomalies may trigger an on-site battery of NDE tools (See Figure 1-1) which would escalate, as needed, in rigor and detail in order to fully appreciate the extent and magnitude of the deterioration and/or damage (System #1). It is desirable that the system is operational from the very beginning of bridge construction in order to record any and all events which would ultimately affect its performance or capacity and to understand their significance in relation to each other (see Figure 1-10). Moreover, there is significant promise in a regular follow-up regimen of truckload and modal impact tests with a

more limited scope, once a rigorous structural baseline is established. As a long-range goal, the bridge health monitor may gain an autonomous nature where sensor measurements are gathered and processed, preliminary decisions regarding bridge health are made, immediate corrective actions (such as closing the bridge to traffic) are made, and communication with a central information and planning system is maintained regularly.

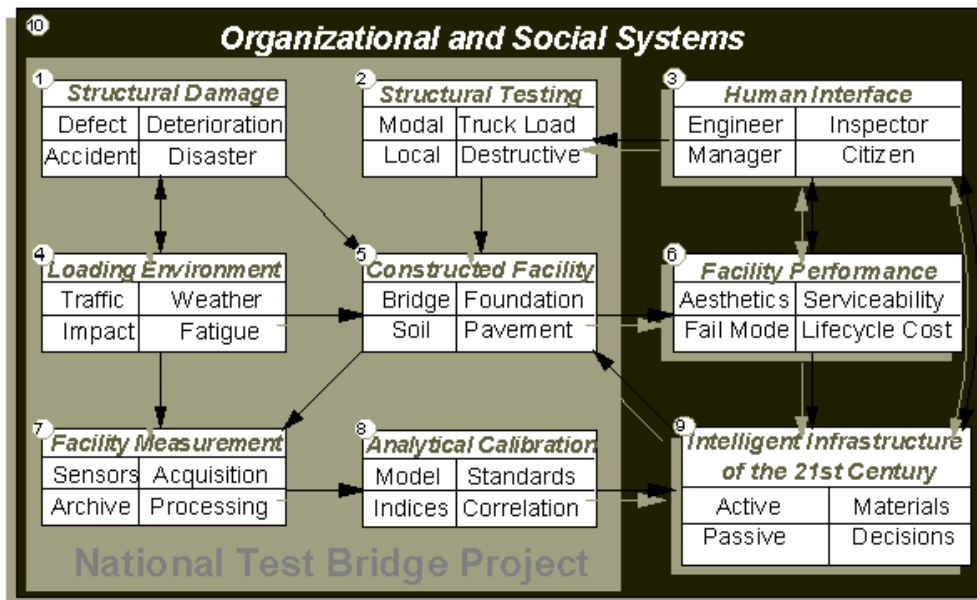


**Figure 1-8: Multi-System Conceptualization of Intelligent Infrastructure**

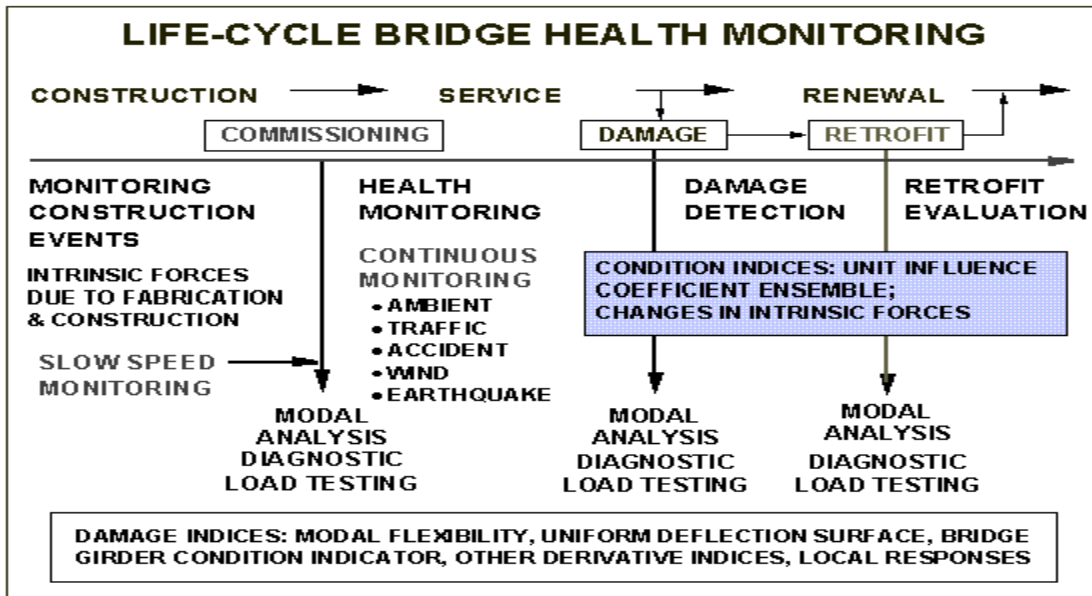


Figure 1-9: NDT Regimen of Structural Evaluation

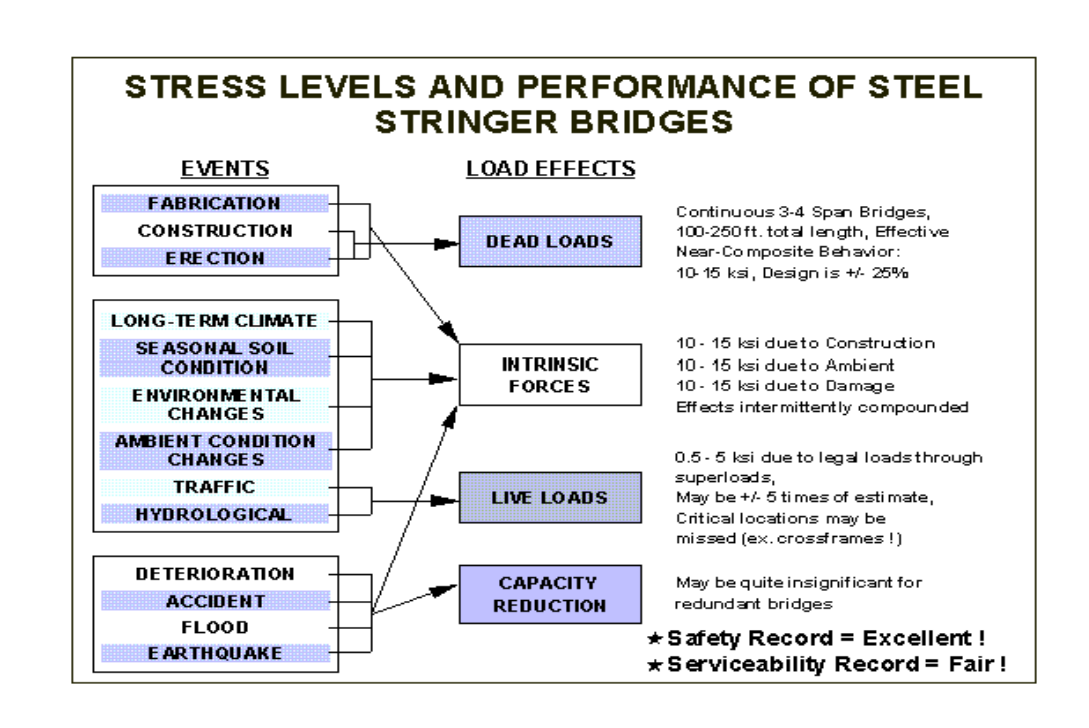


Figure 1-10: Lifetime Assessment of Steel-Stringer Bridges

The broader context of the above NDE technologies and damage detection methods is the rational organization of each according to its merits within a system devoted to monitoring the state-of-health of the structure. This monitoring system may sit resident and on-line at the site of structure in order to provide continuous assessment of its performance; or, the monitoring system may represent the remote bureau of responsible engineers and inspectors which is the typical practice of the present day. In either case, this system takes a hybrid approach for structural monitoring where emphasis is placed upon the optimum interconnection and interaction of several NDE methods and technologies of merit for the given structure. As depicted in Figure 1-11, a three-level hierarchical system can provide this connection [Saradis, 1979]. The first level has immediate access to the measured structural outputs and provides immediate health threshold checks of both the structure and the monitor itself. Higher levels are concerned with less immediate processing and more complex aspects of the structure. The highest level allows planning of monitoring tasks and qualitative decisions regarding the state of the structure. The level of deterioration or damage can be weighted in the context of its probable effects, the structure's lifecycle, and the present safety requirements. Further, an evacuation or routing plan can be organized, communicated, and implemented in a controlled manner. The middle level acts to coordinate the extreme levels of the system. Structural identification is conducted to estimate and update the structural condition states based upon the measured structural outputs. These condition states, in turn, dictate the performance parameters upon which the structural evaluation is made.

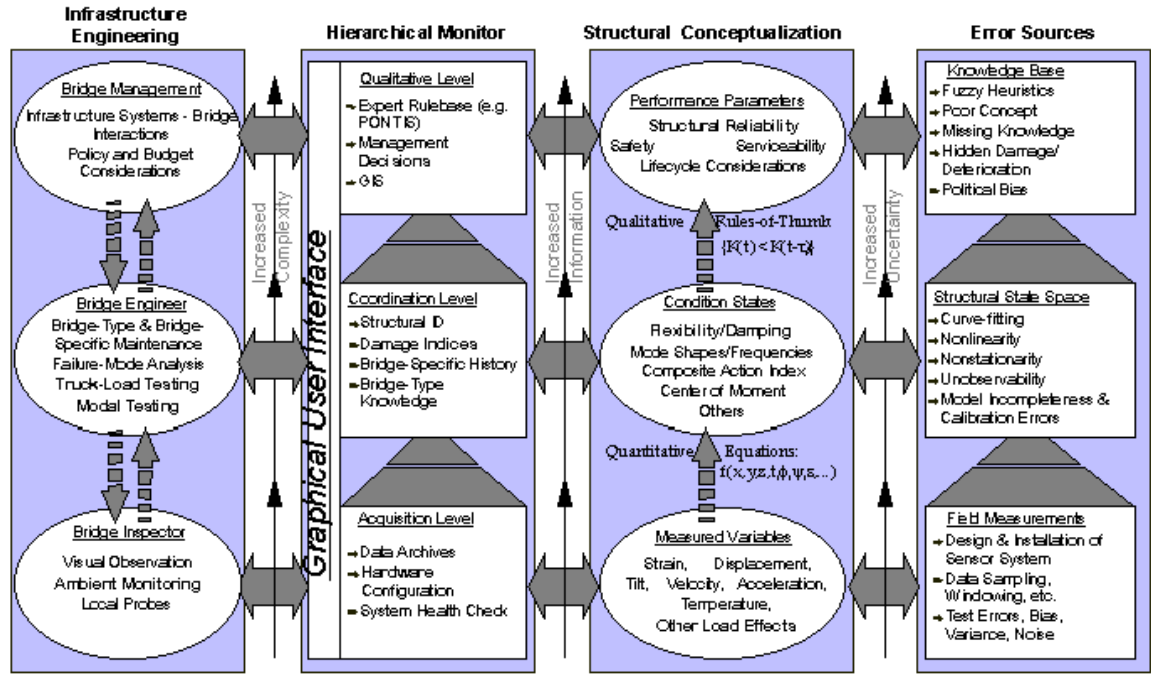


Figure 1-11: Hierarchical Monitor System for Highway Bridges

### 1.2.6. Consensus Terminology for Structural Systems

To foster a national management strategy, Aktan [1995a] developed a general terminology for structural systems with consensus definitions based upon the prevailing notions of today's engineering community. For a structure, *measured output* variables can be obtained from the component materials (mechanical, chemical, and metallurgical characteristics at the microscopic or coupon level), the local mechanical elements (strains, distortions, displacements, velocities, accelerations, rotations, etc.), and the global structure itself (skew, span lengths, elevations, etc.). *Environmental* variables, such as temperature, wind speed, rainfall, humidity are also measured to assess their impact upon the structure. With the exception of a controlled experiment, *service load* forces and their distribution are typically difficult to measure directly, but can be inferred

from the measured outputs. Structural *condition states* are quantitative indices, which cannot be directly measured, are calculated from the measured outputs, and represent the current mechanical behavior of the structure. Typically, each NDE method has its own derived condition states, which form the basis for its structural model. Modal testing, for example, represents the vibrational response of a structure by frequency peaks known as modes and the corresponding structural distortion as mode shapes. Structural identification would classify a structure's response to a known load input by calculation of the mass M, stiffness K, and damping C matrices. Local instrumentation techniques to evaluate section strength or element fatigue may derive condition states such as center of moment, stress envelopes, and load cycle reversal count. *Performance parameters* are those numerical terms or quality concepts used at the highest levels of structural assessment, which are typically uncertain or fuzzy in nature. They describe aesthetics, functionality, serviceability, toughness, safety (in terms of damage and failure mechanisms, and their corresponding capacities and modes), ease of inspection and maintenance, and lifecycle cost.

The related technical committees of ASCE have not yet defined a consensus terminology for condition/damage assessment. This terminology must be defined in conjunction with performance criteria at the critical limit states. Indices such as total and relative drift, span deflection, crack-width and stress-level have been typically used for defining the onset of serviceability and damageability limit-states for common constructed facilities. However, proven relationships between such measurable indices and actual facility performance have not yet been established. For example, in designing common highway bridges, AASHTO recommends span live load deflections to be restricted to 1/800 of the span length. In some cases, however, little

correspondence existed between the deflections calculated in the design and the measured live-load bridge deflections. It follows that “condition” or “damage” are terms which need to be expressed by a set of objective and measurable indices which can be proven to actually relate to the performance of a structure at its design limit states.

We hypothesize that the objective condition assessment of a structure via instrumented monitoring (Figure 1-12) should begin by the measurement of the appropriate responses amongst the large number of possible strains, rotations, displacements and accelerations during operations and/or controlled load tests of the constructed facilities. Subsequently or concurrently, the structural state properties, such as flexibility coefficients, vibrational frequencies, damping coefficients, and mode shapes, should be determined. Performance parameters at the design limit states should be estimated from both the measured responses and the determined state properties, as well as projected into the future. We would further need to characterize the typical set of defects, deterioration and damage mechanisms corresponding to the design, construction, operation and maintenance of a structure, and to understand the impact of these mechanisms upon the measured characteristics as well as expected performance.

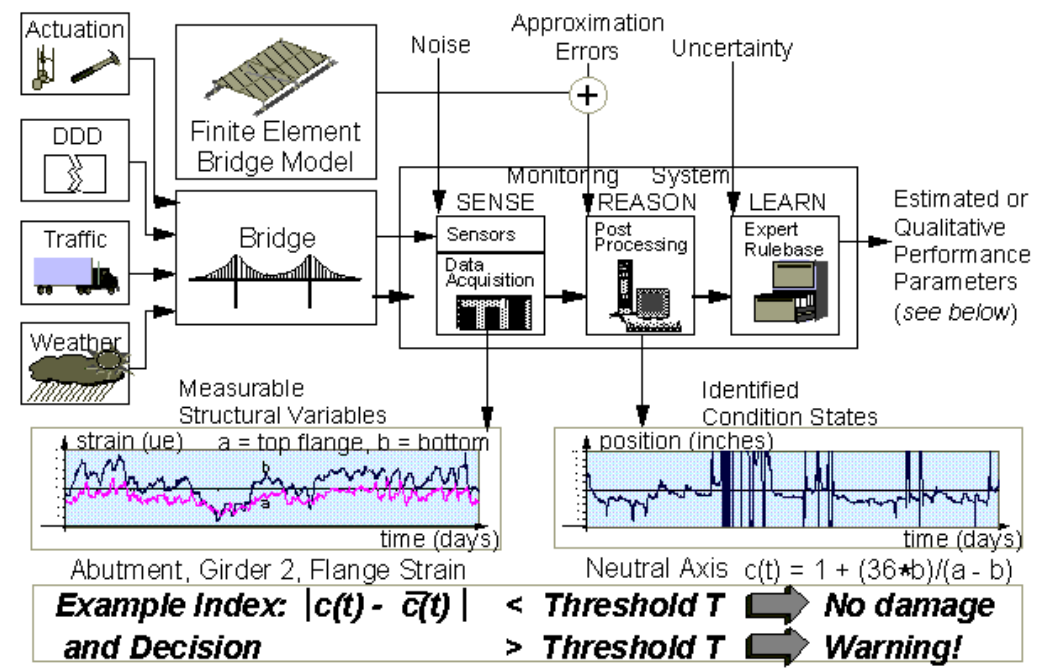


Figure 1-12: System and Strategy for Instrumented Health Monitoring

### 1.3. Objective and Expected Significance of the Research

This research is meant to complement and extend the work currently funded by the Ohio Department of Transportation, the Federal Highway Administration, the National Science Foundation and other agencies through the University of Cincinnati Infrastructure Institute (UCII). The UCII researchers have developed a rational, global condition assessment technique, which addresses the conceptualization and measurement of several unknowns for bridges, which include:

- (a) A lack of quantitative knowledge on the as-built state parameters (e.g., initial stresses, strains and displacements, local and global stiffness) and their variation over time;

(b) A lack of clear and quantitative definitions for the performance parameters (e.g., functionality, serviceability, safety, lifecycle cost, etc.) and relationships between the state and performance parameters; and,

(c) A lack of a clear and complete understanding of the phenomena which influence the state-of-force in a bridge; which lead to changes in state parameters; and/or which lead to a decrease in performance.

Fifteen steel-stringer, four steel truss, two reinforced concrete slab, and one fiber-reinforced polymer (FRP) deck on steel bridge have been tested nondestructively by a variety of techniques, while several of which were tested numerous times. Three decommissioned bridges (two trusses and one stringer bridge) were further tested to damage and failure. A global NDE method was developed based on the structural identification concept, and employing truckload testing, modal impact testing, and instrumented monitoring as its principal experimental tools. The test results are transformed to modal flexibility, which has been demonstrated to be a conceptual, quantitative, comprehensive, and damage-sensitive signature [Rubin, 1983]. Flexibility also provides a conceptual condition index, since it may be used to conveniently obtain the deflected shapes of a bridge under any loading pattern. Another such conceptual signature is the fundamental structural parameter of the unit influence line, the characteristic response at any instrumented bridge node due to the position of a unit load. Both testing approaches will provide best results under controlled loading conditions, which can be performed on a regular basis or in response to suspected or known damage. Ambient monitoring is conducted during the interim to track, document, and alert the bridge engineer to any gradual or sudden changes in these or component damage indices.

The scope and complexity of bridge condition assessment, however, does not permit a simplistic, reductional formulation. A holistic approach has been followed in the design and implementation of UCII research, and includes:

- (a) The strategies, concepts, and tools needed to confidently measure bridge state parameters;
- (b) The lessons learned from instrumented health-monitoring of actual bridge specimens;
- (c) The hardware, software, and analytical and experimental expertise required for linearized structural identification of complex bridges; and,
- (d) The concept of bridge-type-specific behavior mechanisms that have so far been identified for steel-stringer bridges.

Based on the principal attributes that influence state and performance, it is possible to rationally classify steel-stringer bridges into several groups of like behavior, each of which can then be represented through a statistical population of bridges. Once the statistical population is rigorously tested and studied, practical, type-specific global condition assessment procedures can then be developed for the whole group. The UCII researchers have extensively tested and monitored three steel-stringer bridges in Cincinnati (Figure 1-13) and have just contracted with ODOT to test another thirty-four steel-stringer bridges throughout Ohio. Twenty-four of these bridges to be tested will be essentially in good condition but will cover a wide range of structural parameters, including number and length of spans, skew, non/composite design, integral/stub abutment, etc. in order for a more diverse database. The other ten bridges to be tested will be the lowest rated bridges of greatest concern in the state of Ohio.

## UCII National Bridge Testbed Sites

(1994-present)



Figure 1-13: National Test Sites in Cincinnati, Ohio

### 1.3.1. Instrumented Monitoring of a Bridge in Service

Various controlled and uncontrolled experimental approaches are possible for field testing of highway bridges. Based on instrumentation, these may be classified as: (a) Geometry monitoring; (b) diagnostic testing; (c) long-term monitoring of incremental responses; and, (d) long-term monitoring starting from construction. Following a complete experimental evaluation of the bridge conditions, and understanding all the critical responses which need to be measured, it is possible to design an instrumented monitor system for an improved understanding of its day-to-day and seasonal behavior under traffic and environmental influences. This effort permits the evaluation of bridge performance by correlating the service level strain, displacement, and force states in the critical elements of the bridge to what is considered optimum.

Such a system has been in operation at a test bridge in Cincinnati (HAM-42-0992, Figure 1-14) for the past six years. Several observations were made from the collected data (e.g., Figure 1-15), including:

- 1) A reliable bridge monitor, consisting of long-term vibrating wire strain gages and high-speed conventional sensors hard wired into an on-site data-acquisition system, can be achieved;
- 2) Traffic loading was most observable at the lower girder flange near the midspans, and the recorded deflection and strain were substantially less than that required of the bridge design; and,
- 3) Temperature effects were most significant at the bridge supports, especially the integral abutments, and recorded strain over the annual thermal cycle would far exceed that of any recorded truck traffic.

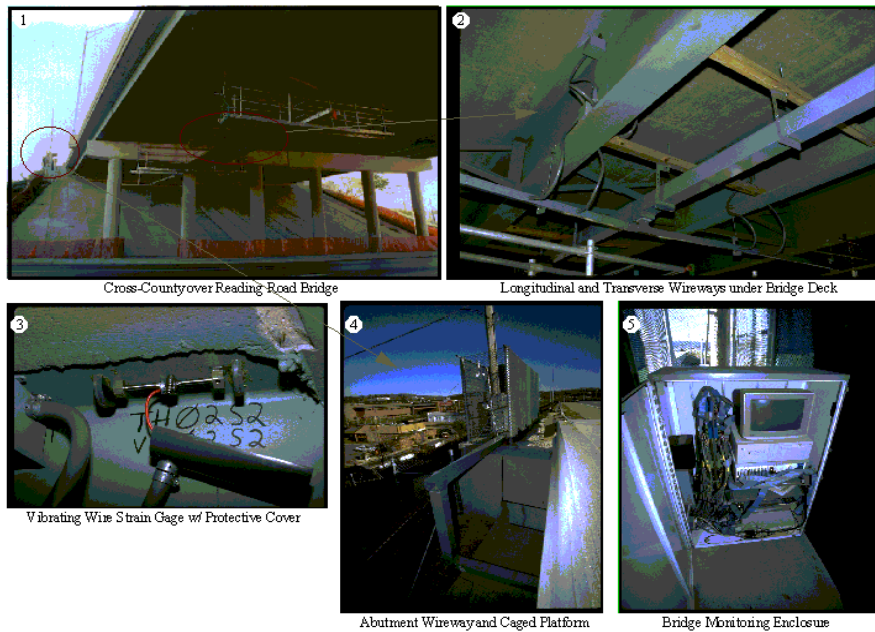


Figure 1-14: Implemented Bridge Health Monitor, HAM-42-0992

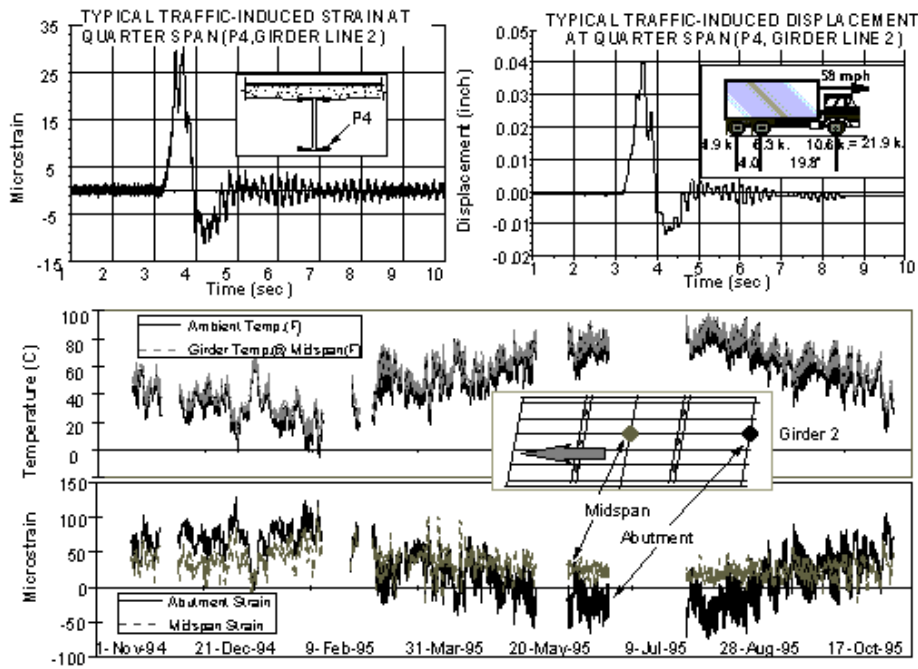


Figure 1-15: Typical Responses to Traffic and Long-Term Environmental Inputs

### 1.3.2. Lifetime Monitor of a Constructed Bridge

Bridge officials have expressed the need for exploring instrumented health monitoring of critical bridges. Several states such as Ohio and New York have issued contracts for the installation of monitoring systems. On the other hand, there has been little scientific investigation of the issues in instrumented bridge monitoring. A variety of transducers have been mounted on bridges and data has been acquired. However, guidelines are needed for interpreting bridge response data and relating this to health. The objective of a second UCII research project is to understand and document the actual absolute state-of-stress in a typical jointless continuous composite reinforced concrete deck-on-steel stringer bridge, together with the corresponding causative effects. The stresses were measured starting from fabrication and construction and through the initial year of service. In conjunction with this, a systematic and rigorous study for establishing the most reliable and feasible sensors, data-acquisition systems and data processing techniques that will optimally serve for long-term bridge health monitoring was pursued.

This objective will be accomplished by collecting a complete set of strain, distortion, inclination, displacement, vibration, and temperature response data for a typical test specimen: the three-span, 170 foot Cross-County Highway over Hamilton Avenue bridge (HAM-126-0881, Figure 1-16). This semi-composite bridge is a unique research opportunity in that it was designed with an unusually small end span to middle span ratio (0.45) and because it incorporates both continuous and integral construction. A complete sensor suite, including a weigh-in-motion (WIM) roadway scale, was incorporated within the construction plans and drawings for the bridge. The intent and necessity of collaboration with the bridge contractor must be emphasized for a successful project

such as this. A dedicated monitoring system began operation in tandem with the bridge construction in March 1995, commencing with construction of the drilled shaft pier foundations. The foundation and substructure were instrumented with embedded concrete strain and temperature gages, welded pile strain gages, inclinometer conduit, soil pressure sensors, and others. Relevant atmospheric effects at the site are monitored with a weather station. The steel superstructure was instrumented with weldable foil and vibrating wire strain gage instrumentation on the beams and the intermediate crossframes. The steel beam instrumentation was monitored during critical shop fabrication procedures and during all subsequent construction and service events. Displacement, tilt, and acceleration instruments were added at subsequent steps of the construction. Modal impact and diagnostic truckload testing were conducted in April and June of 1997, in order to establish the baseline mechanical characteristics of the bridge. The bridge was opened to traffic on October 28, 1997. Two follow-up tests were conducted in May and September 1998.

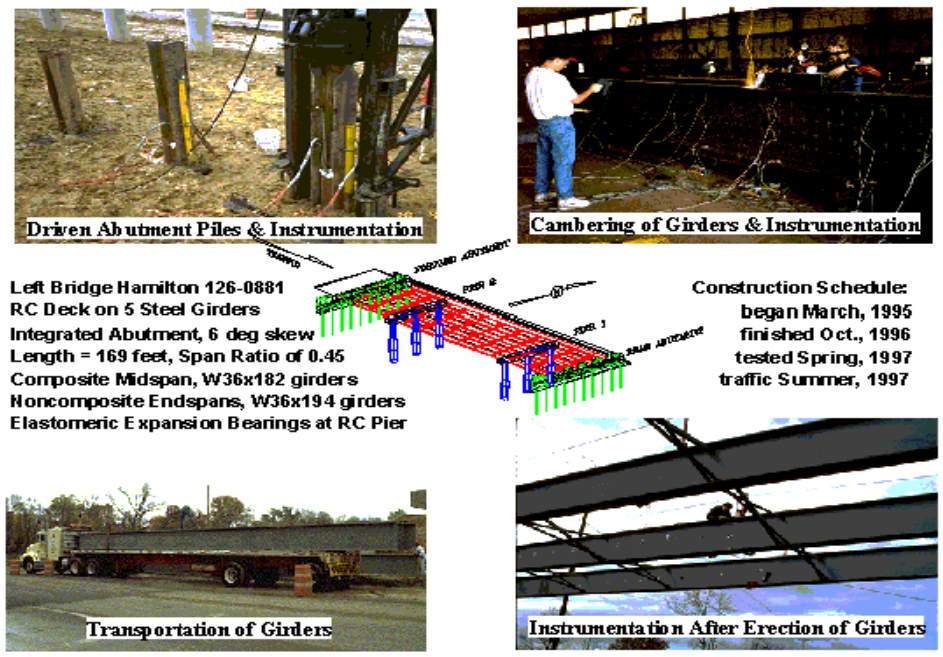


**Figure 1-16: Instrumentation, Testing, and Monitoring of the Construction and Service of a Steel-Stringer Bridge**

Accumulated versus transient stresses and forces will be evaluated by conducting analyses to simulate different episodes of cause and effect in the construction and service stages of the bridge and correlating these with the recorded data. With regards to significant construction events, several discoveries were possible due to the extensive instrumentation (642 channels) which was regularly logged, archived, and subsequently analyzed through a proven methodology.

The fabrication stresses discovered in this research are not explicitly considered for the design of these bridges, but are induced through the cambering process. The measured dead load stresses of the deck and parapet were not uniformly distributed, as assumed by the design, and marginally exceeded design predictions at some locations (see Figure 1-17).

- Fabrication stresses of up to 15 ksi were measured in the stringer web at midspan due to heat cambering
- Dead load stresses of up to 2 ksi were measured in the stringer flange at midspan during placement
- Dead load stresses of up to 10 ksi were measured in stringer flange at midspan due to concrete deck pour
- Dead load stresses of up to 3 ksi were measured in the crossframes due to concrete deck pour

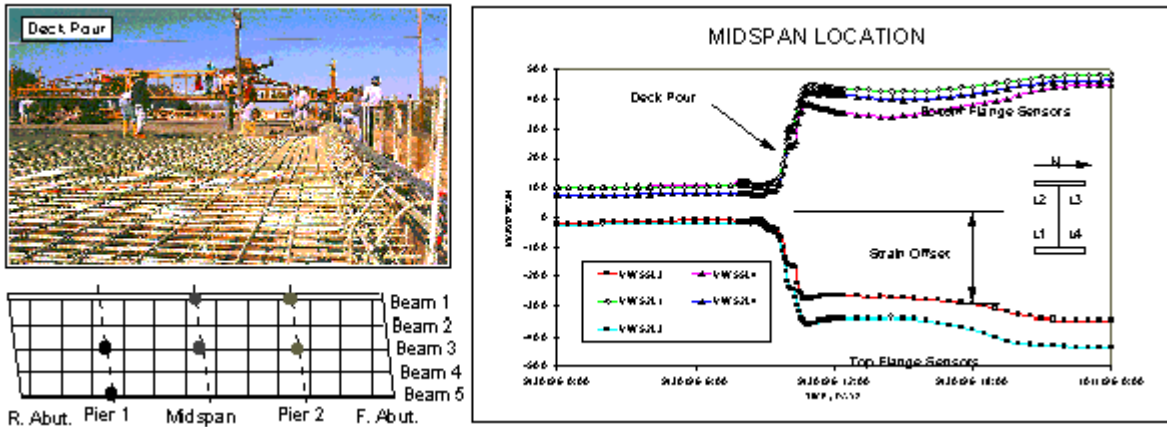


**Figure 1-17: Instrumented Monitoring of Deadload Stresses**

Certain structural details, such as the integral abutments and the welded connections for crossframes and bearing plates (see Figures 1-18, 1-19), were responsible for inducing significant local stresses not explicitly considered in the bridge design. The thermal response of the stringer after encasement indicates that the boundary conditions changed from a simply supported beam to a moment-resisting connection with longitudinal restraints, rather than the roller connection assumed for the integral abutment design.

- Erection stresses of up to -13 ksi were measured in the stringer flange due to welding of bearing plates
- Erection stresses of up to -3 ksi were measured in the stringer flange due to welding of the crossframes
- Change in boundary condition was observed after concrete encasement of the stringers at the abutments

The shrinkage stresses are not explicitly considered for the design of these bridges, but these levels of stress are near or above the cracking threshold for Class S concrete. Significant cracking is observed at the top and bottom deck surfaces corresponding to these critical locations. Cylinder sample tests indicated a low compressive strength of 4400 psi (designed as 4500 psi).

- Shrinkage longitudinal stresses of up to 850 psi were measured at the top rebar layer of the concrete deck
- Shrinkage lateral stresses of up to -550 psi were measured at the bottom rebar layer of the concrete deck

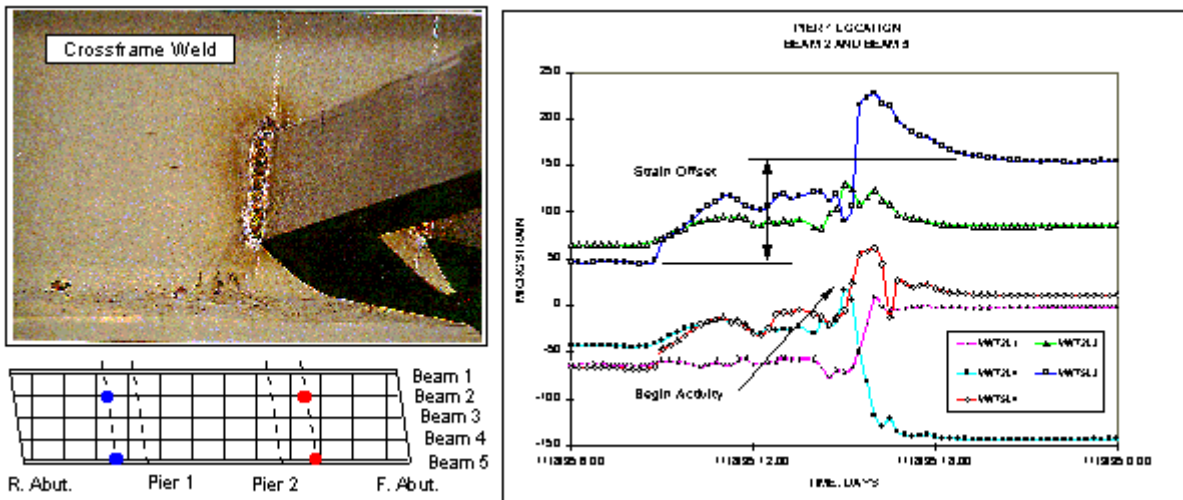


**Figure 1-18: Instrumented Monitoring of Crossframe Weld Stresses**

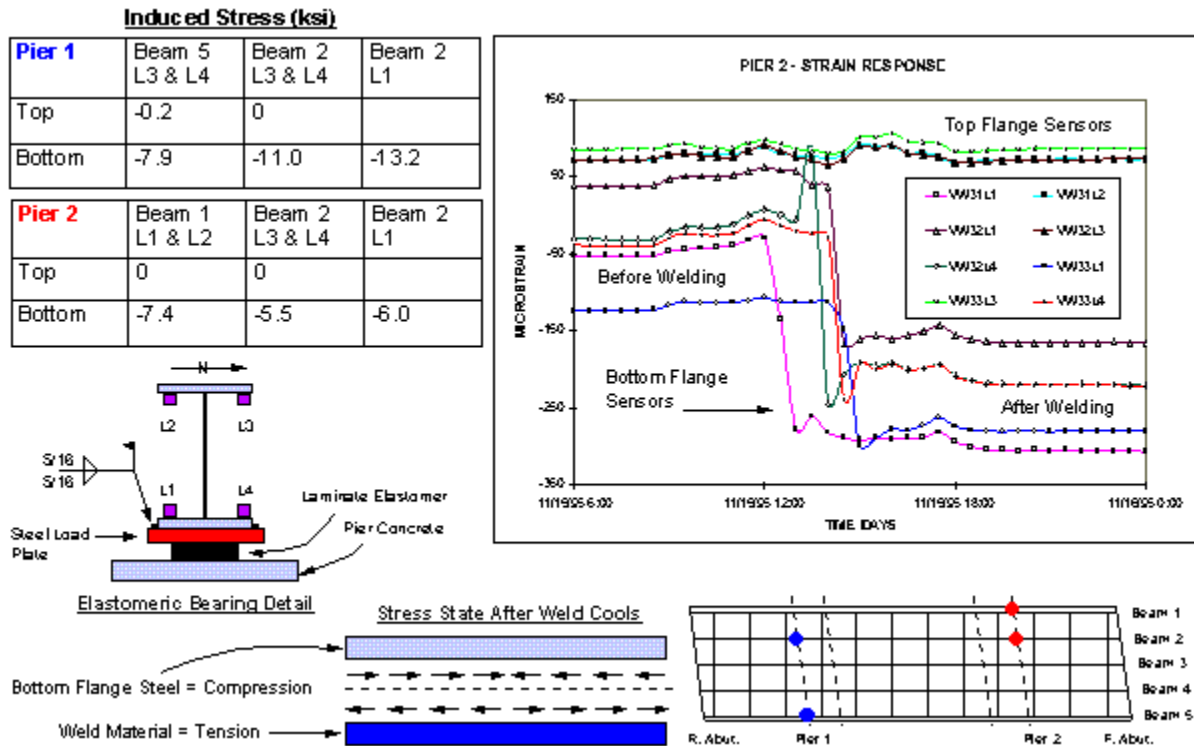
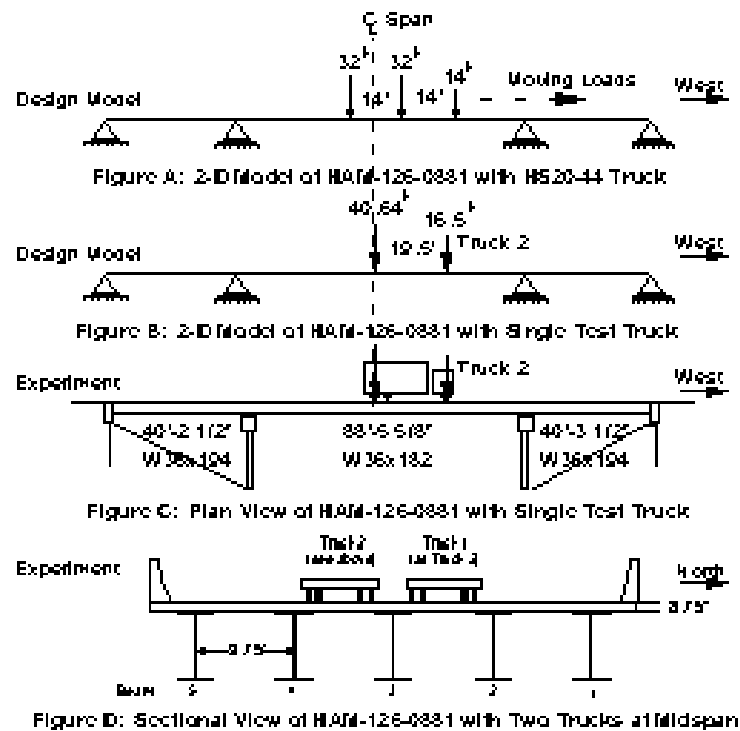


**Figure 1-19: Instrumented Monitoring of Bearing Weld Stresses**

With regards to significant lifetime and service events, several discoveries were possible due to the regular regimen of long-term monitoring, diagnostic truckload and modal impact testing, and structural analysis. Test results are transformed to objective health indices such as modal flexibility or the unit influence line, which have been demonstrated to be conceptual, quantitative, comprehensive, and damage-sensitive signatures.

The live load stresses, moments, and distributions are well within the designed limits. The second and fourth columns of the following table provide a direct comparison of AASHTO design parameters to the actual field test results (see Figure 1-20).

- Static stresses of up to 2 ksi were measured in the stringer flange and crossframes at midspan for a fully-loaded, 3-axle dump truck (57 kips)



Design vs. Identified Structural Parameters	Design		Test	
	Model HS20-44 (Fig. A)	Model 2 Trucks (Fig. B)	Test 1 Truck (Fig. C)	Test 2 Trucks (Fig. D)
Axle Distribution Factor	0.886	0.886	N/a	0.702
Strain (ue) @ Extreme Fiber	360	309	77	159
Stress (ksi) @ Extreme Fiber	10.43	8.96	2.23	4.61
%Stress for Design Load	100%	86%	21%	44%
Live Load Moment ( $M_L$ , k-ft)	815.3	700.7	189	375
% $M_L$ for Design Load	100%	86%	23%	46%

Figure 1-20: Comparison of AASHTO Design Model and Actual Field Experiment

The bridge response to a moving truckload exhibits significant vibrations during and well after the vehicle crossing (Figure 1-21) as compared to the similar bridge, HAM-42-0992 (Figure 1-22). It is believed that these vibrations are caused by traffic excitation of the natural frequency for the structure.

- Modal impact and moving truckload tests both indicate a low natural frequency or first mode of approximately 4.6 Hz due to the low bridge span ratio

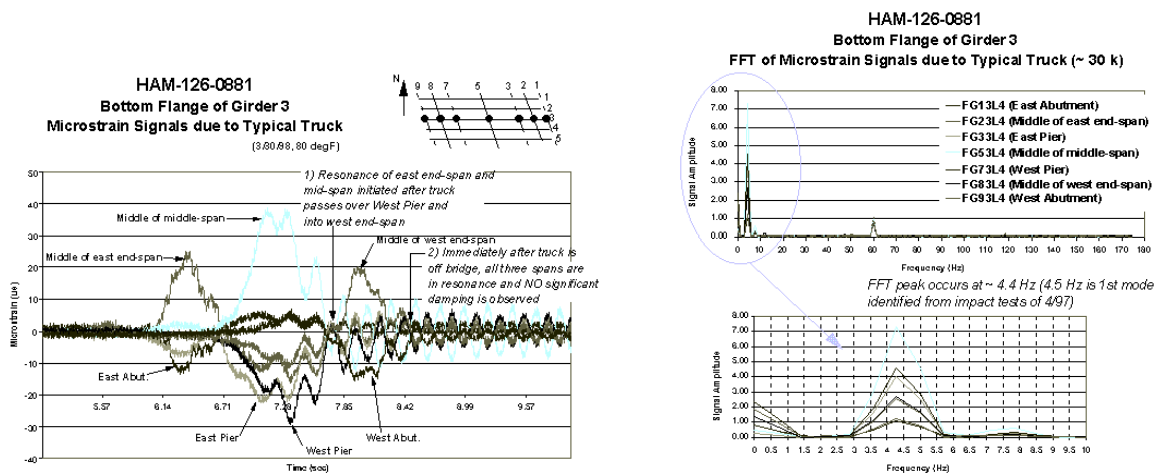


Figure 1-21: Dynamic Response of Bridge, HAM-126-0881

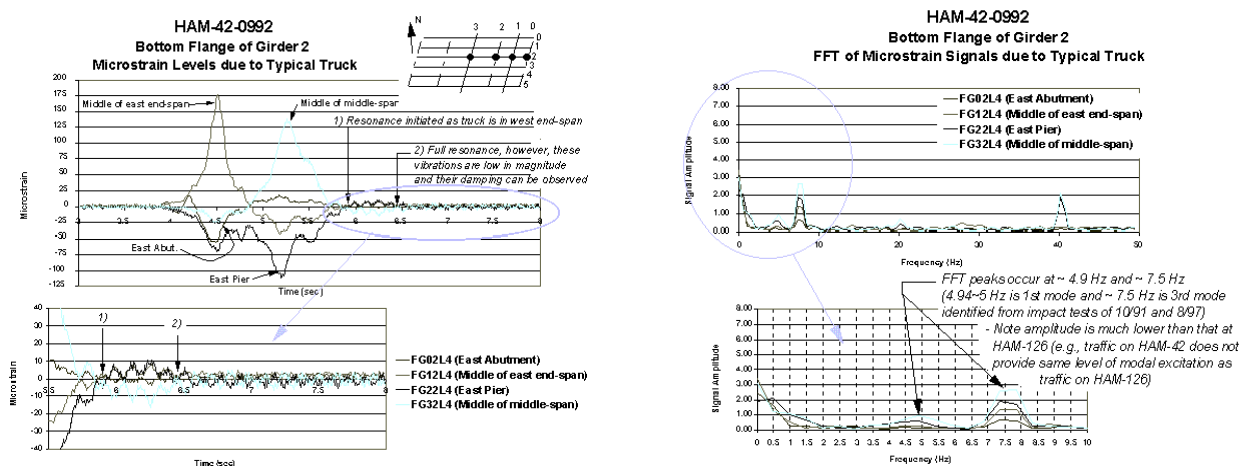
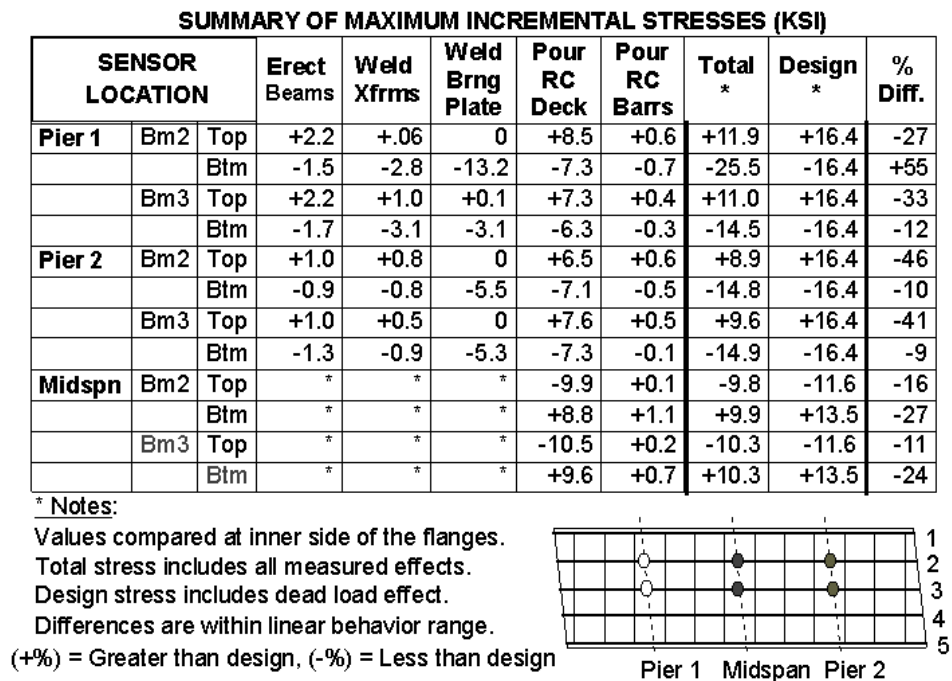


Figure 1-22: Dynamic Response of Bridge, HAM-42-0992

The environmental stresses are not explicitly considered in the bridge design, but these levels of stress far exceed any stress caused by recorded truck traffic (e.g., see Figure 1-15).

- Daily thermal stresses of up to 6 ksi were measured in the stringer flange at the abutment
- Environmental (including thermal) stresses of up to 10 ksi were measured in the stringer flange at the abutment for the entire annual/seasonal cycle

Note that, although the above stresses are indeed additive, the above bounds are local maximums; hence, the worst-case bound is not necessarily represented by their sum. By comparison (Figure 1-23), it is clear that construction and environmental stresses are significant events in a bridge's history, whose significance may not be accurately estimated or even acknowledged within the bridge design or code.



**Figure 1-23: Summary of Lifetime Steel Stresses for Bridge, HAM-126-0881**

Given the conservative nature of most design assumptions and the high level of redundancy inherent with these bridges, the observed stress levels and distributions are not expected to affect the safety of the structure. However, it remains to be seen if they will adversely affect the long-term health and performance of the bridge. For example, it is evident from the controlled truckload tests that most of the unintended composite action between the decking and girders in the end spans has been lost within the first year of service. Significant cracking and efflorescence are observed in the concrete deck and stringer encasement beam corresponding to the locations of the critical environmental stresses. If it is found that these areas later exhibit maintenance problems, new design details or construction practices should be considered.

Bridge monitoring will continue through the coming years of service, and the effect of traffic and environmental forces on these areas will be analyzed. This has been facilitated by the installation of an updated custom-developed monitor software package that automates the data archive and download process via remote phone and/or Internet connection. In addition, a series of truck load tests have been run using both standard 2, 3, and 5 axle truck configurations. Signal processing algorithms allow the direct extraction of unit influence lines from moving truckload test measurements. Sectional moment, impact and distribution factors are then determined and then used to calculate a field identified rating of the bridge. These processing algorithms and condition index calculations are the focus of this research and are discussed in subsequent chapters.

### 1.3.3. Validation of Tools Via Damage Simulation Project

A decommissioned, 3-span steel-stringer bridge, HAM-561-0683, has served as a test specimen in the latter half of 1996 for the evaluation of different concepts, experimental approaches, algorithms, and hardware/software tools for the detection of various types and levels of induced damage (Figure 1-24). Damage scenarios have included the simulation of long-term deterioration such as the loosening and/or breaking of connections, fatigue-fracture, dislocated bearing, corrosion and reduction of effective area and inertia of steel members and connections, loss of chemical bond providing composite action, and cracking and delamination of deck concrete.

The research was designed within the framework of structural identification. The two basic experimental approaches explored were instrumented monitoring and dynamic testing. A monitoring system comprised of temperature, strain, displacement, and acceleration sensors at the critical regions of the test bridge was utilized to record and collect data in several modes: (a) Continuous low-speed monitoring of environmental conditions and bridge responses corresponding to these as well as the damage being induced; (b) high-speed monitoring of responses due to ambient or traffic vibrations; and, the responses under controlled static and crawl-speed truck loading. Modal testing was conducted by impact and by forced excitation, using a new generation of hardware and software which have been developed for bridge modal testing based on research at the Structural Dynamics Research Laboratory of the university. Figure 1-25 illustrates the excellent correlation of the derived and measured flexibility from the two testing methods along a given girder line of the bridge.

The testing methods were repeated several times to determine a statistical error bound for the flexibility estimation due to instrumentation, experimental conditions, and analytical techniques. The tests could confidently detect a 10% change in the sensed local parameter (e.g., strain) during truck loading or in derived flexibility from the modal test; however, this change can correspond to significant and observable damage (e.g. loss of bearing, Fig. 1-24) due to the structural redundancy found in most bridges or it can correspond to the natural variation in flexibility due to seasonal or environmental changes (e.g. backwall resistance to thermal expansion).

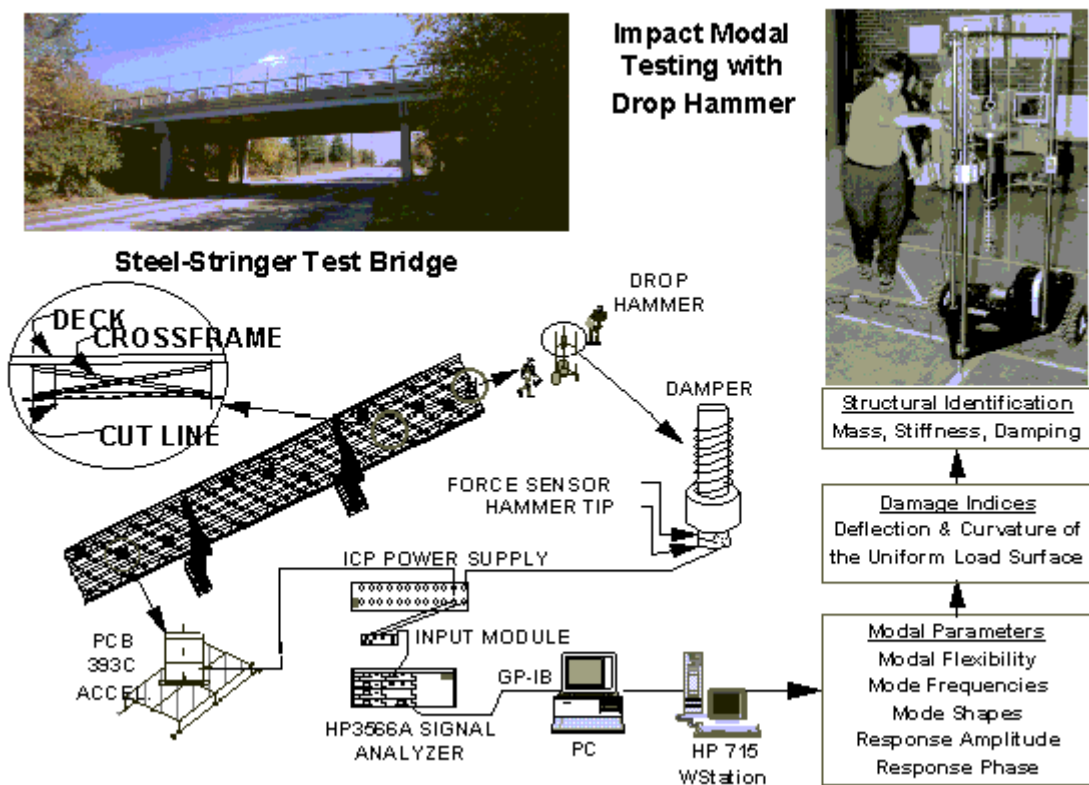


**Figure 1-24: Modal Impact Test System for Detection of Induced Damage**

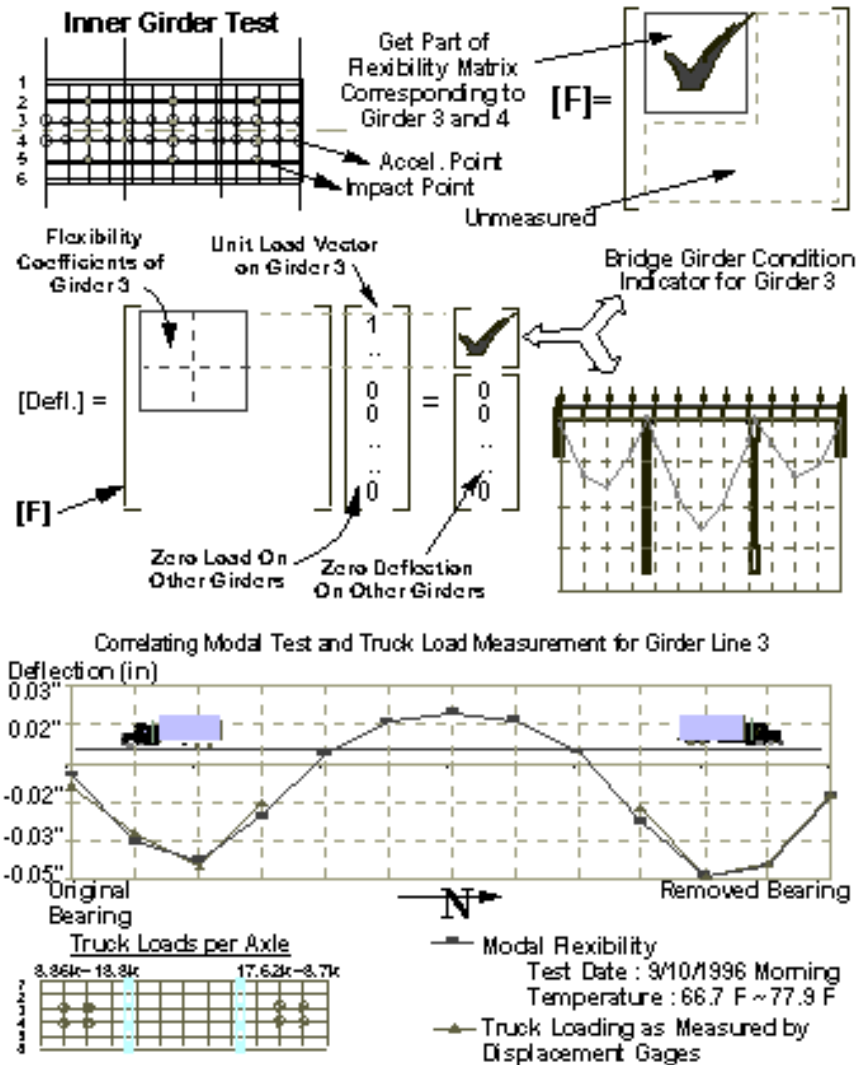


**Figure 1-25: Bridge Girder Condition Indicator and Truckload Verification**

1.4. Problem Statement and Research Deliverables

For a hierarchical monitoring system of an existing structure, the following questions will be asked and solved at each stage in its design:

- A) Given a structure, what are the necessary and desired sets of observable measurands, estimated state parameters, and relevant condition or damage indices?

Step #1: A qualitative manual of the available controlled tests and long-term monitoring procedures, as well as their necessary sensor types and positioning, for a highway steel-stringer bridge. This step is on-going research for this author and the UCII team; however, a large body of work has already been completed over the past six years and has been documented within our final reports for the Reading bridge (Levi, 1996) and Hamilton bridge (Lenett, 2000).

- B) Given a set of measurands, what are the methods and experiments utilized to estimate and cross-check the state parameters of the structure, based upon the available access?

Step #2: A set of quantitative models of varying degrees of complexity for incorporation of ALL measured data from each controlled test and from long-term monitoring. These models include finite element, 2-D grid discretization, MDOF mechanical system, thermo-mechanical analysis, stochastic state-space, Kalman filter, fuzzy or heuristic knowledge, and others. While this author's work has been primarily focused upon the dynamic characterizations (see Chapter 2), significant future effort will be spent upon integration with the traditional structural models provided by the civil engineers.

- C) Given a set of measurands and estimated state parameters, what are the methods or algorithms used for the evaluation of bridge condition and the detection of known or suspected damage mechanisms?

Step #3: The quantitative evaluation of the traditional condition indicators (see Chapter 3) and the most promising damage indices (see Chapter 4) for the assessment of bridge condition and the detection of damage (e.g., the induced damage-types at HAM-561-0683). These indices can be measured under ambient or known loadings and will include structural or member flexibility/damping, deflected mode or structural shapes, modal or other measured frequencies, neutral axis location, influence lines, rating factors, etc.

- D) Given the above set of measurands, estimated state parameters, and damage indices; what are the potential algorithms for localizing and diagnosing the detected (and possibly conflicting) damage mechanisms and their eminent effect upon current and future bridge performance and safety?

Step #4: A predictive algorithm will be designed to utilize the above model set to detect, locate, and identify the induced damage-types for HAM-561-0683 with a probabilistic measure of its uncertainty. Some preliminary or otherwise exploratory results will be provided by this author; however, it is envisioned that this research is beyond the scope of this dissertation.

This research has provided several unique deliverables to the field of expertise:

1. The application, verification, and assessment of truckload testing, modal impact testing, and long-term monitoring procedures, as well as their necessary sensor types and positioning, for several highway bridges. Several steel-stringer bridges are examined within this paper.
2. A reduced set of quantitative models for the estimation and identification of single and multiple span beam response to truckload, traffic, and impact.
3. The quantitative evaluation of the traditional condition indicators and the most promising damage indices for the detection of induced damage-types.
4. The quantitative identification of AASHTO condition indices and their requisite assumptions from the acquired field data.

In this manner, a hierarchical approach to the structural health monitoring system will be designed and built. The final product is envisioned as an on-site continuous Windows-based health monitor which:

- Acquires sensor data at variable sampling speeds,
- Communicates with peripheral devices such as the WIM scale,
- Provides a graphical interface via phone line with a remote engineer,
- Performs simple range and other checks for sensor faults,
- Identifies parameters for a simple beam model of the bridge,
- Detects any structural degradation or damage via NP thresholds,
- Has an open architecture for future expansion or connection.

The current attributes of the bridge health monitor program include (see Figure 1-26):

1. *Remote desktop control* to review and/or initiate monitoring of the instrumented bridge.
2. *Simultaneous high-speed acquisition* of traffic information, video camera, and sensor data from the instrumented bridge for the most recent truck crossing.
3. Field implementation of a continuous, multi-tasking, Windows95 health monitor which acquires sensor data at variable sampling speeds, communicates with peripheral devices, provides a user-friendly and customizable display interface, and allows an open hardware/software architecture for:

- Other structural monitoring applications
- System expansion of instrumentation, reporting, or other functions
- Networked multinode connection of other peripherals, structures, and organizations.

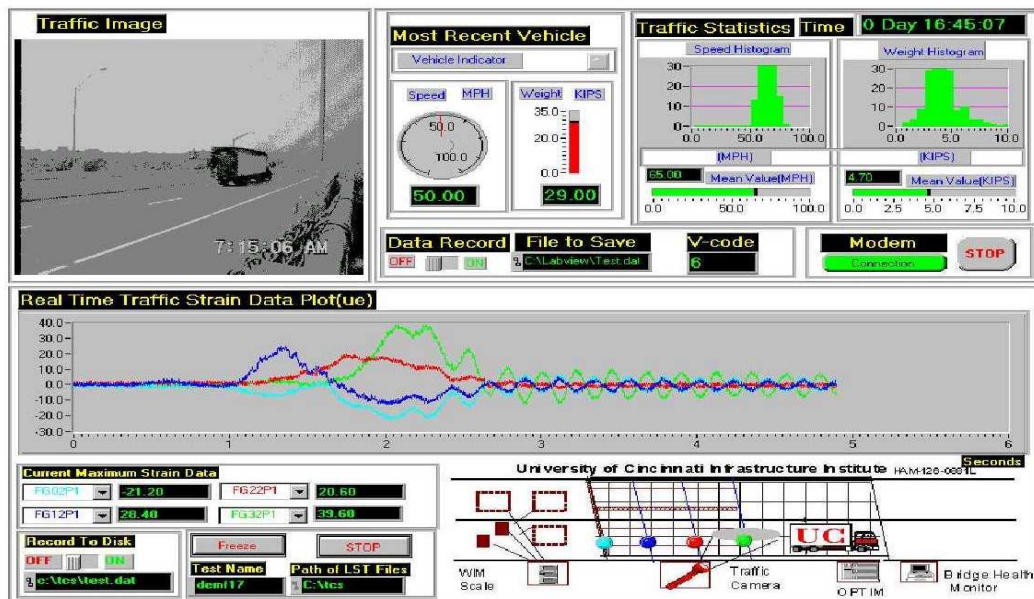


Figure 1-26: Instrumented Health Monitor for Bridge, HAM-126-0881

Future attributes of the bridge health monitor program, based upon results from this research, will include (see Chapter 5):

1. The *automated monitoring program* which switches between high-speed truck monitoring and long-term environmental monitoring, posting regular reports on statistics and evaluated health indices. These can then provide hardcopy reports to the engineer, be posted to the UCII website, and/or trigger alarms based upon pre-defined thresholds. For example:

*Maximum Stress* at the instrumented nodes for both traffic and environmental monitoring.

The location is highlighted on an overhead view of the bridge. This indicates a significant target for the bridge inspector on his/her next visit. This report can provide hardcopy reports to the engineer, be regularly posted to the UCII website (e.g. hourly), and/or trigger alarms based upon pre-defined thresholds.

*Maximum Shift in Neutral Axis* at the instrumented nodes for traffic monitoring. The location is highlighted on an overhead view of the bridge. This indicates a significant target for the bridge inspector on his/her next visit. This report can provide hardcopy reports to the engineer, be regularly posted to the UCII website (e.g. hourly), and/or trigger alarms based upon pre-defined thresholds.

*Remaining Composite Action (RCA)* at the instrumented nodes for traffic monitoring. RCA is considered as the percentage shift of the neutral axis at its measured condition from that of a fully composite section as compared to that of a noncomposite section.

*Unit Influence Line (UIL)* decomposition of measured truckload response at each instrumented node. The actual axle count, weight, and spacing is provided by the WIM scale. Crawl speed of the test truck is the most accurate; however, dynamic filtering allows acceptable comparison of ambient truck traffic.

*Modal Parameter Tracking* for traffic monitoring of instrumented nodes. Frequency, shape, and assurance criteria will be identified based upon real, uncoupled modes. This information is utilized in deriving the UIL from noisy traffic data by using a dynamic filter.

*Impact Factor* at the instrumented nodes for traffic monitoring.

*Distribution Factor* at the instrumented section for traffic monitoring.

*Load Rating* at the instrumented nodes for traffic monitoring. All assumptions such as capacity, concrete strength, axial force, planes remain planes, etc. will be denoted. The derived sectional properties such as modulus, deadload stresses, HS20 liveload stresses, composite action, and moment will be provided. Ratings will be calculated for both inventory and operating levels and for both the allowable stress and load factor methods.

*Remaining Fatigue Life* at the instrumented nodes for traffic monitoring.

2. *Sensor Fault Detection and Diagnostics* for its own system health evaluation and maintenance planning.

In conclusion, the most important contribution of this research is the proven technique for the accurate field identification of bridge parameters (specifically, strain influence lines and modal flexibility) which not only define the structural condition (or health) but are also sensitive to typical damage scenarios. These results are achieved without a finite element model, but can also serve to calibrate such a model for greater spatial precision and the investigation of other possible damage scenarios, repair/retrofit schemes, and other structural considerations.

This contribution is unique to the aforementioned field of expertise and provides a considerable advancement towards the problem of objective and timely assessment of highway bridges.

## 2. Analysis and Identification of a Highway Bridge under Truckload

Parameter estimation is a necessary step in identifying the mechanical model of a structure and is best done by iteration. Sufficient excitation of the structure in terms of amplitude and frequency content is necessary for the parameters to converge upon reliable estimates. Typically, the measured structural variables consist of displacements, rotations, strains, and/or accelerations at discrete points on the structure. The estimated parameters, however, are the characteristic rigidity, stiffness, mass, and damping properties of the structure. This iterative process can be automated on or off-line so as to adapt to or learn new structural properties as environmental, loading, or damage conditions change. Parameters may be updated at a rate dependent upon the complexity of the model and the accessibility of the structure. When compared with past values, the updated model will quantify changes in the structure's parameters that may adversely affect its performance or health, such as its serviceability or its ultimate load capacity.

An optimal estimator is a computational algorithm that processes measurements to deduce a minimum error of the system state by utilizing knowledge of the structure's loading environment, static or steady-state behavior, dynamic or transient response, assumed statistics for measurement noise and error, probabilistic or fuzzy representation of event states and conditional state translations, and initial condition information. One subject of great debate is the merit of time versus frequency domain. Several approaches are documented within the literature, each with its own merits and potential disadvantages [time-domain: Ibrahim, 1977 and 1982, Beck, 1980, and Seibold, 1991; frequency-domain: Chen, 1987, Stubbs, 1990, and Dascotte, 1991]. Many share the burden of computational complexity and sensitivity to erroneous a priori modeling. Each estimation approach is made optimal according to a selected cost or error

functional. Also, each approach is tailored to the desired moment or horizon of estimation: filtering of current measurements, smoothing of past observations, or prediction of future performance. Redundant data, whether it is achieved via repeated sampling or multiple sensor fusion, is desirable to reduce the influence of measurement error.

We need to examine the established methods of representing the load response of bridges to truckload, traffic, and impact. This examination is quite novel as compared to the existing analyses in the literature due to its parallel formulation in the frequency domain. MathCAD software was employed in the mathematics and presentation of this analysis and is appended to this dissertation as Appendix A. We will begin with the assessment of a simply supported beam.

### 2.1. Elastic Deformation of a Beam with a Single Span under Quasi-Static Equilibrium

The deformation of beams is introduced in the study of mechanics and strength of materials. Simple bending theory uses a set of differential equations to relate the internal strains  $\epsilon(x,t)$  and stresses  $\sigma(x,t)$  of a beam to its vertical deflection  $y(x,t)$  or curvatures  $\phi(x,t)$  due to the loading force  $P(x,t)$  or moment  $M(x,t)$  action that causes these deformations.

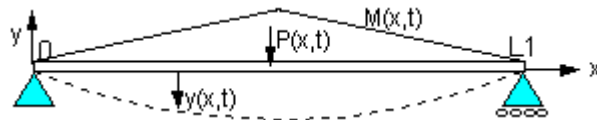


**Figure 2-1: Simply Supported Beam**

where  $y$  = Deflection in inches,  $\frac{\partial y}{\partial x} = \theta$  Rotation,  $\frac{\partial^2 y}{\partial x^2} = \phi$  Curvature.

The analysis of the strength of materials lends us several material properties and their relationships:

$E$  = Young's modulus of elasticity for the material, measured in  $\frac{lbs}{in^2}$  (psi) or  $\frac{1000 lbs}{in^2}$  (ksi),

$\frac{\partial \ell}{\partial x} = \epsilon$  Strain, a dimensionless quantity, oftentimes referred to in  $\mu\epsilon = 10^{-6}\epsilon$  or Microstrain,

$\epsilon E = \sigma$  Stress, measured in  $\frac{lbs}{in^2}$  (psi) or  $\frac{1000 lbs}{in^2}$  (ksi). Also note that 1 kip = 1,000 lbs.

Although the deformation is indeed a three-dimensional phenomenon, strain and stress are considered as axial parameters for this beam analysis where positive values occur due to tensile forces and negative values occur due to compressive forces. When a vertical point load is applied to a beam, the top fibers will act in compression and the bottom fibers in tension as the beam bends in resistance. For symmetrical cross sections, the tensile elongation is found to be equal to the compressive shortening [French, 1996].

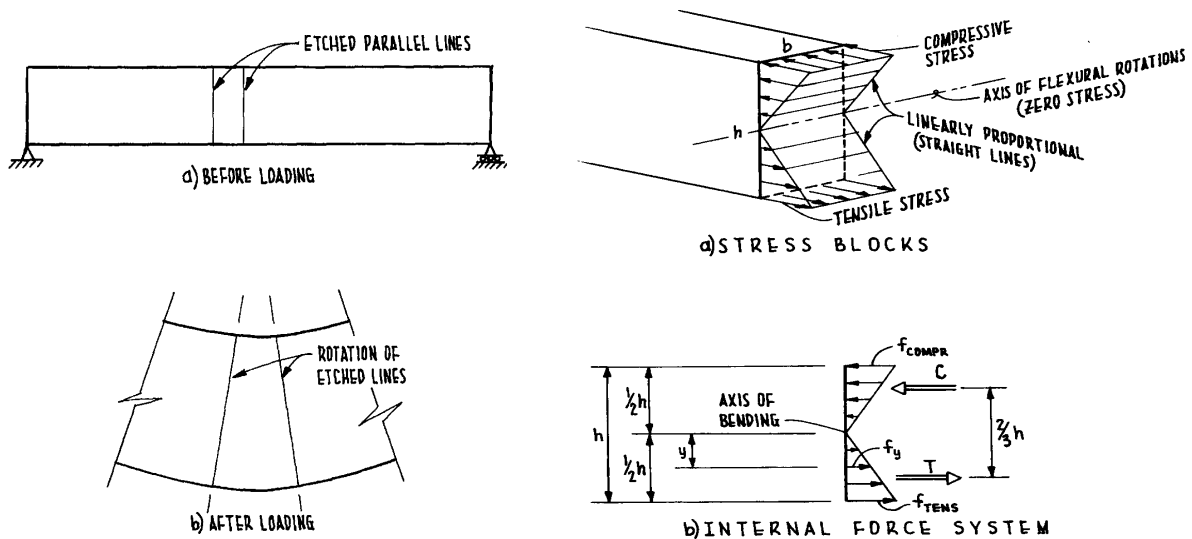


**Figure 2-2: Bending Theory for a Simply Supported Beam**

The planar moment of inertia, I, is the bending moment or torque required to produce 1 psi of stress at a distance of 1 inch from the axis of bending. It is defined by the geometric shape of the beam and allows the following beam flexure equation. The sectional parameters of moment and modulus, constants for the given cross section, are described here.

$$\frac{\sigma I}{y} = M, \text{ Moment or torque for the beam about its bending axis, measured in kip-in or kip-ft}$$

$$\frac{I}{y_{\max}} = S, \text{ Sectional modulus for the geometric cross-section of the beam, measured in } in^3$$

where y is measured down from the axis of bending (as in Figure 2-2). The axis of bending is referred to as the neutral axis, because the stress is zero at this location in the cross section. If there are no other forces acting upon the beam, then the neutral axis coincides with the geometric centroid for the beam.

The above variables and equations for the bending and strength of a beam yield the following relationship between moment and curvature for the cross section and a second-order linear differential equation to relate deflection with the moment action for the beam:

$$\frac{\partial^2 y}{\partial x^2} = \phi = \frac{\epsilon_b - \epsilon_t}{h} = \frac{1}{h} \left( \frac{My_b}{EI} - \frac{My_t}{EI} \right) = \frac{M}{EI} \left( \frac{y_b - y_t}{h} \right) = \frac{M}{EI}$$

$$EI y(x,t) = \int_0^x \int_0^x M(x,t) \partial^2 x + C_1 x + C_2$$

where h is the beam height, the product EI is known as the flexural rigidity of the beam, and the subscripts t and b indicate the top and bottom chord of the beam, respectively. Note again that yt

and  $y_b$  are arbitrarily measured down from the axis of bending (as in Figure 2-2). In general, deflection  $y(x,t)$  is defined opposite of but parallel with gravity in a vertical plane that is tangential to the  $x$  axis of the beam (as in Figure 2-1).

A simply supported beam (see Figure 2-1) is ideal for static determination. The constants  $C_1$  and  $C_2$  of the above integration are determined from boundary conditions or, more precisely, from the conditions imposed upon the beam by its supports. The supports of a simply supported beam are a pin (which allows free rotation but no axial movement) and a roller (which is free to rotate and move axially). The roller is included so that the beam is free to move axially due to thermal contraction and elongation and, therefore, satisfies the assumption #10 below. If the bending moment  $M(x,t)$  can be represented by a single function (e.g.,  $y(x,t)=Y\sin(\pi x/L)$ ), then only two unknowns need to be determined by imposing two boundary conditions (i.e.,  $y(0,t)=0$  and  $y(L,t)=0$ ). If the moment is represented by  $N$  functions, then  $2N$  unknowns need to be determined by imposing  $2N$  boundary conditions. This latter case is usually determined by enforcing continuity of both deflection and slope across the  $N$  functions (i.e.,  $y_0(x_1,t)=y_1(x_1,t)$  and  $\partial_0(x_1,t)=\partial_1(x_1,t)$ ).

The beam flexure equation and the moment-curvature relationship is based upon and limited by several assumptions [Beer, 1992, Rossow, 1996].

1. Small strains and deformations: so that geometry changes are negligible and slopes are small.
2. Bernoulli Theorem of Bending: plane sections before bending will remain plane after bending.

3. Homogeneity: beam material is consistent throughout the cross section.
4. Hooke's Law: beam material has a linear stress-strain relationship as defined by the modulus of elasticity,  $E$ , and it is the same in both tension and compression.
5. Vertical symmetry: to ensure that the stress distribution is symmetric, that the  $y$  axis is the principal axis, the shear center will lie on the  $y$  axis, and bending without twisting will occur.
6. Straight beam design: although it can be extended to curved beams if the ratio of depth to radius of undeformed curvature is small.
7. Prismatic beam design: beam is long, slender, and has a constant cross section, although the latter can be relaxed if the change in cross section is gradual and continuous.
8. Stability under bending: cross section is to maintain integrity and shape under bending action (which may not occur for thin-walled elements).
9. One dimension: all deformation is to occur in the  $x$ - $y$  plane (i.e., no lateral or torsional behavior).
10. No axial load: only bending is considered.
11. Superposition: the deformation for the simultaneous application of two or more loads is equal to the sum of their respective deformations

Shear is considered as a planar force or load that produces a “slicing” effect upon a structural member. One of the more easily visualized cases of direct shear stress is that in a bolt or rivet that joins two plates together. The effect of the load is to slice the connection into two pieces. Shear can also be the internal force for a structure that is tangential to the section upon which it acts. For a simple beam in flexure, shear and moment are changing even over a short segment (see Figure 2-3). Here, it is assumed that both increase to the right (i.e.,  $V_2 > V_1$ ,  $M_2 > M_1$ ).

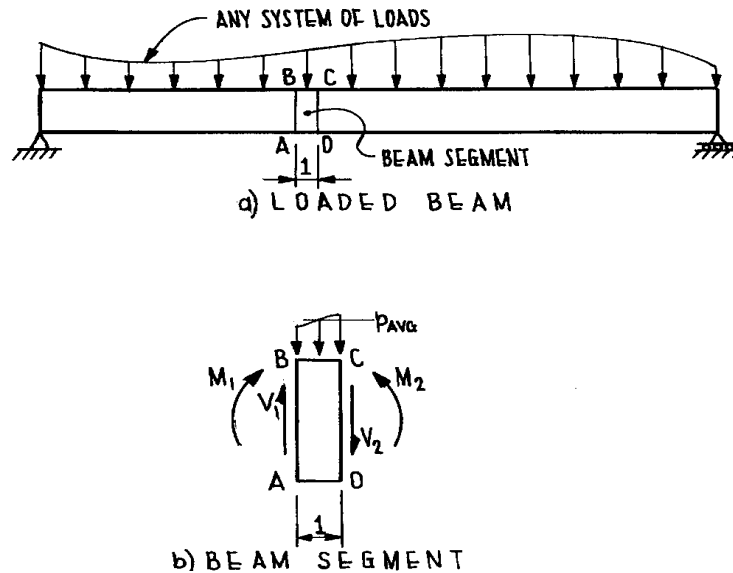


**Figure 2-3: Equilibrium of Forces for a Unit Cross Section of Beam**

The mathematical laws of static equilibrium yield the following equations:

$$\frac{\partial V}{\partial x} = \frac{V_2 - V_1}{1} = -p_{AVG} = -p(x, t)$$

$$\frac{\partial M}{\partial x} = \frac{M_2 - M_1}{1} = V_1 - \frac{p_{AVG}}{2} = V_1 + \frac{V_2 - V_1}{2} = V_{AVG} = V(x, t)$$

which will yield the following second-order linear differential equation to relate moment with the applied load:

$$\frac{\partial^2 M}{\partial x^2} = \frac{\partial V}{\partial x} = -p(x, t)$$

$$M(x, t) = \int_0^x \int_0^x -p(x, t) \partial^2 x + C_3 x + C_4$$

which, when combined with the above equations for beam flexure and the moment-curvature relationship, will yield the following fourth-order linear differential equation to relate deflection with the applied load:

$$\frac{\partial^4 y}{\partial x^4} = \frac{1}{EI} \frac{\partial^2}{\partial x^2} M = \frac{1}{EI} \frac{\partial}{\partial x} V = \frac{-p(x,t)}{EI}$$

$$EI y(x,t) = \int_0^x \int_0^x \int_0^x \int_0^x -p(x,t) dx + \frac{1}{6} C_1 x^3 + \frac{1}{2} C_2 x^2 + C_3 x + C_4$$

A simply supported beam (see Figure 2-1) is again ideal for static determination. The constants C1 and C2 are determined from the above boundary and continuity conditions for deflection and slope. The constants C3 and C4 are determined by the condition of free rotation at the supports (i.e., M(0,t)=0 and M(L,t)=0). If the moment is represented by N functions, then continuity is enforced across the N functions (i.e., M0(x1,t)=M1(x1,t)).

### 2.1.1. Ideal Beam Response to a Slowly Moving Point or Axle Load

If a point load  $p(x,t) = P\delta(x-a)$  is considered for a simply supported beam (as in Figure 2-1), where  $\delta(x-a)$  is the Dirac delta function known as the unit impulse function in the time domain, then two equations are required for both deflection,  $y(x,a)$ , and moment,  $M(x,a)$ , corresponding to positions before and after the load position (see Appendix A1):

$$M0(x, a) := -P \cdot \frac{(-L1 + a)}{L1} \cdot x \quad \text{for } x < a$$

$$M1(x, a) := -P \cdot \frac{(-L1 + a)}{L1} \cdot x - P \cdot (x - a) \quad \text{for } a < x$$

$$y0(x, a) := \frac{1}{6} \left[ -P \cdot \frac{(-L1 + a)}{L1} \right] \cdot x^3 + \frac{-1}{6} \cdot P \cdot a \cdot \frac{(-3 \cdot a \cdot L1 + 2 \cdot L1^2 + a^2)}{L1} \cdot x \quad \text{for } x < a$$

$$y1(x, a) := \frac{1}{6} \left[ -P \cdot \frac{(-L1 + a)}{L1} \right] \cdot x^3 - P \cdot \left( \frac{1}{6} \cdot x^3 - \frac{1}{2} \cdot a \cdot x^2 \right) + \frac{-1}{6} \cdot P \cdot a \cdot \frac{(2 \cdot L1^2 + a^2)}{L1} \cdot x + \frac{1}{6} \cdot P \cdot a^3 \quad \text{for } a < x$$

where a = axial position of the load, L1 = L or the length of the beam in inches or feet, and P = magnitude of the load in lbs or kips. Note that the deflection remains to be scaled by the flexural rigidity EI, which has been arbitrarily set to unity for this example. For the following MathCAD examples and plots, the units of feet and kips have been arbitrarily used; thus, the deflection is represented in feet and moment is represented in kip-ft. Note that the equations are linear with respect to the load P.

The above equations are also functions of the applied load position, a. An influence line is defined as a graphical or formulaic presentation of the variation in magnitude of a force, moment, deflection, or other parameter at a single fixed point in a structure as a function of position of an applied unit load on the structure. The key concept is that the load position is now the functional variable and the structural response is determined for a fixed point on the structure. The unit influence line (UIL) is normalized for a point load of 1 kip or 1,000 lbs. The assumptions and limitations for the beam flexure equation and the moment-curvature relationship still hold. Due to superposition, an influence line is especially helpful to a bridge engineer to understand the effects of various loads at different positions and/or orientations (e.g.,

point, uniform, etc.) on the structure and identify the maximum or worst-case loading scenarios for condition assessment. For example, the response to a slowly moving truckload can be determined by adding the weighted sum of influence lines corresponding to each axle weight (see Figure 2-4) [Turer, 1997 and 1999].

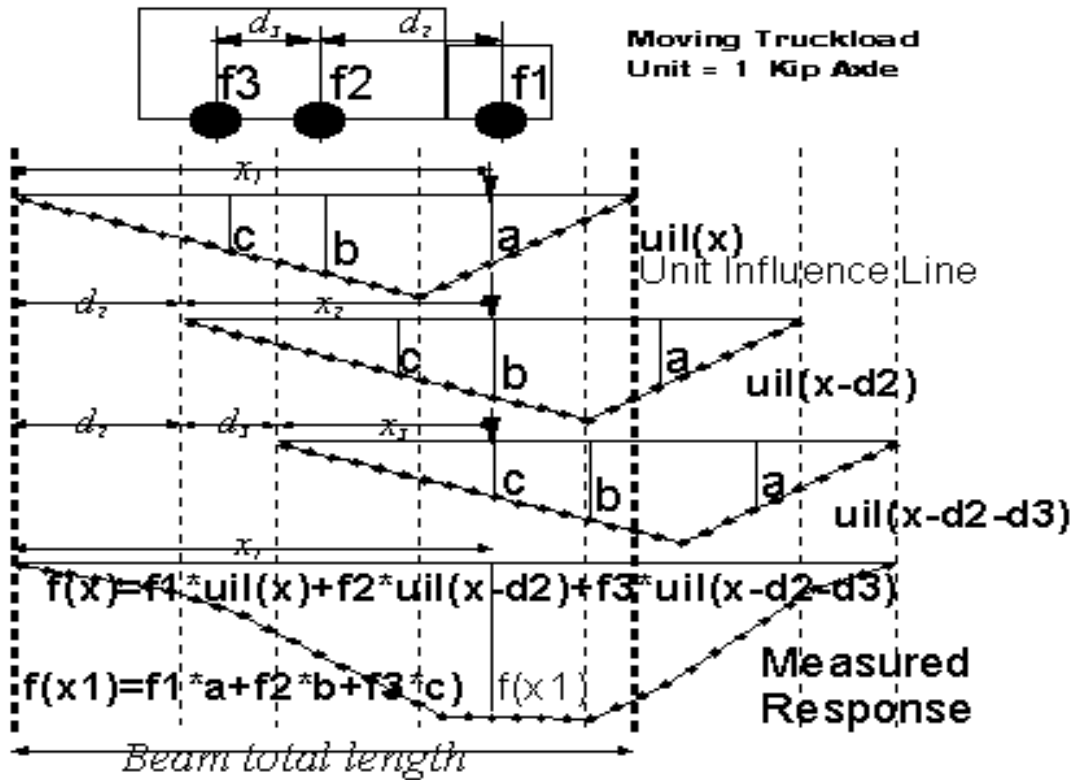
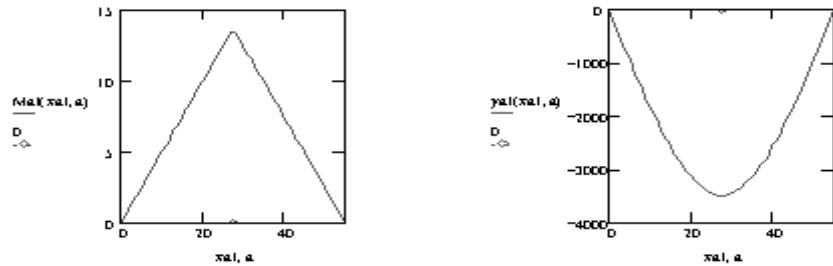


Figure 2-4: Truckload Response Determined from Influence Lines

In MathCAD, the above two sets of equations were combined to form one equation for both deflection  $y_{a1}(x,a)$  and moment  $M_{a1}(x,a)$ . The beam length ( $L_1=55$  feet) was specified as the length of the first span for one of our local instrumented bridges, HAM-42-0992. The point load ( $P=1$  kip) was fixed at midspan ( $a=27.5$  feet) and the two functions were plotted for the variable

$x=xa1$ . Figure 2-5 illustrates the characteristic triangular shape for moment and the half-sinusoidal shape of  $-P*L^3/48EI \sin(\pi x/L)$  for deflection. The influence lines for the midspan (i.e.,  $x$  is fixed at 27.5 feet and  $a$  is varied over the beam length) are identical to the responses in Figure 2-5 and are therefore not plotted. It can be shown that the maximum point load response for both deflection and moment occurs at the midspan of the structure when the load is also positioned at the midspan. A slowly moving, two-axle truckload can be simulated by superimposing two weighted influence lines (i.e.,  $y2P = y(x,a) * P1 + y(x,a-S) * P2$ , where  $P1$  and  $P2$  are the axle loads and  $S$  is the axle spacing). Figure 2-6 illustrates the moment and deflection responses to a slowly moving truckload with  $P1=1$  kip,  $P2=2$  kip, and  $S=10$  feet. Note that in both plots the deflection remains to be scaled by the flexural rigidity  $EI$ , which has been arbitrarily set to unity for this example.



**Figure 2-5: Moment and Deflection for a Point Load and the UIL at Midspan of an Ideal Beam**

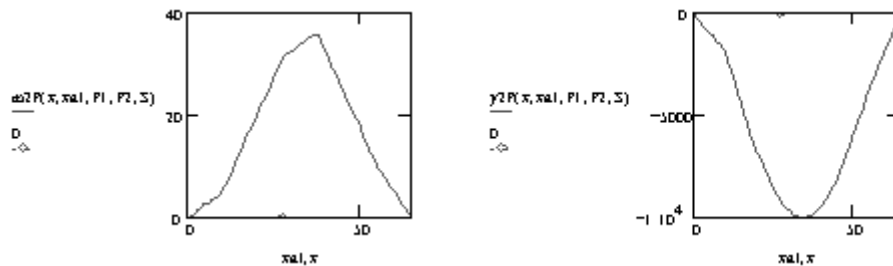


**Figure 2-6: Moment and Deflection for a Simulated Truckload at Midspan of an Ideal Beam**

Since this model does not incorporate dynamics of any manner, this truckload simulation represents an ideal experiment that is free from all dynamic disturbances. For example, the vehicle would have to move slow enough such that dynamics of the structure and of the truck itself are insignificant. This assumption is sometimes referred to as a quasi-static experiment or as a crawl-speed truckload test. In a section below for this chapter, we will model the generalized dynamic behavior of the beam and its effect upon a truckload experiment. In future chapters, we will examine if this assumption is realizable in practice.

Irregardless of sensor position, it will be shown that both influence lines can be represented by the Fourier summation of sinusoidal loading modes,  $p(n,t) = P*\phi(n,v*t)$ , where  $P$  is the axle weight and  $\phi(n,x)$  is the derived bending modes for the beam. For example, the deflection influence line for the midspan,  $y_1(L/2,a)$ , can be approximated by the first loading mode shape of the beam,  $\phi(1,a) = \sin(\pi a/L)$ , when it is scaled by the peak deflection at midspan,  $y(L/2,L/2) = -P*L^3/48EI$ . Further, for any sensor location  $L/i$ , there are  $i-1$  loading modes required to represent the beam deflection. For example, midspan ( $L/2$ ) is represented by one loading mode while quarter span ( $L/4$ ) is represented by three loading modes. The moment response, however, must be represented by many sinusoidal loading modes due to its triangular shape. Moment requires much more information than deflection to represent it in the time domain.

The simulated beam responses for deflection and moment to a crawl-speed point load are transformed to the frequency domain,  $f_y2P(f)$  and  $f_m2P(f)$  respectively. Note again that the beam responses are the influence line for a beam. Magnitude,  $M_{fy2P}(f)$  and  $M_{fm2P}(f)$ , and

phase angle,  $P_{fy2P}(f)$  and  $P_{fM2P}(f)$ , are plotted in the following figures for the case of 10 mph and 50 mph truck speed. Note that in all plots the deflection remains to be scaled by the flexural rigidity  $EI$ , which has been arbitrarily set to unity for this example. The units of feet and kips have been arbitrarily used; thus, the deflection is represented in feet and moment is represented in kip-ft. Phase is represented in degrees from  $-180$  to  $180$ . Frequency is provided in hertz (Hz) along the horizontal axis of the plots. For this example, it is assumed that the data system has a sample speed of 500 Hz and that 5x oversampling is employed beyond the time window of interest in order to provide a better spectral resolution in the frequency domain. The spectral resolution,  $f_{min}$ , is 0.053 Hz and 0.226 Hz for the 10 mph and 50 mph cases, respectively.

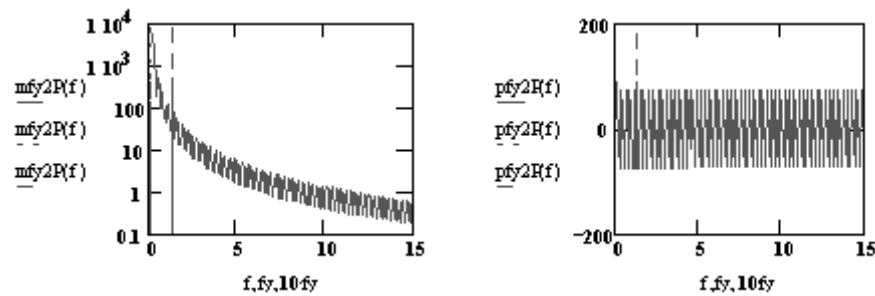


**Figure 2-7: Deflection Magnitude and Phase for Point Load of Simple Beam at 10mph**

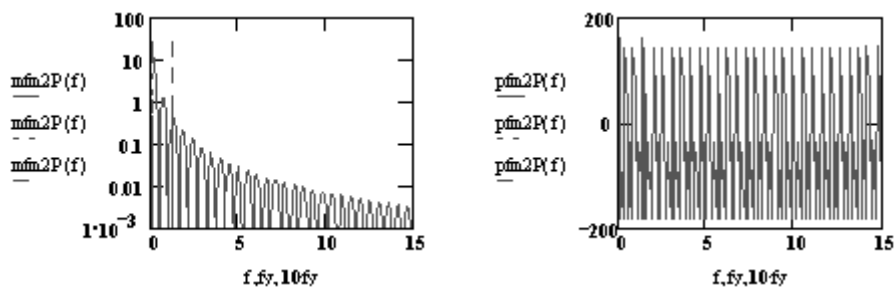


**Figure 2-8: Moment Magnitude and Phase for Point Load of Simple Beam at 10mph**

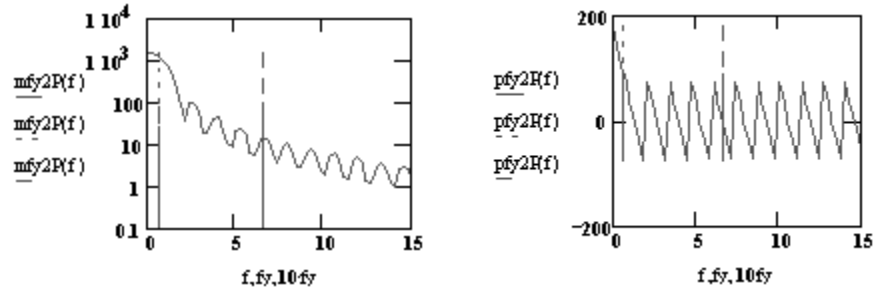


**Figure 2-9: Deflection Magnitude and Phase for Point Load of Simple Beam at 50mph**

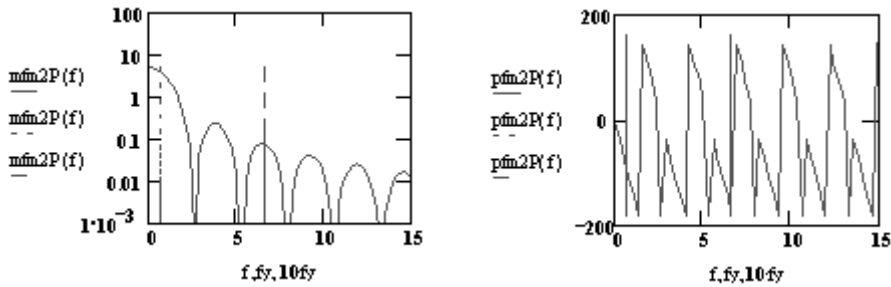


**Figure 2-10: Moment Magnitude and Phase for Point Load of Simple Beam at 50mph**

It is observed that the midspan responses can be approximated for a beam by a series of spectral modes at  $k \cdot f_y = V/(2L)$ , where  $V$  is the truck velocity in feet/second,  $L$  is the span or beam length, and  $k = \{1,4,6,8, \dots\}$  and  $\{1,5,10,15, \dots\}$  for deflection and moment, respectively. This frequency  $f_y$  will be referred to as the first loading frequency or mode. The first loading frequency is plotted for each case above and is 0.133 and 0.667 Hz for the 10mph and 50mph examples, respectively. For any sensor location  $L/i$ , there are  $i-1$  loading modes observed in the frequency response spaced at intervals of the first loading mode  $f_y$ . For example, midspan ( $L/2$ ; hence,  $i=2$ ) is represented by one loading mode while quarter span ( $L/4$ ) is represented by three loading modes at  $f_y$ ,  $2f_y$ , and  $3f_y$ . This is more apparent in the moment response due to its triangular shape (see Appendix A2 and Figure 2-11). Moment requires much more information than deflection to represent it in the frequency domain. Note that as velocity is increased, the

bandwidth is increased by the same factor; otherwise, the signal for a faster loading remains unchanged in its form.

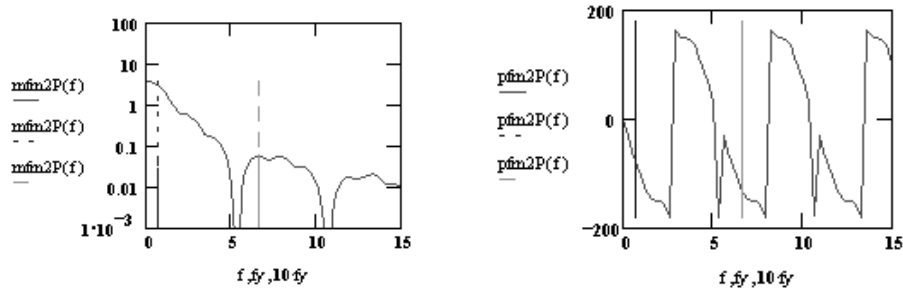


**Figure 2-11: Moment Magnitude and Phase for Point Load of Quarter Span at 50mph**

Deflection of a simple beam at midspan due to a moving point load is approximated in the time domain as a sinusoidal pulse:

$$\text{Simy}(t) := \left[ \sin\left(\frac{\pi \cdot V \cdot t}{L1}\right) \cdot \Phi(t) + \sin\left(\frac{\pi \cdot V \cdot (t - \frac{L1}{V})}{L1}\right) \cdot \Phi\left(t - \frac{L1}{V}\right) \right] \cdot y0\left(\frac{L1}{2}, \frac{L1}{2}\right)$$

where  $\Phi(t) := 1$  for  $t \geq 0$  and  $\Phi(t) := 0$  for  $t < 0$

Moment of a simple beam at midspan due to a moving point load is represented in the time domain as a triangular pulse:

$$\text{Simm}(t) := \left[ \Lambda\left(\frac{L1}{V}, t - \frac{L1}{2 \cdot V}\right) \right] \cdot M0\left(\frac{L1}{2}, \frac{L1}{2}\right)$$

where  $\Lambda(T, t) := \frac{T}{2} - |t|$  for  $-T \leq t \leq T$ , and  $\Lambda(T, t) := 0$  for  $t < -T$  and  $t > T$

Note that a time delay is represented by a complex exponential in the frequency domain:

If  $y(t) \leftrightarrow Y(f)$ , then  $y(t-T) \leftrightarrow Y(f) e^{-i2\pi fT}$

Deflection of a simple beam at midspan due to a moving point load is approximated in the frequency domain as the sum of two equal second order poles, where one pole is delayed by  $L1/V$ :

$$\text{Sim2y}(f) := y_0\left(\frac{L1}{2}, \frac{L1}{2}\right) \cdot \frac{L1}{\pi \cdot V \cdot \left(1 - \frac{4 \cdot f^2 \cdot L1^2}{V^2}\right)} \cdot \left(1 + e^{-i \cdot 2 \cdot \pi \cdot L1 \cdot \frac{f}{V}}\right) \quad \text{where } y_0\left(\frac{L1}{2}, \frac{L1}{2}\right) := \frac{-L1^3}{48EI}$$

Moment of a simple beam at midspan due to a moving point load is represented in the frequency domain as the sinc function, delayed by  $L1/2V$ :

$$\text{Sim2n}(f) := M_0\left(\frac{L1}{2}, \frac{L1}{2}\right) \cdot \frac{L1}{2 \cdot V} \cdot \left[\frac{\sin\left(\pi \cdot L1 \cdot \frac{f}{2 \cdot V}\right)}{\left(\pi \cdot L1 \cdot \frac{f}{2 \cdot V}\right)}\right]^2 \cdot e^{-i \cdot \pi \cdot L1 \cdot \frac{f}{V}} \quad \text{where } M_0\left(\frac{L1}{2}, \frac{L1}{2}\right) := \frac{L1}{4}$$

Figures 2-12 and 2-13 compare the above Fourier transforms (FT) for the approximated time responses with the Fast Fourier transforms (FFT) determined from the MathCAD program. From both the FT plots and their equations, note that appreciable attenuation of the signal magnitude occurs beyond the frequency or bandwidth of  $10f_y$ . This occurs also for sensor locations off of the midspan (e.g., quarter span response, Figure 2-11). To examine the bandwidth further, the simulated beam responses for deflection and moment to a crawl-speed point load are inversely transformed back to the temporal domain,  $if_{y2P}(t)$  and  $if_{M2P}(t)$

respectively. The performance of an ideal low-pass filter is examined in terms of the mean squared error of the filtered beam responses as compared with those initially simulated above,  $y2P(t)$  and  $M2P(t)$ . It was found that acceptable recovery of the influence lines occurred when the filter cut-off frequency was set to include any spectra that was within approximately forty decibels or 1% of the DC or steady-state magnitude for the signal. This was generally found to occur within one decade of the frequency  $f_y$  of the loading mode due to its second order nature. Hence, the cut-off frequency,  $f_c$ , for the ideal low-pass filter used to recover the time signal from the frequency domain should be set greater than  $10f_y = 5V/L$ . We will show in a future section of this chapter that if the beam has multiple spans, then the shortest span should be used in this determination.

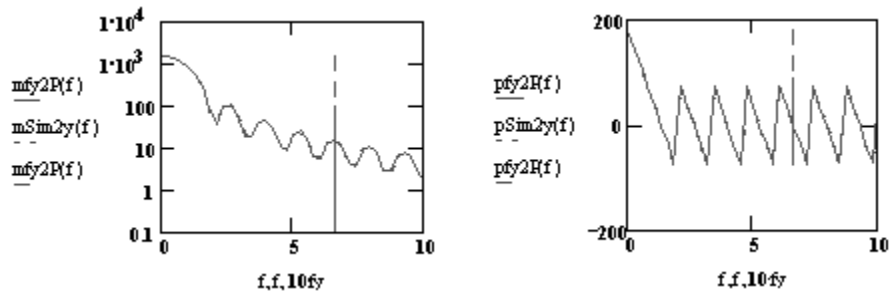


**Figure 2-12: Deflection Magnitude and Phase Comparison of FT and FFT for Point Load, 50mph**

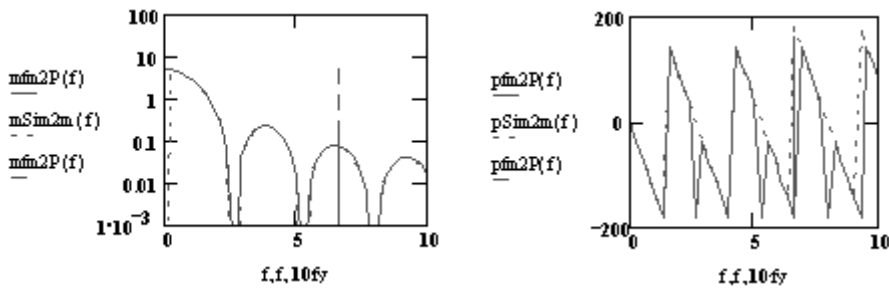


**Figure 2-13: Moment Magnitude and Phase Comparison of FT and FFT for Point Load, 50mph**

### 2.1.2. Ideal Beam Response to a Slowly Moving Truckload

The simulated beam responses for deflection and moment to a 2-axle crawl-speed truckload are also transformed to the frequency domain. As the same MathCAD program was utilized to generate these plots, the functions  $f_{y2P}(f)$  and  $f_{M2P}(f)$  are again used to represent deflection and moment as above.

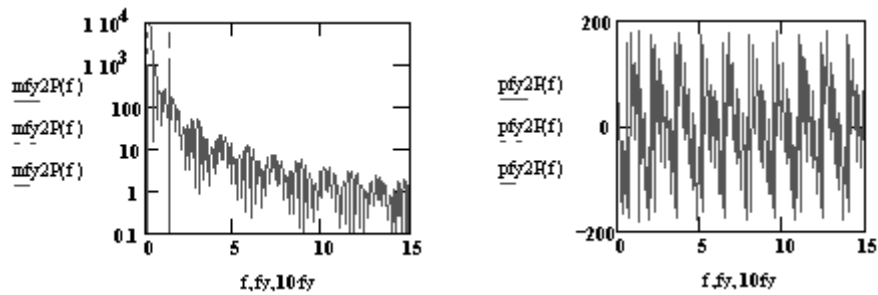


**Figure 2-14: Deflection Magnitude and Phase for Truckload of Simple Beam at 10mph**

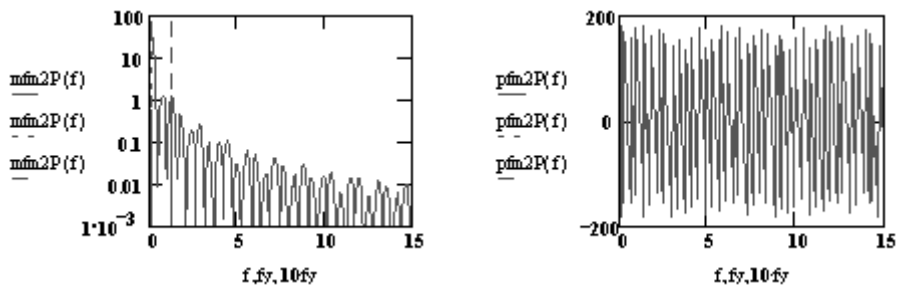


**Figure 2-15: Moment Magnitude and Phase for Truckload of Simple Beam at 10mph**

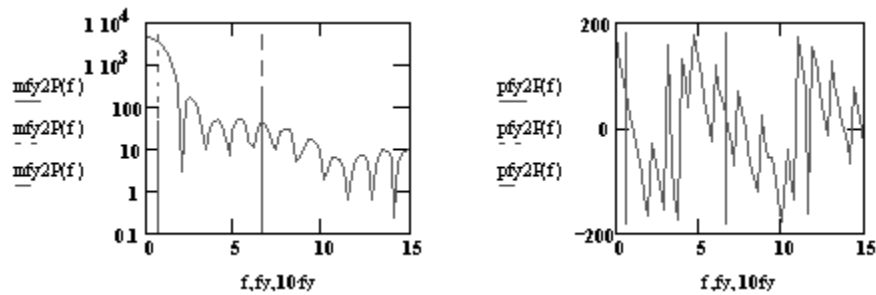


**Figure 2-16: Deflection Magnitude and Phase for Truckload of Simple Beam at 50mph**

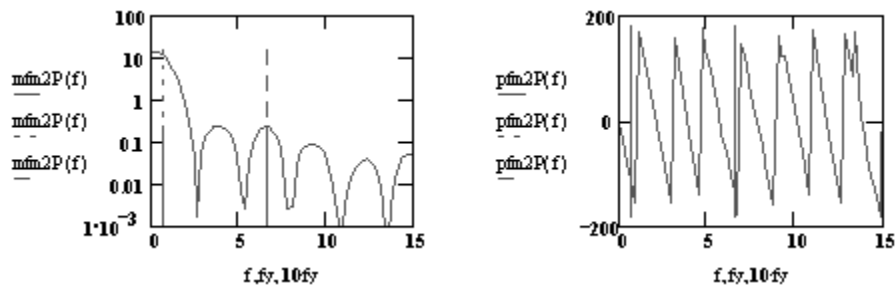


**Figure 2-17: Moment Magnitude and Phase for Truckload of Simple Beam at 50mph**

It is observed again that the loading modes occur at intervals of  $f_y = v/(2L)$ . The responses also contain a series of alternating anti-resonance and resonance modes which are spaced at intervals of the 2<sup>nd</sup> axle frequency,  $f_S = v/(2S)$ , where  $S$  is the spacing of the truck axles. Thus, the spectral signal is the superposition of the loading modes at  $kf_y$  intervals due to the influence of the truck weight and the beating modes at  $nf_S$  intervals due to the out-of-phase spacing of the two axles. The loading modes clearly dominate the magnitude in the frequency domain. Hence, the bandwidth for the two-axle response is comparable with that of the one-axle or point load response.

Deflection of a simple beam at midspan due to a moving truckload is approximated in the time domain as two sinusoidal pulses, with one delayed by the axle spacing  $S/V$  and each weighted by their respective axle weights  $P1$  and  $P2$ :  $\text{Sim2y}(t) = \text{Simy}(t)*P1 + \text{Simy}(t-S/V)*P2$

Moment of a simple beam at midspan due to a moving truckload is represented in the time domain as two triangular pulses, with one delayed by the axle spacing  $S/V$  and each weighted by their respective axle weights  $P1$  and  $P2$ :  $\text{Sim2m}(t) = \text{Simm}(t)*P1 + \text{Simm}(t-S/V)*P2$

Deflection of a simple beam at midspan due to a moving truckload is approximated in the frequency domain as the sum of four equal second order poles delayed by  $0$ ,  $L1/V$ ,  $S/V$ , and  $(L1+S)/V$ :

$$\text{Sim2y}(f) := y0\left(\frac{L1}{2}, \frac{L1}{2}\right) \cdot \frac{L1}{\pi \cdot V \cdot \left(1 - \frac{4 \cdot f^2 \cdot L1^2}{V^2}\right)} \cdot \left(1 + e^{-i \cdot 2 \cdot \pi \cdot L1 \cdot \frac{f}{V}}\right) \cdot \left(P1 + P2 \cdot e^{-i \cdot 2 \cdot \pi \cdot S \cdot \frac{f}{V}}\right)$$

$$\text{where } y0\left(\frac{L1}{2}, \frac{L1}{2}\right) := \frac{-L1^3}{48EI}$$

Moment of a simple beam at midspan due to a moving truckload is represented in the frequency domain as the sinc function, delayed by  $L1/2V$ :

$$\text{Sim2n}(f) := M0\left(\frac{L1}{2}, \frac{L1}{2}\right) \cdot \frac{L1}{2 \cdot V} \cdot \left[\frac{\sin\left(\pi \cdot L1 \cdot \frac{f}{2 \cdot V}\right)}{\left(\pi \cdot L1 \cdot \frac{f}{2 \cdot V}\right)}\right]^2 \cdot e^{-i \cdot \pi \cdot L1 \cdot \frac{f}{V}} \cdot \left(P1 + P2 \cdot e^{-i \cdot 2 \cdot \pi \cdot S \cdot \frac{f}{V}}\right)$$

$$\text{where } M0\left(\frac{L1}{2}, \frac{L1}{2}\right) := \frac{L1}{4}$$

Note that the only difference between the Fourier transform equation for one-axle and two-axle loading is the latter time delay function in parenthesis due to the axle spacing,  $(P1 + P2\exp(-i2\pi Sf/V))$ .

Figures 2-18 and 2-19 compare the above Fourier transforms (FT) for the approximated time responses with the Fast Fourier transforms (FFT) determined from the MathCAD program. From both the FT plots and their equations, note that appreciable attenuation of the signal magnitude occurs beyond the frequency or bandwidth of  $10f_y$ . The performance of an ideal low-pass filter is examined in terms of the mean squared error of the filtered beam responses as compared with those initially simulated above,  $y_2P(t)$  and  $M_2P(t)$ . It was found again that acceptable recovery of the influence lines occurred when the filter cut-off frequency was set to include any spectra that was within forty decibels or 1% of the DC or steady-state magnitude for the signal. This was generally found to occur within one decade of the frequency  $f_y$  of the loading mode due to its second order nature. Hence, the cut-off frequency,  $f_c$ , for the ideal low-pass filter used to recover the time signal from the frequency domain should be set greater than  $10f_y = 5V/L$ . We will show in a future section of this chapter that if the beam has multiple spans, then the shortest span should be used in this determination. Note that as velocity is increased, the bandwidth is increased by the same factor; otherwise, the signal for a faster loading remains unchanged in its form.

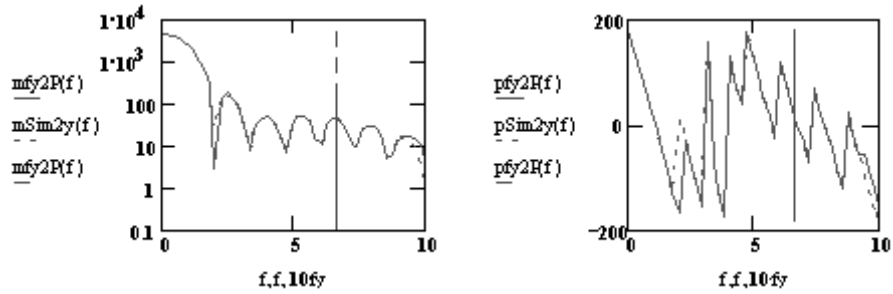


**Figure 2-18: Deflection Magnitude and Phase Comparison of FT and FFT for Truckload at 50mph**

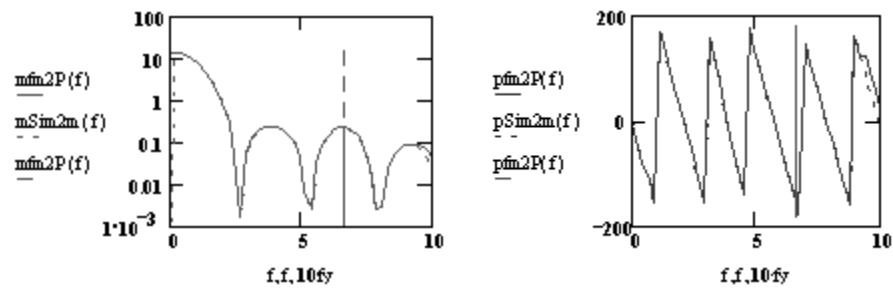


**Figure 2-19: Moment Magnitude and Phase Comparison of FT and FFT for Truckload at 50mph**

We will continue in the following section with the assessment of a simply supported beam with multiple spans.

## 2.2. Elastic Deformation of a Beam with Multiple Spans under Quasi-Static Equilibrium

Simple bending theory will again define a set of differential equations to relate the internal strains  $\epsilon(x,t)$  and stresses  $\sigma(x,t)$  of a beam to its vertical deflection  $y(x,t)$  or curvatures  $\phi(x,t)$  due to the loading force  $P(x,t)$  or moment  $M(x,t)$  action that causes these deformations. We will examine the symmetrical case of three spans (i.e., equal endspan lengths of  $L1=(L3-L2)$ , which may or may not be equal to the middle span length  $(L2-L1)$ ) that is quite common for steel-

stringer bridges. Note that the deflection is necessarily zeroed at each support, while the moment is nonzero.

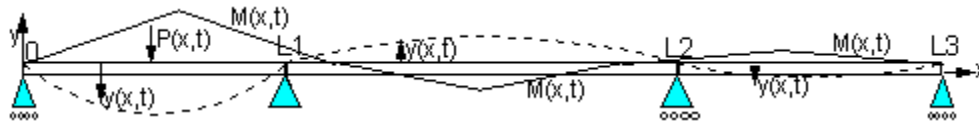


**Figure 2-20: Simply Supported Beam with Three Spans**

The beam flexure equation, the moment-curvature relationship, and its assumptions still apply for a simply supported beam with multiple spans. As depicted in Figure 2-20, the moment and deflection must be identified with  $N+1$  functions for a beam with  $N$  spans. The four constants for each of the integrated  $N+1$  differential equations are determined from boundary conditions or, more precisely, from the conditions imposed upon the beam by its supports and by continuity. The pin and roller supports of a simply supported beam will impose  $N+2$  boundary conditions (i.e.,  $M(0,t)=0$ ,  $M(LN,t)=0$ , and  $y(L_i,t)=0$  where  $i = \{1,2,3,\dots,N\}$ ). The remaining  $3N+2$  unknowns are determined by enforcing continuity of deflection, slope, and moment across the  $N$  functions (i.e.,  $y_0(x_1,t)=y_1(x_1,t)$ ,  $\vartheta_0(x_1,t)=\vartheta_1(x_1,t)$ , and  $M_0(x_1,t)=M_1(x_1,t)$ ).

### 2.2.1. Ideal Multi-Span Beam Response to a Slowly Moving Point or Axle Load

If a point load  $p(x,t) = P\delta(x-a)$  is considered for a simply supported beam with three symmetrical spans (as in Figure 2-20), where  $\delta(x-a)$  is the Dirac delta function known as the unit impulse function in the time domain, then four equations are required for both deflection,  $y(x,a)$ , and moment,  $M(x,a)$ , corresponding to positions before and after the load position in the loaded span

and for positions in the unloaded spans. Further, the four equations must be reformulated depending upon whether the loaded span is an endspan (see Appendix A3) or the middle span (see Appendix A4). Appendix A5 puts all of this together within a MathCAD program to address the same issues and concepts that were examined for the single span case.

In MathCAD, the above four sets of equations were combined to form one equation for both deflection  $y_1(x,a)$  and moment  $M_1(x,a)$ . The span lengths ( $L_1=55$ ,  $L_2=133$ ,  $L_3=188$  feet) were specified for one of our local instrumented bridges, HAM-42-0992. The point load ( $P=1$  kip) was fixed at the first midspan ( $a=27.5$  feet) and the two functions were plotted for the variable  $x=xa_1$ . Figure 2-21 illustrates the series of characteristic triangular shapes for moment and the half-sinusoidal shapes for deflection. The influence lines for the midspan (i.e.,  $x$  is fixed at 27.5 feet and  $a$  is varied over the beam length) are defined by equation  $y(x,a)$  for deflection and  $M(x,a)$  for moment. Figure 2-22 illustrates that the deflection influence line is again identical to the response in Figure 2-21, but the moment influence line is now zeroed at the supports. It can be shown that the maximum point load response and influence for a given span for both deflection and moment occurs at the middle of that instrumented span of the structure when the load is also positioned at the middle of the given span. A slowly moving, two-axle truckload can be simulated by superimposing two weighted influence lines (i.e.,  $y_2P = y(x,a) * P_1 + y(x,a-S) * P_2$ , where  $P_1$  and  $P_2$  are the axle loads and  $S$  is the axle spacing). Figure 2-23 illustrates the moment and deflection responses to a slowly moving truckload with  $P_1=1$  kip,  $P_2=2$  kip, and  $S=10$  feet.

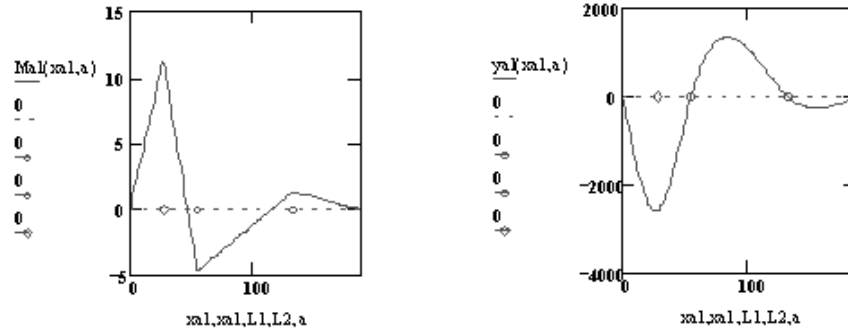


**Figure 2-21: Moment and Deflection for a Stationary Point Load at 1<sup>st</sup> Midspan of a 3-Span Beam**

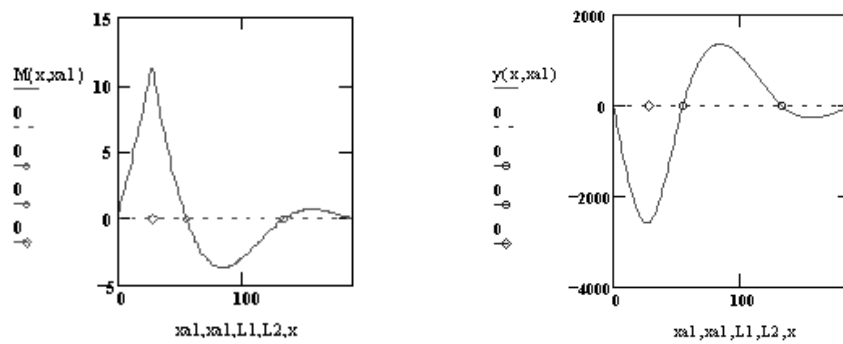


**Figure 2-22: Moment and Deflection for a Moving Point Load at 1<sup>st</sup> Midspan of a 3-Span Beam**

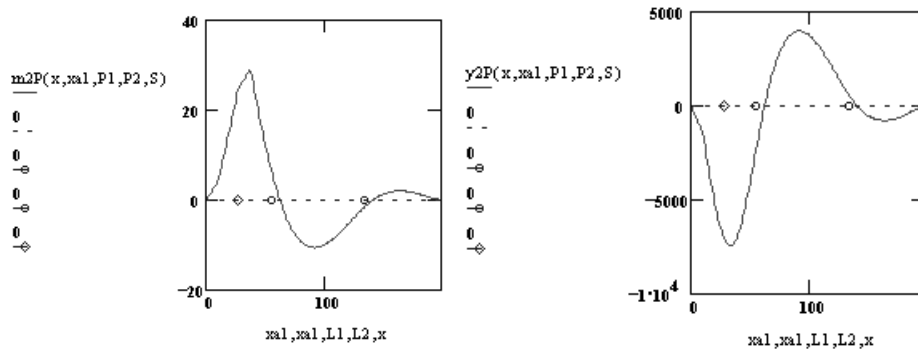


**Figure 2-23: Moment and Deflection for a Simulated Truckload at 1<sup>st</sup> Midspan of a 3-Span Beam**

Since this model does not incorporate dynamics of any manner, this crawl-speed truckload simulation represents an ideal quasi-static experiment that is free from all dynamic disturbances. In the next section, we will model the generalized dynamic behavior of the beam and its effect upon a truckload experiment.

The simulated beam responses for deflection and moment to a crawl-speed point load are transformed to the frequency domain,  $f_y2P(f)$  and  $f_M2P(f)$  respectively. Note again that the beam responses are the influence line for a beam. Magnitude,  $M_{fy2P}(f)$  and  $M_{fM2P}(f)$ , and phase angle,  $P_{fy2P}(f)$  and  $P_{fM2P}(f)$ , are plotted in the following figures for the case of 10 mph and 50 mph truck speed. Note that in all plots the deflection remains to be scaled by the flexural rigidity  $EI$ , which has been arbitrarily set to unity for this example. The units of feet and kips have been arbitrarily used; thus, the deflection is represented in feet and moment is represented in kip-ft. Phase is represented in degrees from  $-180$  to  $180$ . Frequency is provided in hertz (Hz) along the horizontal axis of the plots. For this example, it is assumed that the data system has a sample speed of 500 Hz and that 2x oversampling is employed beyond the time window of interest in order to provide a better spectral resolution in the frequency domain. The spectral resolution,  $f_{min}$ , is 0.074 Hz and 0.370 Hz for the 10 mph and 50 mph cases, respectively.

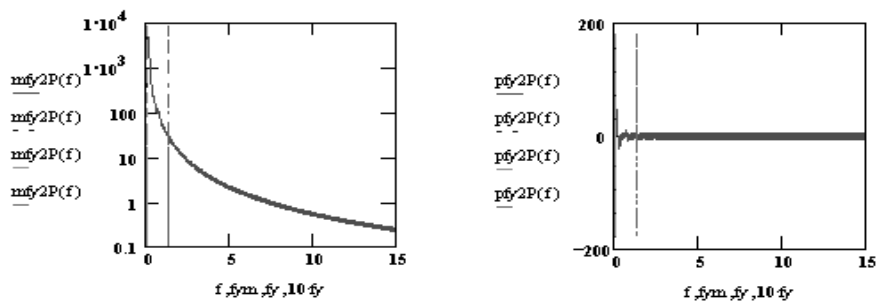


Figure 2-24: Deflection Magnitude & Phase for Point Load of 1<sup>st</sup> Midspan of 3-Span Beam, 10mph

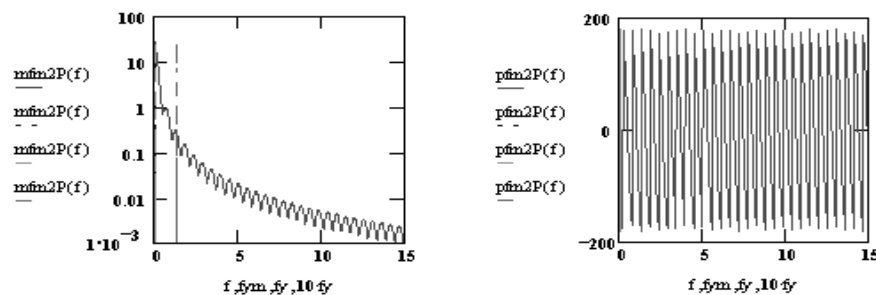


Figure 2-25: Moment Magnitude & Phase for Point Load of 1<sup>st</sup> Midspan of 3-Span Beam, 10mph

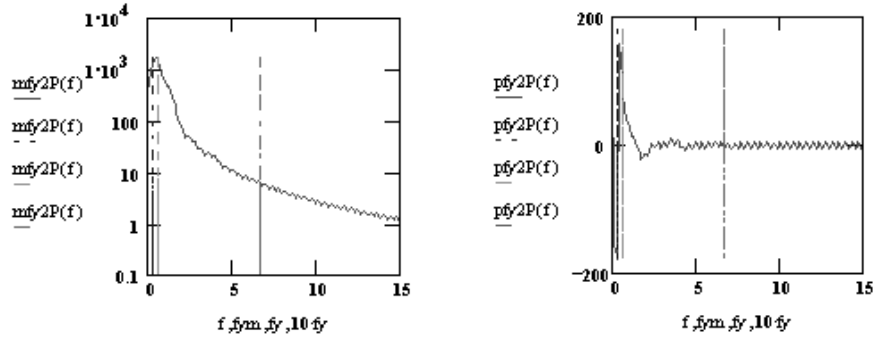


Figure 2-26: Deflection Magnitude & Phase for Point Load of 1<sup>st</sup> Midspan of 3-Span Beam, 50mph

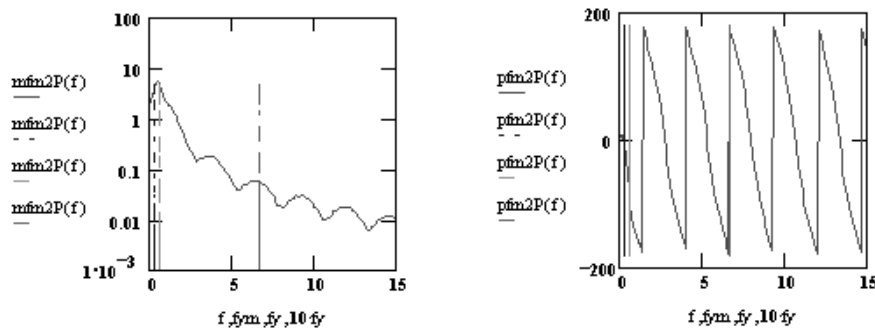


Figure 2-27: Moment Magnitude & Phase for Point Load of 1<sup>st</sup> Midspan of 3-Span Beam, 50mph

It is observed that the first midspan responses can again be approximated for a beam by a series of spectral loading modes at  $k \cdot f_y = V/(2L)$ , where  $V$  is the truck velocity in feet/second,  $L=L1$  is the shortest span or beam length, and  $k = \{1,4,6,8, \dots\}$  and  $\{1,5,10,15, \dots\}$  for deflection and moment, respectively. The first loading frequency is plotted for each case above and is 0.133 and 0.667 Hz for the 10mph and 50mph examples, respectively, of the three-span symmetrical beam representation of the highway bridge, HAM-42-0992. A second loading mode exists at  $k \cdot f_{ym} = V/(2L_m)$ , where  $L_m=(L2-L1)$  is the length of the longer middle span for the bridge. This second loading mode, which is out of phase with the first loading mode, corresponds to the response while the middle span is loaded. The second mode is smaller in magnitude compared to the first mode; however, it does act to cancel the anti-resonance or zeroed points of the first mode. In

addition, the second mode adds visibly to the first peak in magnitude. As the far endspan has the same length as the first span, its response is also represented by or lumped with the loading modes. However, the magnitude of the far endspan's response is very small compared to the instrumented endspan and removing it from the analysis has little significance on assessing the instrumented endspan.

The magnitude is dominated by the loading modes of the shorter span. Note again that appreciable attenuation of the signal magnitude occurs beyond the frequency or bandwidth of 10fy. For other sensor locations, there are again other loading modes observed in the frequency response spaced at intervals of the first loading mode fy. The response to these other loading modes is again found to be insignificant in terms of the signal's bandwidth. Note that as velocity is increased, the bandwidth is increased by the same factor; otherwise, the signal for a faster loading remains unchanged in its form.

Deflection of a multi-span beam at the first midspan due to a moving point load is approximated in the time domain as a series of alternating sinusoidal pulses. The latter pulses are exponentially diminished:

$$\text{Simy}(t) := \left[ \begin{array}{l} \sin\left(\frac{\pi \cdot V \cdot t}{L1}\right) \cdot \Phi(t) + \sin\left(\frac{\pi \cdot V \cdot (t - \frac{L1}{V})}{L1}\right) \cdot \Phi\left(t - \frac{L1}{V}\right) + \dots \\ \dots - e\left(-\frac{\pi \cdot (V \cdot t - L1)}{L1}\right) \cdot \sin\left(\frac{\pi \cdot (V \cdot t - L1)}{L2 - L1}\right) \cdot \Phi\left(t - \frac{L1}{V}\right) - e\left(-\frac{\pi \cdot (V \cdot t - L1)}{L1}\right) \cdot \sin\left(\frac{\pi \cdot V \cdot (t - \frac{L2}{V})}{L2 - L1}\right) \cdot \Phi\left(t - \frac{L2}{V}\right) ] \dots \\ \dots + \frac{L1}{L2 + L3} \left( e\left(-\frac{\pi \cdot (V \cdot t - L2)}{L1}\right) \cdot \sin\left(\frac{\pi \cdot (V \cdot t - L2)}{L3 - L2}\right) \cdot \Phi\left(t - \frac{L2}{V}\right) + e\left(-\frac{\pi \cdot (V \cdot t - L2)}{L1}\right) \cdot \sin\left(\frac{\pi \cdot V \cdot (t - \frac{L3}{V})}{L3 - L2}\right) \cdot \Phi\left(t - \frac{L3}{V}\right) \right) \end{array} \right] \cdot y0\left(\frac{L1}{2}, \frac{L1}{2}\right)$$

Moment of a multi-span beam at the first midspan due to a moving point load is represented in the time domain as a triangular pulse, followed by a series of exponentially diminished, sinusoidal pulses:

$$\text{Simm}(t) = \left[ \begin{array}{l} \Lambda\left(\frac{L1}{V}, t - \frac{L1}{2 \cdot V}\right) + \dots \\ \dots + \frac{L1}{2 \cdot L3} \cdot \left( e^{-\frac{\pi \cdot (V \cdot t - L1)}{L1}} \cdot \sin\left(\frac{\pi \cdot (V \cdot t - L1)}{L2 - L1}\right) \cdot \Phi\left(t - \frac{L1}{V}\right) - e^{-\frac{\pi \cdot (V \cdot t - L1)}{L1}} \cdot \sin\left(\frac{\pi \cdot V \cdot \left(t - \frac{L2}{V}\right)}{L2 - L1}\right) \cdot \Phi\left(t - \frac{L2}{V}\right) \right) \\ \dots - \frac{L1}{8 \cdot L3} \cdot \left( e^{-\frac{\pi \cdot (V \cdot t - L2)}{L1}} \cdot \sin\left(\frac{\pi \cdot (V \cdot t - L2)}{L3 - L2}\right) \cdot \Phi\left(t - \frac{L2}{V}\right) + e^{-\frac{\pi \cdot (V \cdot t - L2)}{L1}} \cdot \sin\left(\frac{\pi \cdot V \cdot \left(t - \frac{L3}{V}\right)}{L3 - L2}\right) \cdot \Phi\left(t - \frac{L3}{V}\right) \right) \end{array} \right] \cdot M0\left(\frac{L1}{2}, \frac{L1}{2}\right)$$

Deflection of a multi-span beam at the first midspan due to a moving point load is approximated in the frequency domain as the sum of two equal second order poles at  $f=V/2L1$  and where one pole is delayed by  $V/L1$ :

$$\text{Sim2yel}(f) := \frac{y0\left(\frac{L1}{2}, \frac{L1}{2}\right) \cdot \pi \cdot V}{L1 \cdot \left[ (\mathbf{i} \cdot 2 \cdot \pi \cdot f)^2 + \frac{\pi^2 \cdot V^2}{(L1)^2} \right]} \cdot \left( \mathbf{1} + e^{-\mathbf{i} \cdot 2 \cdot \pi \cdot L1 \cdot \frac{f}{V}} \right)$$

plus the sum of two additional second order poles at  $f=V/2(L2-L1)$ , exponentially diminished by  $V/L1$ , and where one pole is delayed by  $V/L1$  and the other pole is delayed by  $V/L2$ :

$$\text{Sim2ym}(f) := \frac{-\mathbf{1} \cdot y0\left(\frac{L1}{2}, \frac{L1}{2}\right) \cdot \pi \cdot V}{(L2 - L1)} \cdot \left[ \frac{e^{-\mathbf{i} \cdot 2 \cdot \pi \cdot L1 \cdot \frac{f}{V}}}{\left[ (\mathbf{i} \cdot 2 \cdot \pi \cdot f + \frac{V}{L1})^2 + \frac{\pi^2 \cdot V^2}{(L2 - L1)^2} \right]} + \frac{e^{\frac{L1 - L2}{L1} \cdot \mathbf{i} \cdot 2 \cdot \pi \cdot L2 \cdot \frac{f}{V}}}{\left[ (\mathbf{i} \cdot 2 \cdot \pi \cdot f + \frac{V}{L1})^2 + \frac{\pi^2 \cdot V^2}{(L2 - L1)^2} \right]} \right]$$

plus the sum of two additional second order poles at  $f=V/2(L3-L2)$ , exponentially diminished by  $V/L1$ , and where one pole is delayed by  $V/L2$  and the other pole is delayed by  $V/L3$ :

$$\text{Sim2ye}\lambda(f) := \frac{L1}{L2+L3} \cdot y0\left(\frac{L1}{2}, \frac{L1}{2}\right) \cdot \pi \cdot V \left[ \frac{e^{-i \cdot 2 \cdot \pi \cdot L2 \cdot \frac{f}{V}}}{\left[ \left( i \cdot 2 \cdot \pi \cdot f + \frac{V}{L1} \right)^2 + \frac{\pi^2 \cdot V^2}{(L3-L2)^2} \right]} + \frac{e^{-1} \cdot e^{-i \cdot 2 \cdot \pi \cdot L3 \cdot \frac{f}{V}}}{\left[ \left( i \cdot 2 \cdot \pi \cdot f + \frac{V}{L1} \right)^2 + \frac{\pi^2 \cdot V^2}{(L3-L2)^2} \right]} \right]$$

$$\text{Sim2y}(f) := \text{Sim2ye}l(f) + \text{Sim2ym}(f) + \text{Sim2ye}\lambda(f)$$

Moment of a multi-span beam at the first midspan due to a moving point load is represented in the frequency domain as the sinc function, delayed by  $V/2L1$ :

$$\text{Sim2me}(f) := M0\left(\frac{L1}{2}, \frac{L1}{2}\right) \cdot \frac{L1}{2 \cdot V} \left[ \frac{\sin\left(\pi \cdot L1 \cdot \frac{f}{2 \cdot V}\right)}{\left(\pi \cdot L1 \cdot \frac{f}{2 \cdot V}\right)} \right]^2 \cdot e^{-i \cdot \pi \cdot L1 \cdot \frac{f}{V}}$$

plus the sum of two additional second order poles at  $f=V/2(L2-L1)$ , exponentially diminished by  $V/L1$ , and where one pole is delayed by  $V/L1$  and the other pole is delayed by  $V/L2$ :

$$\text{Sim2mn}(f) := \frac{-1 \cdot M0\left(\frac{L1}{2}, \frac{L1}{2}\right) \cdot \pi \cdot V}{2 \cdot (L2-L1)} \left[ \frac{e^{-i \cdot 2 \cdot \pi \cdot L1 \cdot \frac{f}{V}}}{\left[ \left( i \cdot 2 \cdot \pi \cdot f + \frac{V}{L1} \right)^2 + \frac{\pi^2 \cdot V^2}{(L2-L1)^2} \right]} + \frac{e^{\frac{L1-L2}{L1} \cdot i \cdot 2 \cdot \pi \cdot L2 \cdot \frac{f}{V}}}{\left[ \left( i \cdot 2 \cdot \pi \cdot f + \frac{V}{L1} \right)^2 + \frac{\pi^2 \cdot V^2}{(L2-L1)^2} \right]} \right]$$

plus the sum of two additional second order poles at  $f=V/2(L3-L2)$ , exponentially diminished by  $V/L1$ , and where one pole is delayed by  $V/L2$  and the other pole is delayed by  $V/L3$ :

$$\text{Sim2me}\lambda(f) := \frac{M0\left(\frac{L1}{2}, \frac{L1}{2}\right) \cdot \pi \cdot V}{8 \cdot (L3-L2)} \left[ \frac{e^{-i \cdot 2 \cdot \pi \cdot L2 \cdot \frac{f}{V}}}{\left[ \left( i \cdot 2 \cdot \pi \cdot f + \frac{V}{L1} \right)^2 + \frac{\pi^2 \cdot V^2}{(L3-L2)^2} \right]} + \frac{e^{-1} \cdot e^{-i \cdot 2 \cdot \pi \cdot L3 \cdot \frac{f}{V}}}{\left[ \left( i \cdot 2 \cdot \pi \cdot f + \frac{V}{L1} \right)^2 + \frac{\pi^2 \cdot V^2}{(L3-L2)^2} \right]} \right]$$

$$\text{Sim2n}(f) := \text{Sim2me}(f) + \text{Sim2mn}(f) + \text{Sim2me}\lambda(f)$$

Figures 2-28 and 2-29 compare the above Fourier transforms (FT) for the approximated time responses with the Fast Fourier transforms (FFT) determined from the MathCAD program.

From both the FT plots and their equations, note that appreciable attenuation of the signal magnitude occurs beyond the frequency or bandwidth of  $10f_y$ . This occurs also for sensor locations off of the midspan as well. To examine the bandwidth further, the simulated beam responses for deflection and moment to a crawl-speed point load are inversely transformed back to the temporal domain,  $ify2P(t)$  and  $ifM2P(t)$  respectively. The performance of an ideal low-pass filter is examined in terms of the mean squared error of the filtered beam responses as compared with those initially simulated above,  $y2P(t)$  and  $M2P(t)$ . It was found that acceptable recovery of the influence lines occurred when the filter cut-off frequency was set to include any spectra that was within approximately forty decibels or 1% of the DC or steady-state magnitude for the signal. This was found to occur within one decade of the frequency  $f_y$  of the loading mode due to its second order nature. Hence, the cut-off frequency,  $f_c$ , for the low-pass filter used to recover the time signal from the frequency domain should be greater than  $10f_y = 5V/L$ .

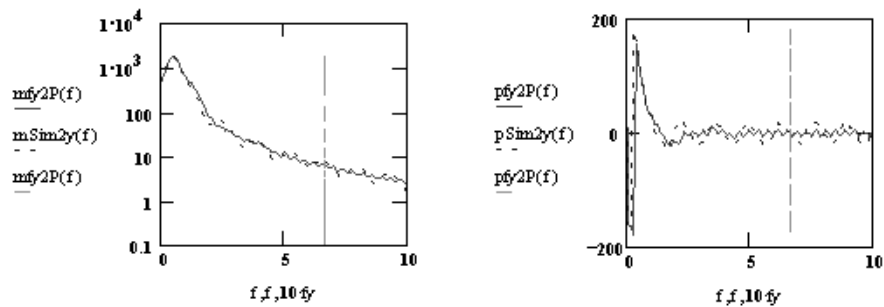


**Figure 2-28: Deflection Magnitude and Phase Comparison of FT and FFT for Point Load, 50mph**

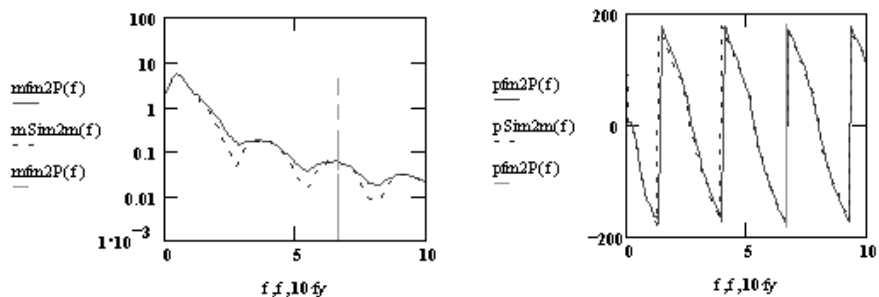


**Figure 2-29: Moment Magnitude and Phase Comparison of FT and FFT for Point Load, 50mph**

2.2.2. Ideal Multi-Span Beam Response to a Slowly Moving Truckload

The simulated beam responses for deflection and moment to a 2-axle crawl-speed truckload are also transformed to the frequency domain. As the same MathCAD program was utilized to generate these plots, the functions  $f_{y2P}(f)$  and  $f_{M2P}(f)$  are again used to represent deflection and moment as above.

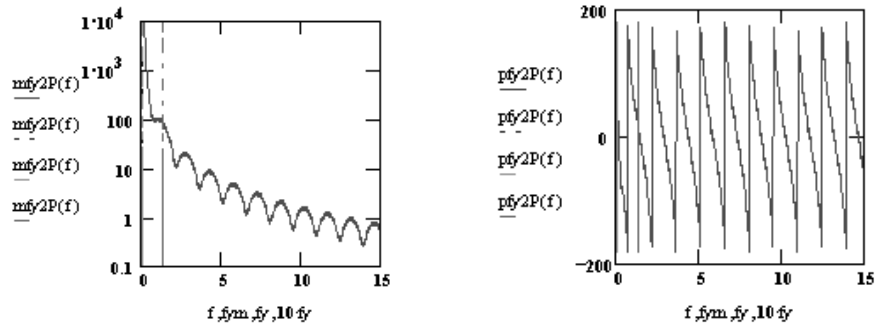


**Figure 2-30: Deflection Magnitude & Phase for Truckload of 1<sup>st</sup> Midspan of 3-Span Beam, 10mph**

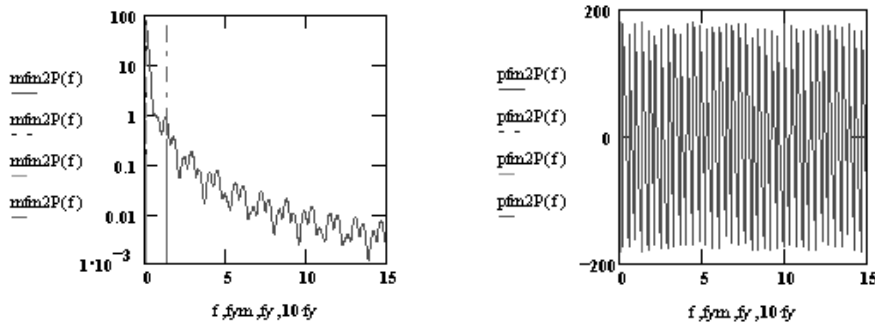


**Figure 2-31: Moment Magnitude & Phase for Truckload of 1<sup>st</sup> Midspan of 3-Span Beam, 10mph**

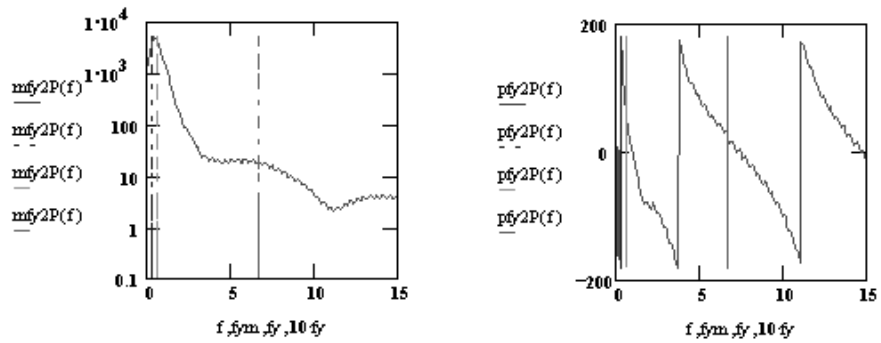


Figure 2-32: Deflection Magnitude & Phase for Truckload of 1<sup>st</sup> Midspan of 3-Span Beam, 50mph

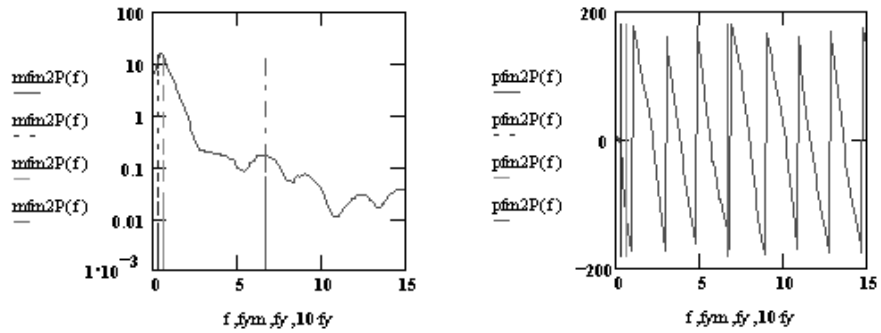


Figure 2-33: Moment Magnitude & Phase for Truckload of 1<sup>st</sup> Midspan of 3-Span Beam, 50mph

It is observed again that the loading modes occur at intervals of  $f_y = v/(2L)$ . The responses also contain a series of alternating anti-resonance and resonance modes which are spaced at intervals of the 2<sup>nd</sup> axle frequency,  $f_S = v/(2S)$ , where  $S$  is the spacing of the truck axles. Thus, the spectral signal is the superposition of the loading modes at  $kf_y$  intervals due to the influence of the truck weight and the beating modes at  $nf_S$  intervals due to the out-of-phase spacing of the two axles. The loading modes clearly dominate the magnitude in the frequency domain. Hence, the bandwidth for the two-axle response is comparable with that of the one-axle or point load response.

Deflection of a multi-span beam at the first midspan due to a moving truckload is approximated in the time domain as two series of sinusoidal pulses  $\text{Sim}_y(t)$  as above, with one delayed by the axle spacing  $S/V$  and each weighted by their respective axle weights  $P1$  and  $P2$ :

$$\text{Sim}_{2y}(t) = \text{Sim}_y(t) \cdot P1 + \text{Sim}_y(t - S/V) \cdot P2$$

Moment of a multi-span beam at the first midspan due to a moving truckload is represented in the time domain as two series of triangular and sinusoidal pulses  $\text{Sim}_m(t)$  as above, with one delayed by the axle spacing  $S/V$  and each weighted by their respective axle weights  $P1$  and  $P2$ :

$$\text{Sim}_{2m}(t) = \text{Sim}_m(t) \cdot P1 + \text{Sim}_m(t - S/V) \cdot P2$$

Deflection of a multi-span beam at the first midspan due to a moving truckload is approximated in the frequency domain as the sum of twelve second order poles:

$$\text{Sim}_{2ye1}(f) := \frac{y_0 \left( \frac{L1}{2}, \frac{L1}{2} \right) \cdot \pi \cdot V}{L1 \cdot \left[ (i \cdot 2 \cdot \pi \cdot f)^2 + \frac{\pi^2 \cdot V^2}{(L1)^2} \right]} \cdot \left( 1 + e^{-i \cdot 2 \cdot \pi \cdot L1 \cdot \frac{f}{V}} \right) \cdot \left( P1 + P2 \cdot e^{-i \cdot 2 \cdot \pi \cdot S \cdot \frac{f}{V}} \right)$$

$$\text{Sim}_{2ym}(f) := \frac{-1 \cdot y_0 \left( \frac{L1}{2}, \frac{L1}{2} \right) \cdot \pi \cdot V}{(L2 - L1)} \cdot \left[ \frac{e^{-i \cdot 2 \cdot \pi \cdot L1 \cdot \frac{f}{V}}}{\left[ (i \cdot 2 \cdot \pi \cdot f + \frac{V}{L1})^2 + \frac{\pi^2 \cdot V^2}{(L2 - L1)^2} \right]} + \frac{e^{\frac{L1 - L2}{L1} \cdot i \cdot 2 \cdot \pi \cdot L2 \cdot \frac{f}{V}}}{\left[ (i \cdot 2 \cdot \pi \cdot f + \frac{V}{L1})^2 + \frac{\pi^2 \cdot V^2}{(L2 - L1)^2} \right]} \right] \cdot \left( P1 + P2 \cdot e^{-i \cdot 2 \cdot \pi \cdot S \cdot \frac{f}{V}} \right)$$

$$\text{Sim}_{2ye2}(f) := \frac{\frac{L1}{L2 + L3} \cdot y_0 \left( \frac{L1}{2}, \frac{L1}{2} \right) \cdot \pi \cdot V}{(L3 - L2)} \cdot \left[ \frac{e^{-i \cdot 2 \cdot \pi \cdot L2 \cdot \frac{f}{V}}}{\left[ (i \cdot 2 \cdot \pi \cdot f + \frac{V}{L1})^2 + \frac{\pi^2 \cdot V^2}{(L3 - L2)^2} \right]} + \frac{e^{-1} \cdot e^{-i \cdot 2 \cdot \pi \cdot L3 \cdot \frac{f}{V}}}{\left[ (i \cdot 2 \cdot \pi \cdot f + \frac{V}{L1})^2 + \frac{\pi^2 \cdot V^2}{(L3 - L2)^2} \right]} \right] \cdot \left( P1 + P2 \cdot e^{-i \cdot 2 \cdot \pi \cdot S \cdot \frac{f}{V}} \right)$$

$$\text{Sim}_{2y}(f) := \text{Sim}_{2ye1}(f) + \text{Sim}_{2ym}(f) + \text{Sim}_{2ye2}(f)$$

Moment of a multi-span beam at the first midspan due to a moving truckload is represented in the frequency domain as the sum of the sinc function and four second-order poles:

$$\begin{aligned} \text{Sim2me1}(f) &:= M0 \left( \frac{L1}{2}, \frac{L1}{2} \right) \cdot \frac{L1}{2 \cdot V} \cdot \left[ \frac{\sin \left( \pi \cdot L1 \cdot \frac{f}{2 \cdot V} \right)}{\left( \pi \cdot L1 \cdot \frac{f}{2 \cdot V} \right)} \right]^2 \cdot e^{-i \cdot \pi \cdot L1 \cdot \frac{f}{V}} \cdot \left( P1 + P2 \cdot e^{-i \cdot 2 \cdot \pi \cdot S \cdot \frac{f}{V}} \right) \\ \text{Sim2me2}(f) &:= \frac{-1 \cdot M0 \left( \frac{L1}{2}, \frac{L1}{2} \right) \cdot \pi \cdot V}{2 \cdot (L2 - L1)} \cdot \left[ \frac{e^{-i \cdot 2 \cdot \pi \cdot L1 \cdot \frac{f}{V}}}{\left[ \left( i \cdot 2 \cdot \pi \cdot f + \frac{V}{L1} \right)^2 + \frac{\pi^2 \cdot V^2}{(L2 - L1)^2} \right]} + \frac{e^{\frac{L1 - L2}{L1} \cdot i \cdot 2 \cdot \pi \cdot L2 \cdot \frac{f}{V}}}{\left[ \left( i \cdot 2 \cdot \pi \cdot f + \frac{V}{L1} \right)^2 + \frac{\pi^2 \cdot V^2}{(L2 - L1)^2} \right]} \right] \cdot \left( P1 + P2 \cdot e^{-i \cdot 2 \cdot \pi \cdot S \cdot \frac{f}{V}} \right) \\ \text{Sim2me3}(f) &:= \frac{M0 \left( \frac{L1}{2}, \frac{L1}{2} \right) \cdot \pi \cdot V}{8 \cdot (L3 - L2)} \cdot \left[ \frac{e^{-i \cdot 2 \cdot \pi \cdot L2 \cdot \frac{f}{V}}}{\left[ \left( i \cdot 2 \cdot \pi \cdot f + \frac{V}{L1} \right)^2 + \frac{\pi^2 \cdot V^2}{(L3 - L2)^2} \right]} + \frac{e^{-1} \cdot e^{-i \cdot 2 \cdot \pi \cdot L3 \cdot \frac{f}{V}}}{\left[ \left( i \cdot 2 \cdot \pi \cdot f + \frac{V}{L1} \right)^2 + \frac{\pi^2 \cdot V^2}{(L3 - L2)^2} \right]} \right] \cdot \left( P1 + P2 \cdot e^{-i \cdot 2 \cdot \pi \cdot S \cdot \frac{f}{V}} \right) \end{aligned}$$

$$\text{Sim2n}(f) := \text{Sim2me1}(f) + \text{Sim2me2}(f) + \text{Sim2me3}(f)$$

Note that the only difference between the Fourier transform equation for one-axle and two-axle loading is the latter time delay function in parenthesis due to the axle spacing,  $(P1 + P2 \exp(-i2\pi S f/V))$ .

Figures 2-34 and 2-35 compare the above Fourier transforms (FT) for the approximated time responses with the Fast Fourier transforms (FFT) determined from the MathCAD program. From both the FT plots and their equations, note that appreciable attenuation of the signal magnitude occurs beyond the frequency or bandwidth of  $10f_y$ . The performance of an ideal low-pass filter is examined in terms of the mean squared error of the filtered beam responses as compared with those initially simulated above,  $y2P(t)$  and  $M2P(t)$ . It was found again that acceptable recovery of the influence lines occurred when the filter cut-off frequency was set to

include any spectra that was within forty decibels or 1% of the DC or steady-state magnitude for the signal. This was generally found to occur within one decade of the frequency  $f_y$  of the loading mode due to its second order nature. Hence, the cut-off frequency,  $f_c$ , for the ideal low-pass filter used to recover the time signal from the frequency domain should be set greater than  $10f_y = 5V/L$ . We will show in a future section of this chapter that if the beam has multiple spans, then the shortest span should be used in this determination. Note that as velocity is increased, the bandwidth is increased by the same factor; otherwise, the signal for a faster loading remains unchanged in its form.

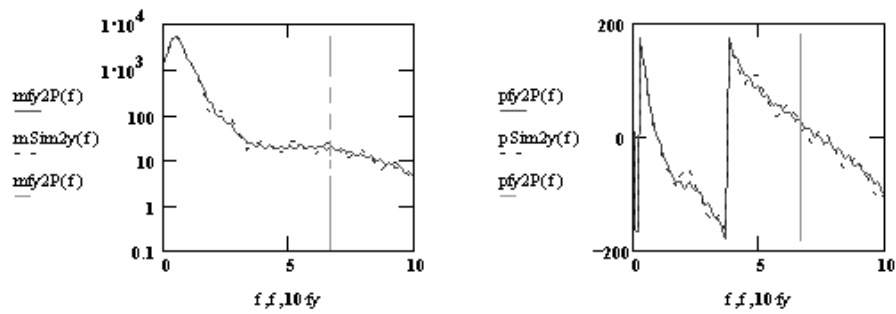


**Figure 2-34: Deflection Magnitude and Phase Comparison of FT and FFT for Truckload at 50mph**

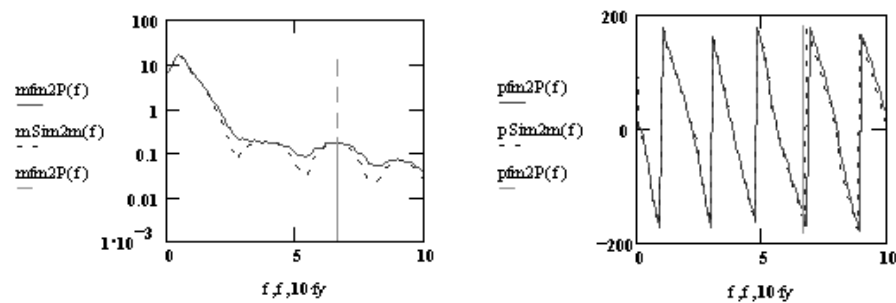


**Figure 2-35: Moment Magnitude and Phase Comparison of FT and FFT for Truckload at 50mph**

We will continue in the following section with the assessment of a simply supported beam under dynamic conditions.

## 2.3. Elastic Deformation of a Beam with a Single Span under Dynamic Conditions

### 2.3.1. The Conventional MKC Lumped Mechanical Model - Temporal and Frequency Domains

Generally, structural identification is considered as the reconciling of a mathematical model based upon first principles with the observed data from a structural experiment consisting of either static or vibrational loading. The conventional mechanical model consists of a second-order, linear dynamical state space governed by the N-dimensional matrices of mass M, stiffness K (or flexibility 1/K), and damping C. Further, the properties of time invariance, statistical stationarity, complete observability, and mechanical reciprocity are assumed for the structural system [Allemang, 1994].

The beam is assumed to be lumped at some N discrete points of the state space. Alternatively, the state space is subdivided into cells and matter is assumed to be lumped at these cells. The resulting dynamic models are ordinary differential equations with time as the only independent variable. For example, the assumption that a solid is a rigid body permits lumping all its mass at its mass center and results in lumped-parameter models of its dynamics. The spatial response of the beam is independent and represented by a mode shape function  $\phi(x)$ , which must satisfy the boundary and continuity conditions [Chopra, 1995, Clough, 1993].

You may recall the following shape functions for an ideal beam, derived in the above sections:

$$\text{Deflection: } \phi(x) := \sin\left(\frac{\pi \cdot x}{L}\right) \cdot y_0\left(\frac{L}{2}, \frac{L}{2}\right); \quad \text{Moment: } \phi(x) := \Lambda(L, x - \frac{L}{2}) \cdot M_0\left(\frac{L}{2}, \frac{L}{2}\right)$$

For a lumped, one-dimensional, second order, single degree of freedom (SDOF) system:

$$m\ddot{x} + c\dot{x} + kx = f(t) \text{ where } \omega_n^2 = \frac{k}{m}, 2\zeta\omega = \frac{c}{m}, \text{ and } \zeta = \frac{c}{\sqrt{4mk}}$$

As a complex quantity, the SDOF frequency response function (FRF) has both magnitude and phase components in polar coordinates:

$$H(\omega) = \frac{1/m}{\sqrt{(\omega_n^2 - \omega^2)^2 + (2\zeta\omega\omega_n)^2}} \quad \theta(\omega) = \tan^{-1} \frac{2\zeta\omega\omega_n}{\omega_n^2 - \omega^2}$$

The characteristic parameters of natural frequency ( $\omega_n$  radians or  $f_n = 2\pi\omega_n$  Hz) and damping ratio  $\zeta$  for the SDOF system can be estimated from both the time and frequency domains (Figure 2-36).

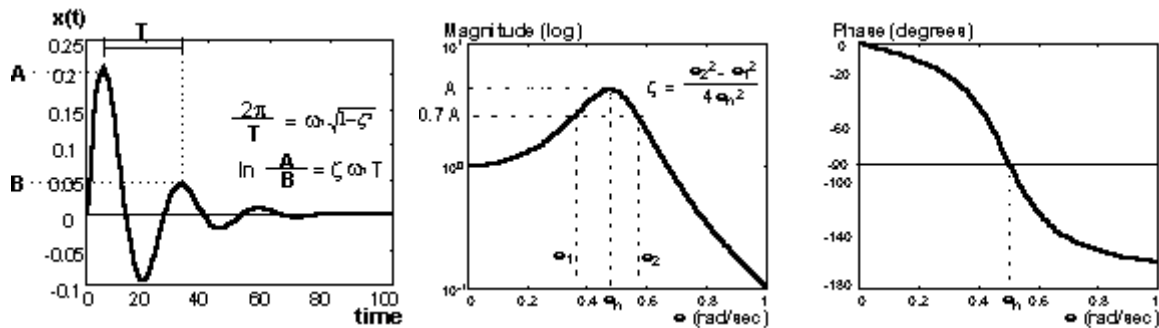


**Figure 2-36: MKC Parameter Estimation From Time or Frequency Domains**

Structural systems are typically underdamped such that the damping ratio  $\zeta$  is less than 0.2. The natural frequency for a highway bridge has been experimentally found to be approximated by  $f_n = 328/L$ , although this typically underestimates the parameter [Cantieni, 1984]. Note that the magnitude of a second order system becomes significant (i.e., not unity) below  $\omega_n/3$ . Hence, the

significant loading modes of the influence line would be separable from the significant dynamic modes in the frequency domain if the loading bandwidth  $f_{cl}=10f_y=5V/L$  was less than the dynamic bandwidth  $f_{cd}=\omega_n/6\pi$ . Hence, it would be desirable for vehicle speed to be less than  $0.011 L\omega_n$  or  $0.067 Lf_n$  or 15 mph.

For a lumped, N-dimensional, second order, multiple degree of freedom (MDOF) system, the mass M, damping C, and stiffness K parameters are now represented as NxN matrices and the response X is now a vector in the state space. The diagonal terms represent the response parameters for the nth mass or node when a unit load is applied at the nth mass or node. The rows represent the response parameters for the nth node when a unit load is slowly moved from node to node (i.e., the influence line). The response magnitude is now represented by N peaks or modes  $\omega_i$  in the frequency domain, although closely spaced modes may be hard to observe depending upon the spectral resolution. The spatial response is now represented by N mode shape functions  $\phi_i(x)$ , which correspond to the eigenvectors of the system. Rayleigh introduced the concept of proportional damping  $C = \alpha M + \beta K$ , such that the eigenvectors are orthogonal to the parameter matrices. With proportional damping, the second order system becomes uncoupled by a coordinate transformation  $X=PY$  and premultiplication by  $P^T$ , where P is the matrix of eigenvectors or mode shapes. An uncoupled MDOF system can be greatly simplified by N independent SDOF systems. Experimental noise, undermodelled dynamics, and other uncertainty may be represented in the mechanical model by including the stochastic vectors of noise V and disturbances W.

A lumped N degree-of-freedom system would consist of the following matrices and vectors:

$$\begin{bmatrix} m_{11} & m_{12} & \cdots & m_{1n} \\ m_{21} & m_{22} & \cdots & m_{2n} \\ \vdots & \vdots & \ddots & \vdots \\ m_{n1} & m_{n2} & \cdots & m_{nn} \end{bmatrix} \begin{Bmatrix} \ddot{x}_1 \\ \ddot{x}_2 \\ \vdots \\ \ddot{x}_n \end{Bmatrix} + \begin{bmatrix} c_{11} & c_{12} & \cdots & c_{1n} \\ c_{21} & c_{22} & \cdots & c_{2n} \\ \vdots & \vdots & \ddots & \vdots \\ c_{n1} & c_{n2} & \cdots & c_{nn} \end{bmatrix} \begin{Bmatrix} \dot{x}_1 \\ \dot{x}_2 \\ \vdots \\ \dot{x}_n \end{Bmatrix} + \begin{bmatrix} k_{11} & k_{12} & \cdots & k_{1n} \\ k_{21} & k_{22} & \cdots & k_{2n} \\ \vdots & \vdots & \ddots & \vdots \\ k_{n1} & k_{n2} & \cdots & k_{nn} \end{bmatrix} \begin{Bmatrix} x_1 \\ x_2 \\ \vdots \\ x_n \end{Bmatrix} = f(t) = \begin{Bmatrix} f_1 \\ f_2 \\ \vdots \\ f_n \end{Bmatrix}$$

$M\ddot{X} + C\dot{X} + KX = M\ddot{X} + (\alpha M + \beta K)\dot{X} + KX = F(t)$  for MDOF system with Rayleigh damping

$$P = \left[ \begin{array}{c|c|c} \begin{Bmatrix} x_1 \\ x_2 \\ \vdots \\ x_n \end{Bmatrix}^{(1)} & \begin{Bmatrix} x_1 \\ x_2 \\ \vdots \\ x_n \end{Bmatrix}^{(2)} & \cdots & \begin{Bmatrix} x_1 \\ x_2 \\ \vdots \\ x_n \end{Bmatrix}^{(n)} \end{array} \right] = [\phi_1 \quad \phi_2 \quad \cdots \quad \phi_n] \text{ where } K\phi_i = \omega_i^2 M\phi_i$$

$$P^T M P = \Lambda_M = \begin{bmatrix} M_{11} & 0 & \cdots & 0 \\ 0 & M_{22} & \cdots & 0 \\ \vdots & \vdots & \ddots & \vdots \\ 0 & 0 & \cdots & M_{nn} \end{bmatrix} \text{ where generalized mass } M_{ij} = \sum_{i=1}^N m_i \phi_i(x_i) \phi_j(x_i)$$

$$P^T K P = \Lambda_K = \begin{bmatrix} K_{11} & 0 & \cdots & 0 \\ 0 & K_{22} & \cdots & 0 \\ \vdots & \vdots & \ddots & \vdots \\ 0 & 0 & \cdots & K_{nn} \end{bmatrix} \text{ where generalized stiffness } K_{ij} = \sum_{i=1}^N EI \phi_i''(x_i) \phi_j''(x_i)$$

$$P^T C P = \alpha I + \beta \Lambda_C \text{ where } \Lambda_C = \begin{bmatrix} \omega_1^2 & 0 & \cdots & 0 \\ 0 & \omega_2^2 & \cdots & 0 \\ \vdots & \vdots & \ddots & \vdots \\ 0 & 0 & \cdots & \omega_n^2 \end{bmatrix}$$

$P^T M P \ddot{Y} + P^T C P \dot{Y} + P^T K P Y = \Lambda_M \ddot{Y} + (\alpha I + \beta \Lambda_C) \dot{Y} + \Lambda_K Y = P^T F(t)$  with Rayleigh damping

or, more simply, a set of N equations  $\ddot{y}_i + 2\zeta_i \omega_i \dot{y}_i + \omega_i^2 y_i = f_i(t) = \Gamma_i F(t)$  with Rayleigh damping

where  $2\zeta_i \omega_i = \alpha + \beta \omega_i^2$  and the mode participation factor is defined as:  $\Gamma_i = \frac{\sum_j \phi_i(x_j) P(x_j)}{\sum_j m_j \phi_i^2(x_j)}$

The mode summation method allows the approximation of the above system with the sum of only a subset of the  $N$  modes, multiplied by the generalized coordinates. For example, if we know that only lower frequency excitation of the beam occurs, then we would be justified in assuming the forced response to be the superposition of only a few of the lower frequency modes. The first three modes may be sufficient:  $x_i = \phi_1(x_i)y_1(t) + \phi_2(x_i)y_2(t) + \phi_3(x_i)y_3(t)$ ; then, only three uncoupled differential equations need to be solved for the temporal response [Chopra, 1995, Clough, 1993].

### 2.3.2. The Generalized MKC Distributed Model – Spatial, Temporal and Frequency Domains

Distributed-parameter models invoke the continuum hypothesis, whereby it is assumed that matter is a medium continuously filling space to which properties are assigned to reflect the statistical mean of the molecular effects. The significant variables are distributed in space and they vary with both time and the spatial coordinates. The resulting dynamic models consist of partial differential equations with time and space coordinates as independent variables. Let us again revisit the free-body diagram for a cross section of the beam (Figure 2-3) and consider the dynamic equilibrium of a moving mass under an external force  $p(x,t)$ . An inertia force  $f = ma$  is added to the above static formulation following D'Alembert's principal:

$$\frac{\partial V}{\partial x} = \frac{V_2 - V_1}{1} = -p(x,t) - m \frac{\partial^2 y(x,t)}{\partial t^2}$$

Based upon the moment-curvature relationship:

$$m \frac{\partial^2 y}{\partial t^2} + \frac{\partial^2}{\partial x^2} \left[ EI \frac{\partial^2}{\partial x^2} \left( y + \beta \frac{\partial y}{\partial t} \right) \right] = -p, \text{ where } \beta = \text{stiffness-proportional damping}$$

This is a simplification of the Timoshenko beam equation because it ignores both the effects of rotational inertia and shear deformation (see above for assumptions and limitations of an ideal beam). Note that mass  $m$ , rigidity  $EI$ , and damping  $\beta$  are considered uniform along the length of the beam.

By separation of variables  $y(x,t)=\phi(x)q(t)$  and the assumed boundary conditions for an ideal beam, it can be shown (see Appendix A6):

There are an infinite number of deflection modes,  $\phi_n(x) = \phi(n,x) = \sin(n\pi x/L)$ .

There are an infinite number of moment modes,  $d^2\phi(n,x)/dx^2 = \phi''(n,x) = -(n\pi x/L)^2 \sin(n\pi x/L)$ .

The mode superposition analysis of a distributed-parameter system is entirely equivalent to that of a lumped-parameter system once the mode shapes and frequencies have been determined, because in both cases the amplitudes of the modal response components are used as generalized coordinates in defining the response of the structure. In principle, an infinite number of these coordinates are available for a distributed system since it has an infinite number of vibrational modes but, in practice, only a finite number of modes are significant. Thus, the distributed case is actually converted into a discrete analysis.

The essential operation is the transformation from the geometric coordinates to the modal coordinates:

$$y(x, t) = \sum_{n=1}^{\infty} \phi_n(x) q_n(t) \cong \sum_{n=1}^{N_y} \phi_n(x) q_n(t), \quad \text{where } N_y = 3 \text{ approximately}$$

$$M(x, t) = \sum_{n=1}^{\infty} EI \phi_n''(x) q_n(t) \cong \sum_{n=1}^{N_m} EI \phi_n''(x) q_n(t), \quad \text{where } N_m = 19 \text{ approximately}$$

Note that it requires the contributions of many more modes to define the triangular moment response. It is far less cumbersome to represent the waveform by two linear equations for each slope (i.e., the triangular pulse function).

By modal orthogonality and the assumed boundary conditions for an ideal beam, it can be shown (see Appendix A6) that there are an infinite number of second order differential equations each associated with a given mode  $i$ :

$$M_n \ddot{q}_n + \beta K_n \dot{q}_n + K_n q_n = -P_n(t) \quad \text{with stiffness-proportional damping } \beta$$

where

$$\text{generalized mass } M_n = \int_0^L m [\phi_n(x)]^2 dx, \quad \text{generalized stiffness } K_n = \int_0^L EI [\phi_n''(x)]^2 dx$$

$$\text{generalized loading force } P_n = \int_0^L p(x, t) \phi_n(x) dx$$

For the modes of deflection for an ideal beam, this simplifies to:

$$M_n = M_{beam}(n) = \frac{mL}{2}, \quad K_n = K_{beam}(n) = \frac{L \cdot EI}{2} \left( \frac{n\pi}{L} \right)^4, \quad P_n = P_{beam}(n) = P \cdot \sin\left( \frac{n\pi Vt}{L} \right)$$

The dynamic frequencies for an ideal beam are then determined by:

$$\omega_n = \sqrt{\frac{K_{beam}(n)}{M_{beam}(n)}} = \frac{n^2 \pi^2}{L^2} \sqrt{\frac{EI}{m}}, \quad f_n = \frac{\omega_n}{2\pi}, \quad \zeta_n = \frac{\beta \cdot K_{beam}(n)}{2\omega_n \cdot M_{beam}(n)} = \frac{\beta EI}{mLV} \left( \frac{n\pi}{L} \right)^3$$

For the endspan of the instrumented bridge, HAM-42-0992, the following parameters have been estimated:  $m=0.03$  kips sec<sup>2</sup> / foot,  $EI=5,500,000$  kips feet<sup>2</sup>, and  $L=55$  feet. If this endspan was not continuous across the full length of the bridge, its natural frequency would be 7 Hz. The midspan has a length of 78 feet and, if noncontinuous, would have a natural frequency of 3.5 Hz.

The deflection  $y(x,t)$  of the beam in response to the generalized loading  $P_{beam}(n)$  is determined by two equations: the particular solution for the differential equation, which represents the beam response during forced excitation by the load; and the complementary solution, which represents the beam's free decay under no excitation after the load has moved off the beam.

The particular solution can be simplified to the following temporal equation:

$$q(n, t) = \frac{P}{K_{beam}(n)} \left( \sin\left(\frac{n\pi V t}{L}\right) - \frac{n\pi V}{\omega_n L \sqrt{1-\zeta_n^2}} e^{-\zeta_n \omega_n t} \sin\left(\omega_n t \sqrt{1-\zeta_n^2}\right) \right)$$

where the first term is the influence line for the beam and the second term is the additional dynamic response of the beam under excitation by a sinusoidal pulse.

The complementary solution can be simplified to the following temporal equation:

$$q(n, t) = \frac{\dot{q}(n, t_d)}{\omega_n \sqrt{1-\zeta_n^2}} e^{-\zeta_n \omega_n (t-t_d)} \sin\left(\omega_n (t-t_d) \sqrt{1-\zeta_n^2}\right) \quad \text{where } t_d = L/V, \text{ the start of free response}$$

Note that the temporal response consists of the sum of three independent responses:

1. The influence line for an ideal beam under moving axle load
2. The dynamic excitation for an ideal beam under moving axle load
3. The dynamic decay for an ideal beam after moving axle load

The influence line (term #1) was considered at length in the above sections.

The dynamic excitation (term #2) is represented in the frequency domain by its Laplace transformation:

$$LB_{beam}(n, v, L, \omega) := \frac{n \cdot \pi \cdot \frac{v}{L} \cdot P}{-1 \cdot K_{beam}(n) \cdot [(\omega \cdot i + \zeta(n) \cdot \omega n(n))^2 + \omega d(n)^2]}$$

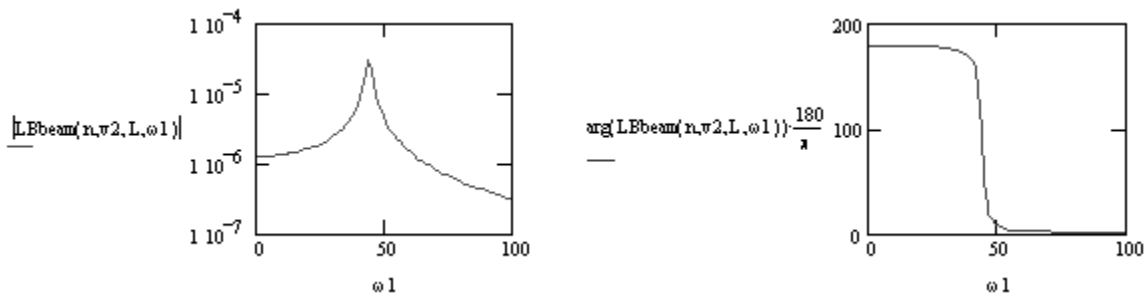


**Figure 2-37: Magnitude and Phase of Dynamic Excitation of Ideal Beam from Point Load, 50mph**

Note that a beam's dynamic excitation is equivalent to the classical second order dynamic system presented above for the standard MKC mechanical model. The system pole is located at  $\omega d$ , which is generally approximated by  $\omega n$  for structural systems due to the low damping.

The dynamic decay is represented in the frequency domain by its Laplace transformation:

$$q_{ss}(n, v, L, P, t, td) := e^{-\zeta(n) \cdot \omega n(n) \cdot (t - td)} \cdot \left[ \frac{dqf(n, v, L, P, td)}{\omega d(n)} \cdot \sin(\omega d(n) \cdot (t - td)) \right]$$

$$LSSbeam(n, v, L, \omega) := \frac{dqf(n, v, L, P, td)}{[(\omega \cdot i + \zeta(n) \cdot \omega n(n))^2 + \omega d(n)^2]} \cdot e^{-td \cdot \omega \cdot i}$$

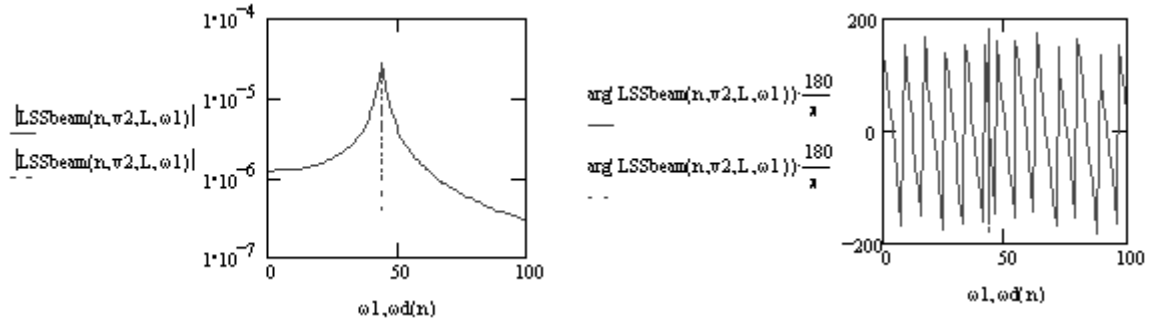


**Figure 2-38: Magnitude and Phase of Free Decay of Ideal Beam after Point Load, 50mph**

Hence, the complete dynamic response of an ideal beam during and after moving axle load is represented in the frequency domain by the sum of its component Laplace transformations:

$$Lfullbeam(n, v, L, \omega) := LFbeam(n, v, L, \omega) + LBbeam(n, v, L, \omega) + LSSbeam(n, v, L, \omega)$$

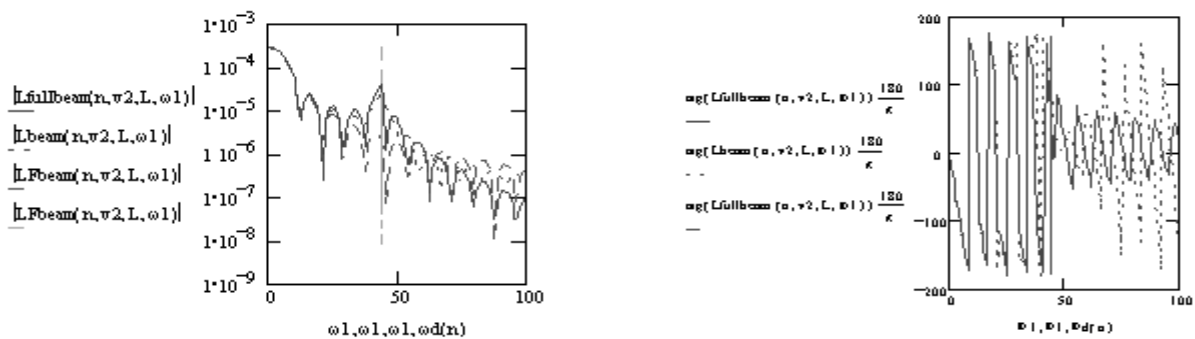


**Figure 2-39: Magnitude and Phase of Full Dynamic Response of Ideal Beam to Point Load, 50mph**

where  $Lbeam(n, v, L, \omega) := LFbeam(n, v, L, \omega) + LBbeam(n, v, L, \omega)$  does not include the free decay.

Note that by including the free decay response, we are simply increasing the disturbance to the influence line response  $L_{beam}$ ; hence, it is best to terminate the signal response after the vehicle has left the beam. However, if the intent is to identify the dynamic characteristics of the beam, then it is best to examine the free decay of the beam just after the vehicle has crossed so that the influence line of the beam is not present in the data.

The temporal response for deflection  $y(x,t)$  is represented by the sum of the dynamic responses  $q(n,t)$  for all modes of the beam, as scaled by its corresponding spatial response  $\phi(n,x)$ . Due to the  $n^4$  term in the denominator for each component of the temporal response, higher order modes have little significance on the solution. The deflection response at the quarterspan is presented here.

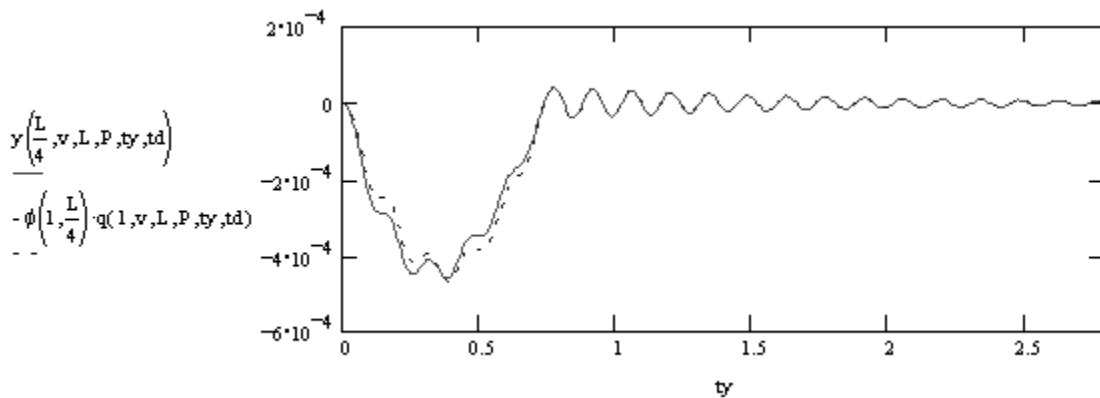


**Figure 2-40: Dynamic Deflection of Ideal Beam to Point Load, 50mph**

Note that the spatial response serves to scale the dynamic response, depending upon the gaged location upon the beam. For any sensor location  $L/i$ , there are  $i-1$  loading modes required to represent the beam deflection. For example, midspan ( $L/2$ ) is represented by one loading mode while quarter span ( $L/4$ ) is represented by three loading modes.

The temporal response for moment  $M(x,t)$  is represented by the sum of the dynamic responses  $q(n,t)$  for all modes of the beam, as scaled by its corresponding spatial response  $\phi''(n,x)$ . Due to the  $n^2$  term in the denominator for each component of the temporal response, higher order modes have less significance on the solution. The triangular moment response to the sinusoidal loading, however, must be represented by many more modes than the deflection. The moment response at the quarterspan is presented next.

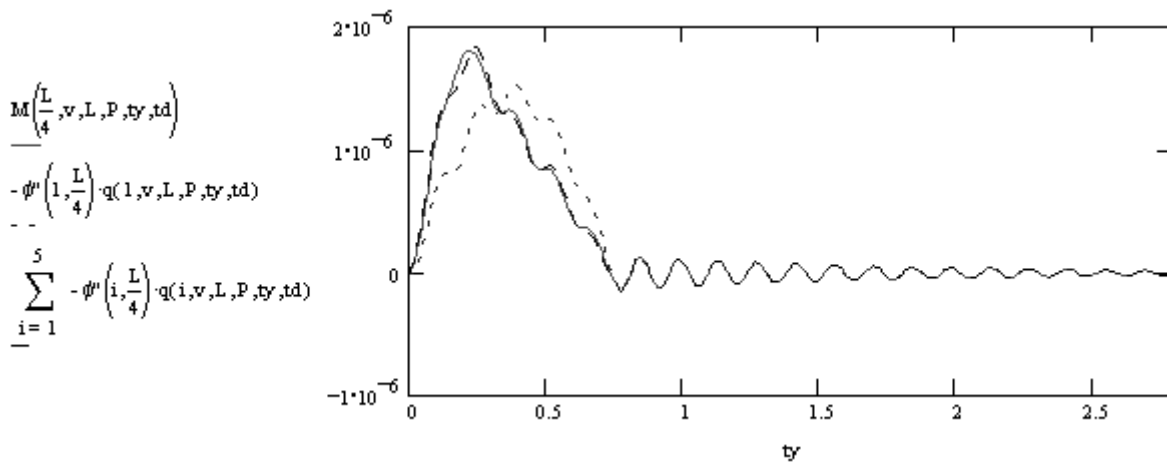


**Figure 2-41: Dynamic Moment of Ideal Beam to Point Load, 50mph**

Figures 2-42 compares the Laplace transform  $L_{fullbeam}$  with the Fast Fourier transforms for the approximated time response  $y(x,t)$  determined from the MathCAD program in Appendix 6. From both the plots and their equations, note that appreciable attenuation of the influence line occurs beyond the frequency or bandwidth of  $10f_y$ . This occurs also for sensor locations off of the midspan as well.

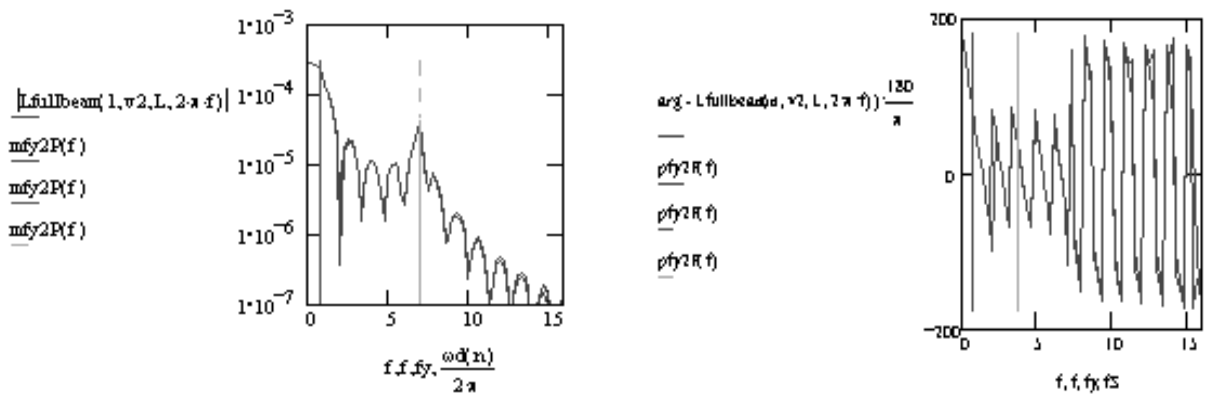


**Figure 2-42: Deflection Magnitude and Phase Comparison of FT and FFT for Point Load, 50 mph**

For a simple beam, it would be desirable for the loading mode frequency  $f_y$  to be separated from the dynamic frequency of the beam  $f_n$  in order to clearly identify the static influence line for the beam. The cut-off frequency for the low-pass filter should be set at  $f_c = 10f_y = 5V/L < f_n/3$ . For a single span beam with the parameters of the endspan for HAM-42-0992,  $5V/L < 7/3$  or  $V < 25.67$  feet/second or 17.5 mph.

#### 2.4. Elastic Deformation of a Single Span under Dynamic Conditions

The generalized model of the dynamic behavior for an ideal beam with multiple spans has been considered by several authors, most notably by Kolousek [Kolousek, 1973, Fryba, 1972, Biggs, 1964]. Kolousek found that the first dynamical mode for a symmetrical 3-span beam lies in between the lower frequency of the longer middle span and the higher frequency of the shorter endspans:

$$\lambda := \text{root} \left[ \left[ \begin{array}{l} \left( 0.000000298 \frac{I1 \cdot K^{12}}{L1} \right) \cdot x^{12} \dots \\ + \left( 0.000071463 \frac{I1 \cdot K^8}{L1} + 0.000031966 \frac{I2}{L2 - L1} \right) \cdot x^8 \dots \\ + \left( 0.019048 \frac{I1 \cdot K^4}{L1} + 0.016667 \frac{I2}{L2 - L1} \right) \cdot x^4 \dots \\ + \frac{-3 \cdot I1}{L1} - \frac{2 \cdot I2}{L2 - L1} \end{array} \right], x \right] \quad \text{where} \quad \omega_n := \frac{\lambda^2}{(L2 - L1)^2} \cdot \sqrt{\frac{E \cdot I2}{m}}$$

$$K := \frac{L1}{L2 - L1} \cdot \left( \frac{I2}{I1} \right)^{.25} \quad \text{where } I1 \text{ and } I2 \text{ are the inertia for the first and second spans, respectively}$$

$$\omega_1 := \frac{\pi^2}{L1^2} \cdot \sqrt{\frac{E \cdot I1}{m}} > \omega_n := \frac{\lambda^2}{(L2 - L1)^2} \cdot \sqrt{\frac{E \cdot I2}{m}} > \omega_2 := \frac{\pi^2}{(L2 - L1)^2} \cdot \sqrt{\frac{E \cdot I2}{m}}$$

However, the simple beam analysis above is sufficient to prove that the dynamic modes of the beam are additive and, hence, separable from the loading modes of the influence line. If the vehicle moves slow, the dynamic modes are easily removed by a low-pass filter at  $f_c = 10f_y$  in the frequency domain. For an ideal beam with multiple spans, it would be desirable for the loading mode frequency  $f_y$  to be separated from the dynamic frequency of the bridge  $f_n$  in order to clearly identify the static influence line for the beam. The cut-off frequency for the low-pass filter should be set at  $f_c = 10f_y = 5V/L < f_n/3$ , where  $L$  is the length of the shortest span. For a beam with the parameters of the endspan for HAM-42-0992, the natural frequency for the bridge is found to be 5 Hz, which lies in between the natural frequency for the endspan at 7 Hz and the middle span at 3.5 Hz. Hence,  $10f_y = 5V/L < 5/3$  or  $V < 18.33$  feet/second or 12.5 mph. For the higher speeds of ambient traffic, some parameter estimation of the first dynamic mode may be required to remove its effect upon the influence line.

## 2.5. The Coupled Dynamic Interaction of Beam and Load

The dynamic interaction between an ideal beam and the loading vehicle has been considered by several authors [Finite element bridge model: Henchi (considering a 7 DOF vehicle), 1998; and Generalized beam model: Hwang (6 DOF vehicle), 1989; Fryba (4 DOF vehicle), 1972; Eymard (2 DOF axle) 1990; Biggs (1 DOF axle), 1964; etc.]. The various conceptualizations for the load may include consideration of each axle's suspension, tire stiffness, and the vehicle pitch and yaw. Many also consider the case of pavement roughness, slope, and discontinuities such as potholes, thermal gaps, cracks, slick spots, etc. However, this coupled (not simply additive) interaction between beam and load requires identification of the vehicle's suspension, pavement condition, and other parameters that are typically unavailable from a truckload test and certainly unavailable from ambient traffic conditions.

For example, Biggs represented the coupled interaction of an ideal beam and a one degree-of-freedom axle load as follows:

$$M_n \ddot{q}_n + \beta K_n \dot{q}_n + K_n q_n = -P_n - K_v \sin\left(\frac{\pi V t}{L}\right) \cdot \left(z - q_n \sin\left(\frac{\pi V t}{L}\right)\right) \text{ for each } n\text{th mode}$$

$$M_v \ddot{z} + \beta_v K_v (\dot{z} - \dot{q} \sin\left(\frac{\pi V t}{L}\right)) + K_v (z - q_n \sin\left(\frac{\pi V t}{L}\right)) = 0 \text{ for the axle's mode}$$

where  $z$  is the axle deflection,  $M_v$  is axle mass,  $K_v$  is axle stiffness,  $\beta_v$  is axle proportional damping

The Swiss Federal Laboratories for Materials Testing and Research (EMPA) reported on hundreds of load experiments over several decades involving fully loaded two-axle tip trucks with leaf springs. Under normal circumstances of pavement roughness, the dynamic wheel loads of such vehicles predominantly occur in two frequency ranges: a) a body bounce mode for the vehicle between 2 and 5 Hz, and b) a wheel hop mode for the second axle between 10 and 15 Hz. The body bounce was found to be excited by relatively long waves of roadway roughness, while the wheel hop was excited by shorter waves. For example, a narrow plank in the roadway was found to amplify the body bounce mode at crawl speeds and the wheel hop mode at speeds above 20 mph. It was concluded that a highway bridge would exhibit a pronounced dynamic response only if its natural frequency lies in the same region as one of the vehicle modes and if pavement roughness can sufficiently excite the coincident vehicle mode. [Cantieni, 1984]

We seek to identify the influence line for the structure. If the test vehicle moves slowly, the vehicular modes and their coupled interaction with the bridge response will be at a higher frequency than the loading modes. The corrupted data is easily removed by a low-pass filter set at a cut-off frequency of  $f_c = 10f_y$  in the frequency domain. Let us assume a vehicle bandwidth of 2 to 6 Hz, hence  $f_c = 10f_y = 5V/L < 2$ , hence  $V < 0.4L$  feet/sec. Of course, this must be checked for each truckload test of each bridge on a case-by-case basis. Remember that the cut-off frequency for the low-pass filter should also be set at  $f_c = 10f_y = 5V/L < f_n/3$ , where  $f_n$  is the natural frequency for the bridge dynamics and  $L$  is the length of the shortest span.. Therefore,  $f_c < 2$  and  $f_n/3$  (feet/sec), whichever is smaller. The speed of the test vehicle is determined accordingly. For the higher speeds of ambient traffic, some parameter estimation of the influence line may be required within the frequency band of the first vehicle mode.

## 2.6. Field Identification of Bridge Influence Lines

Let us now examine the realities of the field identification of influence lines for typical steel-stringer bridges. This objective is accomplished by processing a complete set of strain and displacement response data for three-span, medium-length Cross-County Highway bridges over Reading Road (HAM-42-0992, Figure 1-14) and Hamilton Avenue (HAM-126-0881, Figure 1-16), during several crawl and high speed experiments with various truck vehicles. The bridges incorporate both continuous and integral construction with minimal skew. HAM-126-0881 is also a semi-composite bridge with an unusually small end span to middle span ratio (0.45). The steel superstructure for each bridge was instrumented with weldable foil and vibrating wire strain gage instrumentation on the beams and the intermediate crossframes. The concrete decking for HAM-126-0881 was also instrumented with embedded foil and vibrating wire strain gages during its construction.

Several truckload tests were conducted for HAM-42-0992 on August 5-7, 1997 at various speeds, temperatures, driving paths, and truckloads. Static tests were also conducted at various bridge positions. Figures 2-43 and 2-44 indicate that a consistent influence line for girder strain was obtained regardless of truck load. This result was also found to hold true for the other instrumented locations at various times and temperatures during the test days. Note that the influence line peaks in the time domain at exactly the position of the gage, as predicted by the theory of an ideal beam.

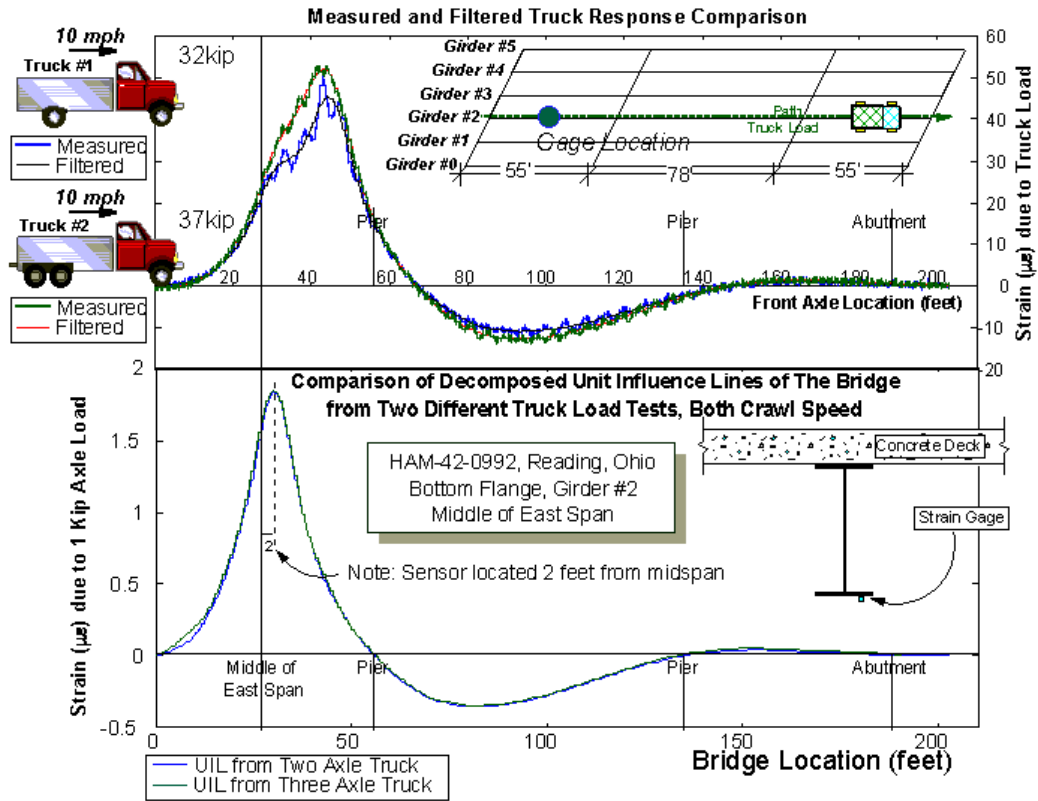


Figure 2-43: Time Responses and UIL for Crawl Truckload Test of Bridge, HAM-42-0992

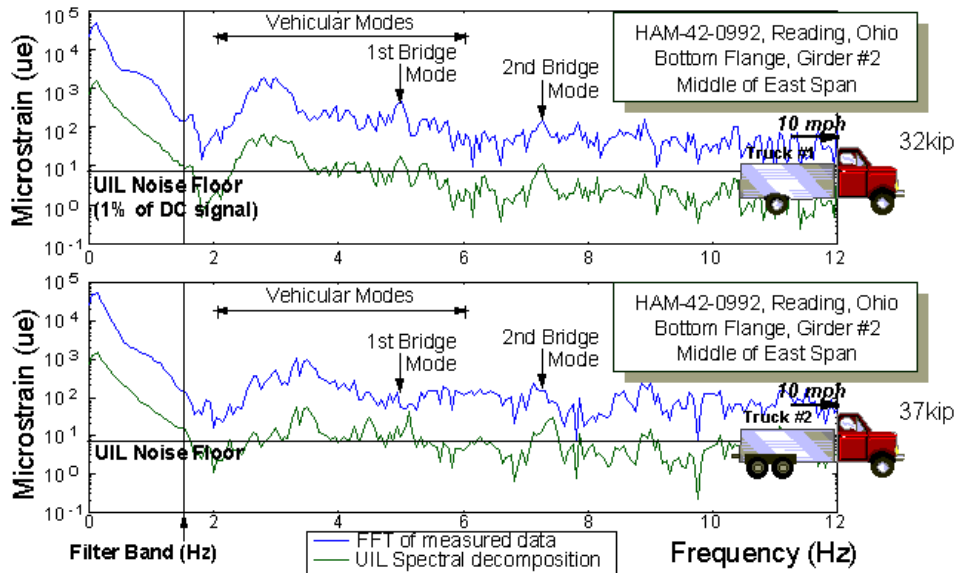


Figure 2-44: Frequency Responses and UIL for Crawl Truckload Test of Bridge, HAM-42-0992

The influence line is determined from the measured truckload response with a Matlab program that performs the following routines:

1. Given tape switch readings at both abutments, determine an average truck speed across the bridge
2. Balance all sensor readings for a zero value when the first truck axle reaches the first tape switch
3. Determine the frequency domain representation for each sensor reading using the FFT function
4. Determine the influence line in the frequency domain by dividing out the phased axle contributions
5. Bandlimit both the sensor reading and influence line in the frequency domain
6. Determine the time domain representation of the bandlimited truck response and influence line
7. Plot and save the results

Truck parameters such as axle spacing and weights were determined at regularly calibrated stations by ODOT. The truck driver was asked to maintain a constant speed and path across the bridge. Of course, this is not physically possible but the variance in these parameters was not found to dramatically affect the test results. In addition, sensitivities for the given values of the program were also checked. For example, a 10% variance in the truck speed causes a 3% variance in the peak strain of the influence line.

As the bridge includes significant unintended composite action between the deck and girder systems, the top flange strain response is approximately zero. Hence, the bottom flange strain response, scaled by the sectional and elastic moduli, represents the sectional moment at the instrumented location. Further, due to this and other realities (e.g., rotational restraint at the supports), the strain response is not perfectly triangular as predicted by ideal beam theory.

The crawl-speed results are removed from any vehicular or bridge modes in the frequency domain for these medium-length bridges. A lowpass filter with a cut-off frequency of 1.5 Hz will still capture the significant spectral components of the influence line ( $f_c > 10f_y = 5V/L = 1.33$  Hz), while removing any dynamic effects from the structure ( $f_c < f_n/3 = 1.67$  Hz) or its interaction with the vehicle ( $f_c < 2$  Hz).

The influence line can now be used to virtually simulate any truck with a given set of axle spacings and weights and crossing the bridge at crawl speed. The simulated truck response from the influence line is found to be essentially equivalent with the actual crawl-speed and static truck responses (Figure 2-45).

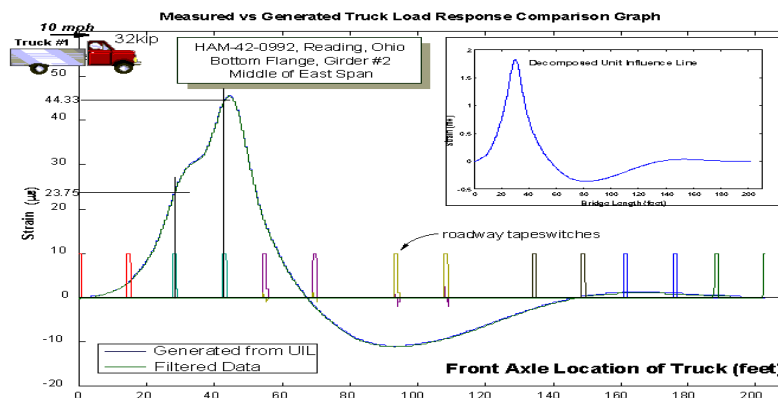


**Figure 2-45: Comparison of Static, Crawl-Speed, and Simulated Truck Responses**

At higher speeds, the influence line and the dynamic modes become overlapped in the frequency domain, as predicted by the ideal beam theory. In Figures 2-46 and 2-47, the first bridge mode and its interaction with the vehicular modes has a notable effect on the sensor readings and determined influence line. In each of the plots, the actual response is compared in the time and frequency domains with that predicted by the influence line previously determined by the crawl-speed experiments. Note that the signal degradation is dependent upon the vehicle type (e.g., 2-axle dump truck vs. 3-axle tandem truck). The response remains untouched in the original frequency band of 1.5 Hz; however, the filter cut-off frequency must now be increased proportionate with the truck speed to 6 Hz. The peak of the influence line is decreased by 6.4% for the dump truck, while it is increased by 2.1% for the tandem. The shape of the influence line is distorted by both trucks, although more noticeable with the tandem. The variance in peak and shape of the influence line is found to increase with increasing truck speed. An ideal compensator for each vehicle type and speed can be determined in the frequency domain in order to correct any deviations from the influence line determined from crawl-speed experiments. Note that the dump truck requires lag compensation, while the tandem requires only slight lead compensation. The actual truck responses (shown after lowpass filtering) are also distorted by the dynamical modes, but the peak variance (-0.16% for the dump truck and -0.46% for the tandem) is bounded by typical experimental limitations. Hence, the influence lines derived by the 40mph test can still provide an accurate simulation of similar truck types, a somewhat less accurate simulation of peak responses for other truck types, and rather questionable simulation of the overall response shape for other truck types.

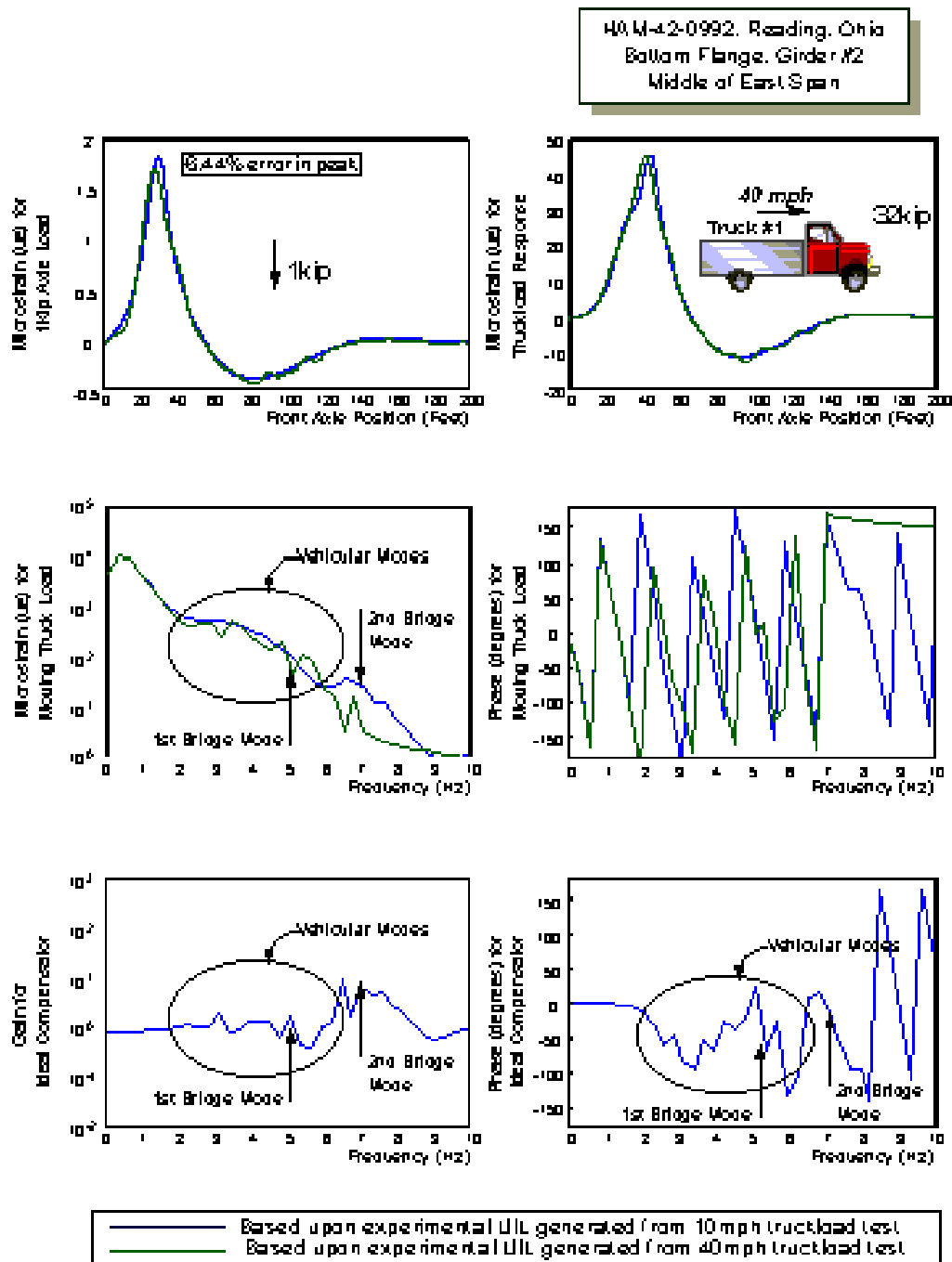


Figure 2-46: Comparison of Measured vs. Simulated Response of Dump Truck at 40 mph

HA M-42-0992, Reading, Ohio  
 Bottom Flange, Girder #2  
 Middle of East Span

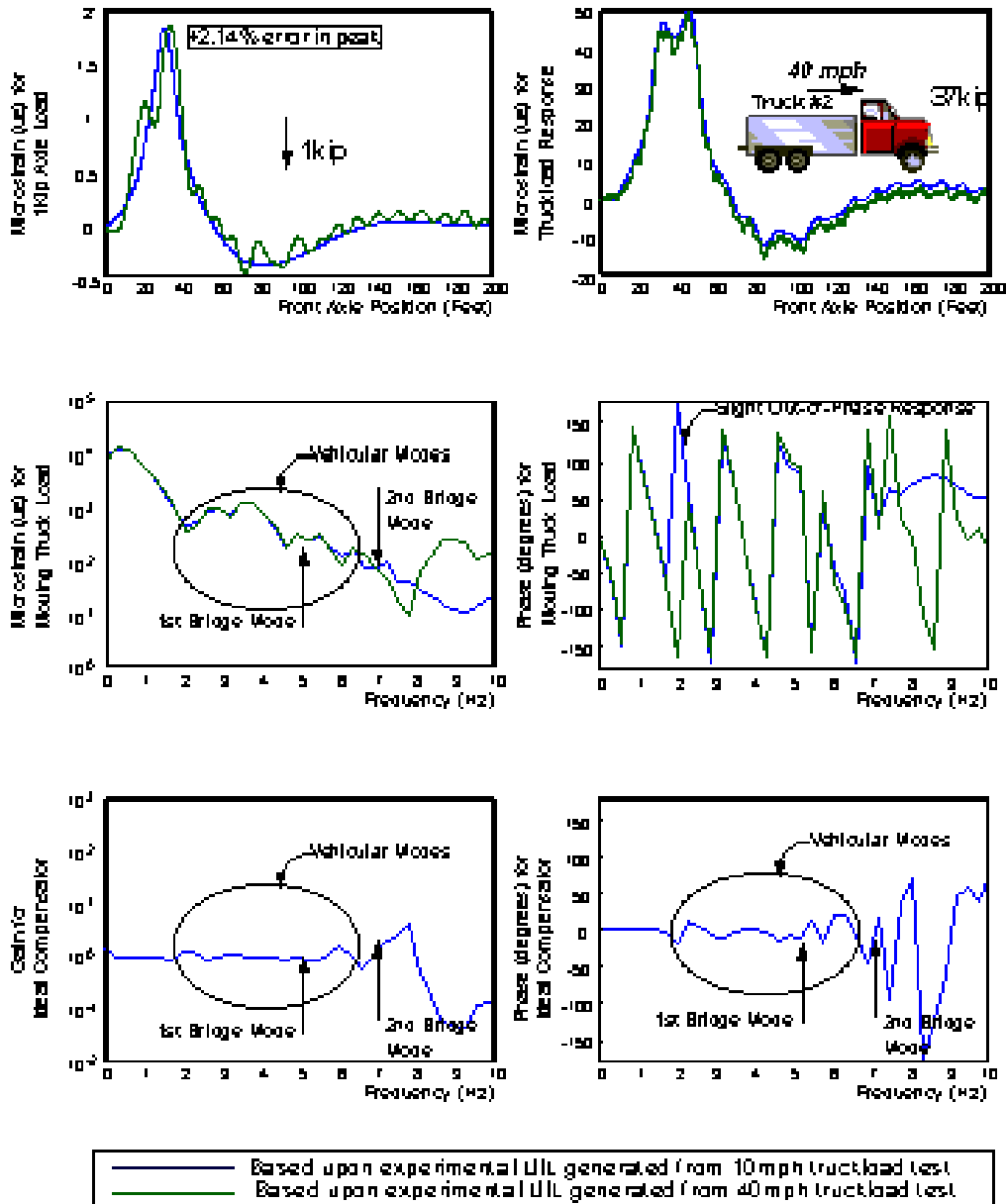


Figure 2-47: Comparison of Measured vs. Simulated Response of Tandem Truck, 40 mph

Several truckload tests were conducted for HAM-126-0881 in May (two tandem trucks) and September (one semi and one dump truck) of 1998 at various speeds, temperatures, driving paths, and truckloads. Static tests were also conducted at various bridge positions. Figures 2-48 and 2-49 indicate that a generally consistent influence line for girder strain was obtained regardless of truck load. A slight exception might be made for the experiments including the five-axle semi-tractor and trailer due to its difficulty in maintaining a consistent speed across the bridge; however, even the semi truck provided a consistent influence line within the instrumented span. These results were also found to hold true for the other instrumented locations at various times and temperatures during the test days/months which bookend the Summer. Note that the influence line peaks in the time domain at exactly the position of the gage, as predicted by the theory of an ideal beam.

In comparison with the results for HAM-42-0992, note that HAM-126-0881 has significant vibration during and after the truck crossing. It is assumed that this is due to its lower natural frequency, which allows for greater interaction between the dynamical modes of the bridge and truck. At all instrumented locations, it is observed from their influence lines that girder #3 (of 5) for HAM-126-0881 experiences less stress than girder #2 (of 6) for HAM-42-0992 for a given unit load as it moves along the rightmost traffic lane (i.e., the most common truck path) for the bridge. This is due to the simple fact that girder #2 (of 6) for HAM-42-0992 lies directly under the load path for the experiment.

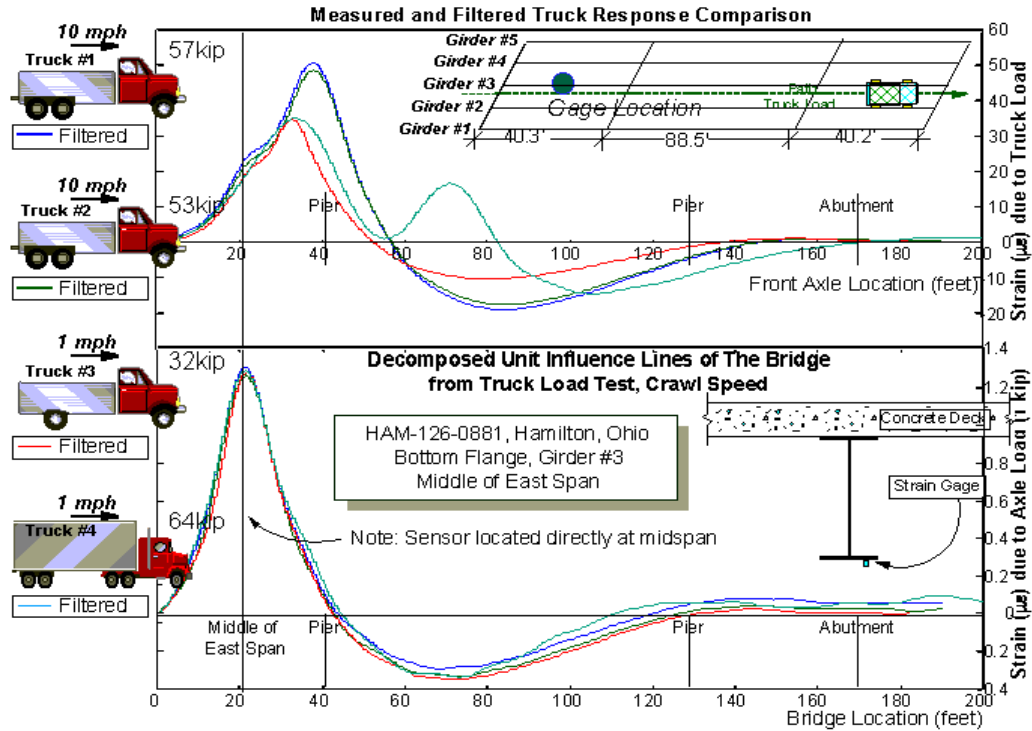


Figure 2-48: Time Responses and UIL for Crawl Truckload Test of Bridge, HAM-126-0881

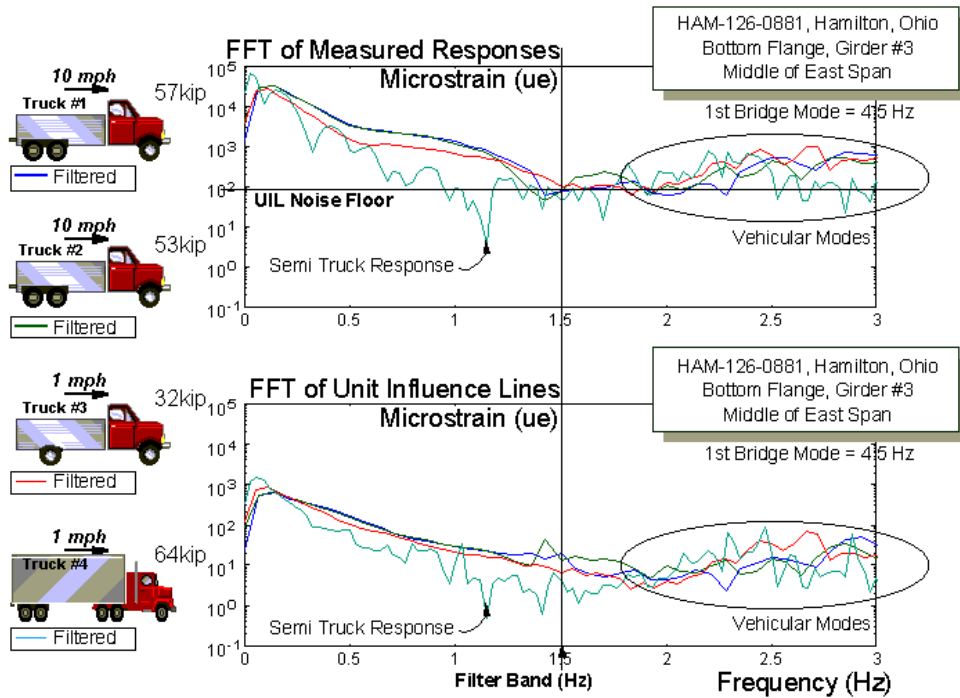
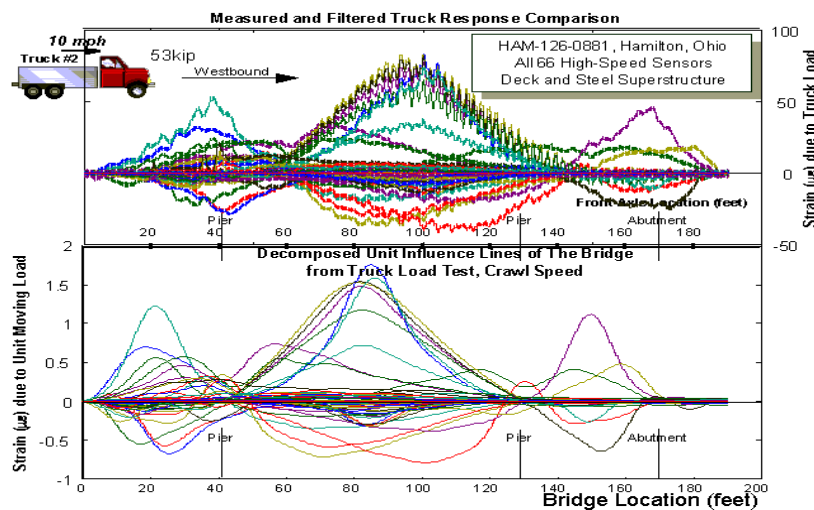


Figure 2-49: Frequency Responses and UIL for Crawl Truckload Test of Bridge, HAM-126-0881

The crawl-speed results are removed from any vehicular or bridge modes in the frequency domain for these medium-length bridges. A lowpass filter with a cut-off frequency of 1.5 Hz will still capture the significant spectral components of the influence line ( $f_c \sim 10f_y = 5V/L = 1.83$  Hz), while removing any dynamic effects from the structure ( $f_c = f_n/3 = 1.5$  Hz) or its interaction with the vehicle ( $f_c < 2$  Hz). Note that we cheated down a bit from the ideal cut-off frequency for the influence line in order to minimize the effects of the first dynamic.

The influence line can now be used to virtually simulate any truck with a given set of axle spacings and weights and crossing the bridge at crawl speed. The simulated truck response from the influence line is found to be essentially equivalent with the actual crawl-speed and static truck responses. Figure 2-50 is included to illustrate the informational complexity and coverage of the instrumented health monitoring system at HAM-126-0881. Note the unbalanced (i.e., unequal and unsymmetrical) response for this bridge design with an unusually low span ratio of 0.45. The designed composite action in the middle span is intact, but the endspans exhibit unintended but partial composite action with the concrete decking.



**Figure 2-50: Influence Lines for All Traffic Sensors of Bridge Monitoring System, HAM-126-0881**

As the endspan exhibits partial composite action, the top flange strain response is nonzero but not equal in magnitude with the bottom flange strain response. Hence, the difference between the bottom and top flange strain responses, scaled by the sectional and elastic moduli, represents the sectional moment at the instrumented location. Further, due to this composite action with the decking and other realities (e.g., rotational restraint at the supports), the strain response is not perfectly triangular as predicted by ideal beam theory (see Figure 2-51). The theoretical microstrain response of a multi-span beam was estimated by scaling the moment response equations for each span (Sim2me1, Sim2mm, and Sim2me2, presented in Section 2.2.2 above) by the non-composite section modulus ( $S = I/y_{\max} = 12,100/36 \text{ in}^3 = 0.1945 \text{ ft}^3$ ), by the elastic modulus ( $E = 29,000 \text{ ksi}/\epsilon = 4.176 \text{ kip}/\text{ft}^2 - \mu\epsilon$ ), and by independent weightings for each span ( $k_1=1.057$ ;  $k_2=1.379$ ;  $k_3=0.1838$ , respectively). Note that the estimate for the first span requires almost no scaling (i.e.,  $k_1 \sim 1$ ), whereas considerable scaling is required for the other spans. The moment equations assume a prismatic beam with a constant cross section along its length (assumption #7, section 2.1 above); however, HAM-126-0881 transitions twice from non-composite W36x194 to fully composite W36x182 beams at the splice plates in the middle span.

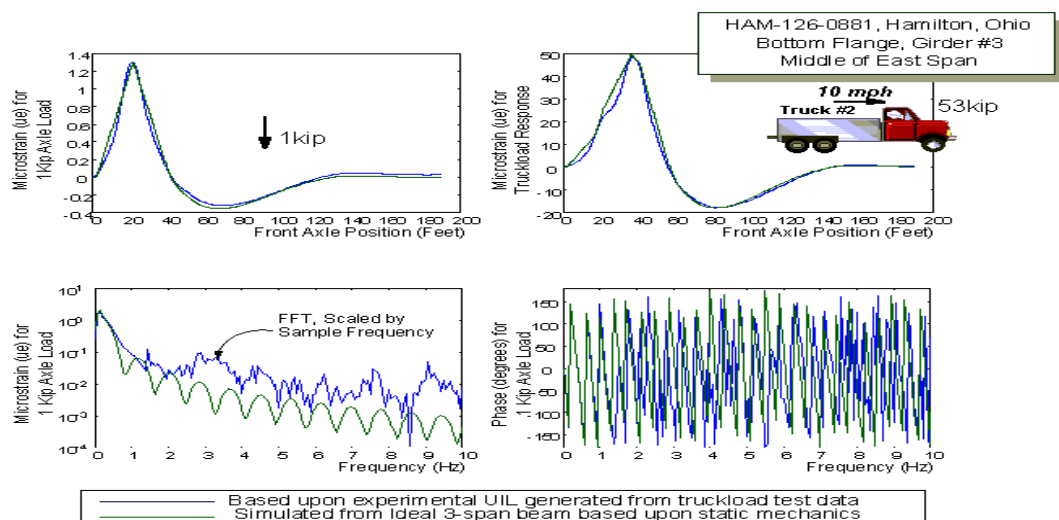


**Figure 2-51: Simulation of Influence Line Using Scaled Moment Equations for Ideal Beam**

At higher speeds, the influence line and the dynamic modes become overlapped in the frequency domain, as predicted by the ideal beam theory. In Figures 2-52, 2-53, and 2-54, the first bridge mode and its interaction with the vehicular modes has a notable effect on the sensor readings and determined influence line. In each of the plots, the actual response is compared in the time and frequency domains with that predicted by the influence line previously determined by the crawl-speed experiments. Note that the signal degradation is dependent upon the vehicle type (e.g., 2-axle dump truck, 3-axle tandem truck, or 5-axle semi truck). The response remains untouched in the original frequency band of 1.5 Hz. The peak of the influence line is decreased by 7.0% for the dump truck and 3.87% for the semi truck, while it is increased by 0.1% for the tandem. The shape of the influence line is distorted by all trucks, although more noticeable with the semi. The variance in peak and shape of the influence line is found to increase with increasing truck speed. An ideal compensator for each vehicle type and speed can be determined in the frequency domain in order to correct any deviations from the influence line determined from crawl-speed experiments. Note that the dump truck requires lag compensation, while the tandem and semi require a series of alternating lead-lag compensation. The actual truck responses (shown after lowpass filtering) are also distorted by the dynamical modes, but the peak variance (-5.22% for the dump truck, -3.74% for the tandem truck, and -2.44% for the semi truck) is bounded by typical experimental limitations. Hence, the influence lines derived by the 50mph test can still provide an accurate simulation of similar truck types, a somewhat less accurate simulation of peak responses for other truck types, and rather questionable simulation of the overall response shape for other truck types.

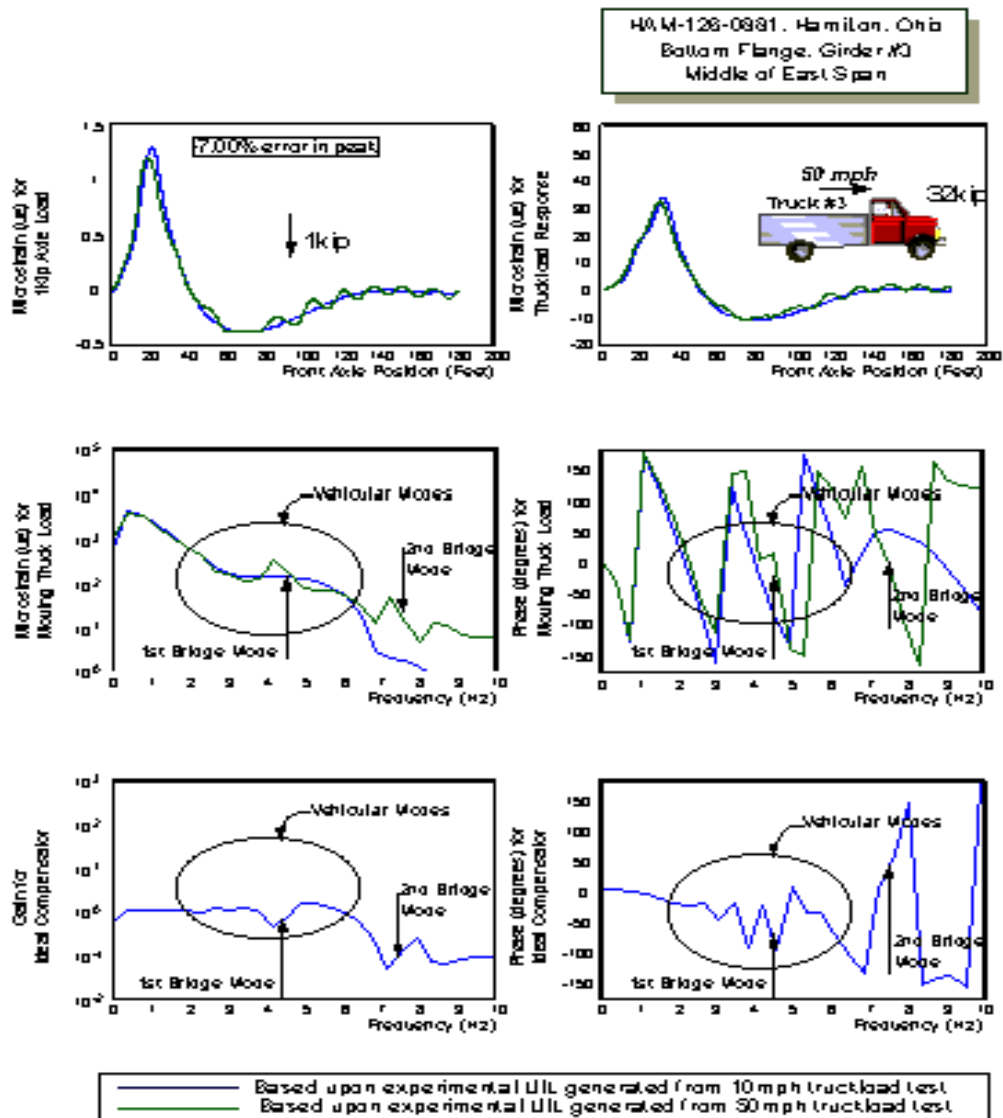


Figure 2-52: Comparison of Measured vs. Simulated Response of Dump Truck at 50 mph

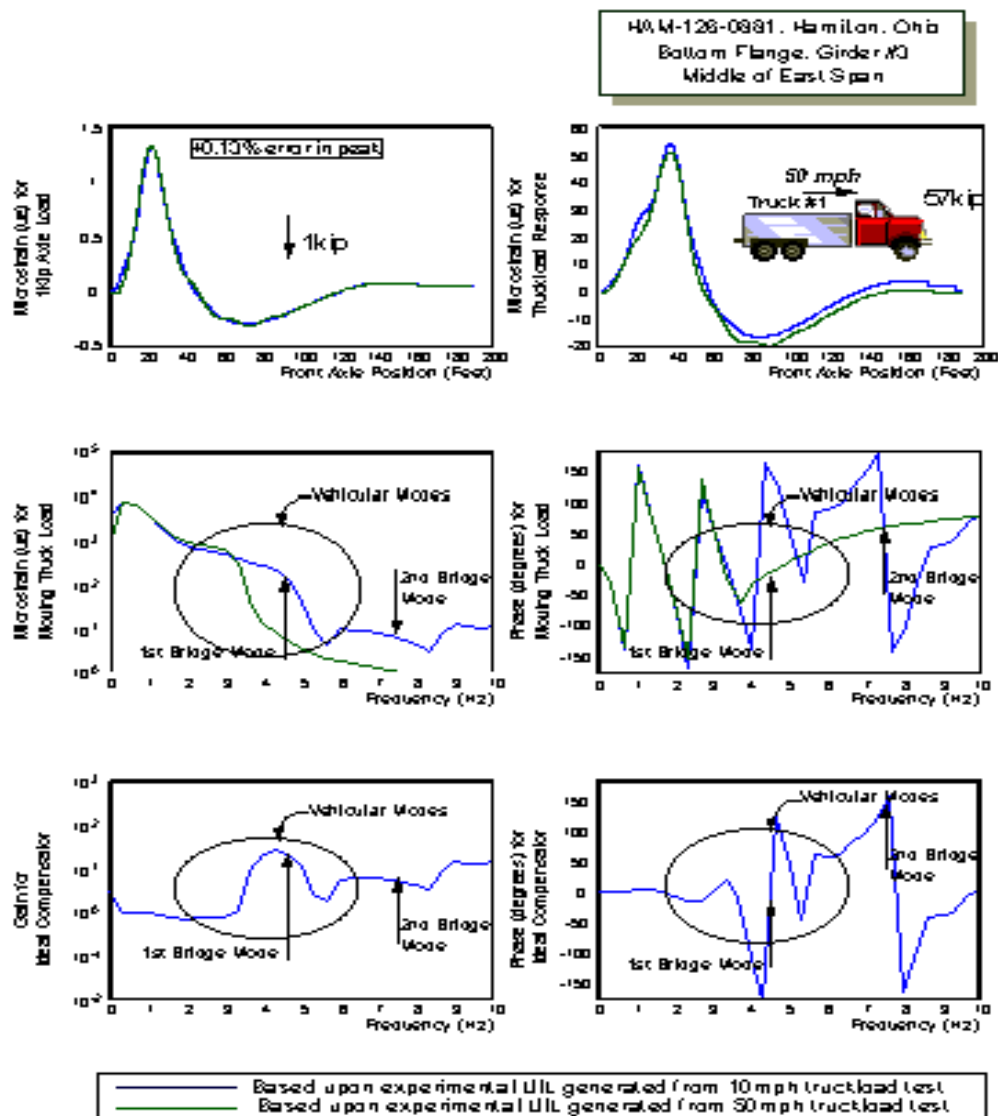


Figure 2-53: Comparison of Measured vs. Simulated Response of Tandem Truck, 50 mph

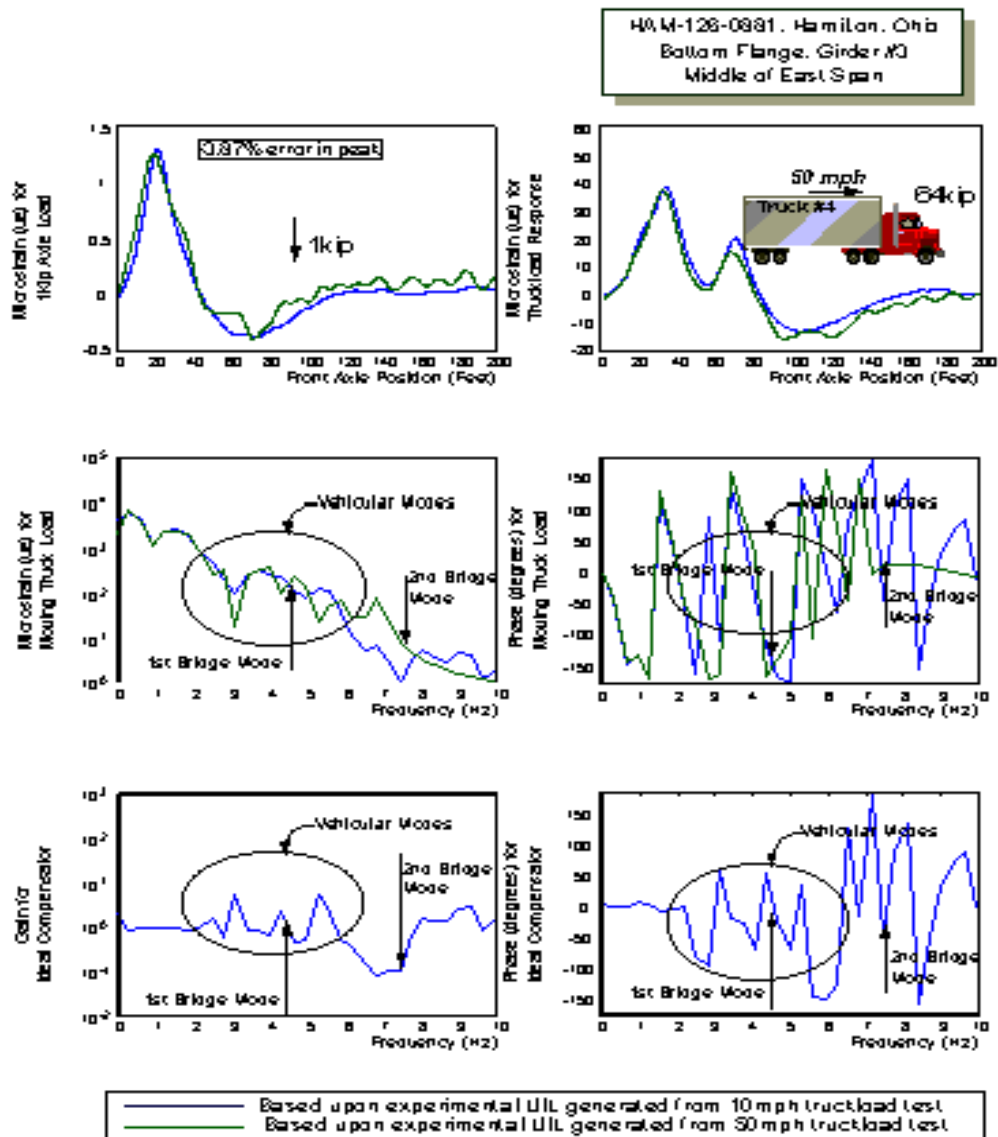


Figure 2-54: Comparison of Measured vs. Simulated Response of Semi Truck at 50 mph

In conclusion, an accurate influence line can be determined by crawl-speed truckload tests given the axle weights, spacings, and speed. The derived influence line is consistent for various truck loads and axle configurations. The maximum speed for an accurate estimate is determined from the shortest span length, the natural frequency of the bridge, and the general bandwidth for vehicle-bridge interaction. A slightly less accurate estimation can be determined from higher speeds, but can be improved in two ways:

1. Comparison against a theoretical simulation of the scaled moment response for an ideal beam, or
2. Adjusted in the frequency domain by an identified compensator based upon the crawl-speed response of the given vehicle.

The accuracy and consistency of this compensation when used in normal traffic circumstances and for the variety of vehicles in the traffic population has yet to be determined.

We will now examine the utilization of the identified influence lines for condition assessment of the steel-stringer bridge under consideration.

### 3. Condition Assessment of a Highway Bridge under Truckload

Linearized condition indices are based on the assumption that a constructed facility may be characterized as incrementally linear at the serviceability limit states. While no soil-foundation-structure system can be strictly linear, the justification in using linearized indices is that most constructed facilities behave linearly in the global sense even when many local nonlinearities, such as due to localized damage in a shake-down state, may exist. In fact, this argument has been the basis of linear analysis for ultimate strength design [ACI 318-95, 1995]. For the general infrastructure management problem, linearized indices offer the advantages that they can be physically conceptualized, can be measured or extracted from measurements during controlled tests at any time, and they can be more easily correlated to facility performance at the serviceability limit states.

Some of the linearized global condition indices that have been proposed for the serviceability limit state of constructed facilities are shown in Table 1. It is noted that an objective index may be classified in terms of whether it corresponds to a modal, numerical or geometric-space conceptualization of the constructed facility. In addition, the indices in Table 1 are classified as either directly measurable through a controlled test, or those that require additional assumptions and analytical and/or numerical modeling of the constructed facility before they may be extracted from the measurements taken during an experiment.

Identification Space	Experimentally Measured Quantities	Post-Processed Indices, <i>No Analytical Model Is Required</i>	Analytically Derived Indices Requiring Structural ID
Modal model	Input: Impact or Swept-sine Excitation; Output: Acceleration; Input and output in time-domain, FRF, or both	Mode frequencies and damping Disp. Mode Shape Vectors Strain Mode Shape Vectors MAC, COMAC, MSF	Strain energy of mode shape  Curvature distribution of a mode shape
Numerical model: w/ assumed forms of M,K,C matrices	<u>Input</u> : Ambient traffic and/or known (truck) load or as in Modal model; <u>Output</u> : strains, tilts, displacements, position, accelerations, etc.	Mode frequencies and damping Mode shapes Modal flexibility coefficients Member influence lines Sectional curvature Neutral axis location	Sectional level properties at any location not instrumented  Parameters derived from stochastic or statistical models
Geometric model: Macro, element or FE forms	Same as in Modal and Numerical models	Global Flexibility Uniform Load Surface (ULS) Sectional Moment and Force Sectional Rating	Global Rating Member level and localized structural properties at any location not instrumented

**Table 3-1: Some Common Linearized Condition Indices For Constructed Facilities**

In evaluating the merits of various condition indices, we need to distinguish between those indices which lend themselves to direct measurement (such as a node acceleration or member strain), those which require a single level of post-processing (such as modal frequencies, influence lines, or flexibility coefficients) and those which require a complete system-identification process (such as element stiffness coefficients). In general, a system-or-structural-identification based condition assessment approach to condition assessment is highly recommended. In the system-identification approach, we would need to generate an a-priori analytical model, design and conduct experiments, conduct parameter identification to calibrate the analytical model, validate its completeness and reality-check by evaluating the physical correspondence of the identified parameters. The resulting field-calibrated analytical model serves as a reality-check on the experiment itself, and for linear (and as a starting point for non-linear) sensitivity analyses which are required for reliability evaluation.

A structural-identification based approach is recommended even when an index used for condition assessment may be a directly measurable one. At the same time, we do have to recognize and take advantage of indices that can be directly quantified during an experiment, or requiring just a single level of post-processing without a complete system-identification process, since these would be easier to conceptualize and to monitor, requiring simpler experiments. The approach of UCII research has been to conduct rigorous studies on statistical samples of a recurring bridge type, utilizing comprehensive experimentation in conjunction with system-identification. This is followed by designing simpler experimentation for objective global condition assessment of the total population. Exploratory studies on just three steel-stringer bridges indicate significant promise in such a bridge-type specific management approach to bridge-types recurring in large quantities [Aktan, 1994c].

For evaluating the sufficiency or relative advantages of different condition or damage indices, we note the following: (a) Acceptable ranges and stationarity of the indices; (b) transformation procedures for relating the measured indices to facility performance at design limit states. This should be conducted in conjunction with identifying any defects, deterioration mechanisms or damage; and, (c) projecting current condition and performance to the future given the expected maintenance, loading environment and service life. Therefore, the criteria for a satisfactory damage detection method should be: (a) Diagnose whether there is damage or not, even when there may not be a baseline. While many indices are useful only if there is a baseline, several may be used in conjunction with structural identification to diagnose damage without a baseline. For example conceptual indices may utilize a rational analytical model as a gauge, or a comparable healthy facility may serve as a baseline to test for anomalous behavior; (b)

Localization, i.e. establishing the boundaries and distribution of any damage; (c) Quantify the extent of the damage and the possible defects, deterioration mechanisms or other loading mechanisms which may have led to the damage; and, (d) Establish the impact of the damage on the global health, i.e. how damage is affecting current and projected performance at the critical limit states.

In addition to or in conjunction with the above criteria, we desire condition indices to be: (a) Sensitive to the effects of common deterioration and damage mechanisms that affect the facility; (b) Directly measurable by practical experimentation, and not requiring extensive post-processing. Some indices may require modal expansion and/or extensive error-prone numerical operations; (c) Robust, i.e. insensitive to experimental errors and uncertainties; and, (d) Conceptual, i.e. directly corresponding to a clear aspect of structural behavior such as deflection, stress, moment, stiffness or flexibility. While some indices, such as the effective flexural rigidity of a member, permit using engineering intuition for damage detection, others with no physical correspondence have been proposed to indicate damage based on an arbitrary scale.

Damage must also be classified according to its spatial context: local material properties, distinct members and their connections, and the complete or global structure. It is interesting that many engineers consider damage as changes in the effective material properties within a structure. Many nondestructive technologies have been developed which can successfully characterize the in-situ properties of construction materials, even through covers and other obstruction [Shickert, 1995]. These tools are very useful in detecting the onset of deterioration (e.g. in a reinforced concrete element or in its chemical bond with steel). For a large-scale constructed facility,

however, it is not possible to presently catalog all of its critical deterioration mechanisms nor pinpoint its critical regions and responses to be investigated. Even if a complete local scan is conducted, it is not clearly understood how local damage affects the complete system performance. Therefore, local scans and measurements can not feasibly and effectively address the problem of global condition and damage assessment.

The AASHTO Manual for Condition Evaluation of Bridges suggests “load testing as an effective means of evaluating the structural performance of a bridge or its selected components. This applies particularly to those bridges which cannot be accurately modeled by analysis, or to those whose structural response to live load is in question. Load evaluation tests are made to determine the magnitude and variation of loads and load effects such as those due to traffic, temperature changes and wind. Diagnostic load tests are performed to determine the effect on various components of a known load on the structure. Proof load testing is designed to directly determine the maximum live load that the bridge can support safely.”

Truck, proof, or other load testing of highway bridges has usually been reserved as an area of academic research due to the complexities, cost, and disturbance to service of such a field experiment. However, when a structure’s computed capacity is less than the desired level of performance, it is usually beneficial to the owner to objectively identify the actual structural response to controlled loading experiments. The constructed bridge will have many inherent mechanisms to resist the applied load and which are generally not considered in the analysis of its capacity. These identified mechanisms include the actual load distribution, impact factor, unintended composite action, participation of superimposed deadload, material properties,

unintended continuity, participation of secondary members, effects of skew, effects of deterioration and damage, unintended bearing restraint, and environmental effects such as thermal stresses [Lichtenstein, 1998].

Diagnostic load tests have traditionally been performed in conjunction with significant analytical modeling (e.g., finite element) of the structure. A nominal model is generated based upon the design, site, inspection report, and other information at hand. Virtual load simulations are conducted with the nominal model in order to determine the appropriate locations for the bridge instrumentation. If static loads are to be employed, then the model will dictate the worst-case position of the trucks. In practice, this preliminary effort is quite often bypassed as the predicted locations by the model are generally intuitive, based upon the first principles already incorporated within the linear model. Further, the number of sensor and truck locations during the test are maximized to the limits of all practical constraints in order to minimize the possibility of overlooking some hidden defect or damage. Crawl-speed tests are preferable because continuous measurement of the load response is recorded for the entire traffic lane (as opposed to a finite set of pre-conceived locations). After the load test, the model is then calibrated based upon some cost function. The calibrated model is then used to virtually determine any of the desired indices at any/all locations for condition assessment and damage detection.

This research provides a novel approach to condition assessment by determining the below indices for the instrumented sections of the bridge from the measured data without the use of a finite element model.

### 3.1. Sectional Indices for Condition Assessment under Truck and Lane Load

The assumptions for an ideal beam (Section 2.1) still apply to the assessment of the following condition indices for a steel-stringer bridge under diagnostic load. The vertical origin will be arbitrarily considered as the outer face of the bottom flange of the steel girder.

#### 3.1.1. Maximum Stress in the Outer Fiber (i.e., Bottom Flange)

The location of maximum stress observed during a set of experiments is certainly a parameter of concern. The response of the instrumented member (e.g. steel flange) can itself be checked against its material capacity for load. If this is tracked over some period of time, this could indicate areas of possible deterioration for the bi-annual inspection. An influence line would provide greater information by normalizing the stress to a unit load and considering the entire length of the load path. However, little assessment of the structure's condition can be made based upon one sensor reading alone.

For HAM-126-0881, the maximum stress occurs in the middle span on the middle girder at the bottom flange during the diagnostic truckload test (see Figure 3-1). The corresponding top flange is near zero, indicating a fully composite section as designed. Note the slight but unintended composite action in the endspans and at the piers. The east span shows greater stress during this and other truckloads and, hence, it will be examined instead of the west span. The response is nearly identical when the truck crosses the bridge in the other (i.e., south) lane due to the symmetry of the bridge.

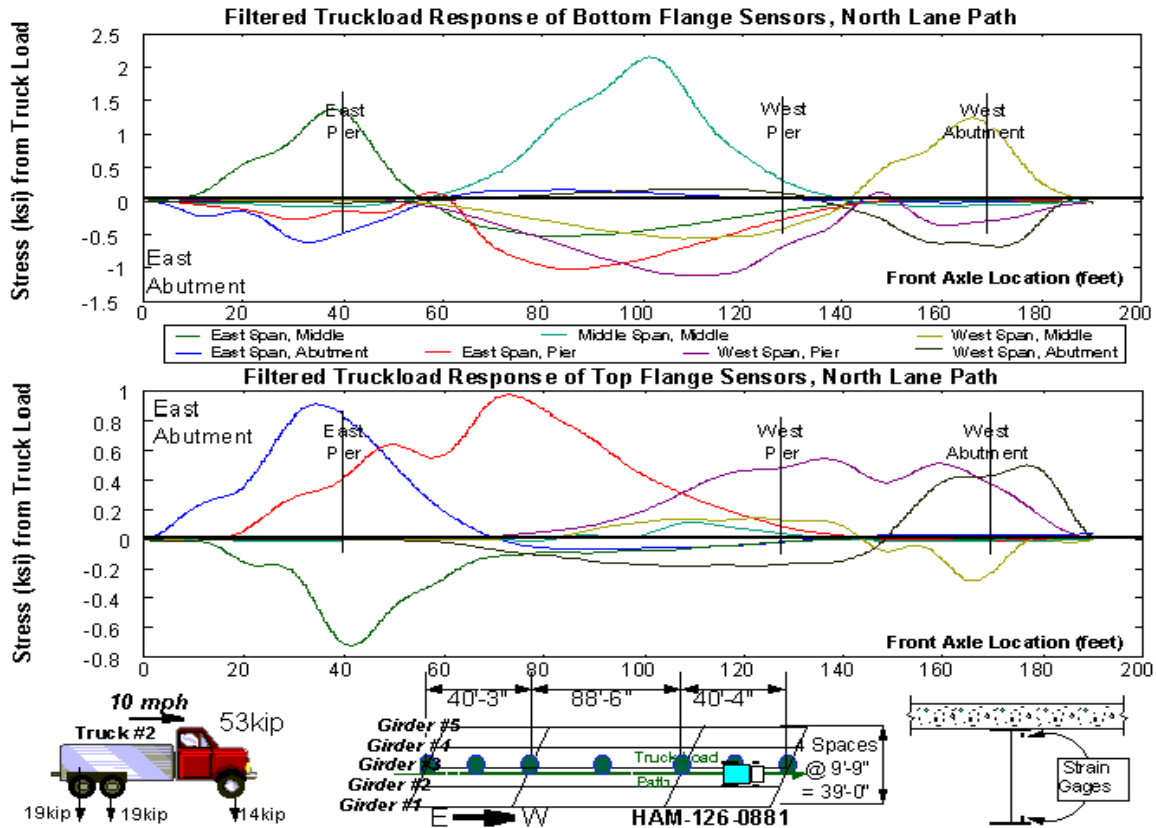


**Figure 3-1: Filtered Truckload Responses for Critical Cross-Sections of HAM-126-0881**

From the determined influence lines, one observes the ideal response discussed in Chapter 2 for the bottom flanges in each span (see Figure 3-2). The top flange lines, however, indicate some nonlinear behavior and do not peak at the same location as the bottom flange lines. This may be due to slip-stick performance of the composite interface with the concrete decking; however, it occurs at every instrumented section including the fully composite middle span. Another hypothesis is that some very local transfer of the load occurs at each crossframe or at other secondary members of the bridge structure. Another observation is that the piers indicate significant axial force when the point load is directly above them. These unexpected but local responses at the top flange and piers have been observed on many other steel-stringer bridges and will be considered further in future research.

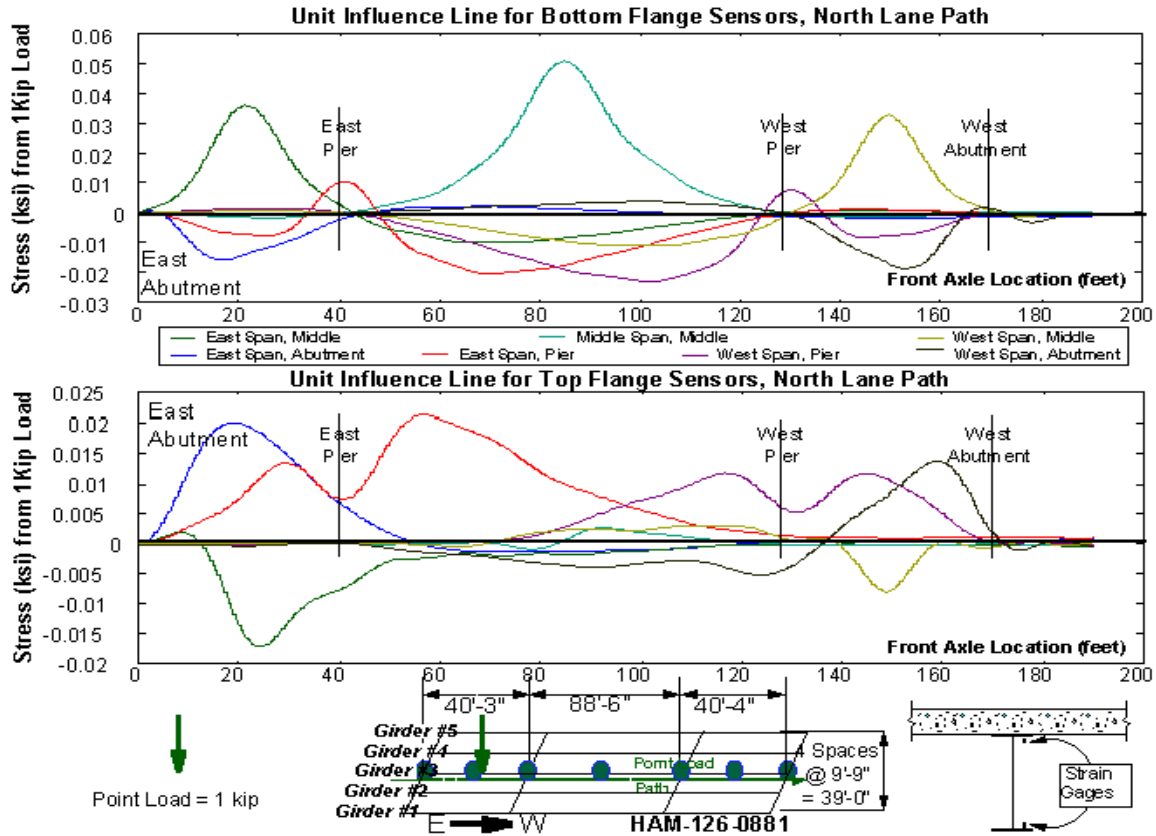


**Figure 3-2: Influence Lines for Critical Cross-Sections of HAM-126-0881**

The NCHRP Manual for Bridge Rating Through Load Testing [Lichtenstein, 1998] simply suggests that the design rating for the bridge could be scaled by the ratio  $K_a = \epsilon_c / \epsilon_m$ , where  $\epsilon_t$  is the maximum strain/stress during the load test and  $\epsilon_c$  is its corresponding theoretical strain/stress due to the test vehicle and its position which produced  $\epsilon_m$ . If the measured stress is less than expected ( $\epsilon_m < \epsilon_c$ , which is quite often the case due to the many inherent but unconsidered mechanisms for load distribution), then the bridge rating is increased. However, if unintended (i.e., not designed) composite action occurs between the steel girder and the concrete decking, then the Manual suggests that the new rating be subsequently reduced by the ratio  $S_{nc} / S_{fc}$ , where  $S_{nc}$  is the sectional modulus for the noncomposite steel beam alone and  $S_{fc}$  is the sectional

modulus for a fully composite deck-on-girder section. Note that  $S_{nc}$  is always less than  $S_{fc}$ . This reduction is equivalent to scaling up the measured stress to discount any effect of the unintended composite action, which might not be sustainable at the higher levels of load required to yield the steel. However, the Manual makes no allowance for partial composite action (see below) and, hence, may be over penalizing the measured stress. Further, the measured stress (and any linear interpolation of it based upon the required rating loads) is generally sufficient to represent the bridge condition for the majority of serviced loads, especially when one considers the safety factors required by the code (see below). In any case, further research is required and, until a consensus is reached, all results should be provided for the discretion of the bridge owner.

### 3.1.2. Modal Frequencies, Shapes, and Weighting

Several researchers have advocated that frequencies, which may be conveniently extracted from ambient or operating responses of most constructed facilities, would serve as condition indices. Relative frequency changes between different modes have been used successfully in crack detection for other structures [Vandiver, 1975, Adams, 1978, Cawley, 1979, Ju, 1986, Meneghetti, 1993]. DeWolf reported good correlation and a linear relationship between ambient temperature and the fundamental frequency of a bridge [DeWolf, 1995]. These authors asserted that once such expected temperature-frequency relations are established for individual bridges, anomalous changes may reveal damage. Research has shown that frequencies of buildings or bridges may shift significantly due to the influence of ambient conditions on the effective boundary conditions and yet remain insensitive to induced damage types [Toksoy, 1993, Lenett, 1997]. The observed modal frequencies from diagnostic truckload tests for HAM-126-0881 and

HAM-42-0992 are illustrated in Figures 1-21 and 1-22, respectively. They correspond to a subset of the identified modes from the impact modal tests conducted for each bridge. Without knowing the input force spectrum, however, it is impossible to rigorously identify the displacement characteristics (e.g., flexibility) from a truckload test. This approach is better suited for modal testing.

Subsequent to several decades of modal test applications with actual large-scale structures, several limitations were discovered for specific local damage types. Cracks were found to have little influence upon the axial stiffness of members and, hence, did not reveal themselves when the global modes were examined. In these modes, the members are behaving much like truss elements. Shifts in the higher-frequency bending modes obtained via local instrumentation, such as strain gages, have been proposed to be more sensitive to the onset of member cracking [Begg, 1976]. This will be explored in Chapter 4.

### 3.1.3. Curvature

As discussed in Section 2.1, the curvature [ $\phi = (\epsilon_b - \epsilon_t)/h$ ] for an instrumented section is approximated by the difference between the bottom and top flange strains divided by the beam height. It will have the same sign as the moment for the section. If the sensors are not located at the outer faces of the flanges, then their distance apart should be used instead of the beam height [ $\phi = (\epsilon_b - \epsilon_t)/(y_{tg} - y_{bg})$ ], where  $y_{tg}$  is the vertical position of the top gage and  $y_{bg}$  is the vertical position of the bottom gage.

Curvature can be considered as the common ground between experiment and theory, as embodied by the moment-curvature relationship. Goble, Schulz, and Commander pioneered the calibration of a two-dimensional finite element model of the bridge by a method that uses curvature as its optimization function [Goble, 1992]. Flexural rigidities of the longitudinal beam ( $EI_g$ ) and lateral diaphragm ( $EI_l$ ) elements were adjusted based upon the field measured curvature for the bridge. The resultant FE model was then used to simulate responses to rating loads in order to assess the condition of the structure. This process was applied successfully to over fifty bridges of various types in thirteen states.

Several researchers have shown that sectional curvature can be an accurate and conceptual health index for a structure, specifically in the detection and localization of damage. Stubbs compares the distribution of flexural strain energy, as related to the measured member curvature, of a mode shape along a beam-element before and after damage [Stubbs, 1985]. The index has been successful in detecting even small damage during a field experiment where a bridge girder was deliberately damaged [Stubbs, 1995]. Changes in modal frequencies and shapes were not observed until the girder was completely severed. Zhang and Aktan considered the curvature of the uniform load surface, as determined from the identified modal flexibility matrix, for damage detection [Zhang, 1993 and 1995].

#### 3.1.4. Neutral Axis Location

As discussed in Section 2.1, the neutral axis occurs at the axis of bending for the section where the stress is zero for an applied vertical load (see Figure 2-2). If there are no other forces acting upon the beam (assumption #10 for an ideal beam), then the neutral axis coincides with the geometric centroid for the beam. The centroid for the typical steel I-beam used in typical steel-stringer design lies at the vertical center of the girder. If additional cover plates were added to the top and/or bottom flanges for improved load capacity, the centroid would be slightly off-center accordingly. If composite action, whether designed or unintended, occurs between the steel beam and the concrete decking, then the centroid is raised substantially above the beam center depending upon the bond integrity. If full composite action is designed by welding shear studs to the top of the beam and encasing the top flange within the concrete decking, then the centroid of the composite section is raised to the top flange of the beam. The steel beam is almost entirely in tension and the concrete decking is completely in compression for a fully composite section in bending under a vertical load.

The location of the neutral axis [ $y_{\text{max}} = \epsilon_b / \phi + y_{\text{bg}}$ ] for each instrumented section can be determined from the top and bottom flange strain measurements during a diagnostic load test (see Figure 3-3). The composite action for the instrumented section can itself be checked against the designed performance. Note that the neutral axis for the middle span remains above fully composite location for most of the truckload test, while the east span and pier indicate varying levels of composite action depending upon the truck position. The east span and pier indicate noncomposite behavior as the truck approaches the east pier. If this is tracked over some period

of time, this could indicate areas of possible deterioration for the bi-annual inspection. An influence line would provide greater information by normalizing the stress to a unit load and considering the change in the neutral axis over the entire length of the load path.

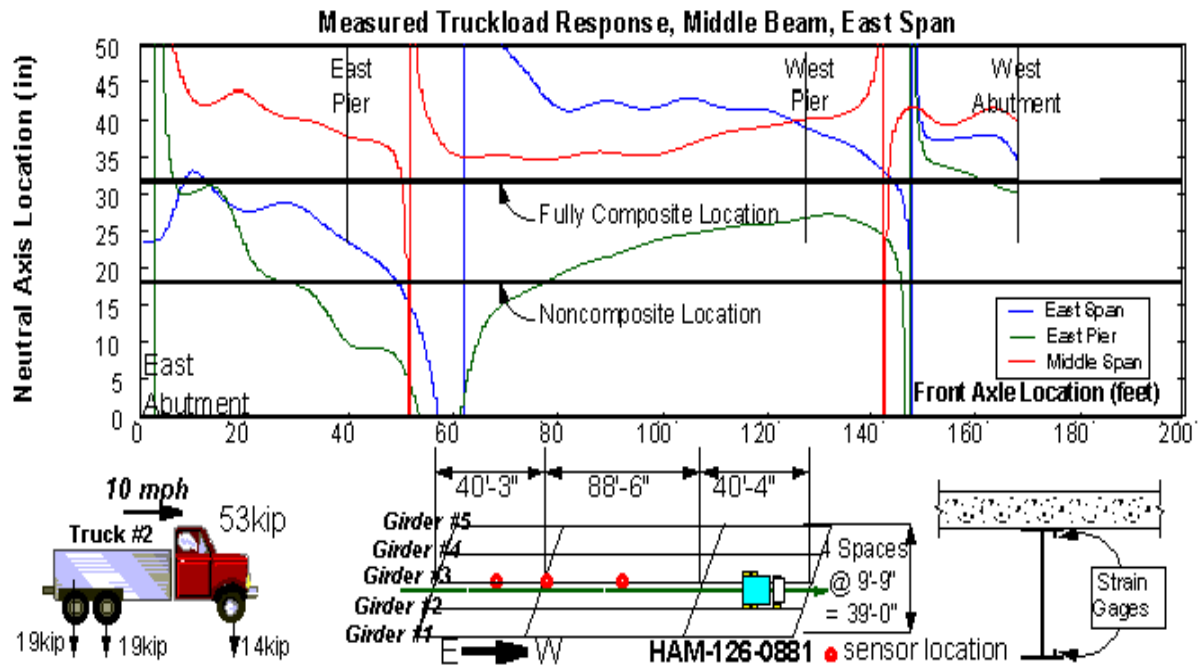


**Figure 3-3: Neutral Axis Location during Truckload of HAM-126-0881**

Note that the design parameters (e.g., neutral axis location) for the middle span and east pier are presented in greater detail in Appendix B1.

### 3.1.5. Truckload Moment

Assessment of the sectional capacity will now reach a theoretical crossroads after determination of the neutral axis location. First, the implications of unintended composite action must be considered in determining sectional inertia, moduli, moment, and capacity rating. Steps may be taken later in the analysis to discount its advantages to the load rating (e.g., capacity can be based upon the steel beam alone, estimated stresses for the rating loads can be increased, etc.); however, if the measured data indicates that the structure exhibited some level of composite action, then its sectional indices must be calculated accordingly. Second, the assumption (#10) of no axial force for an ideal beam must be reviewed. While strains due to axial forces can be induced (e.g., due to rotational restraint at the supports), it is assumed that their magnitude will be insignificant as compared to those due to flexure.

A fully composite section (i.e., designed as per 10.38 and 10.50 of the AASHTO Specifications) exhibits a linear and continuous strain profile through the entire section (see Figure 3-4).

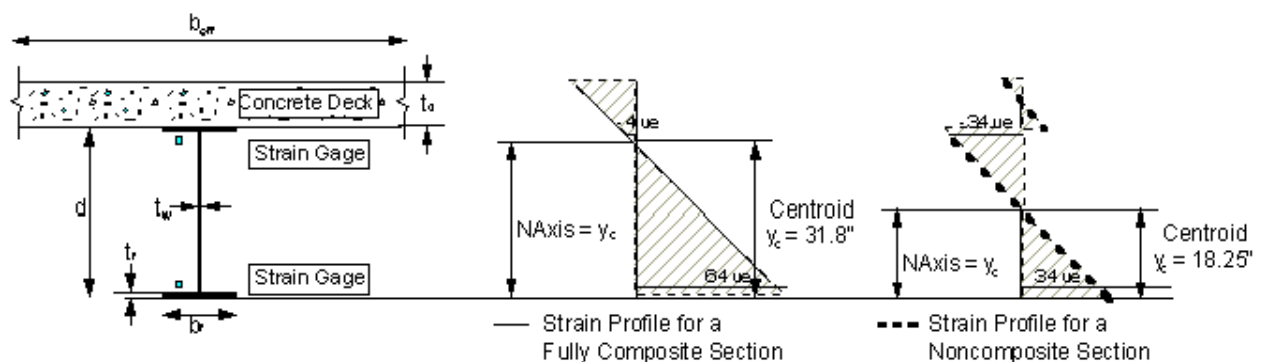


**Figure 3-4: Ideal Behavior for a Fully Composite and Noncomposite Section of East Span**

It incorporates an effective width  $b_{\text{eff}}$  of the concrete decking in its inertia and capacity for load.

The effective width is defined by Specification 10.38.3 as the smaller of:

- 1) One-fourth of the span length (L),
- 2) The distance center to center or spacing of the girders ( $S_g$ ), or
- 3) Twelve times the thickness of the deck. ( $12 t_d$ )

The deck thickness generally dominates the specification. In accounting for this composite system, the cross-sectional area of the decking is reduced to an equivalent area of steel by the strength ratio of their elastic moduli ( $n_{\text{eff}} = E_s / E_c$ , where  $E_s = 29000$  ksi and  $E_c = 57\sqrt{f'_c} \sim 3600$  ksi, although  $E_c$  may vary considerably between 2500 and 4500 as per Specification 10.38.1.3).

Thus, one may now calculate the geometrical inertia  $I_t$  and centroid  $y_t$  of the composite section.

$$y_s = h/2, y_c = t_d/2, A_c = \frac{b_{\text{eff}} \cdot t_d}{n_{\text{eff}}}, I_c = \frac{b_{\text{eff}} \cdot t_d^3}{12 \cdot n_{\text{eff}}}, A_t = A_s + A_c, y_t = \frac{A_s y_s + A_c y_c}{A_s + A_c}, I_t = I_s + I_c + A_s (y_s - y_t)^2 + A_c (y_c - y_t)^2$$

If the measured location of the neutral axis  $y_{\text{naX}}$  does not coincide with the determined centroid location  $y_t$  for a fully composite section, one has at least two methods that will account for this discrepancy and yet still allow for a linear and continuous strain profile for the section.

## Method 1: Fully Composite with Nonzero Axial Force

The assumption of no axial force is removed. An axial force is assumed to be acting upon the section such that the centroid is shifted to the neutral axis location. This can be illustrated as a simple shifting to the left or right of the ideal strain profile of the section along the horizontal axis (see Figure 3-5).

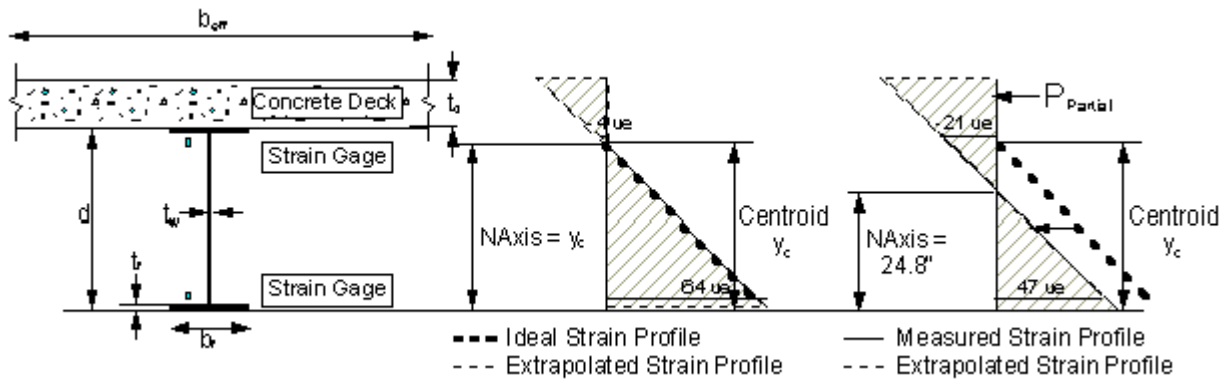


**Figure 3-5: First Method of Estimating the Section Moment for East Span**

$$y_1 = y_t, \quad I_1 = I_t, \quad S_1 = \frac{I_t}{y_t}, \quad K_1 = \frac{y_t - y_{tg}}{y_t - y_{bg}}, \quad P_1 = A_t \cdot E_s \frac{\epsilon_t - \epsilon_b K_1}{1 - K_1}, \quad M_1 = \frac{(\epsilon_b E_s - P_1 / A_t) I_t}{(y_t - y_{bg})}$$

This method may be especially appropriate for those sections that are actually designed as per the AASHTO Code, as was the middle span of HAM-126-0881. Note that there is a continuous and linear decrease in the strain as you move vertically up through the section (see Figure 3-6). Also, note that the embedded sensors in the concrete deck indicate similar behavior laterally for the section; this serves to corroborate the theoretical assumption of an effective deck width of at least the beam spacing. It is conceivable that a larger width of the concrete deck is acting in load distribution than expected.

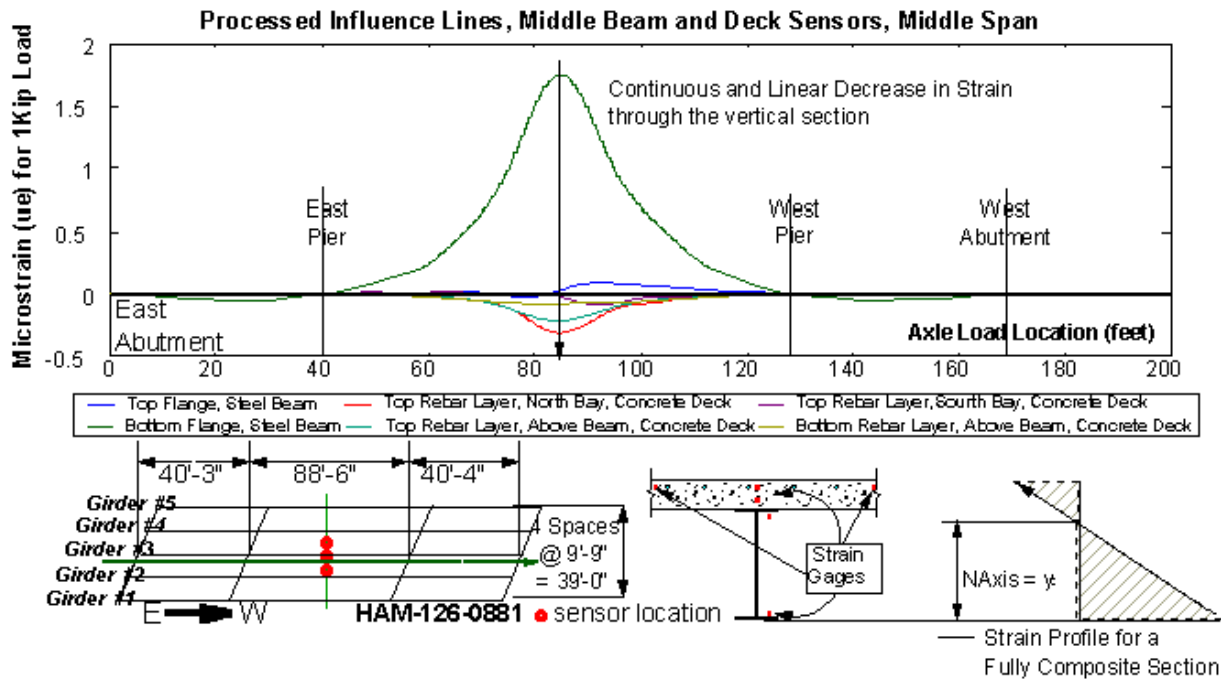


**Figure 3-6: Measured Strain Profile for Fully Composite Section of HAM-126-0881**

An influence line would provide greater information by normalizing the stress to a unit load and considering the change in the sectional moment and axial force over the entire length of the load path. In addition, rating loads may be simulated with the influence line and the resultant moments may be compared with other instrumented sections on the bridge and with the expected values from design (discussed further below).

### **Method 2: Fully Composite with No Axial Force**

The assumption of the code specification for effective deck width is removed. The effective deck width is recalculated to force the geometric centroid to coincide with the neutral axis location. This can be illustrated as both a rotation and translation of the strain profile of the section about the vertical axis (see Figure 3-7).

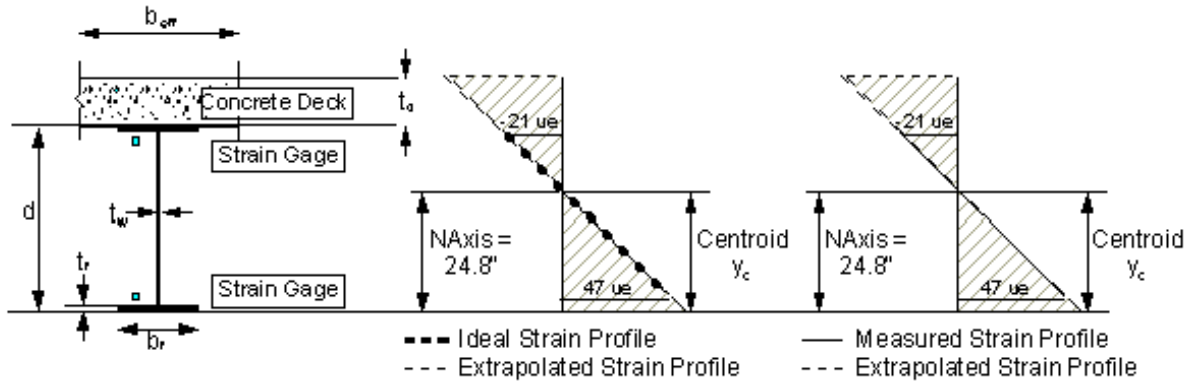


**Figure 3-7: Second Method of Estimating the Section Moment for East Span**

$$y_2 = y_{max}, \quad b_{eff2} = \frac{n_{eff} A_s (y_s - y_2)}{t_d (y_2 - y_c)}$$

$$A_{c2} = \frac{b_{eff2} \cdot t_d}{n_{eff}}, \quad I_{c2} = \frac{b_{eff2} \cdot t_d^3}{12 \cdot n_{eff}}, \quad I_2 = I_s + I_{c2} + A_s (y_s - y_2)^2 + A_{c2} (y_c - y_2)^2$$

$$S_2 = \frac{I_2}{y_2}, \quad P_2 = 0, \quad M_2 = \frac{\epsilon_b E_s I_2}{(y_2 - y_{bg})}$$

Other researchers have suggested modifying other parameters (e.g., deck thickness, strength ratio) to account for the discrepancy between centroid and neutral axis [Chajes, 1997, Elhelbawey, 1999].

This method may be appropriate for those sections designed as fully composite if the estimated axial force  $P_1$  is nonzero. The larger estimate for the moment would of course be the more conservative choice. This method may be especially appropriate for those sections exhibiting partial composite action (and not designed as fully composite per the AASHTO Code) because

the estimated moment acting upon such sections is smaller than that determined by Method 1 above. For example, note that there is a discontinuous decrease in the strain for the east span as you move vertically up through the section (see Figure 3-8). Two separate strain profiles exist for the steel beam and concrete decking; however, a similar curvature exists for both systems. Also, note that the embedded sensors in the concrete deck indicate similar behavior laterally for the section; this serves to corroborate the theoretical assumption of an effective deck width of at least the beam spacing. It is conceivable that a larger width of the concrete deck is acting in load distribution than expected.

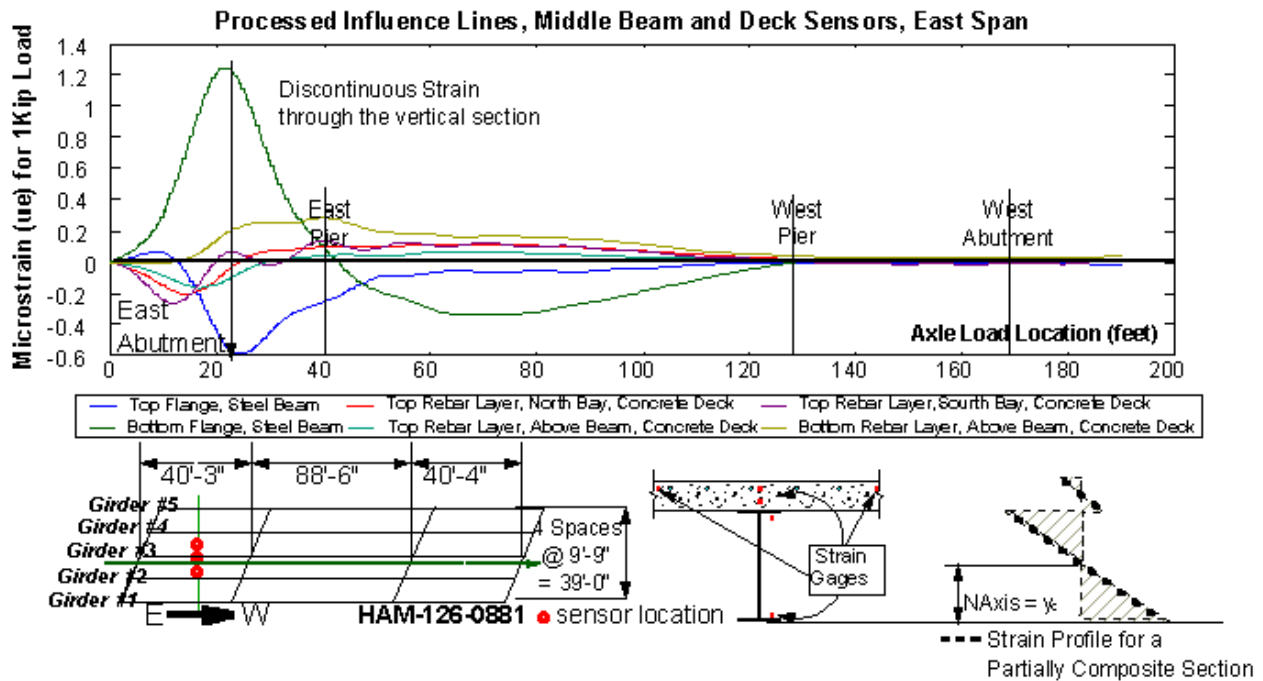


Figure 3-8: Measured Strain Profile for Partially Composite Section of HAM-126-0881

An influence line would provide greater information by normalizing the stress to a unit load and considering the change in the sectional moment and effective deck width over the entire length of the load path. In addition, rating loads may be simulated with the influence line and the resultant moments may be compared with other instrumented sections on the bridge and with the expected values from design (discussed further below).

### **Method 3: Partially Composite with No Axial Force**

Another method is also introduced that will account for the discrepancy between the centroid of a fully composite section and the measured location of the neutral axis. The assumption is made that the section exhibits partial composite action and there exists a discontinuous break in the strain profile of the section. The assumption of the code specification for effective deck width is enforced. No axial force is allowed for the net section; however, an axial force is assumed to be acting upon the steel beam such that its centroid is shifted to the measured neutral axis location. This can be illustrated as a simple shifting to the left or right of the ideal strain profile of the section along the horizontal axis (see Figure 3-9). An equal but opposite axial force is assumed to be acting upon the concrete decking such that the net axial force in the section is zero. The curvature is assumed to be constant for the entire section.

Note that the inertia and centroid cannot be defined for a noncontinuous section. The section modulus is therefore defined by the ratio of estimated moment and the stress at the bottom face of the steel beam.

For Method 3, it is convenient during the rating procedure to define a linear condition index that defines the level of composition action for the deck-on-girder system from none (i.e., zero) to fully composite (one or 100%) based upon the national AASHTO code. Turer suggested the ratio of the axial force in the steel beam as measured relative to that predicted by a fully composite section ( $RCA = P_{\text{Partial}} / P_{\text{Full}}$ ).

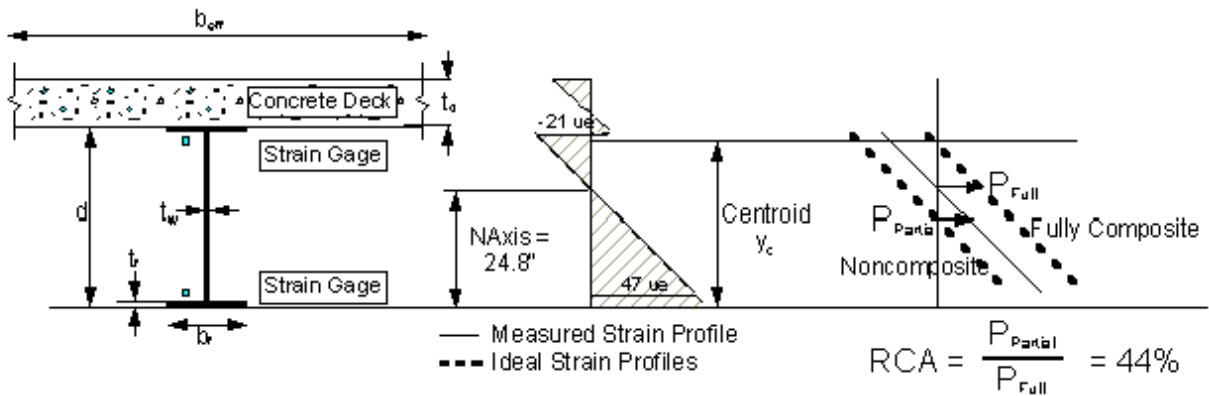


**Figure 3-9: Third Method of Estimating the Section Moment for East Span**

$$K_s = \frac{y_s - y_{ig}}{y_s - y_{bg}}, \quad P_s = A_s \cdot E_s \frac{\epsilon_t - \epsilon_b K_s}{1 - K_s}, \quad M_s = \frac{(\epsilon_b E_s - P_s / A_s) I_s}{(y_s - y_{bg})}$$

$$P_d = -P_s, \quad \epsilon_{td} = \frac{P_d}{A_c E_s} - \frac{t_d \phi}{2}, \quad \epsilon_{bd} = t_d \phi + \epsilon_{td}, \quad M_d = \frac{(\epsilon_{bd} E_s - P_d / A_c) I_c}{(y_c - h)}$$

$$P_3 = 0, \quad M_3 = M_s + M_d - P_s y_s - P_d y_c$$

The section modulus is defined by the ratio of estimated moment and the stress at the bottom face of the steel beam ( $\epsilon_{bs}$ ).

$$\epsilon_{bs} = y_{max} \phi, \quad S_3 = \frac{M_3}{\epsilon_{bs}}$$

It will be shown below that the estimated moment (and, therefore, the section modulus) is very close to that derived by Method 2.

The remaining composite action (RCA) is defined as the ratio of the axial force in the steel beam as measured relative to that predicted by a fully composite section.

$$\varepsilon_{bgc} = (y_t - y_{bg})\phi, \quad \varepsilon_{tgc} = (y_t - y_{tg})\phi, \quad P_{sc} = A_s \cdot E_s \frac{\varepsilon_{tgc} - \varepsilon_{bgc} K_s}{1 - K_s}, \quad RCA = \frac{P_s}{P_{sc}} \cdot 100\%$$

An influence line would provide greater information by normalizing the stress to a unit load and considering the change in the sectional moment and effective deck width over the entire length of the load path. In addition, rating loads may be simulated with the influence line and the resultant moments may be compared with other instrumented sections on the bridge and with the expected values from design (discussed further below).

#### **Method 4: Noncomposite with Axial Force**

The final method assumes that the section exhibits noncomposite action and no estimation of the strain profile in the decking is attempted. An axial force is assumed to be acting upon the steel beam such that its centroid is shifted to the neutral axis location. This can be illustrated as a simple shifting to the left or right of the ideal noncomposite strain profile of the section along the horizontal axis (see Figure 3-10).

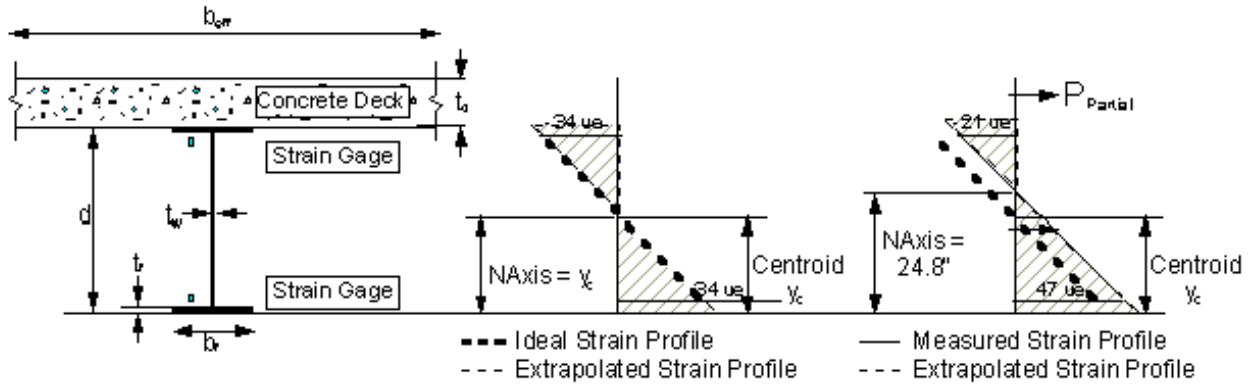


**Figure 3-10: Fourth Method of Estimating the Section Moment for East Span**

$$y_4 = y_s, \quad I_4 = I_s, \quad S_4 = \frac{I_s}{y_s}, \quad P_4 = P_s, \quad M_4 = M_s$$

This method would be applicable in the case where no composite action is indicated with no axial force. An influence line would provide greater information by normalizing the stress to a unit load and considering the change in the sectional moment and effective deck width over the entire length of the load path. In addition, rating loads may be simulated with the influence line and the resultant moments may be compared with other instrumented sections on the bridge and with the expected values from design (discussed further below).

### **Example Estimation of Moments for Truckload Test of HAM-126-0881**

The above methods are employed to analyze the condition of the critical sections from the recorded strains of the instrumented bridge.

Figure 3-11 illustrates the effective deck width calculated by Method 2 and the remaining composite action derived in Method 3. Both parameters are attempts to quantify the partial nature of the composite action for the section; hence, both parameters yield the very same observations about this sectional property as was discussed for the neutral axis location above (see Figure 3-3). Note especially the proportionality between the neutral axis location and the RCA parameter. It will be shown below that RCA is a linear estimation of composite action while effective deck width is exponentially compensated.

Figures 3-12, 3-13, and 3-14 depict the liveload moment that is estimated for the actual test truck along the length of the righthand (i.e., north) lane. Note the similarity between Method 2 and 3 for all sections. These methods compare with Method 1 for the middle span since it was designed as fully composite; however, M2 and M3 are slightly larger than M1 for the middle span because these methods do not allow some of the measured stress to be attributed to axial force. For the east span and pier, M2 and M3 lie in between M1 and M4 for most of the travel path due to the unintended but partial composite action.

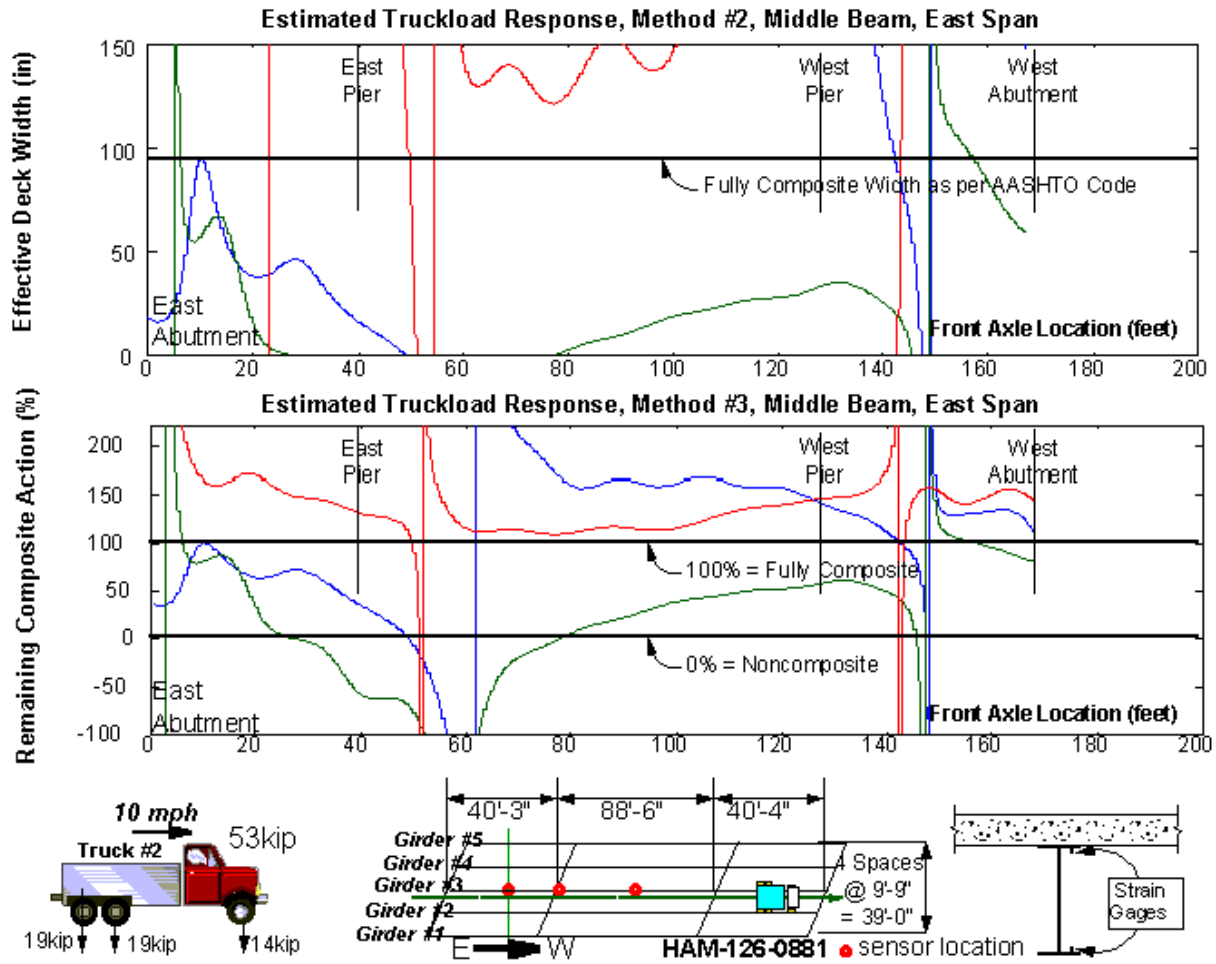


Figure 3-11: Effective Deck Width and RCA for Truckload Test of HAM-126-0881

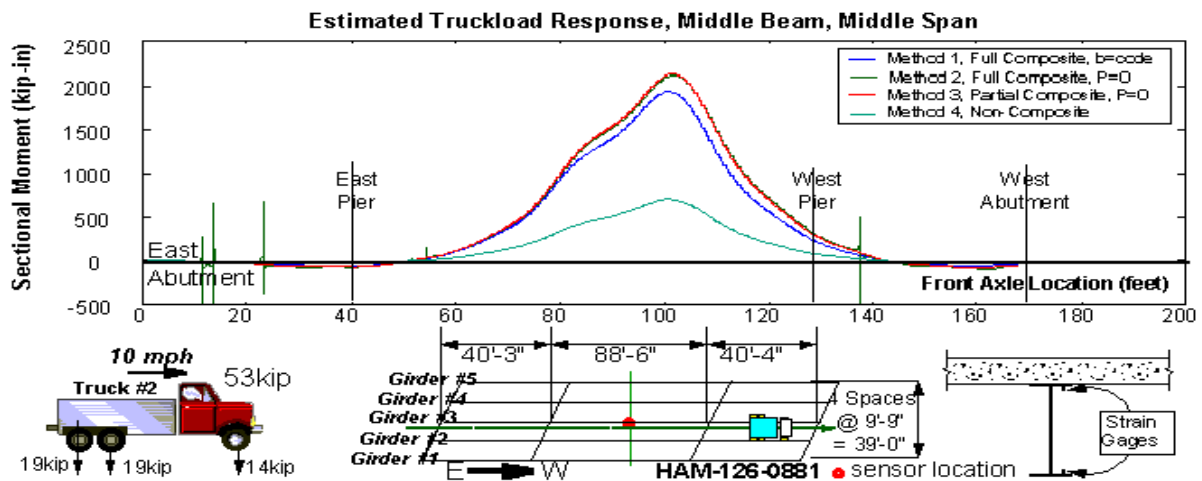


Figure 3-12: Estimated Moment of Middle Span for Truckload Test of HAM-126-0881

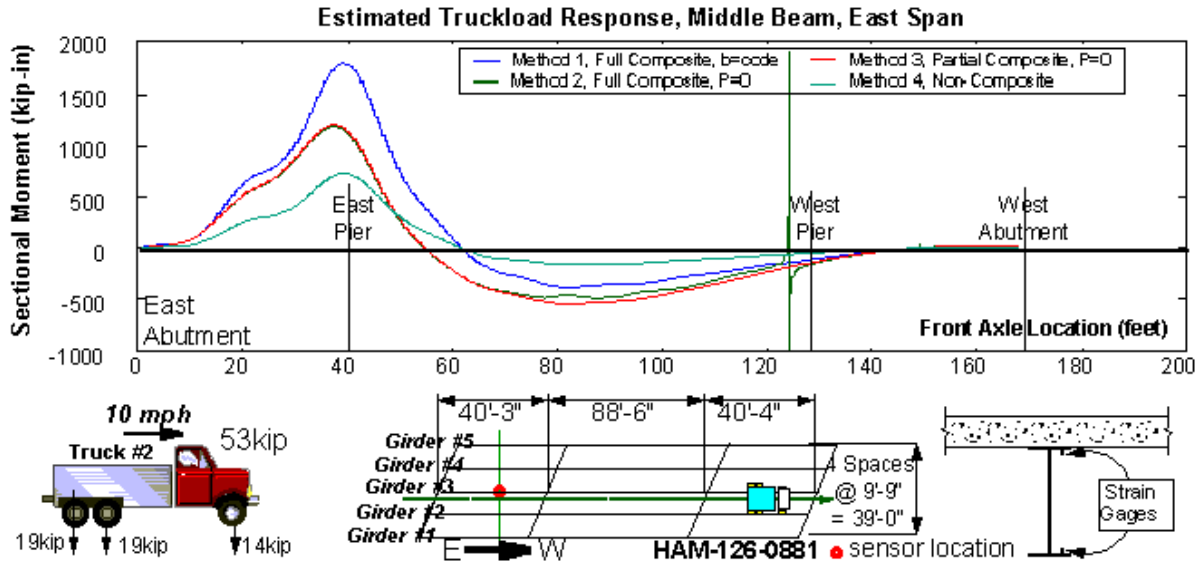


Figure 3-13: Estimated Moment of East Span for Truckload Test of HAM-126-0881

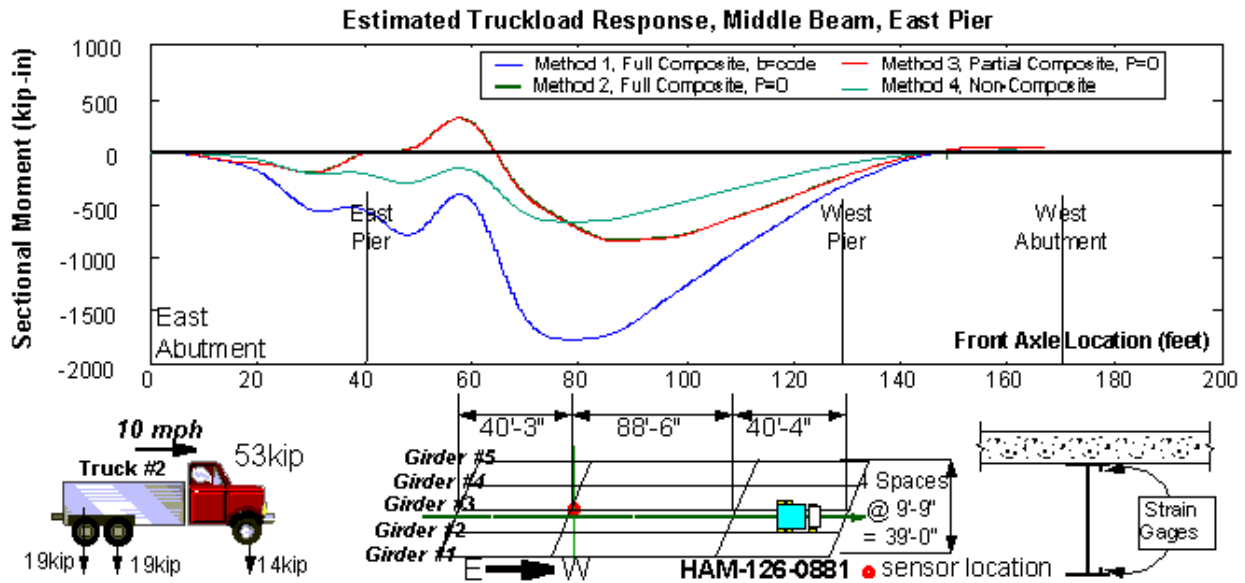


Figure 3-14: Estimated Moment of East Pier for Truckload Test of HAM-126-0881

The identified parameters for the peak liveload (LL) moment are compared with their designed values in Table 3-2. The design was obviously conservative by at least a factor of two in all cases. It must be noted that the design strains correspond to the outer face of the beam flanges,

while the measured/identified strains were located on the inner face; hence, some discrepancy is expected, but not to this extent. Several of the tabularized parameters have not yet been discussed, but will be presented below.

Parameter	Design East Span	Identified East Span	Design East Pier	Identified East Pier	Design Mid Span	Identified Mid Span
Steel Beam	W136x194	As design	W136x194	As design	W136x182	As design
Comp Action	None	Partial	None	None	Full	Full
Bottom Strain	+93 ue	+47 ue	-115 ue	-35 ue	+164 ue	+74 ue
Top Strain	-93 ue	-21 ue	+115 ue	+25 ue	-15 ue	-0.4 ue
Neutral Axis	18.25"	24.8"	18.25"	21.13"	33.2"	34.8"
Curvature	+5.10 ue/in	+2.02 ue/in	-6.30 ue/in	-1.75 ue/in	+4.93 ue/in	+2.19 ue/in
$M_{DL}$	-1097 kip-in	As design	-8680 kip-in	As design	6540 kip-in	As design
$M_{SDI}$	-353 kip-in	As design	-2250 kip-in	As design	2550 kip-in	As design
Impact Factor	0.303	As design	0.265	As design	0.235	As design
Distribution	0.886	0.957	0.886	As design	0.886	0.702
Method 1						
$M_{I,eff}$	N/a	1923 kip-in	N/a	-1683 kip-in	4472 kip-in	1980 kip-in
Axial Force		-71.1 kips		90.0 kips	0	15.8 kips
$M_{DI,eff}$		-1646 kip-in		-13035 kip-in	9845 kip-in	9858 kip-in
$M_{SDI,eff}$		-394 kip-in		-2511 kip-in	2834 kip-in	2837 kip-in
Method 2						
Deck Width		21.8"		7.82"	93"	128"
$M_{I,eff}$	N/a	1238 kip-in	N/a	-821 kip-in	N/a	2132 kip-in
$M_{DI,eff}$		-1413 kip-in		-9959 kip-in		10092 kip-in
$M_{SDI,eff}$		-353 kip-in		-2250 kip-in		2904 kip-in
Method 3						
RCA		44%		19%	100%	111%
$M_{I,eff}$	N/a	1249 kip-in	N/a	-834 kip-in	N/a	2112 kip-in
$M_{DI,eff}$		-1426 kip-in		-10121 kip-in		9994 kip-in
$M_{SDI,eff}$		-353 kip-in		-2250 kip-in		2876 kip-in
Method 4						
$M_{I,eff}$	1789 kip-in	708 kip-in	-2226 kip-in	-723 kip-in	N/a	718 kip-in
Axial Force	0	21.7 kips	0	0		57.2 kips
$M_{DI,eff}$	-1097 kip-in	-1097 kip-in	-8680 kip-in	-8680 kip-in		6540 kip-in
$M_{SDI,eff}$	-353 kip-in	-353 kip-in	-2250 kip-in	-2250 kip-in		2550 kip-in

**Table 3-2: Theoretical and Identified Parameters for Test Truck on Bridge, HAM-126-0881**

For Truck #2, axle weights of 14.3, 19.5, and 19.5 kips, spacing of 15 and 19.4 feet

## **Comparison of Analysis Methods by Simulating Stages of Composite Action**

The above methods are compared and validated by adjusting the strain profile for the east span of the instrumented bridge to represent 0% through 150% composite action (see Figure 3-15). The curvature remains constant for all cases and the profile is simply shifted to the right of the noncomposite case.

The demand or liveload moment remains constant for Methods 1 and 4, as any change in the profile is attributed to axial load. Note that the demand moments estimated by Methods 2 and 3 linearly span the extreme cases as the RCA changes from zero to 100%. Beyond 100%, Method 2 begins to diverge exponentially from Method 3. This exponential relationship is also dramatically observed for the effective deck width; it requires exponentially more deck width to achieve the same incremental improvement in composite sectional strength.

Stress inventory and LFD ultimate moment have not yet been discussed, but they will be presented below. Note that the same relationship between the various methods holds for these parameters as well; Methods 1 and 4 represent the traditional bounds associated with fully and noncomposite behavior while Methods 2 and 3 interpolate (exponentially and linearly, respectively) between and beyond these bounds.

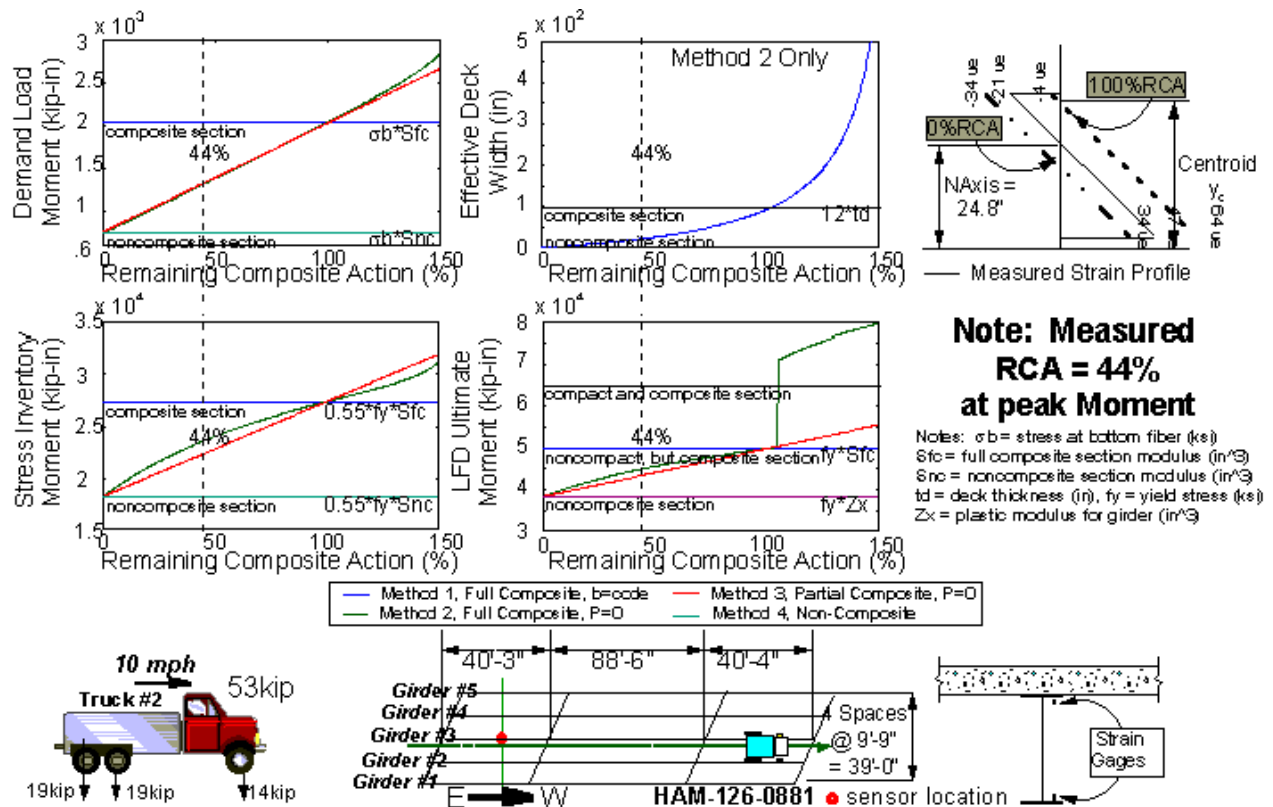


**Figure 3-15: Comparison of Analysis Methods for Various Stages of Composite Action**

### 3.1.6. Distribution Factor

The AASHTO Design Specifications define the distribution factor ( $DF=S/11$ , where  $S$  is the beam spacing in feet) as the maximum fraction of the rating load transferred to any given member at the location of maximum response for the travel path. The remaining portion of the load is carried or distributed among the other members of the superstructure. This equation for distribution factor was originally considered for orthotropic plates, which are free from edge stiffening and skewness of platform, with a vehicle-to-edge distance of one meter [Newmark, 1948]. However, this latter assumption is quite conservative for most bridge designs; further, many bridge designs incorporate some skew and some edge stiffening in the form of parapets or

sidewalks. There are many other mechanisms in addition to beam spacing which contribute to load distribution, including the type and spacing of crossframes and other secondary members, the thickness and strength of the concrete decking, and the stiffness of the girders. Hence, this simplified equation for distribution is generally inaccurate (see Table 3-2, Figure 1-20, and also other research [Moses, 1979, Ghosn, 1986, Goble, 1992, Nowak, 1994, Deatherage, 1995, Kim, 1997, Sartor, 1999]) which further compounds the error in the rating process (see the overconservative estimates for liveload moment above in Table 3-2).

As the distribution factor is intended to scale the designed liveload moment for rating purposes, it should be defined from the identified moments for each girder in the given section. The design truckloads should actually be employed; however, any truck with a significant load can be used assuming linear superposition for the structure. The latter assumption should be checked during the diagnostic load test. The rating load considers the worst-case scenario of side-by-side trucks in each traffic lane for the bridge. Hence, the distribution factor must be sum of the fractions for each single lane loading or, alternatively, the fraction for one multiple lane loading multiplied by the number of lanes.

$$DF_{ij} = \frac{M_{ij}}{\sum_{k=1}^{NG} M_{kj}} = \frac{E_S S_{ij} \epsilon_{ij}}{\sum_{k=1}^{NG} E_S S_{kj} \epsilon_{kj}}$$

$$DF_i = \sum_{j=1}^{NL} DF_{ij} = \sum_{j=1}^{NL} \frac{M_{ij}}{\sum_{k=1}^{NG} M_{kj}} = \sum_{j=1}^{NL} \frac{E_S S_{ij} \epsilon_{ij}}{\sum_{k=1}^{NG} E_S S_{kj} \epsilon_{kj}} \quad \text{Note: } \sum_{i=1}^{NG} DF_i = NL$$

DF=max(DF<sub>i</sub>), where i = # of girder, j = # of lane loaded,

NG = total# of girders, and NL = total# of lanes

It is important to again reiterate that the distribution factor is meant to scale the expected design moment for one rating truckload to the worst-case scenario of all lanes loaded; hence, the sum of distribution factors for the girders should equal the total number of lanes [Kim, 1997].

It has become rather conventional in the above literature regarding diagnostic truckload testing to simplify the above formulation for distribution factor by assuming equivalent section moduli for all girders and under any lane loading. This avoids the entire process of estimating the moment as there is far from any consensus on this matter. The equation then becomes simply a ratio of measured (or projected) strains at the outer face of the bottom flange for the girder and loaded lane under consideration ( $\epsilon_{ij}$ ).

The AASHTO Manual for Condition Evaluation suggests that field measured values of the distribution factor can be used in lieu of the design specification; however, this would seem to just muddy the waters. Instead, the measured stresses can be used directly to estimate the liveload stresses and moment for the design loads and we avoid the use of a distribution factor altogether in the above methodology.

### 3.1.7. Impact Factor

The AASHTO Design Specifications define the impact factor ( $IF=50/(L+125)$ , where  $L$  is the span length in feet) as the fractional increase in the maximum static response for the rating load due to dynamic effects. Dynamic effects for highway bridges have been considered in terms of its incremental change to the static stress and force for many decades [Fuller, 1931]. There are many other mechanisms in addition to span length which contribute to the impact factor, including the dynamic properties (i.e., mass, stiffness, and damping) of the bridge and vehicle, the roughness of the road surface, the slope and orientation of the highway, the truck speed, and the presence of other traffic. Hence, this simplified equation for dynamic increment is generally inaccurate (see Figure 3-16, and also other research [Moses, 1979, Ghosn, 1986, Bahkt, 1989, Goble, 1992, Nowak, 1994, Deatherage, 1995, Kim, 1997, Sartor, 1999]) which further compounds the error in the rating process (see the overconservative estimates for liveload moment above in Table 3-2).

As the impact factor is intended to scale the designed liveload moment for rating purposes, it should be defined from the identified moments for each girder in the given section. It has become rather conventional in the above literature regarding diagnostic truckload testing to simplify the formulation for impact factor by assuming equivalent section moduli for all girders and under any lane loading. This avoids the entire process of estimating the moment as there is far from any consensus on this matter. The formulation then becomes simply a ratio of measured (or projected) strains at the outer face of the bottom flange for the girder and loaded lane under consideration ( $\epsilon_{ij}$ ).

Beyond this matter, there is very little consensus as to the proper calculation of impact factor from measured truckload responses. Bahkt accounts no fewer than eight different methods that researchers have utilized in this endeavor [Bahkt, 1989]. The design truckloads should actually be employed due to the variables noted above; however, it is widely recognized that the code specification (i.e., HS20 truckload) is a fictitious vehicle that is used to mimic the myriad of trucks travelling the highways today. Linear superposition is not possible in considering dynamic increments; hence, it is not possible to readily simulate the dynamic response of the design load from another vehicle's response. The rating load considers the worst-case scenario of side-by-side trucks in each traffic lane for the bridge; however, this can be especially cumbersome if not dangerous to simulate on the highway system. There is no specification regarding vehicle speed for the impact factor; in general, the posted speed is assumed but larger dynamic increments are achievable at higher speeds. A statistical approach seems more appropriate in characterizing the traffic and its dynamic effect upon the bridge [Nowak, 1994].

It has been observed by several researchers that the dynamic increment can be significantly larger if the load is distant from the instrumented section. This can occur due to the ratio of very small signals. Clearly, this has very little merit in defining an impact factor to scale the estimated peak moment for the design load. Cantieni suggested a "zone of direct influence" in order to determine the relevance of a measured impact factor [Cantieni, 1984]. In short, the impact factor should only be calculated for a section when the truckload is located practically overhead (i.e., within the beam spacing).

For this methodology, the impact factor for an instrumented section is determined by considering the ratio of the maxima for the measured and filtered data used to process the influence lines (see Chapter 2).

The AASHTO Manual for Condition Evaluation suggests that field measured values of the impact factor can be used in lieu of the design specification; however, this would seem to just muddy the waters. Instead, the code specification for impact factor is used to scale up the liveload moment for rating purposes in this methodology.

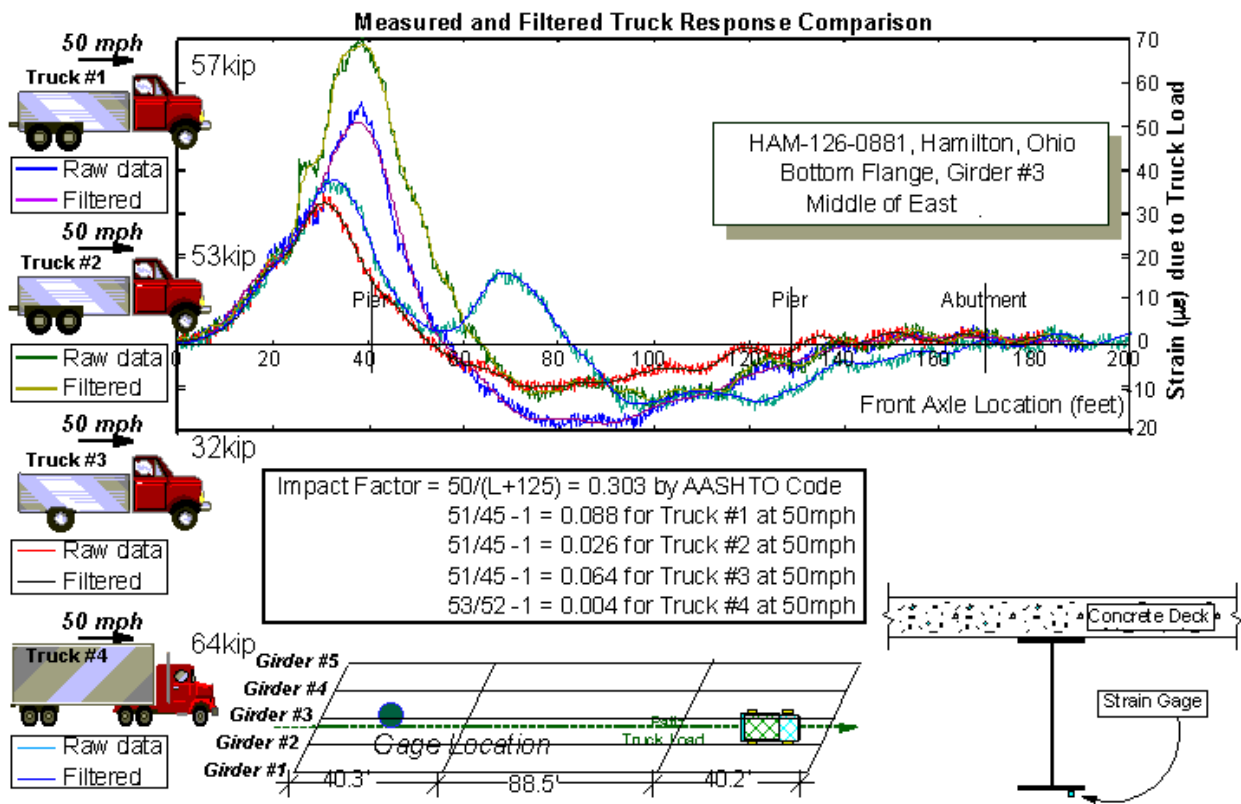


Figure 3-16: Impact Factor for Various Truckload Tests of HAM-126-0881

### 3.1.8. Capacity Load Rating

The design of a structure is based upon a set of loading conditions which the component or element must withstand. In order to form a consistent national basis for design, organizations such as AASHTO have developed methods for defining component and element capacities and a standard set of loading conditions to be considered against such capacities. In bridge engineering, there are two principal methods for design in use today: working stress and limit states. The intent for both methods is for the entire structure to operate well within the elastic or linear range of the constructed material. The point where a material ceases to behave elastically is defined as the proportional or yield limit. Once stress and strain are no longer proportional, the material enters the plastic range and a permanent deformation will occur to the member.

#### **Working or Allowable Stress Method**

For most of the century, the working stress approach was the standard by which bridges and other structural engineering projects were designed. An allowable stress is defined for each structural member to allow a safe margin below the controlling criterion under normal working conditions. Typically, the allowable stress is a fraction of some failure stress for the given material (e.g., yield or buckling stress for steel, compressive strength of concrete, etc.). For steel-stringer bridges, the allowable stress is the yield stress at the bottom flange of the girder ( $f_y$  as per the design plans or per Table 6.6.2.1-1 of the AASHTO Manual for Condition Evaluation) multiplied by a safety factor (SF, defined below).

## **Limit States or Load Factor Method**

By the 1970's, the limit states approach began to gain acceptance by the general engineering community and especially in the design of concrete structures. Concrete behaves linearly only over about half of its total compressive strength; hence, concrete elements designed under the working stress approach utilize much less than half of their capacity. The limit state approach makes use of the entire plastic range for the design of structural members and incorporates unique safety or load factors (LF, defined below) to account for the inherent variability of each loading configuration. Typically, the ultimate moment is defined to be equal to some failure stress for the given section (e.g., shear or plastic moment) which will vary depending upon the level of composite action between the steel girder and the concrete decking.

A belief that is fairly widespread in the transportation community is that the working stress method is overly conservative in the analysis of bridges. The AASHTO Guide states that the load factor method is intended to recognize "the large safety margins present" in the more conventional working stress method. In general, a well maintained bridge with redundant load paths will have a higher rating by the load factor method than with the working stress method. However, the AASHTO Guide emphasizes the use of site specific data and performance histories in the evaluation of the appropriate load factors for the structure; hence, a deteriorated bridge or a design susceptible to certain failure modes can actually be rated lower by the limit states method as opposed to the rote approach of the allowable stress method. The subjectivity of the limit states approach, therefore, places a great deal of responsibility on the design/test engineer and upon the transportation department as a whole.

## **Inventory and Operating Load Ratings**

A quantitative benchmark of the performance of any highway bridge has been standardized by AASHTO. It is not a magic bullet and its assumptions and limits are well known by the transportation field. The load rating, like inspection data, is only a gauge of bridge condition and a component in an overall profile of the structure. Unlike the inspection data, however, the load rating is calculated using analytical rather than subjective methods. One immediate use for the load rating is in the posting of a bridge (i.e., limiting the type and/or weights of vehicles which may pass over the structure). The load rating may also impact any decisions by the transportation department regarding maintenance, rehabilitation, or replacement of the bridge to meet the local, state, and federal requirements for the highway system.

AASHTO differentiates between lower and upper ranges of bridge performance. The lower or inventory range of performance is meant to imply safe use of the highway bridge on a day-to-day basis “for an indefinite period of time”. There are instances, however, when a vehicle has to carry an abnormally large load over the structure. While a structure can withstand these loads on occasion, it is not desirable to have them repeatedly pass over the structure. An upper or operating range of performance is meant to represent the “absolute maximum permissible load level to which the structure may be subjected.”

The inventory and operating rating factors (RF) can be calculated using either the allowable stress or the load factor method and are represented by the ratio of the remaining capacity-to-liveload for the specified design load. For allowable stress method, the remaining capacity is

considered as the factored yield stress reduced by any permanent loads (i.e., deadload,  $D$ , as defined below) upon the structure. For limit states method, the remaining capacity is considered as the ultimate moment reduced by the factored permanent load upon the structure. In the denominator, the liveload ( $L$ ) is increased by the impact factor and, if appropriate, its load factor. A safe structure necessitates that its rating factor is greater than one.

$$RF = \frac{C - LF_1 \cdot D}{LF_2 \cdot L \cdot (1 + IF)}$$

For the evaluation of rating factor for steel-stringer bridges, the following will be utilized by this research:

For Allowable Stress Method:	$LF_1 = LF_2 = 1$
Inventory Rating:	$C = 0.55 f_y$ (stress), $C = 0.55 f_y S_{LL}$ (moment, $M_{ASinv}$ )
Operating Rating:	$C = 0.75 f_y$ (stress), $C = 0.75 f_y S_{LL}$ (moment, $M_{ASopr}$ )
For Load Factor Method:	$C = \text{ultimate moment, } M_{ult}$
Inventory Rating:	$LF_1 = 1.3, LF_2 = 2.17$
Operating Rating:	$LF_1 = 1.3, LF_2 = 1.3$

where  $S_{LL}$  = sectional modulus as defined by the appropriate analytical method (see Section 3.5.1)

## Ultimate Moment by the Four Analysis Methods

The ultimate moment for a fully composite section (i.e., Method 1) is based upon the property of compactness. Symmetrical I-shaped beams are defined as compact if they possess a high resistance to local buckling and they provide proper bracing to resist lateral torsional buckling. Compact sections will therefore form a plastic “hinge” at the ultimate moment. The AASHTO Specification for compactness of a fully composite design is met if the depth or centroid location  $y_a$  for the compressive stress zone or block in the concrete deck is less than the given limit.

$$y_a = \frac{(A_s f_y - A_r N_r f_{yr})}{0.85 \cdot b_{eff} f_c} < \frac{h + t_d}{7.75} \text{ for compactness of a fully composite design}$$

where  $A_r$  = area of rebar,  $N_r$  = #rebars longitudinal in decking for the section,  $f_{yr}$  = yield stress for rebar.

If the section is determined as compact, then the ultimate moment is defined as that moment which causes the section to completely shear (i.e., the stress in every fiber of the beam and every layer of the decking for its equivalent area of steel will meet or exceed the plastic limit  $f_y$ ).  $M_{ult,1} = A_s f_y (y_a - y_s)$ .

If the section is determined as noncompact, then the ultimate moment is defined as that moment which causes the first instance of yielding for the section (i.e., at the outer face of the bottom flange of the steel beam), which is substantially less than that defined for a compact section.

$$M_{ult,1} = S_1 f_y.$$

The ultimate moment for a fully composite section with modified effective width  $b_{eff2}$  for the decking (i.e., Method 2) is also defined by the compactness of the section. However, the effective width and the sectional modulus  $S_2$  is varied depending upon the level of composite action in the section; hence, the ultimate moment also varies accordingly between the two extremes given above. In Figure 3-15, a change in the section's compactness is apparent just after the section exceeds 100% remaining composite action; the ultimate moment is increased to that specified for a compact section simply because the exponential increase in effective deck width has brought the depth  $y_a$  of the compressive block within the specified limits.

The ultimate moment for a partially composite section (i.e., Method 3) is also defined by the compactness of the section. The check for compactness will yield the same results as Method 1 because all of the parameters remain unchanged by Method 3. If the section is determined to be noncompact, then the ultimate moment will vary based upon the section modulus  $S_3$  that is linearly adjusted based upon the level of composite action for the section (see Figure 3-15). If the section is determined to be compact, then this same linear variation is enforced by adjusting the ultimate moment between the two extremes given by Method 1 with the identified RCA for the section.  $M_{ult,3} = RCA [A_s f_y (y_a - y_s) - S_1 f_y] + S_1 f_y$ .

The ultimate moment for a compact and noncomposite beam (i.e., Method 4) is defined as  $M_{ult,4} = Z_x f_y$ . Compactness checks are also relevant for the steel girder, but rolled I-beams are typically fabricated to meet the appropriate specifications. The plastic modulus  $Z_x$  may be calculated directly as that moment which causes the beam to completely shear through the section (i.e., the stress in every fiber of the beam will meet or exceed the plastic limit  $f_y$ ). However, the plastic

modulus is well documented in the literature for the common beam types used in bridge construction.

### **Deadload Moment by the Four Analysis Methods**

Permanent or dead loads on the superstructure are those loads which always remain and act on the bridge throughout its lifetime. The deadload is the aggregate weight of all superstructure elements acting upon the bridge (i.e., the superstructure must bear its own weight). The capacity of the bridge is reduced accordingly and can be significant in and of themselves. The deadload includes the steel girders, the secondary steel members (e.g., crossframes, splice plates, stiffeners), the concrete decking, its layers of reinforcing rebar, and any stay-in-place formwork. By definition, the deadload acts upon the noncomposite section and its moment  $M_{DL}$  is determined from first principals for the steel beam and its supports (as demonstrated in Chapter 2 for a 3-span simply supported beam and in Appendix B1 for HAM-126-0881). The deadload stress is determined from the sectional modulus for the steel beam alone (i.e.,  $\sigma_{DL} = M_{DL}/S_{DL}$ ,  $S_{DL} = I_s/y_s$ ). The effective deadload moment depends upon the section modulus at the event under consideration; during the diagnostic truckload test, the section modulus is determined by one of the four analytical methods (see Section 3.1.5) and the effective deadload moment is similarly determined (i.e.,  $M_{DL\text{eff}} = \sigma_{DL} S_{LL}$ ,  $S_{LL} = \{S_1, S_2, S_3, \text{ or } S_4\}$ ).

A distinction is made regarding deadload that is constructed or placed on the superstructure after the concrete decking has cured and begun working with the steel framing to resist any load. The superimposed deadload includes the concrete sidewalk and parapet, their reinforcement, any wearing surface for the roadway, utilities and their infrastructure, and transportation signing and

lighting. The superimposed deadload moment  $M_{SDL}$  is also determined from first principals for the steel beam alone and its supports. For a section designed as fully composite, AASHTO allows for the superimposed deadload to act upon a partial composite section with a section modulus  $S_{SDL}$  defined by an effective strength ratio of  $3n_{eff}$  (see equations in Section 3.1.5 above). Hence,  $S_{DL} = I_s/y_s < S_{SDL} < S_1 = I_t/y_t$  and the computed stress for superimposed deadload will not be as significant for a fully composite section (i.e.,  $\sigma_{SDL} = M_{SDL}/S_{SDL}$ ) as it would be for a noncomposite design (i.e.,  $\sigma_{SDL} = M_{SDL}/S_{DL}$ ). The effective superimposed deadload moment depends upon the section modulus at the event under consideration; during the diagnostic truckload test, the section modulus is determined by one of the four analytical methods (see Section 3.1.5) and the effective superimposed deadload moment is similarly determined (i.e.,  $M_{SDL_{eff}} = \sigma_{SDL} S_{LL}$ ,  $S_{LL} = \{S_1, S_2, S_3, \text{ or } S_4\}$ ).

### **Truck Liveload Moment and Rating by the Four Analysis Methods**

In general, the principal loading constraint which highway bridges are designed by is truck loading. Given the variety of trucks in use, it was determined that a standard set of design loading caused by truck traffic needed to be developed. In the early part of the century, designers utilized a train of trucks as design loading for their bridges. As the highway trucking industry grew, and along with it truckloads, bridges began to show evidence of overstressing in structural components. In 1944, a suite of hypothetical truck classes designated as H and HS class trucks were developed by AASHTO. These vehicles were created with two and three axles, respectively, set at specified spacing. These truck classes still represent the core standard in use today in the United States. For this research, we will specifically examine the HS20-44 truck classification (see Figure 3-17).

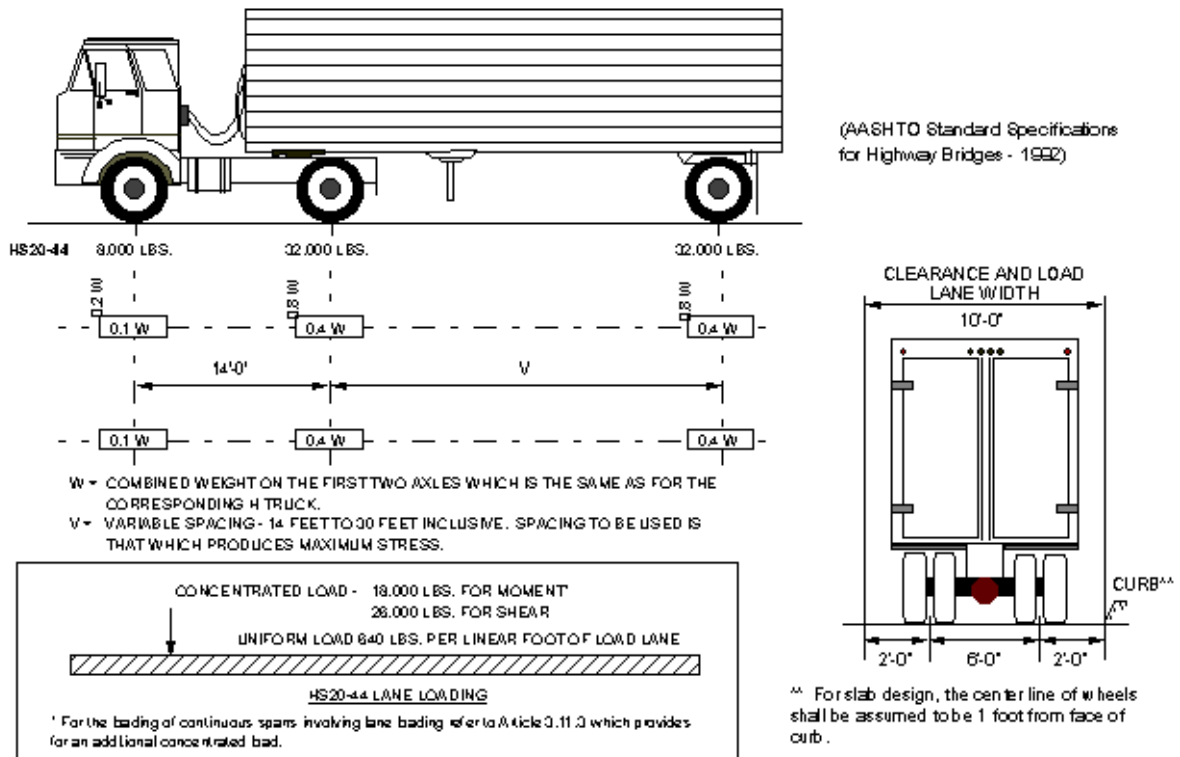


**Figure 3-17: AASHTO Truck and Lane Load Specifications**

The AASHTO specification requires the evaluation of a worst-case scenario where one design truckload is present in each lane. Typically, the maximum response occurs where the trucks are side-by-side in the lanes due to the symmetry of the bridge; however, this may not always be the case (e.g., skewed or curved bridges, damaged structures). A reduction in liveload response is allowed for bridges with three or more lanes (i.e., 10% for three lanes, 25% otherwise) to account for the reduced likelihood that this event will actually occur in the lifetime of the structure. Note that the rear axle spacing for the design truck is variable from 14 to 30 feet to allow for the variability in this parameter in the normal traffic population. For most cases, the smaller axle spacing causes the greater liveload response for the bridge; however, a longer axle spacing may be appropriate for identifying the negative moment at the pier section (based upon the characteristic influence line for a pier support, see Figure 3-2).

The AASHTO design truckload is meant to cover a lateral width of ten feet within a traffic lane width of twelve feet. No fractional lane widths are to be considered in the load rating. The traffic lanes are considered to be spaced evenly across the width of the structure; however, this is generally not the case due to sidewalks, parapets, and traffic shoulders. The AASHTO Manual for Condition Evaluation indicates that “when conditions of traffic movements and volume would warrant it, fewer traffic lanes than specified by AASHTO may be considered”. The Structure Rating chapter of the ODOT Specifications Manual indicates that the “traffic lanes to be used for rating purposes shall be the actual marked travel lanes”. In this paper, the latter specification shall be met and only the marked travel lanes will be considered in the following load ratings.

### **Example Truck Liveload Moment and Rating for HAM-126-0881**

The HS20-44 truckload is virtually simulated in each marked traffic lane by linear superposition of the derived influence lines (see Figure 2-4), weighted by the specified axle weights (see Figure 3-17). The liveload is calculated by each of the four analytical methods and then summarily rated by both the allowable stress and load factor approaches. Inventory and Operating levels are determined for both rating approaches. Note that the corresponding effective deadload  $M_{DLeff}$  and superimposed deadload  $M_{SDLeff}$  moments are used with the calculated liveload  $M_{LL} = \{M_1, M_2, M_3, \text{ or } M_4\}$  moment by the four analytical methods.

The liveload moments calculated for the HS20-44 truckload for the middle span by the four analytical methods are presented in Figure 3-18. The load rating for the middle span is selected as the minimum rating by Method 2 (see Figure 3-19), since the section was designed and is identified as fully composite (see Figure 3-6). Note the similarities between Methods 1, 2, and 3 except with regards to the load factor rating; this discrepancy is due to the distinction between compactness determined by each method (i.e., Methods 1 and 3 indicate noncompact behavior, while Method 2 indicates compact behavior due to its large effective width for the decking). A summary tabulation is presented in Figure 3-20, where the nominal values expected from design (D) are listed in the final row for comparison.

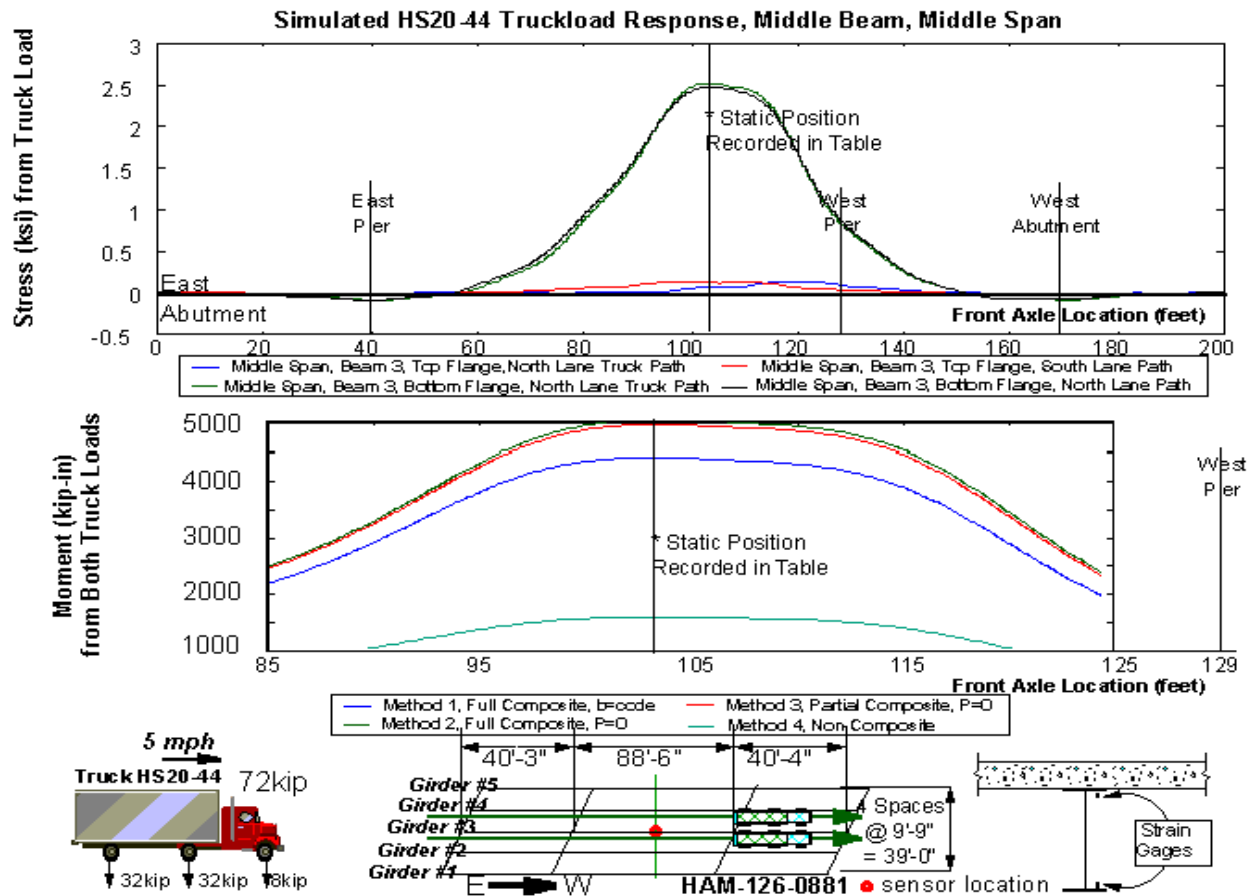
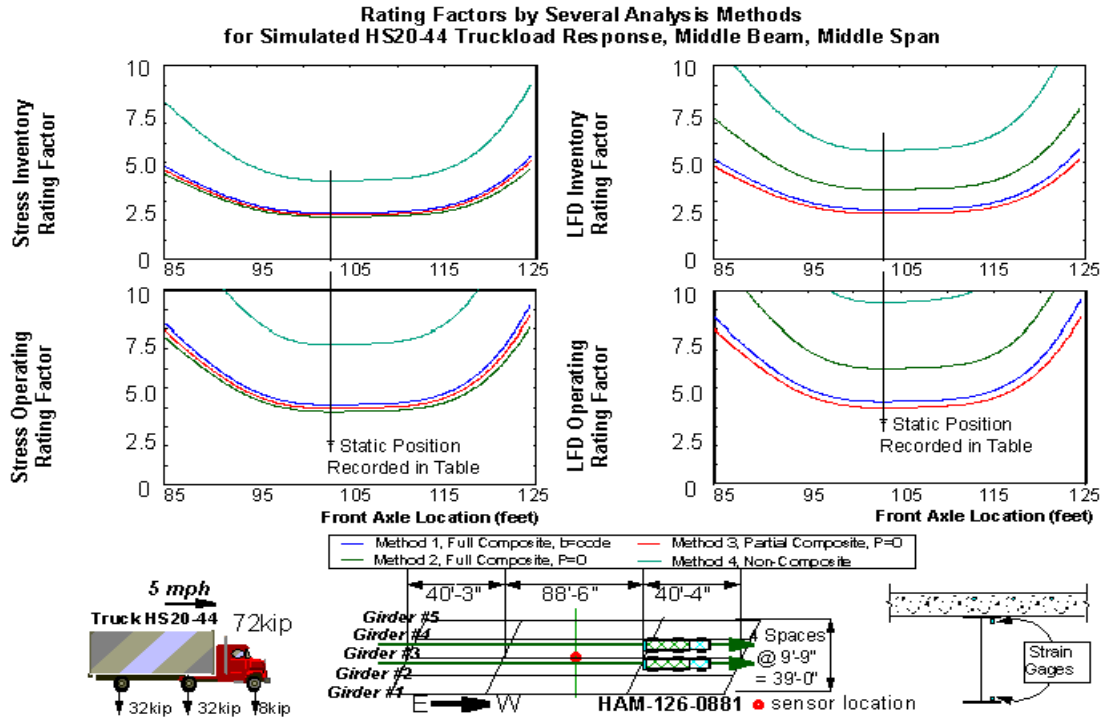


Figure 3-18: Liveload Stress and Moment of Simulated HS20 Truckload for the Middle Span



**Figure 3-19: Rating Factors of Simulated HS20 Truckload for Middle Span**

Analysis Method for Measured Response	Stress Inventory Moment (kip-in)	Stress Operating Moment (kip-in)	Ultimate Moment (kip-in)	Stress Inventory Rating Factor	Stress Operating Rating Factor	LFD Inventory Rating Factor	LFD Operating Rating Factor
<b>1</b> Full Composite, P=65 Effective Deck Width = 93" Centroid Located at 33.2" Live Load = 4,413 kip-in Section Modulus = 938 in <sup>3</sup>	25,798	35,179	46,890	<b>2.40</b>	<b>4.13</b>	<b>2.57</b>	<b>4.29</b>
<b>2</b> Full Composite, P=0 Effective Deck Width = 175" Centroid Located at 36.4" Live Load = 5,053 kip-in Section Modulus = 980 in <sup>3</sup>	26,939	36,735	70,596	<b>2.19</b>	<b>3.76</b>	<b>3.94</b>	<b>6.58</b>
<b>3</b> Partial Composite, P=0 Effective Deck Width = 93" Centroid Located at 33.2" Live Load = 4,975 kip-in Section Modulus = 965 in <sup>3</sup>	27,635	37,684	49,227	<b>2.32</b>	<b>3.96</b>	<b>2.39</b>	<b>3.99</b>
<b>4</b> No Composite, P=139 Effective Deck Width = n/a Centroid Located at 18.17" Live Load = 1,600 kip-in Section Modulus = 622 in <sup>3</sup>	17,107	23,328	35,900	<b>4.06</b>	<b>7.21</b>	<b>5.62</b>	<b>9.38</b>
<b>D</b> No Composite, P=0 Effective Deck Width = n/a Centroid Located at 40" Live Load = 9,790 kip-in Section Modulus = 938 in <sup>3</sup>	25,798	35,179	46,890	<b>1.09</b>	<b>1.86</b>	<b>1.16</b>	<b>1.94</b>

**Figure 3-20: Summary of Condition Assessment Results for Middle Span**

The liveload moments calculated for the HS20-44 truckload for the east span by the four analytical methods are presented in Figure 3-21. The load rating for the east span is selected as the minimum rating by Method 3 (see Figure 3-22), since the section is identified as partially composite (see Figure 3-8). Note the similarities between Methods 2 and 3 in all cases. A summary tabulation is presented in Figure 3-23, where the nominal values expected from design (D) are listed in the final row for comparison.

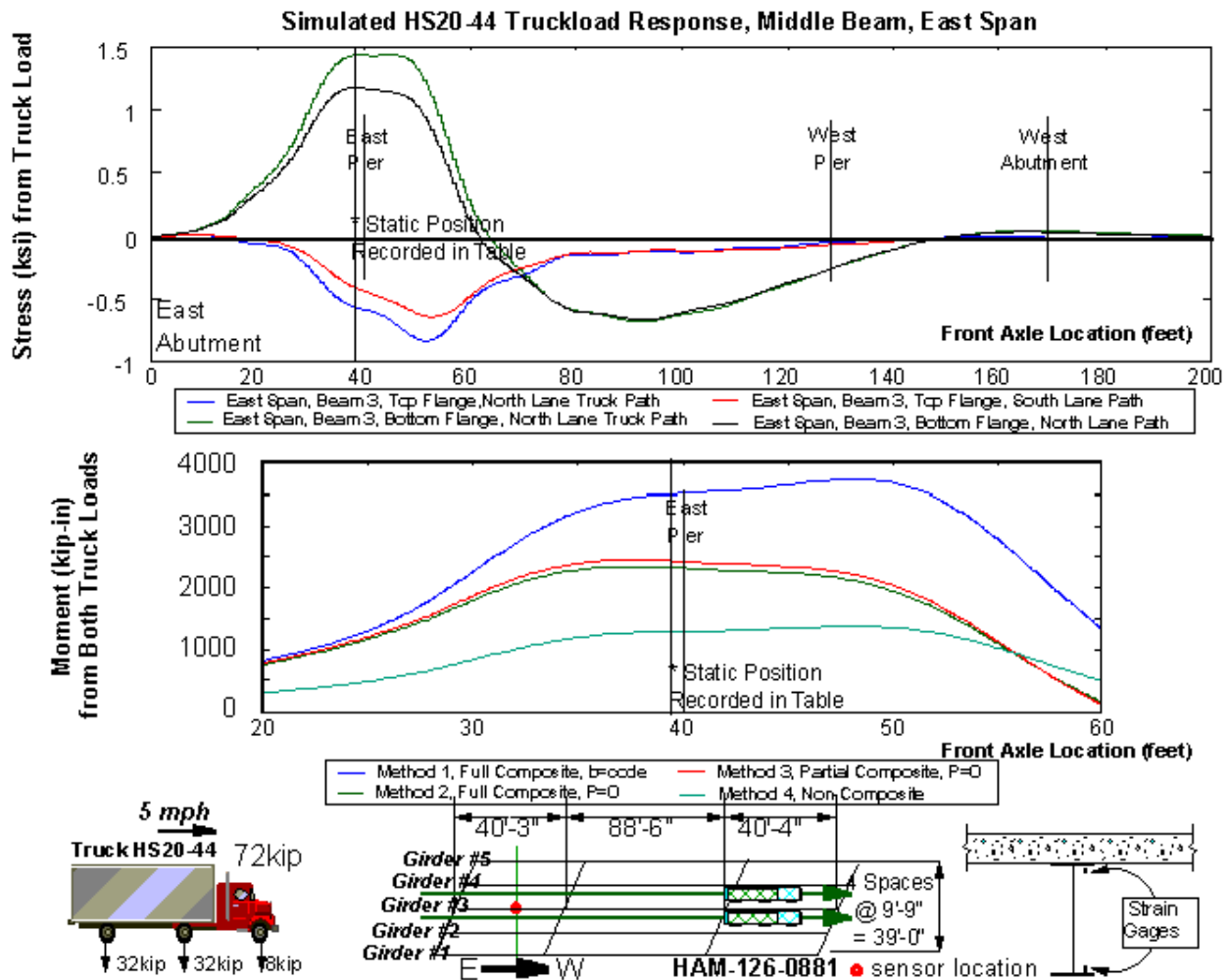
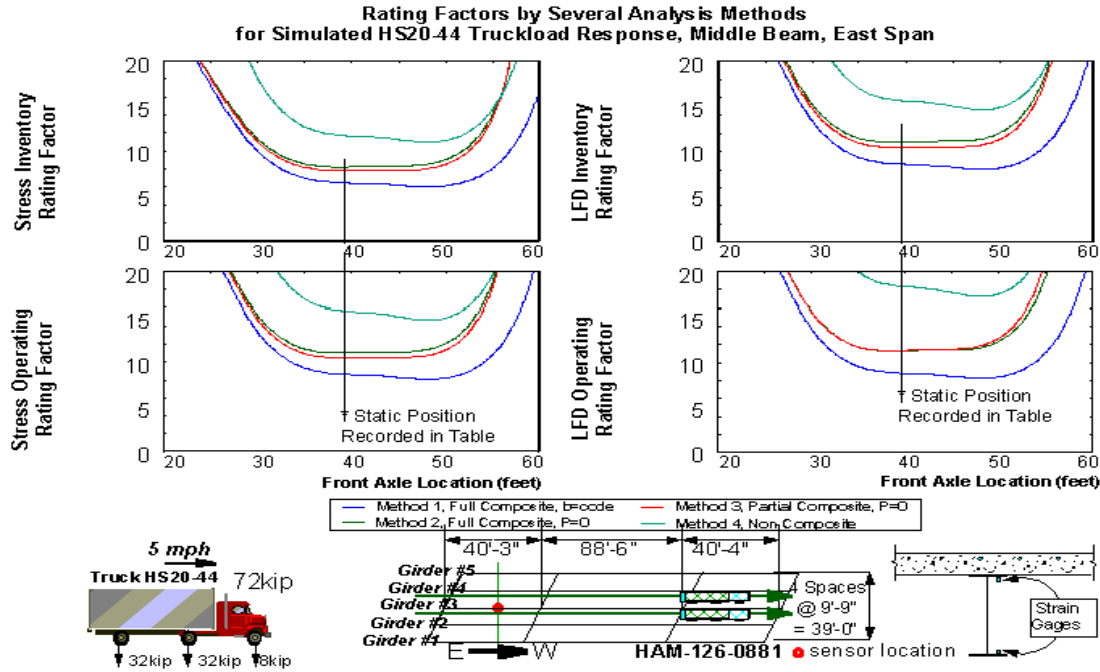


Figure 3-21: Liveload Stress and Moment of Simulated HS20 Truckload for the East Span



**Figure 3-22: Rating Factors of Simulated HS20 Truckload for the East Span**

Analysis Method for Measured Response	Stress Inventory Moment (kip-in)	Stress Operating Moment (kip-in)	Ultimate Moment (kip-in)	Stress Inventory Rating Factor	Stress Operating Rating Factor	LFD Inventory Rating Factor	LFD Operating Rating Factor
<b>1 Full Composite, P=111</b> Effective Deck Width = 93" Centroid Located at 33" Live Load = 3,499 kip-in Section Modulus = 995 in <sup>3</sup>	27,370	37,323	49,764	<b>6.45</b>	<b>8.64</b>	<b>5.30</b>	<b>8.85</b>
<b>2 Full Composite, P=0</b> Effective Deck Width = 27" Centroid Located at 26" Live Load = 2,424 kip-in Section Modulus = 879 in <sup>3</sup>	24,167	32,954	45,762	<b>8.23</b>	<b>11.01</b>	<b>7.02</b>	<b>11.72</b>
<b>3 Partial Composite, P=0</b> Effective Deck Width = 93" Centroid Located at 33" Live Load = 2,442 kip-in Section Modulus = 885 in <sup>3</sup>	22,973	31,327	44,271	<b>7.82</b>	<b>10.44</b>	<b>6.77</b>	<b>11.30</b>
<b>4 No Composite, P=46.5</b> Effective Deck Width = n/a Centroid Located at 18.25" Live Load = 1,288 kip-in Section Modulus = 663 in <sup>3</sup>	18,232	24,863	38,350	<b>11.73</b>	<b>15.68</b>	<b>11.05</b>	<b>18.45</b>
<b>D No Composite, P=0</b> Effective Deck Width = n/a Centroid Located at 18.25" Live Load = 3,711 kip-in Section Modulus = 663 in <sup>3</sup>	18,232	24,863	38,350	<b>4.07</b>	<b>5.44</b>	<b>3.83</b>	<b>6.40</b>

Truck HS20-44 72kip  
32kip 32kip 8kip

Girder #5  
Girder #4  
Girder #3  
Girder #2  
Girder #1  
E     W  
HAM-126-0881 • sensor location  
Spaces @ 9'-9" = 39'-0"

**Figure 3-23: Summary of Condition Assessment Results for East Span**

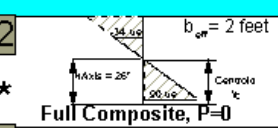
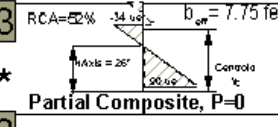
Note that the capacities for the east span as a composite section (i.e., identified by Methods 1, 2, and 3) are significantly higher than the capacity for the noncomposite steel beam (i.e., Method 4) as designed. Although partial composite action is clearly present in the measured data from the diagnostic load test, it is not clear whether this additional strength for the section would actually exist at the allowable stress. Most certainly, the unintended composite action would not remain at the ultimate or plastic moment of the limit state approach. The Structure Rating chapter of the ODOT Specifications Manual indicates that the “members shall be analyzed as to the intended method of design”. In this paper, the ODOT specification shall be met and a reduced load rating will also be determined for any section with unintended composite action. The reduced load ratings by Methods 2 and 3 for the east span are presented in Figure 3-24.

The noncomposite capacities shall be utilized (i.e.,  $M_{ASinv} = 0.55 f_y S_4$ ,  $M_{ASopr} = 0.75 f_y S_4$ , and  $M_{ult} = Z_x f_y$ ).

Further, the effective deadload and superimposed deadload shall be assigned those moments calculated by first principals for a noncomposite beam (i.e.,  $M_{DLeff} = M_{DL}$  and  $M_{SDLeff} = M_{SDL}$ ).

Note that the liveload moment must still be defined by the unintended composite action for the section (i.e.,  $M_{LL} = \{M_1, M_2, \text{ or } M_3\}$ ) to account for the current condition of the structure. It seems contrary to define the liveload by the current bridge condition of partial composite action and yet define the remaining capacity by the assumed noncomposite action at the allowable stress and limit state. However, note that this would lead to a ridiculously large rating factor for the section (i.e.,  $M_3 \sim 2 M_4$ , Figure 3-23).

This modified approach is identical in concept and almost equivalent in practice to that suggested by the NCHRP Manual for Bridge Rating discussed in Section 3.1.1. The significant difference between the NCHRP Manual and this method for rating reduction is the acknowledgement of partial composite action. The NCHRP Manual suggests using the live load moment for full composite action, although this would actually overcompensate for a section with only partial composite action (i.e.,  $M_1 > M_3$ , Figure 3-23).

Analysis Method for Measured Response	Stress Inventory Moment (kip-in)	Stress Operating Moment (kip-in)	Ultimate Moment (kip-in)	Stress Inventory Rating Factor	Stress Operating Rating Factor	LFD Inventory Rating Factor	LFD Operating Rating Factor
 <p>Full Composite, <math>P=0</math></p>	24,167	32,954	45,762	8.23	11.01	7.02	11.72
<p>Live Load Demand 2,334 (kip-in)</p>	18,232	24,863	38,350	6.23	8.33	5.87	9.80
 <p>Partial Composite, <math>P=0</math></p>	22,973	31,327	44,271	7.82	10.44	6.77	11.30
<p>Live Load Demand 2,442 (kip-in)</p>	18,232	24,863	38,350	6.19	8.27	5.83	9.73

Notes: \* Assumes composite action remains at limit state. Capacity includes deck strength.  
 \*\* AASHTO Code. Assumes interface slippage at limit state. Capacity based only upon girder.

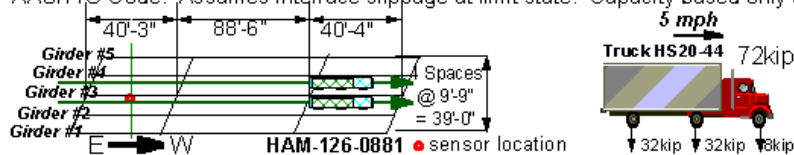


Figure 3-24: Reduced Rating Factors for Unintended Composite Action in East Span

The liveload moments calculated for the HS20-44 truckload for the east pier by the four analytical methods are presented in Figure 3-25. As the pier is designed as a noncomposite section, the load ratings are reduced to remove the effect of unintended composite action upon the remaining sectional capacity. The load rating for the east span is selected as the minimum rating by Method 3 (see Figure 3-26), since the section is identified as partially composite. Note the similarities between Methods 2 and 3 in all cases. A summary tabulation is presented in Figure 3-27, where the nominal values expected from design (D) are listed in the final row for comparison.

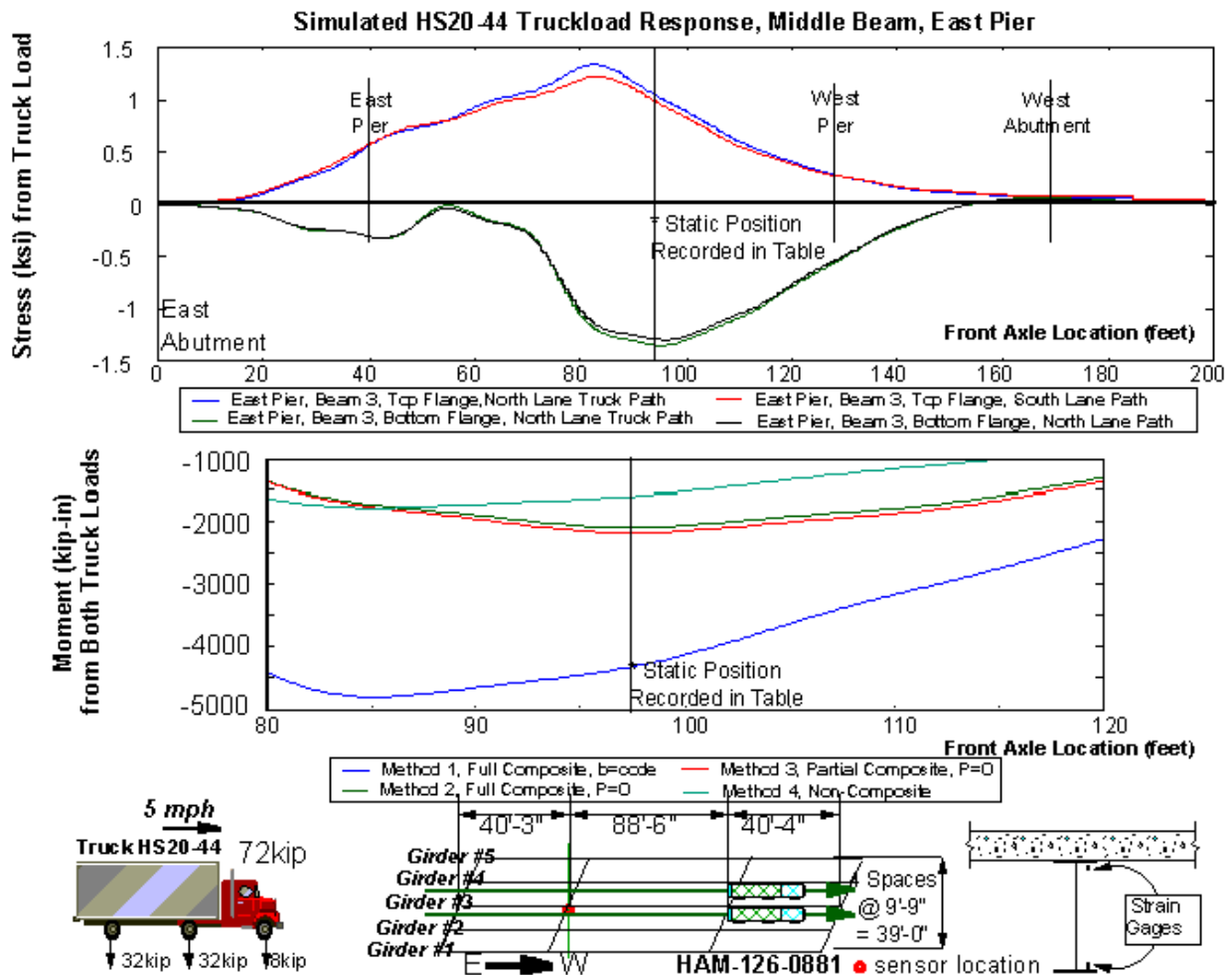
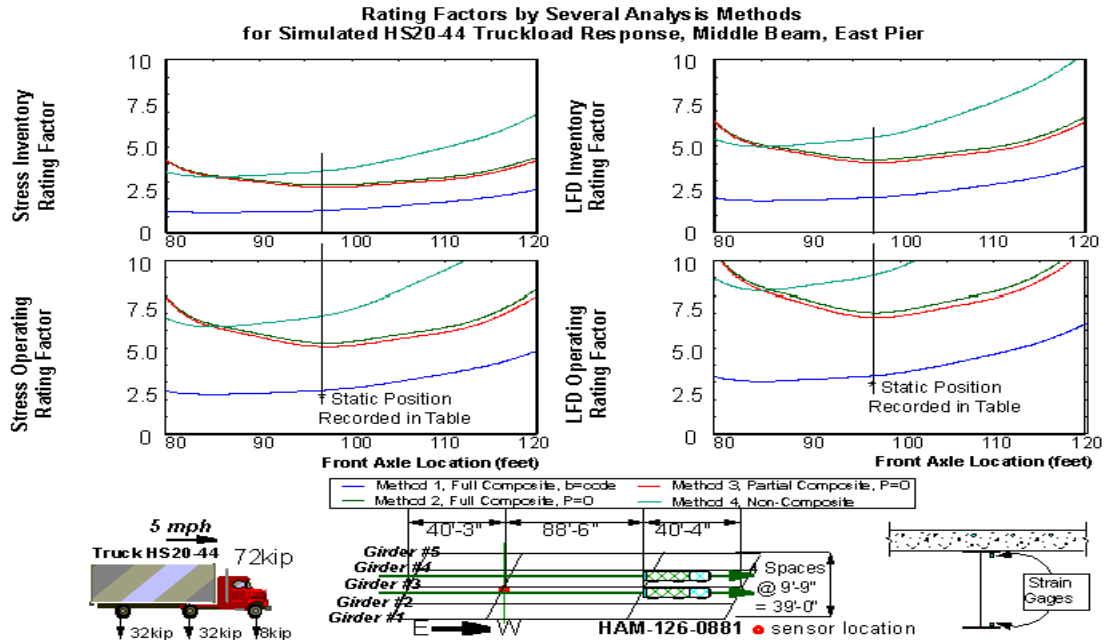
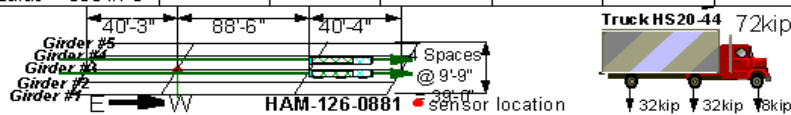


Figure 3-25: Liveload Stress and Moment of Simulated HS20 Truckload for the East Pier



**Figure 3-26: Rating Factors of Simulated HS20 Truckload for the East Pier**

Analysis Method for Measured Response	Stress Inventory Moment (kip-in)	Stress Operating Moment (kip-in)	Ultimate Moment (kip-in)	Stress Inventory Rating Factor	Stress Operating Rating Factor	LFD Inventory Rating Factor	LFD Operating Rating Factor
<b>1 Full Composite, P=229</b> Effective Deck Width = 93" Centroid Located at 33" Live Load = -4,332 kip-in Section Modulus = 995 in <sup>3</sup>	-18,233	-24,863	-38,350	<b>3.91</b>	<b>7.47</b>	<b>5.96</b>	<b>9.95</b>
Assumes interface slippage at limit state. Capacity based only upon girder							
<b>2 Full Composite, P=0</b> Effective Deck Width = 8.3" Centroid Located at 21.2" Live Load = -2,138 kip-in Section Modulus = 765 in <sup>3</sup>	-18,233	-24,863	-38,350	<b>2.70</b>	<b>5.15</b>	<b>4.12</b>	<b>6.87</b>
Assumes interface slippage at limit state. Capacity based only upon girder							
<b>3 Partial Composite, P=0</b> Effective Deck Width = 93" Centroid Located at 33" Live Load = -2,172 kip-in Section Modulus = 777 in <sup>3</sup>	-18,233	-24,863	-38,350	<b>2.66</b>	<b>5.07</b>	<b>4.05</b>	<b>6.76</b>
Assumes interface slippage at limit state. Capacity based only upon girder							
<b>4 No Composite, P=-22.3</b> Effective Deck Width = n/a Centroid Located at 18.25" Live Load = -1,595 kip-in Section Modulus = 663 in <sup>3</sup>	-18,233	-24,863	-38,350	<b>3.62</b>	<b>6.91</b>	<b>5.52</b>	<b>9.21</b>
<b>D No Composite, P=0</b> Effective Deck Width = n/a Centroid Located at 18.25" Live Load = -4,756 kip-in Section Modulus = 663 in <sup>3</sup>	-18,233	-24,863	-38,350	<b>1.21</b>	<b>2.32</b>	<b>1.85</b>	<b>3.09</b>



**Figure 3-27: Summary of Condition Assessment Results for East Pier**

Parameter	Theory East Span	Identified East Span	Theory East Pier	Identified East Pier	Theory Mid Span	Identified Mid Span
Steel Beam	W136x194	As design	W136x194	As design	W136x182	As design
Comp Action	None	Partial	None	None	Full	Full
Bottom Strain	+177.6 ue	+90.5 ue	+312 ue	-90.7 ue	+444 ue	+172 ue
Top Strain	-177.6 ue	-34.2 ue	-312 ue	63.7 ue	-41.2 ue	+6.28 ue
Neutral Axis	18.25"	25.92"	18.25"	21.22"	33.2"	36.44"
Curvature	+9.73 ue/in	+3.67 ue/in	-17.1 ue/in	-4.54 ue/in	+13.3 ue/in	+4.88 ue/in
M <sub>DL</sub>	-1097 kip-in	As design	-8680 kip-in	As design	6540 kip-in	As design
M <sub>SDL</sub>	-353 kip-in	As design	-2250 kip-in	As design	2550 kip-in	As design
Impact Factor	0.303	As design	0.265	As design	0.235	As design
Distribution	0.886	0.957	0.886	As design	0.886	0.702
Method 1					used in rating	
M <sub>I,Leff</sub>	N/a	3499 kip-in	N/a	-4332 kip-in	9790 kip-in	4413 kip-in
Axial Force		-111 kips		228 kips	0	65.1 kips
M <sub>DL,eff</sub>		-1646 kip-in		-8680 kip-in	9845 kip-in	9858 kip-in
M <sub>SDL,eff</sub>		-394 kip-in		-2250 kip-in	2834 kip-in	2837 kip-in
Method 2						used in rating
Deck Width		27.40"		8.26"	93"	175"
M <sub>I,Leff</sub>	N/a	2424 kip-in	N/a	-2138 kip-in	N/a	5054 kip-in
M <sub>DL,eff</sub>		-1453 kip-in		-8680 kip-in		10296 kip-in
M <sub>SDL,eff</sub>		-353 kip-in		-2250 kip-in		2963 kip-in
Method 3		used in rating		used in rating		
RCA		51.88%		20.11%		121.2%
M <sub>I,Leff</sub>	N/a	2442 kip-in	N/a	-2172 kip-in	N/a	4975 kip-in
M <sub>DL,eff</sub>		-1464 kip-in		-8680 kip-in		10137 kip-in
M <sub>SDL,eff</sub>		-353 kip-in		-2250 kip-in		2917 kip-in
Method 4	used in rating		used in rating			
M <sub>I,Leff</sub>	3711 kip-in	1288 kip-in	-4756 kip-in	-1595 kip-in	N/a	1600 kip-in
Axial Force	0	46.5 kips	0	-22.3 kips		139 kips
M <sub>DL,eff</sub>	-1097 kip-in	-1097 kip-in	-8680 kip-in	-8680 kip-in		6540 kip-in
M <sub>SDL,eff</sub>	-353 kip-in	-353 kip-in	-2250 kip-in	-2250 kip-in		2550 kip-in
Capacity, Inv	18230 kip-in	22970 kip-in	-18230 kip-in	-18230 kip-in	25798 kip-in	26380 kip-in
AS Rating, Inv	4.069	7.818	1.213	2.659	1.086	2.193
Capacity, Opr	24860 kip-in	31330 kip-in	-24860 kip-in	-24860 kip-in	35179 kip-in	35970 kip-in
AS Rating, Opr	5.440	10.444	2.315	5.073	1.861	3.764
Ult. Capacity	38350 kip-in	44270 kip-in	38350 kip-in	38350 kip-in	46890 kip-in	64530 kip-in
LF Rating, Inv	3.833	6.771	1.849	4.051	1.158	3.942
LF Rating, Opr	6.400	11.302	3.087	6.762	1.935	6.581

**Table 3-3: Theoretical and Identified Parameters for HS20 Truck on Bridge, HAM-126-0881, Unintended Composite Action is Allowed for Identified Parameters at Limit States**

	Theory	Identified	Theory	Identified	Theory	Identified
Parameter	East Span	East Span	East Pier	East Pier	Mid Span	Mid Span
Steel Beam	W136x194	As design	W136x194	As design	W136x182	As design
Comp Action	None	None	None	None	Full	Full
Bottom Strain	+177.6 ue	+90.5 ue	+312 ue	-90.7 ue	+444 ue	+172 ue
Top Strain	-177.6 ue	-34.2 ue	-312 ue	63.7 ue	-41.2 ue	+6.28 ue
Neutral Axis	18.25"	25.92"	18.25"	21.22"	33.2"	36.44"
Curvature	+9.73 ue/in	+3.67 ue/in	-17.1 ue/in	-4.54 ue/in	+13.3 ue/in	+4.88 ue/in
M <sub>DL</sub>	-1097 kip-in	As design	-8680 kip-in	As design	6540 kip-in	As design
M <sub>SDL</sub>	-353 kip-in	As design	-2250 kip-in	As design	2550 kip-in	As design
Impact Factor	0.303	As design	0.265	As design	0.235	As design
Distribution	0.886	0.957	0.886	As design	0.886	0.702
Method 1	As above	As above	As above	As above	As above	As above
Method 2	As above	As above	As above	As above	As above	As above
Method 3		used in rating		used in rating		
RCA		51.88%		20.11%		121.2%
M <sub>I,eff</sub>	N/a	2442 kip-in	N/a	-2172 kip-in	N/a	4975 kip-in
M <sub>DL,eff</sub>		<i>-1097 kip-in</i>		-8680 kip-in		10137 kip-in
M <sub>SDL,eff</sub>		<i>-353 kip-in</i>		-2250 kip-in		2917 kip-in
Method 4	As above	As above	As above	As above	As above	As above
Capacity, Inv	18230 kip-in	<i>18230 kip-in</i>	-18230 kip-in	-18230 kip-in	25798 kip-in	26380 kip-in
AS Rating, Inv	4.069	<i>6.188</i>	1.213	2.659	1.086	2.193
Capacity, Opr	24860 kip-in	<i>24860 kip-in</i>	-24860 kip-in	-24860 kip-in	35179 kip-in	35970 kip-in
AS Rating, Opr	5.440	<i>8.273</i>	2.315	5.073	1.861	3.764
Ult. Capacity	38350 kip-in	<i>38350 kip-in</i>	38350 kip-in	38350 kip-in	46890 kip-in	<i>46890 kip-in</i>
LF Rating, Inv	3.833	<i>5.830</i>	1.849	4.051	1.158	<i>2.209</i>
LF Rating, Opr	6.400	<i>9.731</i>	3.087	6.762	1.935	<i>3.687</i>

**Table 3-4: Theoretical and Identified Parameters for HS20 Truck on Bridge, HAM-126-0881, Composite Action as Designed is Enforced for Identified Parameters at Limit States, Ultimate Capacity is Limited as per Noncompact but Composite Section**

Note: Changes from the previous table are identified in italics.

Table 3-3 summarizes the condition assessment results for the HS20 truckload rating of HAM-126-0881. Table 3-4 summarizes the reduced rating factors when unintended composite is not assumed for the east span at the allowable stress or limit state. Further, Table 3-4 presents the reduced load factor rating for the middle span when noncompact performance for the section is enforced. The depth of the compressive stress block determined by Method 2 is suspect due to the exponential variation in effective deck width. Hence, the compact nature of the middle span assumed in Table 3-3 is not permitted in Table 3-4. Note that the middle span is the controlling factor in all cases of condition assessment for truckload response.

### **Lane Liveload Moment and Rating by the Four Analysis Methods**

Replacing the train of trucks in the 1935 design code are laneload configurations which approximate a 40kip truck followed by a train of 30kip trucks. To model this, a uniform distributed laneload is used combined with a concentrated force or point load. For the HS20-44 specification, the laneload is 0.64kip per linear foot and the point load is 18kip (see Figure 3-17). Note that the laneload is not necessarily continuous over the length of the structure or even within the length of any given span; the laneload is distributed in order to cause the greatest response for the simulated train of vehicles. For simple span (i.e., noncontinuous) bridges and for positive moment considerations, a single point load is used to determine the maximum liveload response; however, for negative moment evaluation of a continuous bridge design, a second point load (equal in weight to the first point load) is placed in the adjoining span to determine the maximum liveload response (based upon the characteristic influence line for a pier support, see Figure 3-2). Where truckloads generally govern for short span bridges, the laneload generally governs for long and continuous span bridges.

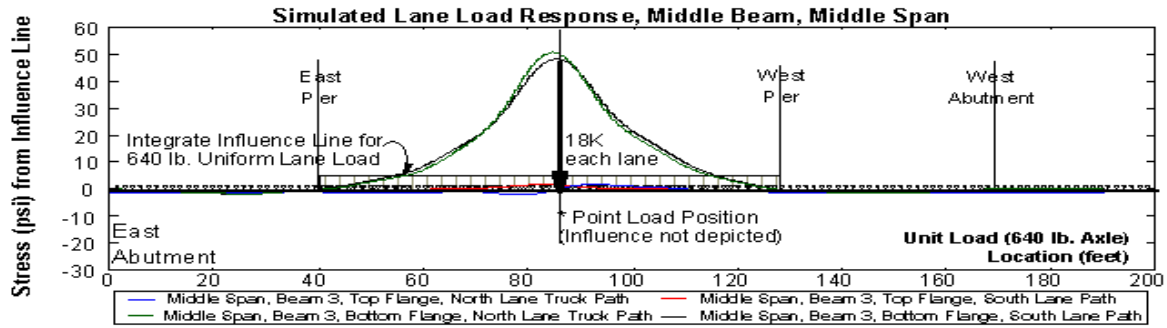
The AASHTO specification requires the evaluation of a worst-case scenario where each design lane is loaded and point load(s) are present in each lane. Typically, the maximum response occurs where the point loads are side-by-side in the lanes due to the symmetry of the bridge; however, this may not always be the case (e.g., skewed or curved bridges, damaged structures). A reduction in liveload response is allowed for bridges with three or more lanes (i.e., 10% for three lanes, 25% otherwise) to account for the reduced likelihood that this event will actually occur in the lifetime of the structure.

The AASHTO design laneload is meant to cover a lateral width of ten feet within a traffic lane width of twelve feet. No fractional lane widths are to be considered in the load rating. The traffic lanes are considered to be spaced evenly across the width of the structure; however, this is generally not the case due to sidewalks, parapets, and traffic shoulders. The AASHTO Manual for Condition Evaluation indicates that “when conditions of traffic movements and volume would warrant it, fewer traffic lanes than specified by AASHTO may be considered”. The Structure Rating chapter of the ODOT Specifications Manual indicates that the “traffic lanes to be used for rating purposes shall be the actual marked travel lanes”. In this paper, the latter specification shall be met and only the marked travel lanes will be considered in the following load ratings.

### **Example Lane Liveload Moment and Rating for HAM-126-0881**

The HS20-44 laneload is virtually simulated in each marked traffic lane by integration of the derived influence lines, weighted by the specified distributed weight (see Figure 3-17). Integration is only performed for that portion of the influence line that would actually magnify the moment for the section (i.e., bottom flange stress should be the same sign as the expected moment for the section, see Chapter 2). The HS20-44 point load(s) are virtually simulated in each marked traffic lane by linear superposition of the derived influence lines (see Figure 2-4), weighted by the specified point load weight (see Figure 3-17). As the middle span has greater influence over the pier than the end span, the first point load is placed in the middle span. The liveload is calculated for the sum of all these stresses by each of the four analytical methods and then summarily rated by both the allowable stress and load factor approaches. Inventory and Operating levels are determined for both rating approaches. Note that the corresponding effective deadload  $M_{DLeff}$  and superimposed deadload  $M_{SDLeff}$  moments are used with the calculated liveload moment by the four analytical methods  $M_{LL} = \{M_1, M_2, M_3, \text{ or } M_4\}$ .

The liveload moments calculated for the HS20-44 laneload for the middle span by the four analytical methods are presented in Figure 3-28. The load rating for the middle span is selected as the minimum rating by Method 2 (see Figure 3-29), since the section was designed and is identified as fully composite (see Figure 3-6). Note the similarities between Methods 1, 2, and 3 except with regards to the load factor rating; this discrepancy is due to the distinction between compactness determined by each method (i.e., Methods 1 and 3 indicate noncompact behavior, while Method 2 indicates compact behavior due to its large effective width for the decking). Note that the HS20 truckload rating is less than the laneload rating.



**Stress (ksi) from Lane and Point Loads**

Beam 3 Middle Span	Lane Load Stress (ksi)	Point Load Stress (ksi)	Total Response
Top Flange	0.08	0.06	0.14
Bottom Flange	1.90	1.78	3.68

**Moment (kip-in) from Total Lane and Point Loads**

Method 1 Full Composite	Method 2 Partial Comp	Method 3 Partial Comp	Method 5 Non Composite
3,262	3,743	3,685	1,182

Full Composite, P=0 Assumption

- RF=3.0, Stress Inventory
- RF=5.1, Stress Operating
- RF=5.3, LFD Inventory
- RF=8.9, LFD Operating

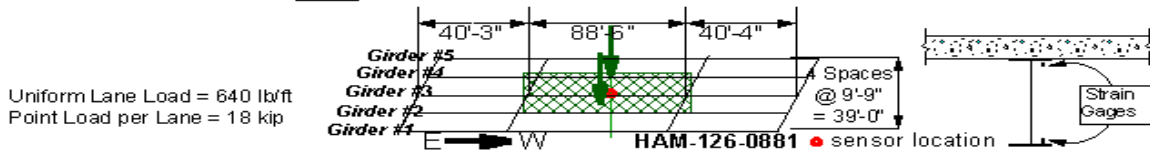


Figure 3-28: Liveload Stress and Moment of Simulated HS20 Laneload for the Middle Span

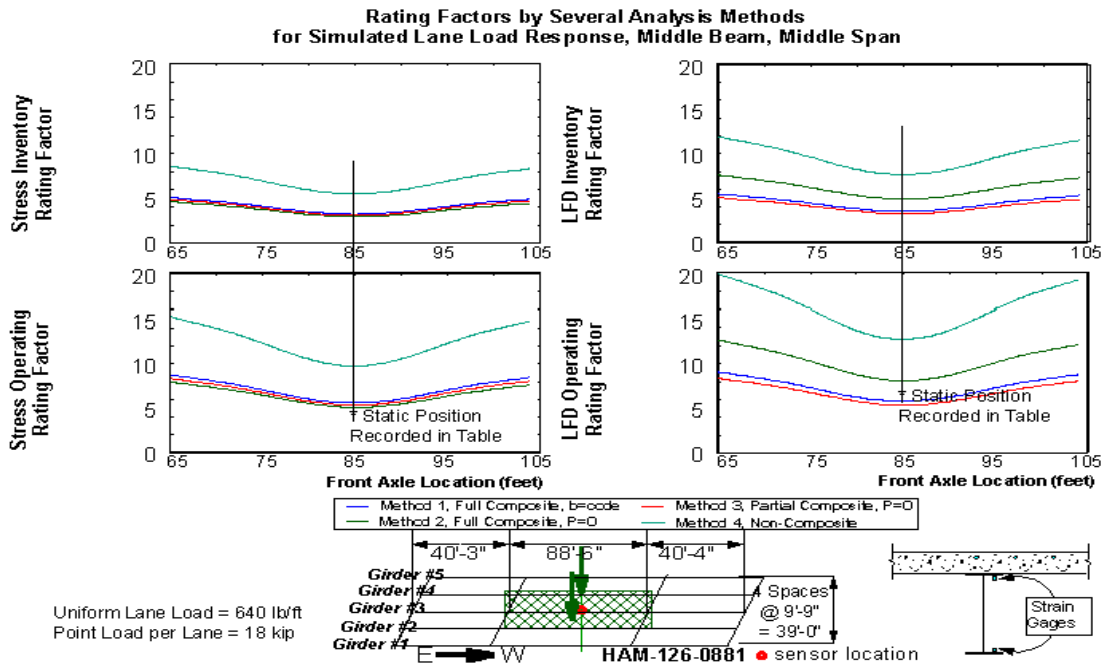
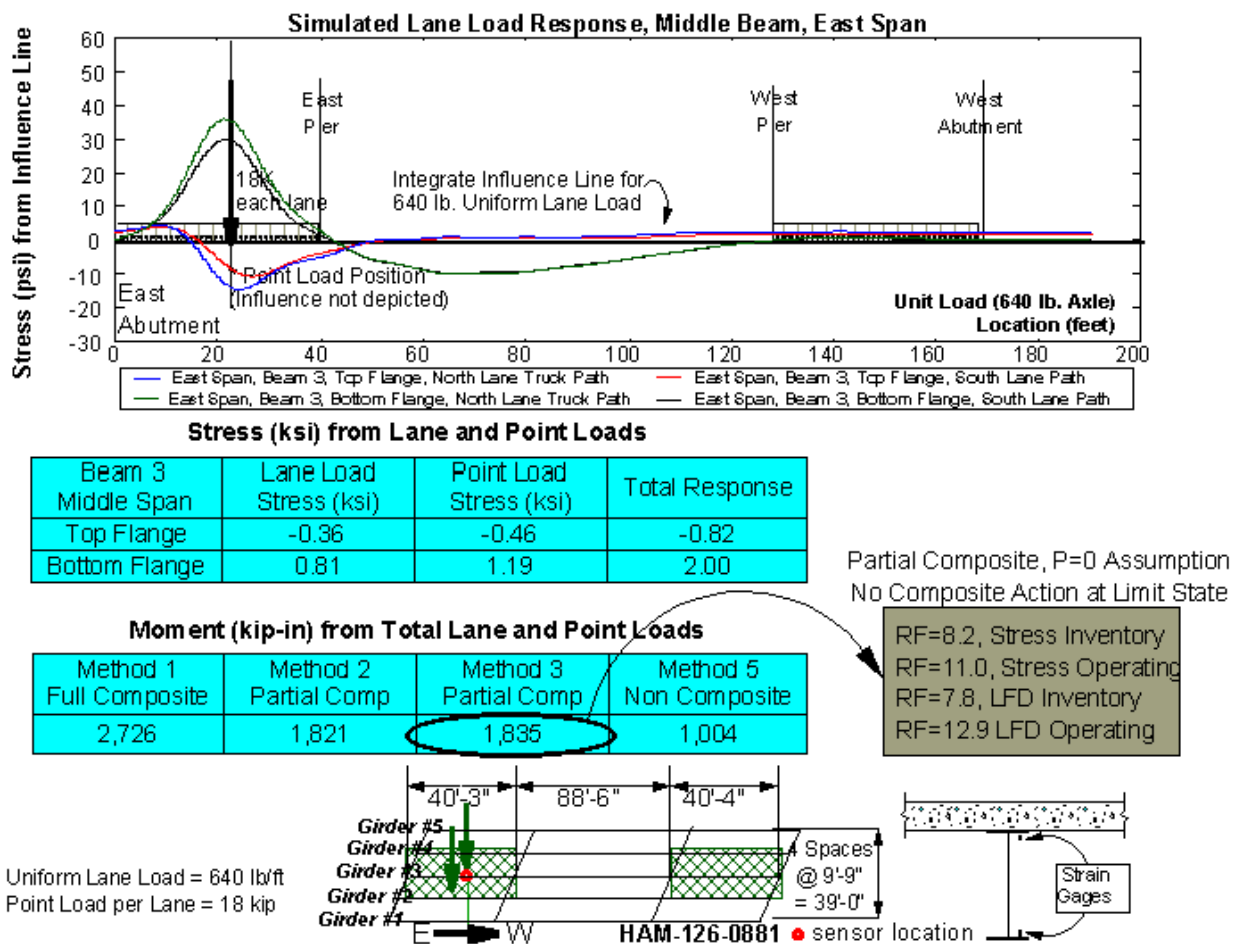
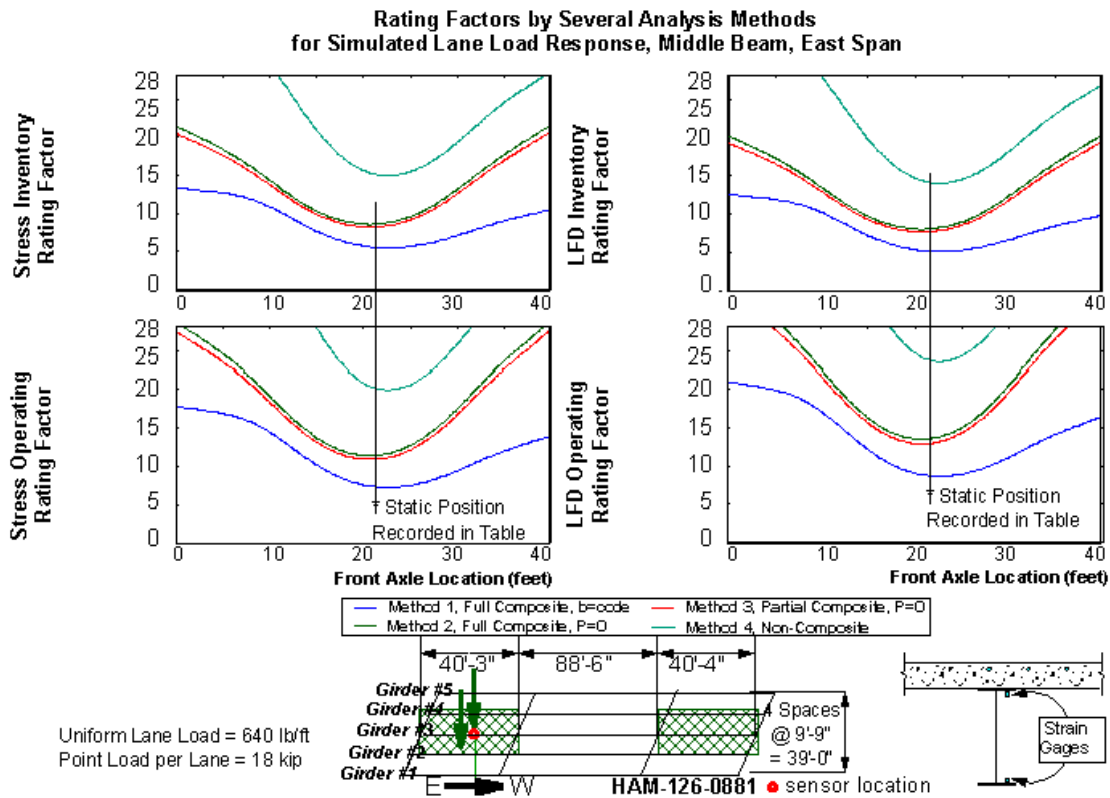


Figure 3-29: Rating Factors of Simulated HS20 Laneload for the Middle Span

The liveload moments calculated for the HS20-44 laneload for the east span by the four analytical methods are presented in Figure 3-30. As the span is designed as a noncomposite section, the load ratings are reduced to remove the effect of unintended composite action upon the remaining sectional capacity. The load rating for the east span is selected as the minimum rating by Method 3 (see Figure 3-31), since the section is identified as partially composite (see Figure 3-8). Note the similarities between Methods 2 and 3 in all cases. Note that the HS20 truckload rating is less than the laneload rating.

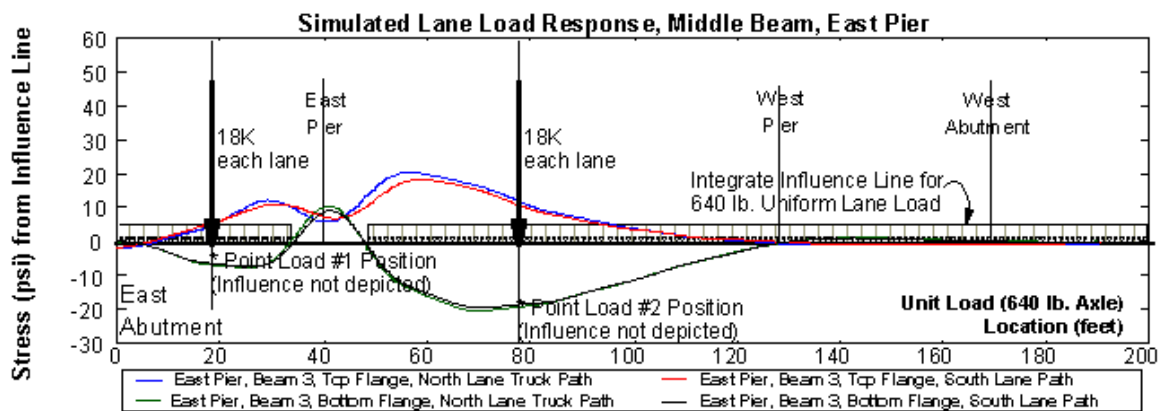


**Figure 3-30: Liveload Stress and Moment of Simulated HS20 Laneload for the East Span**



**Figure 3-31: Rating Factors of Simulated HS20 Laneload for the East Span**

The liveload moments calculated for the HS20-44 laneload for the east pier by the four analytical methods are presented in Figure 3-32. As the pier is designed as a noncomposite section, the load ratings are reduced to remove the effect of unintended composite action upon the remaining sectional capacity. The load rating for the east span is selected as the minimum rating by Method 3 (see Figure 3-33), since the section is identified as partially composite. Note the similarities between Methods 2 and 3 in all cases. Note that the HS20 truckload rating is less than the laneload rating.



**Stress (ksi) from Lane and Point Loads**

Beam 3 Middle Span	Lane Load Stress (ksi)	Point Load #1 Stress (ksi)	Point Load #2 Stress (ksi)	Total Response
Top Flange	1.35	0.41	0.24	2.00
Bottom Flange	-1.44	-0.67	-0.23	-2.34

**Moment (kip-in) from Total Lane and Point Loads**

Method 1 Full Composite	Method 2 Partial Comp	Method 3 Partial Comp	Method 5 Non Composite
-4,200	-1,787	-1,823	-1,546

Partial Composite, P=0 Assumption  
No Composite Action at Limit State

RF=3.2, Stress Inventory  
RF=6.0, Stress Operating  
RF=4.8, LFD Inventory  
RF=8.1 LFD Operating

Uniform Lane Load = 640 lb/ft  
Point Load per Lane = 18 kip

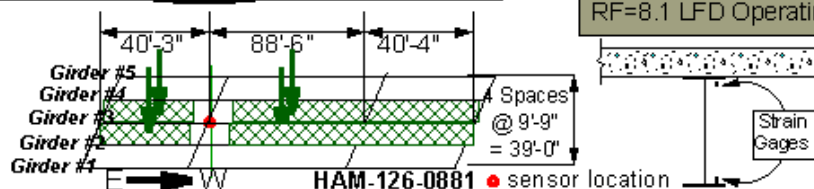


**Figure 3-32: Liveload Stress and Moment of Simulated HS20 Laneload for the East Pier**

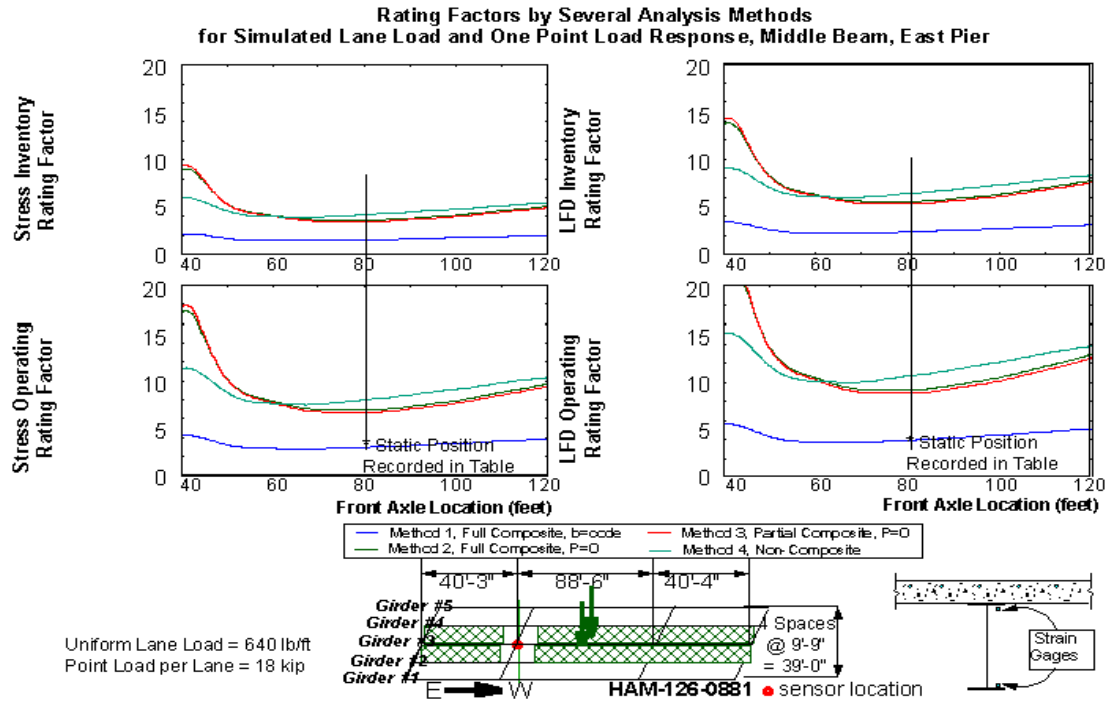


Figure 3-33: Rating Factors of Simulated HS20 Laneload and First Point Load for the East Pier

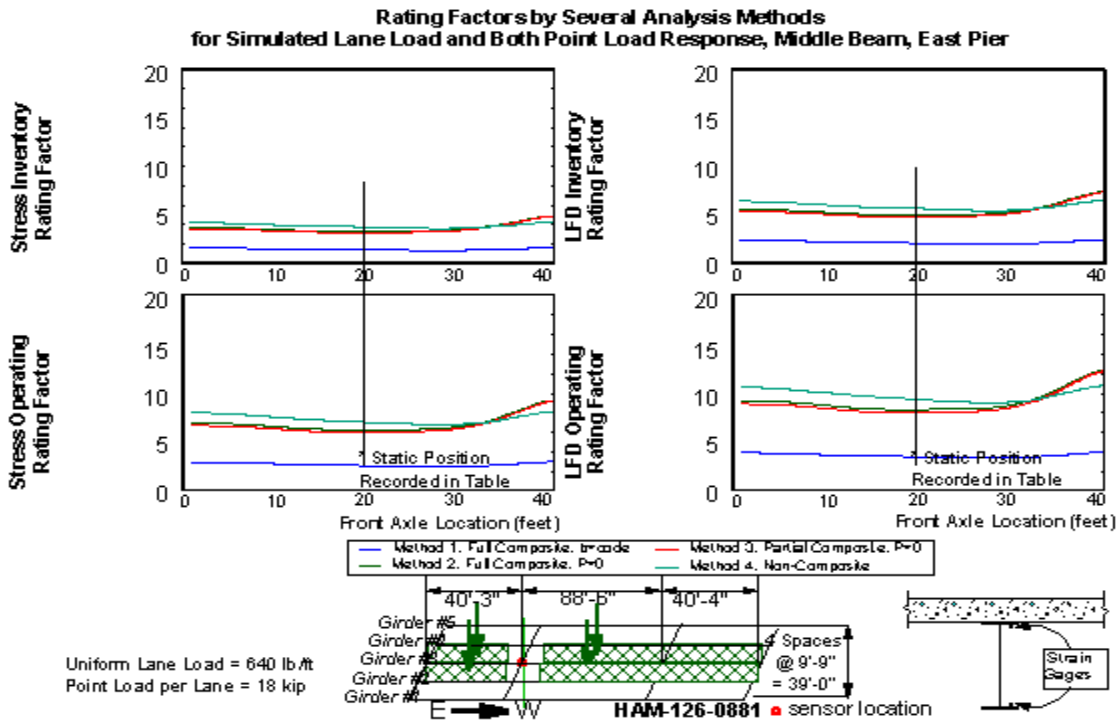


Figure 3-34: Rating Factors of Simulated HS20 Laneload and Both Point Loads for the East Pier

### **Event (e.g., construction) Moment and Rating by the Four Analysis Methods**

A unique opportunity exists for HAM-126-0881 due to the extensive instrumentation and monitoring of the bridge during its construction. The objective for the research project has been to understand and document the actual state-of-stress in a steel-stringer bridge, together with the corresponding causative effects, throughout the construction and service lifetime of the structure. A complete sensor suite was incorporated within the construction plans and drawings for the bridge. Vibrating wire strain gage instrumentation was installed on the steel girders prior to the superstructure construction and monitored continuously by a resident data acquisition system. Several significant events were monitored during construction and some of the results are presented in Figures 1-17, 1-18, 1-19, and 1-23.

Rather than use the expected deadload and superimposed deadload as calculated from first principals, the measured incremental stresses during their corresponding construction events have been used in Table 3-5 to recalculate the HS20 truckload rating factors for both the allowable stress and load factor approaches. Note that, in addition to the actual stresses observed for the concrete deck construction, the new deadload incorporates several other stresses not typically accounted for in the design of a bridge. These include permanent stresses from the beam erection process, the welding of crossframes to form the superstructure, and the welding of bearing plates at the piers. Note that even with these additional stress added to the actual deadload, the conservative design estimate still exceeds that actually measured during construction. The new superimposed deadload is based upon the measured permanent stresses caused by the construction of the bridge parapet. Contrary to design assumptions, the parapet load is not distributed evenly across the structure and very little is actually carried by the critical

middle beam. The deadload and superimposed moments are determined by scaling their stresses by the noncomposite section modulus (i.e.,  $M_{DL} = \sigma_{DL}S_4$ ,  $M_{SDL} = \sigma_{SDL}S_4$ ). The rating factors are all increased due to the reduced deadload.

Although not considered here, the west pier for the second beam experienced significant and permanent stress during the welding of the bearing plate. The total deadload stress for that section is more than twice that calculated for the pier location presented in this research. However, its liveload will be significantly reduced when compared to that of the middle girder and its rating factor is not expected to be critical. Still, this considered further in future research.

### **Environmental (e.g., thermal) Moment and Rating by the Four Analysis Methods**

In addition to construction events, the dedicated monitor for HAM-126-0881 has enabled the examination of considerable although transient environmental stresses on the structure (similar to those stresses measured for HAM-42-0992, Figure 1-15). The rugged steel construction of the vibrating wire strain gages allow for a matched thermal coefficient with the steel beam; hence, zero stress would be measured for thermal cycling of a freely moving steel beam. Any recorded stress is that produced by any restraint upon the beam including bearing friction and, of course, the integral abutment design. Daily as well as seasonal thermal cycling is clearly observed from the measured data. The greatest response occurs at the abutments, but significant stresses were observed for the annual cycle of the sections under consideration (6.67 ksi for the east span and pier, 6.10 ksi for the middle span). The AASHTO Specifications indicate that thermal stresses should not be incorporated within the Inventory rating factor, but can be included within overload considerations by the Operating rating factor.

	Theory	Identified	Theory	Identified	Theory	Identified
Parameter	East Span	East Span	East Pier	East Pier	Mid Span	Mid Span
Steel Beam	W136x194	As design	W136x194	As design	W136x182	As design
Comp Action	None	None	None	None	Full	Full
Bottom Strain	+177.6 ue	+90.5 ue	+312 ue	-90.7 ue	+444 ue	+172 ue
Top Strain	-177.6 ue	-34.2 ue	-312 ue	63.7 ue	-41.2 ue	+6.28 ue
Neutral Axis	18.25"	25.92"	18.25"	21.22"	33.2"	36.44"
Curvature	+9.73 ue/in	+3.67 ue/in	-17.1 ue/in	-4.54 ue/in	+13.3 ue/in	+4.88 ue/in
*M <sub>DL</sub>	-1097 kip-in	-709 kip-in	-8680 kip-in	-9812 kip-in	6540 kip-in	5971 kip-in
M <sub>SDI</sub>	-353 kip-in	-232 kip-in	-2250 kip-in	-66 kip-in	2550 kip-in	435 kip-in
Impact Factor	0.303	As design	0.265	As design	0.235	As design
Distribution	0.886	0.957	0.886	As design	0.886	0.702
Method 1	N/a	N/a	N/a	N/a	As above	N/a
Method 2						used in rating
Deck Width		27.40"		8.26"	93"	175"
M <sub>I,eff</sub>	N/a	2424 kip-in	N/a	-2138 kip-in	N/a	5054 kip-in
*M <sub>DL,eff</sub>		-709 kip-in		-9812 kip-in		9404 kip-in
M <sub>SDI,eff</sub>		-232 kip-in		-66 kip-in		505 kip-in
Method 3		used in rating		used in rating		
RCA		51.88%		20.11%		121.2%
M <sub>I,eff</sub>	N/a	2442 kip-in	N/a	-2172 kip-in	N/a	4975 kip-in
*M <sub>DL,eff</sub>		-709 kip-in		-9812 kip-in		9258 kip-in
M <sub>SDI,eff</sub>		-232 kip-in		-66 kip-in		498 kip-in
Method 4	used in rating		used in rating			
M <sub>I,eff</sub>	3711 kip-in	1288 kip-in	-4756 kip-in	-1595 kip-in	N/a	1600 kip-in
Axial Force	0	46.5 kips	0	-22.3 kips		139 kips
*M <sub>DL,eff</sub>	-1097 kip-in	-709 kip-in	-8680 kip-in	-9812 kip-in		5971 kip-in
M <sub>SDI,eff</sub>	-353 kip-in	-232 kip-in	-2250 kip-in	-66 kip-in		435 kip-in
Capacity, Inv	18230 kip-in	18230 kip-in	-18230 kip-in	-18230 kip-in	25798 kip-in	26380 kip-in
AS Rating, Inv	4.069	6.025	1.213	3.040	1.086	2.639
Capacity, Opr	24860 kip-in	24860 kip-in	-24860 kip-in	-24860 kip-in	35179 kip-in	35970 kip-in
AS Rating, Opr	5.440	8.109	2.315	5.453	1.861	4.175
Ult. Capacity	38350 kip-in	38350 kip-in	38350 kip-in	38350 kip-in	46890 kip-in	46890 kip-in
LF Rating, Inv	3.833	5.731	1.849	4.278	1.158	2.511
LF Rating, Opr	6.400	9.567	3.087	7.142	1.935	4.191

**Table 3-5: Theoretical and Identified Parameters for HS20 Truck on Bridge, HAM-126-0881, Composite Action as Designed is Enforced for Identified Parameters at Limit States, Ultimate Capacity is Limited as per Noncompact but Composite Section, Measured Deadload and Other Construction Stresses are Used**

\* Note: DL Moment now includes the summation of all recorded construction stresses up to and including the pour and cure of the concrete decking (e.g., see Figure 1-23).

	Theory	Identified	Theory	Identified	Theory	Identified
Parameter	East Span	East Span	East Pier	East Pier	Mid Span	Mid Span
Steel Beam	W136x194	As design	W136x194	As design	W136x182	As design
Comp Action	None	None	None	None	Full	Full
Bottom Strain	+177.6 ue	+90.5 ue	+312 ue	-90.7 ue	+444 ue	+172 ue
Top Strain	-177.6 ue	-34.2 ue	-312 ue	63.7 ue	-41.2 ue	+6.28 ue
Neutral Axis	18.25"	25.92"	18.25"	21.22"	33.2"	36.44"
Curvature	+9.73 ue/in	+3.67 ue/in	-17.1 ue/in	-4.54 ue/in	+13.3 ue/in	+4.88 ue/in
*M <sub>DL</sub>	-1097 kip-in	-709 kip-in	-8680 kip-in	-9812 kip-in	6540 kip-in	5971 kip-in
**M <sub>SDL</sub>	-353 kip-in	4171 kip-in	-2250 kip-in	-4699 kip-in	2550 kip-in	4205 kip-in
Impact Factor	0.303	As design	0.265	As design	0.235	As design
Distribution	0.886	0.957	0.886	As design	0.886	0.702
Method 1	N/a	N/a	N/a	N/a	As above	N/a
Method 2						used in rating
Deck Width		27.40"		8.26"	93"	175"
M <sub>I,eff</sub>	N/a	2424 kip-in	N/a	-2138 kip-in	N/a	5054 kip-in
*M <sub>DL,eff</sub>		-709 kip-in		-9812 kip-in		9404 kip-in
**M <sub>SDL,eff</sub>		4171 kip-in		-4699 kip-in		4886 kip-in
Method 3		used in rating		used in rating		
RCA		51.88%		20.11%		121.2%
M <sub>I,eff</sub>	N/a	2442 kip-in	N/a	-2172 kip-in	N/a	4975 kip-in
*M <sub>DL,eff</sub>		-709 kip-in		-9812 kip-in		9258 kip-in
**M <sub>SDL,eff</sub>		4171 kip-in		-4699 kip-in		4811 kip-in
Method 4	used in rating		used in rating			
M <sub>I,eff</sub>	3711 kip-in	1288 kip-in	-4756 kip-in	-1595 kip-in	N/a	1600 kip-in
Axial Force	0	46.5 kips	0	-22.3 kips		139 kips
*M <sub>DL,eff</sub>	-1097 kip-in	-709 kip-in	-8680 kip-in	-9812 kip-in		5971 kip-in
**M <sub>SDL,eff</sub>	-353 kip-in	4171 kip-in	-2250 kip-in	-4699 kip-in		4205 kip-in
Capacity, Inv	18230 kip-in	18230 kip-in	-18230 kip-in	-18230 kip-in	25798 kip-in	26380 kip-in
AS Rating, Inv	4.069	6.025	1.213	3.112	1.086	2.639
Capacity, Opr	24860 kip-in	24860 kip-in	-24860 kip-in	-24860 kip-in	35179 kip-in	35970 kip-in
AS Rating, Opr	5.440	6.725	2.315	3.767	1.861	3.473
Ult. Capacity	38350 kip-in	38350 kip-in	38350 kip-in	38350 kip-in	46890 kip-in	46890 kip-in
LF Rating, Inv	3.833	5.731	1.849	4.322	1.158	2.511
LF Rating, Opr	6.400	8.183	3.087	5.455	1.935	3.489

**Table 3-6: Theoretical and Identified Parameters for HS20 Truck on Bridge, HAM-126-0881, Composite Action as Designed is Enforced for Identified Parameters at Limit States, Ultimate Capacity is Limited as per Noncompact but Composite Section, Measured Construction and Environmental Stresses are Used**

\*\* Note: SDL Moment now includes the summation of all recorded stresses beyond the construction of the concrete decking, including thermal stresses and the construction of the sidewalk/parapet.

The new superimposed deadload is the sum of the measured permanent stresses caused by the construction of the bridge parapet and the maximum thermal stress observed over the annual cycle for the bridge. The superimposed deadload moment is determined by scaling its stress by the noncomposite section modulus. The Operating rating factors are decreased due to the increased deadload (Table 3-6).

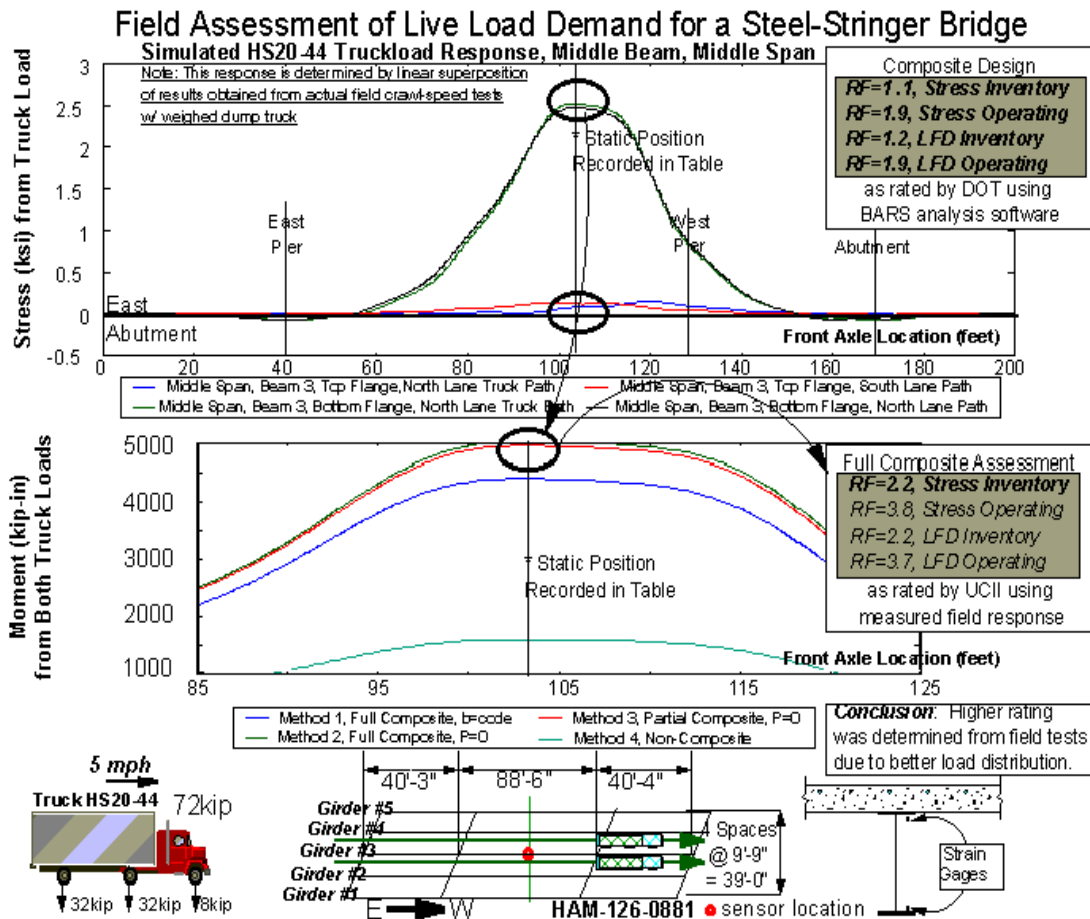


Figure 3-35: Summary of Condition Assessment for Critical Section of HAM-126-0881

## Field Assessment of Dead Load Demand for a Steel-Stringer Bridge

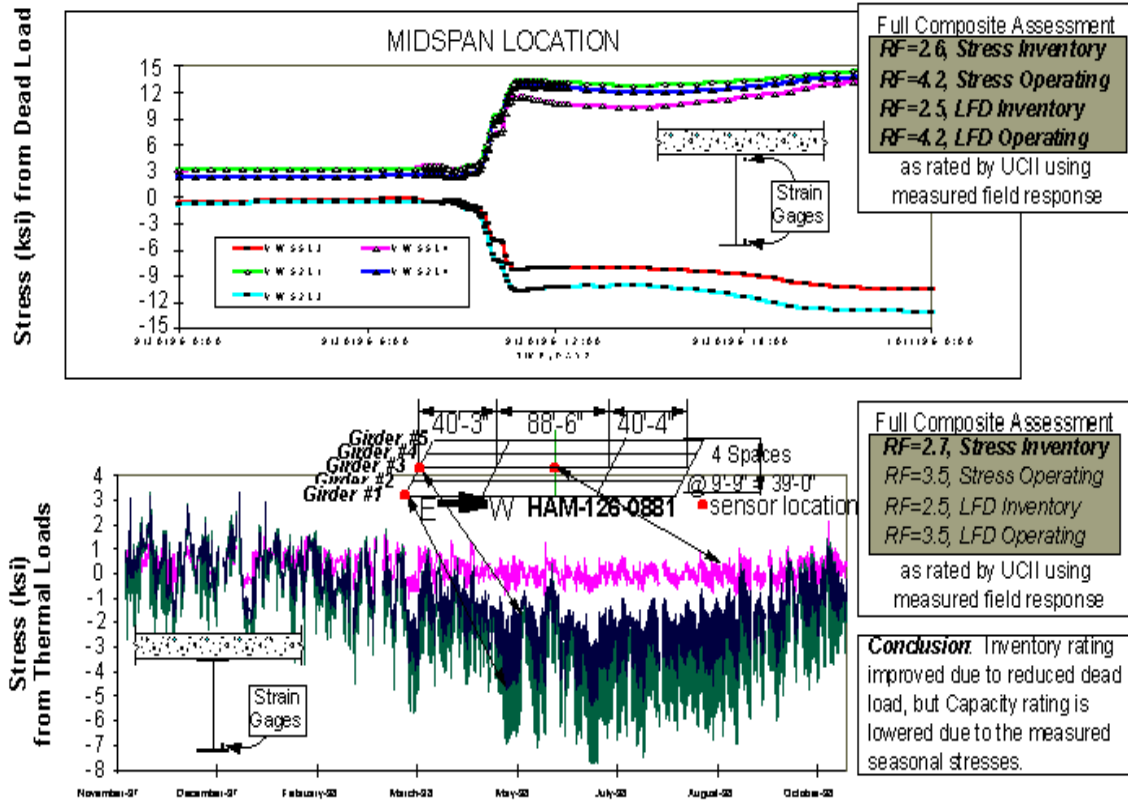


Figure 3-36: Summary of Instrumented Monitoring for Critical Section of HAM-126-0881

### 3.1.9. Remaining Fatigue Life

Fatigue evaluation of highway bridges is also of great concern to the bridge engineer, particularly with older monumental structures that have undergone several episodes of rehabilitation or with suspect connections which were designed before the recent investigation of such phenomena [Fisher, 1984]. Many loading repetitions are required at suspect members, welds, or connections in order to produce a fatigue failure at some time in the future. Generally, all truck loading stresses, whether above or below the allowable range, cause fatigue damage that could result in a fatigue failure. In contrast with the design rating which defines the largest

allowable load corresponding to permanent structural damage, the effects of fatigue loading can best be defined in terms of the total life of the bridge for the given spectrum of service stresses that it experiences each day. To study the fatigue susceptibility of a bridge, the engineer must have the most realistic and precise information to make an accurate assessment, particularly when the live load stresses are used in the cubic equations of the AASHTO code. It would be extremely time-consuming and nearly impossible to attempt to account for all variables in a conventional computer analysis. The only way to obtain precise service information is through continuous field monitoring of the local stress field upon and adjacent to the suspect members, connections, or welds. Similar research is documented in the literature [Moses, 1987a, Ghosn, 1986, Nowak, 1993, Deatherage, 1995, Sartor, 1999].

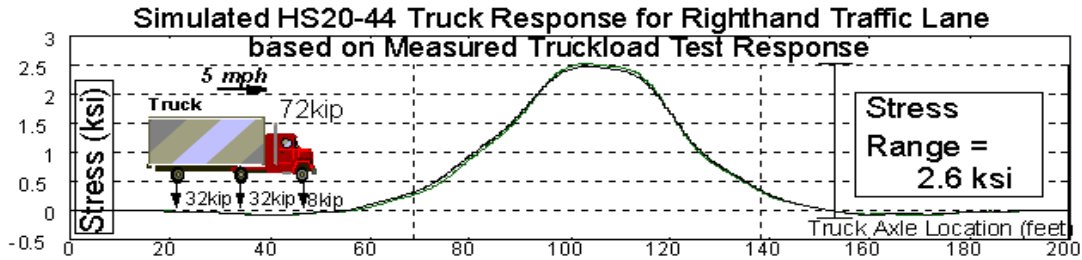
The AASHTO Specifications define a fatigue truck as the standard load to consider in terms of the fatigue for each bridge member. The fatigue truck is an HS15-44 truck type with the very same axle spacing as the HS20-44 truckload (see Figure 3-17) but with the axle weights reduced by 75%. The fatigue truck is virtually simulated in each marked traffic lane by linear superposition of the derived influence lines, weighted by the specified axle weights. A maximum fatigue stress range ( $S_F$ ) is defined for one fatigue truck at any location upon the bridge (e.g., see Figure 3-37). The fatigue stress is scaled by an impact factor of 1.1, regardless of span length, and a reliability factor of either 1.35 or 1.75 depending upon the redundancy of the bridge design. Figure 3-37 illustrates the formulation of remaining fatigue life for the middle span of HAM-126-0881 based upon AASHTO specifications.

Two tests for infinite fatigue life are available:

- If the resultant fatigue stress is less than a predefined limiting stress for the detail category of the member under consideration, then the member is assumed to have infinite fatigue life. Table 3-7 presents the results of this limit test for the middle span, east span, and east pier of HAM-126-0881.
- If the tensile portion of the resultant fatigue stress range is less than the compressive deadload stress (if any) for the member under consideration, then the member is assumed to have infinite fatigue life. Table 3-8 presents the results of this deadload test for the middle span, east span, and east pier of HAM-126-0881.

Note that the pier is examined at both the top and bottom flange due to tensile stress and a poor detail category, respectively. If poorly executed, the welding of the bearing plate to the bottom flange at the pier is considered Category E' by the AASHTO Code (i.e., "base metal at ends of partial length welded coverplates wider than the flange without welds across the ends").

All of the sections under consideration for HAM-126-0881 have passed at least one of the tests for infinite fatigue life. Indeed, it would be unusual for the typical steel-stringer bridge to fail due to fatigue because of the tremendous redundancy built into the design of the structure. In any case, the remaining fatigue life was calculated and is presented in Table 3-9. Note that the middle span has the smallest remaining fatigue life of 669 years!



Fatigue Stress ( $S_F$ ) = 2.6 ksi (0.75) (1.35) (1.10) = 2.9ksi for HS15 Fatigue Truck

$$\text{Remaining Life } (Y_F) = \frac{K \times 10^6}{T_A C (S_F)^3} - A \text{ (years)} = \underline{669 \text{ years}}$$

NOTES	Detail Constant (K) = 68 for fatigue category A
	Lifetime Mean ADTT ( $T_A$ ) = ADTT $\times F_L \times 3.6$ for new bridge w/ 3% annual growth in the traffic population
	Average Daily Truck Traffic = 1500 (presently)
	Outer Lane Traffic ( $F_L$ ) = 0.85 for two lane, one-way traffic
	Effective Number of Stress Cycles (C) = 1 from truck response above
	Age (A) = 1 year for HAM-126-0881 bridge

Figure 3-37: Example Calculation of Remaining Fatigue Life for Middle Span

Member	Detail Category	Compressive HS20 Truck Stress (ksi)	Tensile HS20 Truck Stress (ksi)	Range of HS20 Truck Stress (ksi)	Reliability Factor	Fatigue HS20 Truck Stress (ksi)	Fatigue HS15 Truck Stress (ksi)	Limiting HS15 Truck Stress (ksi)	Limiting Test
Midspan, bottom	A	-0.09	2.52	2.61	1.35	3.88	2.91	8.8	Passed
East span, bottom	A	-0.68	1.44	2.12	1.35	3.15	2.36	8.8	Passed
East pier, top	A	0.00	1.33	1.33	1.35	1.98	1.48	8.8	Passed
East pier, bottom	E'	-1.35	0.06	1.41	1.35	2.09	1.57	0.9	Failed

Notes: HS15 and HS20 Trucks simulated with a worst-case fourteen foot (14') axle spacing.  
Fatigue Stress includes an Impact Factor of 10% and Truck Superposition Factor of 0%

Table 3-7: Limit Test of Stress Range for Infinite Fatigue Life of Detail Category

Member	Detail Category	Tensile HS20 Truck Stress (ksi)	Reliability Factor	Fatigue HS20 Truck Stress (ksi)	Tensile HS15 Truck Stress (ksi)	Compressive Dead Load Stress (ksi)	Limiting Test
Midspan, bottom	A	2.52	1.35	3.75	2.81	0	Failed
East span, bottom	A	1.44	1.35	2.13	1.60	-1.65	Passed
East pier, top	A	1.33	1.35	1.97	1.48	-13.1	Passed
East pier, bottom	E'	0.06	1.35	0.09	0.07	-13.1	Passed

Notes: HS15 and HS20 Trucks simulated with a worst-case fourteen foot (14') axle spacing.  
Fatigue Stress includes an Impact Factor of 10% and Truck Superposition Factor of 0%

Table 3-8: Deadload Test of Tensile Stress for Infinite Fatigue Life of Detail Category

Member	Detail Category	Detail Constant	Fatigue	Fatigue
			HS15 Truck Stress (ksi)	Remaining Life (yrs)
Midspan, bottom	A	68	2.91	669
East span, bottom	A	68	2.36	3590
East pier, top	A	68	1.48	4557
East pier, bottom	E'	1.1	1.57	803087

Given: Lifetime Mean ADTT = 4,590, One effective stress cycle assumed

**Table 3-9: Remaining Fatigue Life for Critical Sections of HAM-126-0881**

In conclusion, diagnostic truckload testing and instrumented monitoring have proven to be valuable but objective methods for the condition assessment of highway bridges. The constructed bridge will have many inherent mechanisms to resist the applied load and which are generally not considered in the analysis of its capacity. The expected deadload and liveload stresses can be checked and identified by this methodology. Further, the bridge may be subjected to unexpected or otherwise undetermined forces by the design which may be measured and used the load rating of the structure.

A suite of condition indices can be processed directly from the measured data to assess the performance of the structure and compare with the nominal design values, including:

- Maximum stress in the outer fiber
- Modal frequencies, shapes, and weighting
- Curvature
- Neutral axis location
- Truckload moment, analyzed by four different methods
- Distribution factor

- Impact factor
- Capacity load rating, analyzed by two different concepts (i.e., working stress and limit states)
  - HS20 Truckload rating, Inventory and Operating
  - HS20 Laneload rating, Inventory and Operating
  - Event rating, Inventory and Operating
  - Environmental rating, Operating
- Remaining fatigue life

This research provides a novel approach to condition assessment by determining the above indices for the instrumented sections of the bridge from the measured data without the use of a finite element model. The derived influence lines can be used to virtually simulate the rating and fatigue loads for immediate field assessment of a highway bridge.

#### 4. Damage Assessment of a Highway Bridge under Truckload

As with the condition indices of Chapter 3, linearized damage indices are based on the assumption that a constructed facility may be characterized as incrementally linear at the serviceability limit states. While no soil-foundation-structure system can be strictly linear, the justification in using linearized indices is that most constructed facilities behave linearly in the global sense even when many local nonlinearities, such as due to localized damage in a shake-down state, may exist. For the general infrastructure management problem, linearized indices offer the advantages that they can be physically conceptualized, can be measured or extracted from measurements during controlled tests at any time, and they can be more easily correlated to facility damage or deterioration at the serviceability limit states.

Some of the linearized global condition indices that have been proposed for the serviceability limit state of constructed facilities are shown in Table 1. Condition indices serve a dual purpose as a damage index in the sense that damage may also be reflected in the poor condition assessment for the structure. For some, this is indeed the metric by which damage should be defined (i.e., only damage which significantly affects the structure's performance should be considered). However, we will show in this chapter that local damage is not always reflected in every condition index for a highway bridge, especially those indices that represent the global structure as a whole (e.g., load rating factor).

In general, a system-or-structural-identification based approach to damage assessment is highly recommended. In the system-identification approach, we would need to generate an a-priori analytical model, design and conduct experiments, conduct parameter identification to calibrate

the analytical model, validate its completeness and reality-check by evaluating the physical correspondence of the identified parameters. The resulting field-calibrated analytical model serves as a reality-check on the experiment itself, and for linear (and as a starting point for non-linear) sensitivity analyses which are required for reliability evaluation. A structural-identification based approach is recommended even when an index used for damage assessment may be a directly measurable one. At the same time, we do have to recognize and take advantage of indices that can be directly quantified during an experiment, or requiring just a single level of post-processing without a complete system-identification process, since these would be easier to conceptualize and to monitor, requiring simpler experiments.

The criteria for a satisfactory damage detection method should be: (a) Diagnose whether there is damage or not, even when there may not be a baseline. While many indices are useful only if there is a baseline, several may be used in conjunction with structural identification to diagnose damage without a baseline. For example conceptual indices may utilize a rational analytical model as a gauge, or a comparable healthy facility may serve as a baseline to test for anomalous behavior; (b) Localization, i.e. establishing the boundaries and distribution of any damage; (c) Quantify the extent of the damage and the possible defects, deterioration mechanisms or other loading mechanisms which may have led to the damage; and, (d) Establish the impact of the damage on the global health, i.e. how damage is affecting current and projected performance at the critical limit states.

In addition to or in conjunction with the above criteria, we desire damage indices to be: (a) Sensitive to the effects of common deterioration and damage mechanisms that affect the facility;

(b) Directly measurable by practical experimentation, and not requiring extensive post-processing. Some indices may require modal expansion and/or extensive error-prone numerical operations; (c) Robust, i.e. insensitive to experimental errors and uncertainties; and, (d) Conceptual, i.e. directly corresponding to a clear aspect of structural behavior such as deflection, stress, moment, stiffness or flexibility. While some indices, such as the effective flexural rigidity of a member, permit using engineering intuition for damage detection, others with no physical correspondence have been proposed to indicate damage based on an arbitrary scale.

Damage must also be classified according to its spatial context: local material properties, distinct members and their connections, and the complete or global structure. It is interesting that many engineers consider damage as changes in the effective material properties within a structure. Many local nondestructive technologies have been developed (see Section 4.1) which can successfully characterize the in-situ properties of construction materials, even through covers and other obstruction [Shickert, 1995]. These tools are very useful in detecting the onset of deterioration (e.g. in a reinforced concrete element or in its chemical bond with steel). For a large-scale constructed facility, however, it is not possible to presently catalog all of its critical deterioration mechanisms nor pinpoint its critical regions and responses to be investigated. Even if a complete local scan is conducted, it is not clearly understood how local damage affects the complete system performance. Therefore, local scans and measurements can not feasibly and effectively address the problem of global damage assessment. Global nondestructive testing methods (see Section 4.2) such as modal impact and truckload testing are suggested by this research.

#### 4.1. Local Nondestructive Diagnostic Techniques (NDT) For Highway Bridges

Diagnostic techniques are becoming common in the evaluation of structural condition and performance. These include techniques to identify the critical parts or elements of the structure, identify the cause of distress, monitor structural performance, warn against failure, and provide statistical data for the development of design and evaluation criteria [Nowak, 1990, Chase, 1995b]. In September 1996, The National Science Foundation sponsored a conference on “Non Destructive Evaluation of Civil Structures and Materials” to discuss the latest developments and applications of nondestructive techniques [NSF, 1996]. A number of nondestructive testing and examination techniques have been applied or are under development by several transportation departments in the nation, as well as by FHWA and NSF funded research. Applications that were used for evaluating bridges fall into the general categories listed below:

- Ultrasonic Evaluation
- Corrosion Surveying by Half Cell Potential
- Acoustic Emission
- Radiographic Testing
- Impact-Echo Techniques
- Infrared Thermography for Concrete Decks
- Ground Penetrating Radar
- Surveying

The following is a very brief description of the non-destructive techniques for complementing the visual inspection. The possible synergy of these techniques will be described in more detail below.

#### 4.1.1. Ultrasonic Evaluation

Ultrasonic evaluation utilizes high frequency sound waves to measure the material properties in order to locate defects. Pulses of ultrasonic energy are launched into the material and detected by specially designed transducers. These pulses are altered as they propagate through the material due to attenuation, reflection and scattering. The output pulse is displayed, processed, and interpreted in terms of the internal structure of the object under investigation based on its relation to the input pulse. Ultrasonic inspection searches flaws in metallic and non-metallic materials, for cracks, voids, delaminations, etc.

#### 4.1.2. Half-Cell Potential

A half-cell test measures the electrical potential of reinforcing steel relative to a standard reaction potential, typically a copper-copper sulfate reaction. The potential of the reinforcing steel is an indication of corrosion activity. Corrosion, an electrochemical process, gives evidence in the form of electrical potential and electrical current. Either can be used as means of detecting corrosion activity in bridge decks. Half-cell testing is executed at the surface of concrete bridge decks and the potentials measured indicate the corrosion of reinforcing steel in the neighborhood.

#### 4.1.3. Acoustic Emission

Acoustic emission is based upon the stress waves produced as a part of the general energy resulting from a change in the stress condition inside a material and specially around hidden and open flaws and defects. AE is often generated by defect related deformation processes such as crack growth and plastic deformation. Thus, the source of AE is the elastic stress field in the material. AE sensors can be embedded in the structure at the critical locations and can perform continuous monitoring.

#### 4.1.4. Radiographic Testing

Radiography is a nondestructive technique for inspecting the internal structure and composition of an object using penetrating radiation (i.e. X-rays, gamma rays, beta particles, neutron or proton beams). Radiography generates an image of internal structure and defects. Quantitative image processing allows for materials characterization, assuring assembly integrity, and determining dimensional measurements. Radiography is particularly appropriate for detecting cracks, voids, and material contaminants. It is frequently used to inspect the quality of welds and brazes. It can be used as material characterization tool, a quality control tool, and as in-service inspection tool.

#### 4.1.5. Impact-Echo Techniques

Impact-echo technique is useful technique to inspect concrete structures, asphalt overlay, bridge decks, and other structures. It is basically a modification of the ultrasonic testing techniques. It detects flaws in concrete such as honeycombing, delaminations, cracks, and voids. The strength of the technique is its simplicity and ease of application. In this method, an impulse is applied to

the object and the response is monitored by the transducer. Both the source of impulse and the receiving transducer are mounted on the same surface of the specimen. Once the impact is done, the introduced waves will travel in the material and are reflected back and forth whenever it meets a boundary with air or a new solid material. The transducer monitors the wave as it is reflected from internal defects, delaminations or external boundaries of the structure. Since the impact-echo technique is geared towards detecting larger flaws and defects, one can afford to use smaller frequencies (e.g., 0.5-25 kHz) than ultrasonic testing. The data acquisition and the transducers needed for the test are simpler and cheaper.

#### 4.1.6. Infrared Thermography

Infrared thermography remotely senses and records surface temperatures and temperature gradients across a field of view. In the field, infrared imaging has sensed and displayed delaminations in bridge decks. Infrared measurements are severely affected by the unpredictable changes in weather conditions. Defects can be identified only on bright sunny days during the solar heating cycle (e.g., 11 a.m.- 3 p.m.) or the cooling cycle (e.g., 11 p.m.- 3 a.m.).

#### 4.1.7. Ground Penetrating Radar

Ground penetrating radar images subsurface objects and defects with high frequency electromagnetic energy. An antenna radiates a short duration pulse which travels through the media until it is reflected back by a change in the media. A profile of the reflection is generated and displayed by a computer system. A cross sectional view of structure beneath the scan path of the antenna is displayed. Thus, depth and location information is provided. It maps rebar in concrete and delaminations in road beds.

#### 4.1.8. Surveying

With the advent of laser based techniques, geodesic surveying equipment has gained high accuracy and excellent field performance. The use of such equipment for monitoring of changes in the bridge geometry can be useful in many cases. The essentials for accurate surveying include adequate record keeping, the appropriate choice of monitored locations and frequency of sightings.

#### 4.2. Global Nondestructive Diagnostic Techniques (NDT) for Highway Bridges

Controlled structural testing, measurement and performance evaluation are well established and have been the cornerstone of the civil engineering profession for centuries [Aktan, Bahkt, Bertero, Cantieni, DeWolf, Fisher, Lichtenstein, Moses, Newmark, Nowak, etc.]. Recent efforts in the literature have been directed towards characterization of the observed ambient and/or service response of the structure (i.e. its healthy condition) and identifying the effect of specific damage events or deterioration mechanisms upon this characterization. Here, the term “characterization” is broadly used to encompass the efforts of mechanical, geometrical, qualitative, fuzzy, neural or any other form of response model for the structure.

##### 4.2.1. Modal Analysis

Modal analysis is a testing technique that uses vibration tests and analytical methods to determine the dynamic characteristics of a structure, such as frequencies, mode shapes, mass, stiffness, and damping, are obtained by this method.

It is performed for four major reasons:

- To understand or identify the structural dynamics of a system
- Troubleshooting of structures experiencing problems in dynamic response
- Validation of analytical models (typically finite element models)
- To contribute in the development of control systems for structures.

Some form of excitation is needed to perform a modal test. This can be either an artificial excitation (e.g., vibration shaker, impact device, an acoustic source, etc.) or natural excitation (e.g., wind, road surface irregularities, or wave action). For modal impact testing, accelerometers are positioned at the coordinates to measure the structure's vibrational response to an applied impact from a custom hammer instrumented with a load cell (see Figure 1-24). Generally, no access below the bridge is required and the bridge may be impact tested in parts so that one or more lanes may remain open to traffic. Frequency domain representation of the measured signals allows immediate derivation of bridge flexibility at the instrumented coordinates (see Figure 1-25).

It has been demonstrated that modal flexibility is a damage sensitive index by conducting modal tests on decommissioned concrete and steel highway bridges which were loaded to various damage states [Toksoy, 1993 and 1994; Aktan, 1994a and 1996c, Lenett, 1997]. Zhang (1993) showed that the uniform load surface and its curvature can provide an accurate and conceptual health index for a structure. A derived flexibility matrix with the appropriate spatial resolution can be used to virtually simulate the deflection basin and influence lines for any span and under any loading pattern upon the bridge. It is possible to check this for spatial anomalies for directly

assessing condition even without a prior experiment. Spatial comparison-checks include: the flexibility of support conditions, the flexibility of symmetric points, the flexibility of similar bridges which are known to be healthy, or the flexibility of a rational analytical characterization. However, the more definitive use of flexibility is that it serves as a baseline for future reference. Any changes in the local flexibility of redundant structures serve as sensitive and reliable indices for damage.

#### 4.2.2. Diagnostic Load Testing & Instrumented Health Monitoring

Instrumentation is installed upon the bridge for static (strain gages, displacement gages, tiltmeters, thermocouples, pressure transducers) and dynamic (accelerometers, velocity transducers) identification of structural parameters. The test duration can vary from a couple of seconds (Crawl speed truck loading, traffic monitoring), to years (continuous monitoring). The loading can be a simple known load pattern (loaded trucks, concrete blocks), environmental loading (wind, temperature, etc.), traffic, earthquake, etc. Using this technique with extensive instrumentation to measure all the critical aspects of bridge response, it is possible to calibrate comprehensive finite-element analytical models that accurately simulate the global behavior as well as the localized forces and distortions of a test bridge.

The AASHTO Manual for Condition Evaluation of Bridges suggests “load testing as an effective means of evaluating the structural performance of a bridge or its selected components”. We suggest that diagnostic truckload tests may also yield sensitive and conceptual damage indices; further, these indices may be processed to define the significance of the detected damage in the

context of overall structural performance or condition. This applies particularly to damage that cannot be accurately modeled by analysis, or to damage whose effect upon the structural response to live load is in question. We also suggest that continuous remote monitoring of a highway bridge to traffic and environmental loading would necessarily prove to be most efficient in the detection of any damage to an instrumented section of the structure. We will show below that damage detection is also possible (although not as likely) for other components of the bridge not instrumented.

Sudden damage to a highway bridge (e.g., vehicle collision) may appear much worse than its actual effect upon the structural performance (e.g., load capacity); quite often, bridges are closed to traffic unnecessarily following sudden damage due to this uncertainty and vice versa. Following the detection of damage, it is usually beneficial to the owner to quickly yet objectively identify the actual structural response to controlled loading experiments. The constructed bridge will have many inherent mechanisms to redistribute the applied load around any local damage and these mechanisms may not be fully considered in the analysis of the damage. These identified mechanisms include the actual load distribution, unintended composite action, participation of superimposed deadload, unintended continuity, and the participation of secondary members. [Lichtenstein, 1998].

Diagnostic load tests have traditionally been performed in conjunction with significant analytical modeling (e.g., finite element) of the structure. However, in the case of a speedy evaluation for damage, all modeling steps can be skipped or at least suspended for later post-processing steps in the experiment. Sensor and truck locations are maximized to the limits of all constraints in order to minimize the possibility of overlooking some hidden defect or damage. Crawl-speed tests are

preferable because continuous measurement of the load response is recorded for the entire traffic lane (as opposed to a finite set of pre-conceived locations). This research provides a novel approach to damage assessment by determining all indices (see Chapter 3) for the instrumented sections of the bridge from the measured data without the use of a finite element model.

A decommissioned, 3-span steel-stringer bridge (HAM-561-0683) was chosen to serve as a test specimen for evaluating the success of different concepts, experimental approaches, algorithms, and hardware/software tools for detecting various types and levels of induced damage to the bridge. Damage detection concepts and tools being the essential prerequisites to health monitoring, this bridge played an important role in the overall research.

#### 4.3. Induced Damage Experiments for Closed Bridge Specimen

A decommissioned bridge (HAM-561-0683, see Figure 4-1) was selected since it is a "typical" steel-stringer bridge, located in Cincinnati and was scheduled for renewal. The bridge specimen was a 130 ft long, 3-span bridge (40', 50', 40') with continuous rolled steel beams and reinforced concrete deck and substructure. The bridge was constructed in 1953. The bridge carried two lanes, one for each traffic direction. Steel sections W27 x 94 and W21 x 73 were used for the inner and outer girders, respectively. Field splices connecting the girders were assembled over the piers, and two cover steel plates were added for high moment concentration to the top and bottom flanges. Although the bridge was designed non-composite, top flanges of the steel girders were partly encased in the reinforced concrete deck. It should be noted that this construction type provides some composite action between the girders and deck slab under traffic stress levels.

The RC deck was 6.5 inches thick and there was an additional 2.5 inches thick bituminous surface on top of concrete deck. At sidewalk sections, the thickness of the concrete slab increased to 20.75 inches.

Simple stub abutments with a single row of piles were used where all the piles are cast-in-place. The abutment was supported by eight 12-in diameter cast-in-place vertical reinforced-concrete piles. Vertical piles were uniformly spaced 5'-6" apart and driven in a single row. The steel girders were rested on the fixed pier bearing plates which were set on the pier head beam which is a 18"x30" reinforced concrete rectangular section, along the transversal direction of the bridge superstructure. The head beam was supported by four reinforced concrete columns (18"x30"). A reinforced concrete rectangular foundation beam with 42"x36" dimensions supported these columns and connected them to nine piles, which were 12-in diameter cast-in-place reinforced concrete.

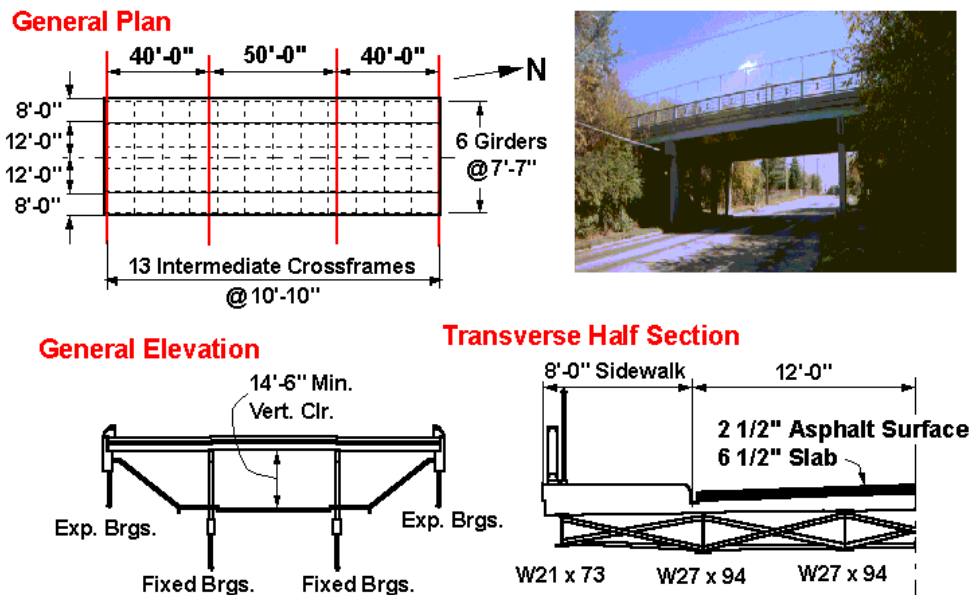


Figure 4-1: General Plans for HAM-561-0683

Field inspections were conducted at the test bridge before and during the research by UCII researchers, ODOT engineers, and experienced engineers from the private sector. It was the common conclusion that this test specimen exhibits extensive deterioration at concrete deck, girders, abutments and expansion joints (see Figure 4-2).

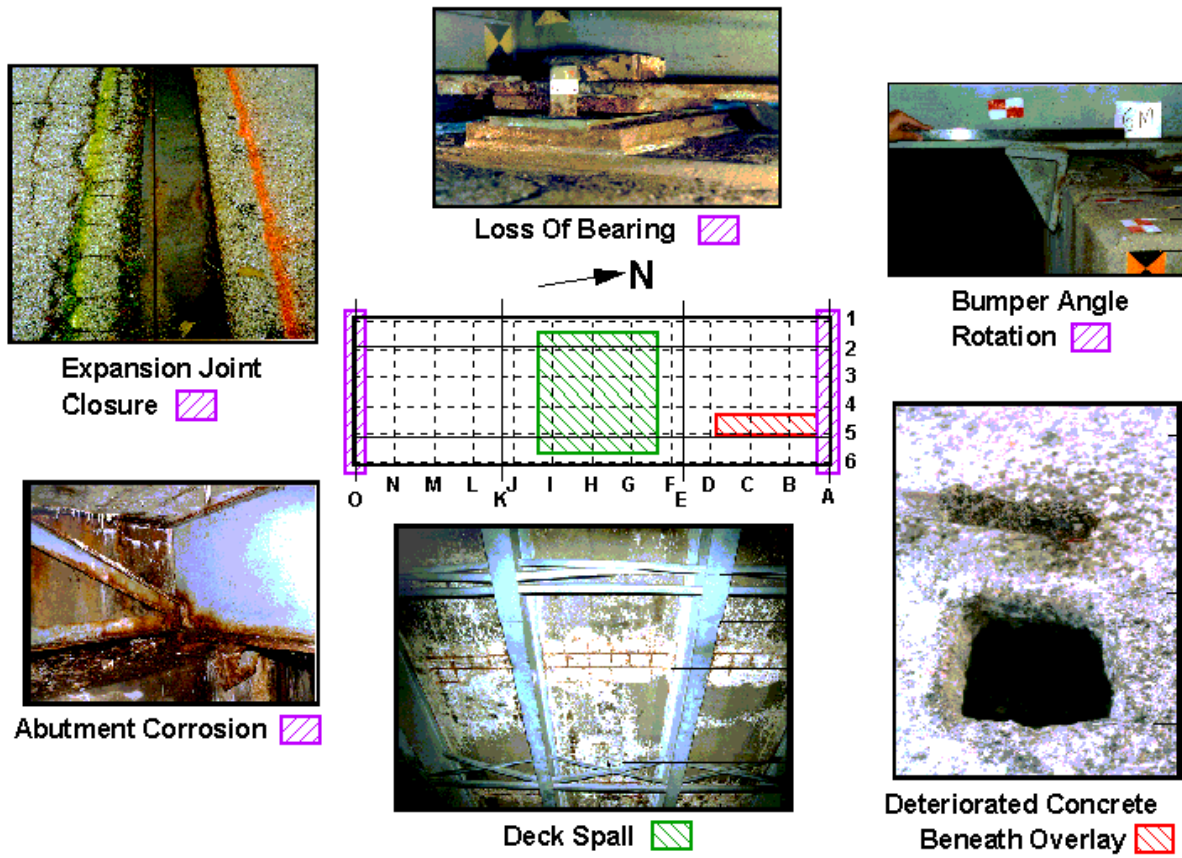
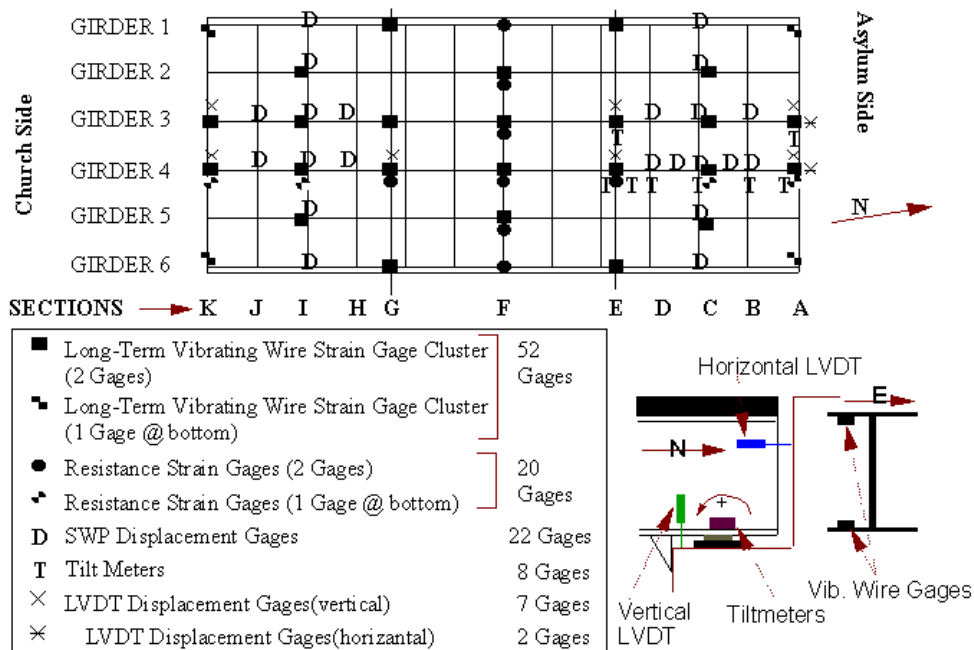


Figure 4-2: Location and Types of Deterioration for HAM-561-0683

The bridge was instrumented and subjected to modal tests and truck load tests in the first month of the project (May 1996) to establish its baseline. A monitoring system (see Figure 4-3) comprised of temperature, strain, displacement, and acceleration sensors at the critical regions of the test bridge was utilized to record and collect data in several modes:

- (a) Continuous low-speed monitoring of environmental conditions and bridge responses corresponding to these as well as the damage being induced;
- (b) high-speed monitoring of responses due to ambient or traffic vibrations; and,
- (c) the responses under controlled static and crawl-speed truck loading.

The two middle girders are heavily instrumented with displacement gages, long-term and resistance strain gages. In addition to these, supports (abutments and piers) and middle of the spans are also instrumented with displacement and strain gages. The north span on Girder 4, is instrumented with tiltmeters.



**Figure 4-3: Instrumentation Plan for HAM-561-0683**

In the first year, the bridge was subjected to a series of deliberately induced damage, simulating typical deterioration and damage scenarios that may affect steel-stringer bridges (see Figure 4-4). Damage scenarios included long-term deterioration effects such as due to the loosening and/or breaking of connections, fatigue-fracture, dislocated bearing, corrosion and reduction of effective area and inertia of steel members and connections, loss of chemical bond providing composite action. Retrofit in terms of stiffening and strengthening of certain bearings and supports was also simulated. Successful simulation of the deterioration, damage, and retrofit scenarios was accomplished through the guidance of an expert panel of ODOT, FHWA, and private consulting engineers. Following each damage or retrofit, researchers conducted their experiments (modal and truck-load tests) and evaluated the results together with the expert panel.

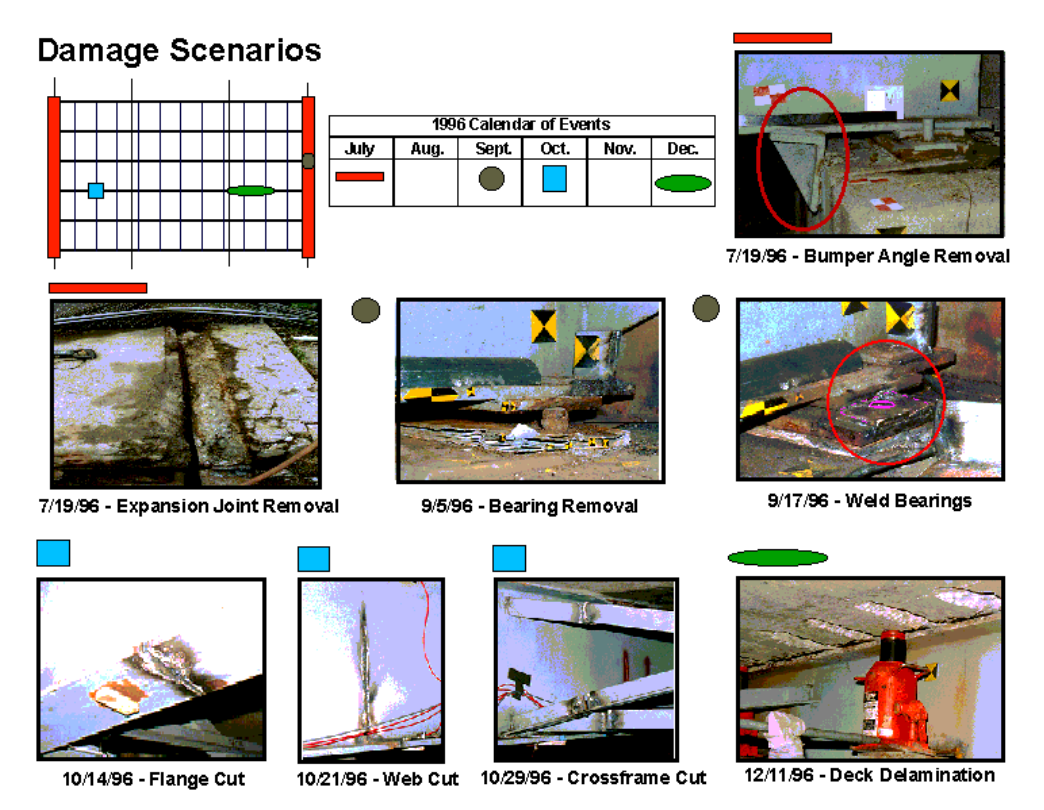


**Figure 4-4: Calendar, Types, and Location of Induced Damages for HAM-561-0683**

For this paper, we will primarily focus our examination of the damage scenarios upon the full flange cut of October 14, 1996. The flange at Section I of Girder 4 in the south span was cut incrementally by torch from the outside edge towards the web on each side. The resultant 0.25” cut was clear through the width and thickness of the bottom flange, adjacent to a crossframe. This damage was meant to somewhat simulate a fatigue crack. The following web and crossframe cuts at the same section were meant to simulate a yielded bottom flange after truck collision due to poor vertical clearance under the bridge. This event is actually quite a common occurrence in practice and the transportation department is often called upon to make a quick judgement about bridge condition after such an event. Truckload and modal impact tests were conducted before and after the damage. Visual inspection by the transportation department and an independent consultant was also conducted before and after the damage to understand the subjective nature of this more traditional approach to nondestructive evaluation.

The assumptions for an ideal beam (Section 2.1) still apply to the assessment of the following condition indices for a steel-stringer bridge under diagnostic load. The vertical origin will be arbitrarily considered as the outer face of the bottom flange of the steel girder.

#### 4.3.1. Sectional Indices for Damage Assessment under Instrumented Monitoring

The vibrating wire gage locations were monitored continuously during the project to capture the temperature and stress distributions, beginning in May 1996. Figure 4-5 shows the endspan gages on girder 4 during the days before and after the flange cut. Two sections are graphed for

comparison, section I where the damage is induced and section C as a corresponding section with no damage. Section C gages show no discernible effect of the damage. The effect of the flange cut is seen at the bottom flange gage reading (I Bottom) as a sudden jump in tension at that location. Since the top flange gage reading is not effected from the damage, it can be concluded that the effect of the flange cut is extremely local. The main question after examining the data was the reason behind the increased tension at the bottom flange gage location after the flange cut. It was concluded that the stresses were transferred back to the sensor location since the gage was only 6 inches from the cut location.

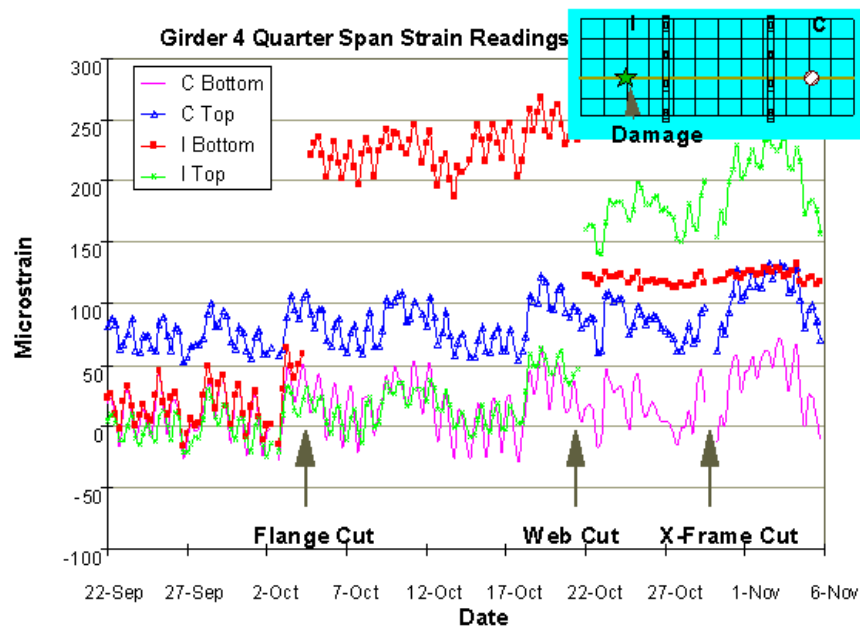


**Figure 4-5: Instrumented Monitoring of Flange Cut for HAM-561-0683**

The web cut can be seen both from bottom and top flange gage readings (I Top & I Bottom) as an increase in tension at top and release of tension at the bottom.

In order to verify the gage readings, analytical strain values are calculated for each damage (Table 4-1). The section is assumed to act compositely under service loads (proven by truck load tests), and the effective width of the concrete section is assumed to be equal to the distance between the girders. As it can be seen from the table, the most obvious characteristic change at the section is the upward movement of the neutral axis. Assuming the total moment on the section does not change, the strain values change at gage levels due to this change in the neutral axis. The change is indicated as an increased tension at the bottom flange location after the full flange cut. The top flange location also shows increasing tension after the web cut whereas the bottom one shows a release in tension. These analytical calculations greatly support the results seen in Figure 4-5.

<b>DAMAGE</b>	<b>Moment of Inertia</b>	<b>% Change</b>	<b>N.A. location (From bottom)</b>	<b>% Change</b>	<b>Strain Change Top (nominal=-1)</b>	<b>Strain Change Bottom (nominal =1)</b>
<b>Nominal</b>	22383.76		25.46		-1.00	1.00
<b>Half Flange Cut</b>	15544.68	30.55	26.46	3.93	-0.46	1.50
<b>Full Flange Cut</b>	9317.76	58.37	27.54	8.19	1.02	2.60
<b>2/3 Web Cut</b>	2737.13	87.77	29.42	15.56	13.95	

**Table 4-1: Comparison of Analytical Section Properties and Strains**

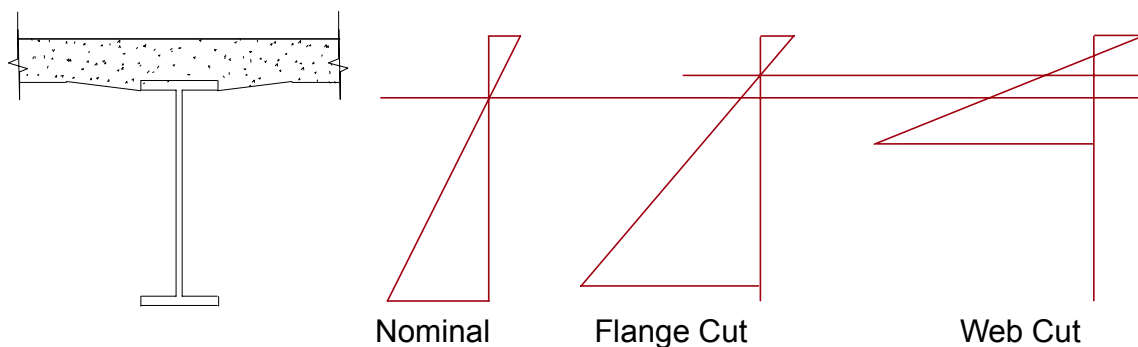


**Figure 4-6: Estimated Sectional Properties due to Induced Damages**

When examining the effect of the daily temperature cycles, the strain readings at section C (non-damaged) follows the daily temperature cycles undisturbed. After the flange cut, the strain readings at section I (damaged) show the daily strain fluctuations superimposed upon the local effects of the damage. After the web cut is completed, the daily strain fluctuations disappear from the bottom flange readings because of the lack of structural continuity at that location; the top flange gages show an increased sensitivity to temperature. It should be indicated that these values are the result of a simple analysis and do not include the three dimensional nature of the structure and grid system.

#### 4.3.2. Sectional Indices for Damage Assessment under Static Truckload

Static loading is a simple and practical method for applying a known load pattern to the test bridge. Static truck load testing was utilized at HAM-561-0683, before and after each damage and repair. The results from these tests are used in two forms: a) Each set of deflection data is compared with the corresponding computed flexibility from the modal test results, b) Before damage and after damage data sets were compared to capture an indication of damage on the gage responses.

A loading combination of 4 loaded trucks (two trucks in each endspan) with average weight of 29.1 kips each is presented in this research. Figures 4-7 and 4-8 show the deflection and strain data collected before and after the flange cut at Girder 4.

The deflection is observed to increase due to a decrease in the stiffness of the member in that location. Although north span deflections remain unchanged, deflections in the south span increased with the severity of the induced damage. The maximum differential deflection occurred with the web cut. The maximum deflection at the damaged location was 0.076" (after the crossframe cut) which corresponds to  $L/6300$ , where  $L$  is the span length. The AASHTO Specifications require that the maximum allowable live load deflection for a conventional highway bridge be limited by  $L/800$ . Even with the flange and  $2/3^{\text{rd}}$  of the web cut, the maximum deflection measured for the given truckload (approximately 40% of the design HS20 truckload) was only  $1/8$  of that value. This shows the redundancy of the structure.

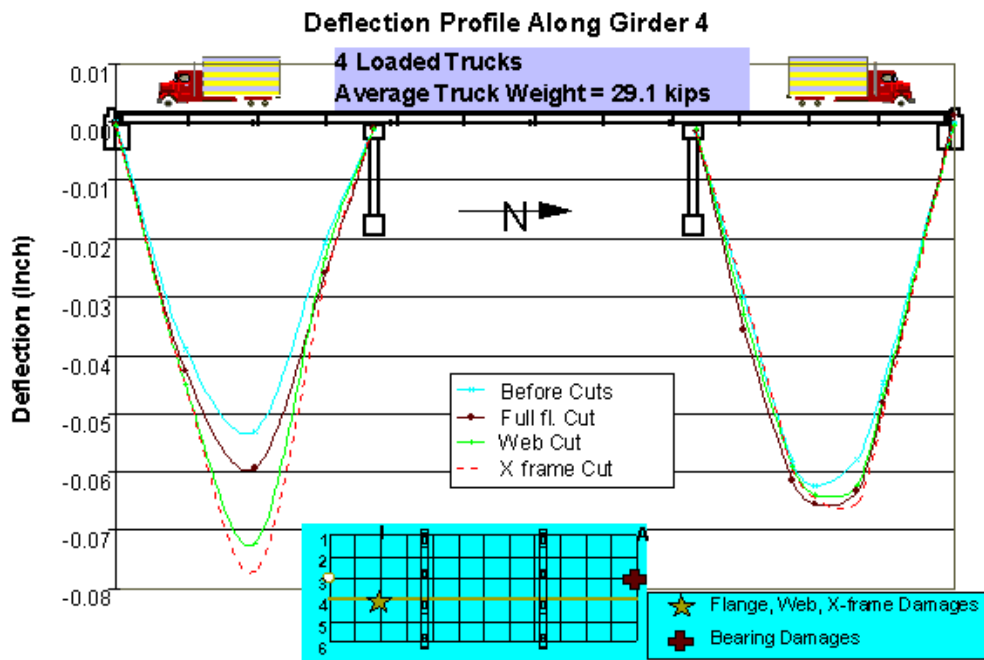


**Figure 4-7: Deflection Profile for Flange, Web, and Crossframe Cuts of HAM-561-0683**

As one might expect, the truckload strains at the cut location have decreased due to the lack of continuity. The amount of decrease in strain is related to the severity of the damage induced. Although the damage induced was highly local, the effects of it can be seen at the abutment and the pier of the same span. The effect was highly dissipated at the north span where no damage is applied. Note that the strain profile is much more sensitive to the induced damages than the deflection profile at each instrumented section. Even with the flange and 2/3<sup>rd</sup> of the web cut, the maximum stress measured (on the adjacent girder in the south span) for the given truckload (approximately 40% of the design HS20 truckload) was only 2.3 ksi, or 7% of the yield stress for the steel beam. This shows the redundancy of the structure.

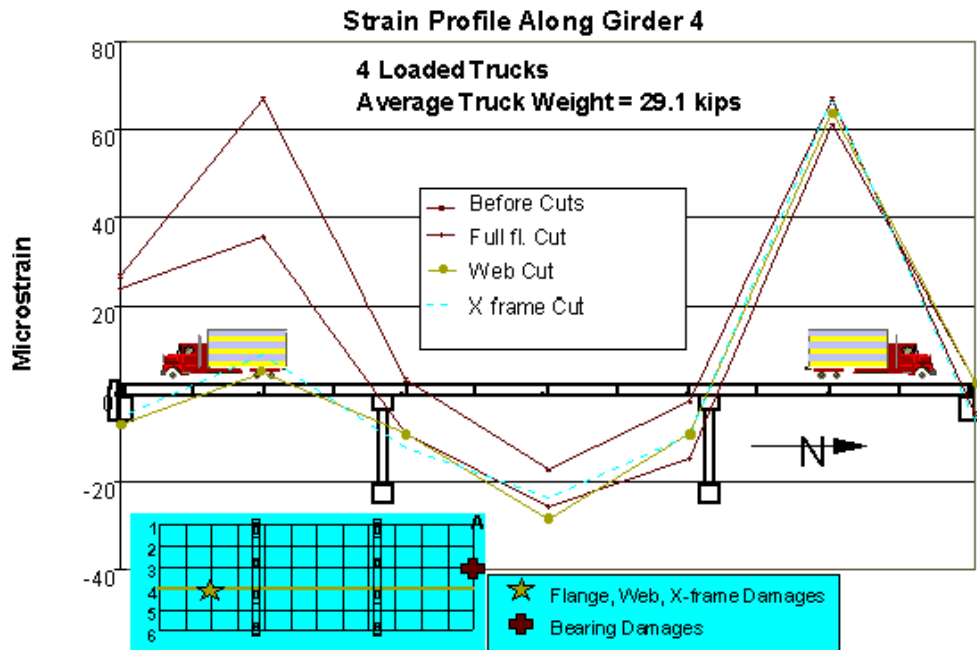


**Figure 4-8: Strain Profiles for Flange, Web, and Crossframe Cuts of HAM-561-0683**

4.3.3. Sectional Indices for Damage Assessment under Modal Impact

One of the important aspects of the Seymour Ave. Bridge research is the opportunity to bring up the synergy between different nondestructive testing methods. A truck loading combination was selected which would accommodate the modal test grid and allow comparison of the determined flexibility with the measured deflections from the instrumented monitor. Two trucks with known wheel loads were positioned on end spans over the middle two girders while the corresponding global displacements and local strains were measured. Figure 4-9 shows good correlation for the two deflection profiles at girder 4 after the web cut. The average deflection differences between the modal and instrumented monitoring responses in these presented data were 0.0037", with maximum differences occurring as 0.009".

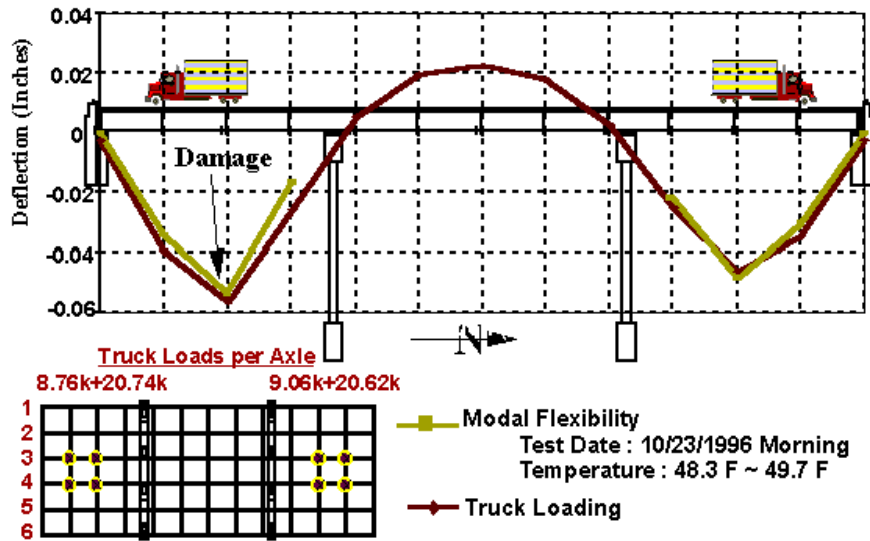


**Figure 4-9: Correlation of Deflection Profiles for Truckload and Modal Tests**

Of many different forms of modal testing, multi-reference impact testing was found to be the most suitable for bridge testing, particularly for bridges with frequencies higher than 4 Hz. Since this type of test could be applied in increments using different grids at different times on the bridge, it was possible to mitigate non-stationarity of the structure. While the bridge's mechanical characteristics may shift over a matter of hours depending on the temperature changes, each individual test could be conducted within an hour or so such that the bridge could remain close to a stationary state during the execution of each test. This was found to be an essential requirement in order to be able to post-process the tests meaningfully.

Depending upon the spatial properties of the test grid and the frequency band of interest, modal flexibility successfully served for both a global and an element-level local condition assessment. The advantage of modal flexibility, even when only two girder-lines could be tested at a time, was that it permitted the experimental evaluation of individual girder deflections under any virtual nodal load, obtained without any analytical characterization or numerical assumption. The deflected shape for a unit nodal load, termed as the Bridge Girder Condition Indicator (*BGCI*), provided a conceptual index of girder condition. While other load patterns may be applied to generate girder deflections which are more sensitive to local damage (e.g. see Figures 4-7 and 4-9), the uniform load pattern permitted the most reliable index since this index was affected the least by modal truncation and experimental errors.

In Figure 4-10, the *BGCI* successfully reveals the relative stiffness of different girders at different spans for before and after each damage cut at the midspan cross-section of Girder 4. The initial flange cut at the latter cross section was detected with the least confidence. One may

conclude that the BGCI reliably and conceptually locates and quantifies the direction and amount of change at a local deflection node in the case of more than 10% change.

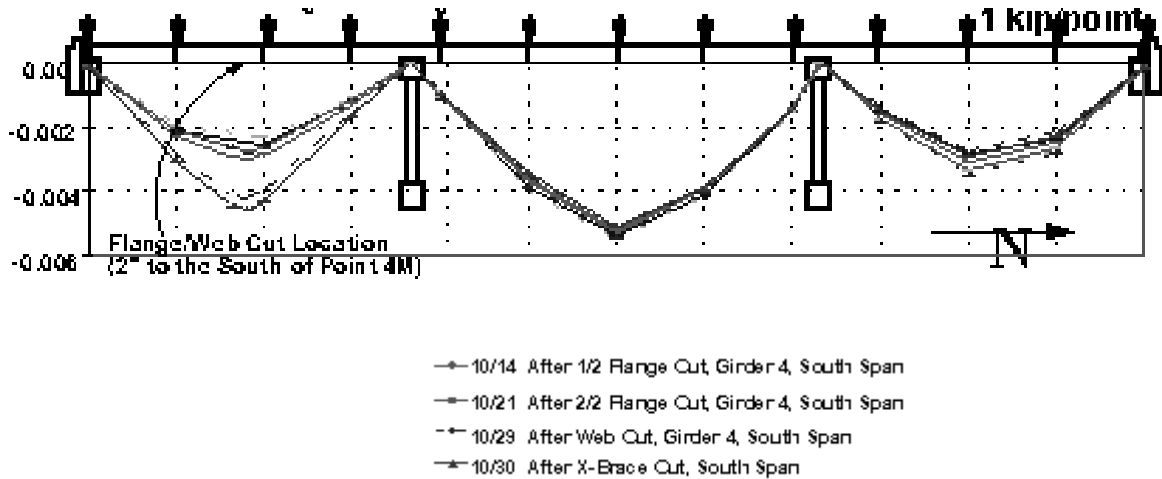


**Figure 4-10: Bridge Girder Condition Indicator of Damage Scenarios for HAM-561-0683**

#### 4.3.4. Sectional Indices for Damage Assessment under Crawl-Speed Truckload

Crawl-speed (i.e., 5mph) truckload tests were conducted in the eastern traffic lane before and after each damage scenario for HAM-561-0863. Such tests could not be performed in the other (i.e., western) traffic lane due to the circumstantial limitations of the bridge site. Data was collected from the all gages except the vibrating wire gages at a 25Hz sample rate. Note that many of the sections were only instrumented at the bottom flange which makes it impossible to calculate most of the indices discussed in Chapter 3.

## **Maximum Stress for Bottom Flange Sensors**

The location of maximum stress observed during a set of experiments is certainly a parameter of concern. The response of the instrumented member can itself be checked against its material capacity for load. If this is tracked for the damage scenarios, this could indicate areas of possible concern for the inspection team. However, an influence line would provide greater information by normalizing the stress to a unit load and considering the entire length of the load path. This provides a highly sensitive and easily conceptualized damage index following the truckload test.

Before and after the flange cut, the maximum stress occurred in the north span on the fourth girder at the bottom flange during the diagnostic truckload test (see Figure 4-8, 4-11, and 4-12). The corresponding top flange at all positive moment regions is near zero, indicating an unintended but fully composite section. With each cut, the damaged section carried less and less load and the crossframe cut removed its last significant load path. After all the cuts to the steel section (i.e., flange, web, and crossframe), the maximum stress occurred in the south span on the third girder at the bottom flange.

Note the significant change in strain influence (28.6%) as compared to the change in deflection for the flange cut (13.6%, see Figure 4-7). The greatest change in strain influence for the instrumented sections occurred immediately adjacent to the damage. The change in strain influence was reduced and yet still sensitive for those instrumented sections that were more distant from the damage. Hence, it is suggested that damage can be easily detected and localized by the strain influence line even when the damaged member itself is not instrumented.

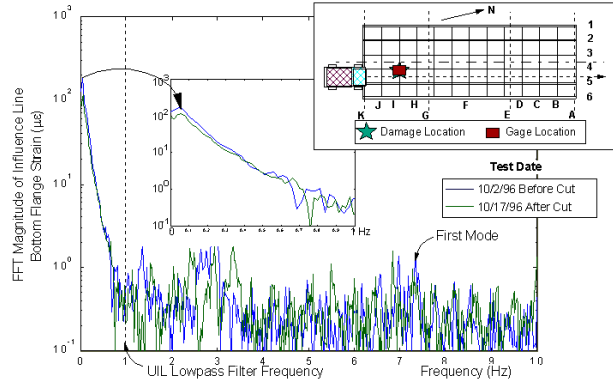
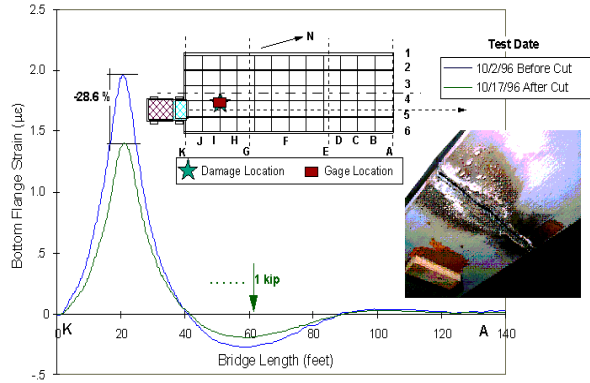


**Figure 4-11: Influence Line Before and After Flange Cut for Bottom Flange of South Span**

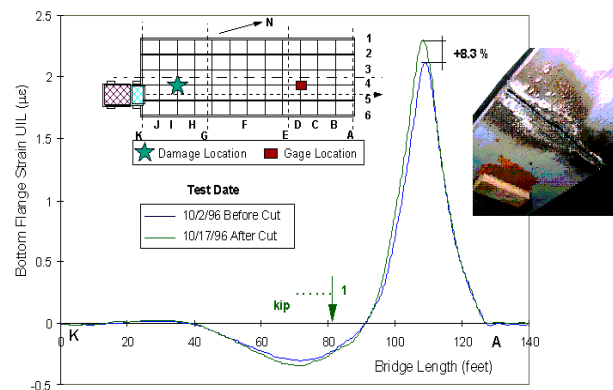
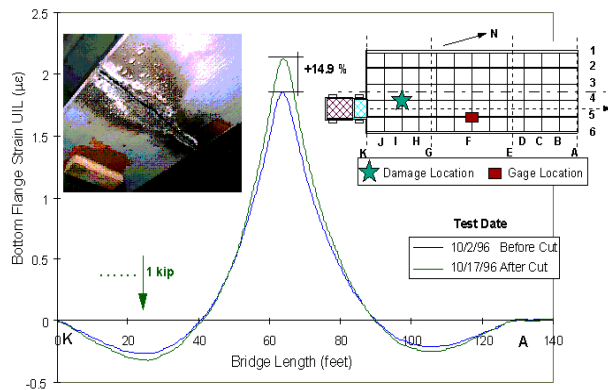


**Figure 4-12: Influence Lines Before and After Flange Cut for Bottom Flange of Other Spans**

The piers indicated very slight composite action, but performed generally in a noncomposite manner as designed. The pier bearings consisted of a thin layer of lead and a small steel plate that was anchored into the concrete of the pier cap. From inspection, it was apparent that there would be high variability in their performance due to the varying levels of deterioration to their seating and connection to both the girder and the pier cap. In addition, there was attempt by the research team to actually fix all of the pier and abutment supports by welding the bearing plates to the girder and their anchors. However, this fixity was not guaranteed nor uniform. Finally,

the structure was observed to have considerable variation in the boundary conditions including settlement, torsional misalignment of girders, varying slope/soil pressure causing shifting and cracking of the backwall and foundation, etc.

The north pier for Girder 4 indicates the expected fixity or restraint of the bridge design, while the south pier appears to have no fixity and is a textbook example of a simple or free support (see Figure 4-13). As the girder cannot transfer any load (axially or in bending) to the south pier, it understandably experiences greater stress and moment during the truckload test. You may recall that HAM-126-0881 also exhibited some axial restraint in the pier influence lines; however, the latter is clearly attributed to the integrated design of its abutments as there is no ambiguity about the boundary conditions of this newly constructed bridge. For HAM-561-0683, there is concern that any of the supports could lose their fixity and thus increase the stress and moment upon the girder in the negative moment region.

Note the greater change in strain influence (19.3%) at the far pier as compared to the change in strain for the near pier for the flange cut (13.9%, see Figure 4-7). Although the sensitivity is still greatest adjacent to the damage, the pier measurements refute the argument that there would be a proportional change with distance from the damage. Further examination is required.

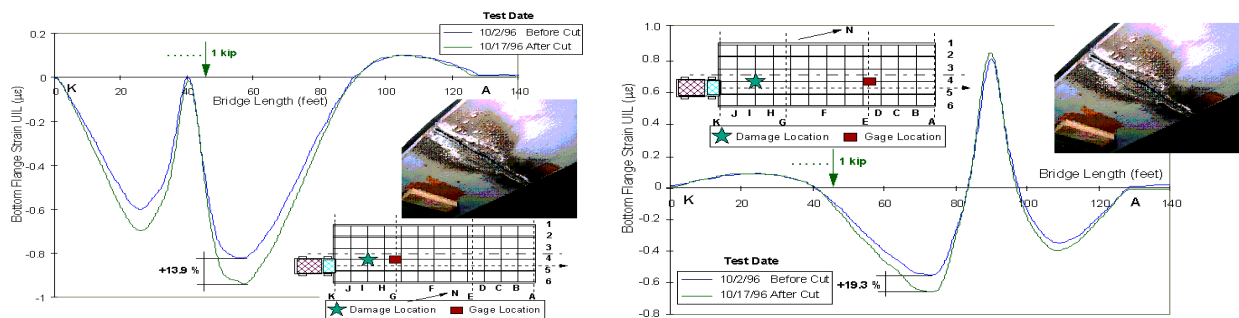


**Figure 4-13: Influence Lines Before and After Flange Cut for Bottom Flange of Piers**

From the influence lines for the positive moment regions, one observes the ideal response discussed in Chapter 2 for the bottom flanges in each span (see Figure 3-2). It must be noted, however, that the top flange influence lines indicate some nonlinear behavior and do not peak at the same location as the bottom flange lines (as was observed for HAM-126-0881 in Chapter 3). This may be due to slip-stick performance of the composite interface with the concrete decking; however, it occurs at every instrumented section. Another hypothesis is that some very local transfer of the load occurs at each crossframe or at other secondary members of the bridge structure. These unexpected but local responses at the top flange and piers have been observed on many other steel-stringer bridges and will be considered further in future research.

### **Capacity Load Rating for Instrumented Sections**

The HS20-44 truckload and laneload are virtually simulated in the east traffic lane by linear superposition of the derived influence lines (see Figure 2-4), weighted by the specified weights (see Figure 3-17). In lieu of the appropriate crawl-speed tests and measurements, estimates based upon bridge design and the static truckload tests are made. The response is assumed to be identical when the truck crosses the bridge in the other lane due to the symmetry of the structure; however, an actual truckload test in all lanes is the appropriate method to assess the condition rating of a bridge. The response at the top flange of the endspan girders has been estimated from the vibrating wire gage measurements during the static truckload experiments; again, strain measurement during the actual crawl-speed truckload test is the appropriate method to assess the condition rating of a structure.

The liveload is calculated for both types of rating load by each of the four analytical methods and then summarily rated by the load factor approach for both the Inventory and Operating levels. Note that the corresponding effective deadload  $M_{DLeff}$  and superimposed deadload  $M_{SDLeff}$  moments are used with the calculated liveload  $M_{LL} = \{M_1, M_2, M_3, \text{ or } M_4\}$  moment by the four analytical methods.

The truckload controls the rating factor for the positive moment regions, while the laneload is found to control the rating for the negative moment regions.

The load ratings for the positive and negative moment regions are selected as the minimum rating by Method 2 (see Figure 3-19) and Method 3 (see Figure 3-26), respectively, based upon their identified level of composite action. Irregardless of the estimated depth of the compressive block in the concrete decking, the section is assumed as noncompact but composite in determining the ultimate moment for the positive moment regions for comparison against other analytical studies. Tables 4-2 and 4-3 summarize the load rating for the composite sections before and after the flange cut, respectively. In addition, all sections are rated as noncomposite to compare against the nominal values. Tables 4-4 and 4-5 summarize the load rating for the noncomposite sections before and after the flange cut, respectively. Table 4-6 summarizes the load rating based upon a simple beam analysis of the design plans.

Girder #4	Capacity (k-ft)	DL <sub>eff</sub> (k-ft)	SDL <sub>eff</sub> (k-ft)	LL (k-ft)	Impact	RF, Inv	RF, Opr
South span	953.15	128.89	41.73	112.19	0.303	2.305	3.848
Middle span	Broken gage	-	-	-	0.286	N/a	N/a
North span	971.03	131.32	42.52	108.57	0.303	2.427	4.051

**Table 4-2: Condition Summary of Positive Moment Regions Before Flange Cut, HAM-561-0683**

Note: Noncompact and unintended composite action assumed at limit state

Girder #4	Capacity (k-ft)	DL <sub>eff</sub> (k-ft)	SDL <sub>eff</sub> (k-ft)	LL (k-ft)	Impact	RF, Inv	RF, Opr
South span	916.58	123.93	40.13	77.38	0.303	3.214	5.366
Middle span	1051.6	156.48	50.67	130.46	0.286	2.149	3.587
North span	954.25	129.04	41.78	115.69	0.303	2.238	3.736

**Table 4-3: Condition Summary of Positive Moment Regions After Flange Cut, HAM-561-0683**

Note: Noncompact and unintended composite action assumed at limit state

Girder #4	Capacity (k-ft)	DL <sub>eff</sub> (k-ft)	SDL <sub>eff</sub> (k-ft)	LL (k-ft)	Impact	RF, Inv	RF, Opr
South span	764.5	90.33	41.73	112.19	0.303	1.869	3.119
South pier	-764.5	-190.75	-82.18	-82.56	0.294	1.767	2.950
Middle span	Gage broken	-	-	-	0.286	N/a	N/a
North pier	-764.5	-190.75	-82.18	-40.08	0.294	3.640	6.076
North span	764.5	90.33	42.52	108.57	0.303	1.928	3.218

**Table 4-4: Condition Summary of Critical Regions Before Flange Cut, HAM-561-0683**

Note: Compact and noncomposite action assumed at limit state

Girder #4	Capacity (k-ft)	DL <sub>eff</sub> (k-ft)	SDL <sub>eff</sub> (k-ft)	LL (k-ft)	Impact	RF, Inv	RF, Opr
South span	764.5	90.33	40.13	38.92	0.303	5.406	9.024
South pier	-764.5	-190.75	-82.18	-93.18	0.294	1.566	2.614
Middle span	764.5	99.42	42.83	130.46	0.286	1.592	2.657
North pier	-764.5	-190.75	-82.18	-56.29	0.294	2.592	4.327
North span	764.5	90.33	41.78	115.69	0.303	1.812	3.025

**Table 4-5: Condition Summary of Critical Regions After Flange Cut, HAM-561-0683**

Note: Compact and noncomposite action assumed at limit state

BARS	Capacity (k-ft)	DL <sub>eff</sub> (k-ft)	SDL <sub>eff</sub> (k-ft)	LL (k-ft)	Impact	RF, Inv	RF, Opr
South span	351.5	153.5	N/a	245.4	0.303	0.711	1.185
South pier	-474.2	-309.7	N/a	-216.2	0.294	1.031	1.718
Middle span	351.5	141.8	N/a	251.3	0.286	0.724	1.206
North pier	-474.2	-309.7	N/a	-216.2	0.294	1.031	1.718
North span	351.5	153.5	N/a	153.5	0.303	0.711	1.185

**Table 4-6: Design Values for Critical Regions, HAM-561-0683**

Note: Compact and noncomposite action assumed at limit state

The condition rating based upon the diagnostic truckload tests indicates that the south pier dominates the assessment for before and after the flange cut. The load rating is reduced by 11.4% at the south pier, which corresponds approximately with the observed change in the strain influence line at that section. Note that the load rating for the damaged section (i.e., the south span) actually increases due to the reduced strain observed during the truckload experiments.

It must be again be reiterated that only a few sections were actually instrumented, some only at the bottom flange, and only one lane was actually loaded during the diagnostic crawl-speed tests.

In comparison with the nominal values, the identified load ratings are just over twice the design ratings for both before and after the flange cut. The design is actually controlled by the positive moment sections instead of the south pier. The combined deadload and superimposed deadload moments compare favorably with the nominal deadload; the liveloads are significantly reduced. Based upon the design capacities, it appears that the nominal values are based upon the outer girders (i.e., Girders #1 and #6) instead of the instrumented Girder #4. Hence, it is rather contrived to quantitatively compare the two; however, it can be stated that the identified condition of even the damaged structure is indeed better than expected based upon a simple design analysis.

#### 4.3.5. Sectional Indices for Damage Assessment by Finite Element Model

Condition assessment of an existing constructed facility is best served by discrete, geometric models taking advantage of any heuristic knowledge-base and, ideally, experimental data from field tests of the structure. This is especially important in the case of HAM-561-0683 where an incomplete set of data from the diagnostic truckload experiments was collected. As discussed above, the lack of instrumentation on the exterior girders makes it rather contrived to compare with the nominal design values. A calibrated model representing the entirety of the structure was prepared to rigorously evaluate the damage scenarios [Griessmann, 1998, Lenett, 1999d]. All available information (e.g., the original design, fabrication/shop drawings, construction, inspection, rating and maintenance records, existing conditions as documented by arms-length-inspection, rebar samples, strength tests of concrete cores, etc.) was utilized in the construction of a preliminary model without idealizing geometric attributes. The FE model served to establish the frequency band of interest, frequency resolution, truck-load positions or modal impact grid, and the reference locations and orientation.

In order to perform FE model calibration, certain structural and material properties within the model, such as moments of inertia and concrete modulus of elasticity, etc. were selected as variables. The idealized internal continuity and external boundary conditions are replaced by appropriate translational and rotational springs to better simulate the local kinematics which have critical impact on the global responses. As field data becomes available, the preliminary FE model of a tested bridge is calibrated to conform to the experimentally determined dynamic characteristics, flexibility, peak strains, deflections, influence lines, etc. (see Figure 4-14). In

addition, modeling assumptions such as linearity, elasticity, reciprocity, stationarity, and others are verified by the field tests.

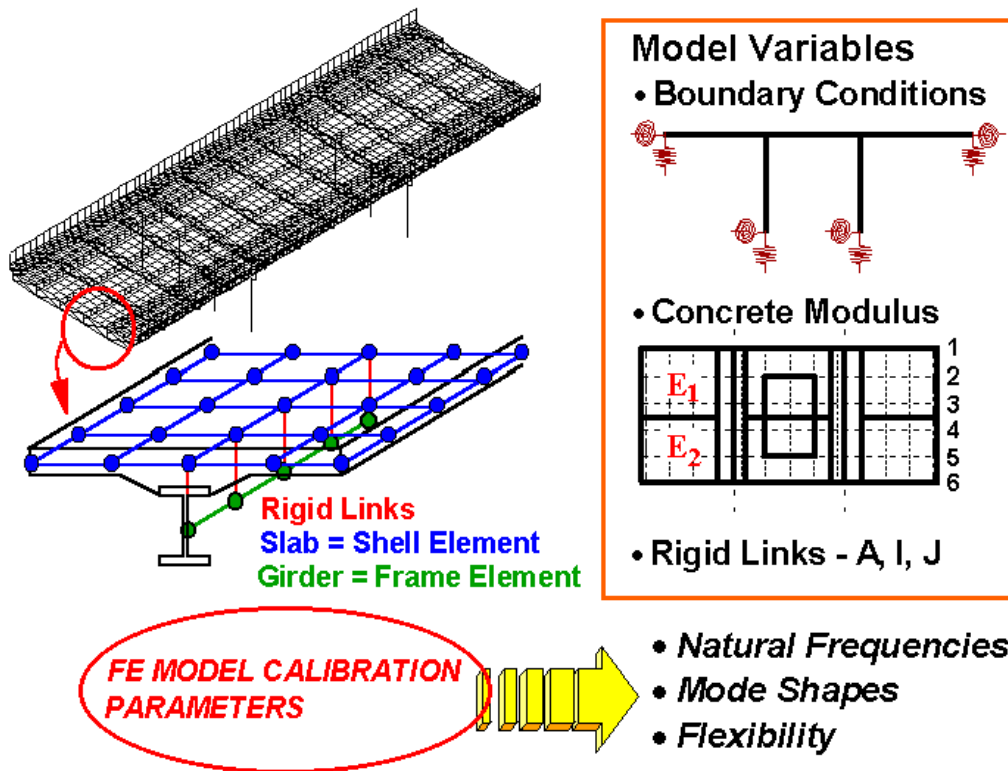


Figure 4-14: Calibration of the Finite Element Model for HAM-561-0683

The field-calibrated FE model now accurately simulates the element stiffnesses and local kinematics at the exterior and interior supports as well as connections. Damage scenarios can now be simulated and evaluated (e.g., the flange and web cuts were represented together as a reduction in beam area and stiffness at the damaged section, as well as reduced stiffness in the rigid link with the concrete decking). In this manner, the actual state and all the critical behavior mechanisms are captured and simulated accurately for the entire structure. Note that the pier bearings are represented as simple supports to consider the worst-case scenario (i.e., any current

fixity will be lost at the limit state) at these sections. Load factor ratings for the test bridge were then computed from the calibrated FE model for both HS20-44 truckload and laneload specifications (see Tables 4-7 and 4-8 for condition summaries of the bridge before and after the cuts to the steel section, respectively). Noncompact and composite action was assumed for the positive moment sections at the limit state; compact and noncomposite action was assumed for the negative moment sections. Truckload dominated the positive moment region, while laneload controlled the negative moment region. Note that the FE model was only adjusted for the entire set of cuts to the flange, web, and crossframes of Section I in the south span.

FEM	Capacity (k-ft)	DL <sub>eff</sub> (k-ft)	SDL <sub>eff</sub> (k-ft)	LL (k-ft)	Impact	RF, Inv	RF, Opr
South span	1064	64.8	-	113.8	0.303	3.050	5.090
South pier	-765	-175.2	-	-83.7	0.294	2.290	3.810
Middle span	976	90.5	-	133.4	0.286	2.310	3.850
North pier	-765	-190.8	-	-93.6	0.294	1.970	3.280
North span	802	63.3	-	111.4	0.303	2.290	3.820

**Table 4-7: Condition Summary of FE Model Before Flange Cut, HAM-561-0683**

Note: Noncompact and composite action assumed for positive moment sections at limit state

Note: Compact and noncomposite action assumed for negative moment sections at limit state

FEM	Capacity (k-ft)	DL <sub>eff</sub> (k-ft)	SDL <sub>eff</sub> (k-ft)	LL (k-ft)	Impact	RF, Inv	RF, Opr
South span	1064	73.7	-	132.4	0.303	2.590	4.330
South pier	-765	-179.8	-	-87.8	0.294	2.150	3.600
Middle span	976	95.6	-	138.0	0.286	2.210	3.690
North pier	-765	-190.3	-	-93.6	0.294	1.970	3.290
North span	802	62.3	-	112.0	0.303	2.280	3.810

**Table 4-8: Condition Summary of FE Model After Flange Cut, HAM-561-0683**

Note: Noncompact and composite action assumed for positive moment sections at limit state

Note: Compact and noncomposite action assumed for negative moment sections at limit state

The condition rating based upon the finite element model indicates that the north pier for an inner girder dominates the assessment for before and after the flange cut. The load rating is actually unaffected by the entirety of the induced damage scenarios. Note that the load rating for the damaged section (i.e., the south span) decreases based upon the increased strains observed for Girder #3 adjacent to the damaged girder. Although Girder #3 was not instrumented during the crawl-speed truckload tests, the model was calibrated to both the static truckload and modal impact tests and can extrapolate this member's behavior. As opposed to the identified condition from truckload (Tables 4-4 and 4-5), the north pier has a liveload that is comparable with the south pier because both are modeled as simple or free supports.

Note that the superimposed deadload is not listed in the summary tables for the finite element model; it is actually more appropriate to consider the effects of deadload and superimposed deadload as one entity for the model. Also, the deadload measurements of the instrumented bridge HAM-126-0881 during its construction indicated that, contrary to design, the superimposed deadload is not uniformly distributed to all girders. Hence, the superimposed deadload used above for the identified load ratings will be removed for direct comparison with the results of the finite element model.

Crawl test	Capacity (k-ft)	DL <sub>eff</sub> (k-ft)	SDL <sub>eff</sub> (k-ft)	LL (k-ft)	Impact	RF, Inv	RF, Opr
South span	No gage on G3						
South pier	-764.5	-190.75	0	-82.56	0.294	2.228	3.719
Middle span	Gage broken						
North pier	Pier is fixed						
North span	971.03	131.32	0	108.57	0.303	2.607	4.352

**Table 4-9: Modified Summary of Critical Regions Before Flange Cut, HAM-561-0683**

Note: Noncompact and composite action assumed for positive moment sections at limit state

Note: Compact and noncomposite action assumed for negative moment sections at limit state

Crawl test	Capacity (k-ft)	DL <sub>eff</sub> (k-ft)	SDL <sub>eff</sub> (k-ft)	LL (k-ft)	Impact	RF, Inv	RF, Opr
South span	No gage on G3						
South pier	-764.5	-190.75	0	-93.18	0.294	1.974	3.295
Middle span	1051.6	156.48	0	130.46	0.286	2.330	3.889
North pier	Pier is fixed						
North span	954.25	129.04	0	115.69	0.303	2.404	4.013

**Table 4-10: Modified Summary of Critical Regions After Flange Cut, HAM-561-0683**

Note: Noncompact and composite action assumed for positive moment sections at limit state

Note: Compact and noncomposite action assumed for negative moment sections at limit state

The deadloads remain greater than those estimated by the finite element model; however, the estimated capacities at the limit state are also greater than those of the model. The liveloads are remarkably close, which is actually the forte of the diagnostic truckload test; the main goal of the truckload test is the identification of the liveload stress, moment, and modulus for the current condition of the instrumented sections. The load ratings are therefore greater than those estimated by the model; however, note that the rating for the south pier still controls the condition assessment of the structure. As noted above, the rating of the south pier and therefore the bridge remains unchanged by the entirety of the induced damage. Although the sectional indices for the damaged span are indeed responsive to even the flange cut, the rating factor for the bridge as a whole is actually insensitive to considerable and visible damage.

#### 4.3.6. Sectional Indices for Damage Assessment by Visual Inspection

By federal law, visual inspections must be performed at least every two years for every highway bridge. The results are placed into the bridge inventory. A routine inspection consists of “sufficient observations and/or measurements to determine the physical and functional condition of the bridge, to identify any developing problems and/or change from inventory or previously

recorded conditions, and to ensure the structure continues to satisfy present service requirements [FHWA, 1990].” The basic strength and weakness of the current bridge management system is that the information supplied to these databases is based upon subjective evaluation of visual inspection alone [Chase, 1995]. Essentially, subjective evaluation of visual data alone does not appear to enhance our understanding of bridge behavior or our ability to rate its condition and performance.

Before and after the steel damage scenario, four bridge engineers were brought to the test specimen to inspect and assess its condition. Two were consulting engineers with over sixty years of experience. The local District engineer and the Director of the Structural Maintenance and Inspection Division for the Ohio Department of Transportation were also included within the expert panel for the project. An initial overall rating for the bridge condition prior to any of the induced damage was a four (4 = poor) by the local district engineer and a five (5 = fair) by the Director. After the flange cut, the entire panel agreed that this damage would need to be immediately repaired due to concerns regarding fatigue; however, safety was not of concern because the load would be distributed to the rest of the superstructure through crossframes and decking. One renowned consultant remarked that the immediate local area would feel the damage, but the bridge as a whole would not notice anything. This correlates with the measured results and estimated ratings from the finite element model (see Table 4-7 and 4-8). Upon the web and crossframe cut, the panel became divided; the transportation officials became quite alarmed and would shut down any bridge in operation with this type of damage whereas the consultants remained unconcerned.

After the final induced damage scenario of deck delamination at the fourth girder in the north span, the expert panel was not concerned because the structure was not designed as a composite system; no detrimental effect was expected from this damage scenario. However, the finite element model estimated that the rating factor for the north pier and the structure was reduced by 5.6% due to the loss in unintended composite action for the section (see Figure 4-15). The damage to the girder-deck interface, which was thought to have no influence upon structural behavior, had reduced the safe load carrying capacity for the bridge. An incomplete understanding of the in situ performance of the structure in combination with the lack of any powerful visual evidence caused the inspectors to misdiagnose the seriousness of the damage.

In practice, truckload tests might help meter the variety of responses to sudden damage; however, it is reassuring to know that the public's trust is safe in the rather conservative hands of the transportation department. It is important to note that any inspection and/or condition ratings determined by a bridge engineer would involve the analysis of many disparate forms of information other than and including the physical appearance and load-carrying capacity of the structure. Maintenance schedules, engineering specifications, and political machinations alike must be delicately yet judiciously administered by our public officials each and every day of the week.



**As-Is Condition**



**Steel Damage**



**Concrete Damage**

Description	BARS RF (ODOT)	FEM RF
Inventory Rating Level	0.711	1.97
Inventory [tons]	256	70.9
Operating Rating Level	1.185	3.28
Operating [tons]	427	118.1

Description	FEM RF
Inventory Rating Level	1.97
Inventory [tons]	70.9
Operating Rating Level	3.29
Operating [tons]	118.4

Description	FEM RF
Inventory Rating Level	1.86
Inventory [tons]	67.0
Operating Rating Level	3.10
Operating [tons]	111.6

**SUBJECTIVE ANALYSIS**

**Fair Condition** - Primary structural elements are sound, but have minor section loss. Secondary elements have significant deterioration.  
**Poor Condition** - Advanced section loss, deterioration or spalling.

**Bridge Inspectors** - Shut down the bridge. The damages need to be repaired immediately.  
**Consulting Engineers** - There really isn't an immediate concern, but the repair would have to be fixed. The bridge can still carry its required capacity.

**Bridge Inspectors** - Not a problem. The bridge was not designed as a composite.  
**Consulting Engineers** - Not a problem. The bridge was not designed as a composite.

**Figure 4-15: Summary Assessment for Induced Damage Project, HAM-561-0683**

In conclusion, diagnostic truckload testing and instrumented monitoring have proven to be valuable but objective methods for the damage assessment of highway bridges. Continuous remote monitoring of a highway bridge to traffic and environmental loading would most likely detect any damage to an instrumented section of the structure and could immediately alert the transportation department of said damage and its likely effect upon structural performance. Following the detection of damage, a controlled truckload test would quickly yet objectively identify the actual structural condition and quantify the allowable traffic load upon the damaged bridge without speculation.

A suite of damage indices can be processed directly from the measured data to assess the presence and location of damage and quantify its effect upon the performance of the structure, including:

- Maximum stress in the outer fiber
- Modal frequencies, shapes, and weighting
- Neutral axis location
- Truckload moment, analyzed by four different methods
- Capacity load rating, analyzed by two different concepts (i.e., working stress and limit states)
  - HS20 Truckload and Laneload rating, Inventory and Operating
- Remaining fatigue life

This research provides a novel approach to condition assessment by determining the above indices for the instrumented sections of the bridge from the measured data without the use of a finite element model. The derived influence lines can be used to detect and localize damage and to virtually simulate the rating and fatigue loads for immediate field assessment of a highway bridge.

## 5. Health Monitoring/Management System for Highway Bridges

Health monitoring is the rational organization of the existing technologies, methods, and concepts each according to its merits within a system devoted to monitoring the state-of-health of a structure. This monitoring system may sit resident and on-line at the site of a structure in order to provide continuous assessment of its performance; or, the monitoring system may represent the remote bureau of responsible engineers and inspectors, which is the typical practice of the present day. In either case, this system takes a hybrid approach for structural monitoring where emphasis is placed upon the optimum interconnection and interaction of several NDE methods and technologies of merit for the given structure.

Two monitoring systems for steel-stringer bridges, HAM-42-0992 and HAM-126-0881, have been in operation for the past six years on a local highway in Cincinnati, Ohio. These projects were discussed in some detail in Chapter 1. Recently, the Ohio DOT contracted with the University of Cincinnati to extend the operation of these systems for at least the next two years.

The millions of miles of bridges, combined with the need to respond swiftly to accidental damage, has also lead several federal institutions to pursue the instrumented monitoring of highway roads and bridges. It is envisioned that the intelligent infrastructure of the future (Figure 1-8) will include a sensor system that will monitor structural condition and alert officials in case it is decided that the reliability of the structure is reduced to an unacceptable level. At a minimum, it has been established that an instrumented bridge health monitoring system will be comprised of a collection of sensors and data-acquisition hardware which will act to collect, archive, and possibly telemeter various bridge measurements such as strains, deflections,

accelerations, temperature, rotation, and others. These measurements will, in turn, be used by bridge engineers to complement the subjective visual inspections and must be sufficient to characterize the structure's response to its ambient loading environment in order to assess structural integrity. This is further depicted in Figures 5-1 and 5-2 for the existing monitoring systems. Detected anomalies may trigger an on-site battery of objective NDE tests that would escalate, as needed, in rigor and detail in order to fully appreciate the extent and magnitude of the deterioration and/or damage. As a long-range goal, the bridge health monitor may gain an autonomous nature where sensor measurements are gathered and processed, preliminary decisions regarding bridge health are made, immediate corrective actions (such as closing the bridge to traffic) are made, and communication with a central information and planning system is maintained regularly.

As depicted broadly in Figure 1-11 and with specific detail for the existing systems in Figure 5-3, a three-level hierarchical system can provide this connection [Saradis, 1979]. The first level has immediate access to the measured structural outputs and provides immediate health threshold checks of both the structure and the monitor itself. Higher levels are concerned with less immediate processing and more complex aspects of the structure. The highest level allows planning of monitoring tasks and qualitative decisions regarding the state of the structure. The level of deterioration or damage can be weighted in the context of its probable effects, the structure's lifecycle, and the present safety requirements. Further, an evacuation or routing plan can be organized, communicated, and implemented in a controlled manner. The middle level acts to coordinate the extreme levels of the system. Structural identification is conducted to estimate and update the structural condition states based upon the measured structural outputs.

These condition states, in turn, dictate the performance parameters upon which the structural evaluation is made.

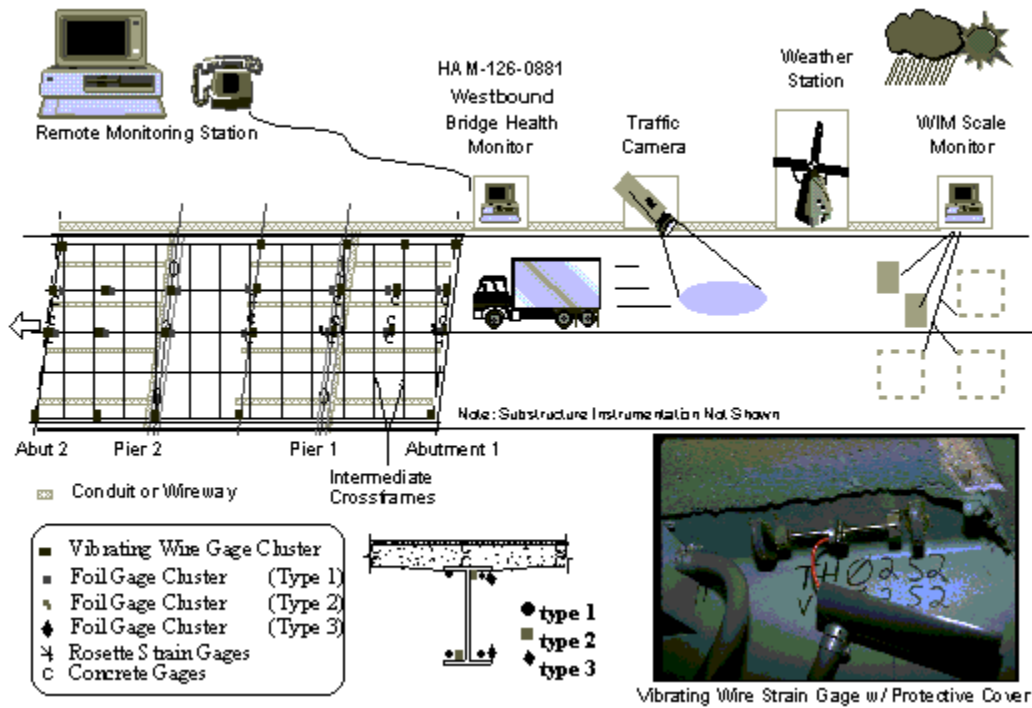


**Figure 5-1: Health Monitoring System for Bridge, HAM-126-0881**

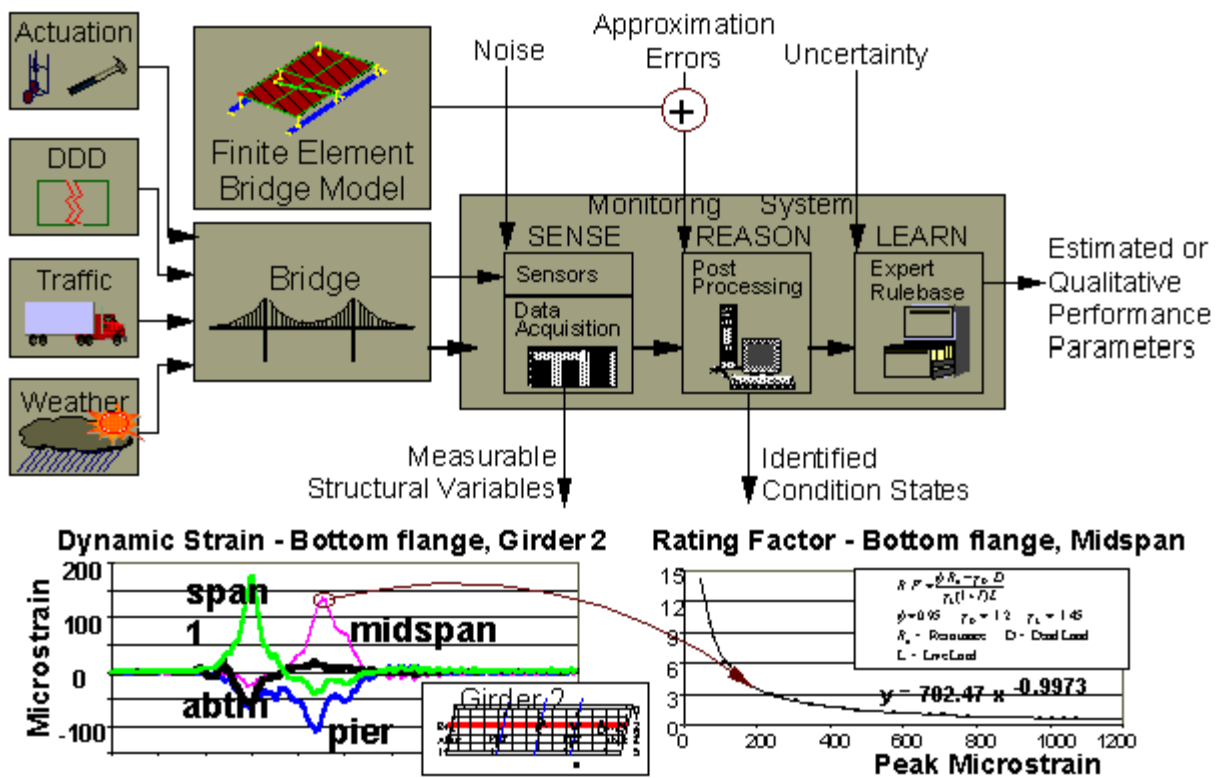
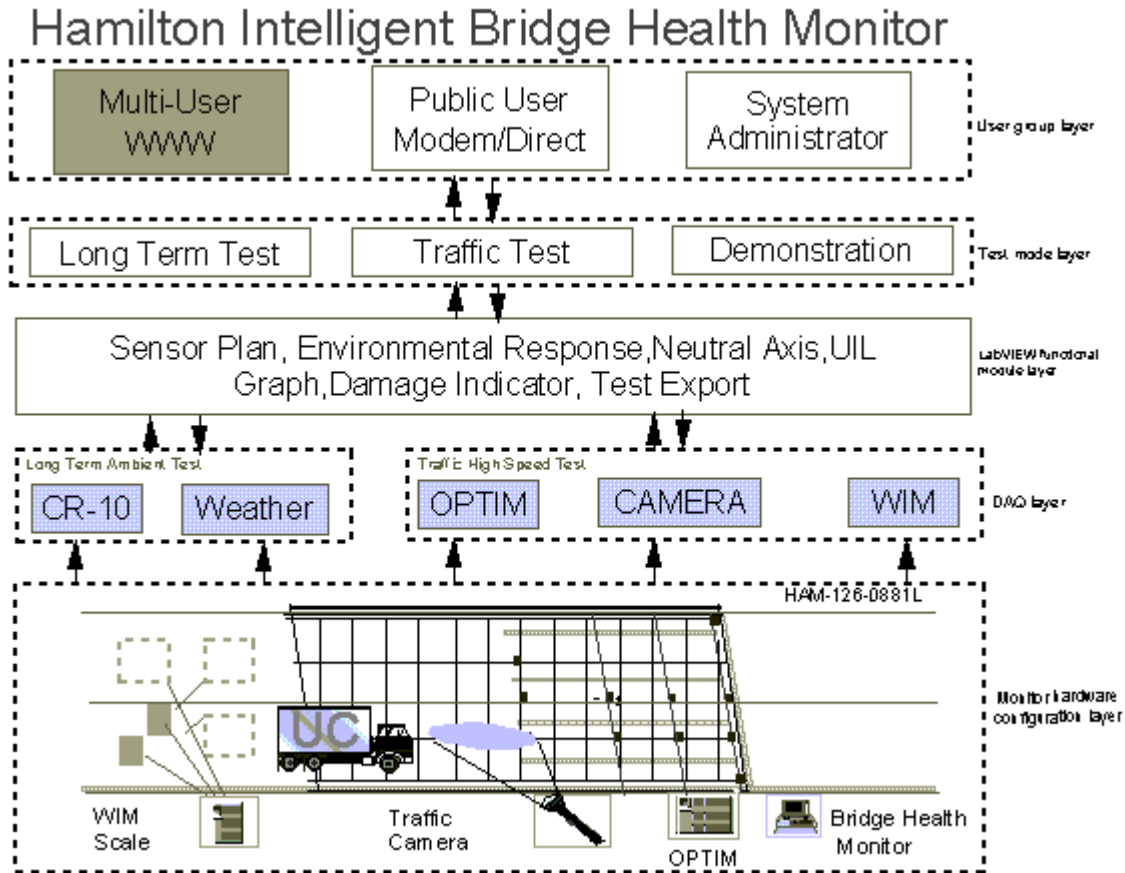


Figure 5-2: Health Decision Strategy for Bridge, HAM-42-0992



**Figure 5-3: System Hierarchy for a Bridge, HAM-126-0881**

### 5.1. Existing System for the Health Monitoring of a Steel-Stringer Bridge

A complete sensor suite, including a weigh-in-motion (WIM) roadway scale, was incorporated within the construction plans and drawings for a typical steel-stringer bridge: the three-span, 170 foot Cross-County Highway over Hamilton Avenue bridge (HAM-126-0881, see Figure 1-16). The objective was to collect a complete set of strain, distortion, inclination, displacement, vibration, and temperature response data for a newly built specimen. A dedicated monitoring system began

operation in tandem with the bridge construction in March 1995, commencing with construction of the drilled shaft pier foundations. The foundation and substructure were instrumented with embedded concrete strain and temperature gages, welded pile strain gages, inclinometer conduit, soil pressure sensors, and others. Relevant atmospheric effects at the site are monitored with a weather station. The steel superstructure was instrumented with weldable foil and vibrating wire strain gage instrumentation on the beams and the intermediate crossframes. The steel beam instrumentation was monitored during critical shop fabrication procedures and during all subsequent construction and service events. Displacement, tilt, and acceleration instruments were added at subsequent steps of the construction. Modal impact and diagnostic truckload testing were conducted in April and June of 1997, in order to establish the baseline mechanical characteristics of the bridge. The bridge was opened to traffic on October 28, 1997. Two follow-up tests were conducted in May and September 1998.

A hierarchical approach was taken in the design and implementation of the structural health monitoring system (Figure 5-3) [Gao, 1998]. The past test and monitoring efforts were lacking in many ways from a systems perspective:

1. DOS-based user interface with standalone operation and imprecise graphics.
2. Uncoordinated data manipulation and synchronization of each acquisition system.
3. Minimal processing and analysis of collected data is supported by each system.
4. Fixed test parameters (e.g. sample speed, channels used, etc.) are enforced by each system.
5. On-site operation and display of the data collection is required.
6. No specific application or information provided for structural health monitoring.

Coordinated sharing and customized display of the collected data and any subsequent processing applications on a multi-tasked, standardized platform is required of today's monitoring systems. Real-time decision making is sought, but not often achieved in practice for the more complex manipulations of the acquired data.

#### 5.1.1. Local Data Acquisition

The bridge health monitoring system implemented by the University of Cincinnati has incorporated five instruments, each their own subsystem of the whole. These instruments are all not necessarily required at a given bridge, nor are the manufacturers a sole source supplier of such equipment for the system. They are described briefly here to elaborate on one specific application of a bridge health monitoring system.

- *Long-term monitoring system* – Vibrating wire gages (e.g., strain, inclination, pressure, temperature, etc.) are wired to relay multiplexers and then to a Campbell Scientific CR-10X datalogger. This technology is based upon frequency measurement of the sensor's plucked wire, which minimizes the errors due to the long cabling required of highway bridges. The steel sensors are ideal for long-term monitoring due to their rugged construction and matched thermal response with the steel superstructure of the bridge. The sensors require one second to excite and measure the vibrating wire. The 16:1 multiplexers will dramatically reduce the cabling costs and effort. The system is rather low in cost due to the minimal system requirements of slow sample speed and digital input counting. There are over 250 vibrating wire gages installed at HAM-126-0881 and three CR10X systems to monitor them. The

provided software allows the user to specify different sensor types, a common sample interval (i.e., every thirty minutes), and a specific download time to the on-site computer via a standard serial interface (IEEE RS-232). LabVIEW procedures have been written to access the standard ASCII file format for this system.

- *Traffic monitoring and testing system* – Several common sensor types (e.g., foil strain, accelerometer, wire potentiometer, LVDT, etc.) are wired directly to an Optim Electronics MEGADAC datalogger. Sample speeds of at least ten times the bandwidth of interest (i.e., up to 20 Hz) are required to completely visualize the bridge response and its properties. Special attention must be paid to the inherent sources of error due to long cable lengths and Wheatstone bridge completion (see Appendix C1). The system is rather competitive in price with other high-end products that provide the integrated components for excitation (up to 10V DC or square wave), amplification (x100), filtering (3-pole Butterworth at 100Hz), digitization (16 bit), and computer acquisition for a broad range of sensors. There have been over 100 sensors installed at HAM-126-0881 for various experiments and the MEGADAC system has handled them all. The provided software allows the user to specify different sensor types, a common sample interval (i.e., 200 Hz), and immediate download to the on-site computer via a General Purpose Interface Bus (GPIB, IEEE RS-488). LabVIEW procedures have been provided to start, monitor, and stop these predefined tests.
- *Weather station* – Several common meteorological sensor types (e.g., ambient temperature, humidity, wind speed, wind direction, etc.) are wired to either an independent data system or directly to one or both of the data systems described above. This information is useful in

either the long-term or traffic-monitoring applications.

- *Video camera* – A BCR424II monochrome video camera was mounted on an aluminum pole next to the bridge approach for a wide and unobstructed view of the bridge traffic. The camera is wired directly to a National Instrument PCI-1408 framegrabber board that is installed in the PCI bus of the onsite computer. A real-time view of the bridge traffic is provided for remote actualization of the operating environment of the structure. Digital frames may be archived in the event of transportation or load violations. Windows-based utility software, as well as a LabVIEW driver, are provided with the framegrabber board for picture display, adjustment, and frame acquisition.
- *Weigh-In-Motion scale* - Several common transportation sensor types (e.g., embedded load scales, piezoelectronic tubes, inductive loops, etc.) are wired to an independent data system purchased by the Ohio DOT. The DAW-100 system by PAT, Inc. is installed at HAM-42-0992, while the PC-126 was plan specified and installed at HAM-126-0881. This is primarily due to the purchasing cycles of the DOT, although the latter system is clearly more advanced than the former in several ways: piezo sensors are employed in addition to loops for vehicle detection, a staggered scale is installed to measure the weights of both tires, a faster processor is used by the on-site computer, and both a digital (IEEE RS-422) and phone modem interface are provided. The provided software allows the user to access the immediate and statistical record of truck class, speed, weight, axle weight, axle spacing, and violation (if any). The accuracy of the WIM system is dependent upon several factors: truck class, speed, load, suspension; pavement roughness, alignment, and slope; environmental

factors (e.g., temperature, wind); and calibration regimen (e.g., Figure 5-4). Research has shown that truck drivers will modify their route or speed, and sometimes even damage the WIM scale, in order to avoid measurement of their loads [Nowak, 1994]. A LabVIEW procedure has been written to access this information via the local digital line through a National Instruments NI-182930E-12 interface board that is installed in the EISA bus of the onsite computer.

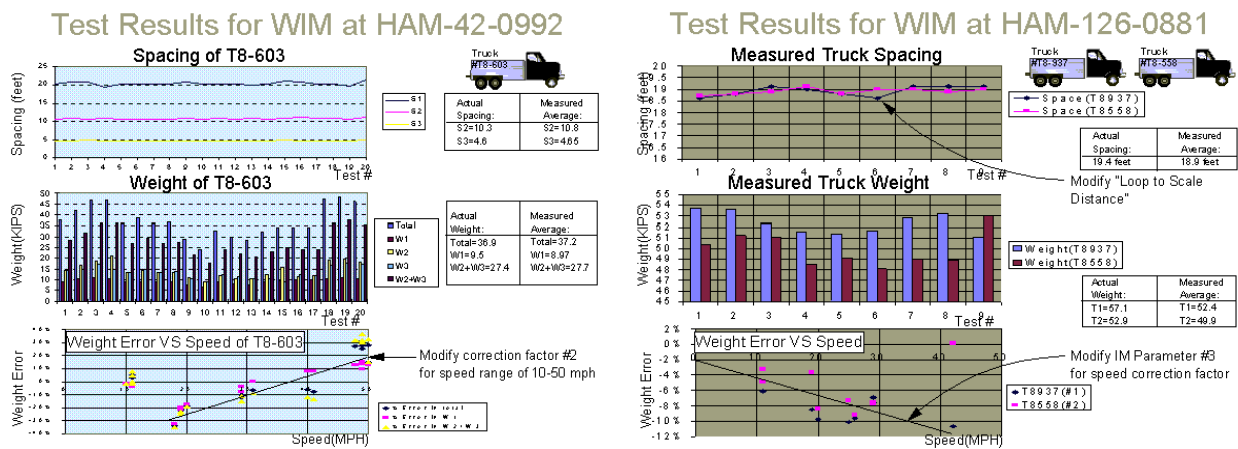


**Figure 5-4: Parameter Accuracy for Weigh-in-Motion Scales**

### 5.1.2. Coordinated Platform

The second functional layer of the system hierarchy (Figure 5-3) was designed to coordinate the many peripheral components of the lowest acquisition layer, manipulate or otherwise process the desired state parameters, and communicate this refined information to its intended audience. This layer must be versatile to simultaneously handle the flow of data from many disparate hardware and software sources via several different protocols and standards. The audience will also consist of many different users, each with their own varied demands for system information.

One user would be the higher decision layer of the system hierarchy, although no such layer has been implemented onsite for the bridge health monitor (see Future Work below). The research team would expect full access to all system parameters and data at this level, while the community at large would be overwhelmed by such access. In addition, some users in each audience may require much greater detail in the provided information, while others may be satisfied with only a cursory review. For example, the general public may be impressed with real-time video, traffic, and structural response and a general report of bridge health, while the DOT bridge engineer may want the full statistical history for specific state or condition parameters. Finally, there are security concerns to consider. Graphical displays and controls must be developed for each audience with staged levels of interaction.

LabVIEW was chosen as the program development application to handle all of the above concerns and to promote an open environment for future expansion and/or revision of the system's hardware or software components. While other programming requires the use of text-based language to create lines of code, LabVIEW uses a graphical programming language, G, to create programs in block diagram, or modular, form. A task is divided into a series of subtasks, which can be further divided again, until a complicated program becomes a collection of simple procedures. This type of programming lends itself to future development and facilitates debugging, as each procedural module is standalone and recyclable. LabVIEW provides an extensive library of mathematical, communication, presentational, and data acquisition functions that can be readily utilized by our application (e.g., all of the hardware protocols discussed above). It supports several platforms (e.g., Windows, Apple Macintosh, etc.). For the chosen Windows platform, it supports features such as Dynamic Data Exchange (DDE), Object Linking

and Embedding, (OLE), and Dynamic Link Library (DLL) which are used for communication between the various software applications discussed above for the onsite computer. LabVIEW also supports features such as Transport Control Protocol (TCP), File Transfer Protocol (FTP), User Datagram Protocol (UDP) which are used for communication between various software applications over the Internet.

Two methods of external data communication have been achieved with the bridge health monitoring system (see Figure 5-5). Analog modem communication over a phone line is sufficient bandwidth (32k bits per second, bps) for remote monitoring and system maintenance by the research team. Digital modem communication over an Asymmetric Digital Subscribe Line (ADSL, up to 1.5M bps) provides the bandwidth for remote streaming of the video, transportation, and structural responses to traffic. ADSL is typically provided by the major telephone companies in highly populated regions for data communication over traditional phone lines.

For the bridge monitoring system at HAM-126-0881, the following was implemented:

- 1) a 10/100 Base-T Ethernet LAN board was installed in the PCI bus of the onsite computer
- 2) a Cisco 675 Router was connected to the Ethernet LAN board, the analog modem, and the phone line
- 3) an account was generated with the ADSL service provider known as Zoomtown, a division of Cincinnati Bell, that routes the data stream to the Internet, and
- 4) an account was generated with an Internet Service Provider (ISP) for data transmission over the Web

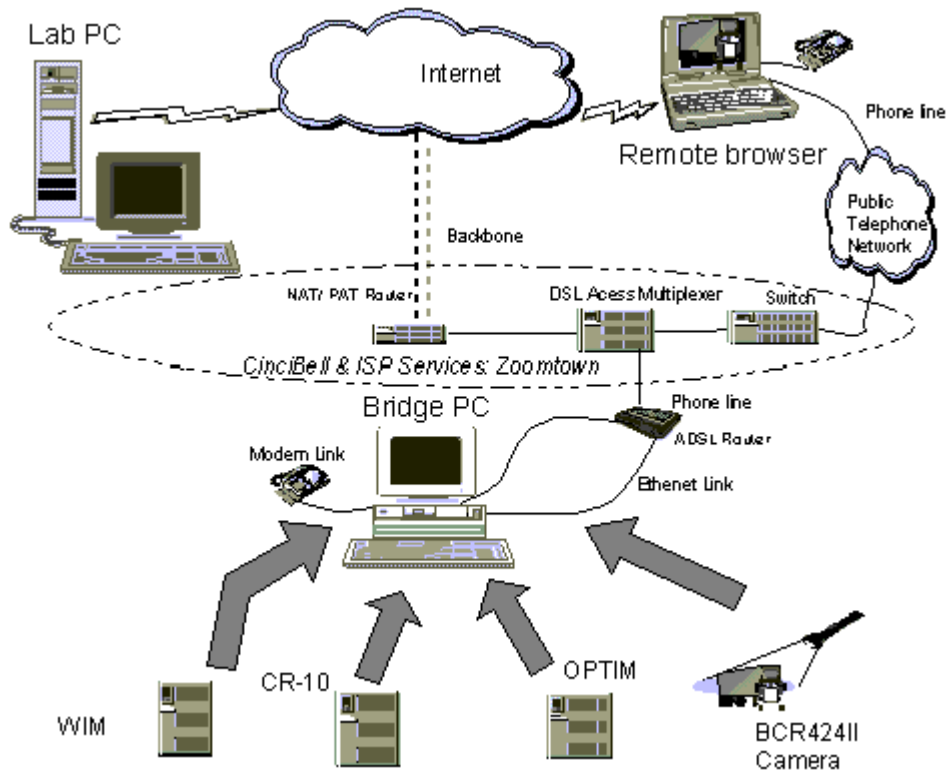


**Figure 5-5: System Diagram for Internet Communication**

LabVIEW modules were designed to push the acquired data files upstream by FTP from the onsite computer to a remote server for offsite processing and archival. The burdensome video frames are compressed into JPEG format before delivery. An estimated 200 kbps bandwidth is required by the bridge health monitoring system (see Table 5-1). The throughput achieved at the remote server depends upon the efficiency of the ADSL and ISP, the onsite computer, the offsite server, and the data path over the Internet. In general, service should be sought which is at least twice the required bandwidth. It should be noted here that the LabVIEW drivers provided for the MEGADAC system limited our sensor sample rate to approximately 25 Hz. This may be sufficient to determine most of the critical state parameters for condition assessment (e.g.,

influence lines), but improved drivers will be considered in future work. Table 5-1 indicates the desired sample rate of 200 Hz.

<b>Data Source</b>	<b>Stream Estimation</b>	<b>Required Data Rate</b>
<b>Weigh-In-Motion Scale</b>	(128 B per vehicle) *	Average: 593 bps
<b>Traffic Monitoring System</b>	(40,000 vehicles per day)	Peak Traffic: 2.96 kbps
<b>Video Camera</b>	(24 channels) * (2 B per channel) * (200 Hz sample)	96 kbps
<b>Long-Term Monitoring System</b>	Uncompressed: 336x262 = 88kB Compressed Frame: 25kB * (0.4 Hz refresh rate)	100 kbps
<b>Total Data Stream</b>	(500 channels) * (2 B per channel) at every fifteen minutes	0.01 kbps
Note: B = byte, b = bit	Note: 1B = 10b (8b character + start bit + stop bit)	198.97 kbps

**Table 5-1: Required Bandwidth for Bridge Health Monitoring System**

The remote server(s) has several implemented tasks, designed to minimize the necessary processing by the onsite computer that should be focused on data acquisition, packeting, and communication.

- a) File Transfer Protocol (FTP) Server – Freeware software, known as the WarFTP Daemon, was configured to receive multithreaded data files corresponding to the above instruments.
- b) Offsite Processing – The received data files are processed into the desired structural state parameters and condition indices by custom LabVIEW procedures. Graphical displays of the received data and processed parameters are readily generated as needed for system maintenance, demonstration, further analysis, reports, or other communications. Existing displays include: video frame of bridge traffic, four selectable channels of scrolling bridge responses along a six (or other) second time axis, current and statistical graphs of vehicle speed, weight, and classification from the WIM scale, etc. (see Figure 5-6)

- c) World Wide Web (WWW) Server – LabVIEW supports the dynamic execution of a Common Gateway Interface (CGI) which posts and animates any LabVIEW display over the Internet. The displays are formatted as Portable Network Graphics (PNG) for lossless compression.
- d) Data Archival – The received data files and processed parameters are stored in a common format for future review and statistical analysis. This archive can easily require 1GB of storage space each month for an active regimen of bridge testing and condition assessment (see Figure 5-7).

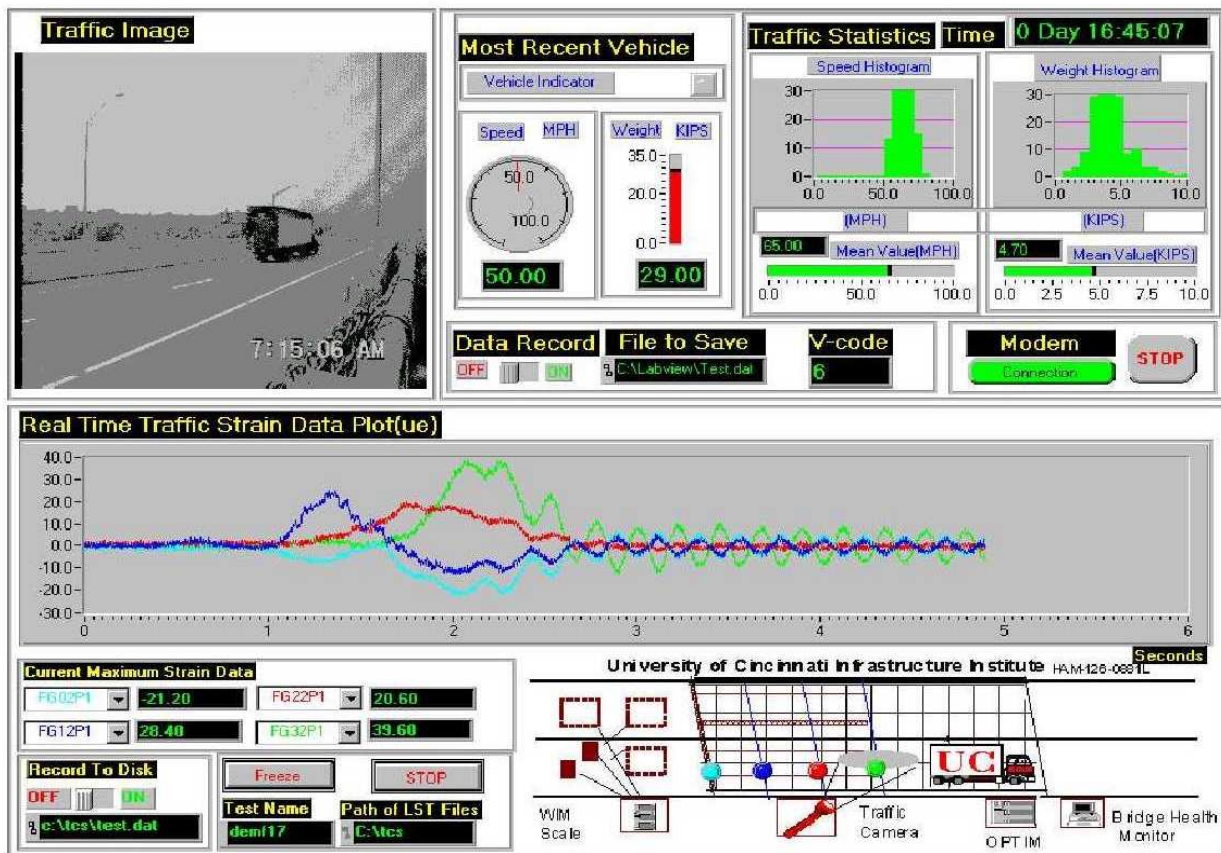
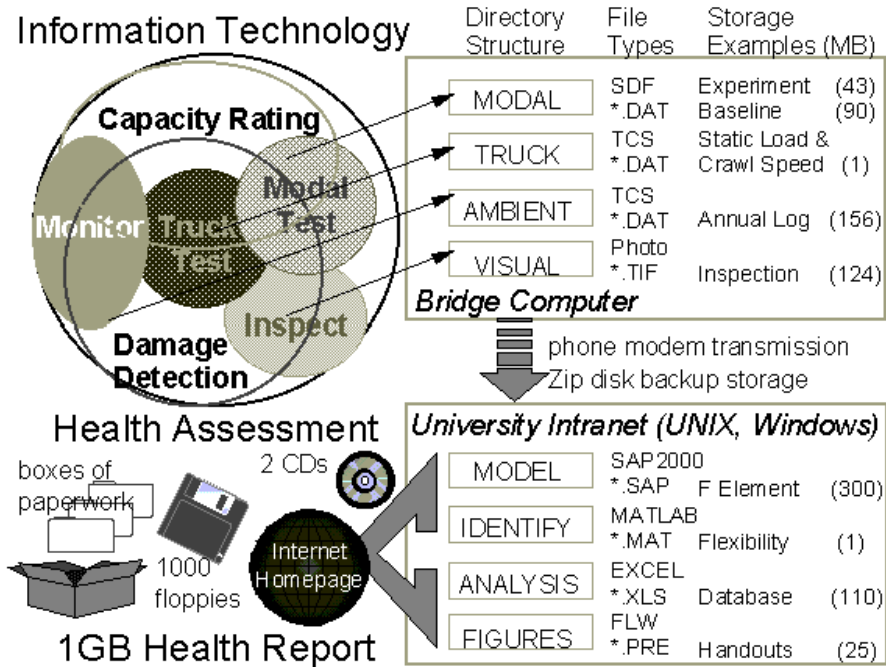


Figure 5-6: Remote Internet Display of Bridge Condition, HAM-126-0881



**Figure 5-7: Information Sources and Required Storage Capacity**

Any remote computer with Internet access can be configured to perform any or all of the above tasks [Zhong, 1999]. For example, a laptop computer can be configured with both the WarFTP Daemon and the LabVIEW procedures so as to provide an Internet demonstration of the bridge health monitoring system anywhere in the world. Alternatively, a dedicated server at the university can be configured for all the above tasks and would provide worldwide access to the system at a specific IP address or Web site.

The onsite computer can also be directed to process and display the data files for the above instruments. This is particularly useful for onsite demonstrations. The analog modem also provides an alternative scheme for remote demonstration by phone line, but this is obviously a less impressive display due to its small bandwidth. Terminal emulation is achieved with the commercial software known as PCAnywhere. Some system control and maintenance needs are

still most readily achieved by terminal emulation. Further, this allows a backup mechanism to debug any interruptions to Internet service and reinitialize the Internet connection without actually driving to the bridge site.

The existing system is a continuous Windows-based health monitor for a remote highway bridge with:

1. *Remote desktop display via the Internet* to review the monitoring of the instrumented bridge by any bridge engineer with access to the World Wide Web.
2. *Remote desktop control via telephone line* to review and/or initiate monitoring of the instrumented bridge by the research team.
3. *Communication with peripheral devices* such as the WIM scale, the various data acquisition systems, and the video camera.
4. *Simultaneous high-speed acquisition* of traffic information, video camera, and sensor data from the instrumented bridge for the most recent truck crossing.
5. *Continuous long-term monitoring* of the structural response to the environment.
6. *Field implementation* of a continuous, multi-tasking health monitor which acquires sensor data at variable sampling speeds, communicates with peripheral devices, provides a user-friendly and customizable display interface, and allows an open hardware/software architecture for:
  - Other structural monitoring applications
  - System expansion of instrumentation, reporting, or other functions
  - Networked multi-node connection of other peripherals, structures, and organizations.

### 5.1.3. Qualitative Decisions

At present, an explicit decision layer suggested by the hierarchical systems concept has not been implemented as such for the bridge health monitoring system. A quantitative decision regarding bridge condition and/or the presence of structural damage will be pursued in future work. However, it is appropriate to consider the existing and venerable system of bridge management by the Department of Transportation as the highest level of our existing and future versions of the monitoring system.

Human judgements in many specialized subject areas, such as bridge management, seem to involve recognition and reasoning methods of a qualitative nature [Bobrow, 1985]. In an expert system, this domain knowledge can be organized in the form of rules or heuristics. Uncertainty can be represented in terms of fuzzy sets and confidence factors. In the simplest form of this approach, the rulebase will form a decision tree where forward reasoning takes into account all the evidence and propagates new rules until all conclusions with their appropriate weighting is reached [Genesereth, 1987]. The current bridge management system for the Department of Transportation, PONTIS, is based upon this approach and relies heavily upon the subjective input of field inspection reports and a condition rating index of 0-9 [PONTIS, 1993]. The exact meaning of each numeric in the index is unclear and varies from engineer to engineer; however, this uncertainty is uncaptured within the knowledge base.

## 5.2. Future Improvements to the Bridge Health Monitoring System

The University of Cincinnati has recently contracted with ODOT to continue and improve upon the existing system for bridge health monitoring.

*The first objective is to continue our documentation of the actual absolute state-of-stress in HAM-126-0881, a jointless continuous composite reinforced concrete deck-on-steel stringer bridge, together with the corresponding causative effects. The stresses have been evaluated from fabrication and construction and through the first year of service. We propose to continue this evaluation well into its service life, especially in light of the significant deck deterioration.*

This objective will be accomplished by the continued collection of a complete set of strain and temperature response data on and in the soil, the substructures (piles or footings, piers and abutments), and the superstructure components (deck and parapet concrete, girders, cross-braces) of the test specimen. Meanwhile, all the relevant atmospheric effects at the site will be monitored. Traffic loading will be automatically monitored by WIM scales and video camera. In addition, an annual regimen of diagnostic testing will be conducted in order to track the mechanical characteristics of the bridge.

*The second objective is to continue the advancement of the state-of-knowledge in feasible and reliable bridge instrumentation, monitoring, and nondestructive evaluation technologies. A remote demonstration of the existing bridge monitoring software has been conducted several*

*times at the headquarters and district offices of ODOT and at professional conferences worldwide. We propose to continue this informational aspect of the project, with further customization based upon the recent feedback from bridge engineers.*

Given the synergy of the on-going research and test specimens, the systematic and integrated development of an automated health monitor for steel-stringer bridges will be pursued. The basic issues that are obstructing an efficient and practical monitor include:

- Limitations in sensor and data-acquisition technologies
- Limitations in state-of-the-art field experimentation
- Uncertainty of actual state and performance properties and quantitative indices
- Uncertainty of natural factors and their potential significance over service loads
- Indices to track changes in state properties due to damage and deterioration
- Optimal integration of human and machine intelligence, specifically:
  - ⇒ Accumulated heuristic know-how and experience on bridge engineering
  - ⇒ Structural testing results and on-line instrumented monitoring data

The most significant challenge is the real-life implementation, graphical display, and efficient representation of such well-researched concepts to the primary end users (i.e. bridge engineers). Specific improvements to the existing monitoring system are discussed below.

To permit periodic impact and truckload testing, continuous long-term monitoring efforts, and development/enhancement of remote monitoring capabilities, the existing instrumentation and hardware at the bridge site will have to be maintained and updated to ensure all significant components are in proper working order.

### 5.2.1. Autonomous Operation

The existing monitoring system, described above, has been utilized primarily for data acquisition and project demonstration. Each instrument is manually configured and operated. The recorded data is transferred to the university for all further processing. No decision is made online by the computer regarding the health or condition of the bridge. The most significant improvement to the monitoring system will be the automation of most of these steps. In addition, the LabVIEW drivers for the MEGADAC must be redesigned for a higher throughput speed for the traffic monitoring procedure.

Auto-triggering of data acquisition: the LabVIEW procedures must be modified to allow for automatic start/stop triggering of the high-speed data system from either installed tape switches on the highway or, preferably, by the installed bridge sensors. The latter may be accomplished by observing the strain response at the abutments. Upon terminating, the data cycle must be reset for the next vehicle crossing.

Synchronization of all data sources: the LabVIEW procedures for collection of the video, bridge response, and vehicle information must be synchronized such that the system may automatically and correctly associate the data files for a common vehicle crossing. Given the uncertainties of the communication delays between the varied hardware and software resources, this effort will largely be a matter of trial-and-error in order to find the correct timing sequence. Some validation can be achieved by comparing the vehicle weight with the magnitude of stress recorded.

Decoupling the response from multiple trucks: this is not a high priority for bridge health monitoring, where a clear one-to-one correspondence is sought between a known input and the measured structural response. However, other applications such as a complete statistics for traffic monitoring will want to pursue this matter [Moses, 1979, Goble, 1992, Nowak, 1994].

Streamlining of system resources: common formats and procedures must be designed, documented, and implemented before a constant informational flow of 1 GB per month has overtaken the available storage facilities. LabVIEW procedures will be written to process the acquired and synchronized data files for the current traffic and the structural response. Most of the raw traffic data may have to be discarded after updating the statistical database and identification of the appropriate state parameters and damage indices. See discussion below.

Real-time decisions regarding structural health: the structural parameters and damage indices will be constantly reviewed for any significant change from their past values. Alarm thresholds will be defined for each parameter and index which maximizes the chance of damage detection, while minimizing the occurrence of false alarms. See further discussion below.

Remote control of monitoring system via the Internet: at present, only a restart button is provided on the website interface. The website should provide user selection of certain variables for the given display. Links must be defined to activate the display of other structural and statistical parameters that may be of interest to a subset of the Internet audience. Most of the system parameters should be available from a password-protected website for adjustment or maintenance by the research team.

Project archival: a standardized account of all project information (e.g., reports, data, figures, photographs, models, etc.) must be established for an ongoing project of this nature. A file structure such as a directory tree should be defined with serial paths representing shared attributes and parallel paths representing redundant attributes. To minimize storage space, data compression and a file linkage scheme should be implemented.

#### 5.2.2. Parameter Processing, Display, and Archival

LabVIEW procedures will be written to process the acquired and synchronized data files for the current traffic and the structural response. As before, these procedures include a custom graphical display of the processed parameter that may be viewed as hardcopy, as a Windows panel at the onsite computer, at the offsite server, or posted and animated upon the server website. The current, worst-case, or statistical version of these processed parameters can be viewed with these panel displays. The state parameters and damage indices may be used to trigger alarms based upon pre-defined thresholds, discussed further below.

*Maximum Stress* at the instrumented nodes for both traffic and environmental monitoring. The location is highlighted on an overhead view of the bridge. This indicates a significant target for the bridge inspector on his/her next visit to check for cracking or other signs of damage, especially if the stress levels have changed significantly since the last inspection.

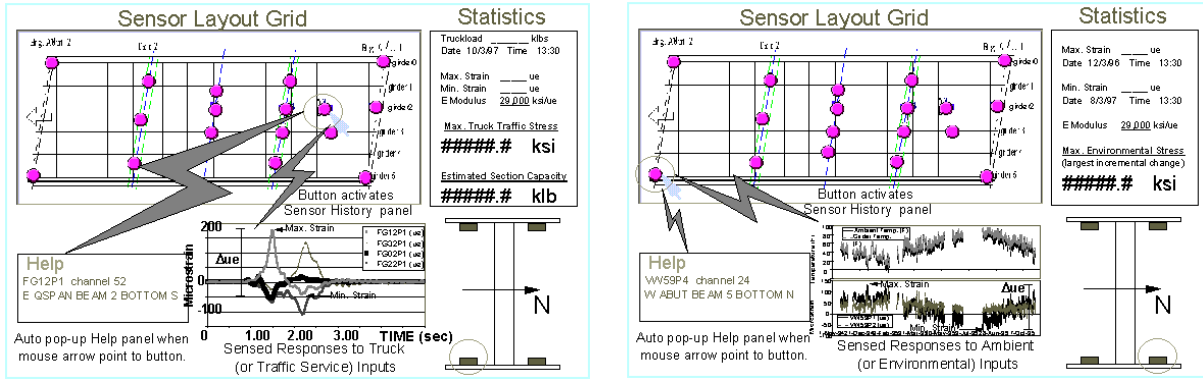


**Figure 5-8: Example Displays of Maximum Stress for Traffic and Environmental Monitoring**

*Maximum Shift in Neutral Axis* at the instrumented nodes for traffic monitoring. Alternatively, *Remaining Composite Action (RCA)* could be provided at the instrumented nodes for traffic monitoring. RCA is considered as the percentage shift of the neutral axis at its measured condition from that of a fully composite section as compared to that of a fully non-composite section. The location is highlighted on an overhead view of the bridge. This indicates a significant target for the bridge inspector on his/her next visit to check for cracking or other signs of the loss of composite action.

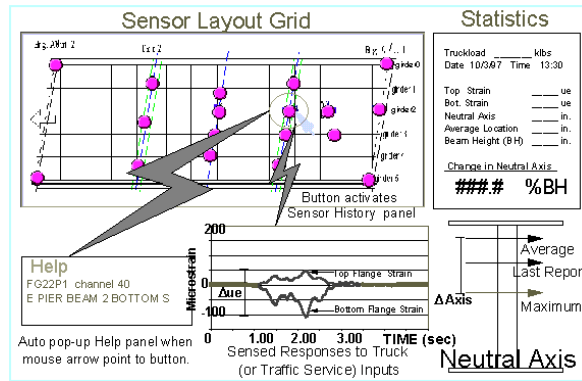


**Figure 5-9: Example Display for Maximum Shift in Neutral Axis**

*Unit Influence Line* (UIL) decomposition of measured truckload response at each instrumented node. The actual axle count, weight, and spacing are provided by the WIM scale. Crawl speed of the test truck is the most accurate; however, dynamic filtering allows acceptable comparison of ambient truck traffic.

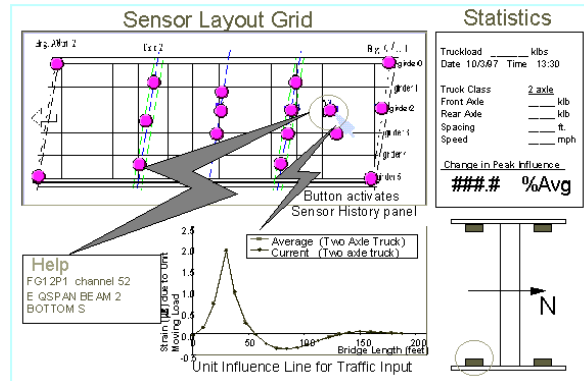


**Figure 5-10: Example Display for Unit Influence Line**

*Modal Parameter Tracking* for traffic monitoring of instrumented nodes. Frequency, shape, and assurance criterions will be identified based upon real, uncoupled modes. This information can be utilized in deriving the UIL from noisy traffic data by using a dynamic filter.

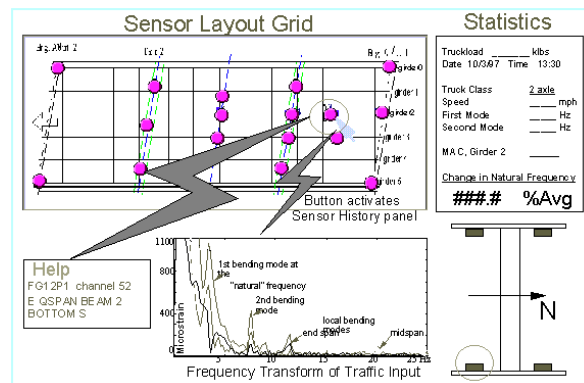


**Figure 5-11: Example Display for Modal Parameters**

*Impact Factor* at the instrumented nodes for traffic monitoring.

*Distribution Factor* at the instrumented section for traffic monitoring.

*Load Rating* at the instrumented nodes for traffic monitoring. All assumptions such as capacity, concrete strength, axial force, planes remain planes, etc. will be denoted. The derived sectional properties such as modulus, deadload stresses, HS20 liveload stresses, composite action, and moment will be provided. Ratings will be calculated for both inventory and operating levels and for both the allowable stress and load factor methods.

*Remaining Fatigue Life* at the instrumented nodes for traffic monitoring. The effects of fatigue loading can best be defined in terms of the total life of the bridge for the given spectrum of service stresses that it experiences each day.

### 5.2.3. Relevant Health Decision Algorithms

The algorithms to be designed for nondestructive testing or on-line health monitoring are to be based upon a mapping from the observable or measurable space to a hypothesis/decision space and therefore imply a decision-making process. In such problems, we have a discrete set of alternative interpretations of the data, we have models for each, and we have optimal estimators for each that allow us to produce statistics that form the basis for efficient and rational assessment of which alternative is most likely to be correct (namely, healthy or damaged performance). This hybrid model approach provides a framework in which it is possible to think about fusing all types of knowledge and information [Levis, 1987]. It also very naturally

reduces data and knowledge to statistics as the basis for higher-level reasoning. The modeling of uncertainty should be "structured" so as to exploit all relevant a priori information about the structure and its ambient environment.

The recommended scheme for damage or fault detection and isolation (FDI) assumes a classical, M-ary hypothesis test with a fixed, singular data sample [Van Trees, 1986]. Our decision will be facilitated by a unique physical manifestation associated with each event (i.e. the magnitude with which each event affects the measurable residual  $r$ ). The fault detection scheme can be optimized by using a generalized likelihood ratio test (GLRT) based upon a degenerated Bayes criterion. The Bayes criterion assumes the a priori determination of the event probabilities and the conditional probabilities for each decision given the occurrence of each event. The Bayes criterion can be degenerated such that only two hypotheses are of importance ( $H_0$  = valid performance,  $H_1$  = fault or damage detected). The likelihood ratio test for our detection scheme compares the absolute value of the residual to the threshold  $T$  and is thus generalized in order to account for any subsequently measurable fault. The threshold  $T$  is originally made quite large while the probability of normal operation is high and subsequently reduced to zero as the probability of damage or a fault increases. Thus, the threshold is varied according to the reliability of the structure.

An alternative approach for the fault detection scheme can be based upon a static threshold given by the Neyman-Pearson (NP) criterion. Here, the conditional probability of false alarms ( $P_0P_{10}$ ) is constrained to remain less than some arbitrarily small value  $\alpha$ , known as the level or significance level of the test. The conditional probability of fault detection ( $P_1P_{01}$ ) is maximized

to some value  $(1-\beta)$ , known as the power of the test. Structural reliability is not incorporated within the Neyman-Pearson criterion and, thus, this information is forfeited for a simpler approach to the fault detection scheme. Pape demonstrated that by looking for resonances outside of the statistically normal behavior, structural members with gross defects could be detected [Pape, 1993]. Note that again this method requires a significant fault signal-to-noise ratio to perform acceptably. Figure 5-12 illustrates the performance of NP and Bayesian thresholding for the redundant hardware of a typical monitoring system assuming Gaussian noise with a standard deviation of  $\sigma_r$  for the observed residual  $r$  [Hunt, 1991, and Walker].

Upon detection of damage, several other decisions must be made:

- 1) Classification as to the nature or origin of the damage must be pursued. Penny, Wilson, and Friswell suggest a least-squares comparison of measured structural frequencies with those simulated for several considered damage cases in order to determine the “most likely” damage case [Penny, 1993].
- 2) Localization of the phenomenon must be pursued. For example, several authors have developed algorithms for crack location in an idealized beam from measured frequency shifts [Meneghetti, 1993, Stubbs, 1994].
- 3) The severity of the damage must be judged and appropriate counter-measures taken.

To achieve this, high level decision making techniques for reasoning under uncertainty and taking actions must be utilized within a hierarchical system program [Figure 5-13, Antsaklis, 1991 and 1993]

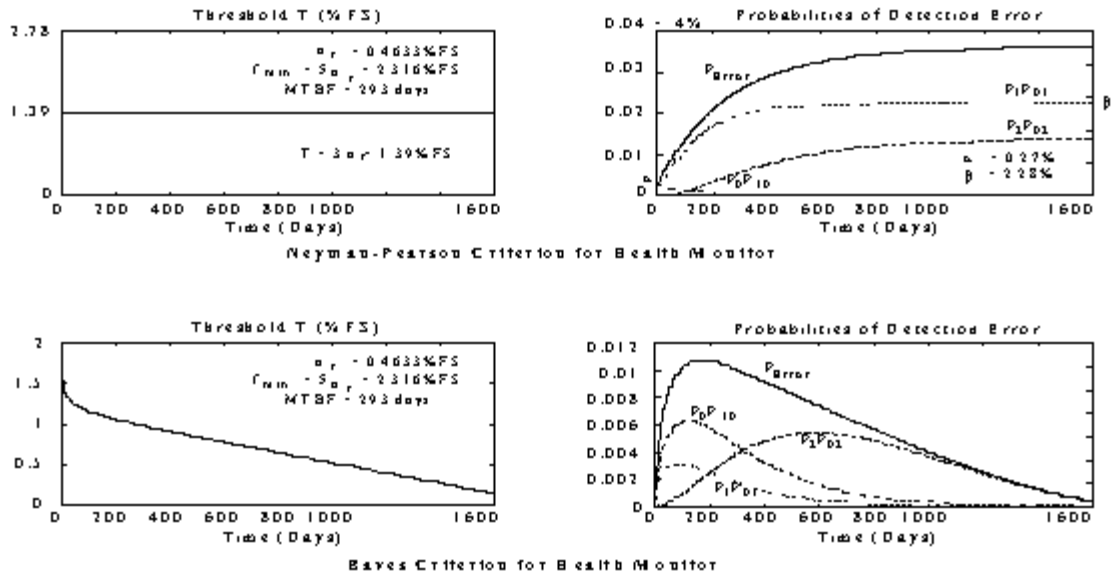


Figure 5-12: Thresholding for Damage Detection

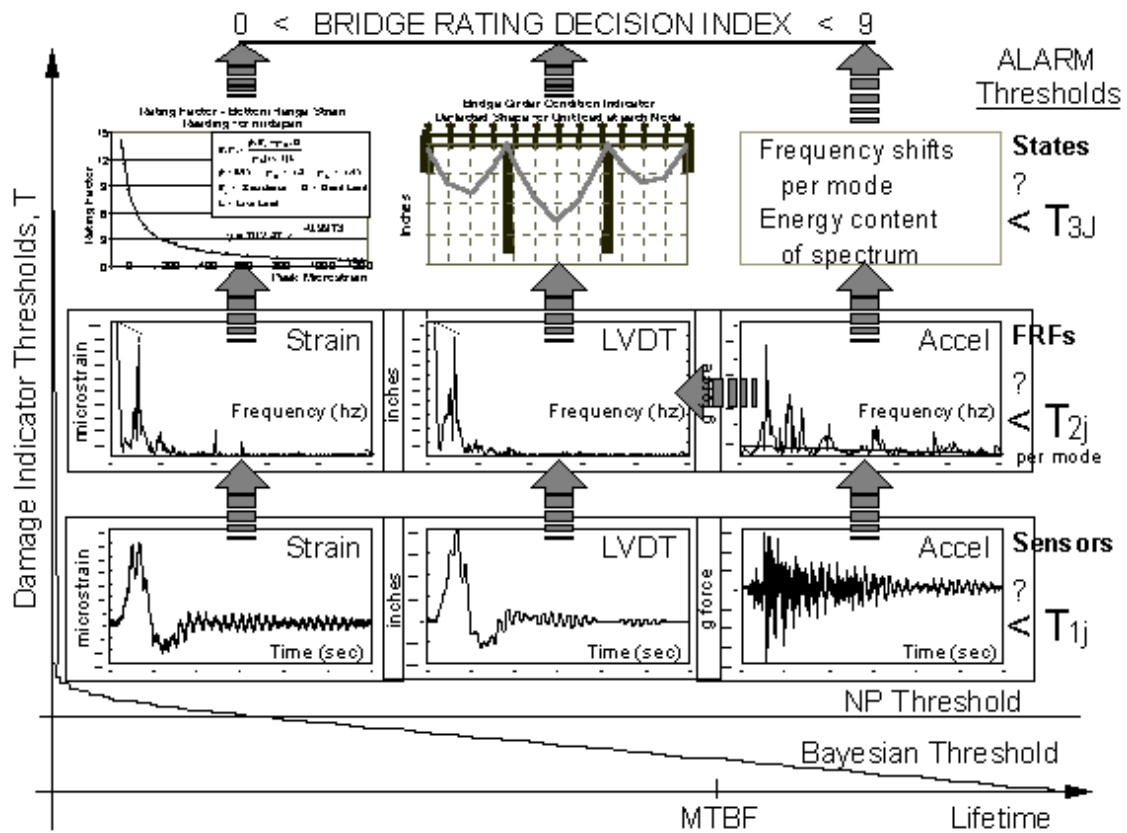
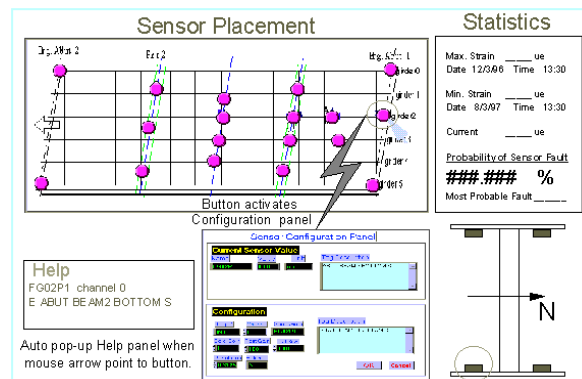


Figure 5-13: Hierarchy of Damage Indicator Thresholds

In addition to supervising, the autonomous monitor must also provide a high degree of tolerance to sensor failures. This implies that the controller should have self-test capability, tolerance of transient errors, adjustable fault detection thresholds, reversible state changes, and protection from invalid external commands. A fault-tolerant measurement system is also designed to take advantage of the benefits of redundancy. Upon validation of the measurement system by fault detection and isolation (FDI) algorithms, a confidence metric can be associated with each measured parameter based upon the derived accuracy. This allows a solid base upon which to build further reasoning about the structure. This status information, presented to the host system (see Figure 5-14), provides a confidence metric with each measured parameter and thus facilitates qualitative reasoning about the current condition of the structure [Garrett, 1987b; Matejka, 1988; Fox, 1983]. For example, in a qualitative monitoring system which can select among alternative performance states during a specific evaluation, the availability of this status information can meaningfully influence this choice by quantifying the confidence associated with each measured variable. Hence, the hierarchy combines local, low-level observation and broader, higher-level reasoning and planning in order to ensure continuous and efficient system performance and knowledge.



**Figure 5-14: Example Display of Sensor Condition Status**

### 5.3. Bridge Management System

It is appropriate to consider the Department of Transportation as the highest level of our existing and future versions of the monitoring system. The current bridge management system for the Department of Transportation, PONTIS, is based upon a qualitative set of expert heuristics and the subjective input of field inspection reports to derive a condition rating index of 0-9 [PONTIS, 1993]. The exact meaning of each numeric in the index is unclear and varies from engineer to engineer; however, this uncertainty is uncaptured within the knowledge base. One outcome of a bridge management system would be a schedule of current and future action(s), if any, required for a specific structure. Planning decisions will influence the decision criteria and certain rules such as “Grouping projects along the same route or in the same vicinity will reduce overall costs” will dramatically effect such decisions. Other rules such as “State resources should be shared equally by all counties and districts” and “Posted bridges should be repaired or replaced” may conflict with each other and some prioritizing of rules must be defined. Decision criteria would range from the acceptable level of each condition index, performance and reliability evaluation for each structural subsystem, the average and projected cost for customary actions; evaluation and planning of options, the state’s current and future budget; political influences; etc.

The algorithms of the previous section will provide a quantitative measure of the current structural condition of the bridge. Thresholding of the condition and damage indices will specifically define any alarm states for the considered scenarios. However, no decision scheme has been introduced to:

- manage any conflict between the various condition or damage indices

- consider and schedule any future actions such as inspection, maintenance, repair, shutdown (or, at the very least, communicate with the DOT management system for such matters)
- consider and detect any damage scenarios beyond the considered scenarios
- compare this structure's response to those of similar bridge types to help estimate the most probable damage scenario, the expected lifecycle cost, potential rehabilitation schemes, etc.
- other bridge management considerations and decisions.

Future work can pursue several complementary approaches to this end.

### 5.3.1. Qualitative or Heuristic Knowledge Base

In an expert system, domain knowledge is captured in the form of rules to which one commits less than total belief. Each rule is a sentence of the form  $X \Rightarrow Y (p_{y|x})$  meaning  $X$  implies or suggests  $Y$  with a conditional weighting or probability of  $p_{y|x}$ . Even when people knowledgeable about these relations might not be able to estimate conditionals, they often can express their ratio (i.e. the likelihood ratio or odds). In a simple version of such a system, the network of statements will form a decision tree or network with a final conclusion as the root node and the primitive pieces of evidence at the tips. Forward reasoning in such a tree starts by taking into account all the evidence at the tips, propagating this evidence to establish new probabilities for antecedents of rules higher in the tree, and continuing until the probability of the end conclusion is determined. These reasoning methods depend on strong assumptions about conditional independence and consistency of the subjective probabilities.

An onsite programming shell, utilizing a qualitative description of the mechanisms which link performance to the measurable parameters, can be pursued to locally capture the qualitative decision process which is presently utilized by the Department of Transportation [Adams, 1995, Chen, 1995b]. A prototype knowledge base for other processes controlled primarily by expert rules yielded significant and dramatic results [Garrett, 1987b, Matejka, 1987]. A schedule of achieve or prevent events  $E = \{A_1, \dots, A_n, P_1, \dots, P_m\}$  (e.g., inspection, maintenance, repair, shutdown) is defined with respect to the performance goals for the structure (e.g. safe load capacity for the given traffic and environmental loads). At each step of the monitor's cycle, the rulebase of expert heuristics is referenced to draw inferences about the current state (e.g. state at instant  $k$ ,  $S(k) = E_i$ ). The fundamental or driving concept for the QPA inference engine is that the likelihood of the achieve events  $p(S=A_i)$  is maximized while the probability of the prevent states  $p(S=P_i)$  is minimized; a constant endeavor to reduce the state entropy while directing the process towards desirable end goals (see Figure 5-15). Conflict resolution is handled by a ranking or prioritization of the structural states based on their relative importance to the goals. This qualitative description allows in-situ determination of the decision path  $P = \{S(0) = E_i, C_i, S(1) = E_j, \dots, C_j, S(k) = \text{goal}\}$  because of the reduced computational load.

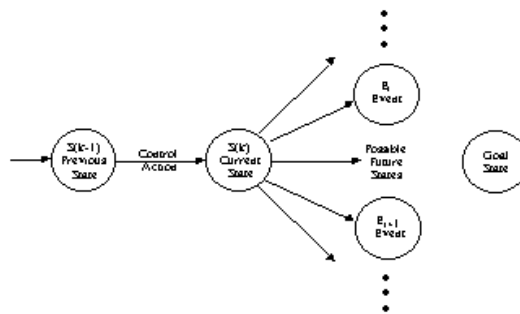


**Figure 5-15: Management Decision Tree for Identified Structural Condition States**

### 5.3.2. Adaptive or Neural Algorithms for Learning

Adaptive or self-learning methods are also possible with both quantitative and qualitative approaches. The notion of learning systems has primarily been developed in the fields of artificial intelligence, cybernetics, and biology as a method to mimic the human ability to understand new concepts. Of late, neural networks have gained much attention for their recognition of patterns in symbolic lists, expert systems have demonstrated the creation of new rules for a knowledge base with inference algorithms, and fuzzy sets have shown an aptitude for generalization or interpolation about a given set of functional mappings. [Genesereth, 1987; Kosko, 1992; Zimmerman, 1992]

Adaptive or self-learning methods are also possible with both quantitative and qualitative approaches. For example, parameter estimation is a necessary step in identifying the mechanical model of a structure and is best done by iteration. Sufficient excitation of the structure in terms of amplitude and frequency content is necessary for the parameters to converge upon reliable estimates. Typically, the measured structural variables consist of displacements, rotations, strains, and/or accelerations at discrete points on the structure. The estimated parameters, however, are the characteristic rigidity, stiffness, mass, and damping properties of the structure. This iterative process can be automated so as to adapt to or learn new structural properties as environmental, loading, or damage conditions change. Parameters may be updated at a rate dependent upon the complexity of the model and the accessibility of the structure. When compared with past values, the updated model will quantify changes in the structure's parameters

that may adversely affect its performance or health, such as its serviceability or its ultimate load capacity.

Much research has also been dedicated to the utilization of neural networks for structural health monitoring [Ghaboussi, 1993, Chen, 1995a]. Multiple-layer perceptrons are trained via the back propagation method upon analytically simulated damage scenarios for a finite element model of the structure. Several engineering fields have explored this concept: Aerospace [Tsou, 1993], mechanical [Worden, 1993], and civil [Elkordy, 1993]. The National Center for Earthquake Engineering Research has suggested the use of a neural network monitoring system for structural damage detection [Elkordy, 1994]. Here, two sets of neural networks were developed for the physical and analytical model of a five-story steel frame. Results were comparable for eleven induced damage scenarios consisting of an increased loss to the bracing area for the first and second floors. Elkordy emphasizes that the unique interpolative and adaptive nature of a neural network makes it particularly suited to this implementation as “no one structural characterization/signature is universally applicable.” In the same sense, however, it must also be appreciated that the neural network is not universally applicable; specifically, a trained network can have difficulty identifying the signature for a damage scenario which was not represented in its simulation set. In the state space mapping for the neural network, there can be significant error associated with a damage set that requires extrapolation beyond its trained or observed subspace.

### 5.3.3. Statistical Knowledge Base of Common Bridge Types

It is believed that field testing a statistical sample of the bridge population would provide sufficient information and insight regarding typical behavior of recurring bridge types. Bridge type-specific management would classify bridges of similar construction into types and, thus, facilitate group management based upon condition assessment techniques that focus upon these similarities. This works contrary to the widely held notion that every bridge is a unique structure. While there is justification in this premise when we consider that no two bridge-foundation-soil systems will have exactly the same geometric, material, and boundary conditions, there is evidence that the mechanisms of stiffness and strength will be similar within a population corresponding to the same bridge type.

Steel-stringer bridges are the most common bridge type in the Ohio inventory. The average age of its approximately 12,000 steel-stringer bridges is approaching fifty years, which is the expected lifespan for such bridges. 82% are continuous, 7% are of composite design, and 4% have integral abutments; although, the recent trend has been towards these three attributes. Typically, steel-stringer bridges are built with Jersey barriers and the most common supports are slide (42%) and rockers (26%) bearings; the recent trend has been towards the use of neoprene elastomeric bearings.

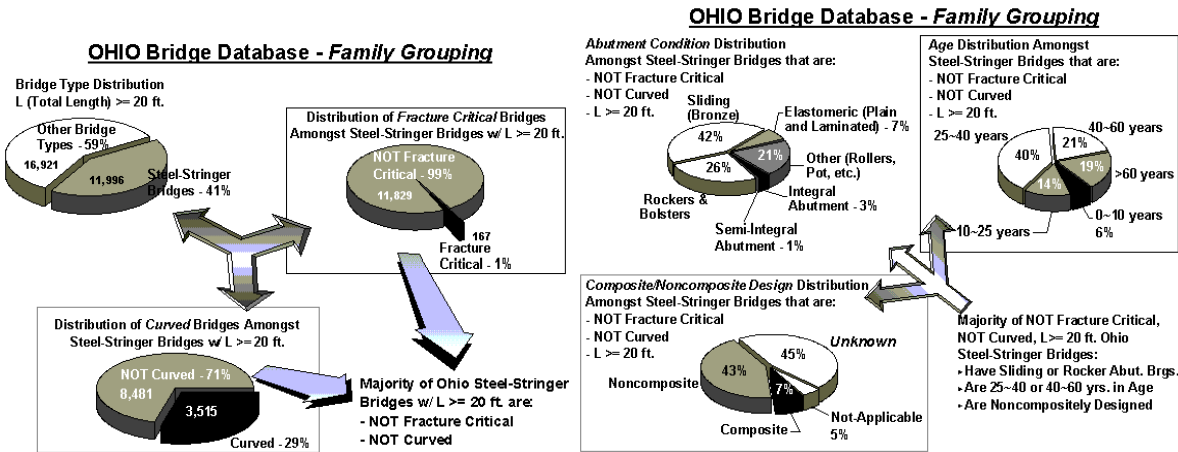


**Figure 5-16: Statistics for Steel-Stringer Bridges in Ohio**

The success of their management is dependent upon objective, accurate, and detailed data and other information provided as a basis for their evaluation and planning decisions. Yet, experimental testing of every single bridge would require an enormous effort that may not be affordable. On the other hand, type-specific management would seek to test and monitor only a sample population in order to obtain generic information about steel-stringer bridges. This would help conduct experiments and analysis on other samples in a more feasible manner. For example, instrumentation and testing of most bridges may not be necessary once the effect of traffic, the environment, and various geometric, material, and boundary conditions upon the general behavior mechanisms and state parameters are clearly understood. In addition, the most common forms of defect, deterioration, and damage will be cataloged for the bridge type and their effect must also be clearly delineated from the design constraints and loading environment.

The field data (impact test data, instrumented monitoring data) acquired from the statistical sample would be used to calibrate a two-dimensional grid or a three-dimensional finite-element

model of each bridge. In addition to observing the actual field data, studying the field calibrated models for each bridge within the statistical sample would permit observation of behavior patterns and characteristics (e.g., deflections, natural frequencies, etc.) that are similar amongst the representative bridges. An envelope for such bridge parameters could be defined for the given bridge type. These similarities would then be incorporated into a “generic” model that could be used to simulate the general behavior of the bridge type. For example, a model would exist which could be used to analytically represent the general behavior of any steel-stringer bridge within the Ohio inventory. Moreover, this generic grid model could be customized for a particular steel-stringer bridge by permitting the specification of foundation type, abutment type, bearing type, non-composite action, composite action, span lengths, etc., and incorporating ODOT damage report and inspection rating information. The resulting model could therefore be used to compute capacities and rating factors for the steel-stringer bridge in question.

The University of Cincinnati has recently been contracted to test and evaluate thirty (30) structures in order to develop such a statistical database for steel-stringer bridges. The sample size of 30 bridges proposed for testing is based on standard statistical methods. The argument proceeds as follows: Suppose that a given bridge parameter,  $X$ , is to be estimated based on the sample mean of a population of measurements  $(X_1, X_2, X_3, \dots, X_N)$ . Then, it is intuitively obvious that the quality of the estimate is a function of both the population size,  $N$ , and the quality of the measurements,  $(X_1, X_2, X_3, \dots, X_N)$ . This intuition can be quantified as follows: The probability that the estimation error (i.e.,  $X - X_{Mean}$ ) exceeds some limit  $e$  can be described by the equation

$$P(|X - X_{Mean}| \leq M\sigma) = e$$

where  $\sigma$  denotes the standard deviation of the measurement distribution (i.e., a measure of the quality of the measurement data), and  $M$  is a function of the sample size and is plotted in Figure 5-16. In order to obtain a parameter estimate with a 99% probability of being within 1 standard deviation of the actual parameter value, the estimate should be based on a population sample size of at least 30.

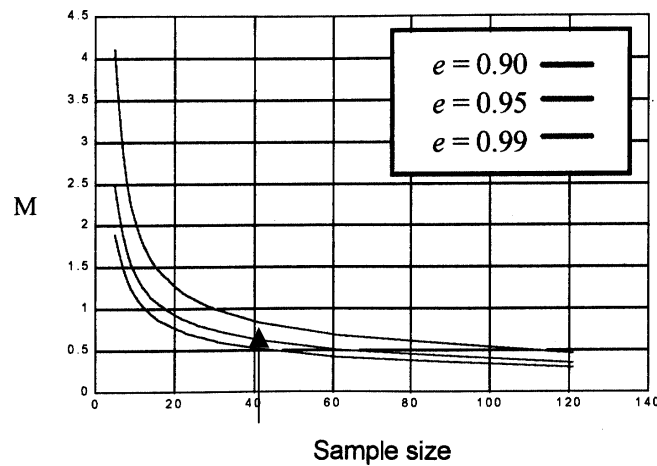


**Figure 5-17: Statistical Confidence for Sample Size**

The specimens will represent various ages, design attributes, construction attributes, condition, and records of performance for steel-stringer bridges. The field testing – impact and/or truck-load testing – of these bridges will yield experimental, objective information which can be used as a statistical baseline of what may be considered normal and customary behavior for this type of bridge. A health monitoring system for a steel-stringer bridge should be designed to take advantage of this statistical database. First, it may be used to modify the above decision schemes (e.g. the probability of failure SNR for a given damage scenario, the likelihood for a given heuristic). Second, it may be used to weight such decision thresholds for the resolution of any conflicts based upon the statistical concept of normal bridge behavior.

## 6. Conclusions

### 6.1. General Overview of the Research

The problem of objective global condition assessment is the transformation of the traditional process of subjective rating and evaluation to one which objectively incorporates all the past, present and future systems and properties which affect performance, into a more meaningful expression for the global health of a structure. The two fundamental concepts which provide the basis for this transformation are structural reliability and structural identification. Moreover, by utilizing actual operating or decommissioned facilities as test-specimens in conjunction with laboratory and analytical-numerical-computational support for the research, and interacting with practicing engineers, a reasonable check and balance is maintained between academic imagination and vision, the current state-of-the-art research tools, and the actual states of engineering education and practice. The three basic and distinct experimental approaches offering the greatest promise for feasibly generating objective and detailed information about the mechanical characteristics and loading mechanisms of an operating structure are dynamic testing, diagnostic truckload experiments, and instrumented monitoring.

The constructed bridge will have many inherent mechanisms to resist the applied load and which are generally not considered in the analysis of its capacity. These identified mechanisms include the actual load distribution, impact factor, unintended composite action, participation of superimposed deadload, material properties, unintended continuity, participation of secondary members, effects of skew, effects of deterioration and damage, unintended bearing restraint, and

environmental effects (e.g., thermal stresses). The AASHTO *Manual* envisions the future use of diagnostic tests under truckloads for load rating. Fatigue evaluation of highway bridges is also of great concern to the bridge engineer, particularly with older monumental structures that have undergone several episodes of rehabilitation or with suspect connections which were designed before the recent investigation of such phenomena. The only way to obtain precise service information is through continuous field monitoring of the local stress field upon and adjacent to the suspect members, connections, or welds. This research has demonstrated how the influence line can be reliably identified from controlled or service loadings and then used to immediately provide a capacity rating for the instrumented section and/or an estimation of the remaining fatigue life for the instrumented member/connection based upon the relevant AASHTO codes.

The most important contribution of this research is the proven technique for the accurate field identification of bridge parameters (specifically, strain influence lines and modal flexibility) which not only define the structural condition (or health) but are also sensitive to typical damage scenarios. These results are achieved without a finite element model, but can also serve to calibrate such a model for greater spatial precision and the investigation of other possible damage scenarios, repair/retrofit schemes, and other structural considerations. This contribution is unique to the aforementioned field of expertise and provides a considerable advancement towards the problem of objective and timely assessment of highway bridges. Sudden damage to a highway bridge (e.g., vehicle collision) may appear much worse than its actual effect upon the structural performance (e.g., load capacity); quite often, bridges are closed to traffic unnecessarily following sudden damage due to this uncertainty and vice versa. Following the detection of damage, it is usually beneficial to the owner to quickly yet objectively identify the

actual structural response to controlled loading experiments. Alternatively, continuous remote monitoring of a highway bridge to traffic and environmental loading would most likely detect any damage to an instrumented section of the structure and could immediately alert the transportation department of said damage and its likely effect upon structural performance.

The proposed management strategy for civil structures is simply an extension of the hierarchical approach wherein objective mechanical fundamentals are utilized as a starting point for increasingly sophisticated process models or knowledge. In an on-site data-acquisition system, measureable parameters feed an intelligent monitor which contains knowledge of the relationship between structural variables and the desired goal or performance state. This knowledge may consist of mathematical models, statistical classification, and expert heuristics. The challenge is to capitalize on the complementary strengths of each method in a hybrid controller. Decisions are made regarding the bridge health based upon real-time simulations and identification of the current state of the structure. This insitu evaluation of the structure distinguishes intelligent structural monitoring from the traditional approach of annual inspection and remote management.

In this manner, a hierarchical approach to the structural health monitoring system will be designed and built. The final product is envisioned as an on-site continuous Windows-based health monitor which:

- Acquires sensor data at variable sampling speeds,
- Communicates with peripheral devices such as a video camera or traffic scale,
- Provides a graphical interface via Internet and phone line with a remote engineer,

- Performs simple range and other checks for sensor faults,
- Identifies parameters for a simple beam or grid model of the bridge,
- Detects any structural degradation or damage via NP thresholds,
- Has an open architecture for future expansion or connection.

The current attributes of the bridge health monitor program include:

1. *Remote desktop control* to review and/or initiate monitoring of the instrumented bridge.
2. *Simultaneous high-speed acquisition* of traffic information, video camera, and sensor data from the instrumented bridge for the most recent truck crossing.
3. Field implementation of a continuous, multi-tasking, Windows95 health monitor which acquires sensor data at variable sampling speeds, communicates with peripheral devices, provides a user-friendly and customizable display interface, and allows an open hardware/software architecture for:

- Other structural monitoring applications
- System expansion of instrumentation, reporting, or other functions
- Networked multinode connection of other peripherals, structures, and organizations.

Future attributes of the bridge health monitor program, based upon results from this research, will include an *automated monitoring program* which switches between high-speed truck monitoring and long-term environmental monitoring, posting regular reports on statistics and evaluated health indices, including: maximum traffic stress, maximum environmental stress, neutral axis location, remaining composite action, dynamic parameters, influence line, impact factor, distribution factor, capacity load rating, remaining fatigue life, etc. These can then

provide hardcopy reports to the engineer, be posted to the UCII website, and/or trigger alarms based upon pre-defined thresholds.

Structural identification by these methods should further remain as a potent tool in the case of: intelligent infrastructure applications; construction with new materials such as FRP composites applications; long-span, monumental, and/or critical lifeline structures which require continuous health-monitoring; and, historic structures which require preservation design. Perhaps the most important need for structural identification applications today is rationalizing the manner in which we design, inspect, evaluate, maintain and renew bridges and other components of the civil infrastructure system.

## 6.2. Specific Review of the Dissertation

This dissertation concerns the conceptualization and validation of a novel approach for the accurate and timely evaluation of steel-stringer highway bridges. The most important contribution of this research is the application of signal processing algorithms within the context of systems integration for the field identification of bridge state parameters (specifically, strain influence lines and modal flexibility). The identified parameters for a given cross-section of the bridge are then processed into condition indices according to structural and material fundamentals. It is observed that certain condition indices are also quite sensitive to induced damage scenarios. These results are achieved without a finite element model, but can also serve to calibrate such a model for greater spatial precision and the investigation of other possible damage scenarios, repair/retrofit schemes, and other structural considerations.

Chapter 1 introduces the current problems of the infrastructure and relevant findings by this and other researchers in the area of nondestructive evaluation and instrumented monitoring of highway bridges. Presently, a large portion of the nation's inventory of highway bridges are considered functionally obsolete or structurally deficient. The transportation department is mandated to manage this crumbling inventory on an underfunded budget. Design and rating assessment is based upon rather simplistic beam models which are notorious for their inaccurate yet conservative estimates of load capacity. Condition assessment is based upon the rather subjective and highly variable process of bi-annual visual inspection. Research by this and other engineers has pursued several avenues to a more objective solution to design and assessment, including field experimentation and instrumented monitoring of actual bridge specimens and finite element modeling at various levels of complexity in representing elements and their interaction. It is clear from such research that a steel-stringer bridge will have many inherent mechanisms to resist the applied truckloads, thermal effects, deterioration, damage scenarios, or other forces induced during construction and/or service. These findings are generally not considered in practice. One contribution of this dissertation is to draw attention to such discrepancies between practice and reality and to suggest methods for the quantitative evaluation of bridge condition in light of such measured forces.

Chapter 2 is primarily focuses upon the analytical formulation and field identification of influence lines for the instrumented locations of a highway bridge. The simplistic beam model used in bridge design is investigated in both the spatial/time and frequency domains based upon first principals of structural engineering. A quasi-static formulation assuming simple supports is presented for both a single span beam and a symmetrical three-span beam. The crawl-speed response for a noncomposite beam to both a moving point load (i.e., influence line) and two-axle truckload are considered. This dissertation is quite novel as compared to the existing analyses in the literature due to its parallel formulation in the frequency domain. A generalized beam model is employed to represent the dynamical response of the beam to such loading. It is found to be additive to the static response in terms of an infinite number of spatial modes of increasing temporal frequency. The response bandwidth for the influence line is estimated and found to be proportional to vehicle speed; a clear separation from higher frequency disturbances is possible by adjusting the test vehicle's speed accordingly. Other dynamic considerations such as vehicle-beam interaction, condition of the riding surface, etc. remain essentially unmodeled. Field experiments with several trucks of varying configurations yield rather consistent estimations for the influence lines of two bridge specimens; less than 3% error for controlled tests and less than 10% variation in results from normal traffic speeds (i.e. 50mph). This dissertation provides a unique approach to identification of the influence line from experimental data compared to other efforts in the literature; typically, this step is accomplished through a finite element model of varying complexity which requires substantial effort to calibrate (and, quite often, results in non-uniform levels of accuracy for each modeled element). Further, it provides a relatively continuous representation of the influence line for the entire load path of the vehicle instead of just a discrete set of static truckload positions.

Chapter 3 presents the various condition indices that can be directly derived from the measured truckload responses and the identified influence lines. This dissertation is again novel compared to other academic pursuits in the literature because no finite element model is employed in determining the condition indices for each instrumented section. Rather, sectional properties and parameters are deduced from the governing principals of mechanics and strength of materials. Significant consideration is given to the assessment of partial composite action, as is observed from the neutral axis location in comparison with the geometric centroid for the non and fully composite sections. Two methods are introduced to identify the liveload demand, sectional capacity, and load rating factor in light of any partial composite action for the instrumented section. It is found that the usual assumption in practice of one of these two extremes (i.e., either full or noncomposite interaction between the beam and decking) will lead to considerable error in the capacity load rating of highway bridge. The design process is generally conservative in such matters. However, such assumptions in the evaluation of field measurements can lead to significant underestimation of the liveload demand.

This research had the unique opportunity to instrument, measure, and verify such concepts during the actual construction of a local steel-stringer bridge. Both positive and negative moment regions are accommodated by the methodology. The identified influence lines are used to virtually simulate any truckload under consideration, including design truck or lane loads (e.g., HS20-44) and fatigue truckloads. The constructed bridge was controlled by truck loading of the center span due to its rather unique span ratio; however, the bridge capacity was at least twice that suggested by the design. The remaining fatigue life for the constructed bridge was found to be essentially infinite due to its highly redundant design, even after consideration of the

high stresses measured during the welding of the bearing plates at the piers. The measured deadload upon the critical girder was considerably less than predicted by design. Although not considered by design, the measured environmental stresses were much larger than any design load responses; however, the decreases in liveload demand and deadload more than outweighed such factors in the rating. All of these results are quite beyond the state-of-practice and their integration within this dissertation is uncommon if not unique in the academic literature.

Chapter 4 seeks to employ these very same condition indices in the detection and localization of induced damage scenarios on a decommissioned steel-stringer bridge. Continuous monitoring allows the immediate identification of a change to the system; however, without traffic excitation, it would not be possible to distinguish structural damage from sensor malfunction. The identified influence line is found to be highly sensitive to a very localized flange cut of the steel girder; further, this sensitivity remains significant in distant spans and on other beam lines such that immediacy of the installed instrument is desirable but not necessary to detect damage. Localization based upon proximity to the sensor with the largest change is probable, but this did not apply at support sections due to varying levels of deterioration to their designed fixity. Strain measurements were found to be much more sensitive than displacement; however, displacement sensors are generally much easier to install than strain gages. Capacity load rating was found to be insensitive to the flange cut because it represents the entirety of the very deteriorated structure. Again, this dissertation provides a unique approach to damage assessment in that all indices are determined quickly and accurately from the measured signals without the use of a finite element model. However, results compared favorably with an independently calibrated FE model for the bridge before and after the damage.

The final chapter presents an application of the above and other systems concepts for the implementation of a dedicated health monitoring system to the constructed bridge. A hierarchical system has been successfully employed to measure, process, and transmit video images, vehicle statistics, and structural responses to highway traffic over the Internet. Existing and future issues for this application are discussed. In addition, the potential of this research to improve upon the management of the bridge inventory by the transportation department is considered for several theoretical approaches.

## 7. References

AASHTO (1983 and 1989). *Manual for Maintenance Inspection of Bridges*. American Association of State Highway and Transportation Officials, Washington, D.C.

AASHTO (1989 and 1995). *Guide Specification for Strength Evaluation of Existing Steel and Concrete Bridges*. American Association of State Highway and Transportation Officials, Washington, D.C.

AASHTO (1990). *Guide Specification for Fatigue Evaluation of Existing Steel Bridges*. American Association of State Highway and Transportation Officials, Washington, D.C.

AASHTO (1994a). *Manual for Condition Evaluation of Bridges*. American Association of State Highway and Transportation Officials, Washington, D.C.

AASHTO (1994b). *Guide Specification for Distribution of Loads for Highway Bridges*. American Association of State Highway and Transportation Officials, Washington, D.C.

ACI 318-95 (1995). *Building Code Requirements for Structural Concrete*. American Concrete Institute, Committee 318, Farmington, MI.

Adams, R.D., Cawley, C.J., Pye, P., and Stone, B.J. (1978). "A Vibration Technique for Non-Destructively Assessing the Integrity of Structures." *Journal of Mechanical Engineering Science*, Volume 20, pp. 93-100.

Adams, T.M., and Sianipar, P.R.M. (1995). "Project and Network Level Bridge Management," Proceedings, *ASCE Transportation Congress*, San Diego, CA.

Aktan, A.E., and Raghavendrchar, M. (1990). "Nondestructive Testing and Identification for Bridge Rating: Pilot Project." *FHWA Research Report 90-1*, Department of Civil & Environmental Engineering, University of Cincinnati, Ohio, May.

Aktan, A.E., Chuntavan, C., Toksoy, T., and Lee, K.L. (1992a) "Bridge Nondestructive Evaluation by Structural Identification: 1. Description of the Methodology." Proceedings, *Third Workshop on Bridge Engineering Research in Progress*, Sponsored by the National Science Foundation, Department of AMES, University of California, San Diego, La Jolla, CA, November.

Aktan, A.E., Zwick, M., Miller, R., and Shahrooz, B. (1992b). "Nondestructive and Destructive Testing of Decommissioned Reinforced Concrete Slab Highway Bridge and Associated Analytical Studies." *Transportation Research Record 1371*, TRB, National Research Council, Washington, D.C., pp. 142-153.

Aktan, A.E. (1993a). "A Summary of Important Findings Resulting from University of Cincinnati's Bridge Research for ODOT." presentation invited by the *AASHTO Bridge Committee*, AASHTO Meeting, Denver, May.

Aktan, A.E., Chuntavan, C., Lee, K.L., and Toksoy, T. (1993b). "Structural Identification of a Steel Stringer Bridge." *Transportation Research Record 1393*, TRB, National Research Council, Washington, D.C., pp. 175 - 185.

Aktan, A.E., Lee, K.L., Chuntavan, C., and Aksel, T. (1994a). "Modal Testing for Structural Identification and Condition Assessment of Constructed Facilities." Proceedings, *12th International Modal Analysis Conference*, Honolulu, Hawaii, January.

Aktan, A.E., Lee, K.L., Naghavi, R., and Hebbbar, K. (1994b). "Nondestructive and Destructive Experimental Studies of Two 80-year-old Truss Bridges." paper accepted by *TRB Committee A2C05* for presentation at the 1994 Annual Meeting and for publication by the Transportation Research Record.

Aktan, A.E., Chuntavan, C., Lee, K.L., and Farhey, D.N. (1994c). "Nondestructive Testing and Identification for Bridge Rating, Phase 2: Steel-Stringer Bridges." FHWA, *Report FHWA/OH-95/021*, Washington, D.C., April.

Aktan, A.E., Farhey, D.N., and Dalal, V. (1995a). "Issues in Rating Steel-Stringer Bridges." *Transportation Research Record 1476*, TRB, National Research Council, Washington, D.C.

Aktan, A.E., Farhey, D.N., Hunt, V.J., Helmicki, A.J., Brown, D., and Shelley, S. (1995b). "Objective Bridge Condition Assessment." Proceedings, *International Symposium on Non-Destructive Testing in Civil Engineering*, Berlin, Germany, September.

Aktan, A.E., Hunt, V.J., Lally, M.J., Stillmaker, R.B., Brown, D., and Shelley, S. (1995c). "Field Laboratory for Modal Analysis and Condition Assessment of Highway Bridges." Proceedings, *13th International Modal Analysis Conference*, Nashville, Tennessee.

Aktan, A.E., and Farhey, D.N. (1996a). "Condition and Reliability Assessment of Constructed Facilities." *ACI Special Publication*, American Concrete Institute.

Aktan, A.E., Farhey, D.N., Hunt, V.J., Lenett, M., Levi, A. (1996b). "Objective Bridge Condition Assessment." Proceedings, *Structural Materials Technology - An NDT Conference*, Technomic Publishing, Lancaster, Pennsylvania, pp. 228-232.

Aktan, A.E., and Yao, J.T.P. (1996c). "On Structural Identification of Constructed Facilities." Proceedings, *Structures Congress XIV*, ASCE, Chicago, Illinois, April.

Aktan, A.E., Dalal, V., Helmicki, A., Hunt, V., Lenett, M., Catbas, N., and Levi, A. (1996d). "Objective Bridge Condition Assessment for Serviceability." Proceedings, *Third Conference on Nondestructive Evaluation of Civil Structures and Materials*, University of Colorado at Boulder, September.

Aktan, A.E., Farhey, D.N., Brown, D.L., Dalal, V., Helmicki, A., Hunt, V., and Shelley, S. (1996e). "Condition Assessment for Bridge Management." *Journal of Infrastructure Systems*, ASCE, Vol. 2, No. 3, pp. 108-117, September.

Aktan, A.E., Helmicki, A.J., and Hunt, V.J. (1996f) "Issues in Health Monitoring for Intelligent Infrastructure." Proceedings, *US/Japan Workshop on Smart Structures Technology*, National Science Foundation, College Park, MD.

Aktan, A.E., Helmicki, A.J., and Hunt, V.J. (1996g) "Issues Related to Intelligent Bridge Monitoring." Proceedings, *ASCE Structures Congress*, Chicago, IL, April.

Aktan, A.E., Brown, D., Farrar, C., Helmicki, A., Hunt, V., and Yao, J. (1997a). "Objective Global Condition Assessment." Proceedings, *15th International Modal Analysis Conference*.

Aktan, A.E., Farhey, D.N., Helmicki, A.J., Hunt, V.J., Lee, K.L, and Levi, A. (1997b). "Structural Identification for Condition Assessment: Experimental Art." *Journal of Structural Engineering*, No. 1674, ASCE, December.

Aktan, A.E., Helmicki, A.J., and Hunt, V.J. (1997c). "Structural Identification for Condition Assessment of Civil Infrastructure." Proceedings, *American Control Conference*, Albuquerque, NM.

Aktan, A.E., Helmicki, A.J., Dalal, V., and Hunt, V.J. (1997d). "Instrumented Monitoring and Nondestructive Evaluation of Highway Bridges." Proceedings, *ASCE Structures Congress*, Portland, OR, April.

Aktan, A.E., Helmicki, A.J., and Hunt, V.J. (1998a). "Issues in Health Monitoring for Intelligent Infrastructure." *Journal of Smart Materials and Structures*, IOP Publishing Ltd., No. 7, July.

Aktan, A.E., Catbas, N., Turer, A., and Zhang, Z. (1998b). "Structural Identification: Analytical Aspects." *Journal of Structural Engineering*, ASCE, Vol. 124, No. 7, July, pp. 817-829.

Alamapalli, S. and Fu, G. (1994). "Automatic Instrumentation for Remote Structure Monitoring." Proceedings, *NDT Conference*, New Jersey Department of Transportation, February.

Allemang, R.J., and Brown, D.L. (1982), "A Correlation Coefficient for Modal Vector Analysis." Proceedings, *First International Modal Analysis Conference*, Orlando, Fl..

Allemang, R.J. (1994). *Vibrations: Experimental Modal Analysis*. UC-SDRL-CN-20-263-663/664, Department of Mechanical, Industrial, and Nuclear Engineering, University of Cincinnati, April.

Anderson, B., and Moore, J. (1979). *Optimal Filtering*. Prentice-Hall, New Jersey.

Antsaklis, P., Passino, K., and Wang, S. *Autonomous Control Systems: Architecture and Fundamental Issues*. Department of Electrical and Computer Engineering, University of Notre Dame, Notre Dame, IN.

Antsaklis, P., Passino, K., and Wang, S. (1991). "An Introduction to Autonomous Control Systems." *Journal of IEEE Control Systems*, Volume 11, Number 4, June.

Antsaklis, P., Passino, K. (1993). *An Introduction To Intelligent And Autonomous Control*. Kluwer Academic, Boston, MA.

Bahkt, B., and Pinjarkar, S.G. (1989). "Dynamic Testing of Highway Bridges – A Review," *Transportation Research Record*, No. 1223, TRB, National Research Council, Washington, D.C., pp. 93-100.

Bahkt, B., and Jaeger, L.G. (1990). "Bridge Testing – A Surprise Every Time," *Journal of Structural Engineering*, ASCE, Vol. 116, No. 5, May, pp. 1370-1383.

Bahkt, B., and Jaeger, L.G. (1992). "Ultimate Load Test of Slab-On-Girder Bridge," *Journal of Structural Engineering*, ASCE, Vol. 118, No. 6, June, pp.1608-1624.

Bahkt, B., and Jaeger, L.G. (1995). "Utilization of Service Loads in Bridge Evaluation," *Bridge Evaluation, Repair, and Rehabilitation*. Kluwer Academic Publishers, Netherlands.

Barrish, R. (1997). *Instrumented Monitoring of a Reinforced Concrete Slab on Steel Stringer Highway Bridge Through Construction: Concrete Elements*, Masters Thesis, Department of Civil and Environmental Engineering, University of Cincinnati, Cincinnati, OH.

Beer, F., and Johnston, E.R. (1992). *Mechanics of Materials*. McGraw-Hill, New York, NY.

Begg, R.D. (1976). "Structural Integrity Monitoring Using Digital Processing of Vibration Signals." Proceedings, *8th Annual Offshore Technical Conference*, Houston, pp. 305-311.

Bertero, V.V., and Bresler, B. (1971), "Developing Methodologies for Evaluating the Earthquake Safety of Existing Buildings." *Report No. UCB 71-13*, University of California, Berkeley.

Biggs, J. (1964). *Introduction to Structural Dynamics*. McGraw-Hill Book Company, New York, NY.

Blevins, R. (1979). *Formulas for Natural Frequency and Mode Shape*. Van Nostrand Reinhold Company, New York, NY.

Bobrow, D. (1985). *Qualitative Reasoning About Physical Systems*. MIT Press, Cambridge, MA.

- Buckland, J., Musgrave, J., and Walker, B. (1992). *On-Line Implementation Of Nonlinear Parameter Estimation For The Space Shuttle Main Engine*. National Aeronautics and Space Administration, NASA Technical Memorandum 106097, Washington, D.C.
- Burdette, E.G., and Goodpasture, D.W. (1988). "Correlation of Bridge Load Capacity Estimates with Test Data," *NCHRP Report*, No. 306, Transportation Research Board, National Research Council, Washington, D.C.
- Cantieni, R. (1984). "Dynamic Load Testing of Highway Bridges," *Transportation Research Record*, No. 950, TRB, National Research Council, Washington, D.C., pp. 141-148.
- Casas, J.R., and Aparicio, A.C. (1994). "Structural Damage Identification From Dynamic-Test Data." *Journal of Structural Engineering*, Vol. 120, No. 8.
- Catbas, F., Lenett, M., Brown, D., Doebling, S., Farrar, C., and Turer, A. (1997) "Modal Analysis Of Multi-Reference Impact Test Data For Steel Stringer Bridges." Proceedings, *Fifteenth International Modal Analysis Conference*, Orlando, FA.
- Cawley and Adams, R.D. (1979). "The Location of Defects in Structures From Measurements of Natural Frequencies." *Journal of Strain Analysis*, Vol.14, No.2, pp. 49-57.
- Chajes, M.J., Mertz, D.R., and Commander, B. (1997). "Experimental Load Rating of a Posted Bridge," *Journal of Bridge Engineering*, ASCE, Vol. 2, No. 1, February, pp. 1-10.
- Chance, J., Tomlinson, G.R., and Worden, K. (1994). "A Simplified Approach to the Numerical and Experimental Modeling of Dynamics of a Cracked Beam." Proceedings, *12th International Modal Analysis Conference*, pp. 778-785.
- Chase, S.B. (1995a). "Keynote Address: FHWA NDE Contract Research, An Overview." Proceedings, *North-American Workshop on Instrumentation and Vibration Analysis of Highway Bridges*, Sponsored by: FHWA, NSF, and ODOT, University of Cincinnati Infrastructure Institute, Ohio, July.
- Chase, S.B. (1995b). SPIE Proceedings, *Nondestructive Evaluation of Aging Bridges and Highways*.
- Chen, J.C., and Garba, J.A. (1987). "Structural Damage Assessment Using a System Identification Technique." Proceedings, *Workshop on Structural Safety Evaluation Based on System Identification Approaches*, Lambrecht/Pflaz, Germany.
- Chen, J.C., and Garba, J.A. (1988). "*On-Orbit Damage Assessment for Large Space Structures*." *AIAA Journal*, Vol. 26, No. 9, pp. 1119-1126.
- Chen, S., and Sungkon, K. (1995a). "Neural Network Based Sensor Signal Monitoring of Instrumented Structures," *Restructuring: America and Beyond*. Proceedings, Structures Congress XIII, ASCE, Boston, Massachusetts, April, pp.52-55.

- Chen, S., and Sungkon, K. (1995b). "Logic-Based Object-Oriented Modeling for Health Monitoring of Instrumented Structures," *Restructuring: America and Beyond*. Proceedings, Structures Congress XIII, ASCE, Boston, Massachusetts, April, pp.783-786.
- Chen, Y., and Swamidas, A. (1994). "Dynamic Characteristics and Modal Parameters of a Plate with a Small Growing Surface Crack." Proceedings, *12th International Modal Analysis Conference*, pp. 1155-1161.
- Chopra, A. (1995). *Dynamics of Structures*. Prentice Hall, Englewood Cliffs, NJ.
- Clinton, President, and Gore, Vice President (1993). "Technology For America's Economic Growth, A New Direction To Build Economic Strength." Inaugural Address to the Nation, February 22.
- Clough, R., and Penzien, J. (1993). *Dynamics of Structures*. McGraw-Hill, New York, NY.
- Coppolino, R.N., and Rubin, S. (1980). "Detectability of Structural Failures in Offshore Platforms by Ambient Vibration Monitoring." Proceedings, *12th Annual Offshore Technology Conference*, Houston, Vol. 4, pp. 101-110.
- Crohas, H., and Lepert, P. (1982). "Damage-Detection Monitoring Method for Offshore Platforms is Field-Tested." *Oil & Gas Journal*, February, pp. 94-103.
- Dascotte, E. (1991). "Applications of Finite Element Tuning Using Experimental Modal Data." *Sound and Vibration*, Volume 25, pp. 22-26.
- Deatherage, J.H., Sanders, M.D., Goodpasture, D.W., and Burdette, E.G. (1995). "Controlled Load Tests on a Four-Girder Steel Bridge," *Transportation Research Record*, No. 1476., TRB, National Research Council, Washington, D.C., pp. 106-116.
- DeRusso, D.M., Roy, R.J., and Close, C.M. (1966). *State Variables for Engineers*. John Wiley & Sons, Inc., New York.
- DeWolf, J., Coon, P., O'Leary, P. (1995). "Continuous Monitoring of Bridge Structures." *IABSE Reports*, Issue 73, Zurich, Switzerland, pp. 935-940.
- Doebling, S., Farrar, C., Prime, M., and Shevitz, D. (1996). "Damage Identification and Health Monitoring of Structural and Mechanical Systems from Changes in Their Vibration Characteristics: A Literature Review." *Report LA-13070-MS*, Los Alamos National Laboratories.
- Duggan, D.M., Wallace, E.R., and Caldwell, S.R. (1980). "Measured and Predicted Vibrational Behavior of Gulf of Mexico Platforms." Proceedings, *12th Annual Offshore Technology Conference*, Houston, Vol. 4, pp. 92-100.

Dunker, K.R., and Rabbat, B.G. (1993). "Why America's Bridges Are Crumbling." *Scientific American*, March, pp. 66-72.

Elhelbawey, M., Fu, C.C., Sahin, M.A., and Schelling, D.R. (1999). "Determination of Slab Participation from Weigh-In-Motion Bridge Testing," *Journal of Bridge Engineering*, ASCE, Vol. 4, No. 3, August, pp. 165-173.

Elkordy, M., Chang, K., and Lee, G. (1993). "Neural Network Trained by Analytically Simulated Damage States." *ASCE Journal of Computing in Civil Engineering*, Volume 7, Number 2, pp. 130-145.

Elkordy, M., Chang, K., and Lee, G. (1994). "A Structural Damage Neural Network Monitoring System." *Microcomputers in Civil Engineering*, Volume 9, pp. 83-96.

Emami-Naeini, A., Akhter, M., and Rock, S. (1985). "Robust Detection, Isolation, and Accommodation for Sensor Failures." Proceedings, *American Control Conference*, p.1129.

Ewins, D.J. (1984). *Modal Testing: Theory and Practice*, John Wiley & Sons, Inc..

Eymard, R., Guerrier, F., and Jacob, B. (1990). "Dynamic Behavior of Bridge Under Full Traffic." *Bridge Evaluation, Repair, and Rehabilitation*. edited by Nowak, Kluwer Academic Publishers, Netherlands.

Farrar, C.R. (1994). "Dynamic Characterization and Damage Detection in the I-40 Bridge Over the Rio Grande." LA-12767-MS, Los Alamos National Laboratories, Los Alamos, NM.

Farrar, C.R., and Cone, K.M. (1995). "Vibration Testing of the I-40 Bridge Before and After the Introduction of Damage." Proceedings, *13th International Modal Analysis Conference*, Nashville, Tennessee, pp. 203-209.

FHWA, (1990). *Bridge Inspector's Training Manual*, Federal Highway Administration , Publication No. FHWA-PL-93-017, Washington, D.C.

FHWA, (1993). *The Status of the Nation's Highways, Bridges, and Transit: Conditions and Performance*, Federal Highway Administration , Washington, D.C.

Fisher, J. (1984). *Fatigue and Fracture in Steel Bridges*. John Wiley & Sons, New York, NY.

Fisher, R.A. (1912). "On an Absolute Criterion for Fitting Frequency Curves." *Messenger of Math*, Volume 41.

Fleming, J.F., and Mayers, D.F. (1961). "Dynamic Response of Highway Bridges," *Journal of Structural Engineering*, ASCE, Vol. 87, No. 7, pp. 31-61.

Fox, M., Lowenfeld, S., and Kleinosky, P. (1983). *Techniques for Sensor-Based Diagnosis*. Robotics Institute, Carnegie-Mellon University, Report No: CMU-RI-TR-83-7, Pittsburgh, PA.

- Fox, C.H.J. (1992). "The Location of Defects in Structures: A Comparison of the Use of Natural Frequency and Mode Shape Data." Proceedings, *10th International Modal Analysis Conference*, San Diego, California, Vol. 1, pp. 522-528.
- Fuller, A.H., Eitzen, A.R., and Kelly, E.F. (1931). "Impact on Highway Bridges." *ASCE Transactions*, Vol. 95, Paper 1786, pp. 1089-1117.
- French, S. (1996). *Determinate Structures*. Delmar Publishers, New York, NY.
- Fryba, L. (1972). *Vibration of Solids and Structures Under Moving Loads*. Noordhoff International Publishing, Groningen, Netherlands.
- Gai, E., Harrison, J., and Daly, K. (1979). "Generalized Likelihood Test for FDI in Redundant Sensor Configurations." *Journal of Guidance, Control, and Dynamics*, Vol. 2, January.
- Gai, E., Harrison, J., and Daly, K. (1979). "FDI Performance of Two Redundant Sensor Configurations." *IEEE Transactions on Aerospace and Electronic Systems*, Vol. AES-15, No. 3, May, p.405.
- Gao, Y. (1998). *Intelligent Bridge Health Monitoring System: High Speed Data Acquisition And Graphical User Interface Design*. Masters Thesis, Department of Electrical and Computer Engineering and Computer Science, University of Cincinnati, Cincinnati, OH.
- Garrett, P. (1987a). *Computer Interface Engineering for Real-Time Systems*. Prentice-Hall, Englewood Cliffs, NJ.
- Garrett, LeClair, and Wee (1987b). "Qualitative Process Automation vs. Quantitative Process Control." Proceedings, *American Control Conference*, Minneapolis, MN, June.
- Garrett, P., Heyob, J., Hunt, V., LeClair, S., and Patterson, O. (1993). "Decoupled Flux Control for Molecular Beam Epitaxy." *Journal of IEEE Transactions on Semiconductor Manufacturing*, Vol. 6, No. 4, November.
- Gelb, A. (1989). *Applied Optimal Estimation*. The Analytical Sciences Corporation, MIT Press, Cambridge, Massachusetts.
- Genesereth, M. and Nilsson, N. (1987). *Logical Foundations of Artificial Intelligence*. Morgan Kaufmann Publishers Inc., Palo Alto, CA.
- Gertler, J. (1988). "Survey of Model-Based Failure Detection and Isolation in Complex Plants." *IEEE Control Systems*, December, pp. 3-11.
- Ghaboussi, J. (1993). "An Overview of the Potential Applications of Neural Networks in Civil Engineering." Proceedings, *ASCE Conference on Structural Engineering in Natural Hazards Mitigation*, Volume 2, pp. 1324-1330.

Ghanem, R., and Shinozuka, M. (1995). "Structural-System Identification: Theory." *Journal of Engineering Mechanics*, ASCE, Vol. 121, No. 2, pp. 255-264, February.

Ghosn, M., Moses, F., and Gobieski, J. (1986). "Evaluation of Steel Bridges Using In-Service Testing," *Transportation Research Record*, No. 1072, TRB, National Research Council, Washington, D.C., pp. 71-78.

Goble, G., Schulz, J., and Commander, B. (1992). "Load Prediction and Structural Response," *Final Report*, FHWA Project DTFH61-88-C-00053, Department of Civil, Environmental, and Architectural Engineering, University of Colorado, Boulder, CO, September.

Griessmann, A. (1998). *Subjective vs. Objective Analysis for the Condition Evaluation of Bridges*, Masters Thesis, Department of Civil and Environmental Engineering, University of Cincinnati, Cincinnati, OH.

Grimmelsman, K. (1997). *Instrumented Monitoring of a Reinforced Concrete Slab on Steel Stringer Highway Bridge Through Construction: Steel Elements*, Masters Thesis, Department of Civil and Environmental Engineering, University of Cincinnati, Cincinnati, OH.

Grzybowski, M., and Meyer, C. (1992). *Damage Prediction for Concrete With and Without Fibre Reinforcement*, Department of Civil Engineering and Engineering Mechanics, Columbia University, New York, April.

Gudmunson, P. (1982). "Eigenfrequency Changes of Structures Due to Cracks, Notches, or Other Geometrical Changes." *Journal of the Mechanics and Physics of Solids*, Vol. 31, pp. 329-345.

Hambly, E.C. (1991). *Bridge Deck Behavior*, 2nd edition, New York.

Hancock, J. (1966). *Signal Detection Theory*. McGraw-Hill, New York, NY

Helmicki, A. (1991a). "Rocket Engine Health Monitoring: A System's Perspective." *NASA/ASEE Summer Faculty Fellowship Report*, NASA Marshall Space Flight Center, August.

Helmicki, A., Kuo., F., and Vallely, D. (1991b). "Rocket Engine Health Monitoring and Control: Some Connections and Their Implications." Proceedings, *Third Annual Health Monitoring Conference for Space Propulsion Systems*, Cincinnati, OH, November.

Helmicki, A., Sayweed, S., Ksenia, K., and Kuo., F. (1993). "Health Monitoring and Control for the STME: A Case Study." Proceedings, *Fifth Annual Health Monitoring Conference for Space Propulsion Systems*, pp. 128-141, Cincinnati, OH, April.

Helmicki, A., Jaweed, S., and Kolcio, K. (1994). "Liquid Rocket Engine Modeling for Condition Monitoring and Control." *30th Joint Propulsion Conference*, Indianapolis, IN, June.

Helmicki, A.J., Aktan, A.E., and Hunt, V.J. (1995) "Issues in Implementation of Structural Monitoring to Constructed Facilities for Serviceability with Damageability Considerations." Proceedings, *American Control Conference*, Seattle, WA.

Helmicki, A.J., Aktan, A.E., and Hunt, V.J. (1997). "Issues in Bridge Control Systems Applications." *Journal of Infrastructure*, Vol. 2, No. 4, pp.30-40, April.

Helmicki, A., Hunt, V., Dalal, V., and Aktan, A.E. (1999a). "Information Technology in Civil Infrastructure Systems: Multi-Modal Testing and Monitoring of a Highway." *Structural Health Monitoring*, Stanford Press.

Helmicki, A., Lenett, M., Greismann, A., Hunt, V., and Aktan, A.E. (1999b). "Structural Identification Based Condition Assessment: A Demonstration of Methods Applied to a Laboratory Scale Model Testbed." Proceedings, *1999 American Control Conference*, San Diego, CA, June.

Henchi, K., Fafard, M., Talbot, M., and Dhatt, G. (1998). "An Efficient Algorithm for Dynamic Analysis of Bridges Under Moving Vehicles Using a Coupled Modal and Physical Components Approach," *Journal of Sound and Vibration*, Vol. 212, No. 4, pp. 663-683.

Hogue, T.D., Aktan, A.E. and Hoyos, A. (1991). "Localized Identification of Constructed Facilities." *Journal of Structural Engineering*, ASCE, Vol. 117, No. 1, January.

Horak, D.T. (1988). "Failure Detection in Dynamic Systems with Modeling Errors." *Journal of Guidance, Control, and Dynamics*, Vol. 11, No. 6, p. 508, November.

Hunt, V. (1989). "Dual-Difference Redundant Structure in Fault-Tolerant Control." Proceedings, *Fifth Aerospace Applications of Artificial Intelligence Conference*, Dayton, OH.

Hunt, V. (1991). *Redundant Structures for Fault-Tolerant Control*. Master's Thesis, Department of Electrical and Computer Engineering, University of Cincinnati, Cincinnati, OH, December.

Hunt, V.J., Levi, A., Dietz, D., Sobecks, B., Helmicki, A.J., and Aktan, A.E. (1994). "Issues in Bridge Instrumentation and Monitoring." Proceedings, *Spring Conference on Experimental Mechanics*, SEM, Baltimore, Maryland, June.

Hunt, V.J., Levi, A., Sobecks, B., Helmicki, A.J., and Aktan, A.E. (1995). "Progress Report on Bridge Instrumentation and Monitoring." Proceedings, *Spring Conference on Experimental Mechanics*, SEM, Grand Rapids, Michigan, June.

Hunt, V.J., Helmicki, A.J., and Aktan, A.E. (1997a). "Informational Issues in Bridge Health Monitoring." Proceedings, *International Workshop on Structural Health Monitoring*, Stanford, CA.

- Hunt, V.J., Helmicki, A.J., and Aktan, A.E. (1997b). "Instrumented Monitoring and Nondestructive Evaluation of Highway Bridges." Proceedings, *Infrastructure Condition Assessment Conference*, ASCE, Boston, MA.
- Hunt, V.J., Turer, A., Gao, Y., Levi, A., and Helmicki, A.J. (1998). "Instrumented Monitoring and Nondestructive Evaluation of Highway Bridges." Proceedings, *Structural Materials Technology - An NDT Conference*, Technomic Publishing, Lancaster, Pennsylvania, April.
- Hunt, V., Shell, M., Turer, A., Lenett, M., Helmicki, A., Barrish, R., and Aktan, A.E. (1999). "Design Verification and Performance Monitoring of a Recently Constructed Steel-Stringer Bridge." Proceedings, *Society of Experimental Mechanics Annual Conference*, Cincinnati, OH, June.
- Huria, V., Lee, K.L., and Aktan, A.E. (1993). "Nonlinear Finite Element Analysis of a RC Slab Bridge." *Journal of Structural Engineering*, ASCE, 119(1), January, pp. 88-107.
- Hwang, E.-S., and Nowak, A. (1989). "Dynamic Analysis of Girder Bridges," *Transportation Research Record*, No. 1223, TRB, National Research Council, Washington, D.C., pp. 85-92.
- Ibanez, P. (1972). "Identification of Dynamic Structural Models from Experimental Data." *Engineering Report #UCLA-ENG-7725*, University of California at Los Angeles.
- Imbsen, R.A., Lui, W.D., Schamber, R.A., and Nutt, R.V. (1987). "Strength Evaluation Of Existing Reinforced Concrete Bridges." *NCHRP Report #292*, TRB, Washington D.C.
- Ismail, F., Ibrahim, A., and Martin, H.R. (1990). "Identification of Fracture Cracks From Vibration Testing." *Journal of Sound and Vibration*, Vol. 140(2), pp. 305-317.
- Ju, F., and Mimovich, M. (1986). "Modal Frequency Method in Diagnosis of Fracture Damage in Structures." Proceedings, *4th International Modal Analysis Conference*, Vol. 2, pp. 1168-1174.
- Ju, F. (1988). "Experimental Diagnosis of Fracture Damage in Structures by the Modal Frequency Method." *Journal of Vibration, Acoustics, Stress, and Reliability in Design*, Vol. 110, October, pp. 456 - 463.
- Ju, F. (1993). "Structural Dynamic Theory in Health Monitoring." *Vibration, Shock, Damage, and Identification of Mechanical Systems*, ASME, Vol. 64, pp. 39-46.
- Kalman, R.E. (1960). "A New Approach to Linear Filtering and Prediction Problems." *Journal of Basic Engineering*, March, pp. 35-46.
- Kim, J.T., and Stubbs, N. (1995). "Model-Uncertainty Impact and Damage-Detection Accuracy in Plate Girder." *Journal of Structural Engineering*, ASCE, October, pp. 1409-1417.

Kim, S., and Nowak, A. (1998). "Load Distribution and Impact Factors for I-Girder Bridges," *Journal of Bridge Engineering*, ASCE, Vol. 2, No. 3, August, pp. 97-104.

Kolmogorov, A.N. (1941). "Interpolation and Extrapolation von Stationaren Zufalligen Fogen." *Bulletin of the Academy of Science, USSR, Ser. Math* 5, pp. 3-14.

Kolousek, V. (1973). *Dynamics in Engineering Structures*. Butterworth & Co., London, England.

Kosko, B. (1992). *Neural Networks for Signal Processing*. Prentice-Hall, New Jersey.

Lenett, M., Catbas, N., Hunt, V., Aktan, A., Helmicki, A., and Brown, D. (1997). "Issues in Multi-Reference Impact Testing of Steel-Stringer Bridges." Proceedings, *15th International Modal Analysis Conference*.

Lenett, M. (1998). *Global Condition Assessment Using Modal Analysis and Flexibility*. Doctoral Dissertation, Department of Civil and Environmental Engineering, University of Cincinnati, Cincinnati, OH.

Lenett, M., Hunt, V., Helmicki, A., Catbas, F., and Aktan, A.E. (1999a). "Condition Assessment of a Decommissioned Bridge Using Nondestructive Experimental Methods." Proceedings, *Society of Experimental Mechanics Annual Conference*, Cincinnati, OH, June.

Lenett, M., Helmicki, A., Hunt, V., and Aktan, A.E. (1999b). "Condition Assessment and Damage Identification of a Steel Stringer Bridge using System Identification Methods." Proceedings, *1999 American Control Conference*, San Diego, CA, June.

Lenett, M., Catbas, N., Hunt, V., Aktan, A.E., Helmicki, A., and Brown, D. (1999c). "Condition Assessment of Commissioned Infrastructure Using Modal Analysis and Flexibility." Proceedings, *17th International Modal Analysis Conference*, Kissimmee, FL, February.

Lenett, M., Griessmann, A., Helmicki, A.J., and Aktan, A.E. (1999d). "Subjective and Objective Evaluations of Bridge Damage," *Transportation Research Record*, No. 1688, TRB, National Research Council, Washington, D.C., pp. 76-86.

Lenett, M., Hunt, V., Helmicki, A., and Aktan, A. (2000a). "Instrumentation, Testing and Monitoring of a Newly Constructed Reinforced Concrete Deck-On-Steel Girder Bridge - FHWA Project Report." *Report UC-CII-00*, University of Cincinnati, Infrastructure Institute, Cincinnati, OH.

Lenett, M.S., Hunt, V.J., Helmicki, A.J., and Turer, A. (2000b) "Health-Monitoring of the Ironton-Russell Truss Bridge." Proceedings, *Condition Monitoring and Diagnostic Engineering Management (COMADEM)* Conference, Houston, TX, December.

- Lenett, M.S., Helmicki, A.J., and Hunt, V. (2000c) "Multi-Reference Impact Testing of FRP Bridge Deck Material." Proceedings, *18th International Modal Analysis Conference*, San Antonio, TX, February.
- Lenett, M.S., Brown, D.L., Hunt, V., and Helmicki, A.J. (2000d) "Performing Bridge Condition Assessment With Spliced Multi-Reference Impact Data." Proceedings, *18th International Modal Analysis Conference*, San Antonio, TX, February.
- Lenett, M., Hunt, V.J., Helmicki, A.J., and Turer, A. (2001). "Health-Monitoring of the Ironton-Russell Bridge for Rating Purposes." Proceedings, *Transportation Research Board*, Washington, D.C., January.
- Levi, A., Hunt, V., Helmicki, A., and Aktan, A. (1996). "Instrumentation, Testing and Monitoring of Reinforced Concrete Deck-On-Steel Girder Bridges - FHWA Project Report." *Report UC-CII-96*, University of Cincinnati, Infrastructure Institute, Cincinnati, OH.
- Levi, A., Hunt, V., Helmicki, A., and Aktan, A. (1997). "Instrumented Monitoring and Diagnostic Load Testing of Steel Stringer Bridges." Proceedings, *15th International Modal Analysis Conference*.
- Levi, A. (1997). *Instrumented Monitoring & Diagnostic Load Testing For Condition Assessment And Evaluation Of Bridges*. Doctoral Dissertation, Department of Civil and Environmental Engineering, University of Cincinnati, Cincinnati, OH.
- Levis, A.H. (1987). "Challenges to Control: A Collective View." *IEEE Transactions on Automatic Control*, Vol. AC-32, No. 4, April.
- Li, D., Zhung, H., and Wang, B. (1989). "The Principle and Technique of Experimental Strain Modal Analysis." Proceedings, *7th International Modal Analysis Conference*, pp.1285-1289.
- Lichtenstein, A.G. (1992). "Bridge Rating Through Nondestructive Load Test." *Proposed Manual for Bridge Rating through Load Testing*, NCHRP 12-28(13)A, August.
- Lichtenstein, A.G. (1998). "Manual for Bridge Rating through Load Testing," *NCHRP Research Results Digest*, No. 234, Transportation Research Board, National Research Council, Washington, D.C., November.
- Lieven, N.A.J., and Ewins, D.J. (1988). "Spatial Correlation of Mode Shapes, The Coordinate Mode Assurance Criterion (COMAC)." Proceedings, *6th International Modal Analysis Conference*, pp. 690-695.
- Lim, T.W. (1991). "Structural Damage Detection Using Modal Test Data." *AIAA Journal*, 29(12), pp. 2271-2274.

- Loland, O., and Dodds, J.C. (1977). "Experience in Developing and Operating Integrity Monitoring System in North Sea." Proceedings, *8th Annual Offshore Technology Conference*, Vol. 2, pp. 313-319.
- Massicotte, B., Picard, A. (1994). "Monitoring of a Prestressed Segmental Box Girder Bridge During Strengthening." *Prestressed Concrete Institute Journal*, Volume 39, No. 3, pp. 66-80, May-June.
- Matejka, R. (1988). *A Real-Time Environment for Qualitative Process Control*. Master's Thesis, Electrical and Computer Engineering, University of Cincinnati, Cincinnati, OH, June.
- Mayes, R.L. (1992). "Error Localization Using Mode Shapes." Proceedings, *10th International Modal Analysis Conference*, San Diego, CA.
- Mayes, R.L. (1995). "An Experimental Algorithm for Detecting Damage Applied to the I-40 Bridge Over the Rio Grande." Proceedings, *13th International Modal Analysis Conference*, Nashville, Tennessee, pp. 219-225.
- Mazars, J. (1986). "A Model of Unilateral Elastic Damageable Material and its Application to Concrete." Proceedings, *Fracture Toughness and Fracture Energy of Concrete*, F.H. Wittmann, ed. Elsevier, New York, NY, pp. 61-71.
- Mazurek, D., and DeWolf, J. (1990). "Experimental Study of Bridge Monitoring Technique." *Journal of Structural Engineering*, ASCE, Vol. 116, No. 9, pp. 2532-2549, September.
- McGillem, C., and Cooper, G. (1984). *Continuous and Discrete Signal and System Analysis*. CBS College Publishing, New York, NY.
- Meneghetti, U., and Maggiore, A. (1993). "Crack Detection By Sensitivity Analysis." Proceedings, *12th International Modal Analysis Conference*, pp. 1292-1298.
- Moses, F. (1979). "Weigh-In-Motion System Using Instrumented Bridges," *Transportation Engineering Journal*, ASCE, Vol. 105, No. 3, May.
- Moses, F., Ghosn, M., and Snyder, R. (1984). "Application of Load Spectra to Bridge Rating." *Transportation Research Record*, No. 950, Vol. 1, pp. 45-53, Transportation Research Board, National Research Council, Washington, D.C., September.
- Moses, F., Schilling, C.G., and Raju, K.S. (1987a). "Fatigue Evaluation Procedures for Steel Bridges," *NCHRP Report*, No. 299, Transportation Research Board, National Research Council, Washington, D.C.
- Moses, F., and Verma, D. (1987b). "Load Capacity Evaluation of Existing Bridges," *NCHRP Report*, No. 301, Transportation Research Board, National Research Council, Washington, D.C.

Moses, F., Lebet, J.P., and Bez, R. (1994). "Applications of Field Testing to Bridge Evaluation." *Journal of Structural Engineering*, ASCE, Vol. 120, No. 6, June.

National Council on Public Works Improvement (1988). *Fragile foundations: America's public works*, Final report to the President and Congress, Washington, D.C.

Natke, H., Tomlinson, G., and Yao, J.T.P. (1993). *Safety Evaluation Based On Identification Approaches Related to Time-Variant and Nonlinear Structures*. Vieweg and Sohn Verlagsgesellschaft, Germany.

Newmark, N.M. (1959). "A Method of Computation for Structural Dynamics," *Journal of Engineering Mechanics*, ASCE, Vol. 85, No. 3, pp. 67-94.

Newmark, N.M., and Rosenblueth, E. (1971). *Fundamentals of Earthquake Engineering*, Prentice-Hall, New Jersey.

Nowak, A., and Tharmabala, T. (1988). "Bridge Reliability Evaluation Using Load Tests." *Journal of Structural Engineering*, ASCE, Vol. 114, No. 10, October.

Nowak, A. (1990). *Bridge Evaluation, Repair, and Rehabilitation*. Kluwer Academic Publishers, Netherlands.

Nowak, A., and Hong, Y.-K. (1991a). "Bridge Live Load Models," *Journal of Structural Engineering*, ASCE, Vol. 117, No. 9.

Nowak, A., Hong, Y.-K., and Hwang, E.-S. (1991b). "Modeling Live Load and Dynamic Load," *Transportation Research Record*, No. 1290, TRB, National Research Council, Washington, D.C., pp. 110-118.

Nowak, A., Nassif, H., and Frank, K. (1993). "Fatigue Load Spectra for Steel Girder Bridge." *Transportation Research Record*, No. 1072, TRB, National Research Council, Washington, D.C.

Nowak, A., Laman, J., and Nassif, H. (1994). "Effect of Truck Loading on Bridges," *Research Report UMCE 94-22*, Department of Civil and Environmental Engineering, University of Michigan, Ann Arbor, MI.

NSF, National Science Foundation (1992). *Civil Infrastructure Systems Research*. Report of the Civil Infrastructure Systems (CIS) Workshop, CIS Task Committee, April 15.

NSF, National Science Foundation (1993). *Civil Infrastructure Systems Research: Strategic Issues*, Report of the Civil Infrastructure Systems (CIS) Task Group, National Science Foundation.

NSF, National Science Foundation (1996). *Proceedings, 3<sup>rd</sup> Conference on Nondestructive Evaluation of Civil Structures and Materials*, Boulder, CO, co-editors Schuller, M., Woodham, D.

Office of Technology Assessment (1991). "Delivering The Goods: Public Works Technologies, Management, And Finance." *Report OTA-SET-477*, U.S. Congress, Washington, D.C.

Osegueda, R.A., Dsouza, P.D., and Qiang, Y. (1992). "Damage Evaluation of Offshore Structures Using Resonant Frequency Shifts." *Serviceability of Petroleum, Process, and Power Equipment*, ASME, PVP-Vol. 239, MPC-Vol. 33, pp. 31-37.

Pandey, A.K., Biswas, M., and Samman, M.M. (1991). "Damage Location From Changes in Curvature Mode Shape." *Journal of Sound and Vibration*, Vol.145(2), pp. 321-332.

Pape, D.A. (1993). "A Modal Analysis Approach to Flaw Detection in Ceramic Insulators." *Proceedings, 11th International Modal Analysis Conference*, pp. 35-40.

Papoulis, A. (1984). *Probability, Random Variables, and Stochastic Processes*. McGraw-Hill, New York, NY.

Pasco, T.J. (1993). *A Monitored System of Bridges: Random Thoughts*. Director, Office of Advanced Research, Federal Highway Administration.

Patent #08/131,536 (1995). *A Hierarchical Control System for Molecular Beam Epitaxy*, Sponsor: Manufacturing Research Group, Materials Laboratory, WPAFB (1988-1993).

Peebles, P. (1987). *Probability, Random Variables, and Random Signal Principles*. 2nd Ed., McGraw-Hill, New York, NY.

Peng, S. (1984). "A Pragmatic Approach in Rating Highway Bridges." *Transportation Research Record*, No. 950, Vol. 1, pp. 53-59, Transportation Research Board, National Research Council, Washington, D.C., September.

Penny, J.E.T., Wilson, D.A.L., and Friswell, M.I. (1993). "Damage Location in Structures Using Vibration Data." *Proceedings, 11th International Modal Analysis Conference*, pp. 861-867.

Peterson, W.S., and Kostem, C.N. (1973). "Dynamic Analysis of Beam-Slab Highway Bridges," *Highway Research Record*, No. 428, pp. 57-63.

Pinjarkar, S.G., Guedelhoefer, O.C., Smith, B.J., and Kritzler, R.W. (1990). "Nondestructive Load Testing For Bridge Evaluation And Rating." *NCHRP Report No. 12-28(13)*, Transportation Research Board, TRB, National Research Council, Washington, D.C., February.

PONTIS (1993). "A Network Optimization System for Bridge Improvements and Maintenance." *Publication FHWA-SA-93-083, Version 2.0, User's Manual*, U.S. Department of Transportation, Federal Highway Administration, Washington, D.C.

Poor, V. (1988). *An Introduction to Signal Detection and Estimation*, Springer-Verlag, New York, NY.

- Pugachev, V.S. (1965). *Theory of Random Functions and Its Application to Control Problems*. Addison-Wesley Publishing Company, Reading, Massachusetts.
- Qian, L., Gu, S.N., and Jiang, J.S. (1990). "The Dynamic Behavior and Crack Detection of a Beam with a Crack." *Journal of Sound and Vibration*, Vol.138(2), pp. 233-243.
- Raemer, H.R. (1969). *Statistical Communications Theory and Applications*. Prentice-Hall, Englewood Cliffs, NJ.
- Raghavendrachar, M., and Aktan, A.E. (1992). "Flexibility By Multireference Impact Testing For Bridge Diagnostics." *Journal of Structural Engineering*, ASCE, 118(8), August, pp. 2186-2203.
- Rayleigh, J.W.S. (1894). *The Theory of Sound*, Dover, New York.
- Rice, S.O. (1944). "Mathematical Analysis of Random Noise." *Bell System Technical Journal*, Volume 23, July.
- Reising, R.M.W., Shahrooz, B., Hunt, V.J., Lenett, M., et al. (2000). "Performance Of A Five-Span Steel Bridge With Fiber Reinforced Polymer Composite Deck Panels." Proceedings, Transportation Research Board, Washington, D.C., January.
- Rossow, E. (1996). *Analysis and Behavior of Structures*. Prentice-Hall, Upper Saddle River, NJ.
- Rubin, S., and Coppolino, R. (1983). *Flexibility Monitoring Evaluation Study*, Minerals Management Service, U.S. Department of the Interior, Washington, D.C.
- Salawu and Williams (1994). "Damage Location Using Vibration Mode Shape." Proceedings, *12th International Modal Analysis Conference*, pp. 933-939.
- Sanayei, M., and Saletnik, M. J. (1995). "Parameter Estimation of Structures from Static Strain Measurements; Part I, Formulation." *Journal of Structural Engineering*, ASCE, July.
- Saridis, G. (1979). "Toward the Realization of Intelligent Controls", *Proceedings of the IEEE*, Vol. 67, No. 8, August.
- Sartor, R.R., Culmo, M.P., and DeWolf, J.T. (1999). "Short-Term Strain Monitoring of Bridge Structures," *Journal of Bridge Engineering*, ASCE, Vol. 4, No. 3, August, pp. 157-164.
- Schulz, J., Commander, B., Goble, G., and Frangopol, D. (1995). "Efficient Field Testing and Load Rating of Short and Medium Span Bridges," *Structural Engineering Review*, Vol. 7, No. 3, Pergamon Press, Elsevier Science Ltd., Great Britain, pp. 181-194.

Schwartz, M. (1959). *Information Transmission, Modulation, and Noise*. 1st Ed., McGraw-Hill, New York, NY.

Schwartz, M., and Shaw, L. (1975). *Signal Processing: Discrete Spectral Analysis, Detection, and Estimation*. McGraw-Hill, New York, NY.

Shannon, C., and Weaver, W. (1949). *The Mathematical Theory of Communication*. University of Illinois Press, Urbana, Illinois.

Shickert, G., and Wiggerhauser, H. (1995). *International Symposium on Non-Destructive Testing in Civil Engineering (NDT-CE)*, Berlin, Germany, September.

Shinozuka, M., and Ghanem, R. (1995). "Structural-System Identification: Experimental Verification." *Journal of Engineering Mechanics*, ASCE, Vol. 121, No. 2, pp. 265-273, February.

Slater, G.L., and Shelley, S.J. (1993). "Health Monitoring of Flexible Structures Using Modal Filter Concepts." *Smart Structures and Intelligent Systems*, SPIE, Vol. 1917, pp. 997-1007.

Snyder, R., and Moses, F. (1985). "Application of In-Motion Weighing Using Instrumented Bridges," *Transportation Research Record*, No. 1048, TRB, National Research Council, Washington, D.C.

Soliman, M., and Kennedy, J. (1986). "Simplified Method for Estimating Thermal Stresses in Composite Bridges," *Transportation Research Record*, No. 1072., TRB, National Research Council, Washington, D.C., pp. 23-31.

Somaprasad, H. R., Toksoy, T., Yoshikiyuki, H. and Aktan, A. E. (1991). "Closed-loop Modal Testing of a 27-Story Reinforced Concrete Flat-Core Building." *Technical Report NCEER-91-0016*, Department of Civil and Environmental Engineering, University of Cincinnati, Ohio, July.

Stubbs, N. (1985). "A General Theory of Non-Destructive Damage Detection in Structures." *Proceedings, 2nd International Symposium on Structural Control*, University of Waterloo, July.

Stubbs, N., and Oseguada, R.A. (1990). "Global Non-Destructive Damage Evaluation in Solids." *The International Journal of Analytical and Experimental Modal Analysis*, Vol 5, No. 2, pp. 67-97.

Stubbs, N., Kim, J.T., and Farrar, C.R. (1995). "Field Verification of a Nondestructive Damage Localization and Severity Estimation Algorithm." *Proceedings, 13th International Modal Analysis Conference*, Nashville, Tennessee, pp. 210-218.

Toksoy, T., and Aktan, A.E. (1993). "Bridge Condition Assessment By Modal Flexibility." *Proceedings, International Conference on Nondestructive Testing on Concrete in the Infrastructure*, Dearborn, Michigan, Society for Experimental Mechanics, June, pp. 21-39.

Tsou, P. and Shen, M.-H. (1993). "Structural Damage Detection and Identification Using Neural Networks." *AIAA Journal*, Volume 32, Number 1, pp. 176-183.

Turer, A. (1997). *Stresses And Damage Predictions Of Steel Stringer Bridges Using Finite Element Modeling Techniques And Unit Influence Line Decomposition Method*. Masters Thesis, Department of Civil and Environmental Engineering, University of Cincinnati, Cincinnati, OH.

Turer, A., and Aktan, A.E. (1999). "Issues in Superload Crossing of Three Steel-Stringer Bridges in Toledo, Ohio," *Transportation Research Record*, No. 1688, TRB, National Research Council, Washington, D.C., pp. 87-96.

Utku, S., Norris, C., and Wilbur, J. (1991). *Elementary Structural Analysis*. McGraw-Hill, New York, NY.

Valavanis, K. (1986). *A Mathematical Formulation for the Analytical Design of Intelligent Machines*. Doctoral Dissertation, Department of Computer and Systems Engineering, Rensselaer Polytechnic Institute, Troy, NY, October.

Van Trees, H. (1986). *Detection, Estimation, and Modulation Theory*. John Wiley & Sons, New York, NY.

Vandiver, J.K. (1975). "Detection of Structural Failure on Fixed Platforms by Measurement of Dynamic Response." Proceedings, *7th Annual Offshore Technology Conference*, Vol. 2, pp. 243-252.

Vandiver, J.K. (1977). "Detection of Structural Failure on Fixed Platforms by Measurement of Dynamic Response." *Journal of Petroleum Technology*, pp. 305-310.

Walker, B. (1994a). "Evaluating Performance and Reliability of Automatically Reconfigurable Aerospace Systems Using Markov Modeling Techniques." *Journal of NATO ASI Series F Computer And Systems Sciences*, Volume 120, Springer-Verlag, New York, NY, pp. 101-126.

Walker, B., and Huang, K.-Y. (1994b). "FDI by Extended Kalman Filter Parameter Estimation for the Industrial Actuator Benchmark." IFAC Proceedings, 2nd Symposium On Fault Detection, Supervision And Safety For Technical Processes, Volume 2, Espoo, Finland, pp. 507-513.

Walker, B., et al. *Fault-Tolerant Control Systems*. Department of Aerospace Engineering, University of Cincinnati, Cincinnati, OH, to be published.

Walpole, R., and Myers, R. (1985). *Probability and Statistics for Engineers and Scientists*. MacMillan Publishing, New York, NY.

Warren, G.E., and Malvar, L.J. (1994). "Structural Assessment of Reinforced Concrete Piers Using The Impact Load Method" *Journal of Experimental Techniques*, Vol. 18, No.3, pp.15-21.

- Warren, G.E., and Malvar, L.J. (1995). "Evaluation of Permanent Monitoring Sensors on Navy Piers." Proceedings, *ASCE Structures Congress XIII*, Boston, MA., pp. 28-43.
- Weber, C. (1987). *Elements of Detection and Signal Design*. Springer-Verlag, New York, NY.
- Wiener, N. (1949). *The Extrapolation, Interpolation, and Smoothing of Stationary Time Series*. John Wiley & Sons, Inc., New York.
- Wiener, N. (1961). *Cybernetics*. M.I.T. Press, Cambridge, MA.
- Whalen, A. (1971). *Detection of Signals in Noise*. Academic Press, New York, NY.
- Woodward, P.M. (1953). *Probability and Information Theory With Applications to Radar*. Pergamon, London.
- Worden, K., Ball, A. and Tomlinson, G. (1993). "Neural Networks for Fault Location." Proceedings, *11th International Modal Analysis Conference*, pp. 47-54.
- Yuen, M.F. (1985). "A Numerical Study of the Eigenparameters of a Damaged Cantilever." *Journal of Sound and Vibration*, Vol.103(3), pp. 301-310.
- Yao, G.C., Chang, K.C., and Lee, G.C. (1992). "Damage Diagnosis of Steel Frames Using Vibrational Signature Analysis" *Journal of Engineering Mechanics*, ASCE, 118(9), pp. 1949-1961.
- Yao, J.T.P. (1985). *Safety and Reliability of Existing Structures*. Pitman Publishing Company, Boston, MA.
- Yao, J.T.P. (1996). "Risk Possibility and Probability of Civil Systems." *Workshop on Uncertainty: Models and Measures*, Lambrecht/Pfalz, Germany, July.
- Zhang, Z. (1993). "Error Study of Bridge Test." *12th International Modal Analysis Conference*, Hawaii.
- Zhang, Z., and Aktan, A.E. (1995). "Modal Test Based Damage Indices For Constructed Facilities." Proceedings, *13th International Modal Analysis Conference*, Nashville, Tennessee.
- Zhong, E. (1999). *Internet Based Remote Bridge Health Monitoring Real-Time Data Communication and Graphical User Interface Design*, Master's Thesis, Department of Electrical and Computer Engineering and Computer Science, University of Cincinnati, Cincinnati, OH.
- Zimmerman, H.J. (1992). *Fuzzy Set Theory and its Applications*. 2nd ed., Kluwer Academic Publishers, Boston.
- Zwick, M., Toksoy, T., and Aktan, A.E. (1992). "Nondestructive Evaluation And Destructive Testing Of A Highway Bridge." *Paper # IBC 92-8, International Bridge Conference*, Pittsburgh.

## APPENDIX A1

Elastic Deformation of the Middle of a Single Span Beam under Crawl Truckload

## Elastic Deformation of a Single Span Beam under Static Equilibrium

We assume a stationary point load  $w(x) = P\delta(x-a)$ .  
 Supports are located at  $x = \{0, L1\}$ .

Note that the moment  $M(x)$ , slope  $\theta(x)$ , and deflection  $y(x)$  equations below remain to be scaled by the modulus of elasticity  $E$  and the beam inertia  $I$ , which are considered uniform for the beam.

$$M_0(x) := C_1 \cdot x$$

$\# = 0$ , indicates  $0 < x < a$

$$M_1(x) := C_1 \cdot x - P \cdot (x - a)$$

$\# = 1$ , indicates  $a < x < L1$

$$\theta_0(x) := \frac{1}{2} \cdot C_1 \cdot x^2 + C_2$$

$$\theta(x) = \int M(x) \, dx$$

$$\theta_1(x) := \frac{1}{2} \cdot C_1 \cdot x^2 - P \cdot \left( \frac{1}{2} \cdot x^2 - a \cdot x \right) + C_2$$

$$y_0(x) := \frac{1}{6} \cdot C_1 \cdot x^3 + C_2 \cdot x + C_3$$

$$y(x) = \int \theta(x) \, dx$$

$$y_1(x) := \frac{1}{6} \cdot C_1 \cdot x^3 - P \cdot \left( \frac{1}{6} \cdot x^3 - \frac{1}{2} \cdot a \cdot x^2 \right) + C_2 \cdot x + C_3$$

given

$$M_0(0) = 0$$

$$M_0(a) = M_1(a)$$

$$M_1(L1) = 0$$

$$\theta_0(a) = \theta_1(a)$$

$$y_0(0) = 0$$

$$y_0(a) = y_1(a)$$

$$y_1(L1) = 0$$

$$\text{find}(C_1, C_2, C_3, C_2, C_3) \rightarrow \begin{bmatrix} 1 - \frac{1}{55} \cdot a \\ \frac{1}{2} \cdot a^2 - \frac{55}{3} \cdot a - \frac{1}{330} \cdot a^3 \\ 0 \\ -\frac{55}{3} \cdot a - \frac{1}{330} \cdot a^3 \\ \frac{1}{6} \cdot a^3 \end{bmatrix}$$

$$M0(x, a) := -P \cdot \frac{(-L1 + a)}{L1} \cdot x \qquad L1 \equiv 55 \qquad L2 := 133 \qquad L3 := 188 \qquad P \equiv 1$$

$$M1(x, a) := -P \cdot \frac{(-L1 + a)}{L1} \cdot x - P \cdot (x - a)$$

$$y0(x, a) := \frac{1}{6} \left[ -P \cdot \frac{(-L1 + a)}{L1} \right] \cdot x^3 + \frac{-1}{6} \cdot P \cdot a \cdot \frac{(-3 \cdot a \cdot L1 + 2 \cdot L1^2 + a^2)}{L1} \cdot x$$

$$y1(x, a) := \frac{1}{6} \left[ -P \cdot \frac{(-L1 + a)}{L1} \right] \cdot x^3 - P \cdot \left( \frac{1}{6} \cdot x^3 - \frac{1}{2} \cdot a \cdot x^2 \right) + \frac{-1}{6} \cdot P \cdot a \cdot \frac{(2 \cdot L1^2 + a^2)}{L1} \cdot x + \frac{1}{6} \cdot P \cdot a^3$$

Note: If the solution is also solved for both a and P, all coefficients are simply multiplied by P.  
P is simply a scale multiple for the system solution.

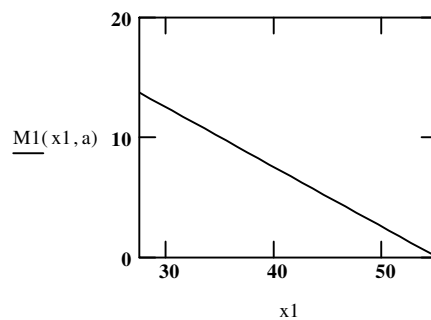
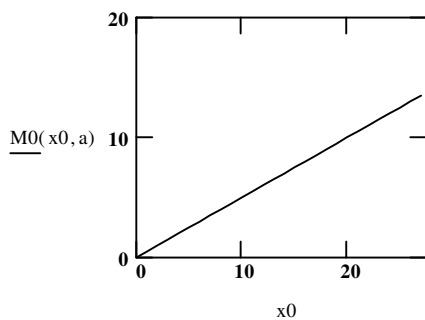
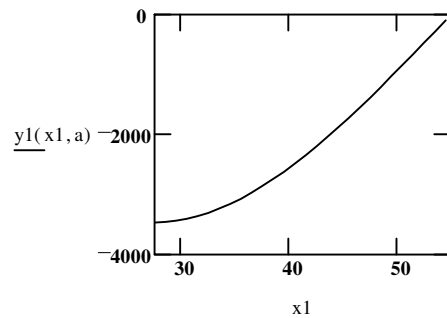
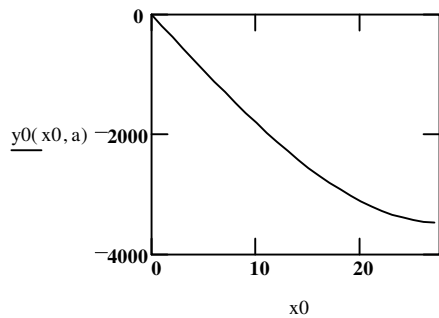
Solution for Cross-County Hwy, Reading Road Bridge (HAM-42-0992)  
(i.e., for the Instrumented Eastern Span)

$$L1 \equiv 55 \qquad L2 := 133 \qquad L3 := 188 \qquad P \equiv 1$$

$$a := 27.5 \quad a, \text{ Location of Unit Load}$$

$$x0 := 0.. a$$

$$x1 := a.. 55$$



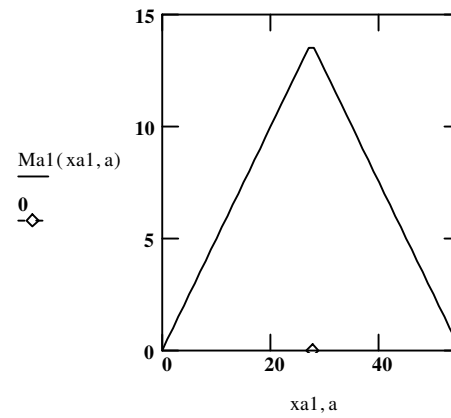
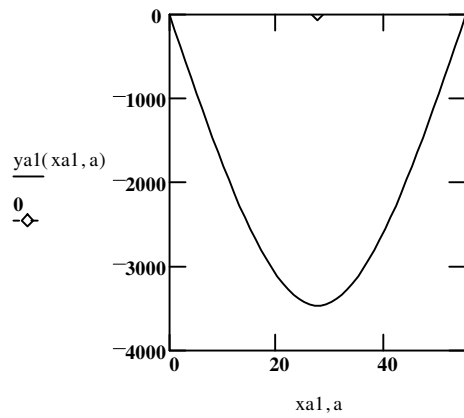
### Beam Response to Stationary Unit Load

$$y_{a1}(x, a) := \text{if}(x < 0, 0, \text{if}(x < a, y_0(x, a), \text{if}(x < L1, y_1(x, a), 0)))$$

$$M_{a1}(x, a) := \text{if}(x < 0, 0, \text{if}(x < a, M_0(x, a), \text{if}(x < L1, M_1(x, a), 0)))$$

$a = 27.5$     Location,  $a$ , of Stationary Unit Load

$x_{a1} := 0..L1$



Circle indicates support locations, Diamond indicates the Stationary Load

### Determination of the Unit Influence Line

(i.e., Beam Response at a Given Node to a Moving Unit Load)

$$y(x, a) := \text{if}(a < 0, 0, \text{if}(a < L1, yal(x, a), 0))$$

$$\psi(x) := \text{if}\left(x < 0, 0, \text{if}\left(x > L1, 0, \sin\left(\frac{\pi \cdot x}{L1}\right) \cdot y\left(\frac{L1}{2}, \frac{L1}{2}\right)\right)\right)$$

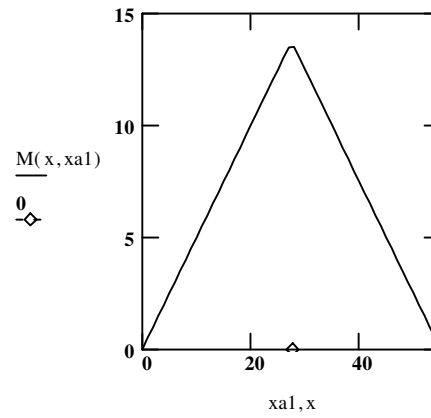
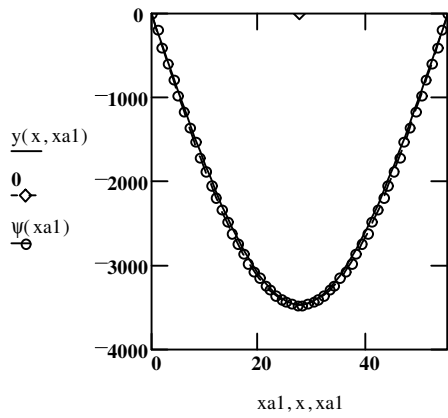
$$M(x, a) := \text{if}(a < 0, 0, \text{if}(a < L1, Mal(x, a), 0))$$

$\psi(x)$  is the first mode, scaled by the peak midspan deflection

$x = 27.5$

Location,  $x$ , of Bridge Sensor Node

Unit Influence Lines are determined by holding  $x$  constant and varying  $a$



Circle indicates support locations, Diamond indicates the Bridge Sensor Node

### Beam Response at a Given Node to a Moving Axle Load

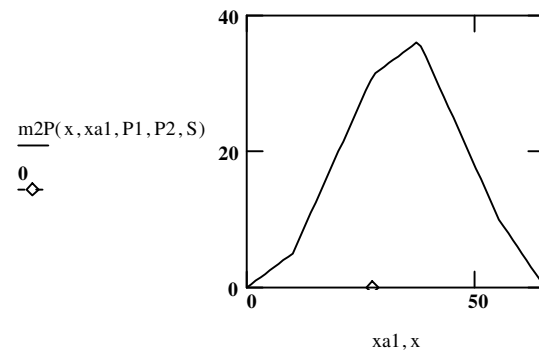
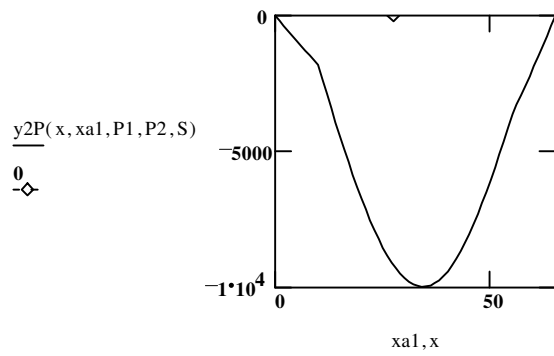
Here, we consider a single axle load P1 and velocity V.

$$y2P(x, a, P1, P2, S) := y(x, a) \cdot P1 + y(x, a - S) \cdot P2$$

$$m2P(x, a, P1, P2, S) := M(x, a) \cdot P1 + M(x, a - S) \cdot P2$$

P1 = 1      P2 = 2      S = 10      x = 27.5    Location, x, of Bridge Sensor Node

xa1 := 0..(L1 + S)·oversample



Circle indicates support locations, Diamond indicates the Bridge Sensor Node

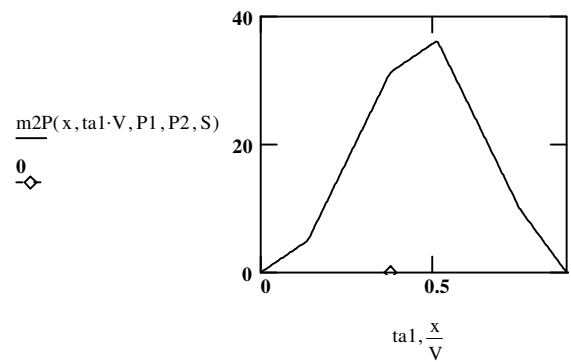
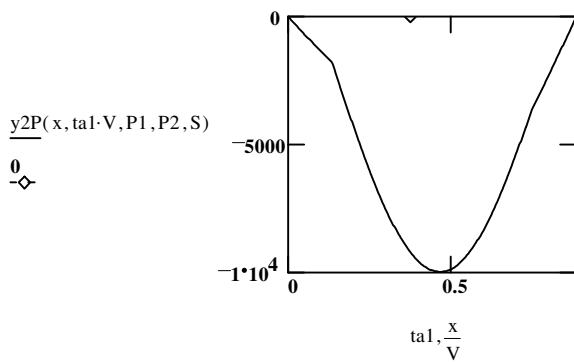
### Transform the Spatial System to the Time Domain

This assumes that the Monitoring System is sampling at a rate of SRate.

$$\text{SRate} := 500 \text{ Hz} \quad R := \frac{1}{\text{SRate}} \quad R = 2 \cdot 10^{-3} \text{ seconds}$$

$$\text{mph} = 50 \quad V := \text{mph} \cdot \frac{5280}{60 \cdot 60} \quad V = 73.333 \text{ feet/second} \quad f_y := \frac{V}{2 \cdot L1} \text{ loading frequency} \\ f_y = 0.667$$

$$\text{ta1} := 0, R \cdot \frac{(L1 + S) \cdot \text{oversample}}{V} \quad \frac{L1 + S}{V} = 0.886 \text{ seconds}$$



Circle indicates support locations, Diamond indicates the Bridge Sensor Node

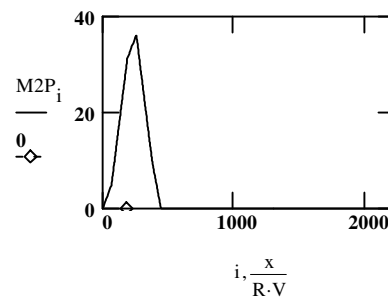
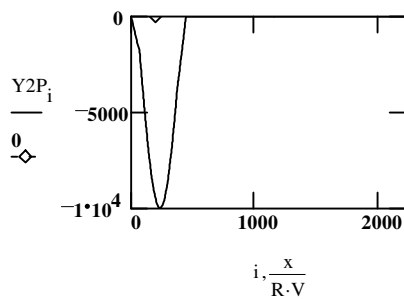
### Transform the Temporal System to the Frequency Domain

$$\text{Tct} := \frac{(L1 + S) \cdot \text{oversample}}{V \cdot R} \quad \text{Tct} = 2.216 \cdot 10^3 \quad \text{Total \# of data samples} \quad i := 0 \dots \text{Tct}$$

$$Y2P_i := y2P(x, i \cdot R \cdot V, P1, P2, S)$$

$$M2P_i := m2P(x, i \cdot R \cdot V, P1, P2, S)$$

Create temporal vectors for the evaluated functions above.



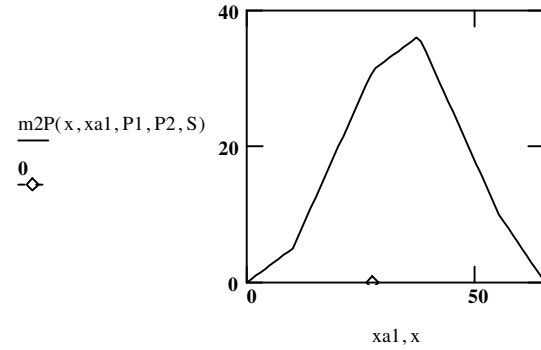
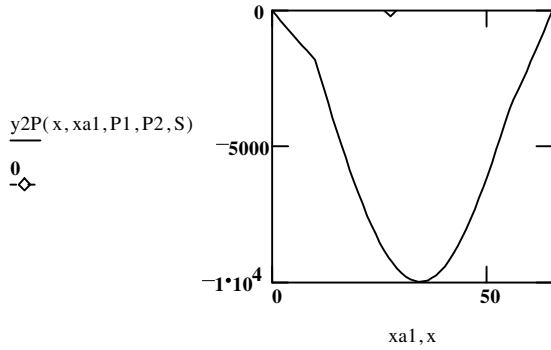
Circle indicates support locations, Diamond indicates the Bridge Sensor Node

Beam Response at a Given Node to a Moving Axle Load, w/ Oversampling

Here, we consider a single axle load P1 and velocity V.  
 P1=1 P2=2 S=10

mph=50 x=27.5 oversample=5

Location, x, of Bridge Sensor Node xa1 := 0..L1 + S



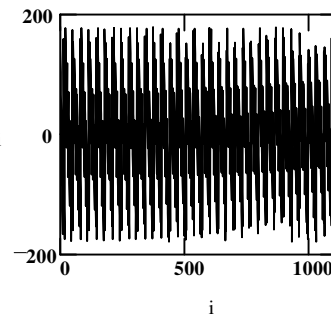
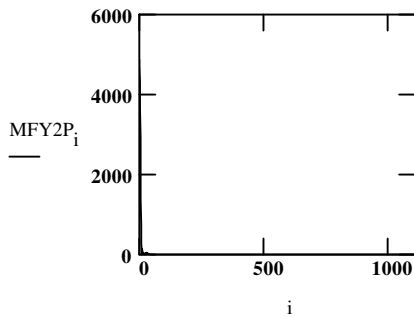
$$F_{max} := \frac{1}{2 \cdot R} \quad F_{max} = 250 \quad \text{FFT Bandwidth}$$

$$f := 0, \frac{1}{T_{ct} \cdot R} \dots F_{max} \quad f_{min} := \frac{1}{T_{ct} \cdot R} \quad \frac{1}{T_{ct} \cdot R} = 0.226$$

$$FY2P := CFFT(Y2P) \cdot T_{ct} \cdot R \quad fy2P(f) := FY2P_{f \cdot T_{ct} \cdot R}$$

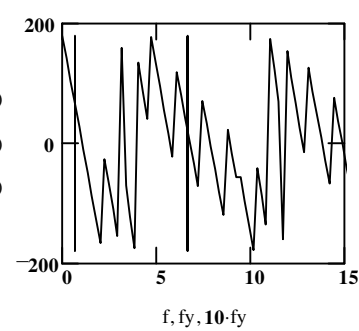
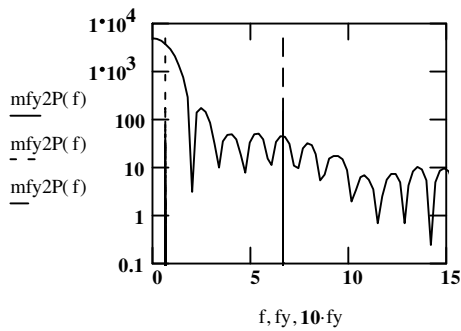
$$MFY2P := |FY2P| \quad \text{FFT Magnitude} \quad mfy2P(f) := MFY2P_{\text{floor}(f \cdot T_{ct} \cdot R)} \quad mfy2P(0) = 4.874 \cdot 10^3$$

$$PFY2P_i := \text{if}(FY2P_i = 0, 0, \arg(FY2P_i) \cdot \frac{180}{\pi}) \quad \text{FFT Phase Angle} \quad pfy2P(f) := PFY2P_{\text{floor}(f \cdot T_{ct} \cdot R)} \quad pfy2P(0) = 180$$



Plot according to the frequency axis for the system bandwidth, BW.

BW := 15 fy = 0.667



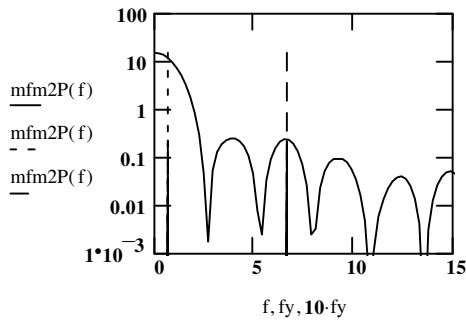
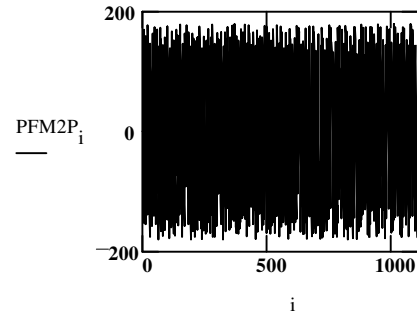
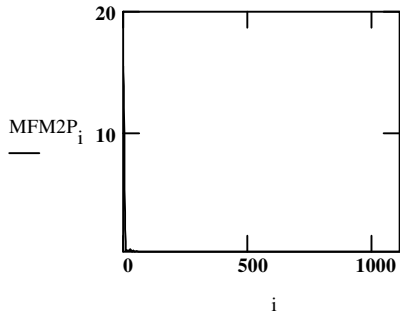
$$mfy2P(0) = 4.874 \cdot 10^3$$

$$pfy2P(0) = 180$$

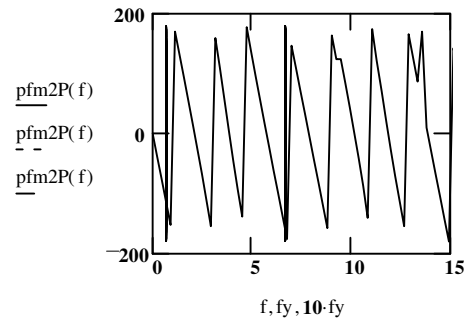
$$FM2P := CFFT(M2P) \cdot Tct \cdot R \quad fm2P(f) := FM2P_{f \cdot Tct \cdot R}$$

$$MFM2P := \overline{|FM2P|} \quad \text{FFT Magnitude} \quad mfm2P(f) := MFM2P_{\text{floor}(f \cdot Tct \cdot R)} \quad mfm2P\left(\frac{0}{Tct \cdot R}\right) = 15.468$$

$$PFM2P_i := \text{if}\left(FM2P_i = 0, 0, \arg(FM2P_i) \cdot \frac{180}{\pi}\right) \quad \text{FFT Phase Angle} \quad pfm2P(f) := PFM2P_{\text{floor}(f \cdot Tct \cdot R)} \quad pfm2P(0) = 0$$



$$mfm2P(0) = 15.468$$



$$pfm2P(0) = 0$$

Depending upon the gage location, certain modes become insignificant due to the structural symmetry.

$$\frac{mfy2P(10 \cdot fy)}{mfy2P(0)} = 9.347 \cdot 10^{-3} \quad \frac{mfm2P(10 \cdot fy)}{mfm2P(0)} = 0.016$$

Note that the magnitude for both signals is dramatically reduced at  $f = 10 \cdot fy = 10 \text{ V/L1}$ .  
 $fy = 0.667$

### Compare the Spectral System to the Ideal Fourier Transforms

Deflection is represented by the sum of two negative sinusoids of period  $2L1/V$  seconds.

One sinusoid is delayed by a half period in order to cancel out the first. Both are multiplied by the unit step.

One axle response in time domain:

$$\text{Simy}(t) := -1 \cdot \sin\left(\frac{\pi \cdot V \cdot t}{L1}\right) \cdot \Phi(t) - \sin\left[\frac{\pi \cdot V \cdot \left(t - \frac{L1}{V}\right)}{L1}\right] \cdot \Phi\left(t - \frac{L1}{V}\right) \quad \text{where } \Phi(t) = 1 \text{ for } t \geq 0 \text{ and } \Phi(t) = 0 \text{ for } t < 0$$

The second axle is represented by the same function, but delayed by  $S/V$  seconds.

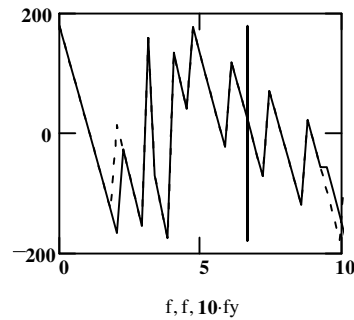
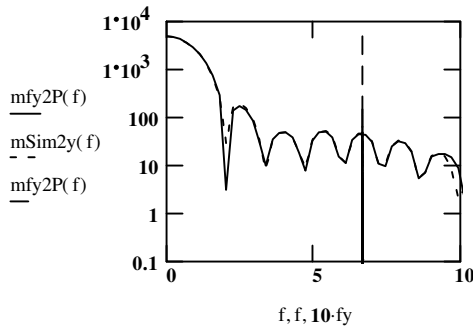
$$\text{Sim2y}(t) := \text{Simy}(t) \cdot P1 + \text{Simy}\left(t - \frac{S}{V}\right) \cdot P2$$

The MathCAD continuous Fourier transform for this ideal sinusoidal time representation for deflection is:

$$\text{Sim2y}(f) := \frac{-\text{mfy2P}(0)}{2 \cdot (P1 + P2) \cdot \left(1 - \frac{4 \cdot f^2 \cdot L1^2}{V^2}\right)} \cdot \left(1 + e^{-i \cdot 2 \cdot \pi \cdot L1 \cdot \frac{f}{V}}\right) \cdot \left(P1 + P2 \cdot e^{-i \cdot 2 \cdot \pi \cdot S \cdot \frac{f}{V}}\right)$$

where  $\text{mfy2P}(0)$  = DC magnitude for the MathCAD transform

$$\text{mSim2y}(f) := \left| \text{Sim2y}(f) \right| \quad \text{pSim2y}(f) := \text{if}\left(\text{Sim2y}(f) = 0, 0, \arg(\text{Sim2y}(f)) \cdot \frac{180}{\pi}\right) \quad \text{BW} := 10$$



The plots do not completely match because the time representation  $\text{fy2P}$  is not exactly sinusoidal.

Compare DC magnitude of continuous Fourier transform to the discrete frequency representation  $\text{mfy2P}(0)$ :

$$y0\left(\frac{L1}{2}, \frac{L1}{2}\right) \cdot \frac{L1 \cdot 2 \cdot (P1 + P2)}{\pi \cdot V} = -4.965 \cdot 10^3 \quad \text{mfy2P}(0) = 4.874 \cdot 10^3 \quad \text{pfy2P}(0) = 180$$

\* Note:  $Tct$  is used to adjust for MathCAD derivation and  $R$  is used to adjust the discrete Fourier transform

The continuous Fourier transform for this triangular time representation for deflection is as follows:

$$\text{Sim2y}(f) := y0\left(\frac{L1}{2}, \frac{L1}{2}\right) \cdot \frac{L1}{\pi \cdot V \cdot \left(1 - \frac{4 \cdot f^2 \cdot L1^2}{V^2}\right)} \cdot \left(1 + e^{-i \cdot 2 \cdot \pi \cdot L1 \cdot \frac{f}{V}}\right) \cdot \left(P1 + P2 \cdot e^{-i \cdot 2 \cdot \pi \cdot S \cdot \frac{f}{V}}\right)$$

where  $y0(L1/2, L1/2) = -L1^3/48EI$

Moment is represented by a triangular pulse of period  $L1/V$  seconds.  
The signal is delayed by a half period to account for causal behavior.

One axle response in time domain:

$$\Lambda(T, t) := \frac{T}{2} - |t|$$

$$\text{Simm}(t) := \Lambda\left(\frac{L1}{V}, t - \frac{L1}{2 \cdot V}\right)$$

where  $\Lambda(T, t) = T/2 - t$  for  $0 < t < T$  and  
 $\Lambda(T, t) = T/2 + t$  for  $-T < t < 0$  and  
 $\Lambda(T, t) = 0$  for  $t < -T$  and  $t > T$

The second axle is represented by the same function, but delayed by  $S/V$  seconds.

$$\text{Sim2m}(t) := \text{Simm}(t) \cdot P1 + \text{Simm}\left(t - \frac{S}{V}\right) \cdot P2$$

The MathCAD continuous Fourier transform for this triangular time representation for moment is as follows:

$$\text{Sim2m}(f) := \frac{\text{mfm2P}(0)}{(P1 + P2)} \cdot \left[ \frac{\sin\left(\pi \cdot L1 \cdot \frac{f}{2 \cdot V}\right)}{\left(\pi \cdot L1 \cdot \frac{f}{2 \cdot V}\right)} \right]^2 \cdot e^{-i \cdot \pi \cdot L1 \cdot \frac{f}{V}} \cdot \left( P1 + P2 \cdot e^{-i \cdot 2 \cdot \pi \cdot S \cdot \frac{f}{V}} \right)$$

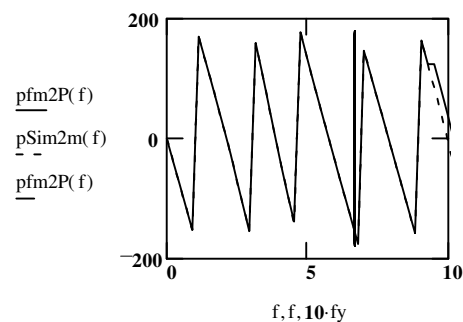
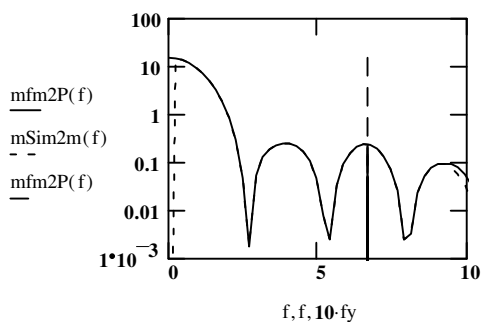
where  $\text{mfm2P}(0) = \text{DC magnitude for the MathCAD transform}^*$

$$\text{mSim2m}(f) := \text{if}\left(\text{Sim2m}(f) = 0, .000000001, \overline{|\text{Sim2m}(f)|}\right)$$

$$\text{mSim2m}(0) = 1 \cdot 10^{-9}$$

$$\text{pSim2m}(f) := \text{if}\left(\text{Sim2m}(f) = 0, 0, \arg(\text{Sim2m}(f)) \cdot \frac{180}{\pi}\right)$$

MathCAD does not evaluate the sinc function properly at  $f=0$ .



Compare DC magnitude of continuous Fourier transform to the discrete frequency representation  $\text{mfm2P}(0)$ :

$$M0\left(\frac{L1}{2}, \frac{L1}{2}\right) \cdot \frac{L1}{2 \cdot V} \cdot \frac{1}{2} \cdot (P1 + P2) = 15.469$$

$$\text{mfm2P}(0) = 15.468$$

$$\text{pfm2P}(0) = 0$$

\* Note: Tct is used to adjust for MathCAD derivation and R is used to adjust the discrete Fourier transform

The continuous Fourier transform for this triangular time representation for moment is as follows:

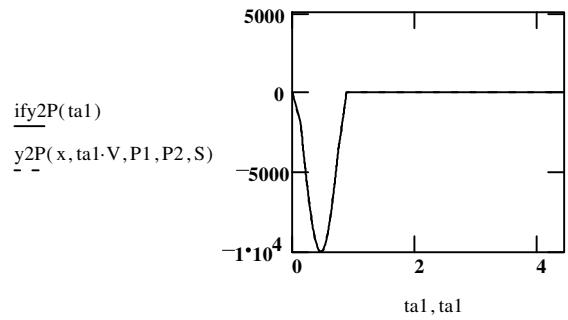
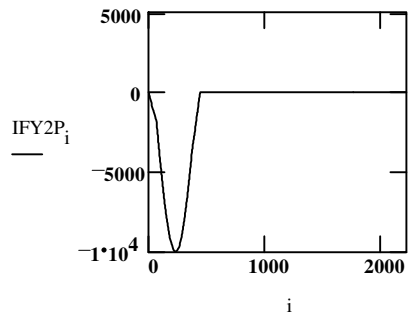
$$\text{Sim2m}(f) := M0\left(\frac{L1}{2}, \frac{L1}{2}\right) \cdot \frac{L1}{2 \cdot V} \cdot \left[ \frac{\sin\left(\pi \cdot L1 \cdot \frac{f}{2 \cdot V}\right)}{\left(\pi \cdot L1 \cdot \frac{f}{2 \cdot V}\right)} \right]^2 \cdot e^{-i \cdot \pi \cdot L1 \cdot \frac{f}{V}} \cdot \left( P1 + P2 \cdot e^{-i \cdot 2 \cdot \pi \cdot S \cdot \frac{f}{V}} \right)$$

where  $M0(L1/2, L1/2) = L1/4$

Transform the Spectral System back to the Time Domain

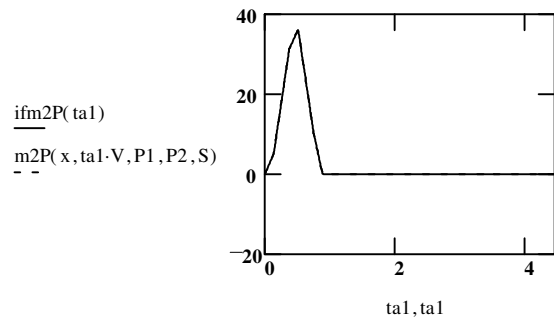
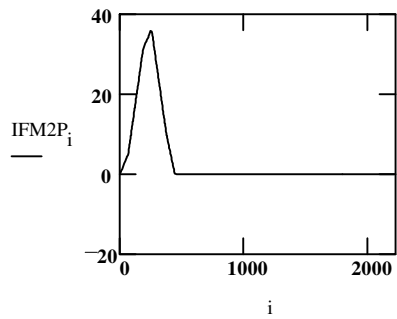
$$\text{IFY2P} := \text{ICFFT}\left(\frac{\text{FY2P}}{\text{Tct}\cdot\text{R}}\right)$$

$$\text{ify2P}(\text{ta1}) := \text{IFY2P}_{\text{floor}\left(\frac{\text{ta1}}{\text{R}}\right)}$$



$$\text{IFM2P} := \text{ICFFT}\left(\frac{\text{FM2P}}{\text{Tct}\cdot\text{R}}\right)$$

$$\text{ifm2P}(\text{ta1}) := \text{IFM2P}_{\text{floor}\left(\frac{\text{ta1}}{\text{R}}\right)}$$



Transform the Spectral System back to the Time Domain  
with a Low-Pass Dynamic Filter

Here, we apply an ideal low-pass filter at a cut-off frequency of  $F_{co}$ .  
The mean squared error, MSE, of the filtered signal compared to the original signal is plotted.

$$F_{co} := 10 \cdot f_y \text{ Hz} \quad F_i := \text{floor}(F_{co} \cdot T_{ct} \cdot R) \quad F_i = 29 \quad \text{vectorial index of } F_{co} \quad T_{ct} - F_i = 2.187 \cdot 10^3$$

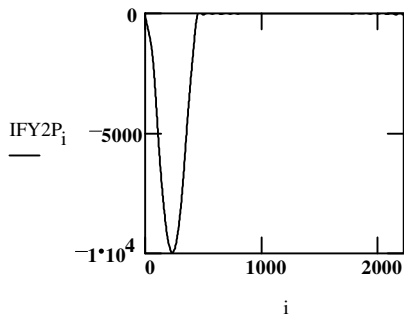
$$f_i := F_i + 1, F_i + 2 \dots T_{ct} - F_i \quad F_{co} = 6.667$$

$$FY2P_{f_i} := 0 \quad IFY2P := \text{ICFFT} \left( \frac{FY2P}{T_{ct} \cdot R} \right)$$

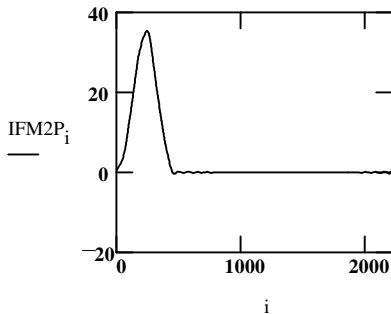
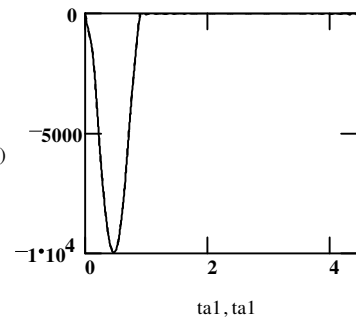
$$\text{ify2P}(ta1) := IFY2P_{\text{floor} \left( \frac{ta1}{R} \right)}$$

$$FM2P_{f_i} := 0 \quad IFM2P := \text{ICFFT} \left( \frac{FM2P}{T_{ct} \cdot R} \right)$$

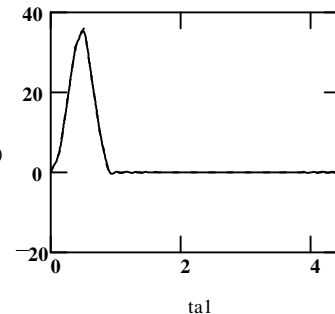
$$\text{ifm2P}(ta1) := IFM2P_{\text{floor} \left( \frac{ta1}{R} \right)}$$



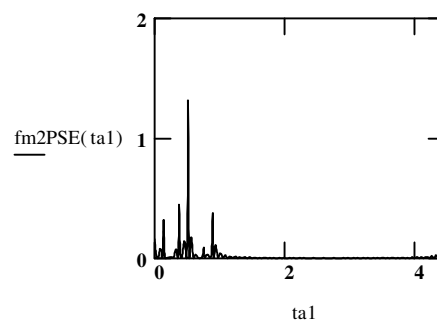
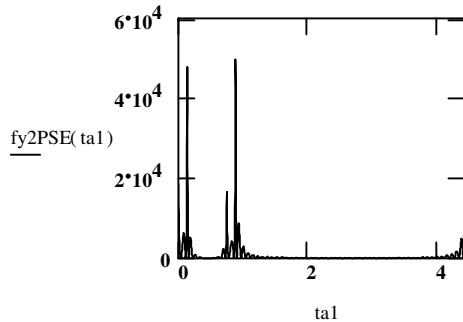
$$\frac{\text{ify2P}(ta1)}{y2P(x, ta1 \cdot V, P1, P2, S)}$$



$$\frac{\text{ifm2P}(ta1)}{m2P(x, ta1 \cdot V, P1, P2, S)}$$



$$fy2PSE(ta1) := (y2P(x, ta1 \cdot V, P1, P2, S) - \text{ify2P}(ta1))^2 \quad fm2PSE(ta1) := (m2P(x, ta1 \cdot V, P1, P2, S) - \text{ifm2P}(ta1))^2$$



$$fy2PMSE := \sum_{ta1} \frac{fy2PSE(ta1)}{T_{ct}} \quad fy2PMSE = 839.324$$

$$fm2PMSE := \sum_{ta1} \frac{fm2PSE(ta1)}{T_{ct}} \quad fm2PMSE = 0.018$$

## APPENDIX A2

### Elastic Deformation of the Quadrant of a Single Span Beam under Crawl Truckload

## Elastic Deformation of a Single Span Beam under Static Equilibrium

We assume a stationary point load  $w(x) = P\delta(x-a)$ .  
 Supports are located at  $x = \{0, L1\}$ .

Note that the moment  $M(x)$ , slope  $\theta(x)$ , and deflection  $y(x)$  equations below remain to be scaled by the modulus of elasticity  $E$  and the beam inertia  $I$ , which are considered uniform for the beam.

$$M_0(x) := C_1 \cdot x$$

$\# = 0$ , indicates  $0 < x < a$

$$M_1(x) := C_1 \cdot x - P \cdot (x - a)$$

$\# = 1$ , indicates  $a < x < L1$

$$\theta_0(x) := \frac{1}{2} \cdot C_1 \cdot x^2 + C_2$$

$$\theta(x) = \int M(x) \, dx$$

$$\theta_1(x) := \frac{1}{2} \cdot C_1 \cdot x^2 - P \cdot \left( \frac{1}{2} \cdot x^2 - a \cdot x \right) + C_2$$

$$y_0(x) := \frac{1}{6} \cdot C_1 \cdot x^3 + C_2 \cdot x + C_3$$

$$y(x) = \int \theta(x) \, dx$$

$$y_1(x) := \frac{1}{6} \cdot C_1 \cdot x^3 - P \cdot \left( \frac{1}{6} \cdot x^3 - \frac{1}{2} \cdot a \cdot x^2 \right) + C_2 \cdot x + C_3$$

given

$$M_0(0) = 0$$

$$M_0(a) = M_1(a)$$

$$M_1(L1) = 0$$

$$\theta_0(a) = \theta_1(a)$$

$$y_0(0) = 0$$

$$y_0(a) = y_1(a)$$

$$y_1(L1) = 0$$

$$\text{find}(C_1, C_2, C_3, C_2, C_3) \rightarrow \begin{bmatrix} 1 - \frac{1}{55} \cdot a \\ \frac{1}{2} \cdot a^2 - \frac{55}{3} \cdot a - \frac{1}{330} \cdot a^3 \\ 0 \\ -\frac{55}{3} \cdot a - \frac{1}{330} \cdot a^3 \\ \frac{1}{6} \cdot a^3 \end{bmatrix}$$

$$M0(x, a) := -P \cdot \frac{(-L1 + a)}{L1} \cdot x \quad L1 \equiv 55 \quad L2 := 133 \quad L3 := 188 \quad P \equiv 1$$

$$M1(x, a) := -P \cdot \frac{(-L1 + a)}{L1} \cdot x - P \cdot (x - a)$$

$$y0(x, a) := \frac{1}{6} \left[ -P \cdot \frac{(-L1 + a)}{L1} \right] \cdot x^3 + \frac{-1}{6} \cdot P \cdot a \cdot \frac{(-3 \cdot a \cdot L1 + 2 \cdot L1^2 + a^2)}{L1} \cdot x$$

$$y1(x, a) := \frac{1}{6} \left[ -P \cdot \frac{(-L1 + a)}{L1} \right] \cdot x^3 - P \cdot \left( \frac{1}{6} \cdot x^3 - \frac{1}{2} \cdot a \cdot x^2 \right) + \frac{-1}{6} \cdot P \cdot a \cdot \frac{(2 \cdot L1^2 + a^2)}{L1} \cdot x + \frac{1}{6} \cdot P \cdot a^3$$

Note: If the solution is also solved for both a and P, all coefficients are simply multiplied by P. P is simply a scale multiple for the system solution.

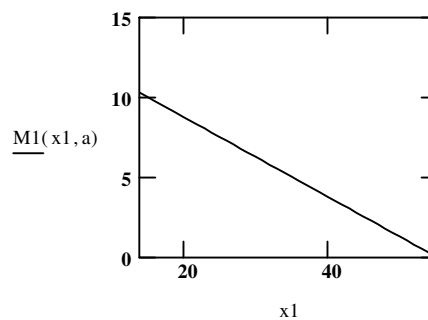
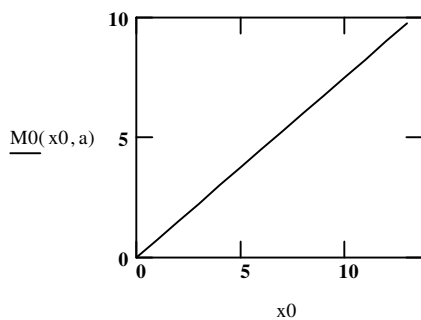
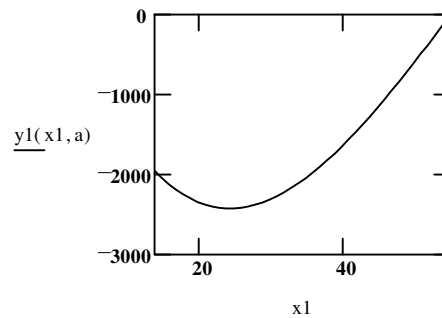
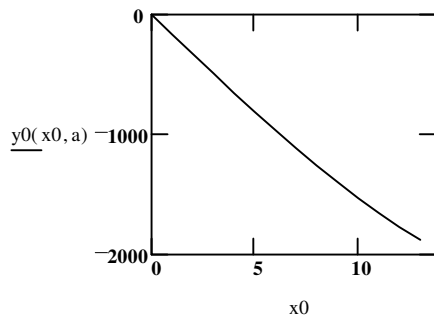
Solution for Cross-County Hwy, Reading Road Bridge (HAM-42-0992)  
(i.e., for the Instrumented Eastern Span)

$$L1 \equiv 55 \quad L2 := 133 \quad L3 := 188 \quad P \equiv 1$$

$$a := \frac{55}{4} \quad \text{a, Location of Unit Load}$$

$$x0 := 0..a$$

$$x1 := a..55$$



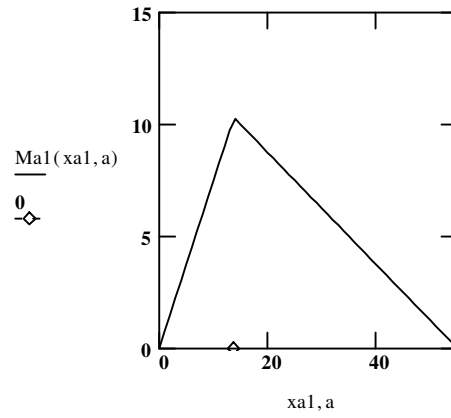
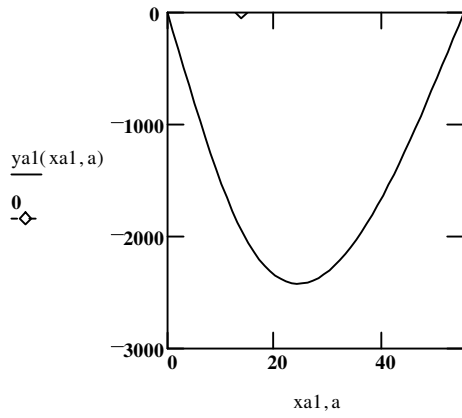
### Beam Response to Stationary Unit Load

$$y_{a1}(x, a) := \text{if}(x < 0, 0, \text{if}(x < a, y_0(x, a), \text{if}(x < L1, y_1(x, a), 0)))$$

$$M_{a1}(x, a) := \text{if}(x < 0, 0, \text{if}(x < a, M_0(x, a), \text{if}(x < L1, M_1(x, a), 0)))$$

$$a := \frac{55}{4} \quad \text{Location, } a, \text{ of Stationary Unit Load}$$

$$x_{a1} := 0..L1$$



Circle indicates support locations, Diamond indicates the Stationary Load

### Determination of the Unit Influence Line

(i.e., Beam Response at a Given Node to a Moving Unit Load)

$$y(x, a) := \text{if}(a < 0, 0, \text{if}(a < L1, yal(x, a), 0))$$

$$\psi(x) := \text{if}\left(x < 0, 0, \text{if}\left(x > L1, 0, \sin\left(\frac{\pi \cdot x}{L1}\right) \cdot y\left(\frac{L1}{2}, \frac{L1}{2}\right)\right)\right)$$

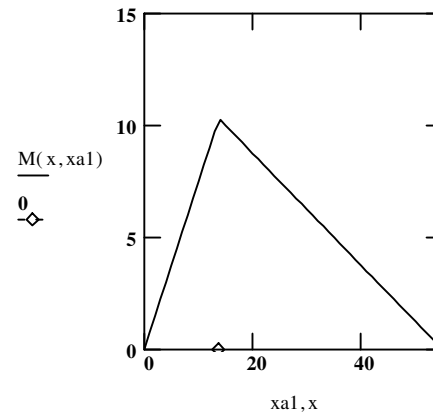
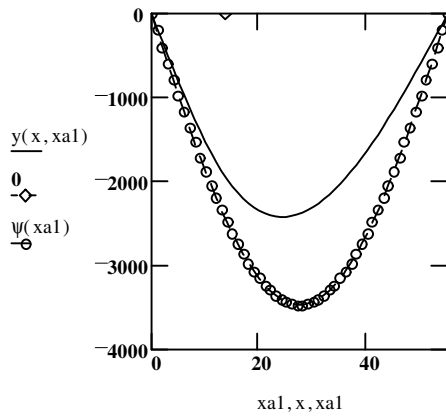
$$M(x, a) := \text{if}(a < 0, 0, \text{if}(a < L1, Mal(x, a), 0))$$

$\psi(x)$  is the first mode, scaled by the peak midspan deflection

$x = 13.75$

Location,  $x$ , of Bridge Sensor Node

Unit Influence Lines are determined by holding  $x$  constant and varying  $a$



Circle indicates support locations, Diamond indicates the Bridge Sensor Node

### Beam Response at a Given Node to a Moving Axle Load

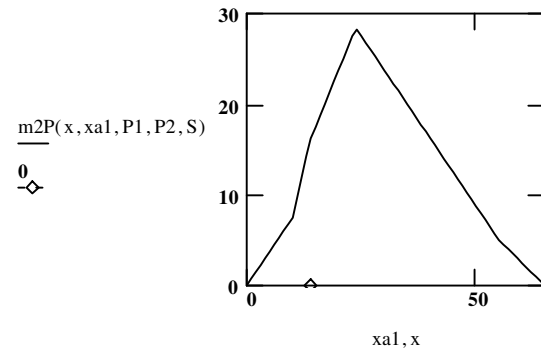
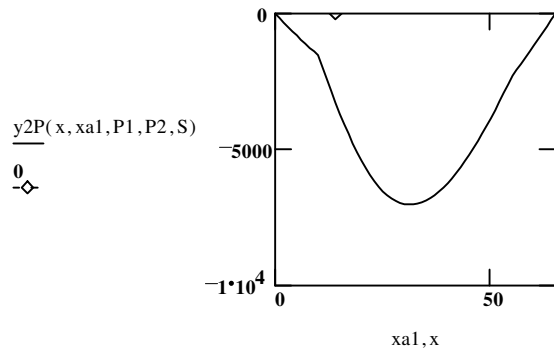
Here, we consider a single axle load P1 and velocity V.

$$y2P(x, a, P1, P2, S) := y(x, a) \cdot P1 + y(x, a - S) \cdot P2$$

$$m2P(x, a, P1, P2, S) := M(x, a) \cdot P1 + M(x, a - S) \cdot P2$$

**P1 = 1      P2 = 2      S = 10      x = 13.75** Location, x, of Bridge Sensor Node

xa1 := 0..(L1 + S)·oversample



Circle indicates support locations, Diamond indicates the Bridge Sensor Node

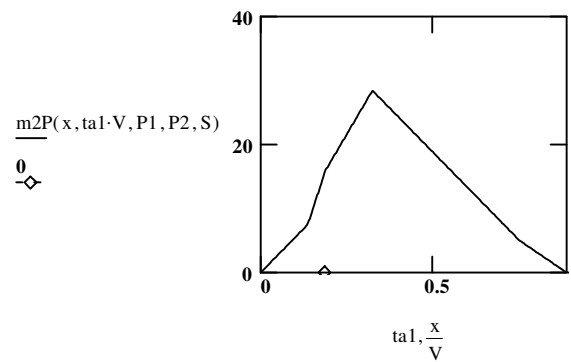
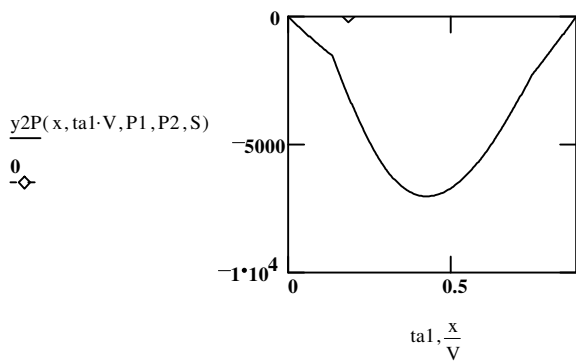
### Transform the Spatial System to the Time Domain

This assumes that the Monitoring System is sampling at a rate of SRate.

$$\text{SRate} := 500 \text{ Hz} \quad R := \frac{1}{\text{SRate}} \quad R = 2 \cdot 10^{-3} \text{ seconds}$$

$$\text{mph} = 50 \quad V := \text{mph} \cdot \frac{5280}{60 \cdot 60} \quad V = 73.333 \text{ feet/second} \quad f_y := \frac{V}{2 \cdot L1} \text{ loading frequency} \\ f_y = 0.667$$

$$\text{ta1} := 0, R \cdot \frac{(L1 + S) \cdot \text{oversample}}{V} \quad \frac{L1 + S}{V} = 0.886 \text{ seconds}$$



Circle indicates support locations, Diamond indicates the Bridge Sensor Node

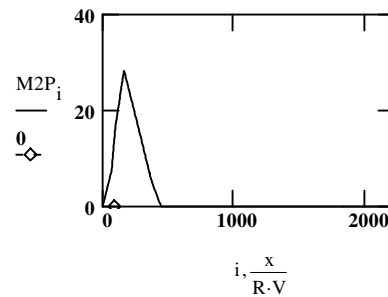
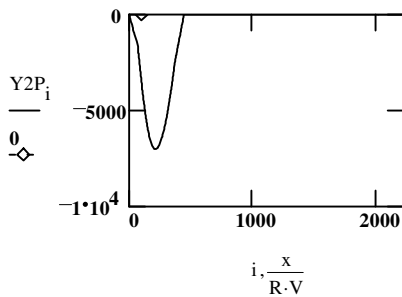
### Transform the Temporal System to the Frequency Domain

$$\text{Tct} := \frac{(L1 + S) \cdot \text{oversample}}{V \cdot R} \quad \text{Tct} = 2.216 \cdot 10^3 \quad \text{Total \# of data samples} \quad i := 0 \dots \text{Tct}$$

$$Y2P_i := y2P(x, i \cdot R \cdot V, P1, P2, S)$$

$$M2P_i := m2P(x, i \cdot R \cdot V, P1, P2, S)$$

Create temporal vectors for the evaluated functions above.

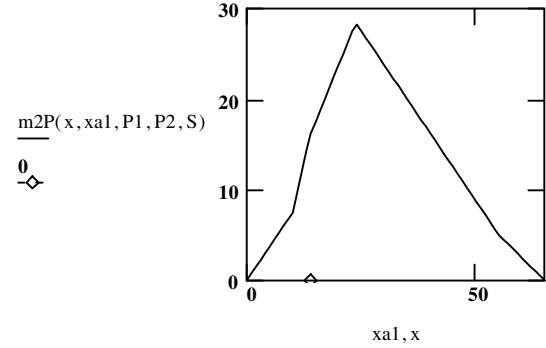
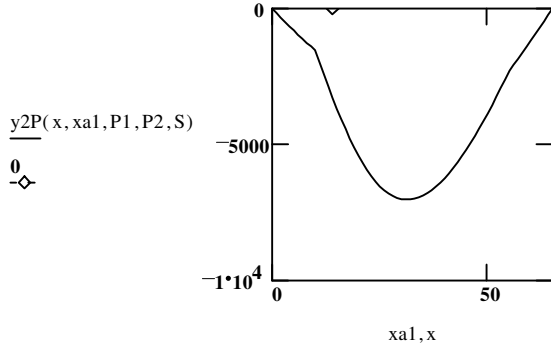


Circle indicates support locations, Diamond indicates the Bridge Sensor Node

Beam Response at a Given Node to a Moving Axle Load, w/ Oversampling

Here, we consider a single axle load P1 and velocity V.  
 P1=1 P2=2 S=10

mph=50  $x = \frac{27.5}{2}$  oversample=5  
 Location, x, of Bridge Sensor Node  $xa1 := 0..L1 + S$



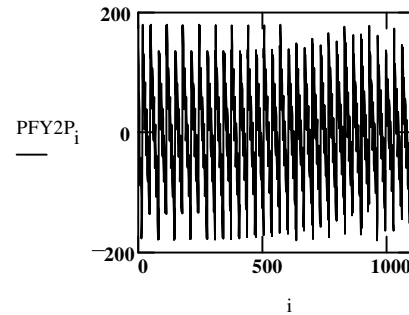
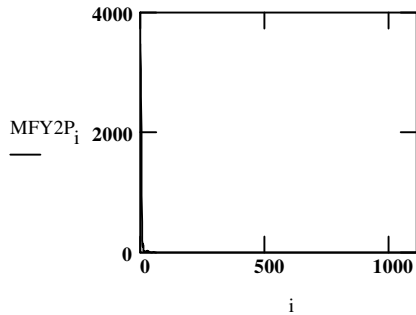
$F_{max} := \frac{1}{2 \cdot R}$   $F_{max} = 250$  FFT Bandwidth

$f := 0, \frac{1}{Tct \cdot R} .. F_{max}$   $f_{min} := \frac{1}{Tct \cdot R}$   $\frac{1}{Tct \cdot R} = 0.226$

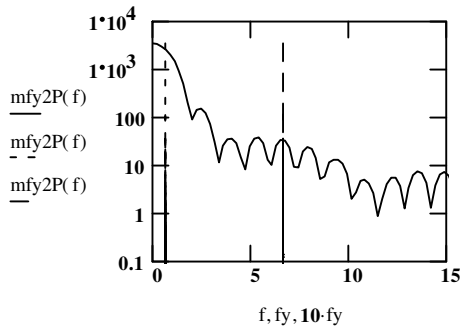
$FY2P := CFFT(Y2P) \cdot Tct \cdot R$   $fy2P(f) := FY2P_{f \cdot Tct \cdot R}$

$MFY2P := |FY2P|$  FFT Magnitude  $mfy2P(f) := MFY2P_{floor(f \cdot Tct \cdot R)}$   $mfy2P(0) = 3.473 \cdot 10^3$

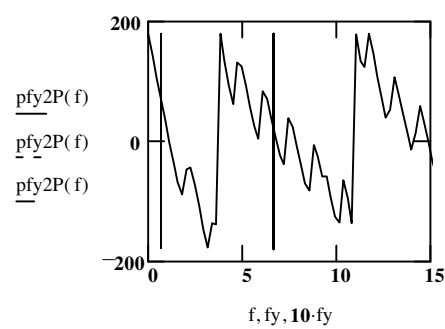
$PFY2P_i := if(FY2P_i = 0, 0, \arg(FY2P_i) \cdot \frac{180}{\pi})$  FFT Phase Angle  $pfy2P(f) := PFY2P_{floor(f \cdot Tct \cdot R)}$   $pfy2P(0) = 180$



Plot according to the frequency axis for the system bandwidth, BW.  $BW := 15$   $fy = 0.667$



$mfy2P(0) = 3.473 \cdot 10^3$

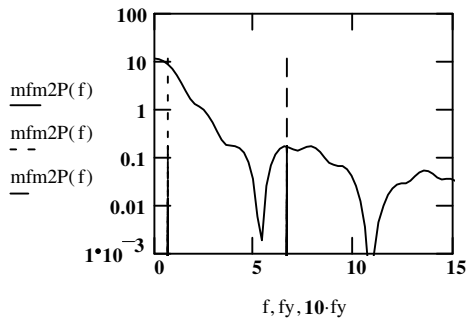
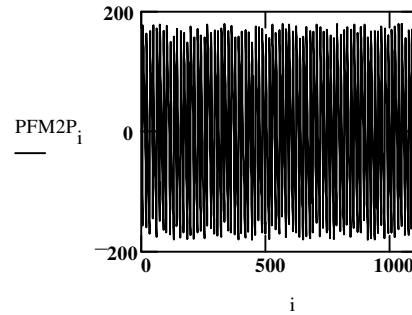
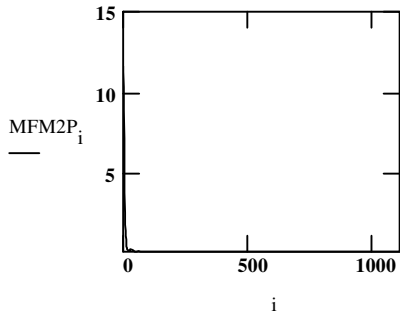


$pfy2P(0) = 180$

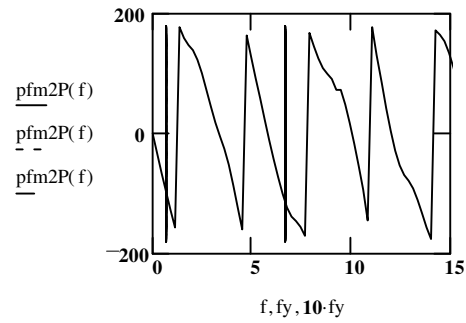
$$FM2P := CFFT(M2P) \cdot Tct \cdot R \quad f_{m2P}(f) := FM2P_{f \cdot Tct \cdot R}$$

$$MFM2P := \overline{FM2P} \quad \text{FFT Magnitude} \quad mfm2P(f) := MFM2P_{\text{floor}(f \cdot Tct \cdot R)} \quad mfm2P\left(\frac{0}{Tct \cdot R}\right) = \mathbf{11.601}$$

$$PFM2P_i := \text{if}\left(FM2P_i = \mathbf{0}, \mathbf{0}, \arg(FM2P_i) \cdot \frac{180}{\pi}\right) \quad \text{FFT Phase Angle} \quad pfm2P(f) := PFM2P_{\text{floor}(f \cdot Tct \cdot R)} \quad pfm2P(\mathbf{0}) = \mathbf{0}$$



$$mfm2P(\mathbf{0}) = \mathbf{11.601}$$



$$pfm2P(\mathbf{0}) = \mathbf{0}$$

Depending upon the gage location, certain modes become insignificant due to the structural symmetry.

$$\frac{m_{fy}2P(10 \cdot fy)}{m_{fy}2P(\mathbf{0})} = \mathbf{9.806 \cdot 10^{-3}} \quad \frac{mfm2P(10 \cdot fy)}{mfm2P(\mathbf{0})} = \mathbf{0.015}$$

Note that the magnitude for both signals is dramatically reduced at  $f = 10 \cdot fy = 10 \cdot V/L1$ .  
 $fy = \mathbf{0.667}$

### Compare the Spectral System to the Ideal Fourier Transforms

Deflection is represented by the sum of two negative sinusoids of period  $2L1/V$  seconds.

One sinusoid is delayed by a half period in order to cancel out the first. Both are multiplied by the unit step.

One axle response in time domain:

$$\text{Simy}(t) := -1 \cdot \sin\left(\frac{\pi \cdot V \cdot t}{L1}\right) \cdot \Phi(t) - \sin\left[\frac{\pi \cdot V \cdot \left(t - \frac{L1}{V}\right)}{L1}\right] \cdot \Phi\left(t - \frac{L1}{V}\right)$$

where  $\Phi(t) = 1$  for  $t \geq 0$  and  $\Phi(t) = 0$  for  $t < 0$

The second axle is represented by the same function, but delayed by  $S/V$  seconds.

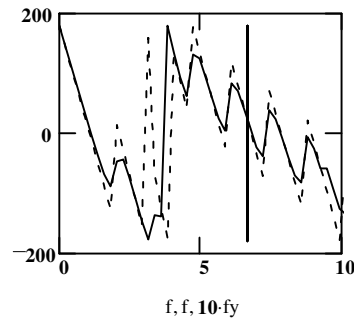
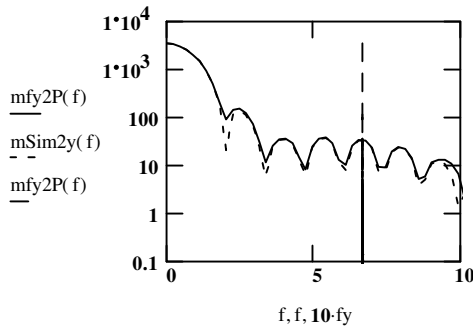
$$\text{Sim2y}(t) := \text{Simy}(t) \cdot P1 + \text{Simy}\left(t - \frac{S}{V}\right) \cdot P2$$

The MathCAD continuous Fourier transform for this ideal sinusoidal time representation for deflection is:

$$\text{Sim2y}(f) := \frac{-\text{mfy2P}(0)}{2 \cdot (P1 + P2) \cdot \left(1 - \frac{4 \cdot f^2 \cdot L1^2}{V^2}\right)} \cdot \left(1 + e^{-i \cdot 2 \cdot \pi \cdot L1 \cdot \frac{f}{V}}\right) \cdot \left(P1 + P2 \cdot e^{-i \cdot 2 \cdot \pi \cdot S \cdot \frac{f}{V}}\right)$$

where  $\text{mfy2P}(0) = \text{DC magnitude for the MathCAD transform}$

$$\text{mSim2y}(f) := \left| \text{Sim2y}(f) \right| \quad \text{pSim2y}(f) := \text{if}\left(\text{Sim2y}(f) = 0, 0, \arg(\text{Sim2y}(f)) \cdot \frac{180}{\pi}\right) \quad \text{BW} := 10$$



The plots do not completely match because the time representation  $\text{fy2P}$  is not exactly sinusoidal.

Compare DC magnitude of continuous Fourier transform to the discrete frequency representation  $\text{mfy2P}(0)$ :

$$y0\left(\frac{L1}{2}, \frac{L1}{2}\right) \cdot \frac{L1 \cdot 2 \cdot (P1 + P2)}{\pi \cdot V} = -4.965 \cdot 10^3 \quad \text{mfy2P}(0) = 3.473 \cdot 10^3 \quad \text{pfy2P}(0) = 180$$

\* Note:  $Tct$  is used to adjust for MathCAD derivation and  $R$  is used to adjust the discrete Fourier transform

The continuous Fourier transform for this triangular time representation for deflection is as follows:

$$\text{Sim2y}(f) := y0\left(\frac{L1}{2}, \frac{L1}{2}\right) \cdot \frac{L1}{\pi \cdot V \cdot \left(1 - \frac{4 \cdot f^2 \cdot L1^2}{V^2}\right)} \cdot \left(1 + e^{-i \cdot 2 \cdot \pi \cdot L1 \cdot \frac{f}{V}}\right) \cdot \left(P1 + P2 \cdot e^{-i \cdot 2 \cdot \pi \cdot S \cdot \frac{f}{V}}\right)$$

where  $y0(L1/2, L1/2) = -L1^3/48EI$

Moment is represented by a triangular pulse of period  $L1/V$  seconds.  
The signal is delayed by a half period to account for causal behavior.

One axle response in time domain:

$$\Lambda(T, t) := \frac{T}{2} - |t|$$

$$\text{Simm}(t) := \Lambda\left(\frac{L1}{V}, t - \frac{L1}{2 \cdot V}\right)$$

where  $\Lambda(T, t) = T/2 - t$  for  $0 < t < T$  and  
 $\Lambda(T, t) = T/2 + t$  for  $-T < t < 0$  and  
 $\Lambda(T, t) = 0$  for  $t < -T$  and  $t > T$

The second axle is represented by the same function, but delayed by  $S/V$  seconds.

$$\text{Sim2m}(t) := \text{Simm}(t) \cdot P1 + \text{Simm}\left(t - \frac{S}{V}\right) \cdot P2$$

The MathCAD continuous Fourier transform for this triangular time representation for moment is as follows:

$$\text{Sim2m}(f) := \frac{\text{mfm2P}(0)}{(P1 + P2)} \cdot \left[ \frac{\sin\left(\pi L1 \cdot \frac{f}{2 \cdot V}\right)}{\left(\pi L1 \cdot \frac{f}{2 \cdot V}\right)} \right]^2 \cdot e^{-i \cdot \pi \cdot L1 \cdot \frac{f}{V}} \cdot \left( P1 + P2 \cdot e^{-i \cdot 2 \cdot \pi \cdot S \cdot \frac{f}{V}} \right)$$

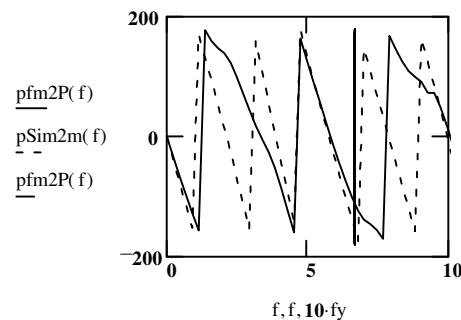
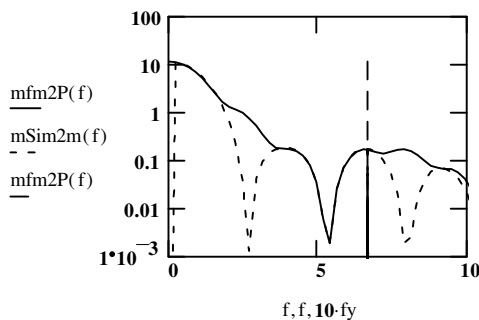
where  $\text{mfm2P}(0) = \text{DC magnitude}$   
for the MathCAD transform \*

$$\text{mSim2m}(f) := \text{if}\left(\text{Sim2m}(f) = 0, .000000001, \overline{\text{Sim2m}(f)}\right)$$

$$\text{mSim2m}(0) = 1 \cdot 10^{-9}$$

$$\text{pSim2m}(f) := \text{if}\left(\text{Sim2m}(f) = 0, 0, \arg(\text{Sim2m}(f)) \cdot \frac{180}{\pi}\right)$$

MathCAD does not evaluate the  
sinc function properly at  $f=0$ .



Compare DC magnitude of continuous Fourier transform to the discrete frequency representation  $\text{mfm2P}(0)$ :

$$M0\left(\frac{L1}{2}, \frac{L1}{2}\right) \cdot \frac{L1}{V} \cdot \frac{1}{2} \cdot (P1 + P2) = 15.469$$

$$\text{mfm2P}(0) = 11.601 \quad \text{pfm2P}(0) = 0$$

\* Note: Tct is used to adjust for MathCAD derivation  
and R is used to adjust the discrete Fourier transform

The continuous Fourier transform for this triangular time representation for moment is as follows:

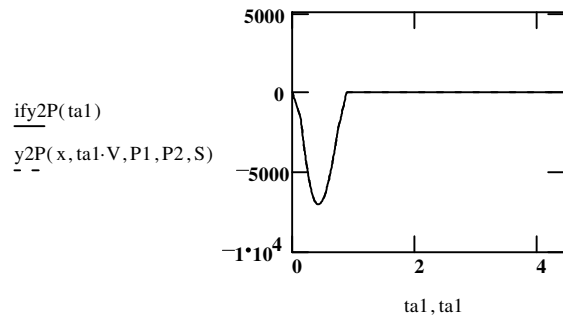
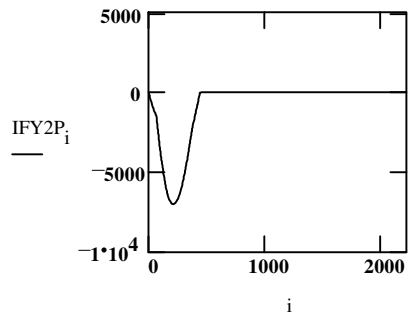
$$\text{Sim2m}(f) := M0\left(\frac{L1}{2}, \frac{L1}{2}\right) \cdot \frac{L1}{2 \cdot V} \cdot \left[ \frac{\sin\left(\pi L1 \cdot \frac{f}{2 \cdot V}\right)}{\left(\pi L1 \cdot \frac{f}{2 \cdot V}\right)} \right]^2 \cdot e^{-i \cdot \pi \cdot L1 \cdot \frac{f}{V}} \cdot \left( P1 + P2 \cdot e^{-i \cdot 2 \cdot \pi \cdot S \cdot \frac{f}{V}} \right)$$

where  $M0(L1/2, L1/2) = L1/4$

Transform the Spectral System back to the Time Domain

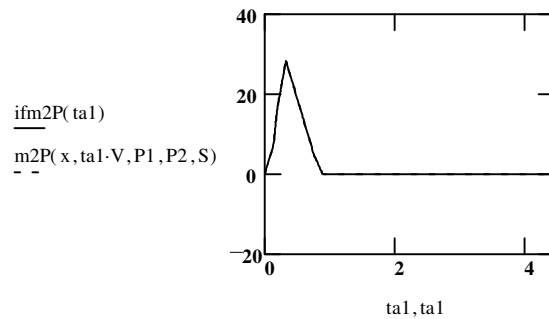
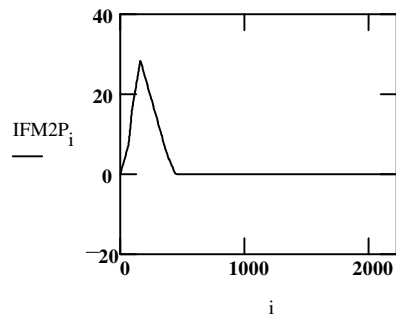
$$\text{IFY2P} := \text{ICFFT}\left(\frac{\text{FY2P}}{\text{Tct} \cdot \text{R}}\right)$$

$$\text{ify2P}(\text{ta1}) := \text{IFY2P}_{\text{floor}\left(\frac{\text{ta1}}{\text{R}}\right)}$$



$$\text{IFM2P} := \text{ICFFT}\left(\frac{\text{FM2P}}{\text{Tct} \cdot \text{R}}\right)$$

$$\text{ifm2P}(\text{ta1}) := \text{IFM2P}_{\text{floor}\left(\frac{\text{ta1}}{\text{R}}\right)}$$



Transform the Spectral System back to the Time Domain  
with a Low-Pass Dynamic Filter

Here, we apply an ideal low-pass filter at a cut-off frequency of  $F_{co}$ .  
The mean squared error, MSE, of the filtered signal compared to the original signal is plotted.

$$F_{co} := 10 \cdot f_y \text{ Hz} \quad F_i := \text{floor}(F_{co} \cdot T_{ct} \cdot R) \quad F_i = 29 \quad \text{vectorial index of } F_{co} \quad T_{ct} - F_i = 2.187 \cdot 10^3$$

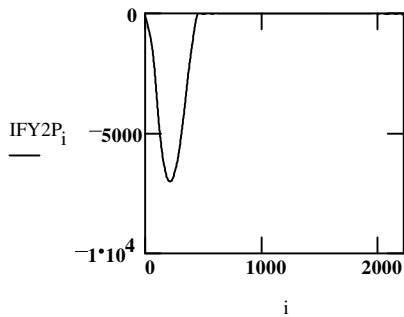
$$f_i := F_i + 1, F_i + 2 \dots T_{ct} - F_i \quad F_{co} = 6.667$$

$$FY2P_{f_i} := 0 \quad IFY2P := \text{ICFFT} \left( \frac{FY2P}{T_{ct} \cdot R} \right)$$

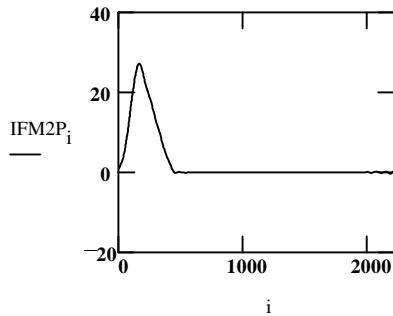
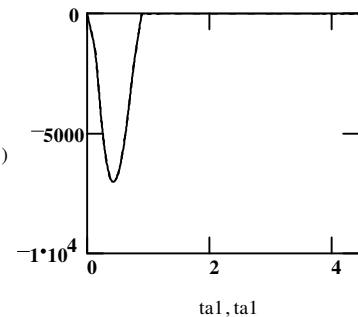
$$ify2P(ta1) := IFY2P_{\text{floor} \left( \frac{ta1}{R} \right)}$$

$$FM2P_{f_i} := 0 \quad IFM2P := \text{ICFFT} \left( \frac{FM2P}{T_{ct} \cdot R} \right)$$

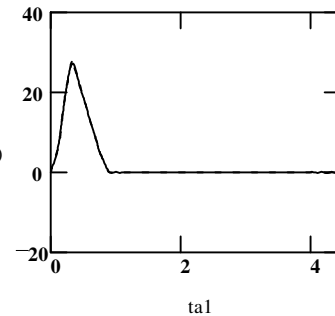
$$ifm2P(ta1) := IFM2P_{\text{floor} \left( \frac{ta1}{R} \right)}$$



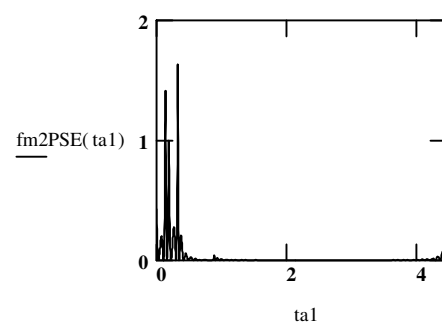
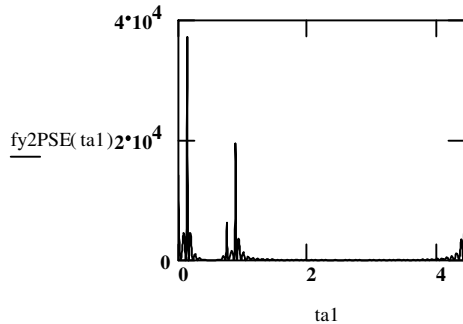
$$\frac{ify2P(ta1)}{y2P(x, ta1 \cdot V, P1, P2, S)}$$



$$\frac{ifm2P(ta1)}{m2P(x, ta1 \cdot V, P1, P2, S)}$$



$$fy2PSE(ta1) := (y2P(x, ta1 \cdot V, P1, P2, S) - ify2P(ta1))^2 \quad fm2PSE(ta1) := (m2P(x, ta1 \cdot V, P1, P2, S) - ifm2P(ta1))^2$$



$$fy2PMSE := \sum_{ta1} \frac{fy2PSE(ta1)}{T_{ct}} \quad fy2PMSE = 487.494$$

$$fm2PMSE := \sum_{ta1} \frac{fm2PSE(ta1)}{T_{ct}} \quad fm2PMSE = 0.026$$

## APPENDIX A3

### Elastic Deformation of the End Span of a Three Span Beam under Static Equilibrium

### Elastic Deformation of a Three Span Beam under Static Equilibrium

We assume a stationary point load  $w(x) = P\delta(x-a)$  located within the first of three spans. Supports are located at  $x = \{0, L1, L2, L3\}$ .

Note that the moment  $M\#(x)$ , slope  $\theta\#(x)$ , and deflection  $y\#(x)$  equations below remain to be scaled by the modulus of elasticity  $E$  and the beam inertia  $I$ , which are considered uniform for the beam.

$$M0(x) := C1 \cdot x$$

$$M1(x) := C1 \cdot x - P \cdot (x - a)$$

$$M2(x) := C2 \cdot (x - L1) + C21$$

$$M3(x) := C3 \cdot (x - L2) + C31$$

$$\theta0(x) := \frac{1}{2} \cdot C1 \cdot x^2 + C02$$

$$\theta1(x) := \frac{1}{2} \cdot C1 \cdot x^2 - P \cdot \left( \frac{1}{2} \cdot x^2 - a \cdot x \right) + C12$$

$$\theta2(x) := C2 \cdot \left( \frac{1}{2} \cdot x^2 - L1 \cdot x \right) + C21 \cdot x + C22$$

$$\theta3(x) := C3 \cdot \left( \frac{1}{2} \cdot x^2 - L2 \cdot x \right) + C31 \cdot x + C32$$

$$y0(x) := \frac{1}{6} \cdot C1 \cdot x^3 + C02 \cdot x + C03$$

$$y1(x) := \frac{1}{6} \cdot C1 \cdot x^3 - P \cdot \left( \frac{1}{6} \cdot x^3 - \frac{1}{2} \cdot a \cdot x^2 \right) + C12 \cdot x + C13$$

$$y2(x) := C2 \cdot \left( \frac{1}{6} \cdot x^3 - \frac{1}{2} \cdot L1 \cdot x^2 \right) + \frac{1}{2} \cdot C21 \cdot x^2 + C22 \cdot x + C23$$

$$y3(x) := C3 \cdot \left( \frac{1}{6} \cdot x^3 - \frac{1}{2} \cdot L2 \cdot x^2 \right) + \frac{1}{2} \cdot C31 \cdot x^2 + C32 \cdot x + C33$$

$$M0(0) = 0$$

$$M0(a) = M1(a)$$

$$M1(L1) = M2(L1)$$

$$M2(L2) = M3(L2)$$

$$M3(L3) = 0$$

$$\theta0(a) = \theta1(a)$$

$$\theta1(L1) = \theta2(L1)$$

$$\theta2(L2) = \theta3(L2)$$

$$y0(0) = 0$$

$$y0(a) = y1(a)$$

$$y1(L1) = 0$$

$$y2(L1) = 0$$

$$y2(L2) = 0$$

$$y3(L2) = 0$$

$$y3(L3) = 0$$

given

$$M_0(0) = 0$$

$$M_0(a) = M_1(a)$$

$$M_1(L_1) = M_2(L_1)$$

$$M_2(L_2) = M_3(L_2)$$

$$M_3(L_3) = 0$$

$$\theta_0(a) = \theta_1(a)$$

$$\theta_1(L_1) = \theta_2(L_1)$$

$$\theta_2(L_2) = \theta_3(L_2)$$

$$y_0(0) = 0$$

$$y_0(a) = y_1(a)$$

$$y_1(L_1) = 0$$

$$y_2(L_1) = 0$$

$$y_2(L_2) = 0$$

$$y_3(L_2) = 0$$

$$y_3(L_3) = 0$$

A3-3



$$L1 \equiv 55$$

$$L2 \equiv 133$$

$$L3 \equiv 188$$

$$P \equiv 1$$

given

$$C1 \cdot L1 - P \cdot (L1 - a) = C21$$

$$C2 \cdot (L2 - L1) + C21 = C31$$

$$C3 \cdot (L3 - L2) + C31 = 0$$

$$\frac{1}{2} \cdot C1 \cdot a^2 + C02 = \left[ \frac{1}{2} \cdot C1 \cdot a^2 - P \cdot \left( \frac{1}{2} \cdot a^2 - a \cdot a \right) \right] + C12$$

$$\left[ \frac{1}{2} \cdot C1 \cdot L1^2 - P \cdot \left( \frac{1}{2} \cdot L1^2 - a \cdot L1 \right) \right] + C12 = C2 \cdot \left( \frac{1}{2} \cdot L1^2 - L1 \cdot L1 \right) + C21 \cdot L1 + C22$$

$$C2 \cdot \left( \frac{1}{2} \cdot L2^2 - L1 \cdot L2 \right) + C21 \cdot L2 + C22 = C3 \cdot \left( \frac{1}{2} \cdot L2^2 - L2 \cdot L2 \right) + C31 \cdot L2 + C32$$

$$C03 = 0 \quad \frac{1}{6} \cdot C1 \cdot a^3 + C02 \cdot a + C03 = \frac{1}{6} \cdot C1 \cdot a^3 - P \cdot \left( \frac{1}{6} \cdot a^3 - \frac{1}{2} \cdot a \cdot a^2 \right) + C12 \cdot a + C13$$

$$\frac{1}{6} \cdot C1 \cdot L1^3 - P \cdot \left( \frac{1}{6} \cdot L1^3 - \frac{1}{2} \cdot a \cdot L1^2 \right) + C12 \cdot L1 + C13 = 0$$

$$C2 \cdot \left( \frac{1}{6} \cdot L1^3 - \frac{1}{2} \cdot L1 \cdot L1^2 \right) + \frac{1}{2} \cdot C21 \cdot L1^2 + C22 \cdot L1 + C23 = 0$$

$$C2 \cdot \left( \frac{1}{6} \cdot L2^3 - \frac{1}{2} \cdot L1 \cdot L2^2 \right) + \frac{1}{2} \cdot C21 \cdot L2^2 + C22 \cdot L2 + C23 = 0$$

$$C3 \cdot \left( \frac{1}{6} \cdot L2^3 - \frac{1}{2} \cdot L2 \cdot L2^2 \right) + \frac{1}{2} \cdot C31 \cdot L2^2 + C32 \cdot L2 + C33 = 0$$

$$C3 \cdot \left( \frac{1}{6} \cdot L3^3 - \frac{1}{2} \cdot L2 \cdot L3^2 \right) + \frac{1}{2} \cdot C31 \cdot L3^2 + C32 \cdot L3 + C33 = 0$$

find(C1, C2, C3, C21, C31, C02, C12, C22, C32, C03, C13, C23, C33) →

$$\left[ \begin{array}{l}
 \frac{-39651}{1778480} \cdot a + \frac{133}{97816400} \cdot a^3 + 1 \\
 \frac{55}{14664} \cdot a - \frac{1}{806520} \cdot a^3 \\
 \frac{-39}{32336} \cdot a + \frac{39}{97816400} \cdot a^3 \\
 \frac{-7315}{32336} \cdot a + \frac{133}{1778480} \cdot a^3 \\
 \frac{2145}{32336} \cdot a - \frac{39}{1778480} \cdot a^3 \\
 \frac{-1051545}{64672} \cdot a - \frac{13217}{3556960} \cdot a^3 + \frac{1}{2} \cdot a^2 \\
 \frac{-1051545}{64672} \cdot a - \frac{13217}{3556960} \cdot a^3 \\
 \frac{29174695}{1261104} \cdot a - \frac{530449}{69360720} \cdot a^3 \\
 \frac{-1339091}{64672} \cdot a + \frac{1339091}{195632800} \cdot a^3 \\
 0 \\
 \frac{1}{6} \cdot a^3 \\
 \frac{-116271925}{160992} \cdot a + \frac{38437}{160992} \cdot a^3 \\
 \frac{420147}{344} \cdot a - \frac{420147}{1040600} \cdot a^3
 \end{array} \right]$$

a := 27.5

x0 := 0..27

x2 := 55..133

$$y0(x, a) := \frac{1}{6} \cdot \left( 1 - \frac{39651}{1778480} \cdot a + \frac{133}{97816400} \cdot a^3 \right) \cdot x^3 + \left( \frac{-1051545}{64672} \cdot a - \frac{13217}{3556960} \cdot a^3 + \frac{1}{2} \cdot a^2 \right) \cdot x$$

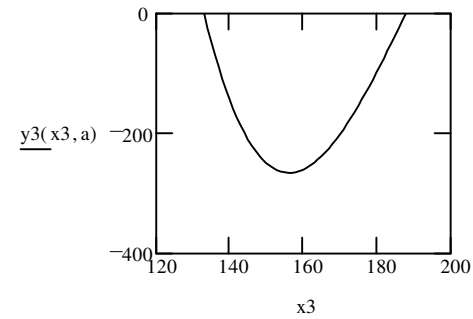
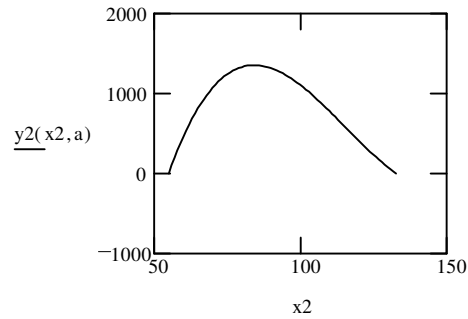
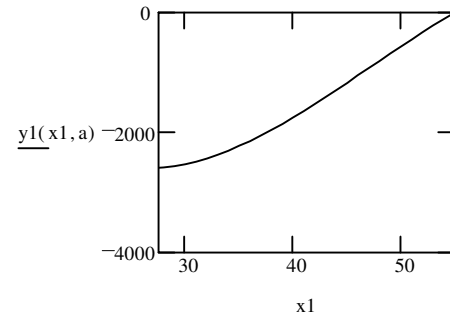
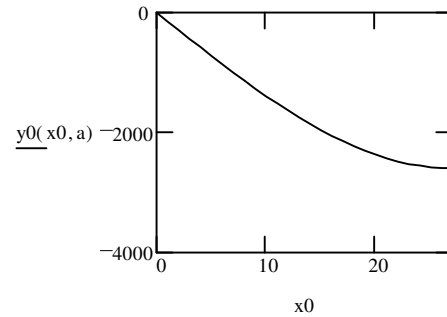
x1 := 27..55

x3 := 133..188

$$y1(x, a) := \frac{1}{6} \cdot \left( 1 - \frac{39651}{1778480} \cdot a + \frac{133}{97816400} \cdot a^3 \right) \cdot x^3 - P \cdot \left( \frac{1}{6} \cdot x^3 - \frac{1}{2} \cdot a \cdot x^2 \right) + \left( \frac{-1051545}{64672} \cdot a - \frac{13217}{3556960} \cdot a^3 \right) \cdot x + \frac{1}{6} \cdot a^3$$

$$y2(x, a) := \left( \frac{55}{14664} \cdot a - \frac{1}{806520} \cdot a^3 \right) \cdot \left( \frac{1}{6} \cdot x^3 - \frac{1}{2} \cdot L1 \cdot x^2 \right) + \frac{1}{2} \cdot \left( \frac{-7315}{32336} \cdot a + \frac{133}{1778480} \cdot a^3 \right) \cdot x^2 + \left( \frac{29174695}{1261104} \cdot a - \frac{530449}{69360720} \cdot a^3 \right) \cdot x + \left( \frac{-116271925}{160992} \cdot a + \frac{38437}{160992} \cdot a^3 \right)$$

$$y3(x, a) := \left( \frac{-39}{32336} \cdot a + \frac{39}{97816400} \cdot a^3 \right) \cdot \left( \frac{1}{6} \cdot x^3 - \frac{1}{2} \cdot L2 \cdot x^2 \right) + \frac{1}{2} \cdot \left( \frac{2145}{32336} \cdot a - \frac{39}{1778480} \cdot a^3 \right) \cdot x^2 + \left( \frac{-1339091}{64672} \cdot a + \frac{1339091}{195632800} \cdot a^3 \right) \cdot x + \left( \frac{420147}{344} \cdot a - \frac{420147}{1040600} \cdot a^3 \right)$$

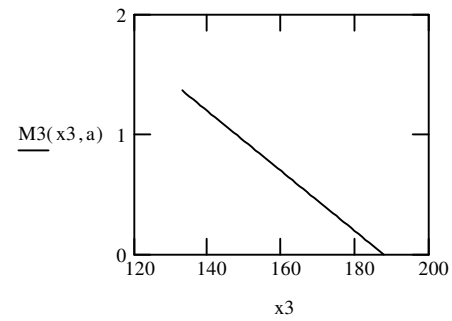
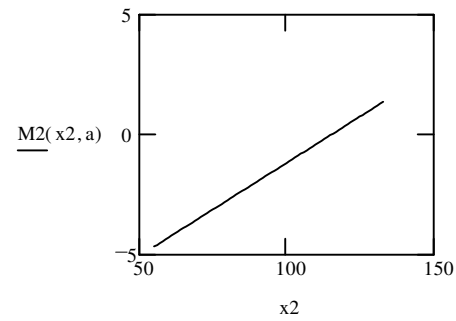
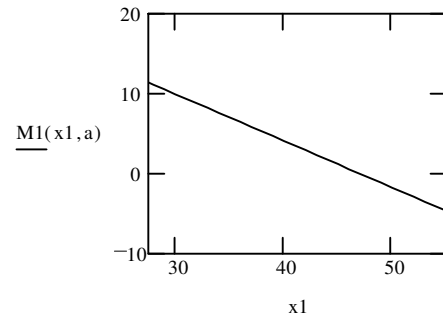
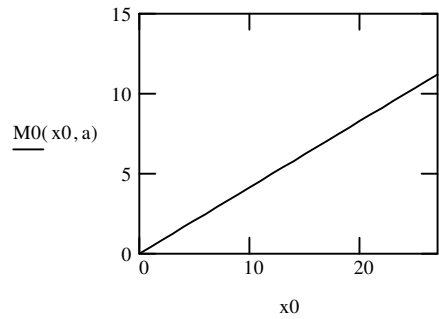


$$M0(x, a) := \left(1 - \frac{39651}{1778480} \cdot a + \frac{133}{97816400} \cdot a^3\right) \cdot x$$

$$M1(x, a) := \left(1 - \frac{39651}{1778480} \cdot a + \frac{133}{97816400} \cdot a^3\right) \cdot x - P \cdot (x - a)$$

$$M2(x, a) := \left(\frac{55}{14664} \cdot a - \frac{1}{806520} \cdot a^3\right) \cdot (x - L1) + \left(\frac{-7315}{32336} \cdot a + \frac{133}{1778480} \cdot a^3\right)$$

$$M3(x, a) := \left(\frac{-39}{32336} \cdot a + \frac{39}{97816400} \cdot a^3\right) \cdot (x - L2) + \left(\frac{2145}{32336} \cdot a - \frac{39}{1778480} \cdot a^3\right)$$

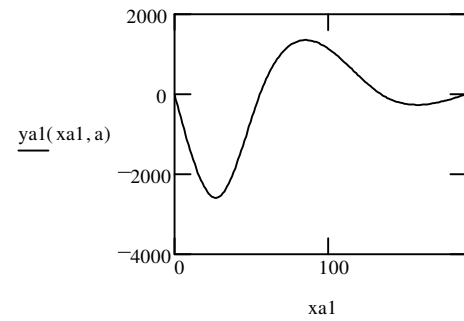


$ya1(x, a) := \text{if}(x < a, y0(x, a), \text{if}(x < L1, y1(x, a), \text{if}(x < L2, y2(x, a), y3(x, a))))$        $0 < a < L1$

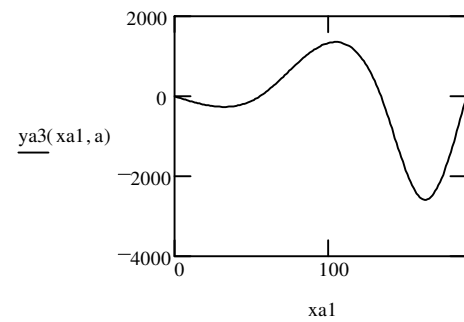
$ya3(x, a) := \text{if}(x > a, y0(L3 - x, L3 - a), \text{if}(x > L2, y1(L3 - x, L3 - a), \text{if}(x > L1, y2(L3 - x, L3 - a), y3(L3 - x, L3 - a))))$

$L2 < a < L3$

$xa1 := 0..188$      $a := 27.5$



$a := 160.5$



## APPENDIX A4

### Elastic Deformation of the Middle Span of a Three Span Beam under Static Equilibrium

### Elastic Deformation of a Three Span Beam under Static Equilibrium

We assume a stationary point load  $w(x) = P\delta(x-a)$  located within the middle of three spans. Supports are located at  $x = \{0, L1, L2, L3\}$ .

Note that the moment  $M\#(x)$ , slope  $\theta\#(x)$ , and deflection  $y\#(x)$  equations below remain to be scaled by the modulus of elasticity  $E$  and the beam inertia  $I$ , which are considered uniform for the beam.

$$M0(x) := C0 \cdot x$$

$\#=0$ , indicates  $0 < x < L1$

$$M0(0) = 0$$

$$M1(x) := C2 \cdot (x - L1) + C21$$

$\#=1$ , indicates  $L1 < x < a$

$$M0(L1) = M1(L1)$$

$$M2(x) := C2 \cdot (x - L1) - P \cdot (x - a) + C21$$

$\#=2$ , indicates  $a < x < L2$

$$M1(a) = M2(a)$$

$$M3(x) := C3 \cdot (x - L2) + C31$$

$\#=3$ , indicates  $L2 < x < L3$

$$M2(L2) = M3(L2)$$

$$M3(L3) = 0$$

$$\theta0(x) := \frac{1}{2} \cdot C0 \cdot x^2 + C02$$

$$\theta1(x) := C2 \cdot \left( \frac{1}{2} \cdot x^2 - L1 \cdot x \right) + C21 \cdot x + C12$$

$$\theta0(L1) = \theta1(L1)$$

$$\theta1(a) = \theta2(a)$$

$$\theta2(x) := C2 \cdot \left( \frac{1}{2} \cdot x^2 - L1 \cdot x \right) - P \cdot \left( \frac{1}{2} \cdot x^2 - a \cdot x \right) + C21 \cdot x + C22$$

$$\theta2(L2) = \theta3(L2)$$

$$\theta3(x) := C3 \cdot \left( \frac{1}{2} \cdot x^2 - L2 \cdot x \right) + C31 \cdot x + C32$$

$$y0(x) := \frac{1}{6} \cdot C0 \cdot x^3 + C02 \cdot x + C03$$

$$y0(0) = 0$$

$$y0(L1) = 0$$

$$y1(x) := C2 \cdot \left( \frac{1}{6} \cdot x^3 - \frac{1}{2} \cdot L1 \cdot x^2 \right) + \frac{1}{2} \cdot C21 \cdot x^2 + C12 \cdot x + C13$$

$$y1(L1) = 0$$

$$y1(a) = y2(a)$$

$$y2(x) := C2 \cdot \left( \frac{1}{6} \cdot x^3 - \frac{1}{2} \cdot L1 \cdot x^2 \right) - P \cdot \left( \frac{1}{6} \cdot x^3 - \frac{1}{2} \cdot a \cdot x^2 \right) + \frac{1}{2} \cdot C21 \cdot x^2 + C22 \cdot x + C23$$

$$y2(L2) = 0$$

$$y3(L2) = 0$$

$$y3(x) := C3 \cdot \left( \frac{1}{6} \cdot x^3 - \frac{1}{2} \cdot L2 \cdot x^2 \right) + \frac{1}{2} \cdot C31 \cdot x^2 + C32 \cdot x + C33$$

$$y3(L3) = 0$$

$$L1 \equiv 55$$

$$L2 \equiv 133$$

$$L3 \equiv 188$$

$$P \equiv 1$$

given

$$C0 \cdot L1 = C21$$

$$C2 \cdot (L2 - L1) - P \cdot (L2 - a) + C21 = C31$$

$$C3 \cdot (L3 - L2) + C31 = 0$$

$$\frac{1}{2} \cdot C0 \cdot L1^2 + C02 = C2 \cdot \left( \frac{1}{2} \cdot L1^2 - L1 \cdot L1 \right) + C21 \cdot L1 + C12$$

$$C2 \cdot \left( \frac{1}{2} \cdot a^2 - L1 \cdot a \right) + C21 \cdot a + C12 = C2 \cdot \left( \frac{1}{2} \cdot a^2 - L1 \cdot a \right) - P \cdot \left( \frac{1}{2} \cdot a^2 - a \cdot a \right) + C21 \cdot a + C22$$

$$C2 \cdot \left( \frac{1}{2} \cdot L2^2 - L1 \cdot L2 \right) - P \cdot \left( \frac{1}{2} \cdot L2^2 - a \cdot L2 \right) + C21 \cdot L2 + C22 = C3 \cdot \left( \frac{1}{2} \cdot L2^2 - L2 \cdot L2 \right) + C31 \cdot L2 + C32$$

$$C03 = 0 \quad \frac{1}{6} \cdot C0 \cdot L1^3 + C02 \cdot L1 = 0$$

$$C2 \cdot \left( \frac{1}{6} \cdot L1^3 - \frac{1}{2} \cdot L1 \cdot L1^2 \right) + \frac{1}{2} \cdot C21 \cdot L1^2 + C12 \cdot L1 + C13 = 0$$

$$C2 \cdot \left( \frac{1}{6} \cdot a^3 - \frac{1}{2} \cdot L1 \cdot a^2 \right) + \frac{1}{2} \cdot C21 \cdot a^2 + C12 \cdot a + C13 = C2 \cdot \left( \frac{1}{6} \cdot a^3 - \frac{1}{2} \cdot L1 \cdot a^2 \right) - P \cdot \left( \frac{1}{6} \cdot a^3 - \frac{1}{2} \cdot a \cdot a^2 \right) + \frac{1}{2} \cdot C21 \cdot a^2 + C22 \cdot a + C23$$

$$C2 \cdot \left( \frac{1}{6} \cdot L2^3 - \frac{1}{2} \cdot L1 \cdot L2^2 \right) - P \cdot \left( \frac{1}{6} \cdot L2^3 - \frac{1}{2} \cdot a \cdot L2^2 \right) + \frac{1}{2} \cdot C21 \cdot L2^2 + C22 \cdot L2 + C23 = 0$$

$$C3 \cdot \left( \frac{1}{6} \cdot L2^3 - \frac{1}{2} \cdot L2 \cdot L2^2 \right) + \frac{1}{2} \cdot C31 \cdot L2^2 + C32 \cdot L2 + C33 = 0$$

$$C3 \cdot \left( \frac{1}{6} \cdot L3^3 - \frac{1}{2} \cdot L2 \cdot L3^2 \right) + \frac{1}{2} \cdot C31 \cdot L3^2 + C32 \cdot L3 + C33 = 0$$

find(C0, C2, C3, C21, C31, C02, C12, C22, C32, C03, C13, C23, C33) →

$$\begin{aligned}
 & \frac{211}{491920} \cdot a^2 + \frac{38437}{26832} - \frac{530449}{11560120} \cdot a - \frac{1}{806520} \cdot a^3 \\
 & \frac{-1}{2028} \cdot a^2 + \frac{3059}{6084} + \frac{5885}{190632} \cdot a + \frac{1}{571896} \cdot a^3 \\
 & \frac{7315}{26832} - \frac{1}{806520} \cdot a^3 + \frac{133}{491920} \cdot a^2 - \frac{3379}{210184} \cdot a \\
 & \frac{211}{8944} \cdot a^2 + \frac{2114035}{26832} - \frac{530449}{210184} \cdot a - \frac{1}{14664} \cdot a^3 \\
 & \frac{-402325}{26832} + \frac{1}{14664} \cdot a^3 - \frac{133}{8944} \cdot a^2 + \frac{185845}{210184} \cdot a \\
 & \frac{-11605}{53664} \cdot a^2 - \frac{116271925}{160992} + \frac{29174695}{1261104} \cdot a + \frac{55}{87984} \cdot a^3 \\
 & \frac{-70235}{43602} \cdot a^2 - \frac{139204450}{65403} + \frac{760858505}{5464784} \cdot a + \frac{5885}{1143792} \cdot a^3 \\
 & \frac{-46018}{21801} \cdot a^2 - \frac{139204450}{65403} + \frac{760858505}{5464784} \cdot a + \frac{5885}{1143792} \cdot a^3 \\
 & \frac{753496205}{160992} - \frac{103007}{4839120} \cdot a^3 + \frac{13699931}{2951520} \cdot a^2 - \frac{348060653}{1261104} \cdot a \\
 & 0 \\
 & \frac{53509225}{2092896} \cdot a^2 + \frac{161865405625}{6278688} - \frac{139204450}{65403} \cdot a - \frac{3025}{36504} \cdot a^3 \\
 & \frac{53509225}{2092896} \cdot a^2 + \frac{161865405625}{6278688} - \frac{139204450}{65403} \cdot a + \frac{3059}{36504} \cdot a^3 \\
 & \frac{-1234603755}{4472} + \frac{3591}{2860} \cdot a^3 - \frac{67342023}{245960} \cdot a^2 + \frac{36401967}{2236} \cdot a
 \end{aligned}$$

$$a := 94 \quad x0 := 0..55 \quad x2 := a..133 \quad x1 := 55..a \quad x3 := 133..188$$

$$y0(x, a) := \frac{1}{6} \cdot \left( \frac{38437}{26832} - \frac{530449}{11560120} \cdot a + \frac{211}{491920} \cdot a^2 - \frac{1}{806520} \cdot a^3 \right) \cdot x^3 + \left( \frac{-116271925}{160992} + \frac{29174695}{1261104} \cdot a - \frac{11605}{53664} \cdot a^2 + \frac{55}{87984} \cdot a^3 \right) \cdot x$$

$$y1(x, a) := \left[ \left( \frac{-1}{2028} \cdot a^2 + \frac{3059}{6084} + \frac{5885}{190632} \cdot a + \frac{1}{571896} \cdot a^3 \right) \cdot \left( \frac{1}{6} \cdot x^3 - \frac{1}{2} \cdot L1 \cdot x^2 \right) + \frac{1}{2} \cdot \left( \frac{2114035}{26832} - \frac{530449}{210184} \cdot a + \frac{211}{8944} \cdot a^2 - \frac{1}{14664} \cdot a^3 \right) \cdot x^2 \right] \dots$$

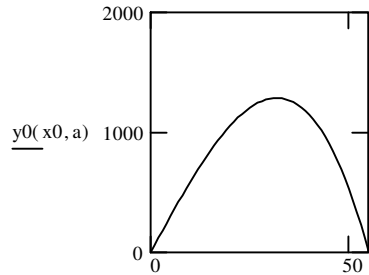
$$+ \left( \frac{-139204450}{65403} + \frac{760858505}{5464784} \cdot a - \frac{70235}{43602} \cdot a^2 + \frac{5885}{1143792} \cdot a^3 \right) \cdot x + \left( \frac{-3025}{36504} \cdot a^3 + \frac{53509225}{2092896} \cdot a^2 + \frac{161865405625}{6278688} - \frac{139204450}{65403} \cdot a \right)$$

$$y2(x, a) := \left[ \left( \frac{-1}{2028} \cdot a^2 + \frac{3059}{6084} + \frac{5885}{190632} \cdot a + \frac{1}{571896} \cdot a^3 \right) \cdot \left( \frac{1}{6} \cdot x^3 - \frac{1}{2} \cdot L1 \cdot x^2 \right) - P \cdot \left( \frac{1}{6} \cdot x^3 - \frac{1}{2} \cdot a \cdot x^2 \right) \right] + \frac{1}{2} \cdot \left( \frac{2114035}{26832} - \frac{530449}{210184} \cdot a + \frac{211}{8944} \cdot a^2 - \frac{1}{14664} \cdot a^3 \right) \cdot x^2 \dots$$

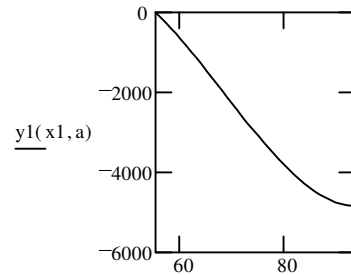
$$+ \left( \frac{-139204450}{65403} + \frac{760858505}{5464784} \cdot a - \frac{46018}{21801} \cdot a^2 + \frac{5885}{1143792} \cdot a^3 \right) \cdot x + \left( \frac{53509225}{2092896} \cdot a^2 + \frac{161865405625}{6278688} - \frac{139204450}{65403} \cdot a + \frac{3059}{36504} \cdot a^3 \right)$$

$$y3(x, a) := \left( \frac{133}{491920} \cdot a^2 + \frac{7315}{26832} - \frac{3379}{210184} \cdot a - \frac{1}{806520} \cdot a^3 \right) \cdot \left( \frac{1}{6} \cdot x^3 - \frac{1}{2} \cdot L2 \cdot x^2 \right) + \frac{1}{2} \cdot \left( \frac{-133}{8944} \cdot a^2 - \frac{402325}{26832} + \frac{185845}{210184} \cdot a + \frac{1}{14664} \cdot a^3 \right) \cdot x^2 \dots$$

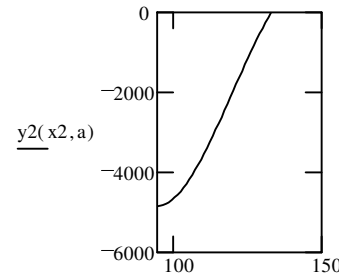
$$+ \left( \frac{13699931}{2951520} \cdot a^2 + \frac{753496205}{160992} - \frac{348060653}{1261104} \cdot a - \frac{103007}{4839120} \cdot a^3 \right) \cdot x + \left( \frac{-67342023}{245960} \cdot a^2 - \frac{1234603755}{4472} + \frac{36401967}{2236} \cdot a + \frac{3591}{2860} \cdot a^3 \right)$$



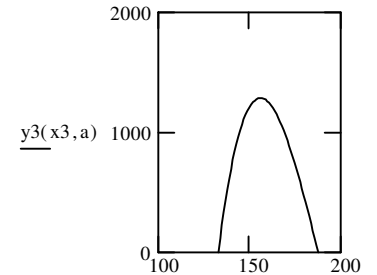
x0



x1



x2



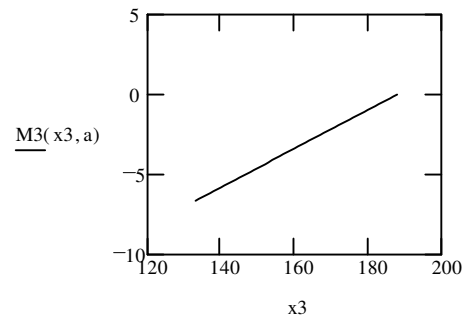
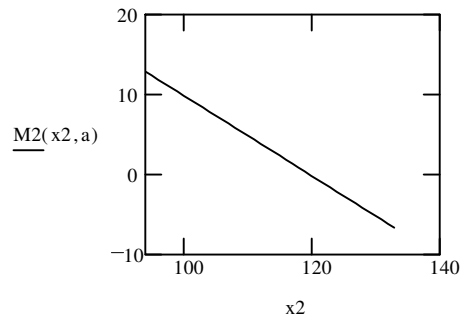
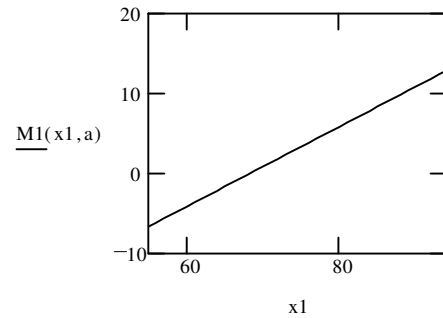
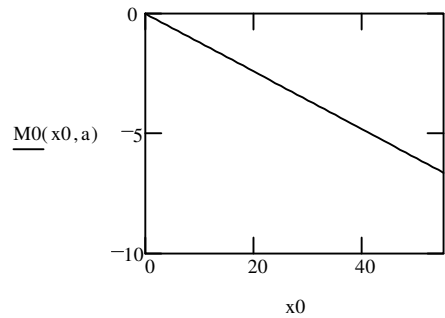
x3

$$M0(x, a) := \left( \frac{38437}{26832} - \frac{530449}{11560120} \cdot a + \frac{211}{491920} \cdot a^2 - \frac{1}{806520} \cdot a^3 \right) \cdot x$$

$$M1(x, a) := \left( \frac{-1}{2028} \cdot a^2 + \frac{3059}{6084} + \frac{5885}{190632} \cdot a + \frac{1}{571896} \cdot a^3 \right) \cdot (x - L1) + \left( \frac{2114035}{26832} - \frac{530449}{210184} \cdot a + \frac{211}{8944} \cdot a^2 - \frac{1}{14664} \cdot a^3 \right)$$

$$M2(x, a) := \left( \frac{-1}{2028} \cdot a^2 + \frac{3059}{6084} + \frac{5885}{190632} \cdot a + \frac{1}{571896} \cdot a^3 \right) \cdot (x - L1) - P \cdot (x - a) + \left( \frac{2114035}{26832} - \frac{530449}{210184} \cdot a + \frac{211}{8944} \cdot a^2 - \frac{1}{14664} \cdot a^3 \right)$$

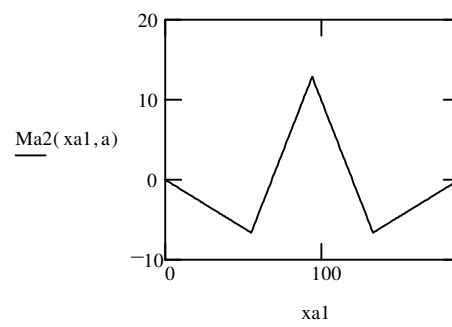
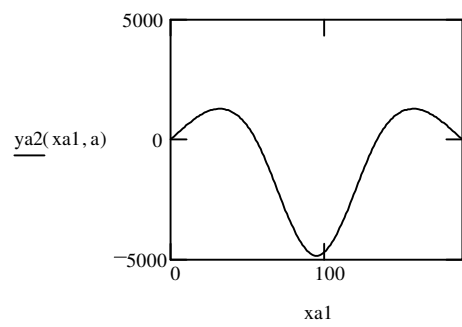
$$M3(x, a) := \left( \frac{133}{491920} \cdot a^2 + \frac{7315}{26832} - \frac{3379}{210184} \cdot a - \frac{1}{806520} \cdot a^3 \right) \cdot (x - L2) + \left( \frac{-133}{8944} \cdot a^2 - \frac{402325}{26832} + \frac{185845}{210184} \cdot a + \frac{1}{14664} \cdot a^3 \right)$$



$$ya2(x, a) := \text{if}(x < 0, 0, \text{if}(x < L1, y0(x, a), \text{if}(x < a, y1(x, a), \text{if}(x < L2, y2(x, a), \text{if}(x < L3, y3(x, a), 0))))))$$

$$Ma2(x, a) := \text{if}(x < 0, 0, \text{if}(x < L1, M0(x, a), \text{if}(x < a, M1(x, a), \text{if}(x < L2, M2(x, a), \text{if}(x < L3, M3(x, a), 0))))))$$

xa1 := 0..188    a := 94    L1 < a < L2



## APPENDIX A5

Elastic Deformation of the End Span of a Three Span Beam under Crawl Truckload

Solution for Cross-County Hwy, Reading Road Bridge (HAM-42-0992)

L1 := 55      L2 := 133      L3 := 188      P := 1

a := 27.5      a, Location of Unit Load

$$y_0(x, a) := \frac{1}{6} \cdot \left( 1 - \frac{39651}{1778480} \cdot a + \frac{133}{97816400} \cdot a^3 \right) \cdot x^3 + \left( \frac{-1051545}{64672} \cdot a - \frac{13217}{3556960} \cdot a^3 + \frac{1}{2} \cdot a^2 \right) \cdot x$$

x0 := 0.. a      x2 := 55.. 133

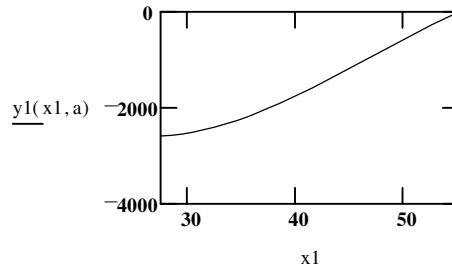
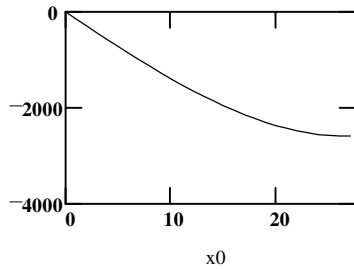
x1 := a.. 55      x3 := 133.. 188

$$y_1(x, a) := \frac{1}{6} \cdot \left( 1 - \frac{39651}{1778480} \cdot a + \frac{133}{97816400} \cdot a^3 \right) \cdot x^3 - P \cdot \left( \frac{1}{6} \cdot x^3 - \frac{1}{2} \cdot a \cdot x^2 \right) + \left( \frac{-1051545}{64672} \cdot a - \frac{13217}{3556960} \cdot a^3 \right) \cdot x + \frac{1}{6} \cdot a^3$$

$$y_2(x, a) := \left( \frac{55}{14664} \cdot a - \frac{1}{806520} \cdot a^3 \right) \cdot \left( \frac{1}{6} \cdot x^3 - \frac{1}{2} \cdot L1 \cdot x^2 \right) + \frac{1}{2} \cdot \left( \frac{-7315}{32336} \cdot a + \frac{133}{1778480} \cdot a^3 \right) \cdot x^2 + \left( \frac{29174695}{1261104} \cdot a - \frac{530449}{69360720} \cdot a^3 \right) \cdot x + \left( \frac{-116271925}{160992} \cdot a + \frac{38437}{160992} \cdot a^3 \right)$$

$$y_3(x, a) := \left( \frac{-39}{32336} \cdot a + \frac{39}{97816400} \cdot a^3 \right) \cdot \left( \frac{1}{6} \cdot x^3 - \frac{1}{2} \cdot L2 \cdot x^2 \right) + \frac{1}{2} \cdot \left( \frac{2145}{32336} \cdot a - \frac{39}{1778480} \cdot a^3 \right) \cdot x^2 + \left( \frac{-1339091}{64672} \cdot a + \frac{1339091}{195632800} \cdot a^3 \right) \cdot x + \left( \frac{420147}{344} \cdot a - \frac{420147}{1040600} \cdot a^3 \right)$$

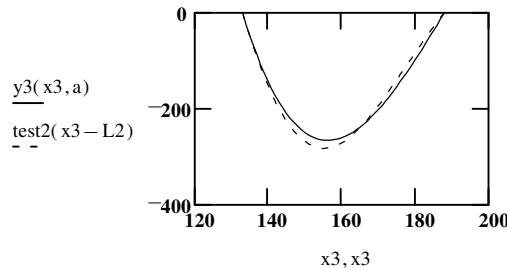
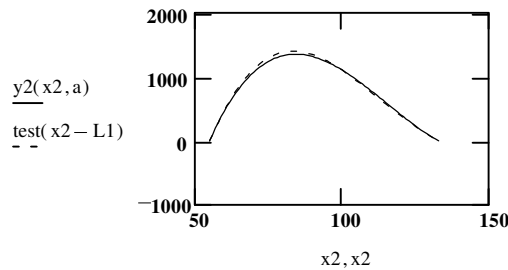
A5-2



$$\text{test}(x) := -1 \cdot y_0\left(\frac{L1}{2}, \frac{L1}{2}\right) \cdot e^{\frac{-x}{L1}} \cdot \sin\left(\pi \cdot \frac{x}{L2 - L1}\right)$$

$$\text{test2}(x) := \frac{L1}{L2 + L3} \cdot y_0\left(\frac{L1}{2}, \frac{L1}{2}\right) \cdot e^{\frac{-x}{L1}} \cdot \sin\left(\pi \cdot \frac{x}{L3 - L2}\right)$$

$$\frac{L1}{L3 + L2} = 0.171 \quad y_0\left(\frac{L1}{2}, \frac{L1}{2}\right) = -2.584 \cdot 10^3$$



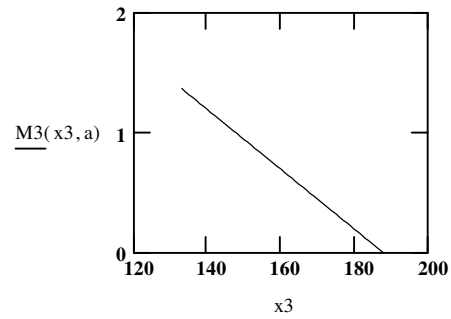
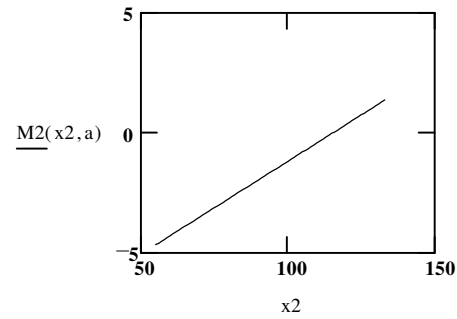
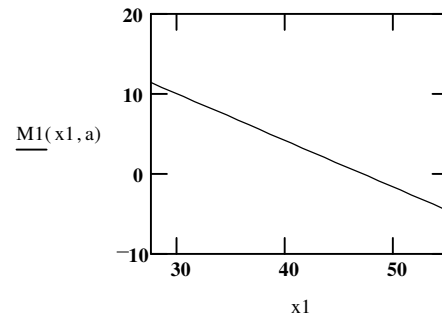
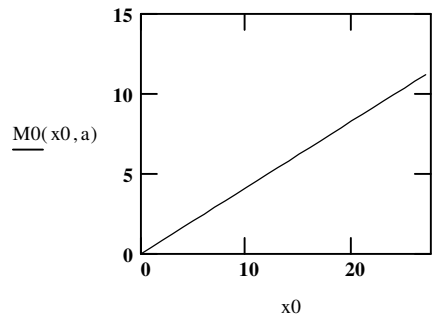
$$M0(x, a) := \left( 1 - \frac{39651}{1778480} \cdot a + \frac{133}{97816400} \cdot a^3 \right) \cdot x$$

$$M1(x, a) := \left( 1 - \frac{39651}{1778480} \cdot a + \frac{133}{97816400} \cdot a^3 \right) \cdot x - P \cdot (x - a)$$

$$M2(x, a) := \left( \frac{55}{14664} \cdot a - \frac{1}{806520} \cdot a^3 \right) \cdot (x - L1) + \left( \frac{-7315}{32336} \cdot a + \frac{133}{1778480} \cdot a^3 \right)$$

$$M3(x, a) := \left( \frac{-39}{32336} \cdot a + \frac{39}{97816400} \cdot a^3 \right) \cdot (x - L2) + \left( \frac{2145}{32336} \cdot a - \frac{39}{1778480} \cdot a^3 \right)$$

A5-3



0 < a < L1, Load in first span

$$ya1(x, a) := \text{if}(x < 0, 0, \text{if}(x < a, y0(x, a), \text{if}(x < L1, y1(x, a), \text{if}(x < L2, y2(x, a), \text{if}(x < L3, y3(x, a), 0))))))$$

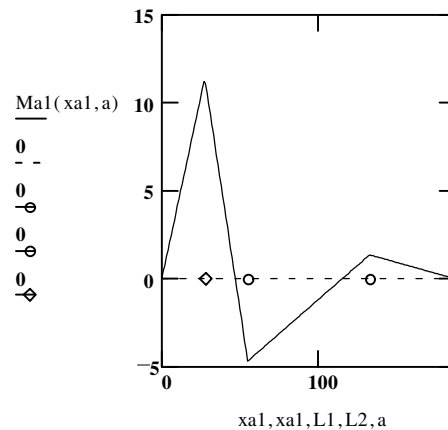
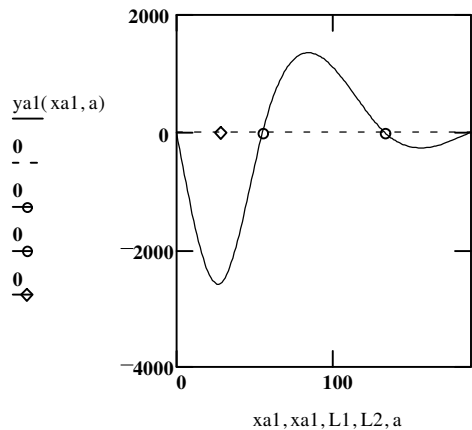
$$Ma1(x, a) := \text{if}(x < 0, 0, \text{if}(x < a, M0(x, a), \text{if}(x < L1, M1(x, a), \text{if}(x < L2, M2(x, a), \text{if}(x < L3, M3(x, a), 0))))))$$

L2 < a < L3, Load in last span

$$ya3(x, a) := \text{if}(x < 0, 0, \text{if}(x > a, y0(L3 - x, L3 - a), \text{if}(x > L2, y1(L3 - x, L3 - a), \text{if}(x > L1, y2(L3 - x, L3 - a), \text{if}(x < L3, y3(L3 - x, L3 - a), 0))))))$$

$$Ma3(x, a) := \text{if}(x < 0, 0, \text{if}(x > a, M0(L3 - x, L3 - a), \text{if}(x > L2, M1(L3 - x, L3 - a), \text{if}(x > L1, M2(L3 - x, L3 - a), \text{if}(x < L3, M3(L3 - x, L3 - a), 0))))))$$

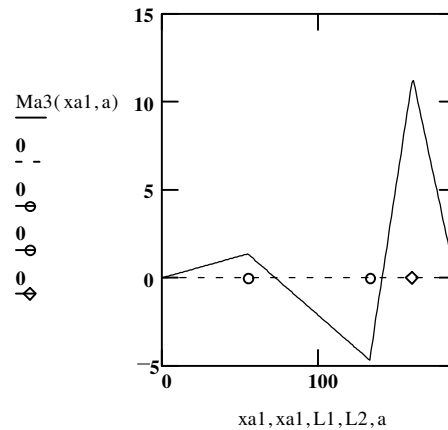
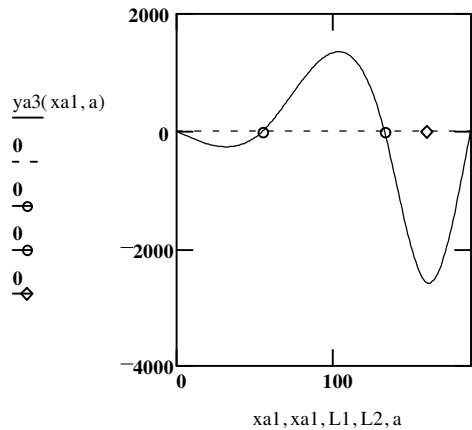
xa1 := 0..188    a := 27.5    Location, a, of Stationary Unit Load



Circle indicates support locations,  
Diamond indicates the Stationary Load

A5-4

a := 160.5    Location, a, of Stationary Unit Load



Circle indicates support locations,  
Diamond indicates the Stationary Load

Determination of the Unit Influence Line  
(i.e., Bridge Response at a Given Node to a Moving Unit Load)



Include:C:\ODOT\Reading\MathCAD\simplebmvh4m.mcd

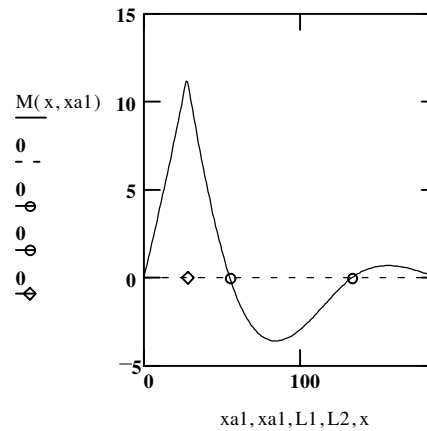
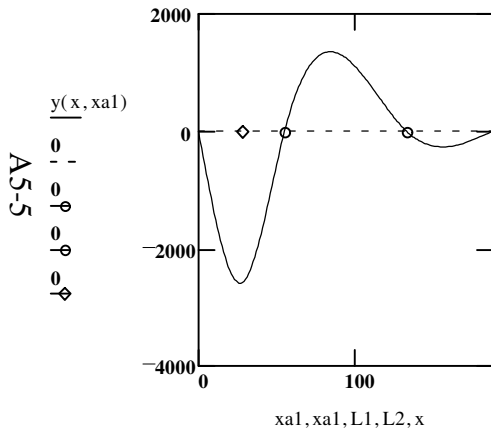
$$y(x, a) := \text{if}(a < 0, 0, \text{if}(a < L1, ya1(x, a), \text{if}(a < L2, ya2(x, a), \text{if}(a < L3, ya3(x, a), 0))))$$

$$M(x, a) := \text{if}(a < 0, 0, \text{if}(a < L1, Ma1(x, a), \text{if}(a < L2, Ma2(x, a), \text{if}(a < L3, Ma3(x, a), 0))))$$

x = 27.5

Location, x, of Bridge Sensor Node

Unit Influence Lines are determined by holding x constant and varying a



$$M0(x, a) := \left( 1 - \frac{39651}{1778480} \cdot a + \frac{133}{97816400} \cdot a^3 \right) \cdot x$$

Circle indicates support locations,  
Diamond indicates the Stationary Load

$$M0\left(\frac{L1}{2}, \frac{L1}{2}\right) = 11.417$$

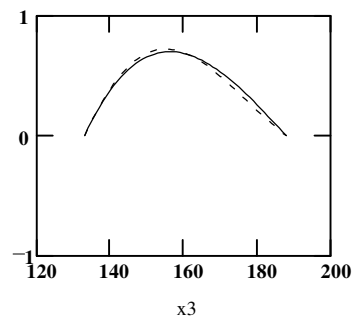
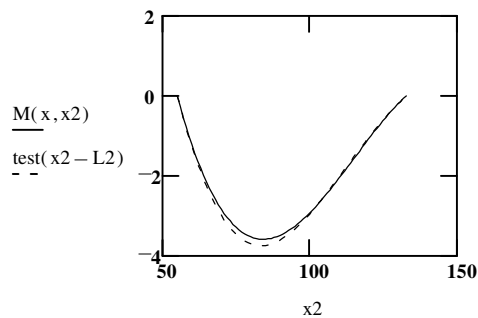
$$\text{test}(x) := \frac{L1}{2 \cdot L3} \cdot M0\left(\frac{L1}{2}, \frac{L1}{2}\right) \cdot e^{\frac{-x}{L1}} \cdot \sin\left(\pi \cdot \frac{x}{L2 - L1}\right)$$

Circle indicates support locations, Diamond indicates the Bridge Sensor Node

$$\text{test2}(x) := \frac{-L1}{8 \cdot L3} \cdot M0\left(\frac{L1}{2}, \frac{L1}{2}\right) \cdot e^{\frac{-x}{L1}} \cdot \sin\left(\pi \cdot \frac{x}{L3 - L2}\right)$$

x2 := 55.. 133

x3 := 133.. 188



### Bridge Response at a Given Node to a Moving Axle Load, w/ Oversample

Here, we consider a 2-axle truck of axle loads P1 and P2, axle spacing of S, and velocity V.

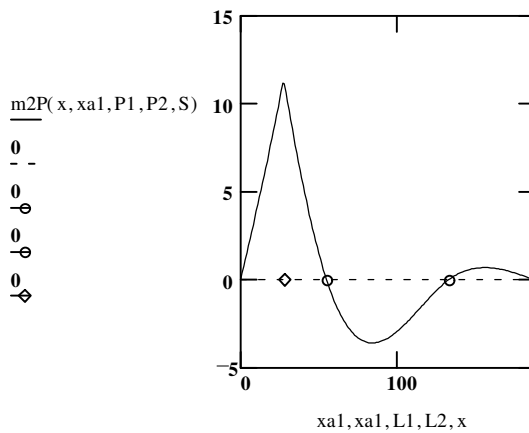
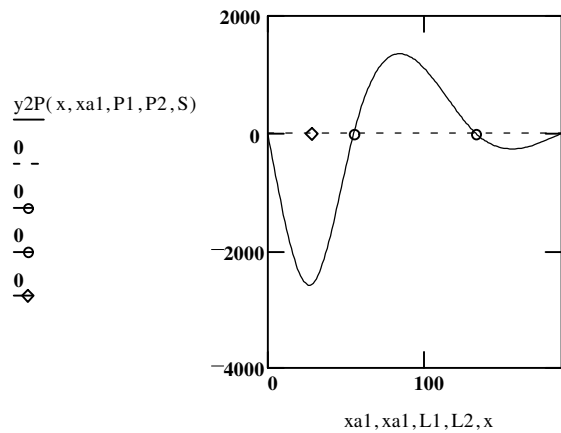
$$y2P(x, a, P1, P2, S) := y(x, a) \cdot P1 + y(x, a - S) \cdot P2$$

$$m2P(x, a, P1, P2, S) := M(x, a) \cdot P1 + M(x, a - S) \cdot P2$$

P1 := 1      P2 := 0      S := 0      x = 27.5      Location, x, of Bridge Sensor Node

xa1 := 0..(L1 + L2 + L3 + S)·oversample      x ≡ 27.5      mph ≡ 50      oversample ≡ 2

A5-6



Circle indicates support locations,  
Diamond indicates the Stationary Load

Circle indicates support locations, Diamond indicates the Bridge Sensor Node

Transform the Spatial System to the Time Domain

This assumes that the Monitoring System is sampling at a rate of SRate.

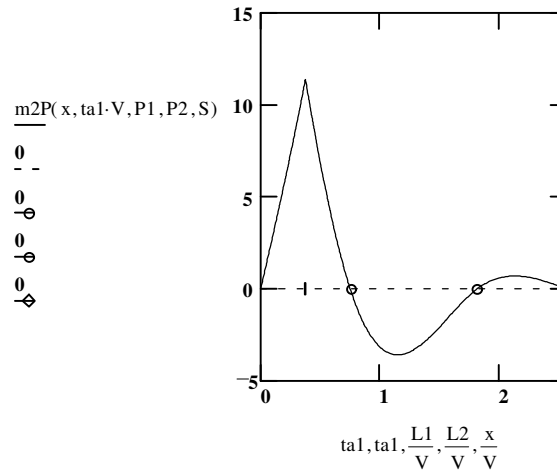
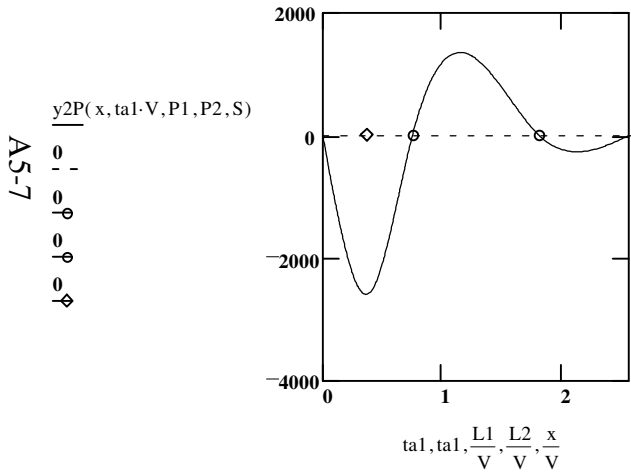
$$\text{SRate} := 500 \text{ Hz} \quad R := \frac{1}{\text{SRate}} \quad R = 2 \cdot 10^{-3} \text{ seconds}$$

$$\text{mph} = 50 \quad V := \text{mph} \cdot \frac{5280}{60 \cdot 60} \quad V = 73.333 \text{ feet/second}$$

$$f_y := \frac{V}{2 \cdot L1} \text{ loading frequency} \quad f_y = 0.667$$

$$f_{ym} := \frac{V}{2 \cdot L2} \text{ loading frequency for midspan} \quad f_{ym} = 0.276$$

$$ta1 := 0, R.. \frac{(L1 + L2 + L3 + S) \cdot \text{oversample}}{V} \quad \frac{188 + S}{V} = 2.564 \text{ seconds}$$



Circle indicates support locations,  
Diamond indicates the Stationary Load

Circle indicates support locations, Diamond indicates the Bridge Sensor Node

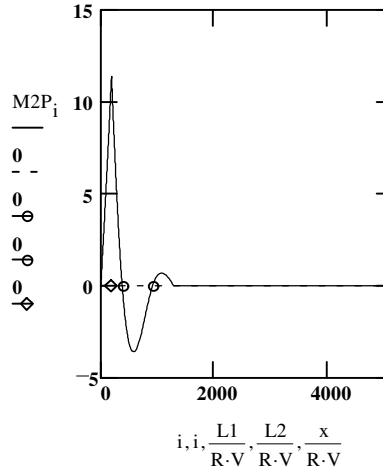
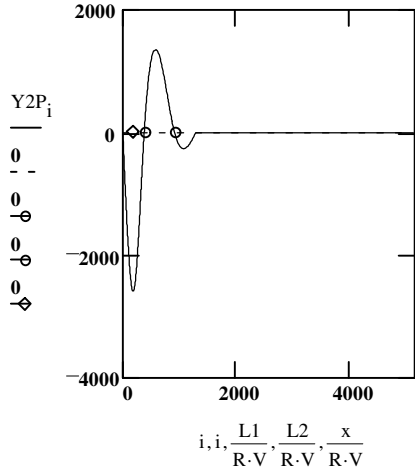
### Transform the Temporal System to the Frequency Domain

$$T_{ct} := \frac{(L1 + L2 + L3 + S) \cdot \text{oversample}}{V \cdot R} \quad T_{ct} = 5.127 \cdot 10^3 \quad \text{Total \# of data samples} \quad i := 0..T_{ct}$$

$$Y2P_i := y2P(x, i \cdot R \cdot V, P1, P2, S) \quad M2P_i := m2P(x, i \cdot R \cdot V, P1, P2, S)$$

Create temporal vectors for the evaluated functions above.

A5-8

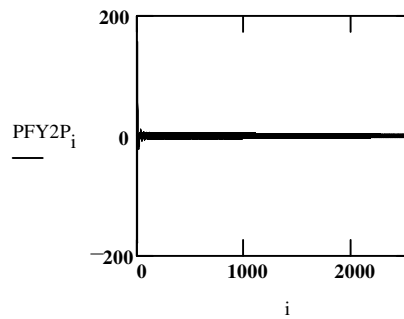
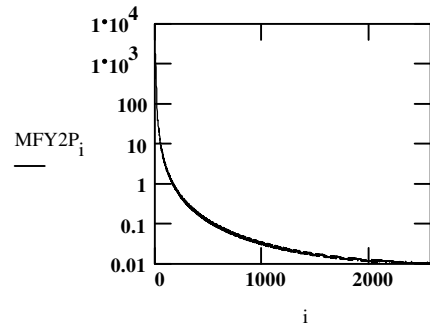


Circle indicates support locations,  
Diamond indicates the Stationary Load

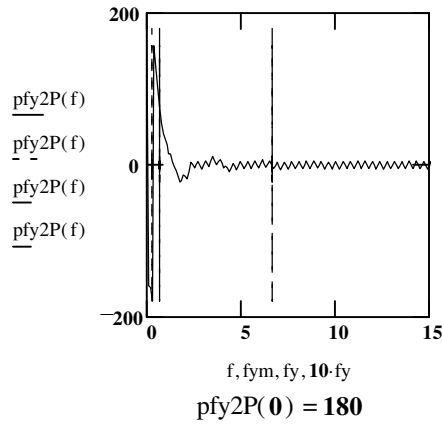
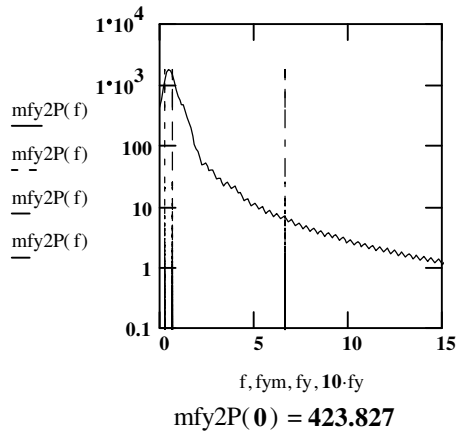
$$FY2P := \text{CFFT}(Y2P) \cdot T_{ct} \cdot R \quad F_{max} := \frac{1}{2 \cdot R} \quad F_{max} = 250 \quad \text{FFT Bandwidth} \quad f := 0, \frac{1}{T_{ct} \cdot R} .. F_{max} \quad f_{min} := \frac{1}{T_{ct} \cdot R} \quad \frac{1}{T_{ct} \cdot R} = 0.098$$

$$MFY2P := \overrightarrow{|FY2P|} \quad \text{FFT Magnitude} \quad mfy2P(f) := MFY2P_{\text{floor}(f \cdot T_{ct} \cdot R)} \quad mfy2P(0) = 423.827$$

$$PFY2P := \overrightarrow{\arg(FY2P)} \cdot \frac{180}{\pi} \quad \text{FFT Phase Angle} \quad pfy2P(f) := PFY2P_{\text{floor}(f \cdot T_{ct} \cdot R)} \quad pfy2P(0) = 180$$



Plot according to the frequency axis for the system bandwidth, BW. BW := 15



$$\frac{\text{mfy2P}(10 \cdot \text{fy})}{\text{mfy2P}(0)} = 0.016$$

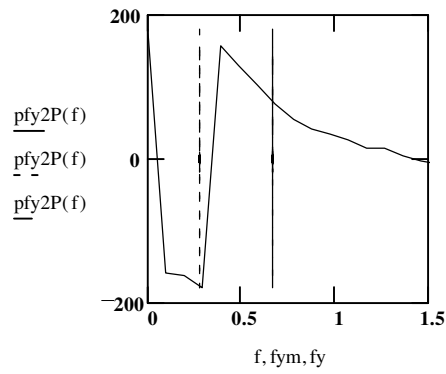
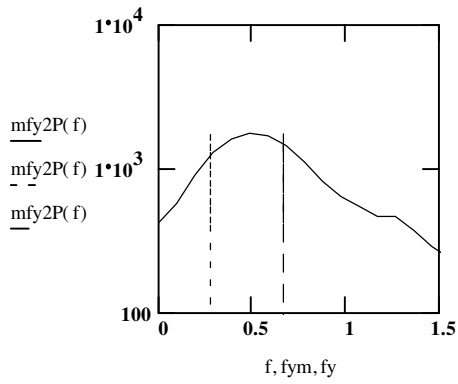
$$\text{fym} = 0.276$$

$$\text{fy} = 0.667$$

Note that the magnitude for both signals is dramatically reduced at  $f = 10 \text{ fy} = 10 \text{ V/L1}$ .

6-5-9

comparison w/ the single span results, the three span spectrum appears dampened in amplitude and phase ; the spectral oscillations are reduced.



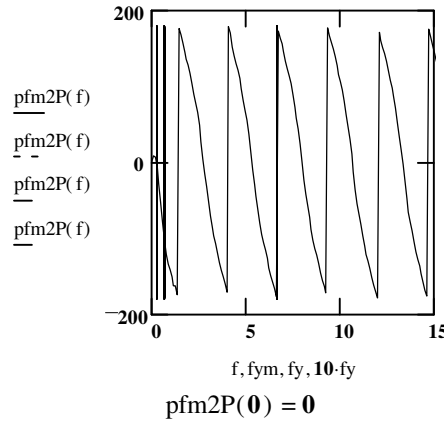
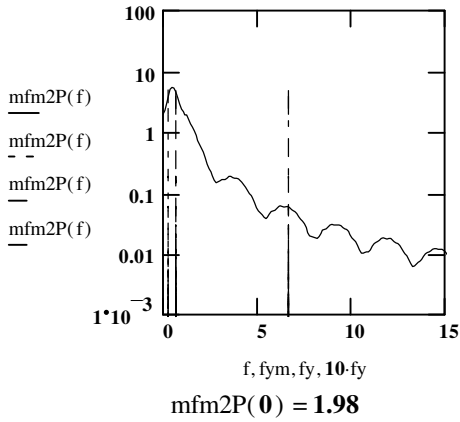
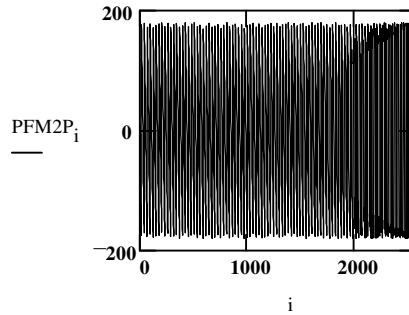
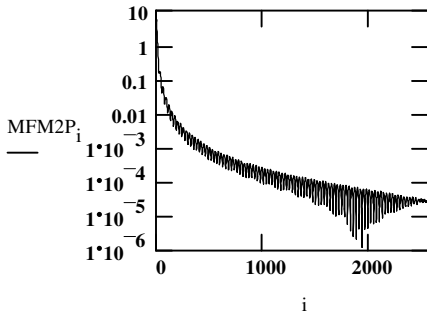
$$FM2P := CFFT(M2P) \cdot Tct \cdot R$$

$$MFM2P := \overrightarrow{|FM2P|} \quad \text{FFT Magnitude}$$

$$PFM2P := \overrightarrow{\arg(FM2P)} \cdot \frac{180}{\pi} \quad \text{FFT Phase Angle}$$

$$mfm2P(f) := MFM2P_{\text{floor}(f \cdot Tct \cdot R)} \quad mfm2P(\mathbf{0}) = \mathbf{1.98}$$

$$pfm2P(f) := PFM2P_{\text{floor}(f \cdot Tct \cdot R)} \quad pfm2P(\mathbf{0}) = \mathbf{0}$$



$$\frac{mfm2P(\mathbf{10 \cdot fy})}{mfm2P(\mathbf{0})} = \mathbf{0.03}$$

$$fym = \mathbf{0.276}$$

$$fy = \mathbf{0.667}$$

Note that the magnitude for both signals is dramatically reduced at  $f = 10 \text{ fy} = 10 \text{ V/L1}$ .

### Compare the Spectral System to the Ideal Fourier Transforms

Deflection is represented by the sum of two negative sinusoids of period  $2L1/V$  seconds. One sinusoid is delayed by a half period in order to cancel out the first. Both are multiplied by the unit step.

One axle response in time domain:

$$\text{Simy}(t) := -1 \cdot \sin\left(\frac{\pi \cdot V \cdot t}{L1}\right) \cdot \Phi(t) - \sin\left[\frac{\pi \cdot V \cdot \left(t - \frac{L1}{V}\right)}{L1}\right] \cdot \Phi\left(t - \frac{L1}{V}\right) \quad \text{where } \Phi(t) = 1 \text{ for } t \geq 0 \text{ and } \Phi(t) = 0 \text{ for } t < 0$$

The second axle is represented by the same function, but delayed by  $S/V$  seconds.

$$\text{Sim2y}(t) := \text{Simy}(t) \cdot P1 + \text{Simy}\left(t - \frac{S}{V}\right) \cdot P2$$

Recall that the equation for deflection in the endspan with the load in the same endspan was as follows:

$$y(x, a) := \frac{1}{6} \cdot \left(1 - \frac{39651}{1778480} \cdot a + \frac{133}{97816400} \cdot a^3\right) \cdot x^3 + \left(\frac{-1051545}{64672} \cdot a - \frac{13217}{3556960} \cdot a^3 + \frac{1}{2} \cdot a^2\right) \cdot x$$

A5-11

The MathCAD continuous Fourier transform for this ideal sinusoidal time representation for deflection is as follows:

$$\text{Sim2ye1}(f) := \frac{y0\left(\frac{L1}{2}, \frac{L1}{2}\right) \cdot \pi \cdot V}{L1 \cdot \left[ (i \cdot 2 \cdot \pi \cdot f)^2 + \frac{\pi^2 \cdot V^2}{(L1)^2} \right]} \cdot \left(1 + e^{-i \cdot 2 \cdot \pi \cdot L1 \cdot \frac{f}{V}}\right) \cdot \left(P1 + P2 \cdot e^{-i \cdot 2 \cdot \pi \cdot S \cdot \frac{f}{V}}\right)$$

$$\text{Sim2ym}(f) := \frac{-1 \cdot y0\left(\frac{L1}{2}, \frac{L1}{2}\right) \cdot \pi \cdot V}{(L2 - L1)} \cdot \left[ \frac{e^{-i \cdot 2 \cdot \pi \cdot L1 \cdot \frac{f}{V}}}{\left[ (i \cdot 2 \cdot \pi \cdot f + \frac{V}{L1})^2 + \frac{\pi^2 \cdot V^2}{(L2 - L1)^2} \right]} + \frac{e^{\frac{L1 - L2}{L1} \cdot i \cdot 2 \cdot \pi \cdot L2 \cdot \frac{f}{V}}}{\left[ (i \cdot 2 \cdot \pi \cdot f + \frac{V}{L1})^2 + \frac{\pi^2 \cdot V^2}{(L2 - L1)^2} \right]} \right] \cdot \left(P1 + P2 \cdot e^{-i \cdot 2 \cdot \pi \cdot S \cdot \frac{f}{V}}\right)$$

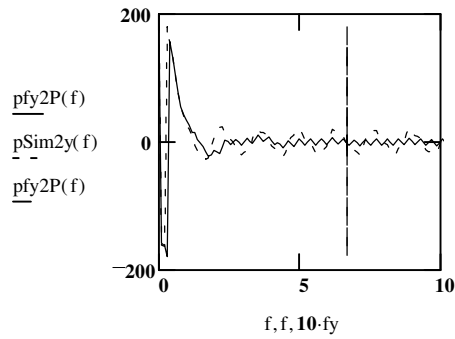
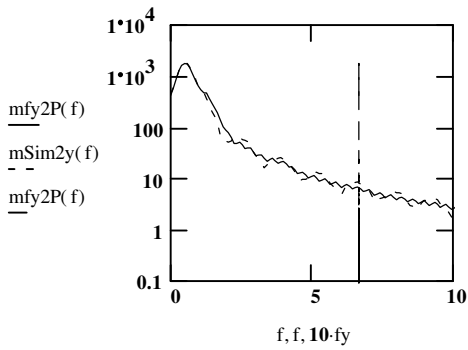
$$\text{Sim2ye2}(f) := \frac{L1}{L2 + L3} \cdot \frac{y0\left(\frac{L1}{2}, \frac{L1}{2}\right) \cdot \pi \cdot V}{(L3 - L2)} \cdot \left[ \frac{e^{-i \cdot 2 \cdot \pi \cdot L2 \cdot \frac{f}{V}}}{\left[ (i \cdot 2 \cdot \pi \cdot f + \frac{V}{L1})^2 + \frac{\pi^2 \cdot V^2}{(L3 - L2)^2} \right]} + \frac{e^{-1} \cdot e^{-i \cdot 2 \cdot \pi \cdot L3 \cdot \frac{f}{V}}}{\left[ (i \cdot 2 \cdot \pi \cdot f + \frac{V}{L1})^2 + \frac{\pi^2 \cdot V^2}{(L3 - L2)^2} \right]} \right] \cdot \left(P1 + P2 \cdot e^{-i \cdot 2 \cdot \pi \cdot S \cdot \frac{f}{V}}\right)$$

$$\text{Sim2y}(f) := \text{Sim2ye1}(f) + \text{Sim2ym}(f) + \text{Sim2ye2}(f)$$

$$\text{mSim2y}(f) := \overline{|\text{Sim2y}(f)|} \quad \text{pSim2y}(f) := \text{if}(\text{Sim2y}(f) = 0, 0, \arg(\text{Sim2y}(f)) \cdot \frac{180}{\pi})$$

BW := 10 where mfy2P(0) is the DC magnitude for the MathCAD transform \*

AS-12



The plots do not completely match because the discrete time representation fy2P is not exactly sinusoidal.

Compare DC magnitude of continuous Fourier transform to the discrete frequency representation mfy2P(0):

$$\text{mSim2y}(0) = 462.311 \quad \text{pSim2y}(0) = 180 \quad \text{mfy2P}(0) = 423.827 \quad \text{pfy2P}(0) = 180$$

\* Note: Tct is used to adjust for MathCAD derivation and R is used to adjust the discrete Fourier transform

Moment is represented by a triangular pulse of period  $L1/V$  seconds.  
The signal is delayed by a half period to account for causal behavior.

One axle response in time domain:

$$\Lambda(T, t) := \frac{T}{2} - |t|$$

$$\text{Simm}(t) := \Lambda\left(\frac{L1}{V}, t - \frac{L1}{2 \cdot V}\right)$$

where  $\Lambda(T, t) = T/2 - t$  for  $0 < t < T$  and  
 $\Lambda(T, t) = T/2 + t$  for  $-T < t < 0$  and  
 $\Lambda(T, t) = 0$  for  $t < -T$  and  $t > T$

The second axle is represented by the same function, but delayed by  $S/V$  seconds.

$$\text{Sim2m}(t) := \text{Simm}(t) \cdot P1 + \text{Simm}\left(t - \frac{S}{V}\right) \cdot P2$$

Recall that the equation for moment in the endspan with the load in the same endspan was as follows:

$$M_0(x, a) := \left(1 - \frac{39651}{1778480} \cdot a + \frac{133}{97816400} \cdot a^3\right) \cdot x$$

A5-13

The MathCAD continuous Fourier transform for this triangular time representation for moment is as follows:

$$\text{Sim2me1}(f) := M0\left(\frac{L1}{2}, \frac{L1}{2}\right) \cdot \frac{L1}{2 \cdot V} \cdot \left[ \frac{\sin\left(\pi \cdot L1 \cdot \frac{f}{2 \cdot V}\right)}{\left(\pi \cdot L1 \cdot \frac{f}{2 \cdot V}\right)} \right]^2 \cdot e^{-i \cdot \pi \cdot L1 \cdot \frac{f}{V}} \cdot \left( P1 + P2 \cdot e^{-i \cdot 2 \cdot \pi \cdot S \cdot \frac{f}{V}} \right)$$

$$\text{Sim2mm}(f) := \frac{-1 \cdot M0\left(\frac{L1}{2}, \frac{L1}{2}\right) \cdot \pi \cdot V}{2 \cdot (L2 - L1)} \cdot \left[ \frac{e^{-i \cdot 2 \cdot \pi \cdot L1 \cdot \frac{f}{V}}}{\left[ \left( i \cdot 2 \cdot \pi \cdot f + \frac{V}{L1} \right)^2 + \frac{\pi^2 \cdot V^2}{(L2 - L1)^2} \right]} + \frac{e^{\frac{L1 - L2}{L1} \cdot i \cdot 2 \cdot \pi \cdot L2 \cdot \frac{f}{V}} \cdot e^{-i \cdot 2 \cdot \pi \cdot L2 \cdot \frac{f}{V}}}{\left[ \left( i \cdot 2 \cdot \pi \cdot f + \frac{V}{L1} \right)^2 + \frac{\pi^2 \cdot V^2}{(L2 - L1)^2} \right]} \right] \cdot \left( P1 + P2 \cdot e^{-i \cdot 2 \cdot \pi \cdot S \cdot \frac{f}{V}} \right)$$

$$\text{Sim2me2}(f) := \frac{M0\left(\frac{L1}{2}, \frac{L1}{2}\right) \cdot \pi \cdot V}{8 \cdot (L3 - L2)} \cdot \left[ \frac{e^{-i \cdot 2 \cdot \pi \cdot L2 \cdot \frac{f}{V}}}{\left[ \left( i \cdot 2 \cdot \pi \cdot f + \frac{V}{L1} \right)^2 + \frac{\pi^2 \cdot V^2}{(L3 - L2)^2} \right]} + \frac{e^{-1} \cdot e^{-i \cdot 2 \cdot \pi \cdot L3 \cdot \frac{f}{V}}}{\left[ \left( i \cdot 2 \cdot \pi \cdot f + \frac{V}{L1} \right)^2 + \frac{\pi^2 \cdot V^2}{(L3 - L2)^2} \right]} \right] \cdot \left( P1 + P2 \cdot e^{-i \cdot 2 \cdot \pi \cdot S \cdot \frac{f}{V}} \right)$$

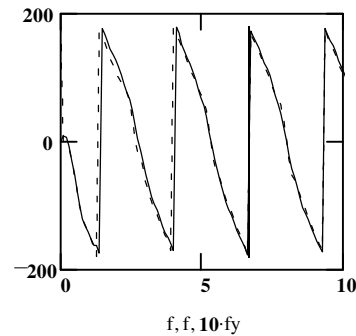
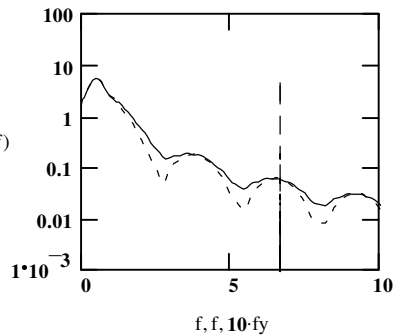
AS-14

$$\text{Sim2m}(f) := \text{Sim2me1}(f) + \text{Sim2mm}(f) + \text{Sim2me2}(f)$$

$$\text{mSim2m}(f) := \text{if}(\text{Sim2m}(f)=0, .00000001, \overline{|\text{Sim2m}(f)|})$$

$$\text{pSim2m}(f) := \text{if}(\text{Sim2m}(f)=0, 0, \arg(\text{Sim2m}(f)) \cdot \frac{180}{\pi}) \quad \text{mSim2m}(0) = 1.571$$

MathCAD does not evaluate the sinc function properly at f=0.



Compare DC magnitude of continuous Fourier transform to the discrete frequency representation  $\text{mfm2P}(0)$ :

$$\text{mSim2m}(0) = 1.571 \quad \text{pSim2m}(0) = 180 \quad \text{mfm2P}(0) = 1.98 \quad \text{pfm2P}(0) = 0$$

MathCAD does not evaluate the sinc function properly at f=0.

\* Note: Tct is used to adjust for MathCAD derivation and R is used to adjust the discrete Fourier transform

## Transform the Spectral System back to the Time Domain

$$\text{SimFY2P}_i := \text{if}\left(i < \frac{\text{Tct}}{2}, \text{Sim2y}(i \cdot \text{fmin}), \text{Sim2y}((\text{floor}(\text{Tct}) - i + 1) \cdot \text{fmin})\right)$$

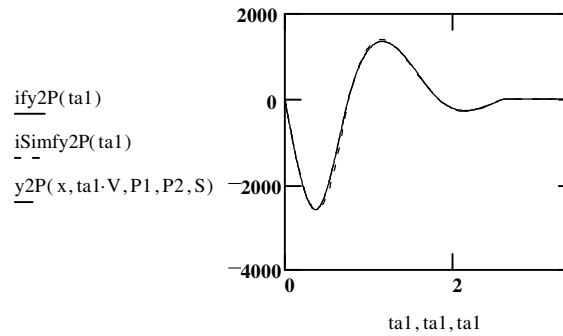
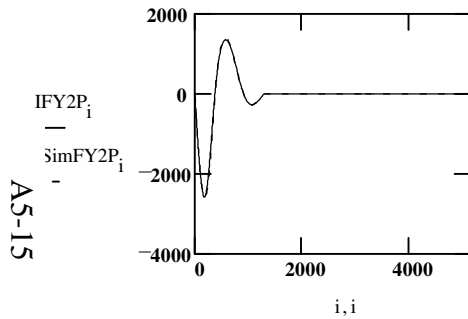
$$\text{SimFM2P}_i := \text{if}\left(i < \frac{\text{Tct}}{2}, \text{Sim2m}(i \cdot \text{fmin}), \text{Sim2m}((\text{floor}(\text{Tct}) - i + 1) \cdot \text{fmin})\right)$$

$$\text{IFY2P} := \text{ICFFT}\left(\frac{\text{FY2P}}{\text{Tct} \cdot \text{R}}\right)$$

$$\text{ISimFY2P} := \text{ICFFT}\left(\frac{\text{SimFY2P}}{\text{Tct} \cdot \text{R}}\right)$$

$$\text{ify2P}(\text{ta1}) := \text{IFY2P}_{\text{floor}\left(\frac{\text{ta1}}{\text{R}}\right)}$$

$$\text{iSimfy2P}(\text{ta1}) := \text{ISimFY2P}_{\text{floor}\left(\frac{\text{ta1}}{\text{R}}\right)}$$

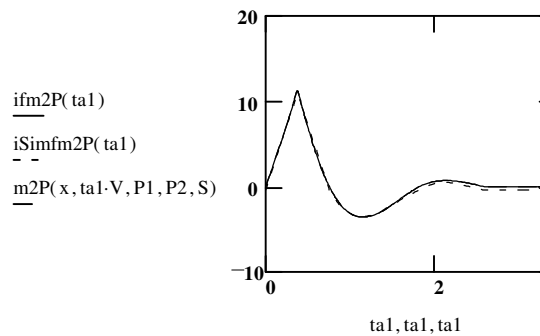
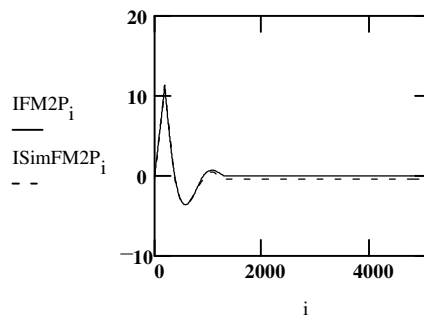


$$\text{IFM2P} := \text{ICFFT}\left(\frac{\text{FM2P}}{\text{Tct} \cdot \text{R}}\right)$$

$$\text{ISimFM2P} := \text{ICFFT}\left(\frac{\text{SimFM2P}}{\text{Tct} \cdot \text{R}}\right)$$

$$\text{ifm2P}(\text{ta1}) := \text{IFM2P}_{\text{floor}\left(\frac{\text{ta1}}{\text{R}}\right)}$$

$$\text{iSimfm2P}(\text{ta1}) := \text{ISimFM2P}_{\text{floor}\left(\frac{\text{ta1}}{\text{R}}\right)}$$



$$\text{ifm2P}(3) = -8.917 \cdot 10^{-15} - 3.155 \cdot 10^{-15} i$$

$$\text{iSimfm2P}(3) = -0.418 - 2.32 \cdot 10^{-6} i$$

MathCAD does not evaluate the sinc function properly at  $f=0$ .

## APPENDIX A6

Elastic Deformation of the End Span of a Three Span Beam under Dynamic Truckload

## Elastic Deformation of a Single Span Beam under Dynamic Equilibrium

Supports are located at  $x = \{0, L\}$ .

Consider the differential equation for the Bournoulli-Euler beam model:

$$\frac{d^2}{dt^2} y(x, t) \cdot m(x) + \frac{d}{dt} y(x, t) \cdot c(x) + \frac{d^2}{dx^2} \left[ EI(x) \cdot \left( \frac{d^2}{dx^2} y(x, t) + a \cdot \frac{d^2}{dx^2} \frac{d}{dt} y(x, t) \right) \right] = p(x, t)$$

Let us assume that mass,  $m(x)$ , viscous damping,  $c(x)$ , Rayleigh or rate-independent damping,  $a$ , and inertia,  $I(x)$ , are all longitudinally uniform.

Seperation of variables

Let  $y(x, t) = \phi(x)q(t)$ .

Let  $\phi'$  represent the spatial derivative and

Then,  $y' = q\phi'$  and  $y'' = q\phi''$ .

Let  $q^*$  represent the temportal derivative.

Arranged according to  $q$ :  $m \phi q^{**} + [c \phi + a E I \phi'''] q^* + E I \phi'''' q = p$

Arranged according to  $\phi$ :  $[a E I q^* + E I q] \phi'''' + [m q^{**} + c q^*] \phi = p$

In the case of free or unforced vibration,  $\phi''''/\phi = -(m q^{**} + c q^*) / EI (a q^* + q) = \beta = \alpha^4$

$$m q^{**} + (c - a\beta EI) q^* - \beta EI q = 0.$$

$$\beta := \alpha^4$$

$$\phi'''' - \beta \phi = 0.$$

The general solution for the former ODE is as follows:

$$q(t) := q(t_0) \cdot e^{-\zeta \cdot \omega_n \cdot t} \cdot \left( \cos(\omega_d \cdot t) + \frac{\zeta}{\sqrt{1 - \zeta^2}} \cdot \sin(\omega_d \cdot t) \right)$$

where

$$\omega_n := \sqrt{\frac{K}{m}} \quad \zeta := \frac{C}{2 \cdot m \cdot \omega_n} \quad \omega_d := \omega_n \cdot \sqrt{1 - \zeta^2} \quad f_n := \frac{\omega_n}{2 \cdot \pi} \quad K := \beta \cdot EI \quad C := c - a \cdot \beta \cdot EI$$

here

The general solution for the latter ODE is  $\phi(x) = C_1 \sin \alpha x + C_2 \cos \alpha x + C_3 \sinh \alpha x + C_4 \cosh \alpha x$ .

For a uniform simply supported beam, deflection and moment are zero at the first support.

$$\phi(0) = 0. \quad \text{Hence, } C_2 + C_4 = 0.$$

$$EI \phi''(0) = 0. \quad \text{Hence, } -\alpha^2 (C_2 - C_4) = 0.$$

$$\text{Hence, } C_2 = C_4 = 0.$$

For a single span beam, deflection and moment are zero at the other end support.

$$\phi(L) = 0. \quad \text{Hence, } C_1 \sin \alpha L + C_3 \sinh \alpha L = 0.$$

$$EI \phi''(L) = 0. \quad \text{Hence, } -\alpha^2 (C_1 \sin \alpha L - C_3 \sinh \alpha L) = 0.$$

$$\text{Hence, } C_3 = 0.$$

Finally, there are an infinite number of solutions of the form:

$\phi(x) = C_1 \sin \alpha x$ , where  $\alpha = n\pi/L$  and  $n$  is any integer.  $C_1$  is arbitrary.

Hence, for a single span beam:

$$\alpha := \frac{n \cdot \pi}{L} \quad \beta := \left( \frac{n \cdot \pi}{L} \right)^4 \quad \omega_n := \sqrt{\frac{\beta \cdot EI}{m}} \quad \omega_n := \frac{n^2 \cdot \pi^2}{L^2} \cdot \sqrt{\frac{EI}{m}} \quad \phi(n, x) := C_{11} \cdot \sin(\alpha \cdot x)$$

Natural Frequency for a 3-span, Symmetrical Beam [Kolousek, 1973]

$$L1 := 55 \quad L2 := 133 \quad \text{feet} \quad m := 0.03 \frac{\text{kips} \cdot \text{sec}^2}{\text{ft}} \quad E := 29000 \cdot 12^2 \frac{\text{kips}}{\text{ft}^2} \quad I1 := \frac{54100 \cdot 0.5}{12^4} \text{ft}^4 \quad I2 := I1$$

Reading bridge, HAM-42-0992

W36x150, Beam spacing of 7' 9", Deck thickness of 8.5"

Mass (m) assumes 150 lb/ft steel and 145 lb/ft<sup>3</sup> concrete

Inertia (I1 and I2) assumes unintended composite action of 50%

$$E \cdot I1 = 5.448 \cdot 10^6 \text{ kips} \cdot \text{ft}^2$$

$$wt := 150 + 145 \cdot \frac{8.5}{12} \cdot \left(7 + \frac{9}{12}\right)$$

$$m := \frac{wt}{32800} \quad m = 0.029$$

$$K := \frac{L1}{L2 - L1} \cdot \left(\frac{I2}{I1}\right)^{.25} \quad \frac{L1}{L2 - L1} \cdot \left(\frac{I2}{I1}\right)^{.25} = 0.705$$

x := 3 Initial guess for MathCAD

$$y := \text{root} \left[ \begin{array}{l} \left( 0.000000298 \cdot \frac{I1 \cdot K^{12}}{L1} \right) \cdot x^{12} \dots \\ + \left( 0.000071463 \cdot \frac{I1 \cdot K^8}{L1} + 0.000031966 \cdot \frac{I2}{L2 - L1} \right) \cdot x^8 \dots \\ + \left( 0.019048 \cdot \frac{I1 \cdot K^4}{L1} + 0.016667 \cdot \frac{I2}{L2 - L1} \right) \cdot x^4 \dots \\ + \frac{-3 \cdot I1}{L1} - \frac{2 \cdot I2}{L2 - L1} \end{array} \right], x$$

$$\lambda1 := K \cdot y \quad \lambda1 = 2.652$$

$$\lambda2 := y \quad \lambda2 = 3.761$$

$$\omega_n := \frac{\lambda1^2}{L1^2} \cdot \sqrt{\frac{E \cdot I1}{m}} \quad \omega_n = 31.953$$

Natural Frequency for 3 continuous spans, with symmetrical lengths (i.e. equal endspans)

$$\omega_n := \frac{\lambda2^2}{(L2 - L1)^2} \cdot \sqrt{\frac{E \cdot I2}{m}} \quad \omega_n = 31.953$$

$$fn := \frac{\omega_n}{2 \cdot \pi} \quad fn = 5.085$$

Natural Frequency for noncontinuous end span

$$\omega1 := \frac{\pi^2}{L1^2} \cdot \sqrt{\frac{E \cdot I1}{m}} \quad \omega1 = 44.84$$

$$f1 := \frac{\omega1}{2 \cdot \pi} \quad f1 = 7.137$$

Natural Frequency for noncontinuous middle span

$$\omega2 := \frac{\pi^2}{(L2 - L1)^2} \cdot \sqrt{\frac{E \cdot I2}{m}} \quad \omega2 = 22.295$$

$$f2 := \frac{\omega2}{2 \cdot \pi} \quad f2 = 3.548$$

Natural Frequency for a 3-span, Symmetrical Beam [Kolousek, 1973]

$$L1 := 40 \quad L2 := 128 \quad \text{feet} \quad m := 0.03 \frac{\text{kips} \cdot \text{sec}^2}{\text{ft}} \quad E := 29000 \cdot 12^2 \frac{\text{kips}}{\text{ft}^2} \quad I1 := \frac{54100 \cdot 0.33}{12^4} \text{ft}^4 \quad I2 := \frac{42000}{12^4}$$

Hamilton bridge, HAM-126-0881

W36x164, Beam spacing of 9' 9.625", Deck thickness of 8.75"

Mass (m) assumes 150 lb/ft steel and 140 lb/ft<sup>3</sup> concrete

Endspan Inertia (I1) assumes unintended composite action of 33%

Midspan Inertia (I2) was designed for 100% composite action

$$E \cdot I1 = 3.595 \cdot 10^6 \text{ kips} \cdot \text{ft}^2$$

$$wt := 194 + 140 \cdot \frac{8.75}{12} \cdot \left( 9 + \frac{9.625}{12} \right)$$

$$m := \frac{wt}{32800} \quad m = 0.036$$

$$K := \frac{L1}{L2 - L1} \cdot \left( \frac{I2}{I1} \right)^{.25} \quad \frac{L1}{L2 - L1} \cdot \left( \frac{I2}{I1} \right)^{.25} = 0.563$$

x := 3 Initial guess for MathCAD

$$y := \text{root} \left[ \left[ \begin{array}{l} \left( 0.000000298 \cdot \frac{I1 \cdot K^{12}}{L1} \right) \cdot x^{12} \dots \\ + \left( 0.000071463 \cdot \frac{I1 \cdot K^8}{L1} + 0.000031966 \cdot \frac{I2}{L2 - L1} \right) \cdot x^8 \dots \\ + \left( 0.019048 \cdot \frac{I1 \cdot K^4}{L1} + 0.016667 \cdot \frac{I2}{L2 - L1} \right) \cdot x^4 \dots \\ + \frac{-3 \cdot I1}{L1} - \frac{2 \cdot I2}{L2 - L1} \end{array} \right], x \right]$$

$$\lambda1 := K \cdot y \quad \lambda1 = 2.1$$

$$\lambda2 := y \quad \lambda2 = 3.731$$

$$\omega_n := \frac{\lambda1^2}{L1^2} \cdot \sqrt{\frac{E \cdot I1}{m}} \quad \omega_n = 27.392$$

Natural Frequency for 3 continuous spans, with symmetrical lengths (i.e. equal endspans)

$$\omega_n := \frac{\lambda2^2}{(L2 - L1)^2} \cdot \sqrt{\frac{E \cdot I2}{m}} \quad \omega_n = 27.392$$

$$fn := \frac{\omega_n}{2 \cdot \pi} \quad fn = 4.36$$

Natural Frequency for noncontinuous end span

$$\omega1 := \frac{\pi^2}{L1^2} \cdot \sqrt{\frac{E \cdot I1}{m}} \quad \omega1 = 61.288$$

$$f1 := \frac{\omega1}{2 \cdot \pi} \quad f1 = 9.754$$

Natural Frequency for noncontinuous middle span

$$\omega2 := \frac{\pi^2}{(L2 - L1)^2} \cdot \sqrt{\frac{E \cdot I2}{m}} \quad \omega2 = 19.422$$

$$f2 := \frac{\omega2}{2 \cdot \pi} \quad f2 = 3.091$$

## Elastic Deformation of a Single Span Beam under Dynamic Conditions

We assume a moving load  $p(x,t) = P\delta(x-vt)$ .

Supports are located at  $x = \{0, L\}$ .

Note that the modulus of elasticity  $E$  and the beam inertia  $I$  are considered uniform for the beam.

$$\frac{d^2}{dt^2} y(x,t) \cdot m(x) + \frac{d^2}{dx^2} \left[ EI(x) \cdot \left( \frac{d^2}{dx^2} y(x,t) + a \cdot \frac{d}{dx^2} \frac{d}{dt} y(x,t) \right) \right] = p(x,t)$$

Let us assume that mass,  $m(x)$ , Rayleigh or rate-independent damping,  $a$ , and inertia,  $I(x)$ , are all longitudinally uniform. Viscous damping,  $c(x)$ , is not considered due to orthogonality assumption.

Separation of variables

Let  $y(x,t) = \phi(x)q(t)$ .

Let  $\phi'$  represent the spatial derivative and

Then,  $y' = q\phi'$  and  $y'' = q\phi''$ .

Let  $q^*$  represent the temporal derivative.

Arranged according to  $q$ :  $m\phi q^{**} + aEI\phi''' q^* + EI\phi'''' q = p$

Arranged according to  $\phi$ :  $[aEIq^* + EIq]\phi'''' + mq^{**}\phi = p$

$$y(x,t) := \sum_{n=1}^{\infty} \phi(n,x) \cdot q(n,t)$$

In the case of forced vibration,

We multiply each of the above PDE terms by  $\phi(r,x)$ , integrate over the beam length, and interchange the order of integration and summation to get the following:

$$\begin{aligned} & \sum_{n=1}^{\infty} \frac{d^2}{dt^2} q(n,t) \cdot \int_0^L m \cdot \phi(n,x) \cdot \phi(r,x) dx \dots = \int_0^L p(x,t) \cdot \phi(r,x) dx \\ & + \sum_{n=1}^{\infty} \frac{d}{dt} q(n,t) \cdot \int_0^L (a \cdot EI \cdot \phi'''(n,x)) \cdot \phi(r,x) dx \dots \\ & + \sum_{n=1}^{\infty} q(n,t) \cdot \int_0^L EI \cdot \phi''''(n,x) \cdot \phi(r,x) dx \end{aligned}$$

By virtue of orthogonality properties of the modes, all terms in each summation vanish except for the case where  $n=r$ , leaving the following:

$$\begin{aligned} \frac{d^2}{dt^2} q(n,t) \cdot \int_0^L m \cdot \phi(n,x)^2 dx \dots &= \int_0^L p(x,t) \cdot \phi(n,x) dx \\ + \frac{d}{dt} q(n,t) \cdot \int_0^L (a \cdot EI \cdot \phi''''(n,x)) \cdot \phi(n,x) dx \dots & \\ + q(n,t) \cdot \int_0^L EI \cdot \phi''''(n,x) \cdot \phi(n,x) dx & \end{aligned}$$

This has the familiar form of the second order ODE for a mechanical MKC system:

$$m \ddot{q} + C \dot{q} + K q = p(t).$$

where:

$$P(n,t) := \int_0^L p(x,t) \cdot \phi(n,x) dx \quad M_{\text{beam}}(n) := \int_0^L m \cdot \phi(n,x)^2 dx$$

$$C_{\text{beam}}(n) := \int_0^L (a \cdot EI \cdot \phi''''(n,x)) \cdot \phi(n,x) dx \quad K_{\text{beam}}(n) := \int_0^L EI \cdot \phi''''(n,x) \cdot \phi(n,x) dx$$

which, by integration by parts, can be simplified to:

$$C_{\text{beam}}(n) := \int_0^L a \cdot EI \cdot \phi''(n,x)^2 dx \quad K_{\text{beam}}(n) := \int_0^L EI \cdot \phi''(n,x)^2 dx$$

For the single span beam,

$$\alpha := \frac{n \cdot \pi}{L} \quad \beta := \left( \frac{n \cdot \pi}{L} \right)^4 \quad \omega_n := \sqrt{\frac{\beta \cdot EI}{m}} \quad \omega_n := \frac{n^2 \cdot \pi^2}{L^2} \cdot \sqrt{\frac{EI}{m}}$$

$$\phi(n,x) := \sin\left(\frac{n \cdot \pi}{L} \cdot x\right)$$

$$\phi'(n,x) := \cos\left(\frac{n \cdot \pi}{L} \cdot x\right) \cdot \frac{n \cdot \pi}{L}$$

$$\phi''(n,x) := -\sin\left(\frac{n \cdot \pi}{L} \cdot x\right) \cdot \left(\frac{n \cdot \pi}{L}\right)^2$$

$$P(n, t) := \int_0^L P \cdot \delta(x, v \cdot t) \cdot \phi(n, x) \, dx \quad P(n, t) := P \cdot \phi(n, v \cdot t) \quad P_{\text{beam}}(n, t) := P \cdot \sin\left(\frac{n \cdot \pi}{L} \cdot v \cdot t\right)$$

$$M_{\text{beam}}(n) := \int_0^L m \cdot \phi(n, x)^2 \, dx \quad M_{\text{beam}}(n) := \frac{1}{2} \cdot \frac{(-\cos(\alpha \cdot L) \cdot \sin(\alpha \cdot L) + \alpha \cdot L)}{\alpha} \cdot m \quad M_{\text{beam}}(n) := \frac{m \cdot L}{2}$$

$$K_{\text{beam}}(n) := \int_0^L EI \cdot \phi''(n, x)^2 \, dx \quad K_{\text{beam}}(n) := \frac{1}{2} \cdot EI \cdot \frac{(-\cos(\alpha \cdot L) \cdot \sin(\alpha \cdot L) + \alpha \cdot L)}{\alpha} \cdot \alpha^4 \quad K_{\text{beam}}(n) := \frac{L \cdot EI \cdot \left(\frac{n \cdot \pi}{L}\right)^4}{2}$$

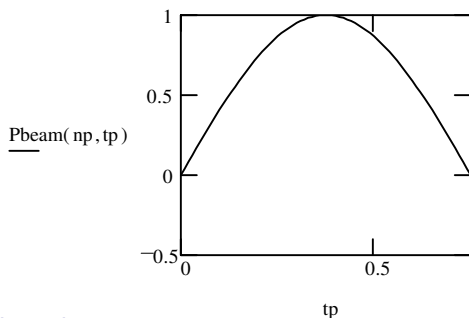
$$C_{\text{beam}}(n) := \int_0^L a \cdot EI \cdot \phi''(n, x)^2 \, dx \quad \text{Based upon the above, } C_{\text{beam}}(n) := \frac{L \cdot a \cdot EI \cdot \left(\frac{n \cdot \pi}{L}\right)^4}{2}$$

### Dynamic Response of a Single Span Beam to a Traversing Load

$$L \equiv 55 \quad P \equiv 1 \quad \text{speed} \equiv 50 \quad v := \text{speed} \cdot \frac{5280}{3600} \quad v = 73.333$$

$$t_p := 0.01 \cdot \frac{L}{v} \quad n_p := 1 \quad n := 1$$

$$P_{\text{beam}}(n, t) := P \cdot \sin\left(\frac{n \cdot \pi}{L} \cdot v \cdot t\right)$$



For all cases of  $n$ , the system input is a forced sinusoid with a frequency  $\omega = n\pi v/L$  for a duration of  $t_d = L/v$ .

After  $t_d$ , the system is unforced and the vibrations are exponentially damped to zero.

$$\omega(n, v, L) := n \cdot \pi \cdot \frac{v}{L} \quad f := \frac{\omega(n, v, L)}{2 \cdot \pi} \quad t_d := \frac{L}{v}$$

$$\omega(n, v, L) = 4.189 \quad f = 0.667 \quad t_d = 0.75$$

given that

$$\omega_n := \sqrt{\frac{K_{\text{beam}}(n)}{M_{\text{beam}}(n)}} \quad \zeta := \frac{C_{\text{beam}}(n)}{2 \cdot M_{\text{beam}}(n) \cdot \omega_n} \quad \omega_d := \omega_n \cdot \sqrt{1 - \zeta^2} \quad f_n := \frac{\omega_n}{2 \cdot \pi}$$

$$\omega_n = 44.177 \quad \zeta = 0.022 \quad \omega_d = 44.166 \quad f_n = 7.031$$

$$\omega(n) := \sqrt{\frac{K_{\text{beam}}(n)}{M_{\text{beam}}(n)}} \quad \zeta(n) := \frac{C_{\text{beam}}(n)}{2 \cdot M_{\text{beam}}(n) \cdot \omega(n)} \quad \omega d(n) := \omega(n) \cdot \sqrt{1 - \zeta(n)^2} \quad f(n) := \frac{\omega(n)}{2 \cdot \pi}$$

In defining the beam response, several coefficients are important to define:

$$\text{partC}(n, v, L, P) := \frac{P}{K_{\text{beam}}(n)} \cdot \frac{1 - \frac{\omega(n, v, L)^2}{\omega(n)^2}}{\left[ \left( 1 - \frac{\omega(n, v, L)^2}{\omega(n)^2} \right)^2 + 4 \cdot \zeta(n)^2 \cdot \frac{\omega(n, v, L)^2}{\omega(n)^2} \right]}$$

Note that

$$\frac{\omega(1, v, L)^2}{\omega(1)^2} = 8.991 \cdot 10^{-3}$$

is very small.

Hence partC reduces to P/Kbeam(n) and partD is approx. zero.

$$\text{partD}(n, v, L, P) := \frac{P}{K_{\text{beam}}(n)} \cdot \frac{-2 \cdot \zeta(n) \cdot \frac{\omega(n, v, L)}{\omega(n)}}{\left[ \left( 1 - \frac{\omega(n, v, L)^2}{\omega(n)^2} \right)^2 + 4 \cdot \zeta(n)^2 \cdot \frac{\omega(n, v, L)^2}{\omega(n)^2} \right]}$$

$$\text{partC}(1, v, L, P) = 6.267 \cdot 10^{-4}$$

$$\text{partD}(1, v, L, P) = -2.649 \cdot 10^{-6}$$

$$\text{partC}(n, v, L, P) := \frac{P}{K_{\text{beam}}(n)}$$

$$\text{partC}(1, v, L, P) = 6.211 \cdot 10^{-4}$$

For the case of zero initial conditions  $q(0) = \dot{q}(0) = 0$ :

$$\text{compA}(n, v, L, P) := -\text{partD}(n, v, L, P)$$

$$\text{compA}(1, v, L, P) = 2.649 \cdot 10^{-6}$$

$$\text{compB}(n, v, L, P) := \frac{\omega(n, v, L) \cdot \text{partC}(n, v, L, P) + \zeta(n) \cdot \omega(n) \cdot \text{partD}(n, v, L, P)}{-\omega d(n)}$$

$$\text{compB}(1, v, L, P) = -5.885 \cdot 10^{-5}$$

$$\text{compB}(n, v, L, P) := \frac{\omega(n, v, L) \cdot \text{partC}(n, v, L, P)}{-\omega d(n)}$$

$$\text{compB}(1, v, L, P) = -5.891 \cdot 10^{-5}$$

The general solution for the forced ODE is as follows:

$$qf(n, v, L, P, t) := \text{partC}(n, v, L, P) \cdot \sin(\omega(n, v, L) \cdot t) + \text{partD}(n, v, L, P) \cdot \cos(\omega(n, v, L) \cdot t) \dots \\ + e^{-\zeta(n) \cdot \omega(n) \cdot t} \cdot (\text{compA}(n, v, L, P) \cdot \cos(\omega d(n) \cdot t) + \text{compB}(n, v, L, P) \cdot \sin(\omega d(n) \cdot t))$$

The first term simplifies to the input forcing function, scaled by the beam stiffness.

The next two terms are not significant, and the final term represents the bouncy response modes.

The temporal derivative of  $qf(t)$  is defined by  $dqf(t)$ :

$$dqf(n, v, L, P, t) := \text{partC}(n, v, L, P) \cdot \cos(\omega(n, v, L) \cdot t) \cdot \omega(n, v, L) - \text{partD}(n, v, L, P) \cdot \sin(\omega(n, v, L) \cdot t) \cdot \omega(n, v, L) \dots \\ + -\zeta(n) \cdot \omega(n) \cdot \exp(-\zeta(n) \cdot \omega(n) \cdot t) \cdot \left( \text{compA}(n, v, L, P) \cdot \cos(\omega d(n) \cdot t) \dots \right) \dots \\ + \exp(-\zeta(n) \cdot \omega(n) \cdot t) \cdot \left( -\text{compA}(n, v, L, P) \cdot \sin(\omega d(n) \cdot t) \cdot \omega d(n) \dots \right) \dots \\ \left( + \text{compB}(n, v, L, P) \cdot \cos(\omega d(n) \cdot t) \cdot \omega d(n) \right) \dots$$

The general solution for the unforced ODE is as follows:

$$q_{ss}(n, v, L, P, t, t_d) := e^{-\zeta(n) \cdot \omega_d(n) \cdot (t - t_d)} \cdot \left[ \begin{array}{l} q_f(n, v, L, P, t_d) \cdot \cos(\omega_d(n) \cdot (t - t_d)) \dots \\ + \frac{dq_f(n, v, L, P, t_d) + \zeta(n) \cdot \omega_d(n) \cdot q_f(n, v, L, P, t_d)}{\omega_d(n)} \cdot \sin(\omega_d(n) \cdot (t - t_d)) \end{array} \right]$$

$$q_{ss}(n, v, L, P, t_d, t_d) = -2.559 \cdot 10^{-5}$$

$$q_f(n, v, L, P, t_d) = -2.559 \cdot 10^{-5} \quad dq_f(n, v, L, P, t_d) = -2.458 \cdot 10^{-3}$$

$$q(n, v, L, P, t, t_d) := \text{if}(t < 0, 0, \text{if}(t < t_d, q_f(n, v, L, P, t), q_{ss}(n, v, L, P, t, t_d))) \quad t_{SS}(n) := \frac{2}{\zeta(n) \cdot \omega_d(n)}$$

$$t_{SS}(1) = 2.05$$

Notes:      the forced system response is defined by the modes  $n\pi v/L$  of the load p.  
               the second term of the forced response is not significant (i.e. the  $\sin(\omega t)$  term dominates).  
               the scaling term of the forced response is approximated by  $P/K_{beam}(n)$ .

Notes:      the unforced system response is defined by the modes  $\omega_d(n)$  of the beam.  
               the modes  $\omega_d(n)$  are approximated by  $\omega_n(n)$  due to the low damping ratio  $\zeta$ .

Example Temporal Response of Beam (Unscaled)

Note: q(t) represents vertical displacement in the direction of gravity (downwards)

Mass	Modulus x Inertia	Viscous Damping	Rayleigh Damping	Mode
$m = 0.03 \frac{\text{kips} \cdot \text{sec}^2}{\text{ft}}$	$EI = 5.5 \cdot 10^6 \text{ kips} \cdot \text{ft}^2$	$c = 0 \frac{\text{kips} \cdot \text{sec}}{\text{ft}^2}$	$a = .001 \text{ sec}$	$np := 1$

$$tq := 0, .01 .. td + tSS(np)$$

$$M_{\text{beam}}(n) := \frac{m \cdot L}{2}$$

$$M_{\text{beam}}(np) = 0.825$$

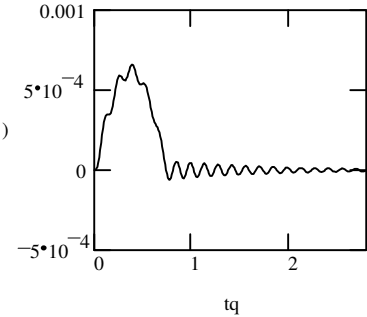
$$K_{\text{beam}}(n) := \frac{L \cdot EI \cdot \left(\frac{n \cdot \pi}{L}\right)^4}{2}$$

$$K_{\text{beam}}(np) = 1.61 \cdot 10^3$$

$$C_{\text{beam}}(n) := \frac{L \cdot a \cdot EI \cdot \left(\frac{n \cdot \pi}{L}\right)^4}{2}$$

$$C_{\text{beam}}(np) = 1.61$$

$q(np, v, L, P, tq, td)$



damping ratio

modal frequency

$$\omega n(np) = 44.177 \quad \zeta(np) = 0.022 \quad \omega d(np) = 44.166 \quad f n(np) = 7.031$$

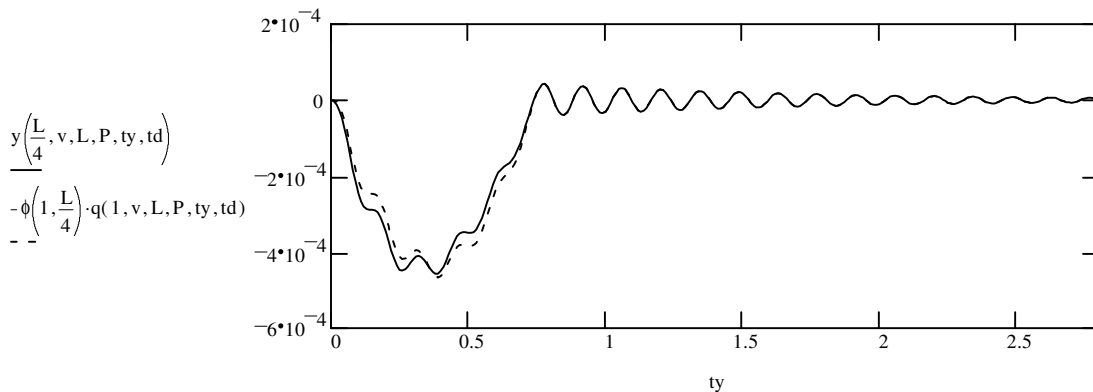
Notes: The damping ratio  $\zeta$  of most structures is less than 0.2

It is observed that higher modes have less significance upon the system response because:

1. Their magnitude is diminished by a factor of  $n^4$
2. Their Rayleigh component of the damping ratio is increased by a factor of  $n^2$

$$y(x, v, L, P, t, td) := \sum_{i=1}^3 -\phi(i, x) \cdot q(i, v, L, P, t, td) \quad ty := 0, .01 .. td + tSS(1)$$

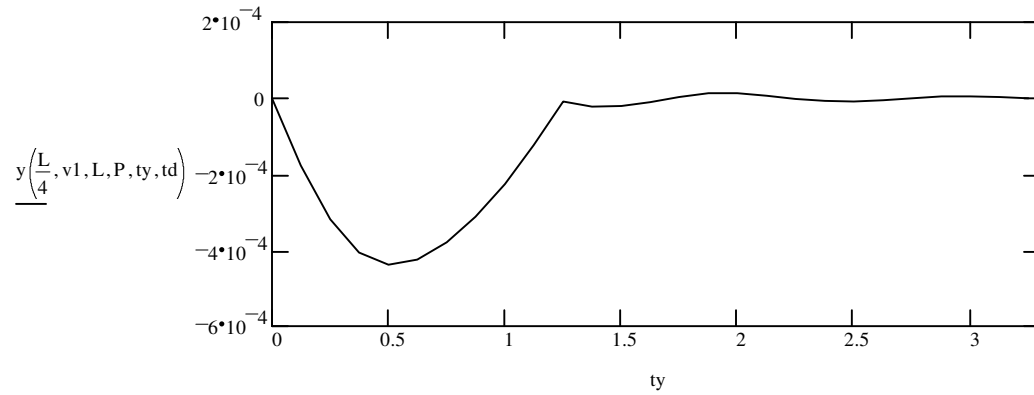
Let us examine the beam's response to an axle load at one quarter of its span length (i.e., the quarterspan)



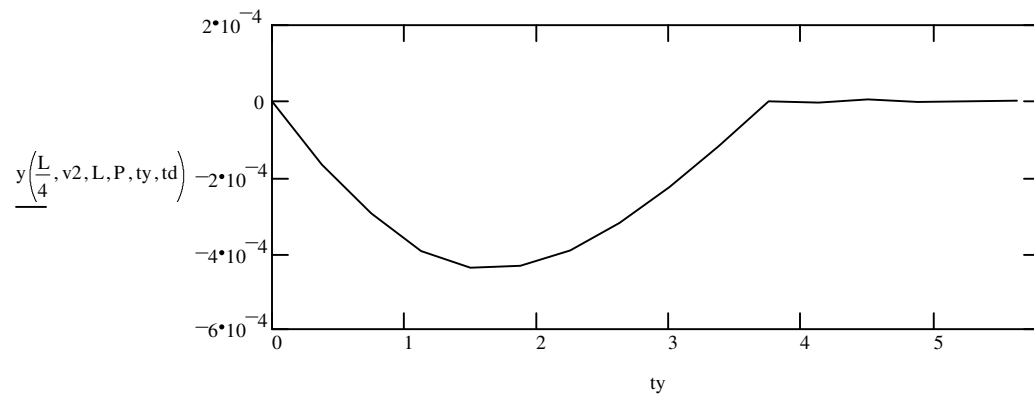
Note that the mode functions  $\phi(n, x)$  simply act to scale the temporal shape, depending upon the gaged location upon the beam.

Let's examine the effect of vehicle speed:

$$v1 := 30 \cdot \frac{5280}{3600} \quad v1 = 44 \quad td := \frac{L}{v1} \quad td = 1.25 \quad ty := 0, \frac{td}{10} .. td + tSS(1)$$



$$v2 := 10 \cdot \frac{5280}{3600} \quad v2 = 14.667 \quad td := \frac{L}{v2} \quad td = 3.75 \quad ty := 0, \frac{td}{10} .. td + tSS(1)$$



Note that, with decreasing vehicle speed, the bouncy beam response is diminished and the vehicle loading duration,  $td$ , is increased. The general loading shape and magnitude remain unchanged.

## Dynamic Response of a Single Span Beam to a Step Load

Here, we consider a system input of  $P(x,t) = P \delta(x-\xi) u(t)$ , where  $u(t)$  is the temporal step function.

$\xi := \frac{L}{2}$  Load position,  $\xi$ , is considered at the beam midspan

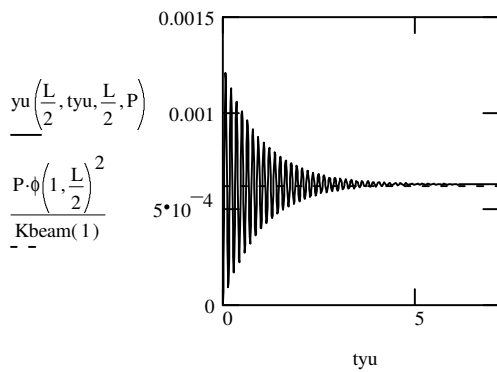
$n := 1$  Let us initially consider the first mode

$P_{beam}(n) := P \cdot \sin\left(\frac{n \cdot \pi \cdot \xi}{L}\right)$        $P_{beam}(n) = 1$       Hence, the input to the MKC system is constant

The complete PDE solution for the step load response is:

$$y_u(x, t, \xi, P) := \sum_{i=1}^5 \frac{2 \cdot P \cdot \phi(i, \xi)}{L \cdot EI \cdot \left(\frac{i \cdot \pi}{L}\right)^4} \left[ 1 - e^{-\zeta(i) \cdot \omega_n(i) \cdot t} \left( \cos(\omega_d(i) \cdot t) + \frac{\zeta(i)}{\sqrt{1 - \zeta(i)^2}} \cdot \sin(\omega_d(i) \cdot t) \right) \right] \cdot \phi(i, x)$$

$$t_{SSu}(n) := \frac{7}{\zeta(n) \cdot \omega_n(n)} \quad t_{yu} := 0, .01 \dots t_{SSu}(1)$$



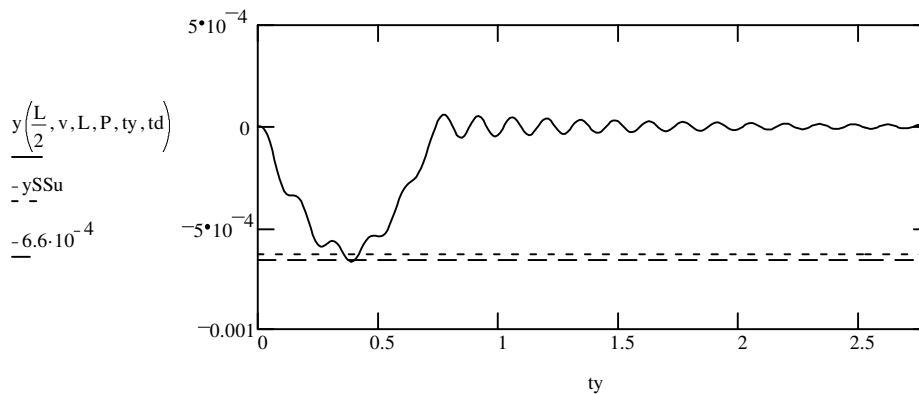
Note that the steady-state displacement  $y_{SSu}$  to a kip load is approximated by considering only the first mode:

$$y_{SSu} := \sum_{i=1}^5 \frac{2 \cdot P \cdot \phi\left(i, \frac{L}{2}\right)^2}{L \cdot EI \cdot \left(\frac{i \cdot \pi}{L}\right)^4} \sim \frac{P \cdot \phi\left(1, \frac{L}{2}\right)^2}{K_{beam}(1)} = 6.211 \cdot 10^{-4}$$

$$y_{SSu} = 6.298 \cdot 10^{-4}$$

$$t_{SS}(n) := \frac{2}{\zeta(n) \cdot \omega_n(n)} \quad t_d := \frac{L}{v} \quad t_y := 0, .01 \dots t_d + t_{SS}(1)$$

Impact Factor (IF) can be assessed by comparing the steady state of the step response  $y_{SSu}$  to the maximum response of the complete axle response at the midspan of the beam.



Dynamic Amplification:

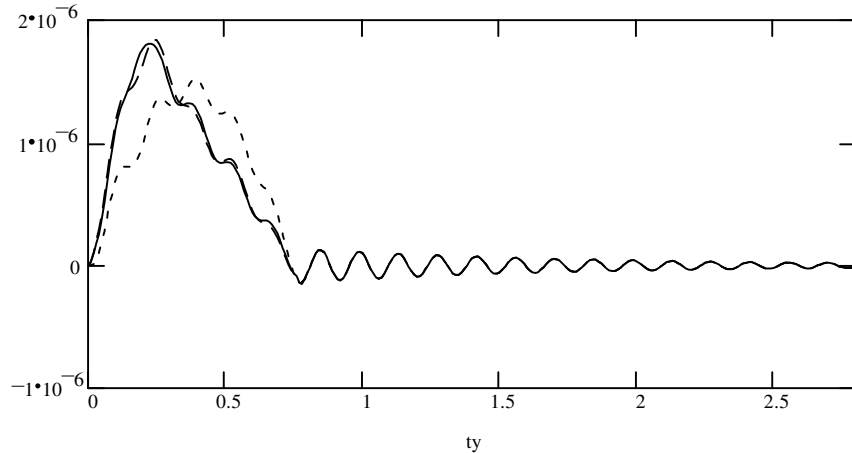
$$IF := \frac{-6.6 \cdot 10^{-4} + y_{SSu}}{-y_{SSu}} + 1$$

$$IF = 1.048$$

Let us examine the moment response for the instrumented node at quarterspan of the beam:

$$M(x, v, L, P, t, td) := \sum_{i=1}^{19} -\phi''(i, x) \cdot q(i, v, L, P, t, td) \quad ty := 0, .01.. td + tSS(1)$$

$$\frac{M\left(\frac{L}{4}, v, L, P, ty, td\right)}{-\phi''\left(1, \frac{L}{4}\right) \cdot q(1, v, L, P, ty, td) - \sum_{i=1}^5 -\phi''\left(i, \frac{L}{4}\right) \cdot q(i, v, L, P, ty, td)}$$



Note that it requires the contributions of many modes to approach the triangular moment response. It is far less cumbersome to represent the waveform by two linear equations for each slope.

In only using the first five loading modes, we approach the triangular waveform, but there is still considerable error in estimating the peak response. The steady-state waveform, however, appears to have converged with only five bridge modes.

In summary, the following # of modes are necessary for an acceptable estimate:

Forced displacement response                      First three load modes,  $\omega = \{\pi v/L, 2\pi v/L, \text{ and } 3\pi v/L\}$

Forced moment response                              First nineteen load modes  $\{n\pi v/L, \text{ for } n=1..19\}$

Steady-state response                                First three beam modes,  $\omega_d \sim \omega_n$

#### Vehicle loading modes

$\omega := \pi \frac{v}{L}$	$\omega = 4.189$	$2 \cdot \omega = 8.378$	$10 \cdot \omega = 41.888$	$19 \cdot \omega = 79.587$	rad/sec	
$f := \frac{\omega}{2 \cdot \pi}$	$f = 0.667$	$2 \cdot f = 1.333$	$10 \cdot f = 6.667$	$19 \cdot f = 12.667$	Hz	speed = 50 mph
	$\frac{f}{5} = 0.133$	$\frac{2 \cdot f}{5} = 0.267$	$\frac{10 \cdot f}{5} = 1.333$	$\frac{19 \cdot f}{5} = 2.533$	Hz	$\frac{\text{speed}}{5} = 10$ mph

#### Beam structural modes

$\omega_n(1) = 44.177$	$\omega_n(2) = 176.708$	$\omega_n(3) = 397.592$
$f_n(1) = 7.031$	$f_n(2) = 28.124$	$f_n(3) = 63.279$

Note that a vehicle at crawl speed has its 19th loading mode at a much lower frequency than the first beam mode. At higher speeds, the modes become overlapped. It is desirable for  $10f < f_n$  in order to observe and clearly estimate the influence line.

## Dynamic Response of a Single Span Beam to a Traversing Vehicle

We assume a second moving load  $p_2(x,t) = P_2\delta(x-vt-S)$ , where  $P_2$  is its load and  $S$  is axle spacing. Due to linear superposition, the beam response for the two axle loads may be solved separately and added.

Characteristics of Second Axle       $P_1 \equiv 1$        $P_2 \equiv 2$        $S \equiv 10$       speed = 50

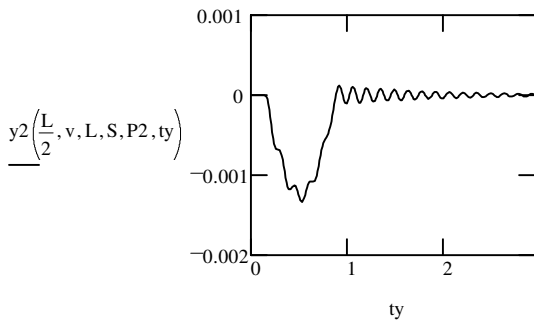
$$P(n,t) := P \cdot \phi(n, v \cdot t) + P_2 \cdot \phi(n, v \cdot t - S) \qquad P_{\text{beam}}(n,t) := P_1 \cdot \sin\left(\frac{n \cdot \pi}{L} \cdot v \cdot t\right) + P_2 \cdot \sin\left[\frac{n \cdot \pi}{L} \cdot (v \cdot t - S)\right]$$

Thus, this second forcing function is again the mode shape series, but phase shifted by  $S$ . The beam properties of mass, stiffness, damping are unchanged.

$$\begin{aligned} t_a &:= \frac{S}{v} & t_a &= 0.136 & \text{Time before 2nd axle reaches the beam} \\ t_d &= 0.75 & & & \text{Time when 1st axle leaves the beam} \\ t_{d2} &:= \frac{S+L}{v} & t_{d2} &= 0.886 & \text{Time when 2nd axle leaves the beam} \\ t_{SS}(1) + t_{d2} &= 2.936 & & & \text{Time for final decay to zero} \end{aligned} \qquad t_y := 0, .01 \dots t_{d2} + t_{SS}(1)$$

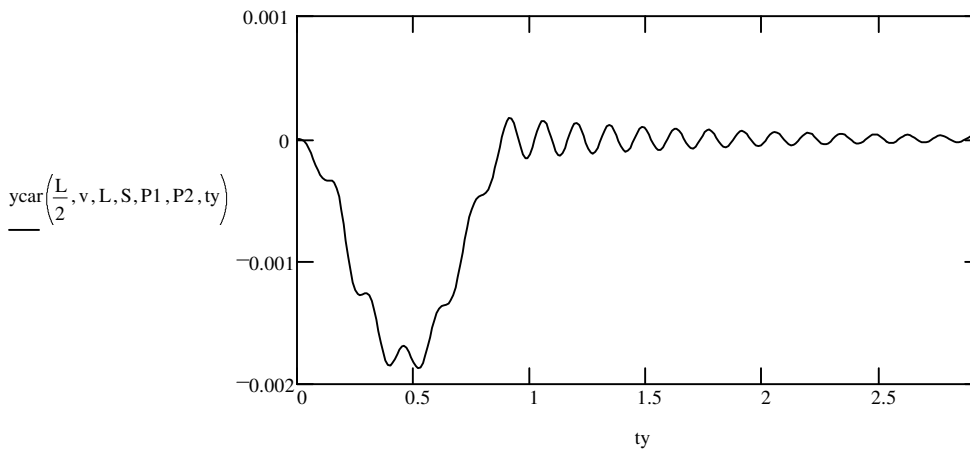
$$y_2(x, v, L, S, P, t) := y\left(x, v, L, P, t - \frac{S}{v}, \frac{L}{v}\right)$$

Beam response to the 2nd axle alone at midspan



Note: Due to boundary conditions, the beam has a definite shape function (as described by the series of mode shapes  $\phi(i,x)$ ) which dictate beam response for the given load distribution. Otherwise, one could imagine the beam assuming some new deformed shape due to the arrival of the second load. The resultant formulation of beam response essentially solves for midspan (i.e. ultimate) displacement  $q(n,t)$  and then scales this by the mode shape for the given gage location.

$$y_{\text{car}}(x, v, L, S, P_1, P_2, t) := y\left(x, v, L, P_1, t, \frac{L}{v}\right) + y_2(x, v, L, S, P_2, t) \quad \text{Full vehicle response at midspan}$$



Laplace Transformation of the Elastic Deformation at Midspan of a Single Span Beam under Dynamic Conditions

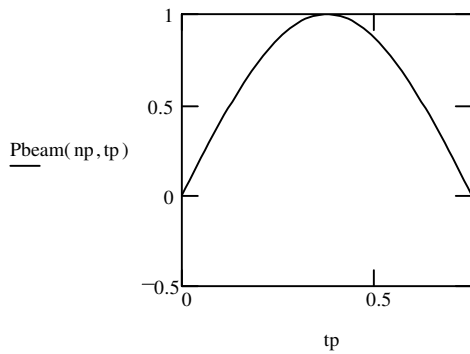
$$L=55 \quad P=1 \quad \text{speed}=50 \quad n:=1 \quad np:=1$$

$$v:=\text{speed} \cdot \frac{5280}{3600} \quad v=73.333 \quad \omega_1:=0, .1.. 10$$

$$f=0.667 \quad td=0.75 \quad tp:=0, .01.. \frac{L}{v}$$

The temporal response Pbeam(n,t)

$$Pbeam(n, t) := P \cdot \sin\left(\frac{n \cdot \pi}{L} \cdot v \cdot t\right)$$

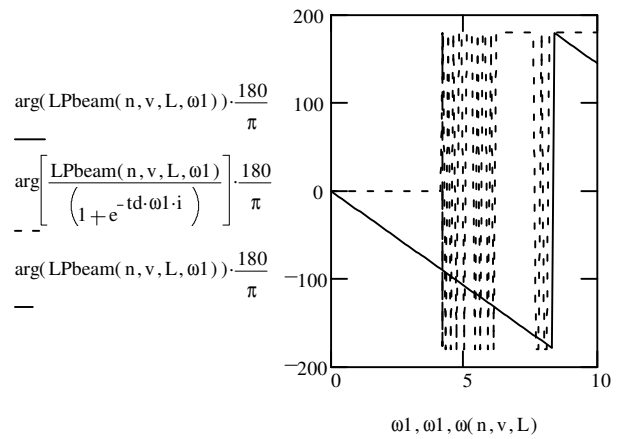
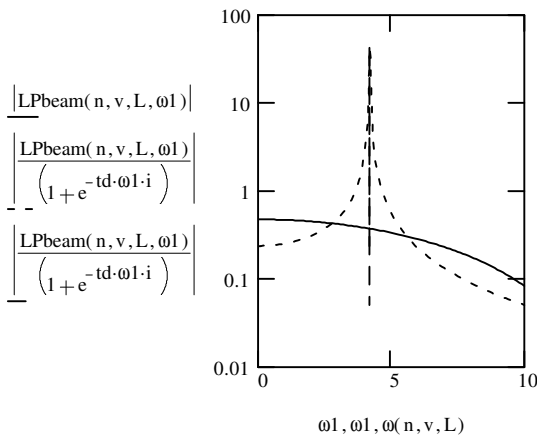


$$\omega(n, v, L) = 4.189 \quad \omega d(1) = 44.166 \quad \zeta(1) = 0.022$$

Its Laplace Transform in the frequency domain

$$LPbeam(n, v, L, \omega) := \frac{P \cdot n \cdot \pi \cdot v}{L \left[ (\omega \cdot i)^2 + \left(\frac{n \cdot \pi \cdot v}{L}\right)^2 \right]} \cdot \left(1 + e^{-\frac{L}{v} \cdot \omega \cdot i}\right)$$

Magnitude and Phase of LPbeam compared to true 2nd order response



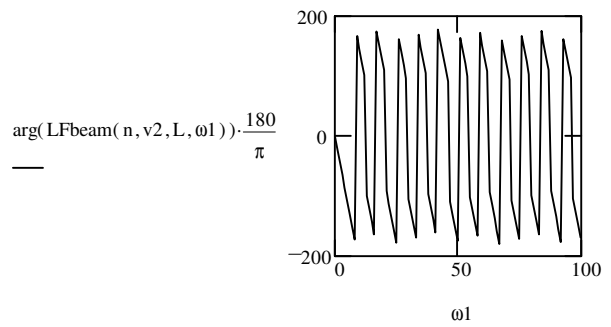
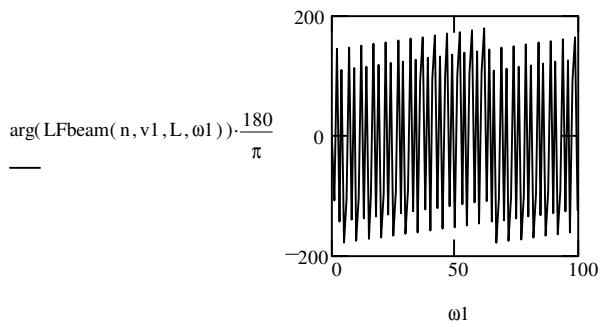
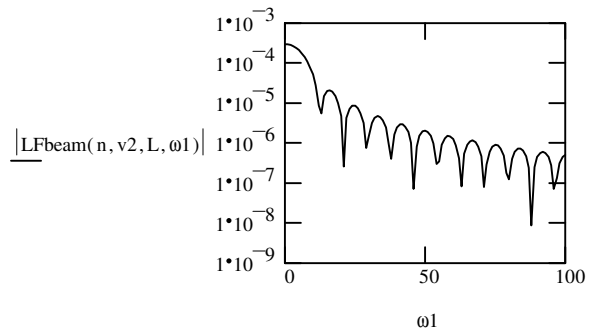
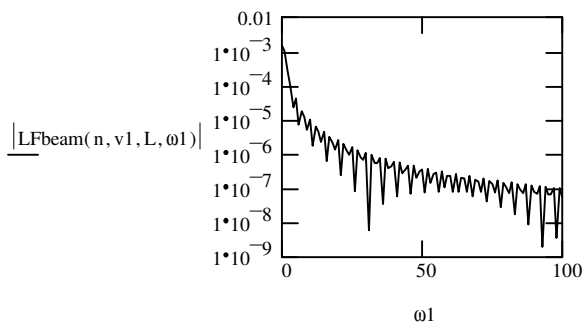
The Laplace transform of the scaled forcing function is:

$$\text{LFbeam}(n, v, L, \omega) := \frac{\text{LPbeam}(n, v, L, \omega)}{\text{Kbeam}(n)}$$

$$\omega_1 := 0, 1..100$$

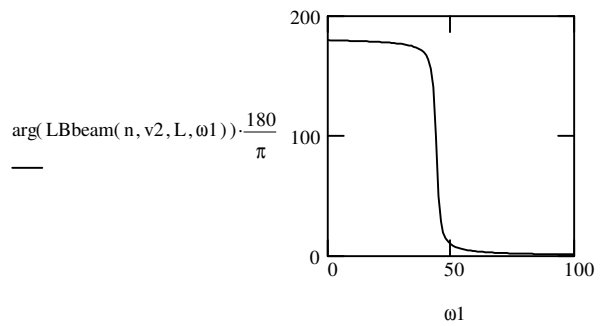
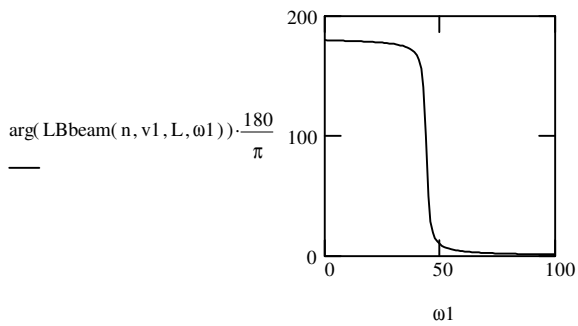
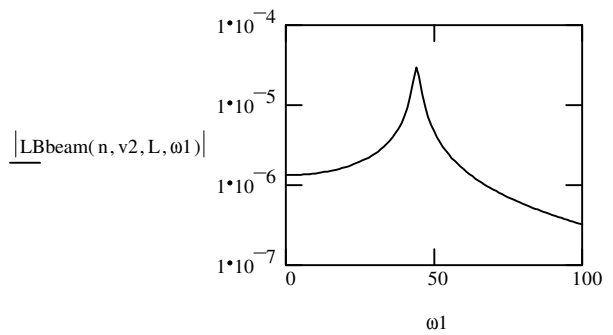
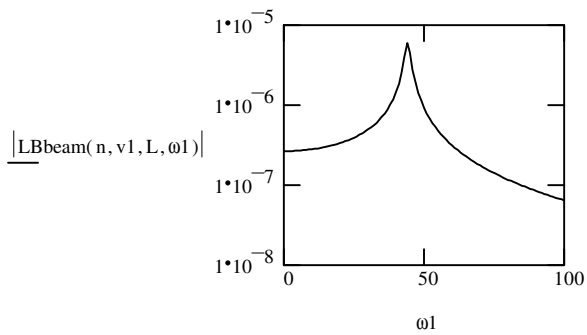
$$\text{speed1} \equiv 10 \quad v_1 := \text{speed1} \cdot \frac{5280}{3600}$$

$$\text{speed2} \equiv 50 \quad v_2 := \text{speed2} \cdot \frac{5280}{3600}$$



The Laplace transform of the beam response is:

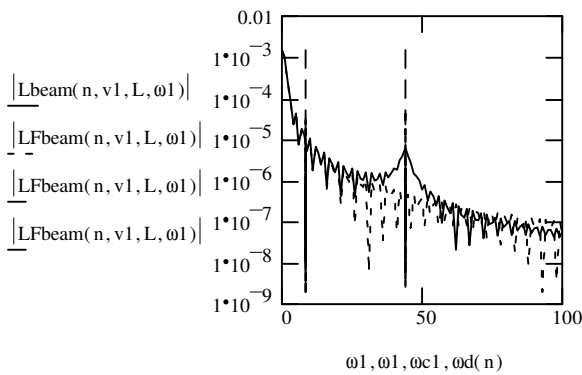
$$\text{LBbeam}(n, v, L, \omega) := \frac{n \cdot \pi \cdot \frac{v}{L} \cdot P}{-1 \cdot K_{\text{beam}}(n) \cdot [(\omega \cdot i + \zeta(n) \cdot \omega n(n))^2 + \omega d(n)^2]}$$



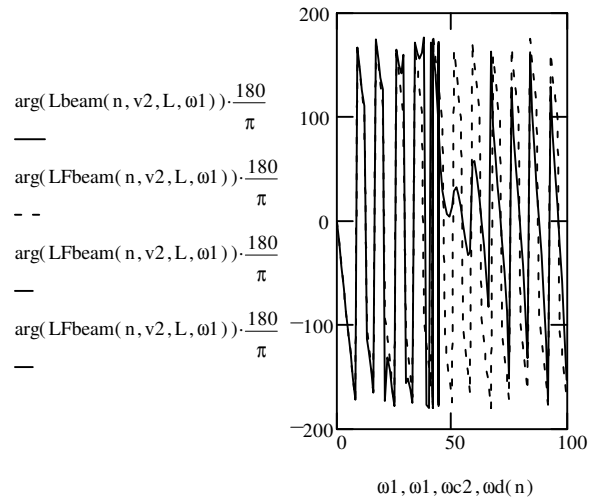
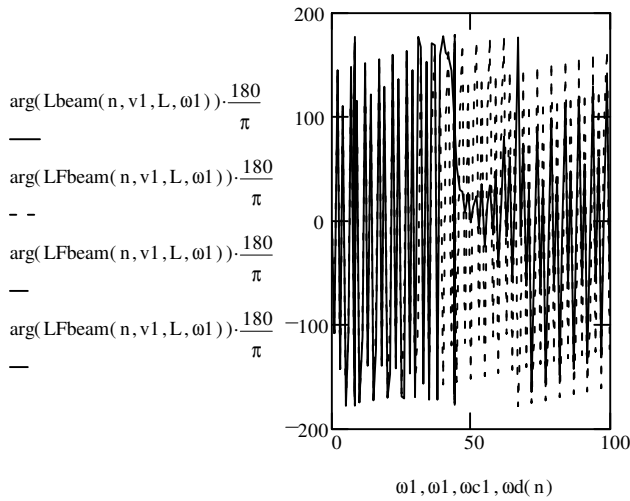
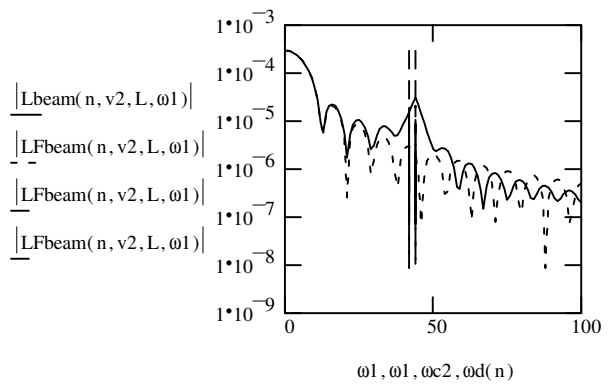
Hence, the Laplace transform of the system response is their sum:

$$L_{beam}(n, v, L, \omega) := LF_{beam}(n, v, L, \omega) + LB_{beam}(n, v, L, \omega)$$

Filter Cutoff Frequency  $fc1 := 10 \cdot \frac{f}{5}$   
 $\omega c1 := fc1 \cdot 2 \cdot \pi$       $\omega c1 = 8.378 \cdot 5$



Filter Cutoff Frequency  $fc2 := 10 \cdot f$   
 $\omega c2 := fc2 \cdot 2 \cdot \pi$       $\omega c2 = 41.888$

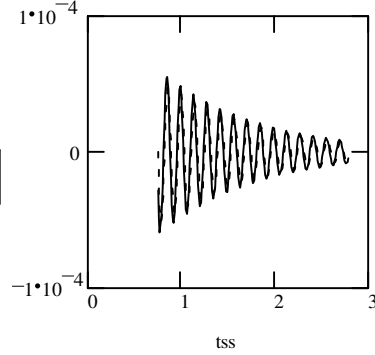


Notes: You may recall that a lowpass filter cutoff of  $10f_y = V/5L$  Hz could still provide a clean forcing signal when no bridge modes were considered. Here, you see that some additional error will pass through the filter, albeit very small, for the crawl speed of 10mph.

The temporal response for the signal's decay

$$tss := td, (td + .01) .. td + tSS(1)$$

$$\underline{qss}(n, v, L, P, tss, td) \\ e^{-\zeta(n) \cdot \omega n(n) \cdot (tss - td)} \cdot \left[ \frac{dqf(n, v, L, P, td)}{\omega d(n)} \cdot \sin(\omega d(n) \cdot (tss - td)) \right]$$

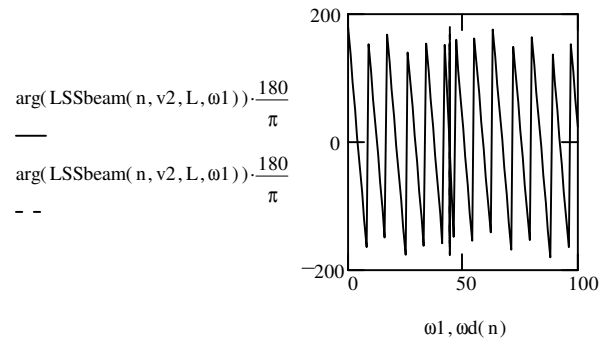
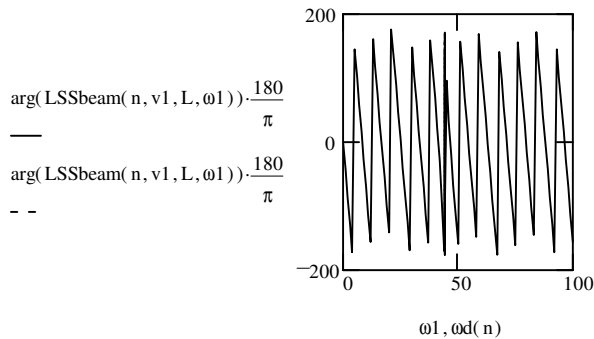
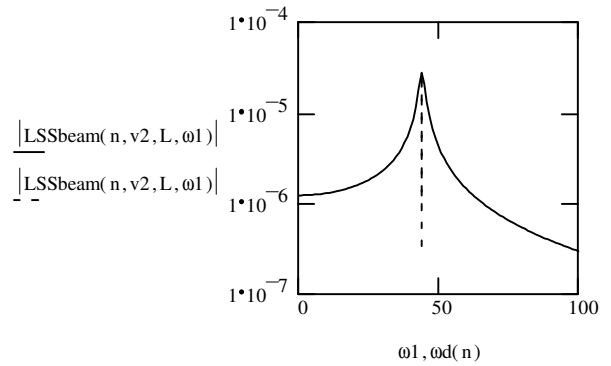
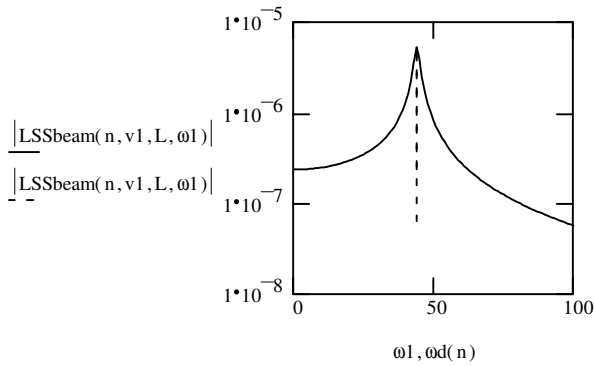


You will note that the decaying response can be approximated by:

$$qss(n, v, L, P, t, td) := e^{-\zeta(n) \cdot \omega n(n) \cdot (t - td)} \cdot \left[ \frac{dqf(n, v, L, P, td)}{\omega d(n)} \cdot \sin(\omega d(n) \cdot (t - td)) \right]$$

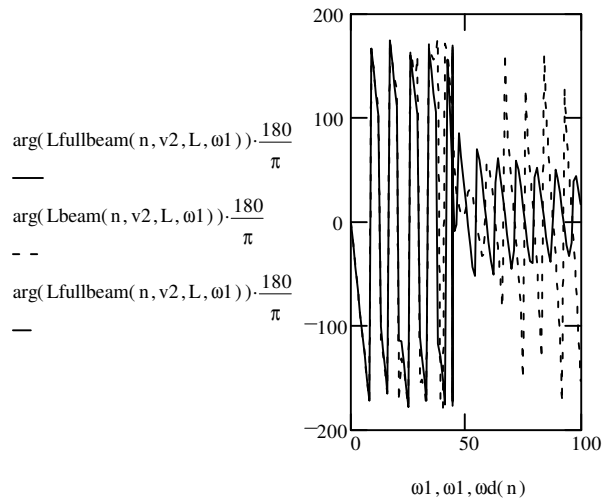
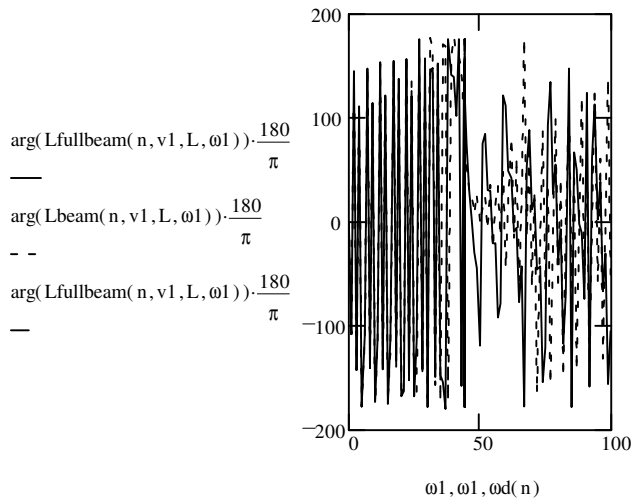
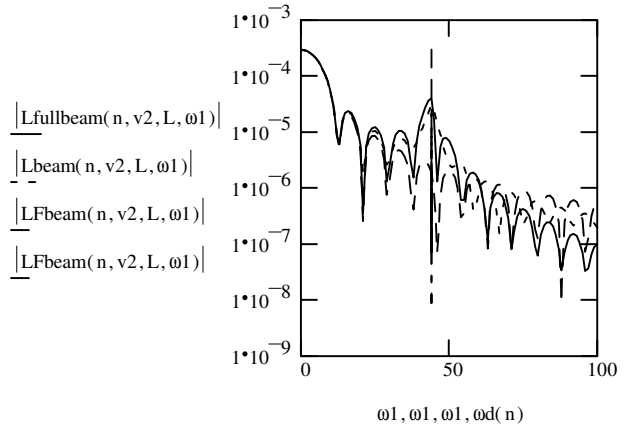
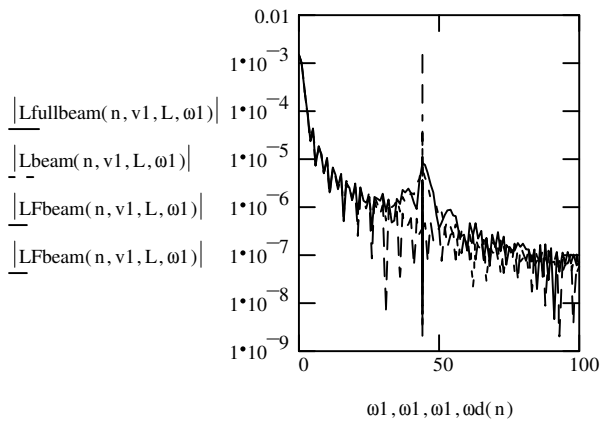
The Laplace Transform of the approximate decaying response function in the spectral domain

$$LSSbeam(n, v, L, \omega) := \frac{dqf(n, v, L, P, td)}{[(\omega \cdot i + \zeta(n) \cdot \omega n(n))^2 + \omega d(n)^2]} \cdot e^{-td \cdot \omega \cdot i}$$



Hence, the Laplace transform of the system response, including the decaying response, is their sum:

$$L_{fullbeam}(n, v, L, \omega) := LF_{beam}(n, v, L, \omega) + LB_{beam}(n, v, L, \omega) + LSS_{beam}(n, v, L, \omega)$$



Notes: The decaying response has effectively doubled the dynamic disturbance to the influence line.

## Transform the Temporal System to the Frequency Domain

This assumes that the Monitoring System is sampling at a rate of SRate.

$$\begin{aligned}
 \text{SRate} &:= 100 \text{ Hz} & R &:= \frac{1}{\text{SRate}} & R &= 0.01 & \text{seconds} & \text{oversample} &:= 5 \\
 \text{mph} &:= 50 & V &:= \text{mph} \cdot \frac{5280}{60 \cdot 60} & V &= 73.333 & \text{feet/second} & f_y &:= \frac{V}{2 \cdot L} & \text{loading frequency} \\
 \text{ta1} &:= 0, R \cdot \frac{L+S}{V} \cdot \text{oversample} & \frac{L+S}{V} &= 0.886 & \text{seconds} & f_S &:= \frac{V}{2 \cdot S} & \text{2nd axle frequency}
 \end{aligned}$$

Note that we are only considering temporal data before td, when the axle leaves the beam.

$$\text{Tct} := \frac{L+S}{V} \cdot \text{oversample} \quad \text{Tct} = 443.182 \quad \text{Total \# of data samples} \quad i := 0.. \text{Tct}$$

$$Y2P_i := y\left(\frac{L}{2}, v, L, P, i \cdot R, \text{td}\right)$$

Create temporal vectors for the evaluated functions above.

$$f1 := 0, \frac{1}{2 \cdot \pi} .. \frac{100}{2 \cdot \pi}$$

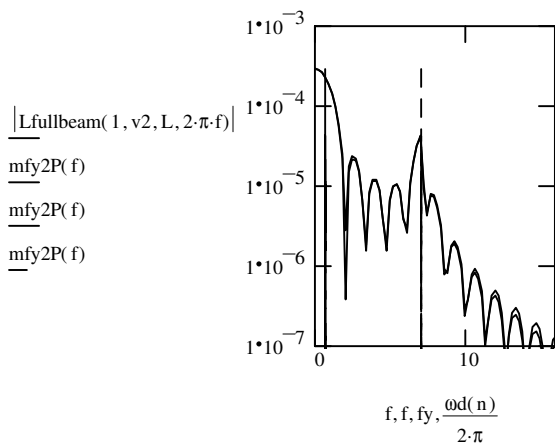
$$\text{Fmax} := \frac{1}{2 \cdot R} \quad \text{Fmax} = 50 \quad \text{FFT Bandwidth} \quad f := 0, \frac{1}{\text{Tct} \cdot R} .. \text{Fmax} \quad \text{fmin} := \frac{1}{\text{Tct} \cdot R} \quad \frac{1}{\text{Tct} \cdot R} = 0.226$$

$$\text{FY2P} := \text{CFFFT}(Y2P) \cdot \text{Tct} \cdot R \quad \text{fy2P}(f) := \text{FY2P}_{f \cdot \text{Tct} \cdot R}$$

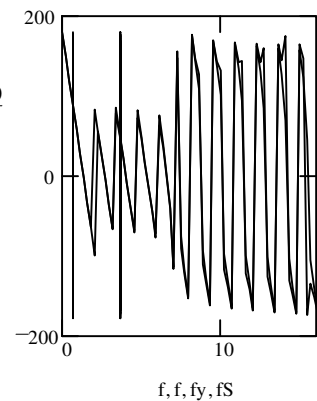
$$\text{MFY2P} := \overline{|\text{FY2P}|} \quad \text{FFT Magnitude} \quad \text{mfy2P}(f) := \text{MFY2P}_{f \cdot \text{Tct} \cdot R} \quad \text{mfy2P}(0) = 2.922 \cdot 10^{-4}$$

$$\text{PFY2P}_i := \text{if}\left(\text{FY2P}_i = 0, 0, \arg(\text{FY2P}_i) \cdot \frac{180}{\pi}\right) \quad \text{FFT Phase Angle} \quad \text{pfy2P}(f) := \text{PFY2P}_{f \cdot \text{Tct} \cdot R} \quad \text{pfy2P}(0) = 180$$

$$n = 1$$



$$\frac{\arg(-L\text{fullbeam}(n, v2, L, 2 \cdot \pi \cdot f)) \cdot 180}{\pi}$$



Hence, the Laplace transformation approximates the ODE solution for beam deflection due to axle loading.

## Dynamic Response of a Single Span Beam at Midspan to a Traversing Vehicle

We assume a second moving load  $p_2(x,t) = P_2\delta(x-vt-S)$ , where  $P_2$  is its load and  $S$  is axle spacing. Due to linear superposition, the beam response for the two axle loads may be solved separately and added.

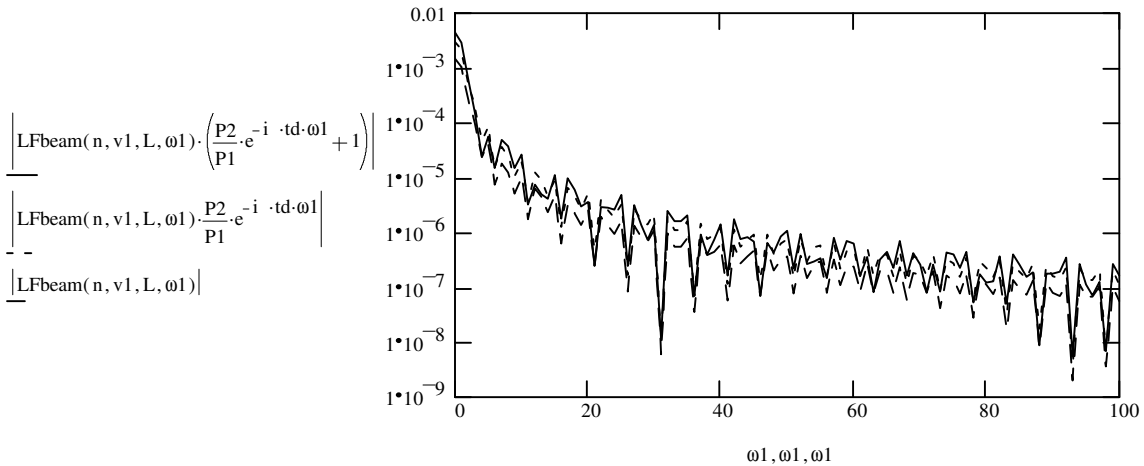
Characteristics of Second Axle       $P_1 \equiv 1$        $P_2 \equiv 2$        $S \equiv 10$       speed = 50

$$P(n,t) := P_1 \cdot \phi(n, v \cdot t) + P_2 \cdot \phi(n, v \cdot t - S) \qquad P_{beam}(n,t) := P_1 \cdot \sin\left(\frac{n \cdot \pi}{L} \cdot v \cdot t\right) + P_2 \cdot \sin\left[\frac{n \cdot \pi}{L} \cdot (v \cdot t - S)\right]$$

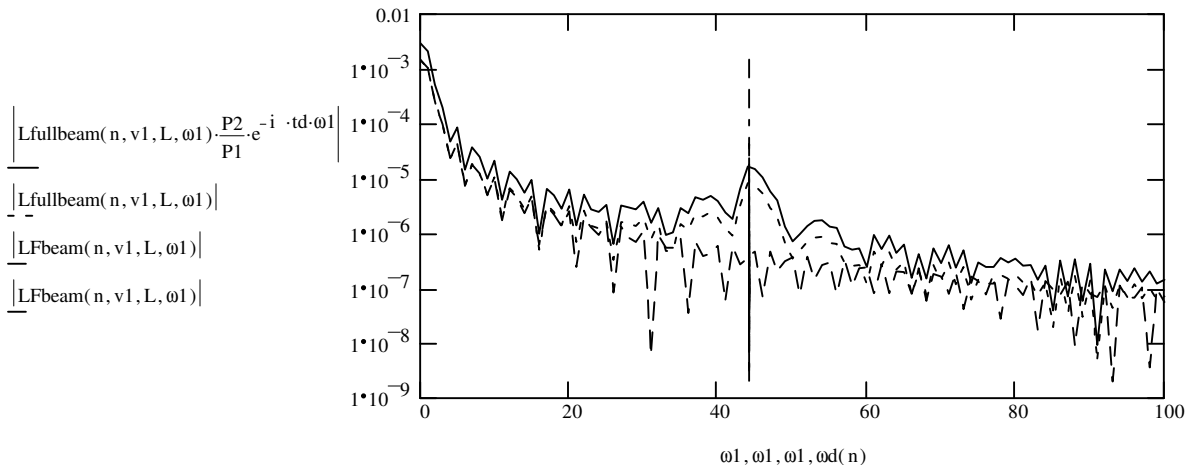
Thus, this second forcing function is again the mode shape series, but phase shifted by  $S$ . The beam properties of mass, stiffness, damping are unchanged.

Temporal delay is represented in the spectral domain by an exponential phase scalar,  $e(-i \cdot t \cdot d \cdot \omega)$ . 2nd axle responses differ from the 1st axle responses only in their phase angle plot.

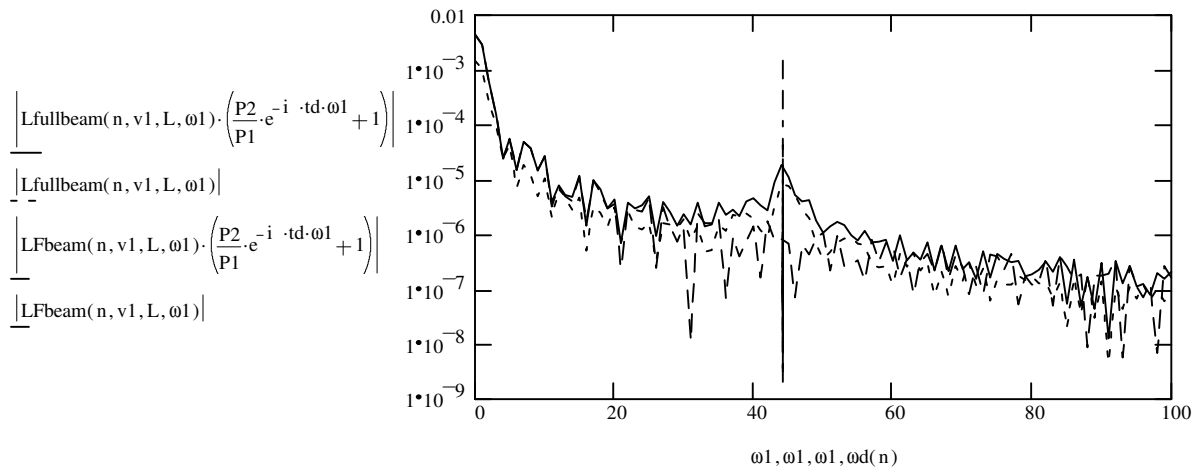
First, let us examine the forced influence response of the beam w/o dynamical mode disturbances. Compared to a single axle response, the total vehicle response is appropriately increased in magnitude, but with the addition of a new loading mode.



The full beam response to the 2nd axle is very similar in magnitude with the 1st axle response.



However, upon adding both axle responses, the whole vehicle response is markedly different.

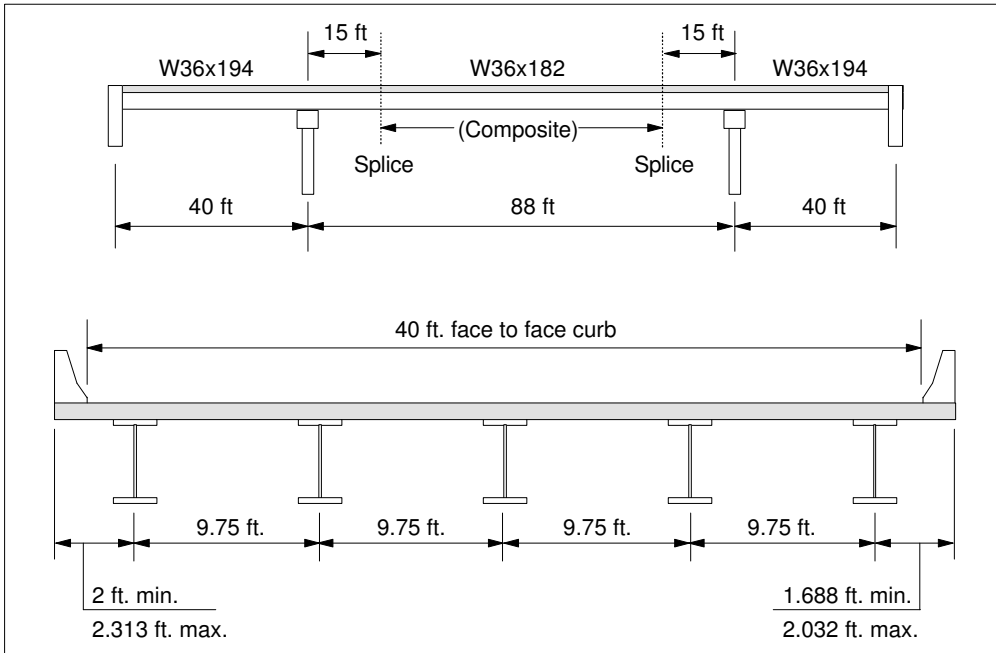


Note the increased discrepancy of the full vehicle response from the disturbance-free response.

APPENDIX B1

Design Calculations for Constructed Bridge, HAM-126-0881

1. **Given:** Hamilton Ave. Bridge (HAM-126-0881L)  
 3 span continuous deck-on-rolled steel beam bridge with integral abutments.  
 (Westbound Traffic Bridge)



- \***Haunch:** Average Haunch Depth = 2"  
 Average Haunch Width = 9" (beyond each edge of flange)
- \***FWS:** (Future Wearing Surface) = 30 psf  
 Note: 1993 ODOT Bridge Design Manual, Sect. 3.2.1.1.2b requires 60 psf FWS.
- \***ADTT:** (Westbound Traffic)  
 1994 ADT = 12,940 >> ADTT = 1423  
 2014 ADT = 16,690 >> ADTT = 1836

**Therefore:** ADTT < 2500 & Major Highway

2. **Determine Effective Flange Width:** (AASHTO 10.38.3.1)

Effective Flange Width is Minimum of:

- ➔ 1/4 Span Length of Girder =  $(0.25)(88')$  = 22'
- ➔ Center to Center Space of Girders = 9.75'
- ➔ 12 Times Min. Slab Thick. =  $(12)(8.75"-1")$  = 93" = 7.75' (Governs)

**Therefore:** Effective Flange Width,  $b_{eff}$  = 93"

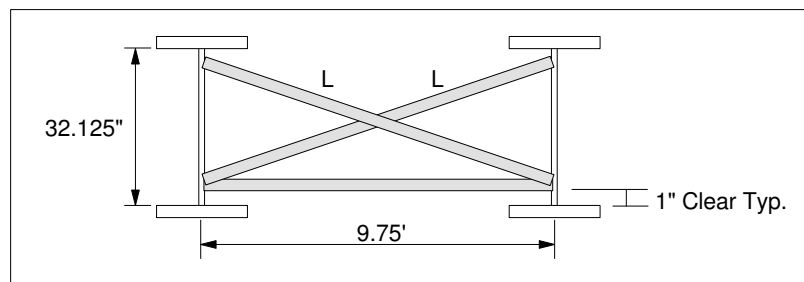
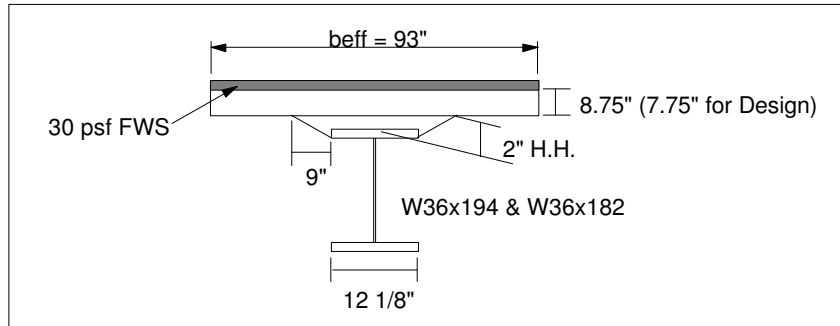
3. **Calculate Dead Load on Girder:** (interior girder) non-composite dead loads

$DL = DL_{slab} + DL_{girder} + DL_{haunch} + DL_{xframe}$

- ➔  $DL_{slab} = (\text{Trib. Width})(\text{Thick.})(\text{Weight conc.}) = (9.75')(8.75"/12"/ft)(0.150 \text{ k/ft}) = 1.07 \text{ k/ft.}$

**3. Calculate Dead Load on Girder:** continued

- ➔  $DL_{\text{haunch}} = (\text{Haunch Width})(\text{Haunch Thick.})(\text{Weight conc.})$
- Haunch Area =  $(12.125'')(2'') + (9''/2 \times 2'')(2) = 42.25 \text{ in}^2$
- $DL_{\text{haunch}} = (42.25 \text{ in}^2 \times 1 \text{ ft}^2/144 \text{ in}^2)(0.150 \text{ k/ft}) = 0.044 \text{ k/ft}$



$$L = [(9.75')^2 + (30.125 \text{ in}/12 \text{ in/ft})^2]^{1/2}$$

$$L = 10.07 \text{ ft.}$$

$$\text{Total Length} = 2(10.07') + (9.75') = 29.89'$$

- ➔  $DL_{\text{xframe}} = L3 \times 3 \times 5/16 @ 14' \text{ spacing}$
- $DL_{\text{xframe}} = \text{xframe wt./spacing} = (29.89')(0.0061 \text{ k/ft})/14' = 0.013 \text{ k/ft}$
- ➔  $DL_{\text{girder}} = W36 \times 182 = 0.182 \text{ k/ft (58')} \ \& \ W36 \times 194 = 0.194 \text{ k/ft (110')}$

Total DL	W36x194	W36x182
Slab + Haunch + Xframe + Girder	1.321 k/ft	1.309 k/ft

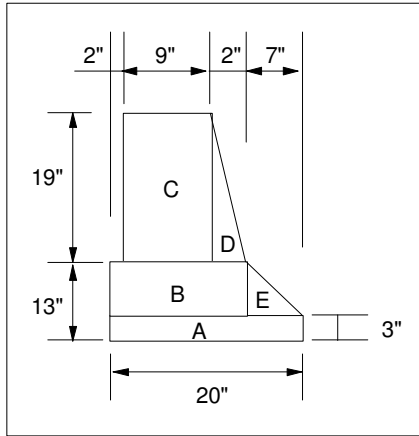
**4. Calculate Superimposed Dead Load:** (interior girder) composite

$SDL = SDL_{\text{parapets}} + SDL_{\text{FWS}}$   
 (AASHTO 3.23.2.3.1.1): Curbs, railings, and wearing surface, if placed after deck is cured, may be distributed equally to all roadway stringers.

- ➔  $DL_{\text{FWS}} = [(\text{Width of Road})(\text{Weight FWS})] / \# \text{ stringers} = (40')(0.30 \text{ k/ft})/5 = 0.240 \text{ k/ft}$

**4. Calculate Superimposed Dead Load:** continued

SDL<sub>parapets</sub>: Calculate area of parapet



Area:

"A" = (3")(20") = 60 in<sup>2</sup>/144 in<sup>2</sup>/ft<sup>2</sup> = 0.417 ft<sup>2</sup>

"B" = (10")(13") = 130 in<sup>2</sup>/144 = 0.903 ft<sup>2</sup>

"C" = (9")(19") = 171 in<sup>2</sup>/144 = 1.188 ft<sup>2</sup>

"D" = (0.5)(2")(19") = 19 in<sup>2</sup>/144 = 0.132 ft<sup>2</sup>

"E" = (0.5)(7")(10") = 35 in<sup>2</sup>/144 = 0.243 ft<sup>2</sup>

Total Area = 2.883 ft<sup>2</sup>

Weight Parapet:

W<sub>parapet</sub> = (Area)(W<sub>conc.</sub>) = (2.883 ft<sup>2</sup>)(0.150 k/ft)  
= 0.432 k/ft

→ SDL<sub>parapet</sub> = [(2 parapets)(Weight parapet)] / # stringers = (2)(0.432k/ft)/5 = 0.173 k/ft

Total SDL	
SDL <sub>FWS</sub> + SDL <sub>parapet</sub>	0.413 k/ft

**5. Calculate Live Load + Impact:**

A wheel load distribution factor and impact factor are calculated and applied to the Live Load moments obtained from a 2D analysis of the structure.

**Determine number of Traffic Lanes:**

AASHTO 3.6.1: The lane loading or standard truck shall be assumed to occupy a 10 feet width.

AASHTO 3.6.2: These loads shall be placed in a 12-foot wide design traffic lanes, spaced across the entire bridge roadway width measured between the curbs.

AASHTO 3.6.3: Fractional parts of design lanes shall not be used but roadway widths from 20 to 24 feet shall have two design lanes each equal to one-half the roadway width.

→ # Traffic Design Lanes = Roadway Width / 12 feet = 40'/12' = 3.33 lanes = 3 lanes

**Determine Distribution of Wheel Loads to Beams:**

AASHTO Table 3.23.1: Distribution of Wheel Loads in Longitudinal Beams

Floor Type: Concrete on Steel Stringers

Bridge Designed for 2 or More Traffic Lanes

→ Wheel Load Distribution Factor = S / 5.5 where S = Avg. Spacing of Beams

→ Axle Load Distribution Factor = WLDF / 2 Wheels per Axle = S / (2 x 5.5) = S / 11

S = 9.75' so S/11 = 9.75'/11 = 0.886

Therefore, multiply live load moments found using axle loads by DF = 0.886 to obtain individual girder moments.

**Therefore: DF = 0.886**

## 5. Calculate Live Load + Impact: continued

### Determine Impact Factor:

AASHTO 3.8.1. Live Loads shall be increased for structural elements in Group A to allow for dynamic, vibratory, and impact effects  
 AASHTO 3.8.1.1: Group A elements - Superstructure, including legs of rigid structures, Piers excluding footings and those portions below groundline, and portions above the groundline of concrete or steel piles that support the superstructure.

AASHTO 3.8.2.1: Impact Formula:  $I = 50 / (L+125)$

I = impact fraction (max. 30 percent)

L = length in feet of the portion of the span that is loaded to produce the maximum stress in the member.

AASHTO 3.8.2.2: Definition of L for uniformity of application

- (a) for roadway floors: the design span length
- (b) for transvers members: the span length of member center to center of supports
- (c) for calc. truck load moments: the span length, or for cantilever arms the length from the moment center the the farthest axle.
- (d) for shear due to truck loads: the length of the loaded portion of the span from point under consideration to the far reaction; except for cantilever arms, use a 30 percent impact factor
- (e) for continuous spans: the length of the span under consideration for positive moment, and the average of two adjacent loaded spans for negative moment.

→ from (e),  $L = 88'$  (Positive Moment) &  $L = (88'+40')/2 = 64'$  (Negative Moment)

Calculate Impact:

$I = 50/(88+125) = 0.235$  (Pos. Moment), Use  $I = 1.235$

$I = 50/(64+125) = 0.265$  (Neg.Moment), Use  $I = 1.265$

**Therefore:**  $I = 1.235$  (+ Moment) &  $I = 1.265$  (- Moment)

## 6. Calculate Girder Section Properties:

**Non-composite Section Properties:** W36x194 & W36x182

W36x194:  $A = 57.0 \text{ in}^2$ ,  $I = 12,100 \text{ in}^4$ ,  $d = 36.49 \text{ in}$ ,  $c = 18.245 \text{ in}$ ,  $S = 664 \text{ in}^3$

W36x182:  $A = 53.6 \text{ in}^2$ ,  $I = 11,300 \text{ in}^4$ ,  $d = 36.33 \text{ in}$ ,  $c = 18.165 \text{ in}$ ,  $S = 623 \text{ in}^3$

**Composite Section Properties:** W36x182 (for Positive LL + I Moment )

→ Calculate Transformed Width of Slab (concrete to equivalent steel)

AASHTO 10.38.1.3: for  $f'c = 4500 \text{ psi}$ , modular ratio  $n = 8 = E_s/E_c$

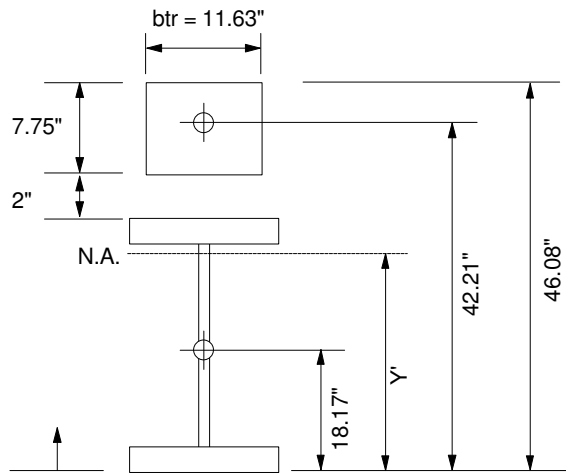
$b_{tr} = b_{eff} / (k)(n)$   $k =$  multiplier to account for creep under dead loads

AASHTO 10.38.1.4:  $k = 1$  for LL+I Moments,  $k = 3$  for SDL Moments

$b_{tr} = 93''/(1)(8) = 11.63''$  for LL+ I Moment

$b_{tr} = 93''/(3)(8) = 3.88''$  for SDL Moment

6. Calculate Girder Section Properties: continued



$$A_{ctr} = (btr)(t) = (11.63)(7.75) = 90.1 \text{ in}^2$$

$$I_{ctr} = (b)(h)^3 / 12 = (11.63)(7.75)^3 / 12 = 451.13 \text{ in}^4$$

Element	A (in <sup>2</sup> )	Y (in)	AY (in <sup>3</sup> )	AY <sup>2</sup> (in <sup>4</sup> )	lo (in <sup>4</sup> )
W36x182	53.6	18.165	973.64	17686.243	11300.00
Slab (k=1)	90.1	42.205	3803.12	160529.737	451.13
Total	143.7		4776.76	178215.98	11751.13

$$I' = \text{Sum } (I_o) + \text{Sum } (AY^2) = 11751.13 + 178215.98 = 189967.11 \text{ in}^4$$

$$Y' = \text{Sum } (AY) / \text{Sum } (A) = 4776.76 / 143.7 = 33.241 \text{ in}$$

$$I_{LL+I} = I' - (\text{Sum } A)(Y')^2 = 189967.11 - (143.7)(33.241)^2 = 31183.77 \text{ in}^4$$

**Therefore:** W36X182 (LL + I)

- ➔  $I_{LL+I} = 31183.77 \text{ in}^4$
- ➔  $Stc = 31183.77 / (46.08 - 33.241) = 2428.83 \text{ in}^3$
- ➔  $Sts = 31183.77 / (36.33 - 33.241) = 10095.10 \text{ in}^3$
- ➔  $Sbs = 31183.77 / (33.241) = 938.11 \text{ in}^3$

**Composite Section Properties:** W36x182 (for Positive SDL Moment) k=3

- ➔  $A_{tr} = (btr)(t) = (3.88)(7.75) = 30.07 \text{ in}^2$
- ➔  $I_{tr} = (btr)(t^3) / 12 = (3.88)(7.75)^3 / 12 = 150.51 \text{ in}^4$

Element	A (in <sup>2</sup> )	Y (in)	AY (in <sup>3</sup> )	AY <sup>2</sup> (in <sup>4</sup> )	lo (in <sup>4</sup> )
W36x182	53.6	18.165	973.64	17686.243	11300.00
Slab (k=3)	30.07	42.205	1269.104	53562.549	150.507
Total	83.67		2242.748	71248.792	11450.507

$$I' = \text{Sum } (I_o) + \text{Sum } (AY^2) = 11450.507 + 71248.792 = 82699.299 \text{ in}^4$$

$$Y' = \text{Sum } (AY) / \text{Sum } (A) = 2242.748 / 83.67 = 26.805 \text{ in}$$

$$I_{SDL} = I' - (\text{Sum } A)(Y')^2 = 82699.299 - (83.67)(26.80)^2 = 22604.16 \text{ in}^4$$

**6. Calculate Girder Section Properties:** continued**Therefore:** W36X182 (SDL)

$$\rightarrow I_{SDL} = 22604.16 \text{ in}^4$$

$$\rightarrow S_{tc} = 22604.16 / (46.08 - 26.80) = 1172.4 \text{ in}^3$$

$$\rightarrow S_{ts} = 22604.16 / (36.33 - 26.80) = 2371.9 \text{ in}^3$$

$$\rightarrow S_{bs} = 22604.16 / (26.80) = 843.4 \text{ in}^3$$

AASHTO 10.38.4.2: A continuous composite bridge may be built with shear connectors either in the positive moment regions or throughout the length of the bridge. The positive moment regions may be designed with composite sections as in simple spans. Shear connectors shall be provided in the negative moment portion in which the reinforcement steel embedded in the concrete is considered a part of the composite section. In case the reinforcement steel embedded in the concrete is not used in computing section properties for negative moments, shear connectors need not be provided in these portions of the spans, but additional anchorage connectors shall be placed in the region of the point of dead load contraflexure in accordance with Article 10.38.5.

**7. Calculate Design Moments:**

Moments were calculated using two programs (Visual Analysis & SAP90) with boundary conditions as pinned at the abutments and rollers at the piers. Because shear connectors are only used for the midspan portion of the bridge, composite properties were used in the analysis only for the W36x182 sections.

**Negative Moment:** (The maximum negative moment occurs at the piers)

DL1: Section properties used in analysis are non-composite W36x194 & W36x182

$$\rightarrow DL1 = -723.59 \text{ k-ft (from Visual Analysis)}$$

SDL: Section properties for analysis are composite W36x182 (n=24) & non-composite W36x194

$$\rightarrow SDL = -187.45 \text{ k-ft (from Visual Analysis)}$$

LL+I: Section properties for analysis are composite W36x182 (n=8) & non-composite W36x194

$$\begin{aligned} \rightarrow LL+I &= (\text{Neg. Moment})(LL+I \text{ factor})(\text{Dist. factor}) = (-447.27 \text{ k-ft})(1.265)(0.886) \\ &= -501.30 \text{ k-ft (Neg. Moment from SAP90 moving load analysis)} \end{aligned}$$

**Positive Moments:** (The maximum positive moment occurs at midspan)

DL1: Section properties used in analysis are non-composite W36x182 & W36x194

$$\rightarrow DL1 = +544.87 \text{ k-ft (from Visual Analysis)}$$

**7. Calculate Design Moments:** Continued

**Positive Moments:** (The maximum positive moment occurs at midspan)

SDL: Section properties used in analysis are composite W36x182 (n =24)  
& non-composite W36x194.

➔ SDL = +212.33 k-ft (from Visual Analysis)

LL+I: Section properties used in the analysis are composite W36x182 (n=8)  
& non-composite W36x194.

➔ LL+I = (Pos. Moment)(LL+I factor)(Dist. Factor) = (920.218)(1.265)(0.886)  
= +1007.27 k-ft (from SAP90 moving load analysis)

Design Moment Summary:

Loading Case	Negative Moment (Piers)	Positive Moment (Midspan)
Non-Composite Dead Load (DL1)	-723.59 k-ft = -8683.08 k-in	+544.87 k-ft = +6538.44 k-in
Composite Dead Load (SDL)	-187.45 k-ft = -2249.40 k-in	+212.33 k-ft = +2547.96 k-in
Live Load + Impact (LL+I)	-501.30 k-ft = -6015.60 k-in	+1007.27 k-ft = +12087.24 k-in

**8. Check Stresses:**

**Negative Moment Region:** Non-composite Section

Check Stresses in rolled beam (W36x194) at Pier Location.

(AASHTO Table 10.32.1A Allowable Stresses - Structural Steel): for High-Strength,  
Low-Alloy Steel.

Compression in extreme fibers of rolled shapes, girders, and built-up sections, subject to  
bending, gross section, when the compression flange is:

(B) Partially supported or is unsupported: (at Piers, bottom flange is compression flange)

$$F_b = \frac{(50 \times 10^6) C_b}{S_{xc}} \left( \frac{I_{yc}}{l} \right) \sqrt{0.772 \frac{J}{I_{yc}} + 9.87 \left( \frac{d}{l} \right)^2} \leq 0.55 F_y$$

C<sub>b</sub> = 1.0 for members where the moment within a significant portion of the unbraced  
segment is greater than or equal to the larger of the segment end moments.

(This is the case at the piers)

l = Length in inches, of unsupported flange between lateral connections, knee braces,  
or other points of support

l = 14 ft. x 12 in/ft = 168 in (crossframes @ 14 ft spacing)

**8. Check Stresses:**

**Negative Moment Region:** Continued

d = depth of girder, in. = 36.49 in

$J = [(bt^3)_c + (bt^3)_t + Dtw^3]/3$  where b and t represent the flange width and thickness of the compression and tension flange, respectively (in<sup>4</sup>).

$$J = [2(12.115 \times 1.26^3) + (36.49 \times 0.765^3)]/3 = 21.60 \text{ in}^4$$

S<sub>xc</sub> = section modulus with respect to compression flange (in<sup>3</sup>) = 664 in<sup>3</sup>

I<sub>yc</sub> = Moment of Inertia of flange about y-axis (in<sup>4</sup>) = (1.26)(12.115<sup>3</sup>)/12 = 186.71 in<sup>4</sup>

$$F_b = (75301.205)(1.11)[(0.0893 + 0.4656)]^{1/2} = 62265.32 \text{ psi} = 62.27 \text{ ksi} > 0.55(50 \text{ ksi})$$

**Therefore: Allowable Stress F<sub>b</sub> = 27.5 ksi**

**Check Negative Moment Bending Stress:**

$$F = M/S_x = (M_{DL1}) + (M_{DL2}) + (M_{LL+I}) / S_x$$

$$F = [(723.59 \text{ k-ft} + 187.45 \text{ k-ft} + 501.30 \text{ k-ft})(12 \text{ in/ft})] / 664 \text{ in}^3 = 25.52 \text{ ksi}$$

**Therefore: F = 25.52 ksi < F<sub>b</sub> = 27.5 ksi, O.K.**

**Positive Moment Region:** Composite Section W36x182

Concrete: f'<sub>c</sub> = 4500 psi, n = 8, (ODOT 402.1.2.B: f<sub>c</sub> = 1500 psi = 1.5 ksi)

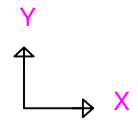
Concrete Stress = M / (3n\*S) for DL2

= M / (n\*S) for LL+I

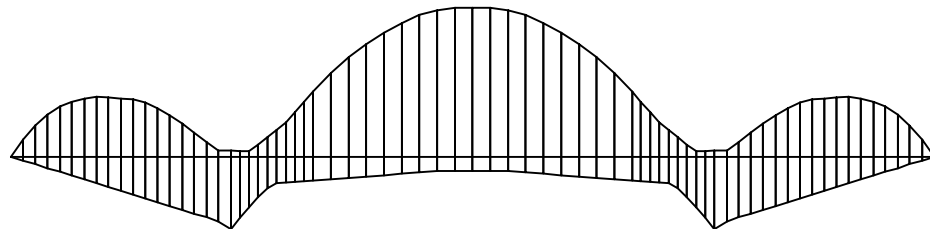
Steel (A572-50): F<sub>y</sub> = 50 ksi, (ODOT 402.1.2.B: F<sub>b</sub> = 27 ksi)

Steel Stress = M / S

Loading Case	Bottom Steel Stress	Top Steel Stress	Concrete Stress
<b>DL1</b>	6538.44 k-in / 623 = 10.495 ksi	6538.44 k-in / 623 = 10.49 ksi	
<b>SDL</b>	2547.96 k-in / 843.4 = 3.021 ksi	2547.96 k-in / 2371.9 = 1.074 ksi	2547.96 k-in / 24* 1172.4 = 0.091 ksi
<b>LL+I</b>	12087.24 k-in / 938.11 = 12.885 ksi	12087.24 k-in / 10095.10 = 1.197 ksi	12087.24 k-in / 8*2428.83 = 0.622 ksi
<b>Total Stress</b>	26.401 ksi < 27.0 ksi O.K.	12.761 ksi < 27.0 ksi O.K.	0.713 ksi < 1.5 ksi O.K.



HAM2D1  
FRAME  
OUTPUT M33  
ENVELOPE ALL

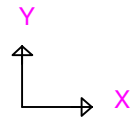


MIN < 6>  
-0.4473E+03  
AT 15.00  
MAX < 4>  
0.9202E+03  
AT 25.78

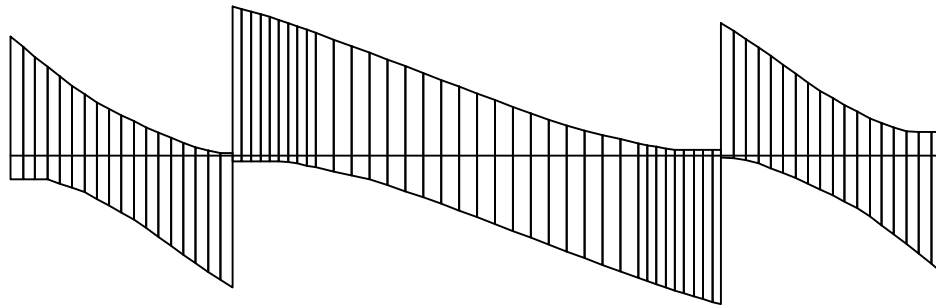
**Moving Load Analysis - Live Load Bending Moment Envelope**

**SAP90**

B1-10



HAM2D1  
FRAME  
OUTPUT V22  
ENVELOPE ALL



MIN < 6>  
-0.6574E+02  
AT 15.00  
MAX < 3>  
0.6574E+02  
AT 0.00

**Moving Load Analysis - Live Load Shear Force Envelope**

SAP90

B1-11

**MOVING LOAD ANALYSIS INPUT FILE (pg 12/13)**

SAP90 MOVING LOAD ANALYSIS - HAMILTON AVE. BRIDGE  
SYSTEM

L=3 :# OF LOAD CASES=3: HS20-44 TRUCK AND LANE, &  
AML

:UNITS ARE KIPS, FT  
:SPAN 1 = 40 ft, SPAN 2 = 88 ft, SPAN 3 = 40 ft  
:AXIS DEFINED X=LT & RT, Y=UP & DOWN, Z=IN &

OUT PAPER

JOINTS

1 X=0 Y=0 Z=0 :INTEGRAL ABUT (MODEL AS PIN)  
2 X=20 Y=0 Z=0 :QUARTER SPAN 1  
3 X=40 Y=0 Z=0 :PIER 1 LOCATION (MODEL AS ROLLER)  
4 X=55 Y=0 Z=0 :SPLICE 1  
5 X=84 Y=0 Z=0 :MIDSPAN  
6 X=113 Y=0 Z=0 :SPLICE 2  
7 X=128 Y=0 Z=0 :PIER 2 LOCATION (MODEL AS ROLLER)  
8 X=148 Y=0 Z=0 :QUARTER SPAN 2  
9 X=168 Y=0 Z=0 :INTEGRAL ABUTMENT 2 (MODEL AS PIN)

RESTRAINTS

1 9 1 R=0,0,1,1,1,0 :ALL JOINTS RESTRAINED IN Z TRANSLATION &  
X,Y ROTATION  
1 9 8 R=1,1,1,1,1,0 :(HINGE) ABUTMENTS RELEASED IN Z ROTATION  
ONLY  
3 7 4 R=0,1,1,1,1,0 :(ROLLER) PIERS RELEASED IN X TRANSLATION, Z  
ROTATION

C UNITS I=ft<sup>4</sup>, A=ft<sup>2</sup>, E=k/ft<sup>2</sup>  
C W36X194 NON-COMPOSITE SECTION - NO SHEAR CONNECTORS USED  
C W36X182 COMPOSITE SECTION - SHEAR CONNECTORS USED

FRAME

NM=2 NSEC=10 :2 SECTION PROPERTIES, 10 FORCE OUTPUT LOCATIONS  
PER MEMBER

1 A=0.3958 I=0.5835,0.5835 E=4176000 :W36X194 NON-COMPOSITE  
2 A=0.9979 I=1.5038,1.5038 E=4176000 :W36X182 COMPOSITE  
1 1 2 M=1 :BEAM 1 BETWEEN NODES 1 & 2, SECTION PROP 1  
2 2 3 M=1 :BEAM 2 BETWEEN NODES 2 & 3, SECTION PROP 1  
3 3 4 M=1 :BEAM 3 BETWEEN NODES 3 & 4, SECTION PROP 1  
4 4 5 M=2 :BEAM 4 BETWEEN NODES 4 & 5, SECTION PROP 2  
5 5 6 M=2 :BEAM 5 BETWEEN NODES 5 & 6, SECTION PROP 2  
6 6 7 M=1 :BEAM 6 BETWEEN NODES 6 & 7, SECTION PROP 1  
7 7 8 M=1 :BEAM 7 BETWEEN NODES 7 & 8, SECTION PROP 1  
8 8 9 M=1 :BEAM 8 BETWEEN NODES 8 & 9, SECTION PROP 1

MOVING LOAD ANALYSIS INPUT FILE (pg 13/13)

BRIDGE

NL=1 UP=Y :#LANES =1, Y DIRECTION UP  
L=1 :LANE1 DEFINITION BLOCK  
S=1  
F=1,2,1 E=0 :SPAN 1, LANE DEFINED BY BEAMS 1 TO 2, NO  
ECCENTRICITY  
S=2  
F=3,6,1 E=0 :SPAN 2, LANE DEFINED BY BEAMS 3 TO 6, NO  
ECCENTRICITY  
S=3  
F=7,8,1 E=0 :SPAN 3, LANE DEFINED BY BEAMS 7 TO 8, NO  
ECCENTRICITY

VEHICLE

NV=3 NG=3 TRUCK=EXACT UNITS=KIP,FT :# OF VEHICLES=3, # OF LOAD  
GROUPS=3  
V=1 TYPE=HS20-44 :VEHICLE 1 =HS20-44 TRUCK  
V=2 TYPE=HS20-44L :VEHICLE 2 =HS20-44 LANE  
V=3 TYPE=AML :VEHICLE 2 =ALTERNATE  
MILITARY LOAD  
G=1 V=1 :LOAD GROUP1=HS20-44 TRUCK  
G=2 V=2 :LOAD GROUP2=HS20-44 LANE  
G=3 V=3 :LOAD GROUP3=ALTERNATE  
MILITARY LOAD

MOVING LOAD

NC=3 MK=2 :3 CASES, MAX OF 2 DATA LINES USED TO DEFINE  
EACH CASE  
C=1 :LOAD CASE 1  
K=MIX L=1 DIR=B G=1 S=1 RF=1.0 :LANE 1, BOTH DIRECTIONS,  
LOAD GROUP 1  
C=2 :LOAD CASE 2  
K=MIX L=1 DIR=B G=2 S=1 RF=1.0 :LANE 1, BOTH DIRECTIONS,  
LOAD GROUP 2  
C=3 :LOAD CASE 3  
K=MIX L=1 DIR=B G=3 S=1 RF=1.0 :LANE 1, BOTH DIRECTIONS,  
LOAD GROUP 3

ENVELOPE

1 B=1,0,0 :ENV#1 = CASE 1 RESULTS  
2 B=0,1,0 :ENV#2 = CASE 2 RESULTS  
3 B=0,0,1 :ENV#3 = CASE 3 RESULTS

## APPENDIX C1

Optimization of the Data Acquisition System, Optim Electronics MEGADAC

## APPENDIX C1

### OPTIMIZATION OF THE DATA ACQUISITION SYSTEM

The complete bridge monitoring system is composed of the bridge, sensors, cabling, the data acquisition system, and the interfacing circuitry. The bridge is the component of interest, but in order to accurately characterize its behavior and eliminate erroneous measurements, the performance of the other components must be understood.

Control or Systems Engineering (open loop control in particular) is a specialty area in electrical and mechanical engineering which has an important bearing on bridge monitoring. There are two fundamental concepts in this field: the concept of a signal and of a system. A signal is a function of one or more independent variables and typically contains information about the behavior or nature of some phenomenon. Time is usually the independent variable and the common dependent variables are temperature, strain, pressure, vibration, etc. Information in a signal is contained in a pattern of variation, and is generally stored in either the amplitude, frequency, or phase of a signal which together completely characterize a time signal. A system is a process that transforms an input signal into an output signal.

Figure is a block diagram that represents  $n$  sensor channels and the corresponding hardware necessary for interfacing signals to a computer for post-processing.

This appendix discusses of the evaluation and optimization of the data acquisition system, and illustrates the software and MEGADAC data acquisition system.

#### **C.1 Fundamental Trade-Offs in Data Acquisition System Design**

In order to select the appropriate data acquisition system for a particular application, the user must have information about the system under test and a concept of the inputs to this system. The following factors should be considered in making a selection:

- Number and types of sensors to be used
- Signal conditioning required for each particular sensor
- Desired sampling rate (defined below)
- Required resolution and accuracy
- Durability of the system
- Memory requirements
- User-friendliness of the system
- Ease of customization and integration with other signal conditioning and data processing hardware/software

Sensor signals are generally continuous functions of time, and an infinite number of points exist in a continuous interval. Digital systems have a limited amount of memory and as a result can only store a finite number of data points. A modern data acquisition system stores sequences of numbers which interpolate the sensor signals, and then utilizes digital signal processing algorithms. A rule in signal processing, known as the Nyquist Criterion, states that in order for a sequence of numbers to accurately interpolate a continuous-time signal, the sampling frequency must be at least twice that of the highest spectral component of that signal (i.e., the highest significant frequency in the Fourier Transform). The oversampling factor is defined as the ratio of the actual sampling frequency to the frequency of the highest spectral component of interest. In terms of the Nyquist Criterion, this means that the minimum oversampling factor required is two. In practice, the oversampling factor is made much greater to provide extra data points for averaging out high frequency noise.

It is important to make the distinction between the per-channel sampling rate ( $f_{PC}$ ) and the total sampling rate ( $f_T$ ). The per-channel sampling rate is the frequency at which a particular sensor is sampled. The total sampling rate is the rate that the data acquisition system must be sampling at in order to obtain the desired per-channel rate. For systems that sample all the sensors in parallel, these parameters are equivalent. However, for many data acquisition systems (such as the MEGADAC 3108DC used in this project), the total sampling rate is a function of the number of sensors employed in a test. These acquisition systems must sequentially obtain one sample from each sensor used in the test before another sampling sweep can be performed. The relation between the fastest per-channel sampling rate and the total sampling rate for this type of acquisition system is given by:

$$f_{PC} = \frac{f_{Total}}{\text{Number of Channels}}$$

The per-channel sampling rate can be set lower, but

the system typically acquires data at this speed and simply remains idle until the sampling period has expired.

There are three fundamental trade-offs involved in data acquisition:

- The trade-off between the per-channel sampling frequency and the sensor count
- The trade-off between the per-channel sampling frequency and memory capacity
- The trade-off between the full-scale range and the resolution

The first trade-off pertains to data acquisition systems which must sequentially sweep through all sensors before a second sweep can begin (described above). As seen from the above equation, if the system is operating at its maximum total sampling rate (so that  $f_{Total}$  is a constant), then the number of sensor channels is inversely proportional to the per-channel or desired sampling rate. Hence, the time required to sample increases with the number of sensors used in a test. The second trade-off is due to the fact that data acquisition systems have a finite amount of memory. When sampling at an extremely high rate, a large amount of data is obtained in a very short time. As a result, the memory buffer of the data acquisition system can fill up and restrict the maximum test duration. The third trade-off results from the quantizing of a signal's amplitude into a fixed number of equal-length steps (i.e., points on the y-axis when plotting signal amplitude vs. time) by the data acquisition system. The total number of these steps is constant for a given data acquisition system. By varying the gain on the data acquisition system, either the full-scale range

can be increased while decreasing resolution, or vice versa. In order to set this gain appropriately, the maximum expected signal amplitude must be considered. The gain is then set so that the full-scale range of signal amplitudes is at least twice the maximum expected signal amplitude, which gives the resolution.

## **C.2 Attributes of the Data Acquisition System Selected for the Project**

The data acquisition system selected for the project was a MEGADAC 3108DC from Optim Electronics. It allows a maximum of 64 sensors to be monitored in parallel, and an expansion chassis can be purchased to increase this capacity. Many different types of signal conditioning modules and A/D circuit cards are available from Optim Electronics for exciting and reading a large number of different sensors. In addition, the MEGADAC 3108DC comes with a user-friendly database management software package, known as the Test Control Software (TCS). Some of the specific features of the MEGADAC 3108DC are listed below [TCS manual and MEGADAC 3108 manual from Optim Electronics]:

- Variable per-channel sampling rates with a total sampling rate of 25,000 samples/sec.
- Both manual and automatic data triggers based on data limits
- Automatic sensor offset correction
- Automatic conversion from voltage to appropriate engineering unit
- A programming language for on-line data manipulation
- Programmable data alarms
- Various ways to display both live and recorded data

The Test Control Software allows tests to be easily defined, documented, and controlled from a 486 PC system under DOS. Hence, a communication interface between the PC and data acquisition system must be established. An AT-GPIB/TNT IEEE-488 parallel interface circuit card from National Instruments was used for this purpose (not standard with the MEGADAC 3108DC package).

Signal conditioning modules are circuit cards required to provide excitation for each sensor and to process the sensor information so that it is presented in a usable form. All the signal conditioning cards were customized with hardware jumpers to set the following:

- The address range of each circuit card
- The gain for each sensor channel
- The passband for the filter on each channel (a filter is a frequency-selective circuit, and the passband is the range of frequencies whose spectral components propagate through the circuit undisturbed)
- The excitation signal for each sensor channel

Terminal blocks are boards which route the signals carried by the sensor cables to the signal conditioning cards via ribbon cable. There are also hardware jumpers on the terminal blocks that must be configured differently depending on the type of sensor.

### **C.3 Test Control Software (TCS)**

Optim developed TCS as a programming tool to simplify the operation of the MEGADAC series of data acquisition systems in terms of defining, recording, and reviewing data acquisition applications. TCS runs within the DOS 640K boundary. Version 5.1.2 of TCS is currently being used by the research team. This section provides a general overview of how TCS is used in conjunction with the MEGADAC 3108DC.

TCS is a menu-driven, window-oriented application software, whose menu selections are presented in a logical sequence of operation. Test procedures are entered in terms of engineering units and time. The user must also define how the data is to be displayed. TCS allows the user to monitor all channels for the test in progress. Channels can be monitored in real-time, using numeric charts, peak values, or graphic plots (up to 30 plots simultaneously).

In addition to the test data manipulation provided by TCS, existing analysis tools such as Excel, dBase, and MATLAB can be used, since the data can be converted to their industry standard data formats (Binary, Floating Point, ASCII, DIF, etc.).

### **C.4 Signal Conditioning Issues**

#### **C.4.1 Vibrating Wire Sensor Signal Conditioning**

A signal conditioning module (AC 3884VW1K) from Optim Electronics was used to excite and read eight Geokon vibrating sensors with associated thermistors. The vibrating wire is excited (i.e., plucked) by an inductive coil which surrounds the wire. Excitation is provided by a square wave whose amplitude varies from 0 to 5 volts, and whose instantaneous frequency varies from 450 to 1000 Hz. The excitation lasts for only 32 cycles and produces an electromagnetic field which causes the sensor to start ringing at its resonant frequency. This resonant frequency is a function of the strain on the structure under test. The vibrating wire sensor encodes this information as a frequency modulated voltage signal, again via the inductive coil. The signal conditioning module demodulates this voltage signal with the setup shown in Figure .

The thermistor portion of the Geokon 4001 is excited with a very stable 1000 micro-amp current source. The resistance of the thermistor varies non-linearly with temperature, and this information is encoded in the resulting voltage drop across the thermistor. The AC 3884VW1K signal conditioning card then conditions this voltage signal with the electronics shown in Figure .

#### **C.4.2 Quarter Bridge Strain Gage and Ambient Weather Sensor Signal Conditioning**

The AD-1 808FB-1 signal conditioning board was selected for use in the project because of its flexibility and features. It can be configured to excite and read a variety of different sensors including full bridge strain gages, quarter bridge strain gages, ambient weather sensors, DC-LVDT's, clip gages, slide wire potentiometers, tiltmeters, accelerometers, and many others. This flexibility is achieved via hardware jumpers. Jumpers on the terminal blocks allow external circuitry (such as the Wheatstone bridge completion resistor network for the Tokyo Sokki

Quarter Bridge sensors and the current-to-voltage conversion resistor for the EASI weather sensors) to be incorporated in the signal conditioning. In addition, jumpers directly on the AD-1 808FB-1 board allow the user to vary the sensor excitation (either 2, 5, or 10 V), the card gain (1 or 100), and the filter passband (any desired range; 0-100 Hz is used in this project). Figure shows a diagram of the AD-1 808FB-1 circuit board. In addition to the flexibility described above, the AD-1 808FB-1 has the advantage of conserving space in the MEGADAC 3108DC chassis because both the excitation circuitry and the signal conditioning circuitry are incorporated on the same circuit card. Thus, if one is not limited by sampling rate constraints, a higher sensor count can be achieved.

#### **C.4.3 Thermocouple Signal Conditioning**

The AD 816TC board connects directly to any E, J, K, R, S, or T-type thermocouple. It has sixteen input channels per module, with a thermal compensation mass, and  $\pm 10$  volts common mode protection. It works with the JP816 jack panel. TCS includes the voltage-to-temperature linearization equations for all popular thermocouples. The AD 816TC board has a card gain of 100, and three-pole 40 Hz filters are available. The AD 816TC card conditions the signal with the electronics shown in Figure .

#### **C.4.4 Analog-to-Digital Conversion Module**

An ADC 3108 circuit card from Optim Electronics was selected as the analog-to-digital (A/D) converter for the project. It is a 16-bit A/D converter implemented with the successive approximation technique and utilizing capacitor technology. The ADC 3108 has the following features:

- Sample-and-hold
- Second tier multiplexing
- Variable post gains of 1, 2, 4, 8, 16, 32, 64, and 128
- Calibration reference voltages
- A channel balance digital-to-analog converter for automatically removing any sensor offset

The maximum total sampling rate with the ADC 3016 is 25,000 samples/sec. Due to overhead in the design of the ADC 3016 and the MEGADAC 3108DC, the maximum per-channel sampling rate is only 10,000 samples/sec., not 25,000 samples/sec., as it ideally should be when using only one sensor in a test. See

Figure for an internal schematic of the ADC 3108.

### **C.5 Cable Selection and Cabling Issues**

Manufacturers of instruments normally standardize the type of cable for each instrument; to do otherwise would create difficulties in supply to the end user. However, the standard type may not be suitable for all applications, and the user should participate in the selection of cable. The following items should be considered for cable selection:

- Length of run
- Frequency and magnitude of signal
- Environment (underground, aerial, etc.)
- Temperature of environment

- Longevity requirements
- Susceptibility to damage (hence, a need for conduit or armoring)
- Proximity to sources of electrical noise

Primary causes of noise are radio frequency interference and electromagnetic interference from sources such as power lines, electrical generators and motors, commercial TV, radio or radar stations, nearby thermostats and other switch closures, welding, and dirty terminals of power line transformers. The best protection against noise is the use of cable shielding. Individually shielded twisted pairs, bundled inside an overall shield, are recommended for all applications. As a rule of thumb, the shield should be grounded with respect to the measuring circuit at one end only so as to avoid any ground loop problems.

Cable splices should not be planned into a system unless there is no alternative. Splices can be a reliability concern due to physical failure or shorting of the connections. Electrical noise may increase due to the loss of shielding at a splice. Although more time consuming, soldered splices should be used instead of crimp splices.

Cabling is a more important issue when using resistance-based gages because of lead wire effects. The lead wire resistance can cause two types of errors. One is due to resistance changes in the wires that are indistinguishable from resistance changes in the gage. This error can be reduced significantly for the quarter-bridge strain gage by utilizing a three-wire connection at the terminal block to balance out the wire resistance within the Wheatstone bridge.

The other error is known as lead wire desensitization. This error reduces as the thickness of the conductor cable increases. This error is quantified in Table for the quarter bridge strain gage. Sense leads can be employed for other gage types to completely remove these cabling errors. This additional pair of cable leads provides direct feedback of the actual gage excitation voltage and the return voltage is reduced proportionately.

During the first phase of the project, AWG-18 six-wire individually shielded twisted pairs were used. Soldered connections were applied where needed. The connections were insulated by water-resistant resin and duct tape for waterproofing.

<b>AWG</b>	<b>Gage Resistance (%) = 120 Ohms</b>	<b>Gage Resistance (%) = 350 Ohms</b>
18	.54	.19
20	.87	.30
22	1.38	.47
24	2.18	0.75

\* per 100 foot of cable at 0.25° Celsius.

**Table C-1: Lead Wire Desensitization Error**

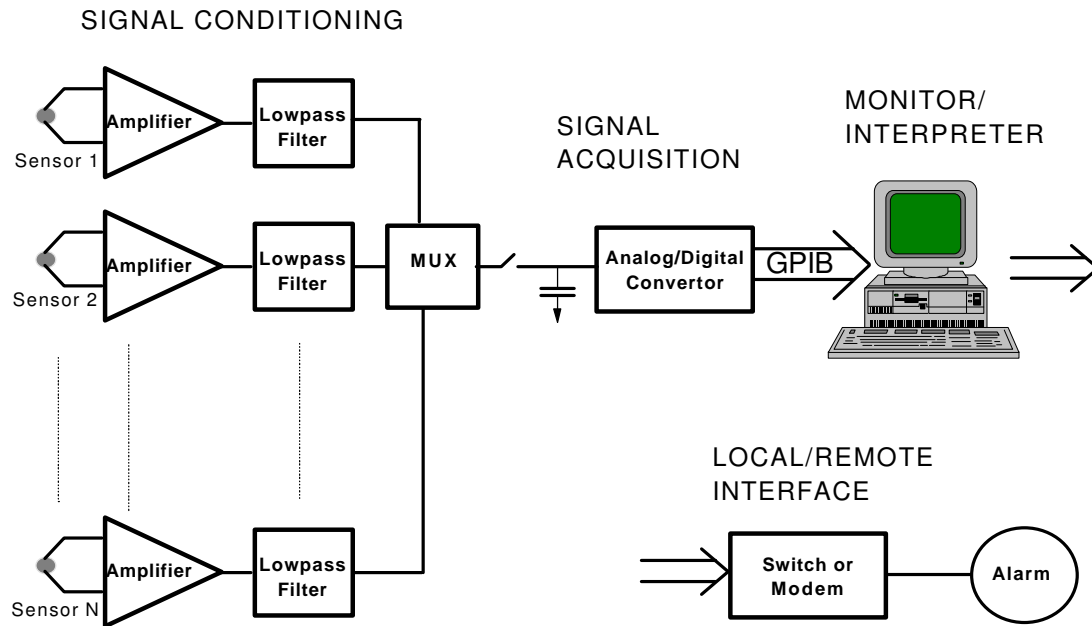


Figure C-1: The Electrical System

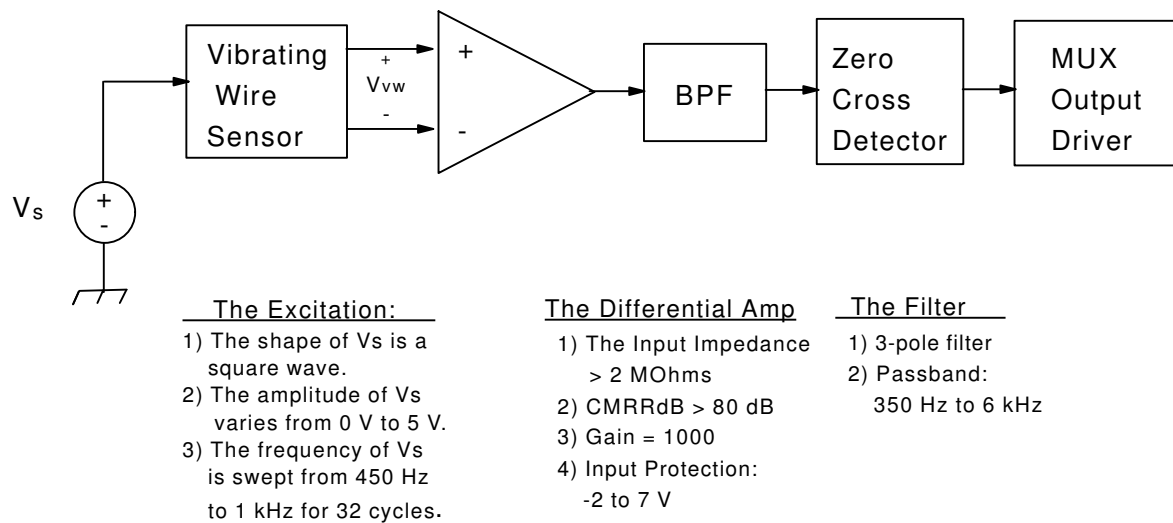
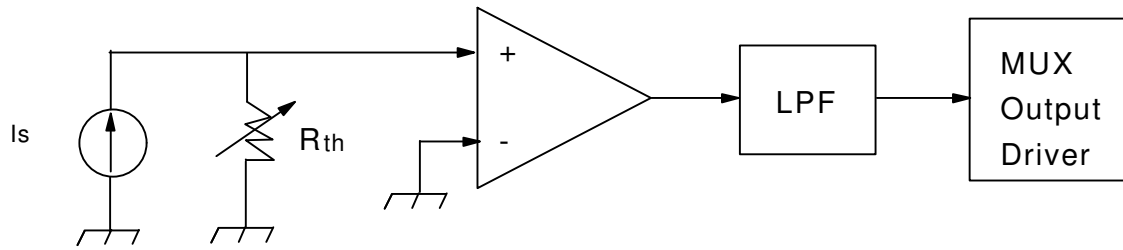


Figure C-2: One Channel of the AC 3884VW1K Circuit Card (Strain Gage Conditioning)

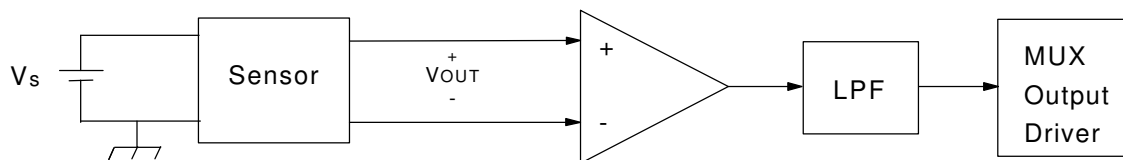


- The Excitation
- 1)  $I_s = 1000$  microAmps
  - 2)  $R_{th}$  = the thermistor
  - 3) The tolerance for this current source is 300 ppm.
  - 4) The tempco for this current source is 60 ppm/C

- The Differential Amp
- 1) The Input Impedance > 2 MOhms
  - 2) CMRRdB > 80 dB at 60 Hz.
  - 3) Gain = 1
  - 4) Input Protection: -12 V to +12 V

- The Filter
- 1) 3-pole filter
  - 2) Cutoff frequency = 100 Hz

Figure C-3: One Channel of the AC 3884VW1K Circuit Card (Thermistor Conditioning)



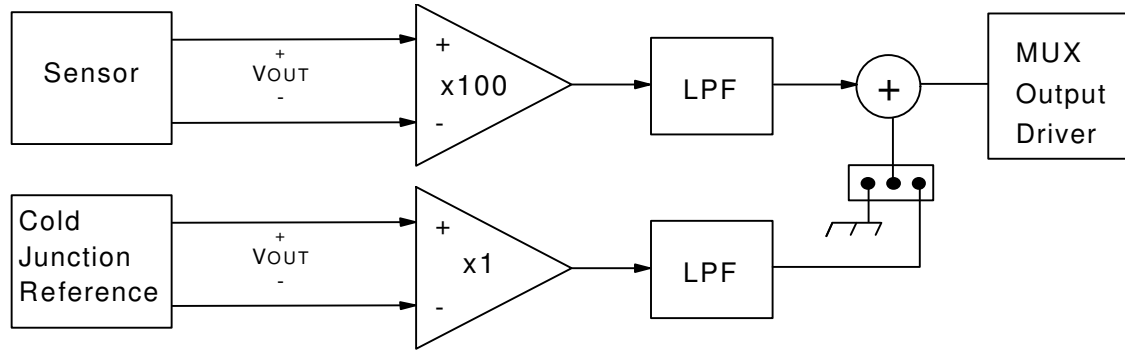
- The Excitation
- 1) The onboard DC voltage supplies are 2, 5, and 10 V (5 V is used for the quarter bridge sensors)
  - 2) External DC voltage supply = 12 V (Used for all weather sensors)

- The Sensors Used with the AD-1 808FB-1
- 1) Quarter Bridge strain gages
  - 2) Ambient temp. sensor
  - 3) Humidity sensor
  - 4) Wind Speed sensor
  - 5) Wind Direction sensor

- The Differential Amp
- 1) The Input Impedance > 20 MOhms
  - 2) CMRRdB > 95 dB at 60 Hz.
  - 3) Gain: 1 or 100
  - 4) FS input
    - a) -10 to +10 V with Gain=1
    - b) -0.2 to 0.2 V with Gain=100
  - 5) BW3-dB = 2 kHz

- The Filter
- 1) 3-pole active Butterworth filter
  - 2) Cutoff frequency = 100 Hz (This is variable)

Figure C-4: One Channel of the AD-1 808FB-1 Circuit Card



The Sensors Used with the AD 816TC  
 Thermocouples used during Cambering Process

The Differential Amp  
 1) The Input Impedance > 10 MOhms  
 2) CMRRdB > 80 dB at 60 Hz.  
 3) Gain: 100  
 4) BW3-dB = 40 kHz

The Filter  
 1) 3-pole active Butterworth filter  
 2) Cutoff frequency = 20 Hz

Figure C-5: One Channel of the AD 816TC Circuit Card

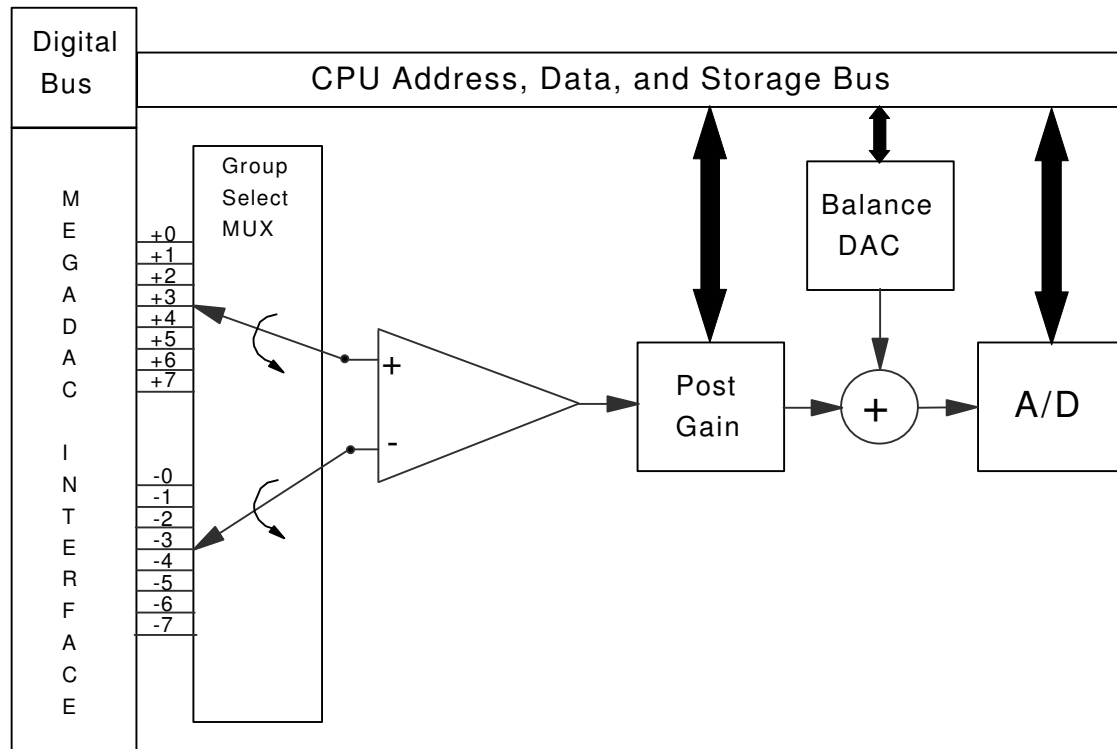


Figure C-6: Schematic of the Internals of the ADC 3108